

AD-A273 661



1



12th International Corrosion Congress

PRECEEDINGS

S DTIC
ELECTE
DEC 09 1993
A

This document has been approved
for public release and sale; its
distribution is unlimited.

September 19-24, 1993
VOLUME 1
Houston, Texas USA

93-29552



7587

COATINGS

NACE
International

93 12 2 096

CORROSION CONTROL FOR LOW-COST RELIABILITY



**12th
International
Corrosion
Congress**

PRECEEDINGS

VOLUME 1

COATINGS

The manuscripts in this volume have been printed from camera-ready copy and have been accepted without editing by NACE International.

Neither NACE International, its officers, directors, members thereof, nor instructors accept any responsibility for the use of the methods and materials discussed herein.

Any goods, products, and/or services mentioned are mentioned as items of information only. Such mention does not constitute an endorsement by NACE International.

The information is advisory only, and use of the materials and methods is solely at the risk of the user.

Printed in the USA. All rights reserved. This book, or parts thereof, may not be reproduced in any form without permission of the copyright owners.

Copyright, NACE International, 1993

ISBN: 1-877914-65-7

Published by

NACE International
P.O. Box 218340
Houston, TX 77218-8340

Accession For	
NTIS	CRA&I <input checked="" type="checkbox"/>
DTIC	TAB <input type="checkbox"/>
Unannounced <input type="checkbox"/>	
Justification	
By	Vol. 1 - 85
Distribution	SD 400
Availability Codes	
Dist	Avail. for Special
A-1	21

NACE
International

DTIC QUALITY INSPECTED 3

Co-Sponsors:

Air & Waste Management Association
American Institute of Chemical Engineers
American Concrete Institute
American Ceramic Society
American Chemical Society
American Iron & Steel Institute
American Society for Testing and Materials
American Society for Nondestructive Testing
American Society of Civil Engineers
American Welding Society
Electric Power Research Institute

The Electrochemical Society
Federation of Materials Societies
Federation of Societies for Coatings Technology
Institute of Clean Air Companies
The Materials Properties Council
Materials Technology Institute of the Chemical Process Industry, Inc.
Minerals, Metals and Materials Society
National Society of Professional Engineers
Steel Structures Painting Council

International Corrosion Council (ICC)*

E. Mattsson, Chairman
Prof. Graham C. Wood, First Vice Chairman
Dr. Michael J. Graham, Second Vice Chairman
vacant, Secretary

Dr. Jose Juan Podesta (Argentina)
Dr. Jose Rodolfo Galvele (Argentina)
David Whitby (Australia)
Prof. Brian W. Cherry (Australia)
Dr. F. Hilbert (Austria)
Prof. Dr. H. Zitter (Austria)
Lucien Clerbois (Belgium)
Prof. Dr. M. Pourbaix (Belgium)
Dr. Leonardo Uller (Brazil)
Dr. Aldo Cordeiro Dutra (Brazil)
Dr. Raicho Raicheff (Bulgaria)
F.W. Hewes (Canada)
Dr. Antonio Pagliero (Chile)
Prof. Ziao Jimei (China)
Prof. Sheng-tai Shih (China)
Prof. Carlos E. Arroyave Posada (Colombia)
Prof. Ruby de Gutierrez (Colombia)
Ing. Juan Fdo. Alvarez (Costa Rica)
Ing. Teresita Calderon Hernandez (Costa Rica)
Ing. Pavel Novak (Czechoslovakia CSSR)
Dr. Jiri Sikac (Czechoslovakia CSSR)
Hans Arup (Denmark)
Prof. Ernst Maahn (Denmark)
Prof. Venice K. Gouda (Egypt U.A.R.)
Prof. A.M. Shams El Din (Egypt U.A.R.)
Dr. Eino Uusitalo (Finland)
Prof. Seppo Ylasaari (Finland)
Prof. Gerard Beranger (France)
Prof. Paul Lacombe (France)
Dr. H. Harzbecker (German Democratic Republic DDR)
Prof. Dr. Hans-Jurgen Engell (Federal Republic of Germany)
Prof. Alfred Rahmel (Federal Republic of Germany)
vacant (Great Britain)
Dr. George W. Greene (Hong Kong)
Prof. Endre Berecz (Hungary)
Dr. Bela Lengyel (Hungary)
Dr. K. Balakrishnan (India)
Dr. K.I. Vasu (India)
R. Kastanya (Indonesia)
Suripto Adiwidjojo (Indonesia)
Dr. A. Afshar (Iran)
Dr. A.R. Mohammed (Iraq)
Prof. J. Yahalom (Israel)

Yesha Berger (Israel)
Prof. Francesco Mazza (Italy)
Prof. Giordano Trabanelli (Italy)
Dr. Hideya Okada (Japan)
Prof. Norio Sato (Japan)
Dr. F.M. Al-Kharafi (Kuwait)
Ali A. Elbasir (Libya)
Dr. Haji Mohamed Mansor Salleh (Malaysia)
Ong Chong Hup (Malaysia)
Dr. Essadiqi El Hachmi (Morocco)
Prof. Salah E. Moujahid (Morocco)
Ir. J.H. van der Veen (Netherlands)
Prof. J.H.W. de Wit (Netherlands)
Les Boulton (New Zealand)
Dr. John R. Duncan (New Zealand)
Prof. Dr. Per Kofstad (Norway)
Prof. Dr. Kemal Nisancioglu (Norway)
Prof. I.H. Khan (Pakistan)
Dra. Agnes de Bosques (Panama)
Dr. Juan Camus (Panama)
Ing. Guillermo Salas Donohue (Peru)
Ing. Marcos Valencia Medrano (Peru)
Prof. Dr. R. Juchniewicz (Poland)
Prof. Dr. S. Mrowec (Poland)
Prof. M. Elisabete Moreira Ameida (Portugal)
Eng Eva Raimann Cabral (Portugal)
Dr. Iba F. Al-Adel (Saudi Arabia)
Dr. B.G. Callaghan (South Africa)
R.T. White (South Africa)
Jose M. Costa (Spain)
Juan J. Royuela (Spain)
Kandage Don Amarasena (Sri Lanka)
A. Mir Amirudin (Sri Lanka)
Prof. Christofer Leygraf (Sweden)
Prof. Dieter Landolt (Switzerland)
Prof. E. Triki (Tunisia)
Prof. Dr. Mustafa Doruk (Turkey)
Prof. Dr. Saadet Uneri (Turkey)
Walter K. Boyd (United States)
Prof. Jerome Kruger (United States)
Prof. Yakov Mikhailovich (USSR)
Prof. V. Ogarev (USSR)
Dr. Bui Thi An (Vietnam)
Prof. Ivan Esih (Yugoslavia)
Prof. Sreten Mladenovic (Yugoslavia)

* Membership as confirmed at ICC meeting in Florence in 1990. A revised membership list will be confirmed at the 1993 ICC meeting.

International Scientific Advisory Committee

R. Baboian
K. Balakrishnan
G. Beranger
J.R. Galvele
R.J. Hussey
P. Kofstad
D.D. Macdonald
F.V. Mazza
T. Murata
R.N. Parkins
A.J.E. Pourbaix
A. Rahmel
J. Kruger
L. Uller
J. Yahalom

Honorary Committee

Edward C. Greco (co-president)
T.J. Hull (co-president)
E.J. Engell
G.C. Wood
M.J. Pourbaix
N. Sato
S.T. Shih
G. Trabanelli

Organizing Committee

Prof. J.H. Payer, Congress President
J. Kruger, Deputy Chairman
W.K. Boyd, Deputy Chairman

V. Agarwala
D. Anderson
B. Ashbaugh
A. Asphahani
R. Baboian
J. Beavers
J. Bennett
S. Dean
S. Dexter
D. Duquette
K. Efird
T. Graedel
M. Graham
H. Hack
R. Hausler
G. Hodge
J. Kolts
D. Kroon
R. Latanision
H. Lawson
B. Lichter
L. Magnon
F. Mansfeld
P. Mayer
D. McCright
J. Montle
C. Nathan
J. Oldfield
R. Parkins
H. Pickering
R. Puyear
R. Rapp
R. Ricker
H. Rossy
L. Scribner
J. Sedriks
D. Sinclair
B. Skerry
S. Smialowska
K. Staehle
B. Syrett
H. Townsend
R. Tuttle
E. Verink
D. Waters



12th
International
Corrosion
Congress

NACE
International

PREFACE

The 12th International Corrosion Congress (ICC) was held September 19-24, 1993 in Houston, Texas USA. The ICC convenes every three years under the auspices of the International Corrosion Council, an international body composed of representatives from more than 40 countries. The goal of the 12th ICC was to stimulate and promote better corrosion control for increased reliability and safety and for reduced costs. This was accomplished through the presentation, discussion and sharing of corrosion science and technology by experts from around the world. In addition to the formal presentations, valuable informal discussions were held throughout the week at the exhibits, breaks and receptions.

The ICC, more than any other meeting, successfully brings together the corrosion community from around the world. The founders of the event and those that assured its continuation are to be commended for their foresight. Now more than ever, we live and work in an international setting. Global markets and global manufacturing demand communication, coordination and cooperation among international technical experts. The documentation and dissemination of corrosion science and engineering is a critical responsibility of the ICC, and this responsibility is met by the high quality and comprehensive nature of the technical presentations and papers. An equally important role of the ICC is its leadership in the fostering and nurturing of the corrosion community. This responsibility is carried out through providing a forum for technical exchange and through the recognition and encouragement of corrosion associations in each member country.

NACE International was the organizing society for the 12th ICC. NACE was a leader in the establishment of the International Corrosion Council and was proud to host the 12th ICC in its hometown during NACE's 50th anniversary year. For more than 50 years NACE has led the way in the documenting and disseminating advances in the science and technology of corrosion control.

The technical program of the 12th ICC consisted of over 400 papers presented in more than 30 technical sessions. Each technical session was co-chaired by a member of the organizing committee and another international corrosion expert. The plenary lectures were given by Professor Norman Hackerman (USA), Professor Dr. Heinz Spahn (Germany), Dr. Tatsuo Kondo (Japan) and Professor Redvers N. Parkins (UK). There were four special workshops within the congress:

- EPRI Workshop on On-Line Monitoring of Corrosion and Water Chemistry for Electric Power Utility Industry
- Oil and Gas Production and Refining Workshop
- Chemical Process Industry Workshop
- International Corrosion Council Workshop

More than 60 displays and exhibits were hosted by companies offering the latest in products and services for preventing materials degradation.

The 12th ICC Organizing Committee was chaired by Professor Payer with Deputy Chairmen W. K. Boyd and J. Kruger. The tremendous efforts of this committee are gratefully acknowledged. A full listing of membership of the Organizing Committee, Honorary Committee, International Scientific Advisory Committee are presented in these proceedings. In recognition of their important contributions to the establishment of the International Corrosion Council, Co-presidents of the 12th ICC were Edward C. Greco, former NACE President, and T.J. Hull, former NACE Executive Director.

The International Corrosion Council meetings at the congress were chaired by Professor Einar Mattsson with First Vice Chairman Professor Graham Wood. The support and guidance of these fellows and the Council are gratefully acknowledged.

Speaking for the many who have contributed so much time and effort into making the 12th ICC a success, we are proud to have served. We encourage the participation of those who will plan and conduct future ICC's. It is a worthwhile effort and contributes significantly to the understanding and control of corrosion around the world.

Joe Payer**
President
12th International Corrosion Congress

** Professor and Chairman,
Department of Materials Science and Engineering,
The Case School of Engineering, Case
Western Reserve University, Cleveland, Ohio

HISTORY OF THE INTERNATIONAL CORROSION COUNCIL AND THE INTERNATIONAL CORROSION CONGRESS

Increasing demands which were being made on materials by space age development, underlined the need for cooperation among and between corrosion scientists and engineers in every country.

The first attempt to promote a forum for the exchange of corrosion information occurred in Great Britain in the early 1960's. Under the auspices of the International Union for Pure and Applied Chemistry and the Minister of the British Council for Science, Sir Henry Melville, a plan was conceived to hold an International Congress on Metallic Corrosion. Lord Melville, with the assistance of U. R. Evans, T. P. Hoar and other British scientists, solicited participation from corrosion specialists throughout the world which resulted in the first International Congress on Metallic Corrosion being held in April, 1961 in London. The meeting proved to be a great success.

One of the attendees at this meeting was Dr. Edward C. Greco, who, at the time, was Vice President of NACE. During the Congress, Dr. Greco and Tenny J. Hull, the Executive Secretary of NACE, had several meetings with Lord Melville regarding future plans for holding such conferences. It was learned that no plans were in progress for a second congress or an international organization, to perpetuate the exchange of corrosion information.

Upon his return to the U.S., and after becoming President of NACE, Dr. Greco, with the aid of T. J. Hull, put together an organization plan for presentation to the NACE Board of Directors. The Board approved the plan for holding a second International Congress on Metallic Corrosion, in connection with the 1963 annual NACE conference to be held in March in New York City. Dr. Greco enlisted the assistance of Frank La Que, Mars Fontana, and Herb Uhlig in contracting internationally known corrosion scientists and engineers for their support and participation. Dr. Greco served as president with La Que and Uhlig as vice-presidents. Honorary vice-presidents included M. Pourbaix of Belgium, H. P. Goddard of Canada, G. Chaudron of France, H. Fischer of Germany, L. Cavalloro of Italy, G. Okomoto of Japan, W. Feitknecht of Switzerland, and R. B. Mears of the United States.

At the second conference, a "draft" charter and by-laws for a permanent council for the ICMC was presented to key people from the participating countries. Reactions were favorable so a meeting with all of the world corrosion scientists was arranged.

The draft charter and by-laws were adopted with some minor changes. It was decided that a Congress would be held every three years and that each member country would have two voting representatives on the permanent council. Dr. Greco was elected the first president, and Dr. Pourbaix the first vice-president. T. J. Hull of NACE was appointed Secretary of the Council. It was also agreed that the third congress would be held in the USSR in 1966. Dr. J. M. Kolotyrkin was to serve as a president of the Moscow conference.

Dr. Greco served as president of the permanent council until the fourth congress held in Amsterdam in 1969, at which time Dr. Pourbaix assumed the presidency of the permanent council, and held that position for the fifth congress in Amsterdam, and the sixth in Sidney.

At the Sidney conference, Bill Hewes of Canada, Dr. Stewart Leach of Great Britain, and T. J. Hull of the United States completed a much needed revision of the by-laws. Dr. H. H. Uhlig of the United States was elected president of the permanent council and served as such through the seventh congress held in 1978 in Rio de Janeiro.

Dr. Leach served as president of the council through the 8th congress in Mainz, Germany. At this conference, Dr. Paul Lacombe of France assumed the presidency of the council.

At the 9th ICMC, hosted by the Canadians in Toronto, Dr. G. Trabanelli was elected president and served through the 10th congress in Madras, India.

Dr. Jerome Kruger of the United States assumed the presidency in Madras and led the congress through the 11th ICC held in Florence, Italy. The 12th congress is being held in Houston, Texas, in 1993.

As noted, distinguished scientists from around the world have served as President of the permanent council. The present council president is Dr. Einar Mattsson of Sweden.

The success of each congress has been insured by the unselfish work of the conference committee chairmen. Some of the most recent host nation chairmen include:

Dr. Dutra	Rio de Janeiro	1978
Dr. Engell	Mainz	1981
Dr. Graham	Toronto	1984
Dr. Mazza	Florence	1990
Dr. Payer	Houston	1993

Through the years, the Council and the ICC have been very successful in promoting and maintaining its objectives. They are:

1. To stimulate, on an international level, research in corrosion science and engineering, and to encourage the broad dissemination of the results of the research.
2. To promote cooperation among and between corrosion scientists and engineers in every country.
3. To provide an organization within whose framework corrosion scientists and engineers can meet to exchange ideas, discuss results of their studies, and publish their findings for the common good.
4. To conserve equipment, materials, and natural resources by focusing the attention of all countries on the waste which is the result of unrecognized and uncontrolled corrosion.
5. To focus attention of agencies in every country on the importance of providing for and supporting research in corrosion science and engineering.
6. To provide a means by which colleagues from every country can associate on a common ground and become better acquainted.

The interest in corrosion worldwide is attested to by the increase in the number of countries who are now members of the permanent council (total 67 in 1993). This insures that the ICC will be perpetuated, and that its influence on a broad area of corrosion and engineering will be continued for the mutual benefit of all countries.

ESTABLISHMENT OF EDWARD C. GRECO AWARD

The International Corrosion Council approved the establishment of the Edward C. Greco Award honoring the founder of the International Corrosion Council and former president of NACE. The first award was presented to Dr. Greco in Houston at the 12th ICC. Subsequent awards will be presented in Houston and at each ICC to the president of the International Corrosion Congress for leadership in the organization and conduct of the Congress.

The increasing demands which were being made on materials by traditional industries and the emerging space age development underlined the need for cooperation among and between corrosion scientists and engineers in every country. The first such attempt to promote a forum for the exchange of corrosion information occurred in Great Britain. Under the auspices of the International Union for Pure and Applied Chemistry and the Minister of the British Council for Science, Sir Henry Melville, a plan was conceived to hold an International Congress on Metallic Corrosion. Lord Melville, with the assistance of U. R. Evans, T. P. Hoar and other British scientists, solicited participation from corrosion specialists throughout the world with the result that the first International Congress on Metallic Corrosion was held in April 1961 in London. The meeting proved to be a great success.

One of the attendants at this meeting was Dr. Edward C. Greco, who at the time was vice-president of NACE. During the Congress, Dr. Greco and T. J. Hull, then executive secretary of NACE, had several meetings with Lord Melville regarding future plans for holding such conferences. It was learned that no plans were in progress for a second congress or an international organization to perpetuate the exchange of corrosion information.

Upon his return to the United States and after becoming president of NACE, Greco, with the aid of Tenny Hull, put together an organization plan for presentation to the NACE Board of Directors. The Board approved the plan for holding a second International Congress on Metallic Corrosion in connection with the 1963 annual NACE conference to be held in March in New York City. Greco enlisted the assistance of Frank La Que, Mars Fontana and Herb Uhlig in contacting internationally known corrosion scientists and engineers for their support and participation. Greco served as president of the Congress with La Que and Uhlig as vice-presidents. Honorary vice-presidents included M. Pourbaix of Belgium, H. P. Goddard of Canada, C. Chaudron of France, H. Fischer of Germany, L. Cavaloro of Italy, G. Okomoto of Japan, W. Feitknecht of Switzerland, and R. B. Mears of the USA.

At the second Congress, a draft charter and by-laws for a permanent Council for the ICC was presented to key people from the participating countries. Reactions were favorable so a meeting with corrosion scientists from around the world was arranged.

The draft charter and by-laws were adopted with some minor changes. It was decided that a congress would be held every three years and that each member country would have two voting representatives on a permanent council. Dr. Greco was elected the first chairman and Dr. Pourbaix the first vice-chairman. T. J. Hull of NACE was appointed secretary of the Council. It was also agreed that the third congress would be held in the USSR in 1966. Dr. J. M. Kolotyrkin was to serve as a president of the Moscow conference.

Dr. Greco served as chairman of the permanent council until the fourth congress held in Amsterdam in 1969, at which time Dr. Pourbaix assumed the chairmanship of the permanent council.

For over 30 years distinguished scientists and engineers from around the world have contributed to and benefitted from the International Corrosion Congress. The interest in corrosion worldwide is attested to by the increase in the number of countries that are now members of the permanent council. This insures that the ICC will be perpetuated and that its influence on a broad area of corrosion science and engineering will be continued for the mutual benefit of all countries.

The vision and diligent efforts of Dr. Edward C. Greco in this endeavor are much appreciated and recognized by the establishment of this award in his name.

PRECEEDINGS CONTENTS

Paper #

Page #

Paper #

Page #

VOLUME 1

PLENARY LECTURES

Corrosion: Its Effect on Society <i>N. Hackerman</i>	Plenary 1
Low-Cost Corrosion Engineering and Risk Potential, Operational and Environmental Safety - nad Irreconcilable Antagonism in the Chemical Process Industry <i>H. Spahn</i>	Plenary 4
Methodology of Predicting Materials Failures in Advance Nuclear Systems <i>T. Kondo</i>	Plenary 20
Corrosion Control by Transferring Knowledge <i>R. Parkins</i>	Plenary 43

COATINGS ON STEEL

514 Advancements in Automotive Corrosion Resistance <i>M. Ostermiller, L. Lee-Piepho, and L. Singer</i>	1
268 Automotive Phosphating Technology 1975 - 1995 <i>R. Miller, M. Petschel Jr., and R. Hart</i>	16
400 Hydrothermal Properties of Protective Polymer Coatings on Steel <i>R. Granata and K. Kovalski</i>	24
293 Corrosion Behavior of Oxide Coated Cold-Rolled and Electrogalvanized Sheet Steel <i>W. Nowak, H. Townsend, and L. Li</i>	42
039 Electrodeposition of Zn-Fe Alloy at High Current Densities <i>L. Yanping and W. Jixun</i>	53A
569 Study of Enameling Properties on the Hot-Rolled Ti-Containing Steel Sheets <i>X. Xiaolian, Z. Kegang, and L. Ri</i>	54

COATINGS

025 Study of Anticorrosion Properties of Metal Arc-Sprayed Coatings on a Carbon Steel for use in Petro Products <i>A. Groysman and V. Belashchenko</i>	63
266 A Discussion on the Role of Cations in Enhancing Internally Coated Metal Container Corrosion Failure <i>W. Tait and K. Handrich</i>	77
085 The Detrimental Effect of Water-soluble Contaminants at the Steel /Paint Interface <i>M. Morcillo</i>	87

106 Anticorrosive Coatings Based on Phase Decomposed Polymer Blends <i>V. Verkholtantsev and M. Flavian</i>	99
097 Application of Electrochemical Impedance Spectroscopy to Study the Efficiency of Anti-Corrosive Pigments in and Epoxy Resin <i>A. Amirovudin, C. Barreau, and D. Thierry</i>	114
046 Determination of Protective Properties of Polymer Coatings from High-Frequency Impedance Data <i>F. Mansfeld and C. Tsai</i>	128
156 Long-Term Electrochemical Characterizations of MIL-P-24441 Epoxy Coated Steel Using Electrochemical Impedance Spectroscopy (EIS) <i>J. Murray and H. Hack</i>	151
073 Electrochemical Methods to Monitor Degradation of Organic and Metallic Coatings <i>T. Simpson</i>	157
096 Determination of Coating Delamination & Underfilm Corrosion during Atmospheric Exposure by Means of Electrochemical Impedance Spectroscopy <i>A. Amirudin, P. Jernberg, and D. Thierry</i>	171
486 Characterization of Corrosion under Marine Coating by Electrochemical Noise Methods <i>D. Mills, G. Bierwagen, D. Tallman, and B. Skerry</i>	182
066 New Accelerated Test Simulating the Atmospheric Undercoat Corrosion <i>A. Martello</i>	195
044 Compatibility of Organic Coatings with Flame Spraying Zn, Al and Zn-Al Alloy Coatings <i>Z. Zhaoqing</i>	204

METALLIC COATING AND SURFACE TREATMENTS

036 Surface Modification by Chemical and Electrochemical Processes <i>F. Mansfeld, V. Wang, S. Lin, and L. Kwiatkowski</i>	219
180 Laser Melting of Plasma Sprayed Alumina Coatings <i>M. Escudero, V. Lopez, A. Jimenez-Morales, E. Vida, and J. Galvan</i>	240
244 Corrosion and Oxidation Behavior of Ti-Al Surface Alloys Formed Using Laser Irradiation <i>A. Khanna, V. Desai, and G. Goswami</i>	250
254 Corrosion and Heat Resistance of Alumina Coated Iron to Alkali Carbonate at 700°C <i>M. Okuyama, T. Noshiro, and S. Kambe</i>	259

Paper #	Page #	Paper #	Page #
319	Corrosion Resistance of Amorphous Plasma Sprayed Coatings <i>N. Bacha and C. Roy</i> 271	193	Evaluation of Corrosion Resistant Coating for Mild Steel <i>M. Trivedi, H. Mandalia, and C. Mital</i> 473
350	Formation of Protective Wearresistant Oxide Coatings of Aluminum Alloys by the Microplasma Methods from Aqueous Electrolyte Solutions <i>A. Timoshenko, B. Opara, and Y. Magurova</i> 280	332	Electrocorrosion-inhibiting Behaviour of Flame Retarding PVC Pressure-sensitive Adhesive Tape <i>W. Tao, H. Ge, and Y. Qing</i> 484
356	Superior Corrosion Resistance by Niobium Coating <i>S. Ylssaari, M. Turkia, and O. Forsen</i> 294		
394	Effects of Laser Transformation Hardening on the Corrosion Resistance of AISI ₃₁₆ Tool Steel <i>L. Yang, S. Jana, S. Tam, L. Lim, and M. Lau</i> 307		
423	A Comparison of the Corrosion Properties of Thick Layers of Chromium and its Alloys with Nickel Deposited from Chromium (III) Electrolytes <i>M. El-Sharif, A. Watson, X. Wang, and C. Chisholm</i> 315		
424	Studies of Chemical Conversion Treatments of Electrodeposited Zinc-Chromium and Zinc-Nickel-Chromium Alloys <i>M. El-Sharif, Y. Su, A. Watson, and C. Chisholm</i> 329		
461	Study of Corrosion Resistance of Electroless Ni-P Plating <i>L. Yi</i> 341		
472	Resistance to Aqueous Corrosion of Steels Protected by a Cr-Si Diffusion Coating <i>X. Wan, G. Wang, and R. Rapp</i> 353		

VOLUME 2

ATMOSPHERIC CORROSION	
335	Materials Damage Caused by Acidifying Air Pollutants - 4 Year Results from an International Exposure Program within UN ECE <i>V. Kucera, A. Coote, J. Henriksen, D. Knotkove, C. Leygraf, and B. Stockle</i> 494
145	Worldwide Data on the Atmospheric Corrosion Resistance of Weathering Steels <i>M. Komp, S. Coburn, and S. Lore</i> 509
040	The Effects of Acid Deposition on the Atmospheric Corrosion Behavior of Structural Materials in California <i>F. Mansfeld, H. Xiao, and R. Henry</i> 529
584	The Influence of Environmental Acidification on the Atmospheric Corrosion of Zinc <i>E. Johansson and M. Linder</i> 549

NON-METALLIC COATINGS ON STEEL SUBSTRATES

150	Flourescent Materials as Corrosion Sensors for Coatings <i>R. Johnson and V. Agarwala</i>	370	230	Techniques Applied to the Analysis of the Atmospheric Corrosion of Low Carbon Steel, Zinc, Copper, and Aluminum <i>A. Fernandez, M. Leiro, B. Rosales, E. Ayllon, F. Varela, C. Gervasi, and J. Vilche</i>	574
175	The Investigation of a New Autodeposition Coating System <i>Z. Pan, D. Qiu, Z. You, and Y. Zhao</i>	379	530	Indoor Gaseous Sulfide and Chloride Pollutants and Their Reaction with Silver <i>L. Volpe and P. Peterson</i>	590
213	The Influence of Absorbed Layers of Silane Coupling Agents on Protective Properties of Polymer Coatings <i>M. Petrunin, A. Nazarov, and N. Mikhailovski</i>	386	222	Field Exposure Studies of Corrosion Products on Metals <i>C. Leygraf, I. Odnevall, D. Persson, and J. Tidblad</i>	600
309	Research of Weather Resistant Bridge Paint and Wear Resistant Primer and Finish for Bridge Cover Plates <i>Y. Shaoyu</i>	398	437B	Protective Rust Layer Formed on Weathering Steel by Atmospheric Corrosion for a Quarter of a Century <i>T. Misawa, M. Yamashita, H. Miyukii, and H. Nagano</i>	612
290	Determination of Water Transport Properties of Organic Coatings with EIS <i>L. Nicodemo, F. Monetta, and F. Bellucci</i>	406	005	Structure of Rust on Weathering Steel in Rural and Industrial Environments <i>H. Townsend, T. Simpson, and G. Johnson</i>	624
324	Characterization of Organic Coatings with Impedance Spectroscopy <i>J. de Wit</i>	420	351	Effects of Seasalt on Corrosion Attacks at 8 Years Exposure of Metals in a Small Geographical Area of the Swedish West Coast <i>J. Gullman</i>	642
331	Substrate Effects on the Corrosion Performance of Coated Steels under Immersed Conditions <i>J. Costa, S. Faidi, and J. Scantlebury</i>	437	305	Chemical Characterization of the Corrosion Products Formed on Plain C Steel, Zinc, Copper, and Aluminum <i>S. Granese, A. Fernandez, and B. Rosales</i>	652
333	Why the Best Performance of Phosphoric Acid Pretreatments when Activated with Aluminium Hydroxide <i>E. Almeida and D. Pereira</i>	449	294	Initial Stages of SO ₂ Induced Atmospheric Corrosion of Zinc Investigated by In-Situ IR Spectroscopy and Time Resolved Trace Gas Analysis; Synergistic Effects of NO ₂ and O ₂ <i>J. Svensson and L. Johansson</i>	662
007	A Unique Plasma Spray Process to Create Corrosion Control Surfaces <i>G. Sweet and W. Bristowe</i>	460			

Paper #	Page #	Paper #	Page #
377	Galvanic Corrosion of Zinc/Steel Under Thin Layer Electrolytes <i>X. Zhang and E. Valeriot</i> 676	102	Plant Measurement Cell for Carrying Out Electrochemical Corrosion Investigations on the Plant <i>G. Wagner and R. Munster</i> 862
416	Experimental Approaches to the Study of Corrosion in Thin Water Layers <i>V. Brusic, G. Frankel, T. Peterson, and S. Huang</i> 687	061	Experience with Neutron Activation for Real-time Corrosion Monitoring in a Urea Plant <i>G. Notten, J. Thoelen, H. Verhoef, and R. Van Sluijs</i> 869
420	Simulation of the Degradation of Limestone and Dolomitic Sandstone under Dry Deposition Conditions <i>S. Haneef, J. Johnson, G. Thompson, and G. Wood</i> 700	330	Corrosion Upsets are Probably More Costly Than You Know <i>A. Perkins</i> 882
308	Dissolution and Precipitation Phenomena in Atmospheric Corrosion <i>T. Graedel</i> 711	378	Automated Ultrasonic Corrosion Mapping <i>C. Sinclair</i> 891
439	Atmospheric Corrosion Model for Zinc and Copper <i>S. Cramer, L. McDonald, and J. Spence</i> 722	104	Adaptive Email Test AZ 90 for Corrosion Monitoring of Glass Lined Reactors <i>J. Hamert</i> 906
043	Defects of Steel Structures Caused by Atmospheric Corrosion <i>D. Knotkova, J. Vlckova, and L. Rozlivka</i> 734		
382	Environmental Effects in the Atmospheric Corrosion of Zinc: An Immersion - Drying Study <i>A. Valencia, R. Perez, C. Arroyave, and S. Mesa</i> 748		
463	Estimate of Economic Damage of large Industrial Cities Infrastruc- ture from Corrosion Caused by Pollutions into Environments <i>A. Lyagh</i> 761B		

CHEMICAL PROCESS INDUSTRY WORKSHOP

092	The Mechanism and Control of Stress Corrosion Cracking of Zirconium in Sulfuric Acid <i>B. Fitzgerald and T. Yau</i> 762	345	Rare Earth Element Effect on Oxidation Behavior of Chromia Forming Alloys <i>L. Ramanathan</i> 914
035	What Has Happened to SA-516-70? <i>T. Phillips and D. Kloss</i> 778	018	A Study of the Metal-Oxide Diffusion Barrier Coatings <i>G. Hengrong, S. Xiaofeng, and S. Biwu</i> 923
028	Corrosion of Weld Zone of Stainless Steels in Industrial Urea Media <i>H. Xizhang, R. Xiaoshan, C. Xiaojun, H. Wenan, and Z. Feng</i> 784	082	High-Temperature Sulfidation Properties and Demixing Process of Sulfide Scale of Fe-25Cr-9Mn Ternary Alloy <i>H. Qi, R. Zhu, and Y. He</i> 934
105	The Fractality of Corroding Metallic Surfaces <i>K. Trethewey, J. Keenan, D. Sargeant, S. Haines, and P. Roberge</i> 795	214	Influence of Nd on Oxidation of Ti-5621S Alloy and Adherence of Oxide Scales <i>L. Meishuan and L. Tiefan</i> 943
379	Methods to Combat Liquid Metal Embrittlement in Cryogenic Aluminum Heat Exchangers <i>S. Wilhelm, R. Kane, and A. McArthur</i> 807	113	High Temperature Corrosion Behavior of Fe-Cr-Al Alloys with and without Y Addition in Pure S_{O_2} Gas Atmosphere <i>Y. Zhang</i> 951B
132	Prevention of Localized Corrosion Caused by Thiosulphate in Paper Mill Environments <i>V. Marichev, T. Saario, and V. Molokanov</i> 826	468	Rupture in a Steam Boiler Tube <i>B. Rezgui and M. Larbi</i> 963
253	Corrosion of Stainless Steels in Kraft Process Liquors <i>A. Klarin, J. Westermarck, S. Ylaseari, J. Aromaa, and O. Forsen</i> 834	069	Na_2SO_4 Deposits Induced Hot Corrosion of Iron Based Alloys at Intermediate Temperatures <i>Y. Zhang, L. Shi, and S. Shih</i> 971
004	The Electrochemical Protection of Nickel in an NaOH + NaCl Solution <i>R. Juchniewicz, W. Sokolski, J. Walaszowski, P. Domzalcki, and B. Pierozynski</i> 849	391	Electrochemical Noise Measurement of Iron in Equimolar $NaNO_3$ - KNO_3 Melt at Various Temperatures <i>I. Singh, G. Venkatachari, and K. Balakrishnan</i> 979
435	Proactive Corrosion Program Improves Process Heater Reliability <i>K. Baumert, B. Heft, and S. Dean</i> 855	114	Corrosion Kinetic Study at High Temperature of the In 657 Super- alloy after Laser Surface Treatment in Contact with the Eutectic Melt 82% $K_2S_2O_7$ - 18% V_2O_5 <i>A. Pardo, E. Otero, F. Perez, and J. Alvarez</i> 987
		316	Performance of Cr-Al Coating on Carbon Steel to Control High Temperature Corrosion due to Ash Deposit <i>G. Navas, C. Leal, E. Baron, and O. Rincon</i> 999
		409	High Temperature Sulfidation of CO-CR Binary Alloys in H_2/H_2O Mixture in Co_3S_4 Stability Region <i>Z. Zurek, M. Zilik, and A. Szuryn</i> 1008

PLANT MATERIALS

- 317 Failure of Alloy 800 Steam Super Heating Coils in Refinery Hydrocracker
M. Islam and H. Shalaby 1022
- 216 The Effect of Blaze on the Mechanical and Corrosion Properties of Isfahan Refinery Distillation Unit Towers
A. Saatchi and A. Pishnamazi 1032
- 367 New Alloys for High Temperature Applications in Incineration Plants
H. Martinz and W. Kock 1039
- 260 Corrosion Evaluation of Materials in Sulfur Compound Environments
M. Teng and I. Yang 1056
- 447 Materials Selection Considerations for Vapor Collection Systems at Marine Tanker Facilities
T. Dunford, K. Lewis, and D. Rein 1064
- 169 Cracking of Weldments in Feed Water Deaerator Systems
T. Gocch, D. Noble, and R. Walker 1076
- 410 Using Fuel Oils with Different Sulphur Content and Treatment of Waste Waters Polluted with Heavy Metals in Thermoelectric Power Plants
L. Dukic 1090B
- 492 Case Study of a Service Water System Piping Corrosion Assessment
R. Tatara, K. Rhoades, and H. Olstowski 1091

VOLUME 3A

CORROSION: MATERIALS PERFORMANCE

- 210 Corrosion-Resistant Amorphous Chromium-Valve Metal Alloys
K. Hashimoto, J. Kim, E. Akiyama, H. Habazaki, A. Kawashima, and K. Asami 1102
- 089 A New Ni-Mo Alloy with Improved Thermal Stability
D. Klarstrom 1111
- 277 Corrosion Behaviour of Stainless Maraging Steel in Acidic Chloride Solutions
M. Viswanathan and K. Balakrishnan 1124
- 372 Electrochemical Characterization of Ni-Based Soft Magnetic Alloys
G. Ball and J. Payer 1132
- 413 Evaluation and Application of the EPR-double Loop Test to Assess the Degree of Sensitisation in Stainless Steels
R. Jargelius-Pettersson and P. Szakalos 1143
- 406 Corrosion Behaviour of Sintered Austenitic Stainless Steels in Sulphate and Chloride Media
E. Angelini, P. Bianco, F. Rosalbino, M. Rosso, and G. Scavino 1154
- 125 Advances in Technology Produce New Materials for Challenging Applications
N. Schmidt and T. DeBold 1170

- 512 Passive Behavior of Niobium and Niobium-Titanium Alloys in Sulfuric Acid Solutions
L. Bulhoes and D. Rehfeld 1183
- 464 The Effects of Microstructure (Cast versus Wrought) on the Wear and Corrosion Properties of a Cobalt-based Alloy
T. Meyer and P. Crook 1191
- 184 Effect of Aging Treatments on the Intergranular Corrosion of 22Cr-5Ni Duplex Stainless Steel
K. Ravindranath, S. N. Malhotra 1202
- 120 Optimized Lean-Pd Titanium Alloys for Aggressive Reducing Acid and Halide Service Environments
R. Schutz and M. Xiao 1213
- 049 Corrosion Characteristics and Applications of Newer High and Low Nickel Containing Ni-Cr-Mo Alloys
D. Agarwal, U. Heubner, and W. Herda 1226
- 178 Duplex Stainless Steels for Demanding Applications
J. Nicholls 1237

CORROSION: MODES AND BEHAVIOR

- 100 Investigation of Modified Schiff Bases for High Temperature Applications in the Area of Tribology
K. Rajan, P. Sen, A. Snelson, V. Agarwala, and A. Conte Jr. 1252
- 255 Corrosion Inhibition of Calcium Chloride Brines
K. Sotoudeh and P. Cote 1262
- 313 The Effect of Temperature and Chloride Concentration on Stainless Steels in Ammonium Chloride Solutions
O. Forsen, J. Virtanen, J. Aromaa, and M. Tavi 1278
- 109 Rest Potential Measurements for Stainless and Low-Alloy Steels in High Temperature Water
A. Charles and J. Congleton 1287
- 215 Managing Galvanic Corrosion in Waters
A. Tuthill 1300
- 119 Combination of Acoustic Emission & Electrochemical Techniques in Erosion-Corrosion Studies of Passive Stainless Steels in Acidic Media
L. Renaud, B. Chapey, and R. Oltra 1315
- 188 Accelerated Corrosion Testing of CrNi Stainless Steels in Nitric Acid by Electrochemical Methods
G. Schanz and S. Leistkow 1327
- 288 Tunneling Corrosion Mechanism of the Hot Forged Austenitic Stainless Steel in Highly Oxidizing Nitric Acid
H. Nagano and H. Kajimura 1341
- 440 Corrosion and Wear in White Cast Iron
S. Watson, S. Cramer, and B. Madsen 1353

ELECTROCHEMICAL TECHNIQUES

- 055 Scanning Microelectrochemical Methods to Study the Corrosion Behavior of Metals
T. Suter and H. Bohni 1367
- 496 PVC Film-Modified Electrodes Studied by EHD Impedance
C. Sousa da Silva, O. Barcia, O. Mattes, and C. Deslouis .. 1378
- 533 Electrochemical Noise Analysis of Iron Exposed to NaCl Solution of Different Corrosivity
F. Mansfeld and H. Xiao 1388
- 139 Characteristics of Electrochemical Noise Generation During Pitting Corrosion
S. Muralidharan, G. Venkatachari, and K. Balakrishnan 1403
- 573 Electrochemical Noise as the Basis of Corrosion Monitoring
A. Legat 1410
- 506 Electrochemical Relaxation Techniques for the Measurement of Instantaneous Corrosion Rates
V. Lakshminarayanan and S. Rajagopalan 1420
- 111 Rapid Evaluation of Corrosion Behavior by Using Random Potential Pulse Method
Y. Sugie and S. Fujii 1430
- 070 Application of Modern Electronic Technique in Corrosion
F. Qiu 1445
- 094 Improvement of Mansfelds Method for Computing Electrochemical Parameters from Polarization Data
G. Rocchini 1450
- 532 Assessment of Corrosion of Laser Surface Alloyed Aluminum & Steel by Electrochemical Technology
R. Li, M. Ferreira, A. Almeida, R. Vilar, K. Watkins, and W. Steen 1460
- 067 Marine Corrosion Resistance of Aluminum and Aluminum-Lithium Alloys
P. Roberge and D. Lenard 1466
- 209 Measuring Corrosion Resistance of Stainless Steels Using the 'Avesta Cell' - Experiences and New Applications
P. Amvig and R. Davison 1477
- 226 Corrosion Resistance and Behavior of Construction Materials Exposed to Dilute Sulfuric Acid at Elevated Temperatures Under Static Conditions
D. Nguyen and R. Daniels 1491

ENVIRONMENTAL CRACKING

- 241 Crack Initiation and Growth of Sensitized Type 304 Stainless Steel in NaF Solution
T. Shibata, T. Oki, and T. Haruna 1509
- 211 Localized Corrosion Problems in Austenitic Stainless Steel Feed-water Heater Tubing
G. Wood 1523
- 063 Stress Corrosion Cracking of Sensitized Type 316 Austenitic Stainless Steel in Pure Sulfuric Acid Solution
R. Nishimura and A. Sulaiman 1532

- 117 The Influence of H⁺ and Cl⁻ Ions on SCC of Austenitic 304SS in Acidic Chloride Solutions at Ambient Temperature
Z. Fang, R. Zhu, and Y. Wu 1542
- 296 Differentiation Between Sulphide Stress Corrosion Cracking in 13% Cr and Duplex Stainless Steels
J. Barker, J. Yu, and R. Brook 1549
- 118 Stress Corrosion Cracking of 321 Austenitic Stainless Steel Single Crystal Under Mode II Loading
L. Qiao, D. She, W. Chu, and C. Hsiao 1560
- 010 Effect of Heat Treatment on SCC Behavior of 40 CrMnSiMo A Steel
S. Jin, S. Li, and X. Liu 1564
- 425 Corrosion Kinetics within Pits or Stress Corrosion
Y. Liu, Y. Cen, and J. Zuo 1572
- 497 Investigation of Mechanical & Environmental Effects on the Occluded Cell withing Stress Corrosion Cracks of 1Cr13 Martensitic Stainless Steel
Y. Liu, Y. Cen, and J. Zuo 1580
- 596 A Fully-Plastic Micro-Cracking Model for T-SCC in Planar-Slip Materials
W. Flanagan, M. Wang, M. Zhu, and B. Lichter 1588
- 509 Improved Stress Corrosion Performance for Alloy 718 via Melt Practice and Heat Treatment Variation
M. Miglin, J. Monter, C. Wade, J. Nelson 1600
- 485 Competition between Anodic Dissolution and Hydrogen Effects During Stress Corrosion Cracking of a 7150 Aluminum Alloy
D. Najjar, O. Moriau, R. Chieragatti, T. Magnin, and T. Warner 1613
- 112 The Peculiarities of Electrochemical Behaviour and Stress Corrosion for Aluminium Alloys with Lithium Additives
V. Sinyavsky 1623
- 122 Cathodic Corrosion and Hydrogen Effect in TiAl & Effects of Hydrogen
W. Chu, K. Gao, J. Jin, and L. Qiao 1637
- 380 Using Real-Time Holography to Monitor Stress Corrosion Cracking Initiation
V. Desai, E. Principe, L. Quian-Falzone, and F. Moslehy ... 1649
- 564 Pre-Crack Fatigue Damage and Crack Initiation under Corrosion Fatigue Conditions
J. Seidel and D. Duquette 1658
- 327 Corrosion Fatigue of Marine Structural Steels in Saline Environments
M. Kermani and F. Abbassian 1671
- 297 Corrosion Fatigue Propagation of Higher Yield Strength Offshore Structural Steel in Artificial Seawater
J. Yu, R. Brook, I. Cole, D. Morahito, and G. Demofonti ... 1692
- 002 Corrosion Fatigue in Fossil-Fueled Boilers
G. Ogundele, E. Ho, and D. Sidey 1702
- 484 Influence of Surface Microcracks on the Corrosion Fatigue Mechanisms of Ferritic and Austenitic Stainless Steels
T. Magnin 1720

- 448 Influence of Applied Potential on Corrosion Fatigue Life and Crack Chemistry of Low Carbon Steel
H. En-Hou, H. Yuma, and K. Wei 1727

VOLUME 3B

INHIBITORS

- 020 Corrosion in Heavy Duty Diesel Engine Cooling Systems
B. Salas 1755
- 053 Synthesis and Study of Different Thioamides as Corrosion Inhibitors
K. Ahmed, S. Oun, and M. Shariff 1743
- 058 Corrosion Resistance of Copper and Copper Alloys Surface Treated with a Benzotriazole Derivative in Sodium Chloride Solutions
F. Zucchi, G. Brunoro, C. Monticelli, and G. Trabanelli 1758
- 078 Study of the Effect of Inhibitors on the Removal of Scale from Mild Steel Surface During Pickling
G. Banerjee and S. Malhotra 1766
- 088 Theoretical Calculation and Experimental Verification of Critical Passivation Concentration of Oxidizing Inhibitors in Acid Solutions
M. Zhao 1773
- 144 Chemical Composition and Structure of Surface Layer Forming in Solutions of Chromate Ions and Corrosion Behaviour of Carbon Steel
E. Enikeev, M. Panov, I. Krashennikova, and
A. Feoktistov 1784
- 149 A Quantum Chemical Study of Inhibition Effect of Isoquinoline Derivatives
L. Yao, M. Lou, P. Kong, E. Kung, and C. Yao 1794
- 200 A Spectroscopic Investigation on Inhibition Mechanism of Dibenzyl Sulfoxide for Iron Corrosion in a Hydrochloric Acid Solution
K. Aramaki, N. Ohno, and H. Nishihara 1804
- 287 The Study on Synergistic Effect of Corrosion Inhibitor
E. Kalman 1814
- 411 Effect of Some Organic Inhibitors on Corrosion of Stainless Steel in Hydrochloric Acid
A. Ismail and S. Sanad 1826
- 508 Corrosion Inhibition Study of Different Azoles on Copper Using Carbon-Paste Electrodes
V. Lakshminarayanan, R. Kannan, and S. Rajagopalan 1854
- 605 Inhibition of the Corrosion of Carbon Steel in Hydrochloric Acid by Phosphonium Species
B. Barker, I. Beech, and F. Walsh 1864

LOCALIZED CORROSION/CREVICES

- 225 Prediction of Crevice Corrosion Resistance of Stainless Steels in Aqueous Environments: A Corrosion Engineering Guide
J. Oldfield, and R. Kain 1876
- 347 Seawater Testing to Assess the Crevice Corrosion Resistance of Stainless Steels and Related Alloys
R. Kain 1889
- 246 Modelling Crevice Corrosion of Fe-Cr-Ni-Mo Alloys in Chloride Solution
P. Gartland 1901
- 284 Crevice Corrosion of a Ni-Based Superalloy in Natural and Chlorinated Seawater
B. Shaw, P. Moran, and P. Gartland 1915
- 300 The IR Mechanism of Localized Corrosion
H. Pickering 1929
- 446 Corrosion Behavior of High Nitrogen Stainless Steels for Biomedical Applications
A. Cigada, G. Rondelli, B. Vicentini, and G. Dallaspezia... 1938
- 470 Nitrogen Bearing Austenitic Stainless Steels - A Promising Replacement for Currently Used 316L Stainless Steel Orthopaedic Implant Material
M. Sivakumar, U. Kamachi-Mudali, and S. Rajeswari 1942
- 471 Pit-Induced Corrosion Failures in Stainless Steel Orthopaedic Implant Devices
M. Sivakumar, U. Kamachi-Mudali, and S. Rajeswari 1949
- 376 Studies on the Environmental Degradation of Metal Matrix Composite Materials
A. Rawat, V. Desai, P. Ramakrishnan, and R. Prasad 1960
- 346 Corrosion Behavior of Alumina/Al and SiC/Al Metal Matrix Composites
P. Nunes and L. Ramanathan 1974
- 252 Effect of Cold-Working on the Crevice Corrosion of Austenitic Stainless Steels
T. Handa, Y. Miyata, and H. Takazawa 1986

LOCALIZED CORROSION/PITTING

- 500 Application of In-Situ Scanning X-ray Fluorescence to Study the Concentration of Metal Ions in Simulated Pits
H. Isaacs, J. Cho, A. Davenport, M. Rivers, and S. Sutton .. 1997
- 599 Pitting Conditions Evolution of 316L Stainless Steels During Aging in Sea Water: A Statistical Approach
M. Ghiazza, D. Festy, J. Leonard, and C. Lemaitre 2005
- 179 Pitting Behaviour of UNS N08904 Stainless Steel in Salt Solutions
V. Gouda and W. Abd-El Meguid 2011
- 086 Corrosion Monitoring of Aluminum Easy-Open Ends by Area Polarization Technique
O. Seri, K. Furuma, and Y. Matsumura 2022
- 565 Passivity and Passivity Breakdown in Sputtered Aluminum and Iron Alloys
Z. Szklarska-Smialowska and R. Inturi 2030

Paper #	Page #	Paper #	Page #
059	Localized Corrosion Phenomena Study in 304L and 316L Stainless Steel Prepared by Power Metallurgy <i>E. Otero, A. Pardo, V. Utrilla, and E. Saenz</i>	392	Effect of Oxygen-Containing Oxidizers on Fe, Cu, and Sn Dissolution Rates in Acidic Sulphate Electrolytes <i>N. Chebotaryova, A. Marshakov, V. Ignatenko, and Y. Mikhailovsky</i>
087	In-Situ Measurement of the Cl^- Concentration Distribution in Two Dimensions of Metal Surface <i>C. Lin</i>	451	Kinetic Study of the PbSO_4 Reduction on Lead Using Rehopping Motion Model <i>C. D'Alkain and H. Mascaro</i>
	2037		2232
	2045		2232

PASSIVITY AND BREAKDOWN

024	Influence of Anions on the Surface Enhanced Raman Spectre of Passive Films Formed on Iron <i>T. Devine and J. Gui</i>	2052
262	Vacancy Condensation as the Precursor to Passivity <i>D. MacDonald</i>	2065
323	Passivity of FeCr Alloys <i>J. de Wit</i>	2077
340A	Passive Oxide Films on Well-Defined Nickel Surfaces: An Examination of Film Growth on Ni(100) with Ex-Situ Scanning Tunneling Microscopy <i>C. Vitus and A. Davenport</i>	2091
371A	Passivity and Pitting Corrosion <i>M. Ives</i>	2096
398	Atomic Structure of Passive Films on Nickel <i>P. Marcus, H. Talah, and V. Maurice</i>	2105
453	The Effect of Temperature on the Passive $\text{Ni}(\text{OH})_2$ Growth on Nickel in 1M NaOH Using Rehopping Motion Model <i>C. D'Alkain and H. Mascaro</i>	2112
071	XPS Study of Passive Films on Stainless Steels in Neutral Solutions <i>A. Rossi, and B. Elsener</i>	2120
567	Passivity of Carbon Steel in Organic Solutions <i>D. Schiffler, P. Moran, and J. Kruger</i>	2131
568	In-situ STM Characterization of Passivity and its Breakdown on Stainless Steels <i>S. Virtanen, A. Schreyer, and H. Bohni</i>	2142
015	An Investigation of the Stability of Transpassivated Film on 304 Stainless Steel <i>G. Song, C. Cao, and H. Lin</i>	2155
130	Photoelectrochemical Studies of the Passive Films on Copper and Brass <i>G. Rajagopal, S. Sathiyarayanan, and K. Balakrishnan</i> ...	2162
212	The Ion-Exchange Behaviour of the Corrodible Metal Surfaces <i>A. Nazarov and M. Petrunin</i>	2175
283	Non-Equilibrium Aluminum Alloys: Effects on Passivity in Chloride Environments <i>E. Principe</i>	2187
315	The Effect of Ion Implantation on the Passivation Behavior of Pure Copper <i>E. Wright, V. Ashworth, B. Procter, and W. Grant</i>	2207

VOLUME 4

CATHODIC PROTECTION

001	Stray Current Interaction in the System of Two Extensive Underground Conductors <i>W. Machczynski</i>	2268
041	An Initial Investigation of Calcareous Deposits Upon Cathodically Polarized Steel in Brazilian Deep Water <i>R. Vianna and G. Pimenta</i>	2278
161	The Isolator/Surge Protector: A Superior Alternative to Polarization Cells <i>T. Scharf</i>	2285
223	Laboratory Evaluation of the Effectiveness of Cathodic Protection in the Presence of Iron Bacteria <i>K. Okamura, Y. Koyama, F. Kajiyama, and K. Kasahara</i>	2293
580	Modification of the Corrosion Environment beneath Disbonded Coatings by Cathodic Protection <i>K. Fink and J. Payer</i>	2302
598	Pipeline Inspection and Rehabilitation - An Overview <i>G. Matocha</i>	2311
607	Prediction of Dynamic Current Density on Cathodically Protected Steel in Seawater at Different Depths <i>R. Griffin, J. Yan, R. White</i>	2324

HYDROGEN EFFECTS

524	Hydrogen Embrittlement in Steels: Mechanical Aspects <i>R. Magdowski</i>	2332
238	Hydrogen Embrittlement in Steels: Metallurgical Aspects <i>M. Speidel</i>	2339
299	Electrochemical Aspects of Hydrogen Embrittlement in Steels: (i) IPZ Model of Hydrogen Permeation (ii) IR Voltage-Induced Hydrogen Charging <i>H. Pickering</i>	2346

Paper #	Page #	Paper #	Page #
147	Predicting the Susceptibility to Hydrogen Embrittlement <i>B. Pound</i> 2356	570	Use of Composite Materials on Offshore Platforms <i>O. Saetre</i> 2529
322	Evaluation of Three Different Surface Modification Techniques for Resisting Hydrogen Embrittlement in Steel <i>S. Chan, C. Ho, and J. Lin</i> 2367	014	Corrosion Performance and Application Limits of Materials in Oil Fields <i>A. Miyasaka and H. Ogaloa</i> 2537
602	Modeling of Nonsteady State Hydrogen Permeation <i>P. Janavicius, S. Amey, J. Payer, and G. Michal</i> 2377	093	Corrosion Resistant Alloys UNS NO9925 and NO7725 for Oil Field and Other Applications <i>E. Hibner and R. Moeller</i> 2548
011	A Sensor for Measuring the Permeation Rate of Atomic Hydrogen and its Applications in HIC Inspection <i>Y. Du</i> 2383	207	Stress Corrosion Cracking Behavior of Austenitic and Duplex Stainless Steels in Simulated Sour Environments <i>K. Saarinen</i> 2566
393	The Mechanism of the Effect of Oxygen-Containing Oxidizers on the Rate of Hydrogen Cathodic Evolution and Hydrogen Permeation into Metal <i>L. Maksaeva, A. Marshakov, Y. Mikhailovsky, and V. Popova</i> 2395	427	Role of Expert Systems in Technology Transfer of Materials for Petroleum Applications <i>S. Srinivasan</i> 2574
342	On Mechanism of Hydrogen Embrittlement of Metals and Alloys <i>Y. Archakow</i> 2405	528	The Effect of Certain Compositional Aspects on the Behavior of Tank and Pipe Linings Under Laboratory and Field Conditions <i>M. Winkler</i> 2585
121	Effect of Composition on Hydrogen Induced Ductile Loss and K_{IH} in Ni-Fe FCC Alloys <i>W. Hu, Y. Wang, W. Chu, and C. Hsiao</i> 2411	549	Methods to Develop a Performance Envelope for Internal Linings in Oilfield Production Environments <i>G. Ruschau, L. Bone III, and O. Moghissi</i> 2601
OIL AND GAS PRODUCTION AND REFINING WORKSHOP		550	Polymer Coating Degradation Mechanisms Related to Hot Production <i>R. Granata, R. MacQueen, and K. Kovalski</i> 2612
490	Corrosion Management <i>D. Milliams</i> 2420	090	Oxidation of Carburised and Coked Heat-Resistant Steels <i>D. Young, D. Mitchell, and W. Kleeman</i> 2625
586	Development of Super _{13Cr} Stainless Steel for CO ₂ Environment Containing Small Amounts of H ₂ S <i>T. Okazawa, T. Kobayashi, and M. Veds</i> 2425	203	The Effect of Environmental Variables on Crack Propagation of Carbon Steels in Sour Media <i>M. Kermani, R. MacCuish, J. Smith, R. Case, and J. Vera</i> .. 2639
587	Corrosion Resistance of 13 and 15% Martensitic Stainless Steels in Oil and Gas Wells <i>O. Hashizume, Y. Miname, and Y. Ishizawa</i> 2439	133	Sulfide Scales for the Protection of Steels in H ₂ S-Containing Atmospheres <i>M. Schulte and M. Schutze</i> 2650
588	Development of Safe Use Limits for Martensitic and Duplex Stainless Steels <i>R. Kane and S. Srinivasan</i> 2451	194	Wall Shear Stress & Flow Accelerated Corrosion of Carbon Steel in Sweet Production <i>K. Efird, E. Wright, J. Boros, and T. Hailey</i> 2662
585	Effect of Flow Velocity on CO ₂ Corrosion Performance of 13Cr, Super 13Cr, and A-Y Duplex Phase Stainless Steels <i>A. Ikeda, M. Ueda, J. Vera, A. Viloria, and J. Morales</i> 2464	307	Effect of Flow Velocity on Carbon Steel CO ₂ Corrosion and Surface Films using a Dynamic Field Tester <i>J. Vera, J. Morales, A. Viloria, A. Ikeda, and M. Ueda</i> 2695
590	The Effect of Temperature on Sulphide Stress Corrosion Cracking Resistance of Martensitic Stainless Steels used in Oil & Gas Industry <i>T. Cheldi, A. Kopliku, A. Cigada, M. Cabrini, G. Rondelli, and B. Vicentini</i> 2482	385	A Proposed Mechanism for Corrosion in Slightly Sour Oil and Gas Productions <i>S. Smith</i> 2695
278	Environment Sensitive Cracking of Titanium Alloys in Offshore Equipment <i>I. Azkarate, H. Flower, I. Aho-Mentila, and L. Lunde</i> 2492	511	Rotating Cylinder Electrode (RCE) Simulation of Flow Accelerated Corrosion in Sweet Production <i>K. Efird, E. Wright, J. Boros, and T. Hailey</i> 2707
478	Stress Cracking & Crevice Corrosion Resistance of Pd-enhanced Ti-38644 Titanium Alloy Products in Deep Sour Gas Well Environment <i>R. Shutz, M. Xiao, and J. Skogsberg</i> 2506	606	Inhibitor Performance in Annular Mist Flow <i>H. Geretsen and A. Visser</i> 2726
099	Study of Oil Aluminium Alloy Pipes With Improved Corrosion Resistance <i>V. Kuznetsova</i> 2520	552	Evaluation of Magnetic Flux Leakage (MFL) Intelligent Pigging Results from Recurring Arctic Pipeline Inspections <i>G. Williamson</i> 2734
		325	Practical Approach to Evaluating a Corrosion and Scale Inhibitor Program in a Gathering System <i>R. Bess, D. Monical, and E. Yanto</i> 2749

Paper #		Page #
579	The Importance of Wettability in Oil and Gas System Corrosion <i>J. Smart III</i>	2758
594	Corrosion Inhibition in Wet Gas Pipelines <i>J. Palmer, J. Dawson, K. Lawson, J. Palmer, and L. Fonczek</i>	2768
574	Behavior of Corrosion Resistant Alloys in Stimulation Acids, Completion Fluids, and Injected Waters <i>R. Kain</i>	2780
553	Effects of Acidizing on High Alloy Springs After H ₂ S Exposure <i>B. Bailey</i>	2795
038	Study of Corrosion Inhibitors in Waste Water Reuse System in the Oilfield <i>L. Zhu</i>	2803B
258	The Preparation of Corrosion Inhibitor for Water Flooding in the Oil-field and Mechanism Evaluation <i>L. Zhu, H. Guangtuan, and Y. Wenjuan</i>	2804
343	Low Cost Material Selection for Produced Water Tank <i>T. Havn</i>	2814

PIPELINE CORROSION

551	Corrosion Prevention on the Iroquois Gas Transmission System by a Reliability Based Design Philosophy <i>T. Hamilton</i>	2823
566	Pitting Corrosion Behaviour of Pipeline Steel in Solutions with Coating Disbonded Area Chemistry and in Bicarbonate Solutions <i>X. Liu, X. Mao, and R. Revie</i>	2831
510	Prediction of Microstructural Effect on Corrosion of Linepipe Steels in Co ₂ - Brine Solution <i>B. Mishra, D. Olson, and M. Salama</i>	2840
250	The Effects of Latex Additions on Centrifugally Cast Concrete for Internal Pipeline Protection <i>R. Buchheit, T. Hinkebein, P. Hlava, and D. Melton</i>	2854
256	A New Process for Internal Welding Joint Corrosion Protection of a Pipeline with Cement Liners <i>L. Fa and C. Jimin</i>	2865
563	Progress Toward a Modified B31G Criterion <i>P. Vieth and J. Kiefner</i>	2869

RELIABILITY AND CORROSION CONTROL OF WELDMENTS/CORROSION RESISTANT ALLOYS

538	Welding of UNS S32654 - Corrosion Properties and Metallurgical Aspects <i>M. Liljas and P. Stenvall</i>	2882
358	Pitting Resistance of Autogenous Welds in UNS S31254 High Alloy Austenitic Stainless Steel <i>B. Ginn and T. Gooch</i>	2895
541	Localized Corrosion of the Unmixed Zone in Nickel-Base Alloy Weldments <i>L. Flasche and H. Ahluwalia</i>	2907

Paper #		Page #
536	Corrosion and Behaviour of SAW Stainless Steel Filler Metals with N ₂ and Mn <i>A. Gil-Negrete</i>	2925
539	Beneficial Effects of Nitrogen Additions on the Micro & Structure Stability & Corrosion 52N & Super Duplex Stainless Steel <i>J. Charles</i>	2926
537	Corrosion Properties of Duplex and Super Duplex Stainless Weld Metals after Isothermal Aging <i>L. Karlsson and S. Pak</i>	2944
459	Corrosion Characteristics of Plasma Weld Surfacing with the Duplex Materials, X2 CrNiMo22 53 and X2 CrNiMoN 257 4 <i>U. Draugelates, B. Bouaifi, A. Stark, I. Garz, and S. Schulze</i>	2959
535	Alloy 625 Weld Overlays for Offshore and Onshore Projects <i>D. Capitanescu</i>	2973
458	Characterization of the Corrosion Behaviour of Surface Welded Protective Claddings of Nickel and Titanium Alloys <i>B. Bouaifi, U. Draugelates, H. Steinberg, J. Gollner, and A. Burkert</i>	2987
540	Some More About Electrochemical Tests to be Performed on the Field as Non-Destructive Quality Control Inspection <i>M. Verneau, F. Dupoirion, and J. Charles</i>	2996

VOLUME 5A

AIRCRAFT

605	The Role of Corrosion in Aging Aircraft <i>G. Koch and T. Bieri</i>	3007
151	Hidden Corrosion - Needs and Requirements <i>P. Bhagat and G. Hardy</i>	3018
196	The Corrosion Prevention & Control Program of the German Air Force for the PA200 Tornado Aircraft <i>J. Fuhr</i>	3033
403	Corrosion Control as a Necessary Treatment Following the Requirements of Aircraft and Environment Safety <i>E. Durig</i>	3043
152	A New Eddy Current Inspection System for Quantitative Corrosion Depth Measurement on A/C Wing Skins <i>H. Grauvogl, F. Regler, and H. Thomas</i>	3058
608	Computer Assisted Aircraft Paint Stripping Technology <i>R. Carnes</i>	3069
185	Accelerating Factors in Galvanically Induced Polyimide Degradation <i>M. Rommel, A. Postyn, and T. Dyer</i>	3077
141	Reducing Aircraft Corrosion with Desiccant Dehumidifiers <i>D. McCarthy, D. Kosar, and S. Cameron</i>	3086
137	Corrosion Contribution to Environmental Cracking Failures of Critical Aircraft Parts <i>J. DeLuccia</i>	3099

Paper #	Page #	Paper #	Page #
474	Use of VCI's (Volatile Corrosion Inhibitors) for Aircraft Protection <i>A. Eydelnant, B. Miksic, and S. Russell</i> 3109	507	Measurement of Corrosion Rate of Reinforcing Steel and Electrical Resistivity of Concrete using Galvanostatic Steady State Polarisation Technique <i>V. Lakshminarayanan, P. Ramesh, and S. Rajagopalan</i> 3295
359	Designing Metallic Surface Coatings for Improved Corrosion Resistance <i>R. Narayan</i> 3118	057	Corrosion and Prevention of Ferrocement Roofing Slabs in Electrical Furnace Processing Workshop <i>H. Sun, M. Chou, and Y. Yong Yang</i> 3308
336	Corrosion Behavior of W Implanted Aluminum <i>J. Fernandes and M. Ferreira</i> 3130	700	Management of Corrosion Control of Reinforced Concrete in the Channel Tunnel <i>A. Pourbaix</i> 3314
428	Development of Chromium Based Composite Coatings for Tribological Applications <i>R. Narayan</i> 3139		
168	Evaluation of Chromate Free Corrosion Inhibited Primers for Airbus Aircrafts <i>C. Matz</i> 3149		
204	Development of a Non-Cyanide Cadmium Pulse Plating Process <i>J. Steppan, D. Rocca, J. Carraway, and V. Agarwala</i> 3156		

AUTOMOTIVE/ACCELERATED TESTING

030	Effect of Surface Impurities on the Corrosion Behavior of Type 434 Stainless Steel <i>R. Baboian</i> 3179
153	Optimization of Corrosion and Wear Properties of Steel Component Surfaces by Controlled Gas Nitriding <i>M. Biestek, A. Czelusniak, J. Iwanow, M. Korwin, W. Liliental, and J. Tacikowski</i> 3188
581	In-Situ Analysis of Corrosion in the Crevice of Automotive Body by A.C. Impedance Measurement <i>S. Fujita and K. Matsamura</i> 3200

CORROSION IN CONCRETE

388	Designing a Reinforced Concrete Against Corrosion in Chloride Containing Environments: Choosing the Cement by Applying a Diffusion Model and Using Electrochemical Methods <i>E. Triki, L. Dhouibi-Hachani, and A. Raharinaivo</i> 3207
337	A Current-Based Criterion for Cathodic Protection of Reinforced Concrete Structures <i>J. Bennett</i> 3220
076	Carbonation of Flyash-Containing Concrete Electrochemical Studies <i>M. Montemor, A. Simoes, M. Ferreira, and M. Salta</i> 3235
301	Performance of Concrete with Microsilica in Chemical Environments <i>N. Berke, T. Durning, and M. Hicks</i> 3242
072	Inspection and Monitoring of Reinforced Concrete Structures - Electrochemical Methods to Detect Corrosion <i>B. Elsner, H. Wojtas, and H. Bohni</i> 3260
302	Evaluation of Concrete Corrosion Inhibitors <i>N. Berke, M. Hicks, and P. Tournay</i> 3271
115	Cathodic Protection of New Steel Reinforced Concrete Structure <i>A. Tvarusko</i> 3287

ELECTRONICS

098	Reliability and Corrosion Testing of Electronic Components and Assemblies <i>J. Sinclair, R. Frankenthal, and D. Siconolfi</i> 3332
131	In-Situ Investigation of the Initial Stages of the Electrochemical Deposition of Metals by Contact Electric Resistance Method <i>V. Marichev</i> 3344
142	Corrosion Study of Polymer-on-Metal Systems Modified by Processing Conditions <i>K. Nenov, P. Nagarkar, D. Mitton, and R. Latanision</i> 3355
157	Quantitative Corrosion Testing of EMI Materials for Aerospace Applications <i>P. Lessner</i> 3366
183	Corrosion of Electronics: Effect of Ionic Particulates <i>R. Frankenthal, R. Lobnig, D. Siconolfi, and J. Sinclair</i> 3378
234	Accelerated Gaseous Corrosion Testing <i>R. Schubert</i> 3385

EXPERT SYSTEMS

289B	How to Formulate Corrosion Knowledge for Expert Systems <i>T. Hakkarainen, and T. Hakkarainen</i> 3396
236	Transforming Computerized Information for its Integration into a Hyper Tutorial Environment <i>P. Roberge</i> 3404
206	Integrated Diagnostic System for Intelligent Processing of Field Inspection Data for Transmission Line Structures <i>P. Mayer and S. Moraes</i> 3413
123	Data Acquisition Update <i>R. Eberlein</i> 3424
048	Corrosion Prediction from Laboratory Tests Using Artificial Neural Networks <i>D. Silverman</i> 3430

LIFE PREDICTION

- 037 The Deterministic Prediction of Failure of Low Pressure Steam Turbine Disks
D. Macdonald and C. Liu 3446
- 228 Prediction of Pitting Damage Functions for Condensing Heat Exchangers
C. Liu, M. Urquidi-Macdonald, and D. Macdonald 3460
- 279 An Estimation of Maintenance Costs Related to Corrosion in Brazilian Electric Power System
A. Marinho Jr. 3477
- 312 Numeric Model for Hydrogen Embrittlement Prediction for Structures Cathodically Protected in Marine Environments
J. Regnier and D. Festy 3484
- 318 Use of Fuzzy Logic as a Decision Making Tool in the Rehabilitation of Concrete Bridge Structures
M. Islam and P. Simon 3489
- 320 The System Analysis of a National Scale Refining Equipment Corrosion Database
Y. Luo 3503
- 455 Interpretation of Electrochemical Impedance Data for Damaged Automotive Paint Films
C. Diaz, M. Urquidi-Macdonald, D. Macdonald, A. Ramamurthy, W. Van Ooij, A. Sabata, M. Strom, and G. Strom 3508
- 456 A Test of the Reliability of Mathematical Modeling of Corrosion
P. Ault Jr. and J. Meany Jr. 3519

VOLUME 5B

- 460 Degradation by Ripple-Load Effect - Impact on Life Prediction
P. Pao, R. Bayles, D. Meyn, and G. Voder 3531
- 465 Some Through-Life Risk/Reliability Considerations for Components Subject to Corrosion - A Safety Assessors View
R. Crombie 3540
- 466 Management of Corrosion in the Power Industry
H. Flitt 3551
- 469 Prediction of Corrosion Rate and Probability on Underground Pipes
Y. Katano, T. Kubo, and Y. Igawa 3561
- 477 A Dominant Flaw Probability Model for Corrosion and Corrosion Fatigue
D. Harlow and R. Wei 3573

MARINE

- 074 The Effects of Complexing Agents on the Corrosion of Copper/Nickel Alloys in Sulfide Polluted Seawater under Impingement Attack
M. Reda and J. Alhajji 3587

- 079 A Study of Flow Dependent Corrosion of Nodular Cast Iron in Arabian Gulf Seawater
A. Al-Hasham, H. Shalaby, and V. Gouda 3600
- 138 Effect of Sulfide Ions on the Corrosion Behavior of Aluminum Alloy (H2O) Synthetic Synthetic Sea Water
M. Valliappan, M. Natesa, G. Venkatachari, and K. Balakrishnan 3613
- 220 Corrosion Protection of Submerged Steel Structures by the Combined Use of Protective Coatings and Impressed Current Cathodic Protection
M. Arponen 3617
- 237 On the Influence of Hydrostatic Pressure on the Corrosion Behavior of 42CD4 Steel in Natural Seawater: A Mossbauer & X-Ray Study
J. Le Breton, J. Teillet, and D. Festy 3634
- 421 Corrosion Characterization of Explosively Bonded Materials in Marine Environment
N. Lindsey 3645
- 432 Corrosion and Stress Corrosion Cracking of a Marine Steel in Artificial and Natural Sea Water
M. Colozar and A. Saatchi 3660
- 441 Environmental Degradation of Polymer Matrix Composite Exposed to Seawater
V. Stolarski, A. Letton, W. Bradley, and R. Cornwell 3671

MICROBIOLOGICALLY INDUCED CORROSION

- 136 The Impact of Alloying Elements on Microbiologically Influenced Corrosion - A Review
B. Little, P. Wagner, M. McNeil, and F. Mansfeld 3680
- 554 Early Stages of Bacterial Biofilm and Cathodic Protection Interactions in Marine Environments
H. Videla, S. Gomez de Saravia, and M. de Mele 3687
- 479 Factors Contributing to Ennoblement of Passive Metals Due to Biofilms in Seawater
P. Chandrasekaran and S. Dexter 3696
- 189 Ennoblement of Stainless Alloys by Marine Biofilms: An Alternative Mechanism
M. Eashwar, S. Maruthamuthu, S. Sathyanarayanan, and K. Balakrishnan 3708
- 249 Characterization of the Bio-Film Formed on a Steel Electrode in Seawater by Analyzing the Mass Transport of Oxygen
D. Festy, F. Mazeas, M. El-Rhazi, and B. Tribollet 3717
- 158 Microfouling Induced Corrosion of Alloys
Z. Ying and W. Qiu 3726
- 555 Microbiological Aspects of the Low Water Corrosion of Carbon Steel
I. Beech, S. Campbell, and F. Walsh 3735
- 190 Anaerobic Corrosion of Steel by Phototrophic Sulfur Bacteria
M. Eashwar, S. Maruthamuthu, S. Sebastian-Raja, and S. Venkatakrishna-Iyer 3747

Paper #	Page #	Paper #	Page #
482	Effect of Biofilms on Crevice Corrosion of Stainless Alloys in Coastal Seawater <i>H. Zhang and S. Dexter</i>	401	Comparative Analysis by AES and XPS of Passive Films on Fe-25Cr-X Model Alloys Formed in Chloride and in Sulfate Solution <i>C. Hubschmid, H. Mathieu, and D. Landolt</i>
304	Role of Metal Uptake by the Mycelium of the Fungus <i>Hormoconis resinae</i> in the MIC of Al Alloys <i>B. Rosales, A. Puebla, and D. Cabral</i>	340B	In-Situ Studies of Passive Film Chemistry Using X-ray Absorption Spectroscopy <i>A. Davenport, J. Bardwell, H. Isaacs, and B. MacDougall</i> ..
217	Electrochemical Noise Analysis as an Indicator of Microbiologically Induced Corrosion <i>A. Saatchi, T. Pyle, and A. Barton</i>	027	Laser Spot Imaging of Passive Films on Stainless Steels <i>P. Schmuki and H. Bohni</i>
480	Use of Nucleic Acid Probes in Assessing the Community Structure of Sulfate Reducing Bacteria in Western Canadian Oil Field Fluids <i>D. Westlake, J. Foght, P. Federak, G. Voordouw, and T. Jack</i>	232	Effect of Rinsing on Analytical Results for Passivity of Amorphous Iron-Chromium-Metalloid Alloys <i>K. Hashimoto, S. Kato, B. Im, E. Akiyama, H. Habakazi, A. Kawashima, and K. Asami</i>
481	Control of Microbial Biofilm by Electrically-Enhanced Biocide Treatment <i>W. Costerton</i>	384	Surface Analytical and Electrochemical Examination of Passive Layers on Cu/Ni Alloys <i>P. Druska and H. Strehblow</i>
483	Use of a Biofilm Electrochemical Monitoring Device for an Automatic Application of Antifouling Procedures in Seawater <i>A. Mollica and G. Ventura</i>	126	Laser Raman and X-Ray Scattering Studies of Corrosion Films on Metals <i>C. Melendres</i>
557	Results of Electrochemical Monitoring of Microbiological Activity <i>G. Nekoksa and G. Licina</i>	544	Studies by Scanning Auger Microscopy of Electrochemical Corrosion: Serendipity and the SAM <i>J. Castle</i>
271	Evaluation of Materials and Coatings for use in Wastewater Lift Stations Subjected to Biologically Induced Corrosion <i>H. Saricimen, M. Shamim, and M. Maslehuddin</i>	545	Alloy Oxidation: Who is in Control as Studied by XPS <i>D. Cocke</i>
		075	Identification of the Chemistry of Corrosion Films Induced on W-Ni-Fe Alloys by Immersion in Aqueous NaCl using XPS <i>A. Mansour and K. Vasanta</i>

SURFACE ANALYSIS TECHNIQUES

363	An ^{18}O /SIMS Study of Oxygen Transport in Thermal Oxide Films Formed on Silicon <i>R. Hussey, G. Sproule, D. Mitchell, and M. Graham</i>	3831
054	SNMS Studies on the Oxidation Behaviour of Titanium Aluminides <i>W. Quadackers, A. Elschner, N. Zheng, and H. Nickel</i>	3842
543	Growth Mechanism of Alumina Scales on FeCrAl Alloys <i>M. Boualam, G. Beranger, M. Lambertin, E. Sciora, R. Hussey, D. Mitchell, and M. Graham</i>	3863
548	Passive Film Studies using Neutron Reflectivity <i>L. Krebs, J. Kruger, G. Long, D. Wiesler, J. Ankner, C. Majczak, and S. Satija</i>	3863
199	Corrosion of Iron in Electrolytic Anhydrous Methanol Solutions with and without Complexing Agents <i>K. Aramaki, M. Sakakibara, and H. Nishihara</i>	3868
135	In-Situ Gravimetry of Corrosion of Iron Thin Films Combined with Surface Analytical Techniques <i>M. Seo and K. Yoshida</i>	3878
445	Passivation of High Alloyed Stainless Steel in HCl at 22°C and 65°C <i>L. Wegrelus and I. Olefjord</i>	3887
505	XPS and Electrochemical Studies of the Dissolution and Passivation of Molybdenum-implanted Austenitic Stainless Steels <i>E. De Vito</i>	3898

NUCLEAR ENERGY AND WASTE STORAGE

282	The Effect of Surface Conditions on the Localized Corrosion of a Candidate High-Level Waste Container <i>D. Dunn, N. Sridhar, and G. Cragolino</i>	4021
303	The Influence of Long-Term Low Temperature Aging on the Performance of Candidate High-Nickel Alloys for the Nuclear Waste Repository <i>F. Hodge and H. Ahluwalia</i>	4031
295	On-Line Monitoring of Corrosion in Field Pipe Gathering Systems <i>K. Lawson, A. Rothwell, L. Fronczek, C. Lange</i>	4046
518	Corrosion Potential Monitoring and Its Simulation in BWR Conditions <i>M. Sakai, N. Ohnaka, and K. Ohsumi</i>	4060

WATER

- 583 Twenty Years of Experience of Dezincification Resistant Brasses in Swedish Tap Water Systems
M. Linder 4069
- 243 Corrosion Protection due to Deaeration using a Hollow Fiber Membrane for Water Distribution Systems in Buildings
T. Fujii, Y. Ochi, Y. Ukena, and Y. Tobisaka 4080
- 609 The Impact of Environmental Consideration on Corrosion Control Economic and Technology
T. Laronge 4088

VOLUME 6**ELECTRIC POWER INDUSTRY WORKSHOP**

- 341 Cutting the Cost of Corrosion and Fouling by Real-time Performance Monitoring
P. Stokes, W. Cox, M. Winters, and P. Zuniga 4093
- 418 Service Water Electrochemical Monitoring Development at Ontario Hydro
A. Brennenstuhl 4102
- 517 Monitoring of Corrosion in a Spray Dryer Absorption FEG Plant
N. Henriksen and J. Kristgeirson 4121
- 476 On Line Monitoring of Fireside Corrosion in Power Plant
D. Farrell 4131
- 521 FSM - A New and Unique Method for Monitoring of Corrosion and Cracking Internally in Piping Systems and Vessels
R. Strommen, H. Horn, and K. Wold 4141
- 582 Experience with Neutron Activation for a Real-time Corrosion Monitoring in a Urea Plant
G. Notten, J. Thoelen, H. Verhoef, and R. van Sluijs 4154
- 311 Monitoring of Microbiological Activity in Power Plants
G. Nekoksa and G. Licina 4166
- 021 Electrochemical Monitoring of Erosion-Corrosion in Multiphase Flows
I. Ehmann, E. Heitz, K. Miers, A. Schnitzler, K. Schroeder, and X. Shimeng 4176
- 419 Monitoring and Prediction of Environmentally Assisted Crack Growth in Stainless Steel Piping
S. Ranganath, T. Diaz, F. Ford, R. Pathania, A. Pickett, S. Ranganath, G. Stevens and D. Weinstein 4185
- 429 Corrosion Monitoring Using Harmonic Impedance Spectroscopy
N. Thompson and B. Syrett 4200
- 576 Electrochemical Noise Methods as a Possible In-Situ Corrosion Sensing Technique
G. Bierwagen, D. Mills, and D. Tallman 4208
- 516 Simultaneous Rig Investigations of Electrochemical and Chemical Corrosion of Low Carbon Steel in Feedwater with Oxygen and Ammonia
A. Sirota, V. Latunin, and V. Donnikow 4219
- 251 Electrochemical Sensors for Application to Boiling Water Reactors
M. Indig 4224
- 321 Electrochemical Potential Monitoring in the Feedwater at the St. Lucie 2 PWR
W. Kassen, J. Seager, and K. Beichel 4237
- 407 On-line Chemistry Control in EDF Nuclear Power Plants
J. Doyen 4259
- 436 Potential Transients, Transmission and Electrochemical Corrosion Detection
H. Isaacs and J. Cho 4267
- 261 Development of Sensors for In-Situ Monitoring of Corrosion and Water Chemistry Parameters for the Electric Power Utility Industry
D. Macdonald, J. Pang, C. Liu, E. Medina, J. Villa, and J. Bueno 4274
- 270 An Electrochemical Sensor for Oxygen and pH in Aqueous Systems
C. Alcock, L. Wang, B. Li, and N. Bakshi 4286
- 310 On-Line Particulate Iron and Sulfur X-Ray Monitor
D. Connolly 4295
- 520 On-Line Dissolution and Analysis of Corrosion Products
M. Robles 4305
- 437A Remote Monitoring of Corrosion Chemicals via Fiber Optic Raman Spectroscopy
L. Jeffers and J. Berthold 4313
- 575 Surface Enhanced Raman Scattering as an In-Reactor Monitor of Phenomena of Interest to the Nuclear Power Industry
T. Devine 4321
- 134 A New Contact Electric Resistance Technique for In-situ Measurement of the Electric Resistance of Surface Films on Metals in Electrolytes at High Temperatures and Pressures
T. Saario and V. Marichev 4325

AUTHOR INDEX

A

Abbassian, F. 1671
 Abd-El Meguid, W. 2011
 Agarwal, D. 1226
 Agarwala, V. 370, 1252, 3156
 Ahluwalia, H. 2907, 4031
 Ahmed, K. 1743
 Aho-Mentila, I. 2492
 Akiyama, E. 1102, 3940
 Al-Hasham, A. 3600
 Alcock, C. 4286
 Alhajji, J. 3587
 Almeida, A. 1460
 Almeida, E. 449
 Alvarez, J. 987
 Amey, S. 2377
 Amirudin, A. 114, 171
 Angelini, E. 1154
 Ankner, J. 3863
 Aramaki, K. 1804, 3868
 Archakow, Y. 2405
 Arnvig, P. 1477
 Aromaa, J. 834, 1278
 Arponen, M. 3617
 Arroyave, C. 748
 Asami, K. 1102, 3940
 Ashworth, V. 2207
 Ault Jr., P. 3519
 Ayllon, E. 574
 Azkarate, I. 2492

B

Baboiian, R. 3179
 Bacha, N. 271
 Bailey, B. 2795
 Bakshi, N. 4286
 Balakrishnan, K. 979, 1124, 1403,
 2162, 3613, 3708
 Ball, G. 1132
 Banerjee, G. 1766
 Barcia, O. 1378
 Bardwell, J. 3921
 Barker, B. 1864
 Barker, J. 1549
 Baron, E. 999
 Barreau, C. 114
 Barton, A. 3786
 Baumert, K. 855
 Bayles, R. 3531
 Beech, I. 1864, 3735
 Beichel, K. 4237
 Belashchenko, V. 63
 Bellucci, F. 406, 2255
 Bennett, J. 3220
 Beranger, G. 3852
 Berke, N. 3242, 3271
 Berthold, J. 4313
 Bess, R. 2749
 Bhagat, P. 3018
 Bianco, P. 1154
 Bieri, T. 3007
 Bierwagen, G. 182, 4208

Biestek, M. 3188
 Biwu, S. 923
 Bohni, H. 1367, 2142, 3260, 3929
 Bone III, L. 2601
 Boros, J. 2662, 2707
 Bouaifi, B. 2959, 2987
 Boualam, M. 3852
 Bradley, W. 3671
 Brennenstuhl, A. 4102
 Bristowe, W. 460
 Brook, R. 1549, 1692
 Brunoro, G. 1758
 Brusic, V. 687
 Buchheit, R. 2854
 Bueno, J. 4274
 Bulhoes, L. 1183
 Burkert, A. 2987

C

Cabral, D. 3773
 Cabrini, M. 2482
 Cameron, S. 3086
 Campbell, S. 3735
 Cao, C. 2155
 Capitanescu, D. 2973
 Capobianco, G. 2255
 Carnes, R. 3069
 Carraway, J. 3156
 Case, R. 2639
 Castle, J. 3982
 Cen, Y. 1572, 1580
 Chan, S. 2367
 Chandrasekaran, P. 3696
 Chapey, B. 1315
 Charles, A. 1287
 Charles, J. 2926, 2996
 Chebotaryova, N. 2223
 Cheldi, T. 2482
 Chieraqati, R. 1613
 Chisholm, C. 315, 329
 Cho, J. 1997, 4267
 Chou, M. 3308
 Chu, W. 1560, 1637, 2411
 Cigada, A. 1938, 2482
 Coburn, S. 509
 Cocke, D. 3991
 Cole, I. 1692
 Congleton, J. 1287
 Connolly, D. 4295
 Conte Jr., A. 1252
 Coote, A. 494
 Cornwell, R. 3671
 Costa, J. 437
 Costerton, W. 3803
 Cote, P. 1262
 Cox, W. 4093
 Cragolino, G. 4021
 Cramer, S. 722, 1353
 Crombie, R. 3540
 Crook, P. 1191
 Czelusniak, A. 3188

D

D'Alkain, C. 2112, 2240, 2248
 Dallaspezia, G. 1938
 Daniels, R. 1491
 Davenport, A. 1997, 2091, 3921
 Davison, R. 1477
 Dawson, J. 2768
 de Wit, J. 420, 2077
 de Mele, M. 3687
 De Vito, E. 3898
 Dean, S. 855
 DeBold, T. 1170
 DeLuccia, J. 3099
 Demofonti, G. 1692
 Desai, V. 250, 1649, 1960
 Deslouis, C. 1378
 Devine, T. 2052, 4321
 Dexter, S. 3696, 3761
 Dhouibi-Hachani, L. 3207
 Diaz, C. 3508
 Diaz, T. 4185
 Domzalcki, P. 849
 Donnikow, V. 4219
 Doyen, J. 4259
 Draugelates, U. 2959, 2987
 Druska, P. 3951
 Du, Y. 2383
 Dukic, L. 10908
 Dunford, T. 1064
 Dunn, D. 4021
 Dupoirion, F. 2996
 Duquette, D. 1658
 Durig, E. 3043
 Durning, T. 3242
 Dyer, T. 3077

E

Eashwar, M. 3708, 3747
 Eberlein, R. 3424
 Efird, K. 2662, 2707
 Ehmann, I. 4176
 El-Rhazi, M. 3717
 El-Sharif, M. 315, 329
 Elschner, A. 3842
 Elsener, B. 2120
 Elsner, B. 3260
 En-Hou, H. 1727
 Enikeev, E. 1784
 Escudero, M. 240
 Eydelnant, A. 3109

F

Fa, L. 2865
 Faidi, S. 437
 Fang, Z. 1542
 Farrell, D. 4131
 Federak, P. 794
 Feng, Z. 784
 Feoktistov, A. 1784

Fernandes, J.	3130
Fernandez, A.	574, 652
Ferreira, M.	1460, 3130, 3235
Festy, D.	2005, 3484, 3634, 3717
Fink, K.	2302
Fitzgerald, B.	762
Flanagan, W.	1588
Flasche, L.	2907
Flavian, M.	99
Flitt, H.	3551
Flower, H.	2492
Foght, J.	3794
Froneczek, L.	2768, 4046
Ford, F.	4185
Forsen, O.	294, 834, 1278
Frankel, G.	687
Frankenthal, R.	3332, 3378
Fuhr, J.	3033
Fujii, S.	1430
Fujii, T.	4080
Fujita, S.	3200
Furuma, K.	2022

—G—

Galvan, J.	240
Gao, K.	1637
Gartland, P.	1915
Garz, I.	2959
Ge, H.	484
Geretsen, H.	2726
Gervasi, C.	574
Ghiazza, M.	2005
Gil-Negrete, A.	2925
Ginn, B.	2895
Glisenti, A.	2255
Gollner, J.	2987
Golozar, M.	3660
Gomez de Saravia, S.	3687
Gooch, T.	1076, 2895
Goswami, G.	250
Gouda, V.	2011, 3600
Graedel, T.	711
Graham, M.	3831, 3852
Granata, R.	24, 2612
Granese, S.	652
Grant, W.	2207
Grauvogl, H.	3058
Griffin, R.	2324
Groysman, A.	63
Guangtuan, H.	2804
Gui, J.	2052
Gullman, J.	642

—H—

Habazaki, H.	1102, 3940
Hack, H.	151
Hailey, T.	2662, 2707
Haines, S.	795
Hakkarainen, T.	3396
Hakkarainen, T.	3396
Hamert, J.	906
Hamilton, T.	2823
Handa, T.	1986
Handrich, K.	77
Haneef, S.	700
Hardy, G.	3018
Harlow, D.	3573
Hart, R.	16
Haruna, T.	1509

Hashimoto, K.	1102, 3940
Hashizume, O.	2439
Havn, T.	2814
He, Y.	934
Heft, B.	855
Heitz, E.	4176
Hengrong, G.	923
Henriksen, J.	494
Henriksen, N.	4121
Henry, R.	529
Herda, W.	1226
Heubner, U.	1226
Hibner, E.	2548
Hicks, M.	3242, 3271
Hinkebein, T.	2854
Hlava, P.	2854
Ho, C.	2367
Ho, E.	1702
Hodge, F.	4031
Horn, H.	4141
Hsiao, C.	1560, 2411
Hu, W.	2411
Huang, S.H.	687
Hubschmid, C.	3913
Hussey, R.	3831, 3852

—I—

Igawa, Y.	3561
Ignatenko, V.	2223
Ikedo, A.	2464, 2680
Im, B.	3940
Indig, M.	4224
Inturi, R.	2030
Isaacs, H.	1997, 3921, 4267
Ishizawa, Y.	2439
Islam, M.	1022, 3489
Ismail, A.	1826
Ives, M.	2096
Iwanow, J.	3188
Jack, T.	3794
Jana, S.	307
Janavicius, P.	2377
Jargelius-Pettersson, R.	1143
Jeffers, L.	4313
Jernberg, P.	171
Jimenez-Morales, A.	240
Jimin, C.	2865
Jin, S.	1564
Jin, J.	1637
Jixun, W.	53A
Johannsson, L.	662
Johansson, E.	549
Johnson, G.	624
Johnson, J.	700
Johnson, R.	370
Juchniewicz, R.	849

—K—

Kain, R.	1876, 1889, 2780
Kajimura, H.	1341
Kajiyama, F.	2293
Kalman, E.	1814
Kamachi-Mudali, U.	1942, 1949
Kambe, S.	259
Kane, R.	807, 2451
Kannan, R.	1854
Karlsson, L.	2944
Kasahara, K.	2293
Kassen, W.	4237

Katano, Y.	3561
Kato, S.	3940
Kawashima, A.	1102, 3940
Keenan, J.	795
Keging, Z.	54
Kermani, M.	1671, 2639
Khanna, A.	250
Kiefner, J.	2869
Kim, J.	1102
Klarin, A.	834
Klarstrom, D.	1111
Kleeman, W.	2625
Kloss, D.	778
Knotkova, D.	494, 561, 734
Kobayashi, T.	2425
Koch, G.	3007
Kock, W.	1039
Komp, M.	509
Kong, P.	1794
Kopliku, A.	2482
Korwin, M.	3188
Kosar, D.	3086
Kovaleski, K.	24, 2612
Koyama, Y.	2293
Krashennikova, I.	1784
Krebs, L.	3863
Kristgeirson, J.	4121
Kruger, J.	2131, 3863
Kubo, T.	3561
Kucera, V.	494
Kung, E.	1794
Kuznetsova, V.	2520
Kwiatkowski, L.	219

—L—

Lakshminarayanan, V.	1410, 1854, 3295
Lambert, M.	3852
Landolt, D.	3913
Lange, C.	4046
Larbi, M.	963
Laronge, T.	4088
Latanision, R.	3355
Latunin, V.	4219
Lau, M.	307
Lawson, K.	2768, 4046
Le Breton, J.	3634
Leal, C.	999
Lee-Picpho, L.	1
Legat, A.	1410
Leiro, M.	574
Leistikow, S.	1327
Lemaitre, C.	2005
Lenard, D.	1466
Leonard, J.	2005
Lessner, P.	3366
Letton, A.	3671
Lewis, K.	1064
Leygraf, C.	494, 600
Li, B.	4286
Li, L.	42
Li, R.	1460
Li, S.	1564
Lichter, B.	1588
Licina, G.	3812B, 4166
Liliental, W.	3188
Liljas, M.	2882
Lim, L.	307
Lin, C.	2045
Lin, H.	2155
Lin, J.	2367

Lin, S.	219
Linder, M.	549, 4069
Lindsey, N.	3645
Little, B.	3680
Liu, C.	3446, 3460, 4274
Liu, X.	1564, 2831
Liu, Y.	1572, 1580
Lobnig, R.	3378
Long, G.	3863
Lopez, V.	240
Lore, S.	509
Lou, M.	1794
Lunde, L.	2492
Luo, Y.	3503
Lyagh, A.	7618

--- —M—

MacCuish, R.	2639
Macdonald, D.	2065, 3446, 3460, 3508, 4274
MacDougall, B.	3921
Machczynski, W.	2268
MacQueen, R.	2612
Madsen, B.	1353
Magdowski, R.	2332
Magnin, T.	1613, 1720
Magurova, Y.	280
Majczak, C.	3863
Maksaeva, L.	2395
Malhotra, S.	1766
Mandalia, H.	473
Mansfield, F.	128, 219, 529, 1388, 3680
Mansour, A.	4009
Mao, X.	2831
Marcus, P.	2105
Marichev, V.	826, 3344, 4325
Marinho Jr., A.	3477
Marshakov, A.	2223, 2395
Martello, A.	195
Martinz, H.	1039
Maruthamuthu, S.	3708, 3747
Mascaro, H.	2112, 2240, 2248
Masleuddin, M.	3813
Mathieu, H.	3913
Matocha, G.	2311
Matsamura, K.	3200
Matsumura, Y.	2022
Mattes, O.	1378
Matz, C.	3149
Maurice, V.	2105
Mayer, P.	3413
Mazeas, F.	3717
McArthur, A.	807
McCarthy, D.	3086
McDonald, L.	722
McNeil, M.	3680
Meany Jr., J.	3519
Medina, E.	4274
Meishuan, L.	943
Melendres, C.	3973
Melton, D.	2854
Mesa, S.	748
Meyer, T.	1191
Meyn, D.	3531
Michal, G.	2377
Miers, K.	4176
Miglin, M.	1600
Mikhailovski, N.	386
Mikhailovsky, Y.	2223, 2395
Miksic, B.	3109

Miller, R.	16
Milliams, D.	2420
Mills, D.	182, 4208
Miname, Y.	2439
Misawa, T.	612
Mishra, B.	2840
Mital, C.	473
Mitchell, D.	2625, 3831, 3852
Mitton, D.	3355
Miyasaka, A.	2537
Miyata, Y.	1986
Miyukii, H.	612
Moeller, R.	2548
Moghissi, O.	2601
Mollica, A.	3807
Molokanov, V.	826
Monetta, F.	406
Monetta, T.	2255
Monical, D.	2749
Montemor, M.	3235
Monter, J.	1600
Monticelli, C.	1758
Moraes, S.	3413
Morahito, D.	1692
Morales, J.	2680
Morales, J.	2464
Moran, P.	1915, 2131
Morcillo, M.	87
Moriau, O.	1613
Moslehy, F.	1649
Munster, R.	862
Muralidharan, S.	1403
Murray, J.	151
Malhotra, S.	1202

--- —N—

Nagano, H.	612, 1341
Nagarkar, P.	3355
Najjar, D.	1613
Narayan, R.	3118, 3139
Natesa, M.	3613
Navas, G.	999
Nazarov, A.	386, 2175
Nekoksa, G.	3812B, 4166
Nelson, J.	1600
Nenov, K.	3355
Nguyen, D.	1491
Nicholls, J.	1237
Nickel, H.	3842
Nicodemo, L.	406
Nishihara, H.	1804, 3868
Nishimura, R.	1532
Noble, D.	1076
Noshiro, T.	259
Notten, G.	869, 4154
Nowak, W.	42
Nunes, P.	1974

--- —O—

Ochi, Y.	4080
Odnevall, I.	600
Ogaloa, H.	2537
Ogundele, G.	1702
Ohnaka, N.	4060
Ohno, N.	1804
Ohsumi, K.	4060
Okamura, K.	2293
Okazawa, T.	2425
Oki, T.	1509

Okuyama, M.	259
Oldfield, J.	1876
Olefjord, I.	3887
Olson, D.	2840
Olstowski, H.	1091
Oltra, R.	1315
Opara, B.	280
Ostermiller, M.	1
Otero, E.	987, 2037
Oun, S.	1743

--- —P—

Pak, S.	2944
Palmer, J.	2768
Pan, Z.	379
Pang, J.	4274
Panov, M.	1784
Pao, P.	3531
Pardo, A.	987, 2037
Pathania, R.	4185
Payer, J.	1132, 2302, 2377
Pereira, D.	449
Perez, F.	987
Perez, R.	748
Perkins, A.	882
Persson, D.	600
Peterson, P.	590
Peterson, T.	687
Petrinin, M.	386, 2175
Petschel Jr., M.	16
Phillips, T.	778
Pickering, H.	1929, 2346
Pickett, A.	4185
Pierozynski, B.	849
Pimenta, G.	2278
Pishnamazi, A.	1032
Popova, V.	2395
Postyn, A.	3077
Pound, B.	2356
Pourbaix, A.	3314
Prasad, R.	1960
Principe, E.	1649, 2187
Procter, B.	2207
Puebla, A.	3773
Pyle, T.	3786

--- —Q—

Qi, H.	934
Qiao, L.	1560, 1637
Qing, Y.	484
Qiu, D.	379
Qiu, F.	1445
Qiu, W.	3726
Quadackers, W.	3842
Quian-Falzone, L.	1649

--- —R—

Raharinaivo, A.	3207
Rajagopal, G.	2162
Rajagopalan, S.	1420, 1854, 3295
Rajan, K.	1252
Rajeswari, S.	1942, 1949
Ramakrishnan, P.	1960
Ramamurthy, A.	3508
Ramanathan, L.	914, 1974
Ramesh, P.	3295
Ranganath, S.	4185
Rapp, R.	353

Ravindranath, K.	1202
Rawat, A.	1960
Reda, M.	3587
Regler, F.	3058
Regnier, J.	3484
Rehfeld, D.	1183
Rein, D.	1064
Renaud, L.	1300
Revie, R.	2831
Rezgui, B.	963
Rhoades, K.	1091
Ri, L.	54
Rincon, O.	999
Rivers, M.	1997
Roberge, P.	795, 1466, 3404
Robles, M.	4305
Rocca, D.	3156
Rocchini, G.	1450
Rommel, M.	3077
Rondelli, G.	1938, 2482
Rosalbino, F.	1154
Rosales, B.	574, 652, 3773
Rossi, A.	2120
Rosso, M.	1154
Rothwell, A.	4046
Roy, C.	271
Rozlivka, L.	734
Ruschau, G.	2601
Russell, S.	3109

—S—

Saarinén, K.	2566
Saario, T.	826, 4325
Saatchi, A.	1032, 3660, 3786
Sabata, A.	3508
Saenz, E.	2037
Saetre, O.	2529
Sakai, M.	4060
Sakakibara, M.	3868
Salama, M.	2840
Salas, B.	1736
Salta, M.	3235
Sanad, S.	1826
Sargeant, D.	795
Saricimen, H.	3813
Sathiyarayanan, S.	2162, 3708
Satija, S.	3863
Scantlebury, J.	437
Scavino, G.	1154
Schanz, G.	1327
Scharf, T.	2285
Schiffler, D.	2131
Schmidt, N.	1170
Schmuki, P.	3929
Schnitzler, A.	4176
Schreyer, A.	2142
Schroeder, K.	4176
Schubert, R.	3385
Schulte, M.	2650
Schulze, S.	2959
Schutze, M.	2650
Schutz, R.	1213
Sciora, E.	3852
Seager, J.	4237
Sebastian-Raja, S.	3747
Seidel, J.	1658
Sen, P.	1252
Seo, M.	3878
Seri, O.	2022
Shalaby, H.	1022, 3600

Shamim, M.	3813
Shaoyu, Y.	398
Shariff, M.	1743
Shaw, B.	1915
She, D.	1560
Shi, L.	971
Shibata, T.	1509
Shih, S.	971
Shimeng, X.	4176
Shutz, R.	2506
Siconolfi, D.	3332, 3378
Sidey, D.	1702
Silverman, D.	3430
Simoes, A.	3235
Simon, P.	3489
Simpson, T.	157, 624
Sinclair, C.	891
Sinclair, J.	3332, 3378
Singer, L.	1
Singh, I.	979
Sinyavsky, V.	1623
Sirota, A.	4219
Sivakumar, M.	1942, 1949
Skerry, B.	182
Skogsberg, J.	2506
Smart III, J.	2758
Smith, J.	2639
Smith, S.	2695
Snelson, A.	1252
Sokolski, W.	849
Song, G.	2155
Sotoudeh, K.	1262
Sousa da Silva, C.	1378
Speidel, M.	2339
Spence, J.	722
Sproule, G.	3831
Sridhar, N.	4021
Srinivasan, S.	2451, 2574
Stark, A.	2959
Steen, W.	1460
Steinberg, H.	2987
Stenvall, P.	2882
Steppan, J.	3156
Stevens, G.	4185
Stockle, B.	494
Stokes, P.	4093
Stolarski, V.	3671
Strehlow, H.	3951
Strom, G.	3508
Strom, M.	3508
Strommen, R.	4141
Su, Y.	329
Sugie, Y.	1430
Sulaiman, A.	1532
Sun, H.	3308
Suter, T.	1367
Sutton, S.	1997
Svensson, J.	662
Sweet, G.	460
Syrett, B.	4200
Szakalos, P.	1143
Szklarska-Smialowska, Z.	2030
Szuryn, A.	1008

—T—

Tacikowski, J.	3188
Tait, W.	77
Takazawa, H.	1986
Talah, H.	2105
Tallman, D.	182, 4208

Tam, S.	307
Tao, W.	484
Tatara, R.	1091
Tavi, M.	1278
Teillet, J.	3634
Teng, M.	1056
Thierry, D.	114, 171
Thielen, J.	869, 4154
Thomas, H.	3058
Thompson, G.	700
Thompson, N.	4200
Tidblad, J.	600
Tiefan, L.	943
Timoshenko, A.	280
Tobisaka, Y.	4080
Tourney, P.	3271
Townsend, H.	42, 624
Trabanelli, G.	1758
Trethewey, K.	795
Tribollet, B.	3717
Triki, E.	3207
Trivedi, M.	473
Tsai, C.	128
Turkia, M.	294
Tuthill, A.	1300
Tvarusko, A.	3287

—U—

Ueda, M.	2464, 2680
Ukena, Y.	4080
Urquidí-Macdonald, M.	3460, 3508
Utrilla, V.	2037

—V—

Valencia, A.	748
Valeriotte, E.	676
Valliappan, M.	3613
Van Sluijs, G.	869, 4154
Van Ooij, W.	3508
Varela, F.	574
Vasanta, K.	4009
Veds, M.	2425
Venkatachari, G.	979, 1403, 3613
Venkatakrishna-Iyer, S.	3747
Ventura, G.	3807
Vera, J.	2464, 2639, 2680
Verhoef, H.	869, 4154
Verkholtantsev, V.	99
Vernieu, M.	2996
Vianna, R.	2278
Vicentini, B.	1938, 2482
Vida, E.	240
Videla, H.	3687
Vieth, P.	2869
Vilar, R.	1460
Vilche, J.	574
Villa, J.	4274
Viloria, A.	2464, 2680
Virtanen, J.	1278
Virtanen, S.	2142
Visser, A.	2726
Viswanathan, M.	1124
Vitus, C.	2091
Vlckova, J.	734
Voder, G.	3531
Volpe, L.	590
Voordouw, G.	3794

—W—

Wade, C.	1600
Wagner, G.	862
Wagner, P.	3680
Walaszkowski, J.	849
Walker, R.	1076
Walsh, F.	1864, 3735
Wan, X.	353
Wang, G.	353
Wang, L.	4286
Wang, M.	1588
Wang, V.	219
Wang, X.	315
Wang, Y.	2411
Warner, T.	1613
Watkins, K.	1460
Watson, A.	315, 329
Watson, S.	1353
Wegrelus, L.	3887
Wei, K.	1727
Wei, R.	3573
Weinstein, D.	4185
Wenan, H.	784
Wenjuan, Y.	2804
Westermarck, J.	834
Westlake, D.	3794
White, R.	2324
Wiesler, D.	3863
Wilhelm, S.	807
Williamson, G.	2734
Winkler, M.	2585
Winters, M.	4093
Wojtas, H.	3260
Wold, K.	4141
Wood, G.	700, 1523
Wright, E.	2207, 2662, 2707
Wu, Y.	1542

—X—

Xiao, H.	529, 1388
Xiao, M.	1213, 2506
Xiaofeng, S.	923
Xiaojun, C.	784
Xiaolian, X.	54
Xiaoshan, R.	784
Xizhang, H.	784

—Y—

Yamashita, M.	612
Yan, J.	2324
Yang, I.	1056
Yang, L.	307
Yanping, L.	53A
Yanto, E.	2749
Yao, C.	1794
Yao, L.	1794
Yau, T.	762
Yi, L.	341
Ying, Z.	3726
Ylasaari, S.	294, 834
Yong Yang, Y.	3308
Yoshida, K.	3878
You, Z.	379
Young, D.	2625
Yu, J.	1549, 1692
Yuma, H.	1727

—Z—

Zhang, H.	3761
Zhang, X.	676
Zhang, Y.	951B, 971
Zhao, M.	1773
Zhao, Y.	379
Zhaoqing, Z.	204
Zheng, N.	3842
Zhu, L.	2803B
Zhu, M.	1588
Zhu, R.	1542
Zhu, R.	934
Zilic, M.	1008
Zucchi, F.	1758
Zuniga, P.	4093
Zuo, J.	1572, 1580

CORROSION, ITS EFFECT ON SOCIETY
BY: NORMAN HACKERMAN
RICE UNIVERSITY AND UNIVERSITY OF TEXAS
AT THE INTERNATIONAL CORROSION CONGRESS
HOUSTON, TX - SEPT. 20, 1993

The recognition of the propensity of metals, noble as well as base, to react with usual environments must be as old as the availability of metals to humans. Certainly early ancestors must have noticed discoloration of native gold and silver, especially after having been handled. More serious effects would not have been noticed before metals began to be used for structural and other such purpose. Without attempting a true historical essay it should be noted that by the time of Robert Boyle the existence of corrosion, as a word as well as a phenomena, had been established. He wrote about it in his "The Works of the Honorable Robert Boyle Epitomized", Book V, Part IV, published in 1675. Indeed, from his writing it is clear that it was already known that activity of the solution (surroundings) as well as reactivity of the metal were both involved.

The serious effects of corrosion undoubtedly coincides largely with the industrial revolution of the 19th century. Certainly there were disturbing effects on metal artifacts, statues, and utensils before that but these were largely discoloration. By virtue of heavy metal ingestion from corroded utensils there must certainly also have been some health effects.

However, with the increasing use of metals in industrial systems, home use, bridges, transportation systems and so on, the impact of metallic corrosion markedly increased. Two major effects are of particular interest, (1). economic and (2). accidents. The latter must be viewed as having economic impact along with its obvious intrusion into human well being. It is likely that health impairment due to corrosion of eating utensils has diminished as a source of human misery.

Consideration of economic effects brings to light the difficult problem of evaluating the cost of corrosion to society. The principal difficulty lies in including avoided costs. Put otherwise, since there is always a cost associated with alleviating or inhibiting the corrosion but no profit, it always appears as a minus. An early estimate of the price the US. paid per annum in the middle of this century was made by H.H. Uhlig (Chem. Eng. News, 97, 2764 (1949). He estimated the cost at about five billion dollars or 2.1% of the then GNP. A later estimate Mat. Perf., 19 (5) 34 (1980) suggested 70 billion in 1975 or

4.2% of that GNP. In fact while direct costs of corrosion prevention can be calculated in principle, in fact only rough estimates are possible and even that is a sizable chore. In any event corrosion, or more generally material deterioration, is an inevitable and costly process and the savings made possible by a knowledgeable cadre of scientists and engineers is of benefit to society in terms of final cost of product and/or of profit.

There is a second, but at least as important, consequence of the practice of corrosion control. Inherent in corrosion processes is the possibility of equipment failure. This may occur from recognizable long term processes or by virtue of sudden loss of function. From the mid nineteenth century problem of sudden failure of steamboilers to the more current rash of chemical plant explosions, failure caused by corrosion has been a source of human misery. Add to this bridge failure, product contamination, sheet metal perforation, and so on and it is clear that improving the resistance of metals to changes which come naturally is an important, even if generally unnoticed, contribution to society.

The obvious question then arises has the corrosion reduction efforts over the last 150+ years to enable enhanced use of metals been effective. The answer must be yes. The use of metals under more and more severe conditions has certainly taken place. Severe conditions of temperature, pH, fluid motion, etc., are now suitably dealt with in many instances. This does not mean that there is no corrosion in such systems, but that it is tolerable. Nor does it mean that it is possible to prescribe in a general way for any conceivable system. For instance, the possibilities of using supercritical water as an oxidant may uncover difficult corrosion problems. The same is true for molten salt and molten metal based systems. Indeed suitable material for processes of this nature may well be a serious, or even an impenetrable, barrier.

The likelihood that the latter will be the case must be based on the fact that thus far solutions, including material substitutions, have generally become available. These solutions have included better materials, treatment of the environment, treatment of the solid surface, less reactive coatings, electrochemical protection, or changes in process conditions which are not detrimental to the product. While the first and last of this series have been most often effective, all have been of value.

Perhaps as important as any finding is that while there are commonalities each system has to be considered individually, and in the final analysis as a system. The individual nature suggests that each system requires a prescription, and this must depend on the corrosion engineers' background and experience. It is also likely that the system changes with time and, therefore it must be monitored so as to alter the treatment as needed. This statement is also pertinent to the suggestion above that one can study parts of the whole but in the real case it is the whole which must be treated.

Considering the complexity the corrosion scientist and engineer has to deal with the progress made to date is notable. With the more recent advent of highly sensitive, inquisitive instruments plus the clearer insight into the complexities of corrosion processes it is likely that dealing with more and more corrosive systems will progress well.

It is heartening to see this gathering of world wide experts at handling corrosion problems of many kinds. It is vital that such meetings are convened as a means of maintaining control in the never-ending battle to make the materials at our disposal serve our various purposes better.

The interactions that take place, not only between engineer and engineer but also between engineer and scientist, will certainly enhance the understanding and capabilities of all who are here. Meetings of this kind of all-encompassing coverage are especially valuable in making it possible for each of us to see the system as a whole. This in turn optimizes each individual's contributions. For reasons cited earlier this is to the advantage of society. Thus your gathering here is not just another meeting but one of real consequence to the human race.

Low-Cost Corrosion Engineering and Risk Potential, Operational and Environmental Safety - an Irreconcilable Antagonism in the Chemical Process Industry ?

H. Spähn
Polytechnic Institute
D-6100 Darmstadt
Grafenstr. 2*

Abstract

Costs of investment, operation and maintenance on the one side and mastering the risk potential of processes on the other have always been of concern to the chemical process industry. From the earliest stage of a new synthesis to maintaining an aging production plant the corrosion expert has to balance risks from either side. Looking at the development of proceeds of a new production facility from point zero on, when capital expenditures for the project in question are effected, we have to recognize three economic essentials: 1. low capital expenditure 2. short project execution time 3. low operating costs. The dent in the income from operation vs. time curve will be determined by the amount of capital expenditure, its width by the time to accomplish the investment, and the point of time when the income from operation starts, and in addition to that, by the gradient at which it increases with production time. The paper tries to exemplify the corrosionist's spheres of influence and his contributions to reconcile the antagonisms indicated.

Key terms: cost considerations, chemical process industries, on-stream electrochemical monitoring

Introduction

Ever since it had been founded 150 years ago the Chemical Process Industry (CPI) had to be aware of the hazards when synthesizing or handling substances. They are twofold if toxic substances have to be handled under pressure (Figure 1). With the development of the Haber-Bosch ammonia synthesis in 1913 the pressures leaped from some six to several hundred atmospheres and the elastic energy stored in pressure bearing walls increased by a factor of at least 10^4 . And yet the integrity of the components had to be maintained under all operating and emergency conditions so that there was no release of toxic or pyrotic substances, no fire or explosion, no deflagration or release of energy by damaging pressure waves nor any throwing off of fragmented pressure vessel parts. The mechanical integrity of vessels, piping and other pressure bearing parts has well been taken care of ever since more than 10 000 boilers had exploded in the USA, Canada and Mexico between 1865 and 1905. This series ended with a disastrous power boiler burst in Massachusetts which took the life of 58 persons, seriously injured 117, and lead to the

* before retirement: head, corporate Development/Materials Eng. Dep., BASF AG, D-6700 Ludwigshafen

development of the ASME Code. Near Düsseldorf, Germany, a power plant boiler burst on account of intergranular stress corrosion cracking again killing 58 persons which gave rise to the foundation of VGB, the German Association of Utilities. Other Codes emerged in other industrialized nations. They all have, however, in common that they take corrosion into account only insofar as global quantities are concerned such as a "corrosion allowance" or, should there be a risk of Stress Corrosion Cracking (SCC), a percentage reduction of allowable net stresses. This is quite understandable regarding the complicated nature of corrosion processes. It is for these reasons that the responsibility for a proper assessment of a process determined corrosion situation rests with the companies and their corrosion experts. It is this very situation which requires the corrosionist's careful approach weighing the ways and means of saving costs of corrosion control measures against component, operational, productional and environmental safety (Figure 2).

Spheres of Influence

Corrosion influences decisions in the CPI in many ways. In extreme cases it may kill the most beautiful new synthesis because it demands such aggressive operational parameters that exorbitant corrosion control costs make the product incompetent. This is, fortunately, the exception, not the rule, and the corrosion engineer must not be blamed for it. In his workaday routine, he has to be helper and mediator in a techno-economic area. He is expected to make decisions which may be, more often than not, of considerable economical consequences. Under the pressure of this routine he seldom resorts to cost accounting which, anyway, is restricted to special cases as shown on Figure 3. Corrosion Economics, in his situation, has to be guided by some simple principle questions such as "When is it justified to select more expensive materials?" (Figure 4). Guided by his professional knowledge and based on concrete, first hand experience he will not pose the question "Which material will last forever?" but instead ask himself "considering the component in question, what will be the consequences if this low cost component will fail?".

No longer bothering the corrosionist now, Figure 5 exemplifies maintenance strategies for components under corrosion load and of different importance for plant availability (i.e. on-stream factor), different component exploitation factors, different risk potentials when failing. Considering the fact that maintenance is just one cost factor this Figure makes plain that low cost corrosion engineering must indeed be guided by pragmatic principles. A systematical compilation of such principles would be beyond the scope of this paper so that a simpler approach has to be taken. It intends to exemplify and highlight noticeable instances in the three characteristic phases shown in Figure 6 which are typical for the CPI. The corrosion expert is challenged and must influence decision making in each of them.

Stage I: New Processes, Research and Development

Developing a new chemical process, be it by a chemical or an engineering company, demands the corrosion engineer's involvement at the earliest point of time. A reliable corrosion prognosis requires time to evaluate the scientific literature, and, based upon this, planning tests and performing them for a long enough time. Take for instance Figure 7. Had the time available been limited to 500 hours, a nominal SCC strength of 500 MPa would have been ascribed to the austenitic-ferritic stainless steel (21Cr-8Ni-2.5Mo(N)) with the highest sustainable nominal SCC stress. At 10 000 hrs the actual value is shown to be 250 MPa, a reduction of 50%. Now, had the 500 hrs-value been used in a strength calculation for components, the result would have been SCC after approximately 1000 hrs under the allowable stress ($2/3 R_{eH} = 300 \text{ MPa}$).

Without discussing anything more a look at Figure 8 reveals two especially difficult stages from the corrosion point of view, viz. 1.) Miniplant stage. Miniplant techniques nowadays allow the chemical engineer to simulate practically all relevant states and dynamic processes in a new synthesis at the same time being able to measure the quantities to be known. In contrast with him the corrosion engineer does not dispose of scale-up procedures which would allow him to directly transfer many of his test results from laboratory to full scale. Consequences: except for the three highest Corrosion Predictability Confidence Levels of Figure 9 he needs again extra time for simulating critical points on a semi-pilot plant scale. 2.) Materials definition. In the crucial stage where the corrosion resistant materials have to be selected it is touch and go for the corrosionist if the supplier of test specimens is unable to produce his material within narrow limits for elements vital for corrosion resistance. Any positive contribution to lower costs from the corrosionist's part might be reversed; instead of having saved money by recommending the leanest alloy close to its resistance borderline there will now be the risk of component failures due to material supplied with lower bound analysis values of critical elements. The situation will be especially serious if passive/active transitions are involved such as in pitting, SCC, and, above all, corrosion fatigue. The consequence of an passive/active transition in the latter case will be a dramatic decay of the corrosion fatigue (CF) strength as exemplified by Figure 10. It is not only that the absolute CF strength value for any given number of cycles is significantly lower in case of a transition from the active to the passive state. As a matter of fact, the difference between the passive and active CF strength values increases steadily with time and number of cycles N , respectively, depending on the passive/active CF system the loss in CF strength in the active state may be up to 50 MPa per decade of cycles.

Stage II: Planning, Engineering, Procurement, Fabrication, Construction

Looking at the development of proceeds of a new production facility from point zero on, when capital expenditures for the project in question are effected, we recognize three economic essentials (Figure 11):

1. low capital expenditure
2. short project execution time
3. low operating costs

The dent in this curve is determined by the amount of capital expenditure, its width by the time to accomplish the investment, and the point of time when the income from operation starts, and in addition to that, by the gradient at which it increases with production time. Any delay in starting up a plant is accumulating a negative cash flow which may, from the day of scheduled start-up on, amount to more than 750 000 \$ per day for large chemical plants. Should this happen, the proceeds of a long production period will have been wasted.

To cope with these essentials already in Stage I requires allotting sufficient time for evaluation and testing and other actions from the part of the corrosionist. In order not to go beyond the limits of this paper no examples for Stage II shall be given. Instead, few catchwords must do:

- are corrosion control measures, planned during the design stage, a small additional expenditure compared to costs of shut-down, lost production etc.?
- can, and if where, the availability index of a plant be hampered from the corrosion side?
- by which weak spots, if any, might there be a potential corrosion induced safety risk?
- where has the economic command of expense and yield been overlooked from the corrosionist?
- has the iron rule "corrosion control has to begin at the design stage" been violated?
- are areas prone to corrosion accessible for nondestructive examination?

Returning to Figure 11 we have to realize that capital cost can easily be calculated whereas considerably more data is needed in order to be able to establish the influence of a corrosion control measure on operating costs. Such measures are causing higher capital cost, a positive or negative change in material cost, energy and labor cost, lower maintenance cost and lower shut-down cost. On the other hand one can, at the time of planning, quite often not decide upon which economic lifetime a plant shall have. Making decisions in such circumstances is difficult, it is true. They must, however, never touch operational safety.

Stage III: Operation, Maintenance

The first example has been chosen in order to illustrate the indication for electrochemical monitoring and its implementation.

In the CPI there are instances where process parameters may temporarily exceed the boundaries set. Should this trigger damaging corrosion processes monitoring may be indicated. The indication is the stronger the higher the economical/safety risks, the likely the extent of damage, the difficulties of repair etc.

SCC, CF, Hydrogen Induced Cracking have these indication characteristics and so does pitting which shall be used as an example. It has been shown conclusively¹ that pitting, once initiated, can be stopped if the stationary potential A is lower than the repassivation potential R . Figure 12 illustrates² the electrochemical situation, Figure 13 the set-up for electrochemical monitoring, Figure 14 its embodiment. When superimposing (according to Wagner-Traudt's mixed potential theory³) the anodic current density-potential curve a with the cathodic curve $c1$ belonging to a weakly oxidizing redox system (Figure 12) we obtain a (stationary) "Mischpotential" A in the passive region. This potential is less noble than the breakthrough potential B for pitting and belongs to the operating conditions within the design values. Now, if during operation a potential excursion to values more noble than the pitting initiation potential P is caused by an influx of a strongly oxidizing redox system (curve $c2$) pits will grow. However, if the potential afterwards drops back to the design values (i.e. to R), repassivation will take place. The pronounced hysteresis in the backward curve is due to the composition of the electrolyte inside the pits; here the acidity is higher (due to the hydrolysis of metal ions), and so is the metal ion and chloride concentration and also the viscosity whereas the oxygen concentration is lower than in the bulk electrolyte. Consequently, more negative potentials are required to re-establish passivity inside pits. Electrochemical measurements such as this³ are powerful means to both monitor potential excursions, and the time it takes until passivation has been restored thus being in a position to counteract any otherwise unforeseeable damage.

The situation worsens even more when fatigue and pitting are superimposed (Mode IV corrosion fatigue⁴). A typical example are tubular heat exchangers (Figure 15). When heat exchanger tube bundles are subjected to a (straight) crossflow of a medium, flow-induced vibrations may be caused if the exchanger does not meet TEMA standards. Fluidelastic instability in such bundles occurs as soon as a critical cross-flow velocity has been reached. At instability, chaotic vibration of the tubes sets in including periodic motion, quasi-periodic oscillation and random vibration so that the tube vibration amplitude will rapidly increase. Should this happen in the presence of a medium causing chloride induced pitting, the corrosion fatigue strength will dramatically decrease (Figure 16) until (pseudo-brittle) corrosion fatigue fracture occurs the location of which (2) is shown on Figure 15. As Figure 17 proves the repassivation potential concept can be applied to the dynamic conditions of CF, too. At potentials below this potential, Mode II-CF⁴ replaces Mode IV-CF⁴. Mode II must, of course, be the design mode under which CF proceeds in the passive state associated with the highest CF strengths of all CF-Modes. It has to be

regained after a potential excursion which will be assured if the stationary open circuit potential is less noble than the repassivation potential, and this is exactly what can be measured and monitored, respectively, cf. Figure 12 with 17.

On-stream electrochemical monitoring is costly not in the sense that investment costs would be outrageous. Its expensive part is the time that has to be allotted to maintaining the set-up (e.g. reference electrodes) by skilled personnel. Depending on the corrosion system to be monitored simpler methods may suffice. Figure 18 is illustrating this for SCC. Compared to U-bend specimens which lack of well-defined stresses and must be taken out for inspection, a test rig of this type will allow to apply well defined tensile stresses and an inspection during a routine round en passant. Should an SCC specimen break, the exterior test head will be free and may be moved.

Failure Analysis

The last point shall emphasize the importance of systematic failure analysis, an enormously effective instrument to lower maintenance costs and a strategic instrument to limit risk. Maintenance in a sense that damaged parts are replaced is neither cost effective nor is it part of an anti-risk strategy. Components which failed can tell us a lot about actual operating conditions and stresses, material misidentification or wrong material selection, inadequate design, unforeseen operating conditions and excursions, respectively (Figure 19). In addition to that, failure analysis must also, in quite a few instances, include specific process engineering or physicochemical considerations. Two examples from this area may visualize this.

The first one is typifying the situation that a metallurgical investigation left no doubt about the cause of a component failure which occurred repetitiously, viz. transgranular SCC. The item damaged was a tubular heat exchanger. If one has to reckon with fouling, it is good practice to have the cooling water go through the tubes where cleaning, inspection and NDE for corrosion are much easier than from the shell side. Figure 20 shows the reverse case combined with the specific situation, that a product (Dicykan) had to be cooled down from high temperatures plus the necessity that, for corrosion reasons, the stainless steel mentioned had to be used for heat exchanger ① (20a). In order to avoid SCC from the cooling water side, this exchanger was cooled in a closed loop by inhibited condensate from the shell side②. The condensate, in turn, was cooled by river water from the shell side. The carbon steel tubes of this exchanger corroded from the shell side, leaked, and chloride-containing river water entered the no longer "closed" cooling water circuit for the austenitic product heat exchanger.

The message of this case has to go back to Stage 2 underlining that team work between chemical and corrosion engineering is one of the prerequisites for failure avoidance thus being able to take the specific requirements of these disciplines into account. It certainly

would have brought about, in the first run up, solution *b* of Figure 19. River water is now repassing through the tube bundle; the inner surface of the tubes has been protected by an organic coating and cannot undergo fouling nor can their outer one, now facing condensate.

The second example addresses the phenomenon that austenitic stainless steels may undergo transgranular SCC in a mysterious manner. It exclusively occurs in organic media which are in contact with a water phase stemming e.g. from ship transport. The enigmatic point in the failure analysis was that such water phases (e.g. in cyclohexane) had extremely small chloride concentrations which could never explain SCC. In a working hypothesis we assumed that organic solvents whose solubility for water increases with temperature, could trigger SCC on hot surfaces because the now available absolute quantities of chlorides can build up critical chloride concentrations during the dynamic evaporation process taking place in a liquid/hot metal interface. As a matter of fact, we could demonstrate this mechanism to work in the set-up shown on Figure 20, in which emulsions of organic solvents and water containing traces of chlorides were producing transgranular SCC of a cold formed 347 SS jacket electrically heated to 150 °C.

The message of this analysis clearly is: whenever there is such a situation any organic liquid must be regarded, in the sense of committing SCC, as guilty and may not be declared innocent before it is clear that it does not show such an increase of water solubility with temperature.

Conclusions

In conclusion the question must be asked whether or not low-cost corrosion engineering and risk potential, operational and environmental safety are indeed an irreconcilable antagonism in the CPI - despite all efforts from the side of corrosionists and so many other disciplines involved. The answer is no when looking for instance into the national pressure vessel statistics of the Fed. Rep. Germany. Since about 15 years the annual rate of persons killed by pressure vessel failures has been 2 to 3 the number of vessels in operation being around one million. Still, failures happen in the CPI and some fifty per cent of them are directly or indirectly due to corrosive actions. The CPI is just as little a zero defect technology as are others. But whenever a failure occurs whose reasons cannot be explained, it must be analyzed. Realizing the losses that failures may entail it is not a matter of pure chance that manufacturing companies and chemical companies as well as insurance companies alike are operating specialized laboratories and testing facilities which perform failure analyses. One cannot have such institutions for next to nothing. However, curtailing expertise in this field will sooner or later have a negative impact on operational and environmental safety and economics. After all, the research for the causes of failures is the only way of finding reliable countermeasures, gaining knowledge and providing feed-back to all parties concerned. Last but not least, failure analysis is the backbone of national and international codes, and finally one of the most powerful instruments to achieve what is equally important to corporations, producers and insurers, viz. minimizing the impact of risk and costs.

References

1. V. Cihal, A. Desestret, M. Froment, G. H. Wagner. *Maschinenmarkt* 76 (1970), p. 1047.
2. G. Heinke. 75 Jahre Materialprüfung der BASF (D-6700 Ludwigshafen: BASF AG, 1987), p. 137.
3. G. H. Wagner. *Stainless Steel* 4, 21 (1992), p. 45.
4. H. Spähn. *Environment Induced Cracking of Metals* (Houston, TX: National Association of Corrosion Engineers, 1990), p. 449

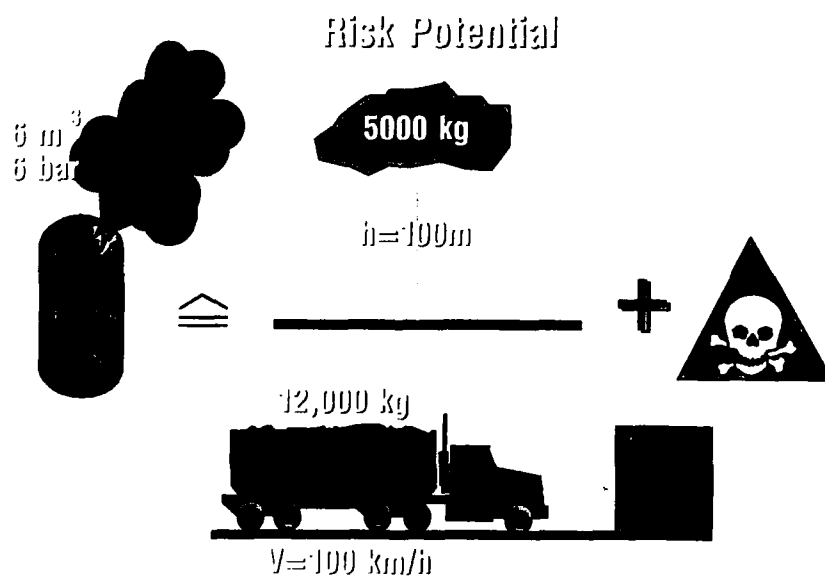


Figure 1. *Risk potential of a simple pressure vessel.*

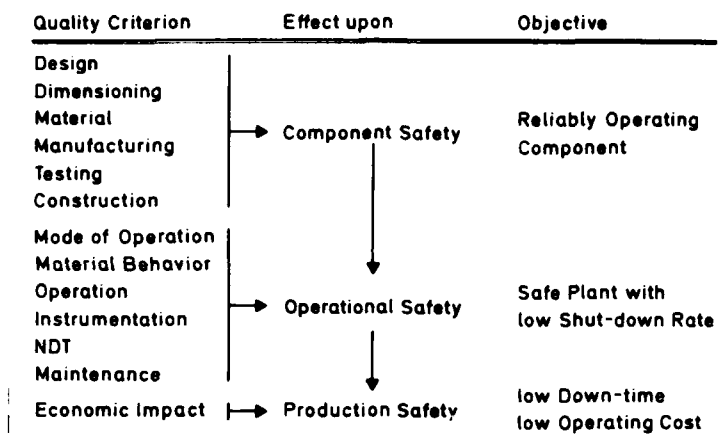


Figure 2. Component, operational and production safety as criteria of plant economics,

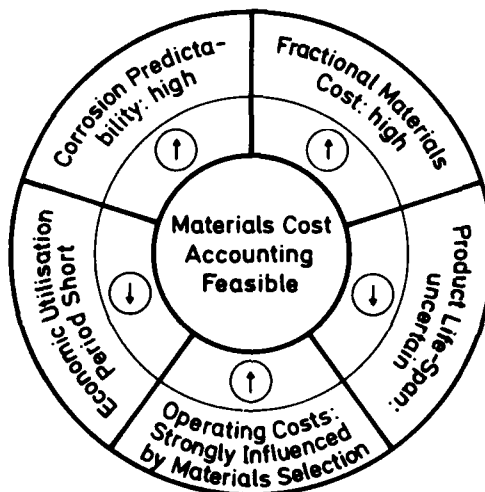


Figure 3. Favorable and unfavorable presuppositions for economic analysis.

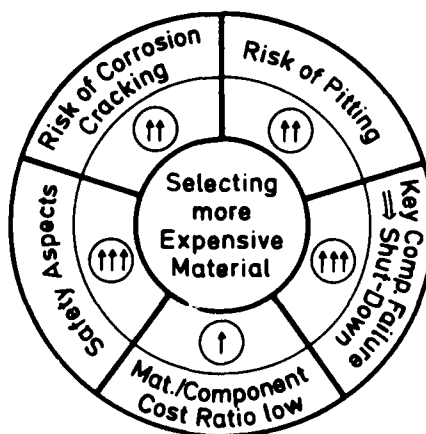


Figure 4. Some reasons for selecting more expensive materials.

Component exploitation, failure risk, and plant availability

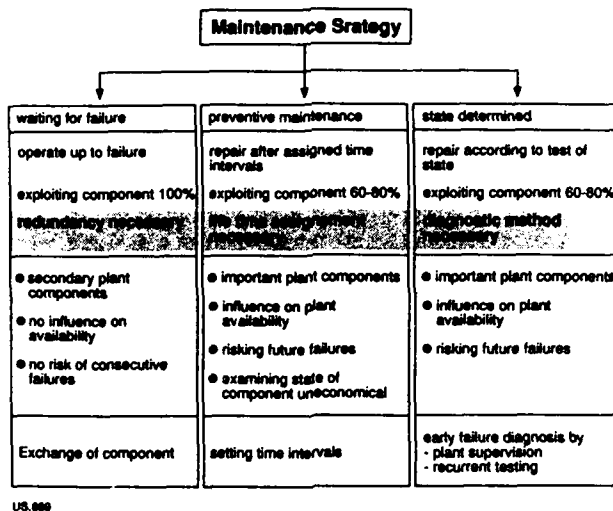


Figure 5. Component exploitation, failure risk, and plant availability.

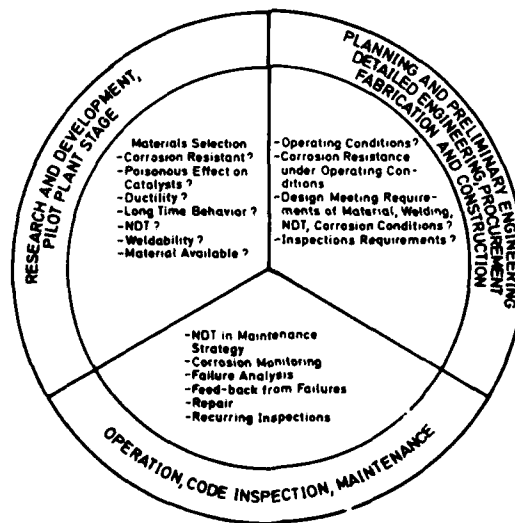
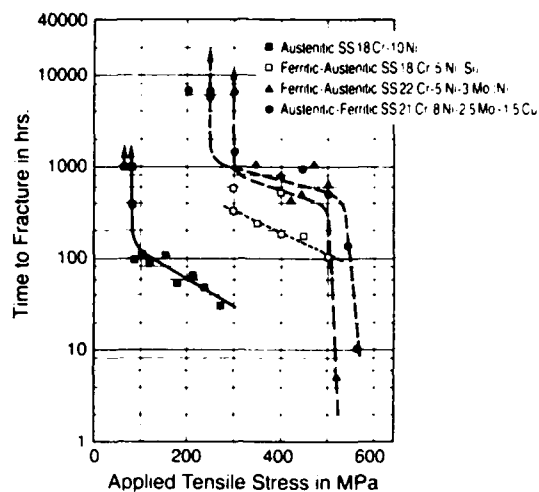


Figure 6. Corrosion and materials engineering requirements in three stages characteristic of the CPI.



US 458

Figure 7. Constant-load SCC tests of long duration (ferritic-austenitic SSs vs. austenitic SS).

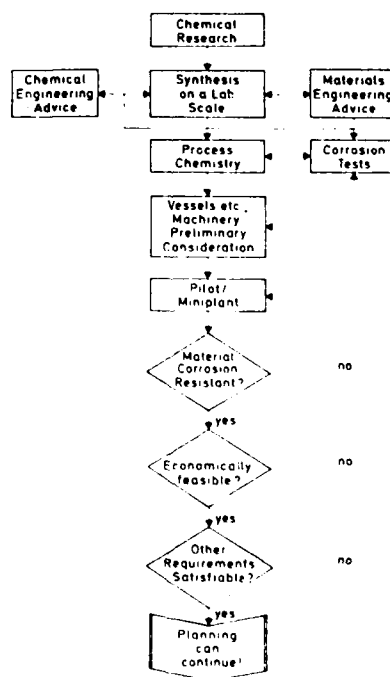


Figure 8. Materials selection in the laboratory/pilot plant stage.

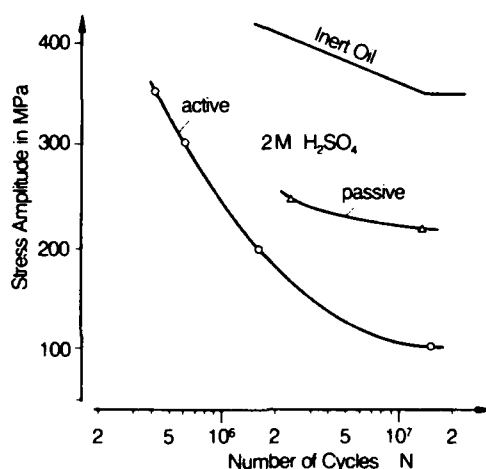


Materials Behavior in Identical Processes
 Behavior of Specimens Exposed in Identical Processes
 Materials Behavior in Similar Processes
 Materials Behavior in Pilot Plants
 Electrochemical/conventional Data from Laboratory Tests
 Non-commercial Reference Publications
 Commercial Reference Publications

NACE-NBS Working Group Corrosion Data Base, Columbia, MD, 24. 6. 1985

Figure 9. Corrosion predictability confidence levels.

**Duplex Steel: CF
 Comparison Active / Passive**



US 434

Figure 10. Corrosion fatigue strength in the active state (Mode I) as compared to the passive state (Mode II) as a function of number of cycles.

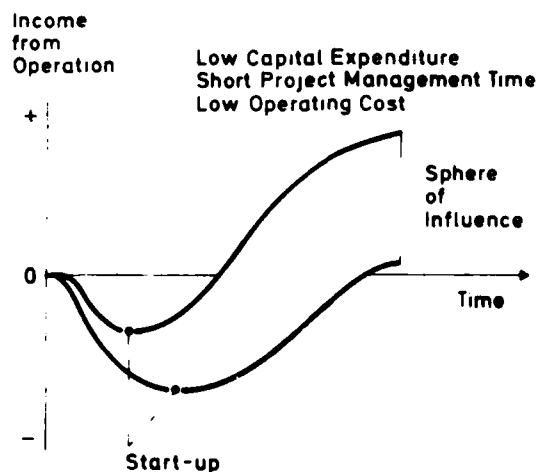


Figure 11. Development of cost and proceeds from project start to production of a new chemical plant.

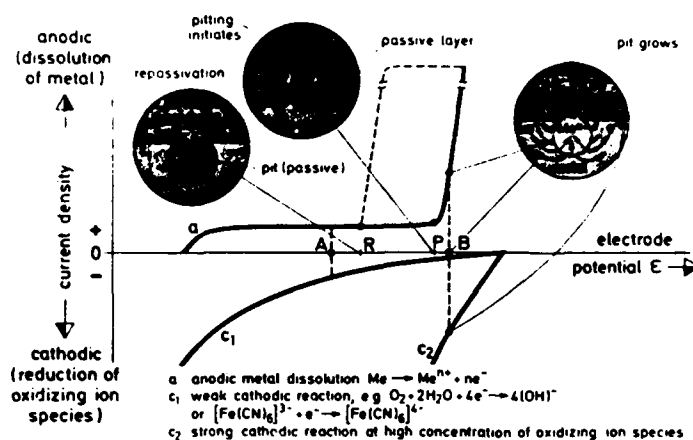


Figure 12. Pitting and its repassivation. Stationary potential: A, repassivation potential for pitting: R, Pit initiation potential: P, pit growth at B, anodic partial current density-potential curve: a, cathodic partial current density-potential curves: c₁ and c₂.

Electrochemical Corrosion Measurement in Plant

Example: installation in a by-pass

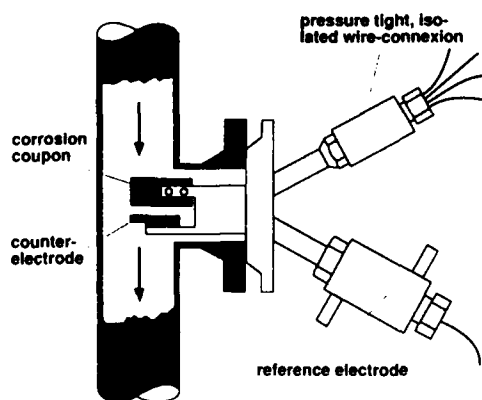


Figure 13. On-stream electrochemical monitoring (continuous measurement of corrosion potentials); polarisation measurements (potentio- or galvanostatically, stepwise etc.).

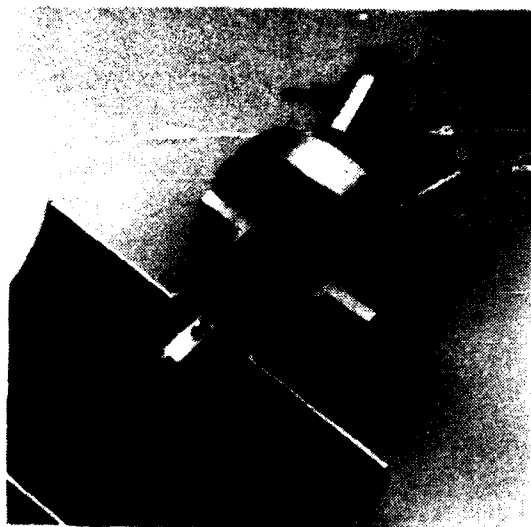


Figure 14. Design of in situ-electrochemical cell.

**Tubular Heat Exchangers:
Areas Endangered by Corrosion**

Endangered Areas:

- ① Stress Corrosion Cracking,
Crevice Corrosion
- ② Corrosion Fatigue
- ③ Erosion Corrosion

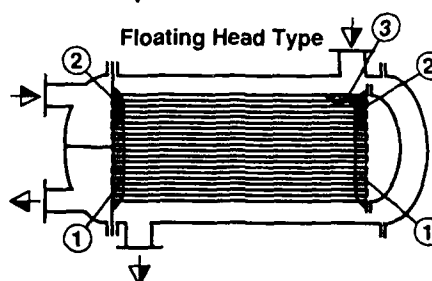
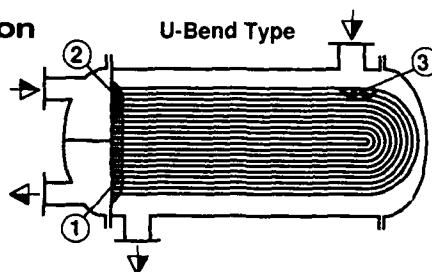
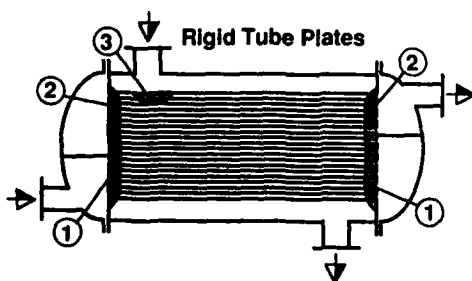


Figure 15. Types and design of the three most common tubular heat exchangers. Areas susceptible to corrosion are indicated.

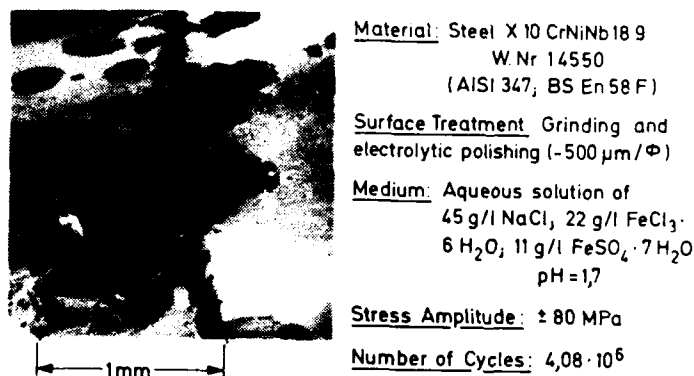


Figure 16. Influence of chloride ions on the corrosion fatigue strength of an austenitic stainless steel.

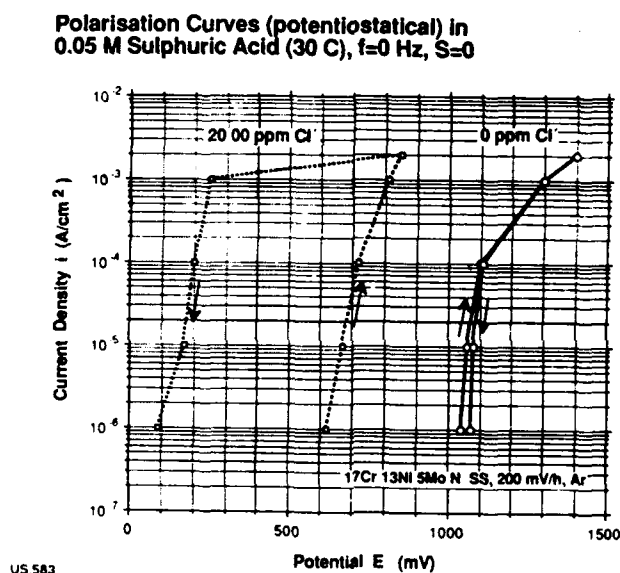


Figure 17. Influence of chloride ions on pitting and repassivation potentials of an austenitic stainless steel.

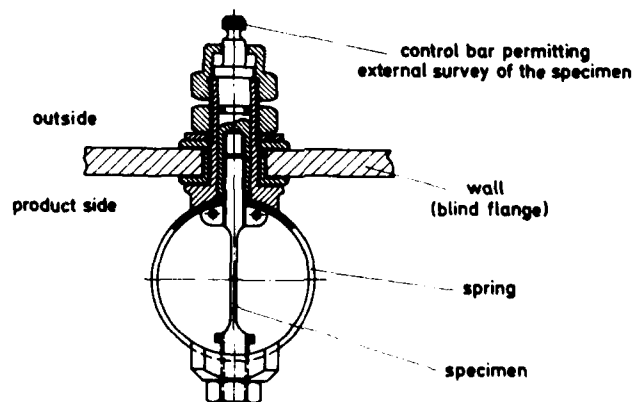


Figure 18. Simple device to control SCC fracture of a specimen under defined tensile stress in a test rig. In contrast to U-specimens fracture can be controlled from outside.

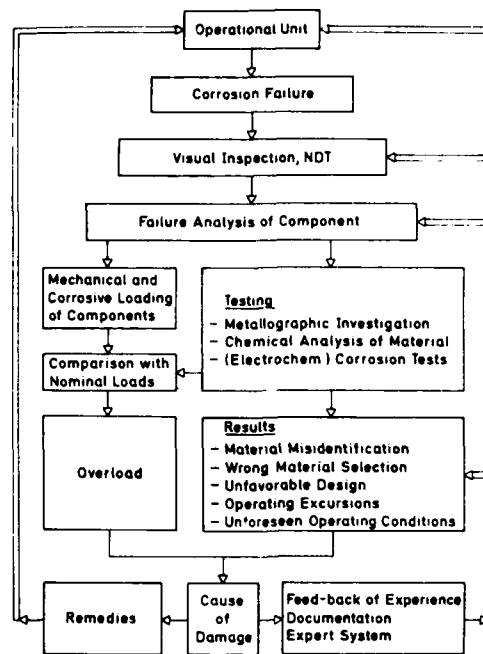


Figure 19. Systematics of corrosion failure analysis.

Avoiding SCC by Changing Flow Direction of River Water

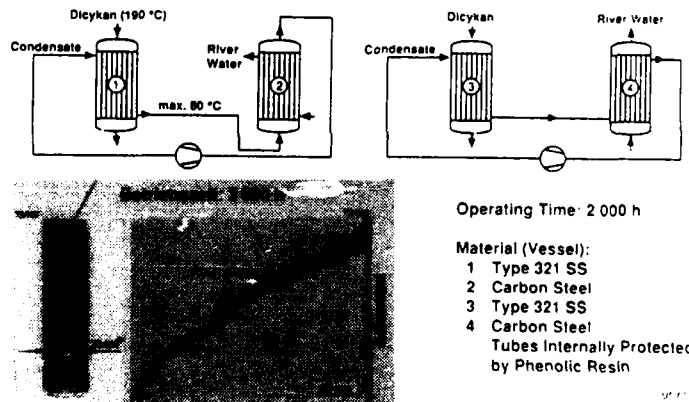


Figure 20. Stress corrosion cracking of heat exchanger tubes caused by river-water leakage in exchanger ② (left); avoidance by a change of grouping heat exchangers (right).

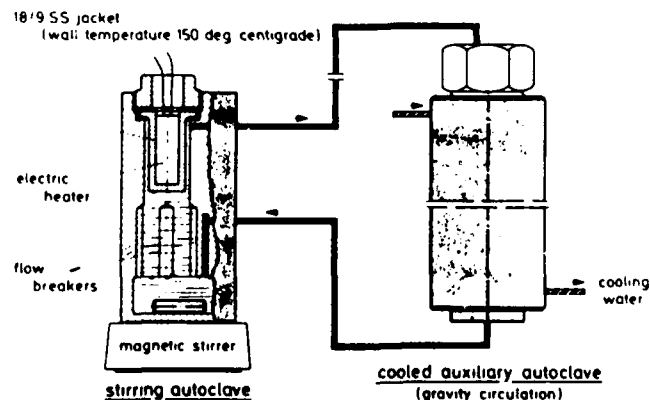


Figure 21. SCC in emulsions of organic solvents containing water with traces of chloride.

Methodology of Predicting Materials Failures in Advanced Nuclear Systems

T. Kondo

**Japan Atomic Energy Research Institute
Tokai-mura, Ibaraki-ken Japan**

Abstract

Experiences in the nuclear power plant operation and the fixing of unexpected component failures, originated mainly from corrosion damages, have led to a base methodology of predicting, correcting and preventing failures. Some analogies of the algorithm developed have been extended to the evolution of reliable materials, their testing and database construction in the development of advanced systems for next generation. An illustrative topic was chosen from the materials development and reliability testing carried out in the development of an advanced HTGR for process heat applications. Possibility and issues in making the similar approach in the case of nuclear fusion is also discussed.

METHODOLOGY OF PREDICTING MATERIALS FAILURES IN ADVANCED NUCLEAR SYSTEMS

Tatsuo Kondo

Japan Atomic Energy Research Institute

1. Introduction

In the last half century the technology of nuclear energy conversion has been developed to accomplish a level of maturity to share a substantial part of the electricity supply in most industrialized nations. In the OECD/NEA member countries, the annual power generation by nuclear systems reached 1.6×10^{12} KWH(23.5%) in 1992, and the annual average growth is estimated to keep about 2% toward the next century.

On the other hand, worries about the safety of nuclear power plants have generated a reluctance to its extensive development and use and some countries are being back to revive more fossil power generation. However, such a trend is supposed to enhance serious dilemma of energy demand and global environment degradation. In longer range, mankind currently has no better alternatives than nuclear energy to cover possible burst of demands as the whole. Although some differences in the degree of urgency may exist among nations, the development of advanced nuclear energy systems with enhanced features of safety, reliability and economics is an indispensable necessity.

The present paper describes about the evolution of the methodology of predicting material degradation and failures in the conventional nuclear power generation and their inheritance to the issues of developing systems for future.

2. Lessons Learned in Operation of LWR (Ref.[1, 2])

The most widely accepted type of nuclear reactor for the current commercial power production is the light water reactor (LWR). The LWR comes in two varieties, the boiling water reactor (BWR) and the pressurized water reactor (PWR). This design features the primary circuit system made of steels with hot ($\sim 300^{\circ}\text{C}$) water and/or steam recirculate through pressure retaining components, ie. Heavy section walled reactor pressure vessel (RPV), piping, steam generators (PWR) or heat exchangers (BWR) and pumps, and the reactor core with fuel elements consisting of sintered ceramic pellets of uranium dioxide contained within tubes (cladding) of the zirconium-based alloy Zircaloy.

The essence of the performance reliability of nuclear reactor in respect of public safety is the prevention of any leakage of radioactive species to the external environment. Insuring the integrity of the structure of multi-barriers - say, fuel

cladding, primary circuit pressure boundary and reactor containment - is one of the main focal points of the reliability/safety efforts. Such efforts have been exercised not only in the reactor systems but also in the spent fuel reprocessing and radioactive waste management.

(1) Nuclear fuel - an area of relative maturity -

The nuclear fuel technology has achieved a relative high level of success in the current normal operation duties. The average occurrence rate of failure is said to be quite low, the order of 10^{-5} rod/reactor year. The technology actually came through some critical steps in the early stage of development. For example internal hydriding of Zircaloy cladding by moisture in the fuel led to a rash of fuel failures in 1970's. The other typical examples well known are; (1) the phenomenon termed as the pellet-cladding interaction(PCI) caused sharp cracking of otherwise ductile material due to the mechanical stress between cladding and swelling fuel pellets. The mechanism has been modeled as a sort of stress corrosion cracking in the exotic high temperature environment inside the tube which contains fission products, such as cesium iodide, decomposed by radiation to an active state. Living inside the cladding with pure zirconium was an effective prevention, and (2) water side corrosion in uniform or localized nodular shaped attacks depending on the type of water chemistry. The theoretical modeling and practical empiricism of improving the art have been established to a fair level, which are favored by the short life cycle of the fuels relative to that of the structural materials. The current interest is to extend the life cycle span or the fuel burn-up for better economy.

(2) Reliability of reactor primary circuit pressure boundaries

The issues of the integrity at the pressure boundaries in the primary circuit system have been given a high priority. The importance is based on the hypothetical scenario on the loss of coolant accident (LOCA). A typical LOCA hypothesis is based on accidental coolant leakage with a rate exceeding the emergency coolant supply. The resultant drying out of the active reactor core can cause a severe damage of fuel elements leading to a possible extensive release of radioactive fission products to external environment. Every LWR commissioned has an emergency coolant supply system with core spray function for fail-safe protection.

(i) The early stage failures

For about a decade after the middle of 1970's, rush of plant outages due to component failures disrupted the credit on reliability of nuclear plant operation, although the known major nuclear incidents such as, Three-Mile Island (1979) and Chernobyl (1986) were not initiated by failure of a component.

The examples of the well known material-originated plant failures are listed in Table 2. All of those happen to be related with corrosion. The failure experiences have indicated some deficiencies in the details of the basic design concept, quality control of materials or fabrication, mismatches between the actual control of operation from the nominal design envelope, eg. Water chemistry, and so forth.

(ii) Corrective actions and countermeasures

Correcting the problem of IGSCC in BWR's by reducing the probability of occurrence through eliminating all the suspected factors has been proved to be very effective. The actions cover the aspects of plant maintenance, material quality and component fabrication, which respectively correspond to water chemistry, materials cracking susceptibility and stress state. Water chemistry controls have been exercised strictly throughout the hot and cold operation stages, and the new technique of the so called hydrogen water chemistry is now being employed to secure marginal protection in some BWR plants. Typical effective counter measures in the hardware aspects are; removal of older or affected welds and replacing them either with the components of SCC resistant modified steels or those with protective cladding. Techniques of heat-sink welding, post weld solution heat treatment and/or an in-situ treatment by induction heating to redistribute residual stresses of the components have been also proved effective. The IGSCC incidents in Japan, for example, have been nearing zero in recent years.

Wide range of research efforts has been invested in combatting the corrosion problems of PWR steam generators including basic mechanism studies up to model boiler tests, and numerous regorous achievements have been made in every phase of work. Corrosion damages of certain types, however, are still persisting in tubes of some plants all over the world. Although difference exists among plants, there have been large variety of damage modes appeared in such a successive way that as one mode is corrected then the other alternatives come to affect. Practically a simple solution has scarcely been derived through anly water chemistry modification without changing hardware design. Complete replacement of faulted units with new ones has been implemented in a significant number of plants. The improved versions are featured with a set of counter-measures, which include the use of the new tubes of corrosion resistant Inconel alloy 690 and stainless steel support plates of improved design in place of the conventional set of Inconel 600 and carbon steel respectively. The replacement has a fate of significant reactor outage and expenses.

Other important corrosion related issues that have been the subjects of intense R&D efforts are the so called crud deposition and the SCC of turbine rotors. The former is the buildup of corrosion product deposits on the heat transfer surfaces in the primary system to cause problems in fuel and steam generator performances

and increase in personnel radiation exposure. Those problems have been corrected to a fair extent by improving water chemistry as the basal procedure, and respectively by replacing Stellite in some specific components with cobalt-free hard surfacing alloys and using improved rotors of mono-block forging in turbines.

(3) Material research for plant safety and life management

As the population of aged plants increases, the focal point of research interest shifts to the direction of predicting the life of components. Among many items, the prediction of the service life of the reactor pressure vessel (RPV) has been recognized with the highest priority. It is based on the views; (1) fracture of RPV causes catastrophic loss of coolant accident (LOCA) leading to a wide range disaster, and (2) RPV is a typical component, of which service life determines the life of total plant. This is due mainly to the difficulty of its refurbishment, which is in contrast to the primary circuit piping. The piping failures by either IGSCC or fatigue generally commence with slow leakage before break (LBB mode) and the defected pipings are readily replaceable.

The time dependent degradation of RPV steel is known in terms mainly of the shift in the ductile-brittle transition temperature (DBTT) occurring with accumulation of neutron exposure dose. The essential life limiting condition of a steel structure can be physically defined with a point where a flaw grows to a limiting (critical) size above which the degraded material cannot resist fracture under a given stress state. The cross point in Fig.1 symbolizes the critical condition in the safe life design aspect of a RPV.

(4) Methodology frameworks established for the prediction and correction

After more than two decades of intensive works, there have been a set of methodology in performing effective approaches to predicting material performances and preventing failures in nuclear service environments. The followings are some stem procedures;

- Analyses on the process and the mode of failures in comparison of laboratory and field experiences
- Identification of key parameters and mechanism modeling
- Application of elementary test methods for mechanism studies and properties examination
- Modification or innovation in materials, component fabrication and plant maintenance
- Formulation of standard test methods and apparatus development, followed

by performance testing and demonstration in controlled environment under either accelerated or closely simulated service conditions

- Developing and maintaining of the database for safe-life design and reliability assessment

During the course of the struggles against those unexpected failures, extensive research efforts were invested in the USA, Europe and Japan over a wide spectrum of R&D areas. Among many significant activities, the roles played by some international cooperative experts' groups must be specially acknowledged.

One very well acted example is a pioneering work by an associated international corrosionists during the early combat. The EPRI Corrosion Advisory Committee(CAC, 1975-1980, leaders; R. W.Staehle and E. Zebroski) acted the issues of the BWR pipe cracking and the PWR steam generator corrosion. The group formulated timely guidelines to attack the environment assisted failure problems in water reactor systems. The basic spectrum of methodology frameworks established there is still alive in the present day research.

The similar but more specified international group was organized after the time of EPRI-CAC. The International Group on Cyclic Crack Growth Rate (ICCGR, 1976-1988) associated with specialists in fracture mechanics, corrosion, water chemistry, etc. volunteered from approx. 50 organizations of 11 countries. This group focussed effort on the rate of fatigue crack growth in RPV steels in high temperature water. Task groups were organized for the mechanism understanding, common test methodology and data acquisition. The most valuable achievement of the activity would be the clear identification of the role of sulfur in steel in accelerating the crack growth. The activity contributed to the successive improvements of the ASME Code Section XI since 1970's by providing dependable guidelines for predicting the life of flaw containing RPV. The knowledge and database yielded are unique in helping the implementation of the concept of damage tolerance design. The tradition is now maintained by the international cooperative group on Environment Assisted Cracking (IGC-EAC).

3. Current Interest in Material Research for Existing Nuclear Systems

In addition to the incentives on high plant capability and availability factors, extending service life of existing plants by refurbishing aged components becomes a growing technology. The difficulty of identifying new sites and costs of building new plants is one of the main driving forces. The extension of average life cycle period is expected to favor not only the economics but also the long-time environmental aspects by minimizing the production of radioactive waste.

(1) Aging studies on component materials

Some studies currently under way are driven by the needs for the methodology of determining the degree of material aging in the residual life evaluation. They are the prerequisites for the plant life extension also and include;

- Neutron irradiation embrittlement
- Thermal embrittlement
- Stress corrosion cracking and intergranular corrosion
- Corrosion fatigue and thermal fatigue cracking
- Deposits due to corrosion, erosion and wear.

In this envelope common interest emphasizes the following specific items;

(a) Irradiation assisted stress corrosion cracking (IASCC): It is a combined effect of corrosion and irradiation on cracking, which affects the life of reactor core internal structure. Evidence indicates that an intergranular type cracking occurs in the austenitic stainless steels without thermal sensitization history when fast neutron dose reaches approximately 5×10^{20} n/cm². Current model assumes possible roles of radiation induced grain boundary segregation /depletion effects induced by neutrons as well as radiolytic effects in the aqueous environment. Practically all the test methodology items developed and applied for IGSCC studies in past are employed with modification to the versions of either post-irradiation or in-situ(pile) testing. A sophistication is required to design and conduct such tests under radiation-shielded remote control. Systematic works by the experts of radiation damage, corrosion and water chemistry are being implemented by an international cooperative group, ICG-IASCC.

(b) Radiation damage mechanism analysis: The phenomenological understanding of the RPV degradation and the regulatory authorized guidelines are already established for the current power generation and the procedures for the surveillance testing in commercial plants has been implemented on a routine basis. A higher level inaccuracy of radiation damage prediction, however, is needed for extended use of RPV. Better understanding of the mechanism concerning the influence of neutron energy spectrum, dose rate, temperature, microstructure, etc. is expected to help interpretation of the surveillance monitoring data. This subject is also being taken care of by an international group on Radiation Damage Mechanism (ICG-RDM)

(2) Material performance issues in the fields of nuclear down-stream

Reliability of the components on the spent fuel reprocessing plant with the current PUREX process is dependent of the performance of metallic structural

materials against aggressive service environment. The working medium, hot nitric acid containing dissolved fuel and fission products, is characterized by complex redox conditions. The trend of the shift of duties from the processing of early metallic fuels to uranium oxide with increasing burn-up levels is drifting the chemical environment to a more critical direction. Such a trend is further pronounced in the stage of processing mixed plutonium-uranium oxide (MOX) fuel from LMFBR's. Research works on prediction and prevention of corrosion damages are under way.

Material issues in the area of radioactive waste storage/disposal are relatively recent additions to the technical areas in the nuclear industry, requiring immediate attention. The current interest is to assess and demonstrate the long-time stability of the waste forms with barrier materials that prevent radionuclides from uncontrolled diffusion to soil. The key factors are the combined effects of a variety of geochemical parameters and radiation. The generation of heat and undesirable chemical species from the waste are to add some complication. Typical object materials currently considered are borosilicate glasses, ceramics and synthetic rocks. Diffusion, advection and sorption of aqueous species transported by ground water through a variety of rock formations has been studied extensively in the past. Regulatory demand for accurate prediction of a minimum of 1000 years may require the most rigorous analyses so that the fatal use of short-time data could convince the public on licensing the system.

4. Advanced Nuclear Systems for Near- and Long Future

There have been variety of design concepts of future nuclear energy conversion systems. Several versions have been developed and promoted in either national or international scale projects based on their potential attractiveness of the mission and technical reality. The followings are those winnowed for near- and long-term future;

- (i) Advanced light water reactors (ABWR and APWR) with improved reliability and/or passive safety for electric power supply in forthcoming decades.
- (ii) Very high temperature versions of gas-cooled reactors (HTGR or VHTR) for non-electric energy supply.
- (iii) Liquid metal fast breeder reactors(LMFBR) for long efficient use of fuel resources through plutonium-based fuel cycle.
- (iv) Thermonuclear fusion reactor for very long-time energy supply with potentials in achieving high level of safety and environmental conservation.

(1) Current status

The order of the above list follows roughly the possible chronology of their

expected commercialization. APWR's have been developed toward the passive safety, as typical in the AP-600 in the US. One type of ABWR is already in the implementing phase. As will be mentioned later, those systems incorporate the feedbacks of experiences strictly so that the former critical issues are eliminated.

Simplified views of the reactor types and the material issues are conveniently summarized in Table 3. Having the neutron damage at elevated temperatures as the major material degradation issues, LMFBR has, however, been believed to have less significant problems in the corrosion aspect. Practically, the long operational experiences up to proto-type reactors have evidenced that the compatibility of steels with liquid sodium is exceptionally high provided by sodium chemistry control(Ref.[1]).

Interesting heritage from the four decades of experiences in the LWR power generation can be found in the development of an advanced HTGR of very high operating temperatures. The approach has followed the methodology steps closely referring to those established in LWR, in which the effects of hot flowing helium containing some traces of chemically reactive impurities has been the source of material performance issues, and the test methodology has employed the simulation of such an environment as one of the reference test conditions.

The fusion power technology is just about to enter its engineering development phase. In order that the fusion is developed to a safe, economical and environmentally acceptable technology, earliest possible brake through of the material issues is among the most critical prerequisites. The performance of the near plasma vacuum wall and the design option for the fuel breeding blanket system with the associated materials issues are current critical spots in the ITER(International Thermonuclear Experimental Reactor) project. A short introductory description on the generic character of the fusion material issues will appear in a later section.

2) ABWR as a direct reflection of operation experience

The world's first two units of ABWR have been licensed in Japan for Tokyo Electric, and are currently under construction. The system was designed originally by General Electric and developed with the cooperation of the Japanese vendors

A typical contrast between the conventional and advanced BWR is illustrated in Fig.2. The piping with recirculating pumps in the primary cooling system is eliminated by use of 10 small internal pumps directly connected to the bottom of RPV. The improved design has removed the traditional fears of piping failure and reduced the burden of inservice inspection on large number of weld joints. Modifications are made in various design aspects so that the insurance levels for the structural integrity and the emergency care are substantially improved.

In addition, the advances in the technology of material manufacturing and

component fabrication, which have already been implemented in the recent versions of the conventional type LWR's, can further substantiate the above changes. For example, the remarkable progress in manufacturing a large heat (approx. 700 tons/batch) of clean steel has increased the potential service life of a modern RPV. Referring to Fig.1 and Fig. 3 jointly and taking the known effects of the residual impurities in steels in the two coordinates, it is suggested that the life prediction scenario for the earlier plants must be amended. The kind of improvement also favors of the integral forging technique to fabricate large pressure components. The total cumulative length of the weld lines even in the conventional type LWR's had already been reduced to about a half of the earlier plants using such a technique. The failure probability of the ABWR is expected to be reduced substantially.

In terms of the component damage prediction, only point which has not been experienced in the conventional system is the direct attachment of the internal pumps to the vessel. Fatigue of the weld-joint at the neck-shaped structure of each pump could be a subject for careful follow-ups. In the current design, an open port is provided for each internal pump for easy access in non-destructive inspection.

5. Materials Research and Performance Predictions in the Development of Future Nuclear Systems

The maturity of the nuclear technology is identified clearly in the generalized methodology of developing materials tailored for the system, testing them for predicting the performance and reliability. The developments made in the field of HTGR in shifting the frontier of service temperature range is one of the typical examples of such a heritage.

(1) High temperature materials technology for advanced HTGR (Ref.[3])

Gas-cooled reactors were first developed in Europe and have been built since 1956. HTGR, equipped with the core of ceramic coated particle fuels embedded in graphite matrix and cooled with helium, has the potential features of achieving high output temperatures with good thermal efficiency and the intrinsic safety for accidental thermal excursions. Despite the successful technical achievements in Germany and the US as the steam-cycle power generating reactor, the system has recently been abandoned from the immediate uses in favor of LWR's. It is believed to be due mainly to some relative minority disadvantages, eg. High capital costs, but not to any technical issue.

(i) Development of process heating reactor and the materials programs

One of the recent studies on the prediction of energy demand in the first quarter of next century indicated that the nuclear energy would have to share about a quarter of the total primary energy supply in the country like Japan where natural

energy resources are limited. Such a fraction corresponds roughly to the current share of the electricity in the total primary energy supply, which means that a portion of nonelectric energy demands must also be covered by nuclear energy in not so long future.

Programs on developing the process heating HTGR have been promoted mainly in Germany and Japan, and the gas coolant outlet temperature of 950°C was demonstrated by the German test reactor AVR (15MWe, 1967-1988). However, the achievement was limited in the coolant within the primary system, while the hardware technology of getting the output of such a temperature level through heat exchangers needed further development in material and structural engineering. Wide range of engineering development programs have been conducted in Germany and Japan during last two decades. Japan has been developing a very high temperature version for the past two decades designed solely to non-electric, the process heating, applications by targeting the secondary system output temperatures at 950 to 1000°C. A 30MW experimental reactor, HTTR (High Temperature Engineering Test Reactor, Fig.4), is under construction for starting operation in 1998. One of the technical features of the HTTR project is to achieve and demonstrate the technology to supply safe and steady nuclear heat at 950°C. The primary helium circuit is designed in a double walled structure, with the inner wall being missioned to resist heat at the high temperature zones, while the outer wall holding the system pressure at a lower temperature, 40 atm / 400°C. The primary system is separated with an intermediate helium-to-helium heat exchanger. The heat is to be utilized for hydrogen fuel production, fossil fuel reforming, direct cycle high efficiency gas turbines and so forth. Basal high temperature technology has been developed and demonstrated by large non-nuclear mockup test systems. For example, the HENDEL loop at JAERI has been operated for years at 1000°C.

Material programs for HTGR have been promoted in several countries since late 1960's which include the tasks of developing and qualifying materials, eg. super alloys for high temperature structures, low alloy steels for RPV, carbon or graphite materials and ceramic coated fuel particles for the reactor core. One challenging task for materials engineers has been to develop and qualify the structural alloys for the intermediate heat exchangers. The initial design target was assigned for the services over 1×10^5 full power reactor hours at 1000°C. The target operating temperature, however, was later modified with a staged strategy, 850 and 950 in the first reactor leaving 1000°C as that for future upgrading. The state of the art of the achievable maximum service temperature for structural metals at the time (1970s) was only 750°C with Incoloy alloy 800, thus shifting the practicable temperature by about 200°C was a technical goal.

(ii) Identifying of key issues and degradation models

Long-term performances of materials have been assumed to be influenced by

the helium-based environment by the consideration of the following factors;

The chemical character of the helium-based hot coolant is defined by the impurity gases which are generated mainly from the interaction of graphite core and moisture. Persisted existence of H_2O , H_2 , CO_2 , CO and CH_4 at the level of 10^{-6} atm has been known from reactor operation experience. The composite effects of this very low but appreciable amount of impurities are rather exotic for some common heat resisting alloys containing Cr as the main oxidation resistant ingredient. Possible degradation processes are stemmed from a difficulty for those alloys in forming protective oxide film in the low oxidizing potential environment. Poorly blocked access of the reactants to the substrate metal would lead to their dissolution and cause metallurgical changes, eg. Internal oxidation, alloy element depletion, carburization or decarburization depending on temperature, alloy composition and environment. There have been structural design concerns on their influence to the life-time mechanical performances creep, fatigue, their interactions and eventual fracture.

(iii) Developing alloys tailored for use in helium-based environments

Basic studies on the oxidation kinetics and microstructural phenomena at the metal-oxide interfaces indicated some unique influence of the HTGR environment. As expected from the low oxidizing potential condition, approx $10^{-23} \sim 10^{-18}$ in effective oxygen pressure, the common elements such as Cr, Mn, Al and Si in alloys are oxidized, while nobler elements such as Mo, W, Fe, Ni and Co are rejected from oxidation. As the consequence, the results of long exposure at elevated temperatures are generally different from those observed in air. The followings are common features of some commercial alloys exposed to the simulated HTGR environment; Chromium and Manganese are incorporated in surface oxide film.. Silicone tends to form oxide particles at metal /oxide film interface, and Aluminum is internally oxidized at grain boundaries unless the content is adequate to form continuous surface film. Such basic observation provided an incentive of improving materials of better compatibility with the specific environment. Combining and compromising the known effects of those elements on the other key properties, eg. Creep resistance, weldability and hot formability, modifying existing common alloys was attempted for the development of candidate materials of near-term application. Based on the LWR experience the mechanism of radioactive dust formation due to incorporation of unoxidized Co was studied, and the results were reflected in alloy modification.

In the HTTR construction - Hastelloy XR, a modified version of the common alloy Hastelloy X, is employed after about 15 years of engineering development. This alloy was formulated by vacuum double melting with optimized contents of

Mn, Si and B as intentional additives, while minimizing Al, Ti and Co as undesirable impurities. There had been a few important findings before and during the development. The coexistence of Cr and Mn in an appropriate range helped forming Cr_2MnO_4 spinel layer outside the Cr_2O_3 film, which was turned out to be quite stable and protective in the helium-based low oxidizing environment even under severe thermal cycling. Fig. 4 illustrates the results of long-time corrosion tests under thermal cycles on the original and improved versions of Hastelloy X. Additional important finding in this line was that the maintaining of a range (30-50ppm) of boron content brought a remarkable improvement in the high temperature strength of base metal and, in particular, the performance of weld joints. An interesting feature of this alloy is that the protective double layer oxide films contribute not only to the corrosion performance but also to the long-time mechanical performances by protecting the depletion of Cr and B from the material. Incorporation of Co in spilled oxide is reduced by several order of magnitude. The factor of improvements in the creep life is estimated to be roughly 5 at 950°C.

Another interesting reflection of the corrosion studies has been shed on the design and development of new alloys tailored for the system. Unlike in air, the addition of Cr for corrosion protection more than several percents does not give any benefit, or even decrease the apparent protective function in the low oxidizing environment. This finding has created a wide range of freedom for the design of alloys because the optimum Cr content in an alloy can be determined by factors other than corrosion protection. In the Japanese nuclear steel making project(1973-1981), a competition in clearing a creep strength requirement at 1000 °C was won by a few Ni-base superalloys designed by the phase computation approach. Following this success, a program of developing the second generation materials for a 1000°C intermediate heat exchanger was initiated at JAERI. Series of testing and analyses have been conducted since 1982 in the optimization of the strength, tube formability, weldability and the corrosion resistance to the helium environment. In the process the Ni based Cr-W ternary alloy system was explored for a best Cr/W ratio in the corrosion resistance along the phase boundary of gamma vs. gamma + alpha-2 at 1000°C, which was the equi-creep-strength line. Repeated cycles of turn-around experiments and analyses have yielded an optimized Ni-18~19Cr - 20~22W(wt.%) based alloy, which contains trace of Yt and B for corrosion resistance and creep strength respectively. The material shows the 1×10^5 h creep-rupture strength at 1000°C exceeding 9.8 MPa in the helium environment, which is believed to be the current highest in the materials plastically formable to seamless tubes. As illustrated in Fig.5, the feature of this new tailored alloy is represented by the balance in the key properties required for structural applications.

(iv) Testing materials in simulated HTGR environment

Testing materials in recirculating helium, doped with the common impurities in reactor coolant was conceived by R.A.U. Huddle of Dragon Project, and the first test was implemented by P. Kofstad in Norway for the project. Later extensive test programs for developing and testing materials for process-heating HTGR have been conducted in Germany and Japan. In the Japanese HTTR Project, a system with functions of continuous cryogenic purification and controlled impurity injection has been operated since 1976 to the present. To this system a various test apparatus are connected for conducting experiments in the simulated HTGR coolant environment. The total engineering test system is organized essentially by an adoption of the methodological principles developed for testing LWR materials in water mainly, and some for LMFBR materials in sodium at elevated temperatures, in which the monitoring and control of the chemistry of test environment play a key role. Beside the tests for alloy development, extensive test matrices on corrosion, creep, fatigue and their interactions have been digested on several heats of prime candidate alloys for over two decades. The results have been accumulated and formulated as an engineering database required for use in structural design and safety reviewing. For the post exposure analyses variety of techniques have also been developed for quantifying the time-dependent progress of the material degradation in the helium-based environment.

The materials performance database for HTGR is now established and utilized. For the Japanese HTTR project, the comprehensive performance data base including creep performance has been prepared for Hastelloy XR. The data contained are to the total cumulative test duration of 5×10^5 h with maximum single test length of about 5×10^4 h per specimen at the temperature ranged 800 to 1000°C, which include also the similar order of corrosion test data. The German PNP program has invested the similar efforts on a few candidate structural materials. In this case two commercial alloys, Inconel alloy 617 and Incoloy 800H, have been tested to form a set of design database with maximum test duration of approx. 7×10^4 h and 1×10^5 h respectively for the creep in the simulated service environment. The combined use of such databases with the mechanical behavior information from the high temperature component tests has contributed in sophisticating the structural design code. Those cover the temperature range beyond the conventional ASME Code Case N-47 where most metallic materials behave non-elastically under strong influence of chemical and /or radiation environments.

The kind of technology bases developed for HTGR are believed to have a potential generic importance in applications to high temperature structures in various advanced energy systems that require a high level of reliability. The design of most advanced energy systems are moving toward higher temperatures, which would automatically employ inert-gas-based media for thermal energy transport.

One of the typical application areas can be found in the nuclear fusion technology.

(2) Materials issue, a critical path for the nuclear fusion power development (Ref.[4])

Nuclear fusion research is the field where extensive international cooperation has been made over years. The materials research for fusion has about 15 years of such a history. Starting with the fundamental studies on the generic issues in radiation damage of structural metals, the spectrum of activity has now expanded to several reactor components and different phenomena. A schematic is shown in Fig. 5, where the materials for the five key components are indicated with a tokamak type experimental reactor. To now number of challenging issues have been identified in each material/component system, and most of those are more or less related with predicting and/or preventing the degradation phenomena that are caused by neutron irradiation. A convenient summary prepared by the IEA international panel is shown in Table 3.

i) Fusion-specific issues and the methodology required

The basic methodology of examining materials behavior in most of the necessary test items in fusion reactor development is essentially common with those grown in either field of LWR, LMFBF or HTGR. The issues in fusion technology, however, are unique in the level of requirement, which are far beyond those achieved in fission. In the present "pre-engineering" stage, there are extensive challenging research works in all over the five material/component disciplines. For example, more than 1000 technical papers have been published in one series of international conferences(ICFRM-1 through -5, Ref.[4]) in last decade. The following are just a few introductory remarks from the authors view point on the matters of near-plasma components.

ii) Neutron effects

The basic technical difficulty and speciality of the materials research in fusion are stemmed from the specific energy spectrum (14.1 MeV) of the neutrons generated by the deuterium-tritium (DT) fusion reaction. The energy level is one order higher than those of fission neutrons. Major differences in the effects relative to fission cases are; higher rate of production of impurity(eg. helium , hydrogen and other solid elements) in materials by nuclear transmutation reaction and the simultaneous formation of cascade structures of more extensive and complex atomic displacements. All the experimental works achieved to date have managed some simulation test methodology using fission reactor neutrons, light- and heavy ions and neutrons from accelerator facilities and electrons. Techniques of testing materials, to be applied under the variety of radiations in the analyses of in-situ or post-exposure modes, have been developed and implemented. Regarding some

nonlinear characters of the flux/fluence dependence of those effects, however, behavior predictions made only through those approximate means are persisting concern, because the risk of deviation must increase with accumulation of neutron fluence.

Unfortunately there is no direct testing means yet for examining such phenomena with adequate flux and fluence of 14 MeV neutrons. This leads to the situation that the materials development to the stages beyond experimental reactors has not been brought to any realistic action yet. The fact is fatal in plasma devices, in their nature and indeed, it is in a sharp contrast to the fission where the use of the test reactor core readily provide a bed for accelerated tests under reasonably simulated neutron spectrum conditions. Only solution conceivable, and actually being explored intensively, is to provide a facility designed specifically for materials testing. Typical is the one equipped with an intense neutron source of the energy spectrum similar to fusion neutrons. Activities such as the FMIT project (1978 -1985) in the US, the conceptual design work in the ESNIT program (1988 -) in Japan and several other efforts have stimulated the current active international collaboration. The trend in the IEA collaboration is to construct an IFMIF (International Fusion Materials Irradiation Facility). This utilizes intense high energy neutrons generated from the deuterium-lithium stripping reaction make with a high current linear deuterium accelerator (Ref.[5]).

In the corrosion aspect, there are some challenging areas in terms of the synergy effects with radiation far more intense than experienced in LWR. The concern of irradiation assisted stress corrosion cracking (IASCC) with a near-term candidate structural material, type 316 stainless steel in the water-cooled version of the ITER design, has been considered as one of the most urgent material/design issues to be resolved.

iii) Plasma-material interactions

Another type of materials problem of rather immediate concern is on the function and endurance of the plasma-facing materials situated inside the vacuum wall. The typical issues involved are such that the mechanical and chemical integrity of the refractory armour materials, eg. Graphite, exposed to the mixed conditions of very high thermal gradient, strong thermal spiking and shocks in the event of plasma disruption and erosion or sputtering due to bombardment with energetic ions or neutral particles emitted from the vacuum-plasma. The matters have been and will be of continued concern among fusion reactor designers in every stage of development.

In the corrosion-relevant aspect, sputtering for example, is of particular interest. Possible resultant contamination of vacuum can cause undesirable quenching of plasma, hence interrupting ignition or stable reactor operation. In particular, chemical sputtering due to residual impurity gases in vacuum dominates

the loss of material from the plasma facing parts in the first wall armours and diverters. In contrast to the problems in high fluence neutron irradiation research, however, realistic experiments have always been possible in this area by using plasma experimental devices at each stage of development.

(iv) Material/blanket option

Option of the type of fuel breeding blanket system influences the structure of a fusion reactor rather drastically. ITER at the current engineering design phase is in the stage of selecting a best set of blanket-coolant -structural material combination out of a few candidate systems. Major criteria of the option are the reliability -safety aspects regarding structural integrity assurance and hazard potentials. Austenitic stainless steel structure cooled with water for breeding blanket of solid lithium compound (ceramics) has been considered as the most realistic choice based on the relative abundance of experience and material database. The major critical drawbacks considered are possible loss of function in the pressure containment structure due to corrosion or neutron induced IASCC, and less attractive thermal properties of the material.

On the other hand, there are two other sets of alternatives with new features but less back ups of database. Each concept has some charm points as well as intrinsic disadvantages. One is the reduced radio-activation versions of ferritic martensitic steels, eg., Fe-8Cr-2W-Ta, V developed for fusion, used with solid breeder cooled with helium or water. The other option is some Vanadium-based alloys used with liquid lithium as a self cooling breeding blanket. The present option for the experimental reactor may not necessarily mean that the system in the future demo-reactor or commercial reactor stage will follow it. The option, however, is highly critical since the establishment of a technology base for one material-environment system require extensive investments of technical and financial efforts and long lead time in practice.

6. Summary

The basic framework of developing and testing materials for reliability assurance on a nuclear energy conversion system have been established through the operation experience of power reactors during last 3 decades.

The methodology established during the course has been applied, either explicitly or implicitly, to the activities in the development of next generation systems. The topics of the high temperature materials development made in last two decades for the programs of direct use of nuclear heat is chosen to examine and demonstrate how the heritage was utilized. Expectation of a further application of the similar methodology to the next step, nuclear fusion development, is described together with its limitation regarding the unique and high levels of the requirements in the nuclear fusion technology. The discussion leads to the necessity of adding an

innovative approach, which is to design and construct an intense neutron test facility for solving complex synergy effects of chemical and radiation environments. These phenomena are believed to form main blind spots in predicting performance and life of materials used in the critical components of fusion reactors.

References

[1] Materials for power reactors in general

J. T. A. Roberts

Structural Materials in Nuclear Power Systems (1981), Plenum Press.

[2] Light water reactor materials

Proc. International Symposium on Degradation of in Nuclear Power Systems
- Water Reactors -, 1st. (1983) through 5th.(1991) issues, NACE

[3] High temperature gas-cooled reactor materials

Nuclear Tech. **66**, (1),(2) and (3) (1984)

[4] Fusion reactor materials

Proc. International Conference on Fusion Reactor Materials (ICFRM)
1st. (1984) through 5th. (1992), J. Nuclear Materials, 133/134(1985),
141/143(1986), 155/157(1988), 179/181(1991), 191/194(1992)

[5] Neutron test facility for fusion material development

T. Kondo, D. G. Doran, K. Ehrlich and F. W. Wiffen
J. Nucl. Mater., **191-194**(1992) 100

Table 1
Typical Examples of Component Failures Originated from Material Damage in Early LWR

DAMAGE MODE	DAMAGE CHARACTER	KEY FACTORS	IMPACTS
Cracking of weld overlay lining in RPV (BWR, mid. 1960's -70's)	Cracking of stainless steel lining, extending to low alloy steel substrate	-SCC susceptibility of improperly welded overlay -Acceleration of fatigue crack growth in hot water with adverse role of sulfur in steel -Thermal vibration with mixing of feed water leading to fatigue	- ASME Code XI amendment -Improved fabrication and design -Enhanced EAC crack growth rate studies
Cracking of stainless steel welds in pipings (BWR, 1970's - early 1980's)	Intergranular cracking at heat affected zones of austenitic stainless steel weldments	-Synergy of ; Intergranular attack, material sensitization and residual tensile stresses due to welding -Oxygen potential due to water radiolysis	-Triple countermeasures: -Water chemistry control -Resistant materials -Stress management -Beginning of EAC studies
Corrosion and mechanical damages of tubes and support plates in steam generators (PWR, 1970's -)	Wall thinning, intergranular corrosion or cracking and denting of Inconel tubes with carbon steel support plates attacked at crevice Fatigue cracking of tubes	-Difficulty in local water chemistry monitoring and control ; Phosphate imbalance and/ or Crevice chemistry deviation leading to Inconel cracking and non-protective corrosion of carbon steel -Hydrodynamic vibration leading to high cycle fatigue	-Successive correction by water chemistry modification to all volatile treatment(AVT), etc.(success limited) -Replacement of steam generators with new versions of improved design

Table 2
Features of Service Environments and Major Material Issues in Current and Future Nuclear Energy Conversion Systems

SYSTEM	SERVICE ENVIRONMENT		KEY ENVIRONMENT FACTORS	DEGRADATION PHENOMENA
	Thermochemical	Radiation		
Water-Cooled Reactor (LWR)	Water ~ 300°C	Mixed thermal and fast neutrons ~10 ²⁰ , n/cm ²	-Electrochemical effects of dissolved electrolytes -Corrosion potentials with radiolytic oxygen	-Stress corrosion cracking -Irrad.- assisted s.c.c. -Corrosion fatigue (RPV) -Irrad. embrittlement (RPV)
Sodium-Cooled Reactor (LMFBR)	Liquid Sodium ~600°C	Fast neutrons ~10 ²³ , n/cm ²	-Carbon transfer -Atomic displacement damage by neutrons	-Creep/fatigue in carburising or decarburizing. environ. -Irrad.- induced creep -Dimensional change by void swelling
Helium-Cooled Reactor (HTGR / VHTGR)	Helium gas ~ 1000°C	Mixed thermal and fast neutrons ~10 ²² , n/cm ² (core materials only)	-Element-selective oxidation -Mass transfer of carbon and boron (Interm. heat exchangers)	-Non-protective oxide film / internal oxidation -Environmentally affected creep and fatigue -Thermal embrittlement
Thermo-Nuclear Fusion Reactor (DT-Tokamak)	Water, liquid lithium or helium gas (under strategic option)	High energy neutrons(14 MeV) ~10 ²³ , n/cm ²	-Synergy of atomic displacement and nuclear transmutation -Synergy of corrosion and irradiation	-Enhanced radiation effects; Ductility loss Irradiation creep, Irradiation assisted s.c.c. Dimensional changes

Table 3

Requirements on Material Research and Database for Nuclear Fusion Power Development
(After "Materials for Fusion", IEA, 1986)

MATERIALS APPLICATION	CRITICAL ISSUES	RANGE OF CONDITIONS
First Wall (a) - Plasma-Interactive / High Heat Flux Components	<ul style="list-style-type: none"> - Rate of erosion and redeposition - Thermal conductivity change - Fatigue - Tritium permeation rate 	Neutron : 14 MeV, up to 100 dpa* Plasma particle: 0.01 to 1 KeV, up to 10^{30} m^{-2} Heat flux: up to 5 MW/m ²
First Wall (b) - Blanket Structural	<ul style="list-style-type: none"> - Mechanical, microstructural and demensional changes - Tritium permeation rate - Compatibility with breeder materials 	Neutron : 14 MeV, up to 200 dpa* Temperature: up to 700°C
Fuel (Tritium) Breeding	<ul style="list-style-type: none"> - Tritium release behavior - Structural integrity - Compatibility with structural materials and coolants - Development and evaluation of neutron multipliers 	Neutron : 14 MeV Burn-up ratio: up to 15% Temperature: 400 - 900°C
Superconducting Magnet	<ul style="list-style-type: none"> - Critical temperature, field and current - fabrication and mechanical stability - Stability of coils 	Radiation doses relatively small Not a critical issue
Special Purpose - Ceramic Insulators - Plasma-Diagnostic Materials	<ul style="list-style-type: none"> - Mechanical and demensional changes - Electrical conductivity and dielectric property changes - Optical property changes 	Neutron; up to 100 dpa*

* note: dpa (displacement per. atom) a unit expressing the extent of atomic displacement damage

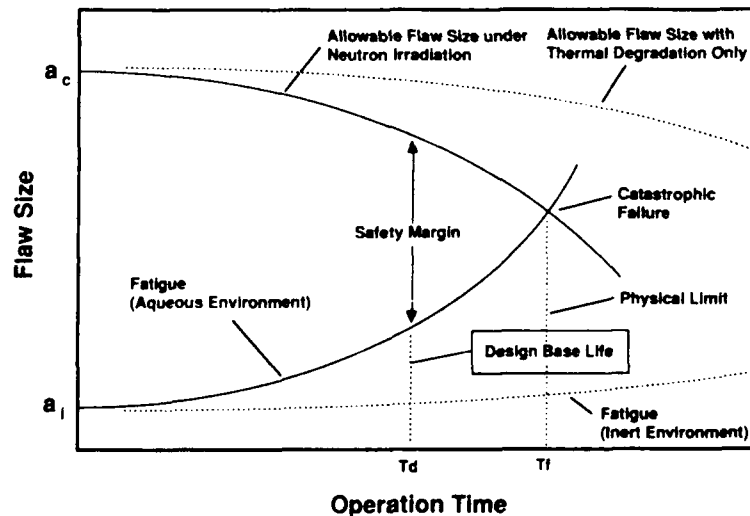


Fig. 1 A definition of service life of a light water reactor pressure vessel

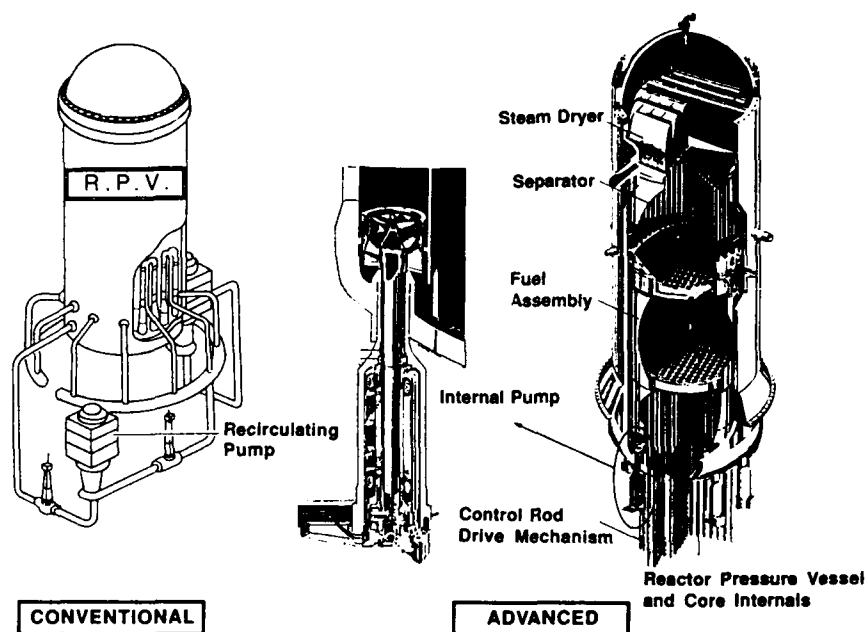


Fig. 2 Typical design features of an advanced boiling water reactor ,ABWR
(after TEPCO document, 1991)

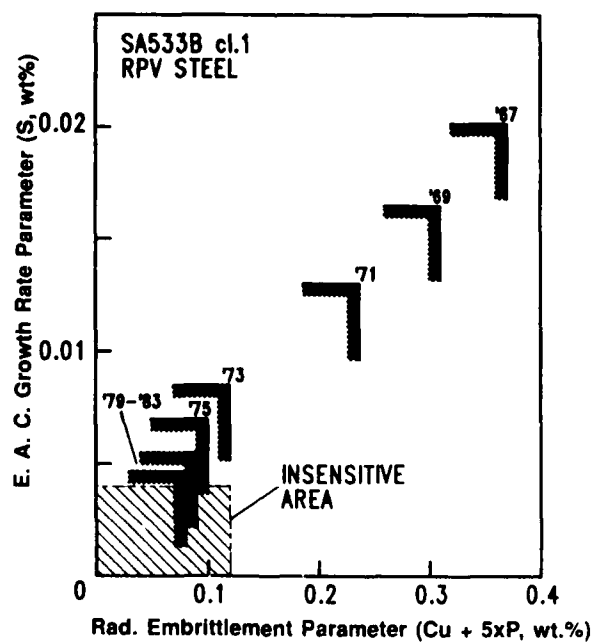


Fig. 3 Progress of Technology of manufacturing nuclear-grade steel for reactor pressure vessel(after JSW data)

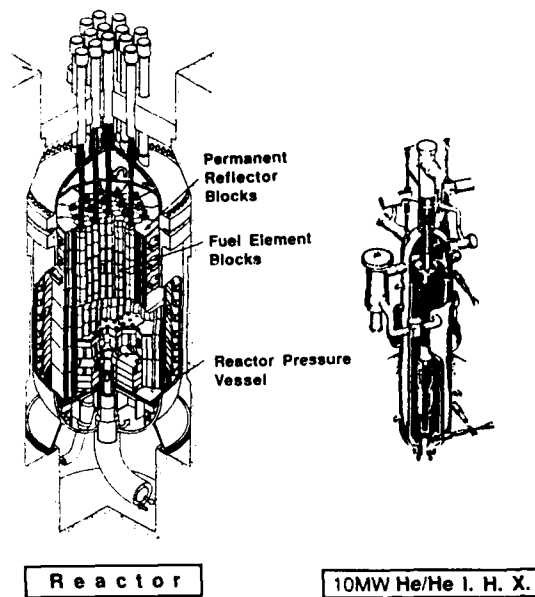


Fig. 4 Major primary system components of HTTR(30MWt)

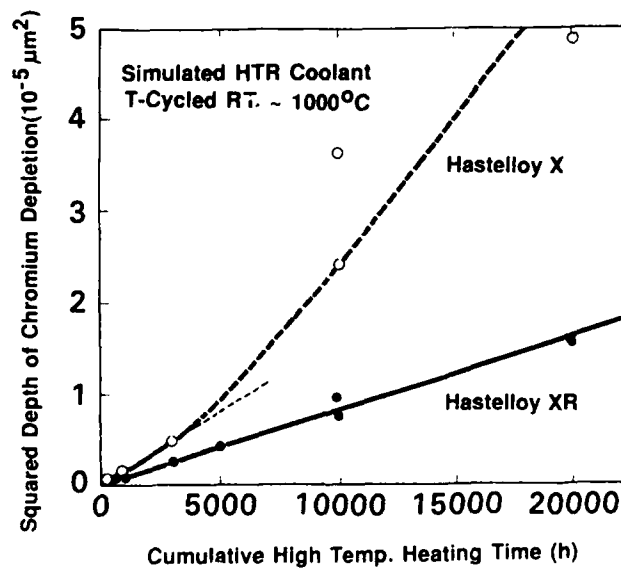


Fig. 5 Long-term exposure test results of nickel-based superalloys

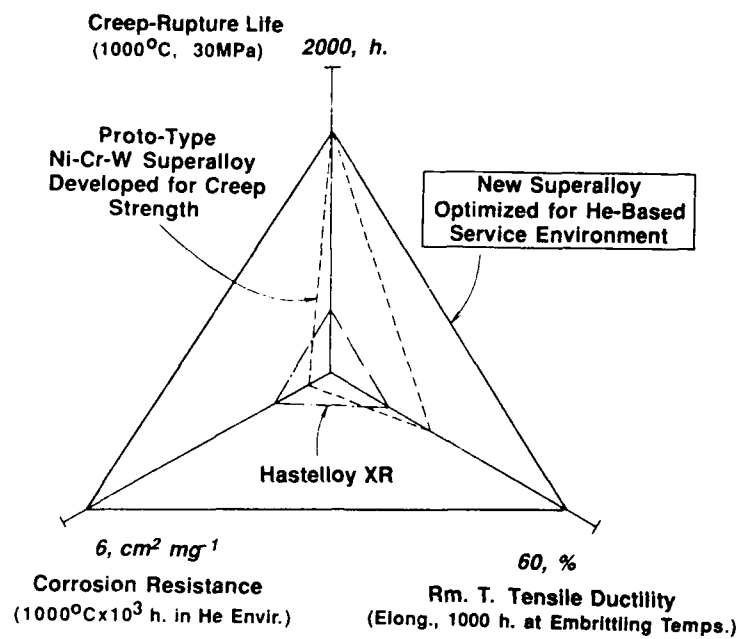


Fig. 6 Progress of alloy development for process-heating HTGR

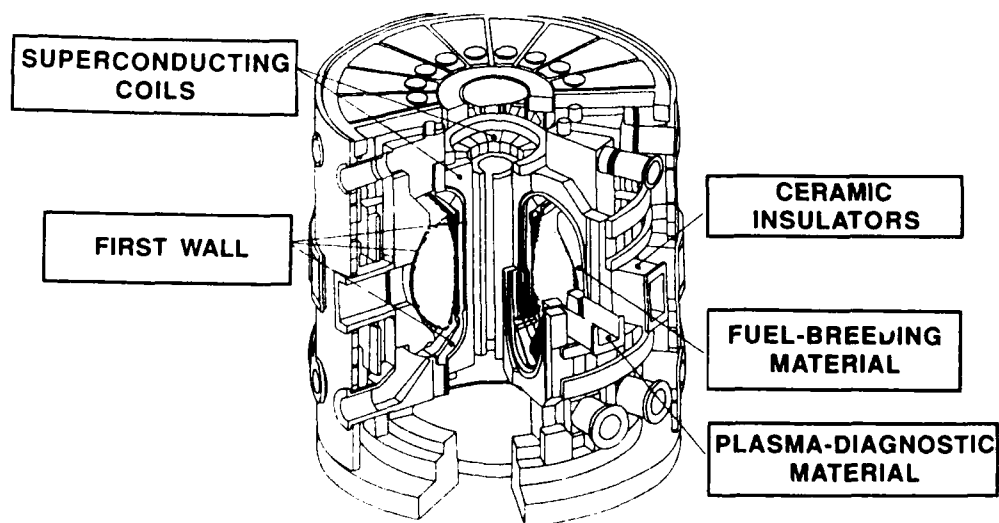


Fig. 7 Key component materials in an experimental fusion reactor

Corrosion Control by Transferring Knowledge.

R.N.Parkins
University of Newcastle upon Tyne
Newcastle upon Tyne NE1 7RU
England

Abstract

The transfer of knowledge implies an educational process and that is what is needed to ensure effective control of much of the waste associated with corrosion. Corrosion societies and associations have an important role to play in this respect and there is room for the development of cooperative programmes between societies in some of these areas, reflecting the international arenas in which many large industrial companies operate. It is probable that many instances of the unnecessary destruction of materials by corrosion results from inadequate engineering design and there is a pressing need to improve matters in that respect. That is not to imply that corrosion specialists have not had a positive impact on corrosion prevention, since there are many examples of successful technology transfer. Perhaps the image of the corrosion prevention community would be improved by dwelling on those successes, and their important contributions to pollution reduction, rather than too often stating how much corrosion costs everyone, with the negativity that such an approach implies.

Key terms: technology transfer, education, research, corrosion costs, pollution.

Technology Transfer

The transfer of science and technology to the fields of corrosion control and prevention has been, and remains, of an order of which the associated industries may be justly proud. Thus, the principles of cathodic protection were first indicated in a paper⁽¹⁾ by Sir Humphrey Davy in 1824, in which he described how zinc anodes could be used to prevent the corrosion of the copper cladding that was applied to the wooden hulls of ships of the British Navy. While the prevention of corrosion of the copper was achieved, it led to fouling of the latter, and the extensive use of cathodic protection did not occur until it was applied to buried pipelines in the U.S.A. after the turn of the century. Its effectiveness in markedly reducing the perforation of pipelines by pitting corrosion has been such that it is now very rare for buried metallic structures not to be subjected to cathodic protection. In similar vein, the development of stainless steels, simultaneously in France, Germany and the U.K. in the early 1900's, has had profound effects in relation to corrosion control in the process industries, a trend that has continued with the relatively recent development of the duplex stainless steels. Organic coatings have been used for the protection of iron for some 2000 years, but understanding of the reasons for their effectiveness has only been achieved in the last half century and

that has led to the development of modern paint systems with life times markedly greater than those employed hitherto. Many other examples could be mentioned of successful events in corrosion control, but perhaps one further example will suffice, if only because it is within the experience of many people. This relates to the marked improvement of the life times of automobile exhaust systems (or mufflers) within about the last decade. Typically, life times have about doubled for most of the more popular mass-produced vehicles, by the simple approach of aluminising the steel and at little increased cost to the system.

Of course, some will argue that the examples quoted, and many others not mentioned, do not invariably result in benefits in relation to corrosion prevention. Thus, cathodic protection, although almost invariably applied to buried pipelines, does not always prevent the latter corroding, nor does stainless steel always display good corrosion resistance. But where a cathodically protected pipeline corrodes, that is most likely to be because the potential was not lowered to a value where the steel was thermodynamically stable, or immune from corrosion, a situation most probably the result of an incorrect potential measurement. That indicates a need for improved methods of potential measurement on buried structures, and their application, since such does not invariably occur, but in relation to the corrosion of stainless steels the solution to the problem is different. It is well established that for stainless steels to display good corrosion resistance requires environmental conditions which allow the maintenance of the chromium oxide film that induces such resistance. Where the environmental conditions have not met that requirement, and corrosion has ensued, does not require more research, but better education of those who made the decisions that led to that result. Indeed, it is probably the case that education, in the broadest sense of that word, is what is needed to ensure effective control of much of the waste currently associated with corrosion, a conclusion that is in agreement with many of the recommendations of the U.K. Committee on Corrosion and Protection (The Hoar Committee) reporting in 1971⁽²⁾.

The Education Problem

Possibly the greatest danger in attempting to create corrosion awareness is that the wrong people are addressed. The vice-presidents or directors of companies invariably will be interested in saving money, if that is a consequence of some application of corrosion control, but they rarely make the technical decisions that cause the problem in the first place. Nor is it the metallurgical or materials engineer who should be the prime target of an awareness campaign, since these are usually subjected to some formal training in corrosion and its prevention. Those who often have a marked impact upon the incidence of corrosion are the detail designers, civil and mechanical engineers, architects of buildings or ships, and so on. There can be few who work in the corrosion area who have not experienced the influence of designers in promoting, say, crevice corrosion or corrosion-related cracking at non-stress relieved

welds. Such examples do not give a complete picture and, in general, it may be stated that those parameters with which design engineers are mostly concerned, such as stress, strain, heat and mass transfer and geometry or shape, can have profound effects upon the incidence of corrosion or otherwise.

Having identified a significant body of people through whom some corrosion prevention technology should transfer, what are the most effective means of ensuring that appropriate actions are taken? One obvious approach for those to be trained in the future is to introduce some formal instruction into their undergraduate training, although how to achieve that, when competition from other subjects to be included in the curriculum is considerable, is another matter. The U.K. 'Committee on Corrosion', (established in 1972 for a limited time of 6 years by the then Secretary of Trade and Industry and charged with implementing the recommendations of the Hoar Committee) recognising the problems associated with the introduction of a formal course on corrosion in the training of most types of engineer, decided upon a somewhat different approach. It had prepared a booklet⁽³⁾ in which emphasis is placed upon the relationships between engineering function or design and corrosion, in the hope that the undergraduate designer will see how the decisions that he makes influences the incidence, or otherwise, of corrosion. Moreover, it was considered that rather than provide a discrete or separate course on corrosion, the subject matter included in the booklet should be incorporated as an integral part of the designers professional courses, thereby avoiding the suggestion that corrosion prevention has the status of a subsidiary subject. How effective that approach has been is not known, although the fact that the booklet has been reprinted suggests that it has been in some demand.

For the practising engineer the problem is somewhat different and while short courses, films and other approaches no doubt provide a useful stimulus to corrosion awareness, it is in the Standards or Codes to which designers resort that answers should be sought. The magnitude of this task is apparent from the experiences of the U.K. 'Committee on Corrosion', which reviewed the adequacy of coverage for corrosion control in British Standards for articles made wholly or partly from metal, examining some 1600 Standards in all. Not surprisingly in such an array of documents, corrosion control receives markedly varying coverage, ranging from none, especially in older Standards, through old practices now outmoded, to vague statements calling for 'protection against the atmosphere', but also to more precisely stated requirements. In the hope of achieving some early responses in this area, the Committee considered that it is probably most important for advice to be readily available in design offices. Such places are usually well stocked with copies of relevant Standards and Codes of Practice, as well as manufacturers literature, but assistance in relation to corrosion prevention is more likely to be conspicuous by its absence. It was considered that what was needed was a series of short guides, aimed at indicating the essential features of a topic in a manner readily understandable by a non-specialist, with, where appropriate, a check list

highlighting the major factors to be considered. The emphasis was on simplicity of use and the route to good practice, rather than detailed explanations, although references to more detailed publications were given where necessary. After the preparation of some 15 such guides, the work of preparing others has been undertaken by the Institute of Corrosion in the U.K..

Quite apart from the education of design engineers in corrosion awareness, industries will continue to need those trained as specialists in corrosion and its prevention. In the U.K., the view has been taken that this is best achieved at the postgraduate level, i.e. after an initial degree in some appropriate discipline. Several university departments, usually of materials science or chemistry, have active research programmes that produce a steady flow of corrosion specialists at the Ph.D. level, while the University of Manchester Institute of Science and Technology (UMIST) not only contributes to that stream but also offers probably the best known Masters Course in the subject. Of course, there are some who feel that Corrosion Science and Engineering should be available as an undergraduate degree course, and possibly such will be offered some time, if it is not already. There are some disadvantages, not the least of which is that, the more specialised an initial degree, the less room for manoeuvre does the holder have in relation to his subsequent employment. Moreover, it is often difficult enough for someone about to enter university to decide between, say, science and engineering, let alone which branch of those fields to study, and there is a school of thought that tends to the view that initial degrees should be more broadly based than is currently the case in most, but not all, universities. The recruitment by those industries concerned with corrosion control of a range of people with initial degrees in chemistry, physics, materials science, and mechanical, chemical or electrical engineering, etc., followed by postgraduate training in areas of corrosion, has probably provided a breadth of experience that has served those industries well and is likely to continue to do so.

Roles of Corrosion Societies

Corrosion societies fulfil an important educational function in arranging meetings of corrosion specialists whereby views and experiences are exchanged through symposia and the like. They also have an important educational role to play, as many of them have recognised in offering formal courses in various branches of corrosion engineering. Many of the courses offered by societies are what are sometimes called transfer courses, covering the principles of corrosion and its prevention, for those whose previous training has been in some other discipline, or they are aimed at a specific branch of corrosion engineering, such as cathodic protection or coatings. Such courses appear to be attractive to corrosion societies because there is a steady demand for them and the costs of their initial development may be recovered at a reasonable rate. It appears likely that, following the trends in other professions, there will be an increasing need for 'updating' courses for corrosion specialists. It may be argued that these tend to be offered currently as short

courses by appropriate universities, but there have been significant developments in, for example, the application of computers to various aspects of corrosion, that may provide additional opportunities for corrosion societies to offer courses.

Since many of the larger companies, especially in the oil and chemical fields, that employ significant numbers of corrosion engineers operate internationally there is a tendency for them to require training courses to be available in different parts of the world. That should ensure that standards in, say, coating inspection should achieve some degree of uniformity and at least one society, NACE International, has been involved in offering its courses on a worldwide basis. While it is recognised that, at least in part, societies offer educational courses for the purpose of raising revenues, nevertheless there would appear to be a case for the development of cooperative programmes between societies in some areas of corrosion control. Obviously, there are differences in the environmental conditions in different parts of the world and these introduce variations in the approaches to corrosion control in particular instances that need to be taken into account in designing training programmes. A society that considers its courses, developed for application in a particular part of the world, are globally applicable, may not invariably be correct and the most appropriate advice on detailed content is likely to be obtained from those who normally work in the area in which a course is to be presented. That may suggest that the obvious body to present training or educational courses in a particular location is that wherein the necessary experience of local conditions exist. But the development of courses and the training of appropriate instructors are, or should be, costly processes and where such expenditure has already been incurred, in relation to a course that would require relatively little modification to be appropriate for presentation in a particular locality, making that modification would appear to be a sensible route to follow. Of course, the cooperating societies in such an exercise need to come to some agreement about sharing surplus revenue and also in the training of appropriate instructors where there are possible language barriers between instructor and instructed.

There is another area in which collaboration between corrosion societies could be beneficial to all and that is in relation to the development of Standards and Codes of Practice. Several corrosion societies, and some whose interests go beyond the fields of corrosion and its prevention, are involved in the preparation of such documents and there are instances of cooperation in these areas. Again, there will be situations where local environmental conditions will necessitate the preparation of documents specific to particular localities, but there are other matters, as with laboratory test methods, for example, where a commonality of approach is likely to be to the benefit of all, but that has not always happened in the past. The Standards and Codes developed by corrosion societies tend, almost inevitably, to be aimed at achieving some uniformity of approach to specific methods of corrosion prevention or testing. But, as

already mentioned, there are many Standards to which engineering design conforms without recognising the built-in corrosion hazards. There is little doubt as to the significant contribution that such Standards make to the incidence of loss of engineering function due to corrosion and so this is an area where there is a very real need for corrosion societies to have a marked influence. While the individuals representing those societies in such endeavour may find the work less immediately rewarding than that associated with writing primary corrosion Standards, nevertheless its impact could be at least of a similar order and there is a need for corrosion societies to enter into a dialogue with those organisations responsible for the preparation of Standards in the fields of civil, chemical, mechanical engineering and the like.

Industry-Government-University Interactions

Concern with the perceived inadequacy of technology transfer of the research output of universities, or other laboratories, to industry has often been expressed and will no doubt continue. But such statements are usually because the person making them is ignorant of the considerable collaboration between universities and industries already existent or because of inadequate understanding of the roles of such bodies. The primary roles of universities are to teach and carry out research, and in teaching they train people for industry, which constitutes an important aspect of technology transfer. Industries are concerned with developing technologies, with all that that implies in economic terms, and which may or may not be dependent on research results. That is not meant to imply that there is not room for improving the interactions between universities and industries, but rather is it to make the point that at least some industrial companies, especially the larger ones, are familiar with much of the relevant research going on in universities, even if those domiciled in academia are sometimes less cognisant of what goes on in industry.

A more important question than that relating to the supposed lack of transfer of knowledge concerns the relevance of some of the research that is prosecuted in university, and indeed other, laboratories. Of course, industry and certain arms of government sponsor research programmes in such laboratories and presumably that research is regarded as relevant by the sponsor. In addition, tradition is such that university researchers carry out particular pieces of research for the very good reason of obtaining a better understanding of why specific events happen, sometimes claiming, perhaps facetiously, that such knowledge will ultimately result in benefits to industry. There is a thought provoking article by IBM Vice President, Science and Technology, John A Armstrong, in a recent issue of MRS Bulletin⁽⁴⁾ that is worth reading in the present context, but where the point is made that the purely cultural argument for scientific research justifies the same level of government support as is accorded to painting, music and the like, which is often at levels about 100 times less than that which science enjoys! Nevertheless, the question remains as to whether we do need information on the

effects of some obscure organic inhibitor on the acid corrosion of gadolinium, or the umpteenth test for intergranular corrosion of sensitized stainless steel, where the successive problems obviously stem from the irrelevance of the environments used in such tests in comparison to plant environments?

Such questions are not entirely trivial, because universities, certainly in Europe and North America, are being financially squeezed and will need to look increasingly at dispersing the research element in their funding on a selective basis. U.K. university departments have, for a few years, been assessed for their research output and central funding is dispersed to universities in a way that reflects those assessments, although whether the (U.K.) Universities Funding Council will retain its nerve in such selectivity remains to be seen. Despite the reductions in defence expenditure in some countries, which have their own implications for reduced research funding, the calls upon government for increasing expenditure on health, education, infrastructure and so on, suggest that the halcyon days for university research in the 1960-80's may not return quickly, if ever. The consequences probably will, and should be selective support for the most relevant research conducted in laboratories of high repute as determined by peer review or other methods of identifying quality. The alternative of distributing funding uniformly between universities will be detrimental to the long term benefits to the taxpayer. As the article⁽⁴⁾ already mentioned succinctly states; "We will be fooling ourselves as a society if, on the one hand, we want university research to help us compete in a world where the merit - i.e. the quality - of products is key, but on the other hand, we are not as a society willing to use merit as the major basis for allocation of research support."

Some will presumably argue that corrosion research is a special case, because many countries have undertaken studies that show the costs of corrosion amount to some few percent of the gross national product, so that money spent on corrosion research is likely to produce a significant return that will outweigh the costs of such research. But is that financial argument valid for the case of corrosion research? Many of the national surveys have concluded that a significant saving against corrosion costs could be achieved by the application of existing knowledge and that the economic solution to many other corrosion problems is to let it happen; few identified specific areas of research for which there was a pressing need and from which the financial returns would be large. Of course, there is a need for continuing research in relation to corrosion and its prevention, as with the inadequacies of the currently used methods of measuring the potentials of buried structures already commented upon, while the developments in composite materials, including those involving fibre reinforced metals and ceramics for high temperature applications, offer opportunities for research that have not yet been fully exploited. There are many other areas where relevant research is needed, but a feasible argument is that, increasingly, these will be funded on a selective basis related to need and to the quality of the reputation of the laboratory in which the work is to be carried out.

The Greenness of Corrosion Prevention.

Having mentioned the national surveys of corrosion costs, and their implications for inculcating corrosion awareness in those who may contribute to such, it may be worthwhile considering these costs further. A reasonable question to ask is, how much has been saved in the time since the numbers became known some 10 - 20 years ago, depending upon the country involved? If that question cannot be answered, other than because the necessary data has not been collected, then the credibility of the initial number is brought into question. There is, in any case, another facet to these numbers and that relates to whether they are meaningful to most people. They are often of the order of national budget deficits in some countries, and therefore national corrosion costs may have been of use initially in gaining the attention of some arms of governments, but does it serve any useful purpose to keep repeating these figures when the average person probably cannot really comprehend them?

There is little doubt of the importance of keeping corrosion awareness in the minds of many people, but maybe what is needed is a new strategy for achieving that objective, even though there will be occasions when the cost approach remains appropriate. Increasingly people are against waste and corrosion is just that. But the environmental implications of corrosion can be quite dramatic, most obviously when corrosion results in leakage of a noxious substance from a containing vessel, but the energy implications of having to replace a corroded structure are worthy of consideration, not only in relation to the long term rise in energy costs but also in relation to their environmental overtones. To replace 1000 kg of steel requires about 380 kg of carbon, if produced from iron ore, and about 140 kg if produced by remelting scrap. Most of the carbon eventually goes into the atmosphere as carbon dioxide, a key gas in global warming, added to which there are acid rain (sulphur dioxide and nitrogen oxides) features involved. Furthermore, the energy implications for fabricating the steel ingot into a useful form will have significant environmental implications. So that a single corrosion pit penetrating the wall of just one joint (≈ 12 m long and weighing ≈ 2600 kg) of high pressure pipeline will require something in excess of 1000 kg of carbon for its replacement, corresponding to some 5 metric tons of carbon dioxide polluting the atmosphere. It may be argued that such numbers again begin to lose the attention of the public and more meaningful units would be helpful. In relation to the 'Green Lights' programme (aimed at installing more efficient lighting systems) in the U.S.A. the Environmental Protection Agency has calculated that to save 1% of the national aggregate electricity demand is the equivalent of taking 4.4 million cars off the roads. It would be a relatively simple matter, using energy consumption as the common denominator, to express the implications of corrosion in similar units, or in whatever form is considered most appropriate for a particular case.

Finally, there is another aspect to selling corrosion prevention in terms of national costs if prevention is not carried out and

which is worthy of more thought. There is an element, at least implied, of negativity in that approach and it may be much more appropriate to sell corrosion prevention in terms of positive achievements. For example, to the public at large, reminding them of how much longer their car exhaust systems last now than they did a decade ago, simply due to better corrosion protection. There are many more similar success stories that can be quoted and such, coupled with the savings in energy consumption and pollution i.e. the greenness of corrosion prevention, may now be more appropriate ways of selling the avoidance of the waste that constitutes corrosion than continuing to repeat national corrosion costs.

References

1. H. Davy, Philosophical Transactions Royal Society, 114 (1824): pp 151, 242, 328.
2. Report of the Committee on Corrosion and Protection, (HMSO, London, 1971) ISBN11 470530 5.
3. R.N.Parkins and K.A.Chandler, "Corrosion Control in Engineering Design", (HMSO, London, 1978) ISBN 0 11 512157 9.
4. J.A.Armstrong, MRS Bulletin, XVIII, 2 (1993): p. 4.

Advancements In Automotive Corrosion Resistance

Michael R. Ostermiller
Corrosion Technology Center
Milford Proving Ground
NAO Validation Center
General Motors Corporation
Milford, Michigan 48380-3726

L. Lee Piepho
Corrosion Technology Center
Milford Proving Ground
NAO Validation Center
General Motors Corporation
Milford, Michigan 48380-3726

Larry Singer
Corrosion Technology Center
Milford Proving Ground
NAO Validation Center
General Motors Corporation
Milford, Michigan 48380-3726

Abstract

This paper discusses the history and development of corrosion protection methods for cars and trucks and details protective measures currently used in the automotive industry. The intent of the paper is to give one a general overview or perspective on automotive corrosion issues and is not all-inclusive.

Included is a brief review of the causes of automotive corrosion and the types of corrosion. There is also a discussion of design, material, and processing factors that are finding wider acceptance in the latest generation of vehicles built worldwide. Coatings, pretreatments and pre-coated steels used to protect vehicles from corrosion are discussed in some detail. Finally, a systems approach to corrosion avoidance is presented as a way to obtain world class performance.

Keywords: corrosion, corrosion avoidance, corrosion protection, corrosion resistance, design, materials, processing, salt, pre-coated steel, primer, pretreatment, phosphate.

Introduction

Prior to the late 1950s, corrosion was not considered a major concern of vehicle owners. Vehicle designs provided for heavy gage steel, and deicing materials were seldom used in the U.S.

However, during this time frame, a major expansion of the U.S. highway system was initiated and many cross-country super-highways and major city transit loops were built. As shipments by truck and railroad increased dramatically and automobile travel expanded, it became necessary to keep these major highways and city loops open year-round in the heavy industrial northeastern U.S. and southern Canada. The readily available and inexpensive commodity of salt (NaCl) was used as the primary means of deicing during the winter. In addition, since salt (NaCl) was not as effective for deicing as was calcium chloride (CaCl_2), the two were frequently mixed. The use of NaCl and CaCl_2 was very effective, so much so that the highway maintenance departments developed the "bare pavement policy." The extensive use of "road salt," as described above, has resulted in corrosion becoming an inland concern as well as a sea coastal concern. With the increased usage of road salt, as shown in figure 1¹, came the increased automotive corrosion problems associated with the most severe salt usage areas. Figure 2 shows the corrosive automotive environments in the U.S. and Canada².

In addition to CaCl_2 usage in the winter, rural communities in the snowbelt and other regions have increased the use of CaCl_2 in the summer months for dust control on unpaved roads. Since CaCl_2 is hygroscopic in nature, deposits on vehicles result in increased time of wetness, thus increasing the localized corrosion environment and subsequent degree of corrosion.

In the same time frame, the use of coal and certain other fossil fuels increased because of population (i.e., cars, home heating, etc.) and industry growth (i.e. chemical, steel, electricity, oil/gas, etc.) resulting in increased pollutants (i.e., SO_2 , NO_x , H_2S) emitted to the atmosphere. When these gases encounter water or related molecules in the atmosphere, they form sulfuric acid (H_2SO_4) droplets and nitric acid (HNO_3) gas which readily dissolves in earthbound rain. Thus, the term acid precipitation or "acid rain." Acid precipitation occurs over large areas of North America, Europe, and Asia. Figure 3 shows the acidity of precipitation along with corrosive automotive environments. The most acidic rainfall occurs in the snowbelt or "salt belt" regions².

In the past 25 years, automotive corrosion has become a more serious concern because the corrosive environment has become more severe and year-round due to the increased road salt and calcium chloride usage (road salt usage has leveled out at approximately 10-11 million tons depending on the severity of the winter), increased atmospheric pollution and contaminants, increased CaCl_2 applications for dust control, and the sea coastal salt laden air conditions. The more severe corrosive environment has necessitated immediate and increased action for the automotive industry to improve the corrosion resistance of cars and trucks worldwide. Appendix 1 lists, in general terms, some of the major advances/events in the industry relative to vehicle corrosion avoidance. Not all advances will be discussed in this paper. The following part of the paper will discuss, in greater detail, the advancements made to improve the corrosion resistance of cars and trucks by applying a systems approach to corrosion avoidance; the system being the coordinated effort between vehicle design, materials, and processing.

Types of Corrosion^{3,4}

Since the corrosion environment has become more severe, a greater burden has been placed on the design engineer to become familiar with the different types of corrosion and the varying susceptibility of materials to particular types of corrosion under specific exposure conditions. Therefore, the following list very briefly describes the various forms of corrosion.

Uniform or General Corrosion - Corrosion that proceeds uniformly over the entire exposed surface (typically referred to as cosmetic corrosion).

Crevice or Concentration Cell Corrosion - Localized corrosion caused by the formation of a potential difference between two areas of metal exposed to different concentrations of dissolved ions in the same solution (typically referred to as perforation corrosion because it results in a perforated substrate).

Galvanic Corrosion - Accelerated attack that occurs when two metals with different potentials or tendencies to corrode are in metal-to-metal contact.

Pitting Corrosion - A form of localized attack at a metal surface where small areas corrode preferentially leading to the formation of cavities.

Stress Corrosion - Form of corrosion occurs where the metal is under the combined influence of sustained tensile stress, either applied or residual, and a corrosive environment.

Intergranular Corrosion - A selective or localized attack at or adjacent to grain boundaries without appreciable attack on the grain.

Exfoliation Corrosion - A laminar type of corrosive attack in which flakes of metal are peeled or pushed from the surface because of the internal stresses created by the corrosion products.

Dealloying or Parting Corrosion - A phenomenon associated with the selective removal of one or more components from an alloy.

Fretting Corrosion - Type of corrosion defined as damage that occurs at the interface of two contacting surfaces, at least one of which is metal, when they are subject to minute slippage relative to each other.

Corrosion Fatigue - The premature fracturing of metal from the exposure to the combined action of corrosion and repeated cyclic stressing.

Filiform (Underfilm) Corrosion - A type of crevice corrosion occurring under protective films.

Erosion Corrosion - The acceleration or increase in rate of deterioration or attack on a metal because of relative movement between a corrosive fluid and a metal surface.

Hydrogen Damage - Mechanical damage of a metal caused by the presence of, or interaction with, hydrogen.

If more extensive information on the various types of corrosion and suggested methods of prevention are needed, reference SAE paper No. 770292 or refer to Corrosion Engineering - M.G. Fontana.⁴

The Evolution Of Corrosion Avoidance

Corrosion incidents or concerns did not occur all at once; that is, they increased in scope and dimension over time directly paralleling the increased severity of the environment.

Total vehicle corrosion avoidance is dependent on a balance between materials, processing, and design. In addition to advancements in those three areas, laboratory and road test procedures have evolved to more accurately predict the corrosion performance of automotive manufacturer and supplier products.

Materials

Pre-Coated Metal^{5,6}

As the corrosion severity increased, pre-coated steels were considered as a replacement for uncoated steels to provide better protection. Hot-dip galvanized steel, a readily available and proven commodity, was chosen. However, the spangled surface associated with hot-dip galvanized steel and its appearance after painting restricted its use to that of less visible areas.

In the early 1970s, hot-dip zinc-iron alloy products were introduced into the automobile industry. Hot-dip zinc-iron alloy is produced by continued heating of the galvanized coil after the zinc bath so that the zinc fully alloys with the steel rather than coating and leaving free zinc on the surface. This produces a smoother, spangle-free surface which gives an acceptable paint appearance. It was first

used for station wagon tailgates, hatch/decklids, and tulip panels. Zinc-iron alloy was more susceptible to paint loss than that of steel. In many cases, most of the paint would lift off to expose the zinc-iron. This gave the material a poor image and limited its usage. Unfortunately, the need for cleaning and phosphate pretreatment different than that of steel was not immediately recognized. Additionally, unlike pure zinc galvanized which produces white corrosion products, zinc-iron will produce red rust which also made it less desirable. Also, when cathodic electrodeposition (ELPO) primer was introduced in 1976, it displayed unacceptable craters in the primer layer, when processed under certain conditions.

Aluminum has been used for some body panels, primarily in hoods and decklids. While desirable from a corrosion standpoint, its usage was made basically for weight savings. Aluminum was susceptible to paint loss also, however, when it did, it displayed white corrosion products, instead of red rust. Aluminum still has phosphate processing concerns to assure a proper coating for paint adhesion, needs special care when attached to steel due to galvanic corrosion susceptibility, and in addition has physical properties (i.e., dent/ding resistance, strength) and cost disadvantages over that of steel that result in limited usage, even today.

The first of the pre-coated steels commonly used by the automobile manufacturers was hot-dip galvanized (HDG) steel containing pure zinc for vehicle rocker panels in the mid-60s. Today, a typical car may have HDG specified for many or all body structural members, including the floor pan, and on all interior surfaces of major body outer panels, which use one sided galvanized steel, and both sides of major body inner panels (i.e., door, hood, decklid inners), which use two-sided galvanized steel.

In the mid-70s, two major breakthroughs occurred when Zincrometal* and electrogalvanized steel became available. The use of these one-side coated materials allowed corrosion protection on the body panel inner surface (Surface B, Figure 4) to prevent perforation while leaving the outer surface (A) uncoated for good paint adhesion and appearance.

Zincrometal* is a one-sided coated steel, with a barrier coat applied to the interior panel surface only. It was the automobile manufacturers' primary choice for exterior panel perforation protection in the late 1970s and early 1980s. A typical arrangement would be to have Zincrometal* on a door or hood outer panel inner surface (B) and uncoated steel on the other panel surfaces (A, C, D - Figure 4). Although laboratory testing showed Zincrometal* to have excellent corrosion properties, accelerated road test and field evaluation showed it was not equivalent to that of pure sacrificial zinc. However, it did add to panel life compared to plain uncoated steel and continues to be used today in the U.S., Europe, and Japan for corrosion protection. In most of these areas today, it's used on the outer panel with two-sided hot-dip galvanized or other alloy steels on the inner panel, ELPO primer, and supplemental cavity coatings/waxes.

Also, a major steel supplier converted an existing galvanizing line to a one-sided electrogalvanized (1EG) line. This material was first introduced in 1977 on quarter panels (Surface B, Figure 4) to prevent perforation where it continued to be used until two-sided galvanized or other zinc alloy steel became available. Since only one 1EG line was built, availability was limited and expansion to other panels was determined on a critical need basis.

In the early 1980s, a minimum spangle HDG steel product was developed for the exterior surface of visible outer and inner body panels (Surfaces A & D, Figure 4). Today, minimum spangle or spangle-free HDG steel is used predominantly on inner panels or secondary surfaces, those surfaces that are only visible during the operation or servicing of the vehicle. Typical zinc coating weights range from 60-100 g/m². Two-sided HDG steel is used for sacrificial protection for both cosmetic (exterior) and perforation (interior) corrosion.

The word "electrogalvanized" typically means to electrolytically plate with pure zinc, although it is possible to electroplate zinc alloys also. In the mid-1980s, the steel manufacturers were getting more and more requests for better paintable steel for exterior body panels, thus, the number of

* Zincrometal is a trademark name of Akzo/Metal Coatings International, Inc.

electrogalvanizing lines increased significantly to meet the demand. The electrogalvanizing process has become regarded as state-of-the-art in the coil coating industry. The most commonly specified zinc coating weights are in the 30-70 g/m² range on the interior and exterior surfaces of the major body outer panels. Thus, since electrogalvanized steel is typically coated on both sides of a panel, it sacrificially protects the body panel from both perforation and cosmetic corrosion. The one advantage of pure zinc on the outside surface (A) is that it sacrificially protects damaged areas and prevents red rust, whereas the other alloy materials display red rust, if damaged. This is true for both electrogalvanized and hot-dip galvanized steel.

Zinc alloy hot-dip and electrogalvanized steels typically contain iron or nickel and were generally introduced in the mid 1980s and have been gaining wider usage lately by domestic, "transplant," and overseas vehicle manufacturers. Typically, the specified coating weights are in the 20-50 g/m² range, which is less than that of currently used pure zinc coatings. As with hot-dip and electrogalvanized steel, one-sided or two-sided zinc alloy steels provide sacrificial protection against perforation and cosmetic exposure, however, on a comparison basis, the lighter pure zinc steels (i.e., 60 g/m²) outperform the heavier zinc alloy steels (i.e., 50 g/m²) for perforation and cosmetic red rust resistance, based on laboratory, trailer, and vehicle road testing.

The latest concept in pre-coated steel is called a composite or "piggyback" coating. This coating combines the sacrificial protection of zinc or zinc alloy with an organic barrier coating for increased perforation corrosion resistance. In this process, a zinc or zinc alloy layer, generally 20-40 g/m², is placed on both surfaces. Then an organic coating is applied to one side which later becomes the interior panel surface of the body panel (B, C, Figure 4). Therefore, a composite-coated panel provides the sacrificial cosmetic corrosion protection to the exterior panel surface (A) and combined sacrificial and barrier coat protection to the interior panel surface (B).

A new product introduction today, in most cases, will typically have pure zinc or zinc alloy coatings on most major body panels and structural members. For example, all four surfaces (A, B, C, D, Figure 4) in a door assembly will have pre-coated steel. Reference American Iron and Steel Institute booklets entitled "Automotive Steels," 1988 and 1989, which display the extensive use of coated steels in vehicles today⁷.

In summary, the major trends in the use of coated sheet steel materials for automotive indicate that pure zinc coating weights are being slightly lowered and zinc alloy coating weights are increasing as costs are being optimized versus corrosion protection versus manufacturability. On an equivalent coating weight basis, pure zinc hot-dip and electrogalvanized steels perform similarly to zinc alloy materials for perforation corrosion resistance. However, for cosmetic corrosion resistance, that is, protection against red rust if the paint on the exterior of the panel is damaged by stone chipping or other incidental damage, the pure zinc products protect against red rust longer than that of other materials, because of their better sacrificial properties. The aforementioned are based on laboratory, trailer, and vehicle road testing.

As shown in figure 5, the different materials will continue to be used for some time by the various automobile manufacturers. Table 1⁸ shows the 1990's trends in coated steel usage by North American vehicle manufacturers. There will probably not be a single choice in the industry but rather a continued mix suited to meet the needs and objectives of a particular manufacturer. The current trend would indicate that pure zinc and zinc alloy materials will be the predominant products specified so that vehicle corrosion performance approaches and potentially surpasses the industry 5 year cosmetic and 10 year perforation objectives. Composite-coated steel, aluminum, and plastics will also find increased usage for specific applications in future vehicle programs.

Processing

The body sheet metal has a variety of different manufacturing related contaminants (e.g., lubricants, rust preventatives, dirt) that must be removed so that the paint system will provide good corrosion durability and appearance. This section will focus on pretreatment, primer, topcoat, and certain paint application process technology advancements. Because these technologies vary within the automotive

industry and even within a company, this discussion will address the generally accepted paint processing practices.

Pretreatment/Phosphate⁸

The first and probably the most important layer of the paint system is the phosphate coating. Even though it is the thinnest coating in the paint system, approximately one-tenth of a mil thick, its importance to corrosion protection is unquestioned because it is the anchor for all subsequent layers. The phosphate coating is actually a conversion coating which produces a layered crystal structure on the top of the uncoated, pure zinc, zinc alloy steel, aluminum, or other surface. The pretreatment process is required to clean the metal, promote paint adhesion, reduce metal-to-paint reactions (particularly galvanized surfaces), and improve corrosion resistance. Typically, the B-I-W, with its variety of materials and different types of contaminants, is processed through this system which means that selection of the phosphate is dependent on the materials mix and type of phosphating process. Thus, since the system cleans the metal or removes the contaminants and applies a phosphate layer, it is commonly referred to as a clean/phosphate system.

Along with zinc and phosphoric acid, other proprietary additives are included in the phosphate stage in order to control the phosphate crystal morphology. This is based on extensive testing which has shown that increased corrosion resistance could be obtained by controlling the size, shape, and orientation of the crystals in the resulting layer.

Some of the developments in phosphate technology over the past decade include:

- Better control of the mill oils, drawing compounds and rust preventatives on steels, along with improved cleaners to assure a clean body for phosphating.
- Better control of the phosphate bath parameters (i.e. temperature, zinc concentration, total acid concentration, free acid concentration) through statistical process control (SPC).
- Measurement of phosphate coating weight in milligram/surface area (i.e. mg/cm²)
- Improved spray zinc phosphate systems and increased use of immersion zinc phosphate systems for better interior cavity coverage and exterior body surface coverage.
- Smaller phosphate crystal size and more uniform coating weight for better paint adhesion, surface finish, and resistance to scribe creepback.
- Optimizing the treatment of car bodies with mixed materials (i.e. aluminum, uncoated steel, zinc-iron, pure zinc, plastic).
- Introduction of nickel and manganese modified zinc phosphates and the controlled addition of fluoride to improve the corrosion resistance and paint adhesion.
- Lower temperature baths to reduce energy costs.
- Development of chrome-free rinses that perform the same as chrome rinses and yet reduce the environmental impact.
- New and improved ELPO materials necessitated better phosphates for paint adhesion.

This list is not all-inclusive, however, it shows some of the more significant improvements in this area during the last decade.

Primer⁹

As seen in the pretreatment area, vast improvements have been made in the primer area also, which is the next step in the process for the B-I-W. These improvements not only include the development of new, tougher, thicker materials, but also major changes in application processes. While many of these changes were driven by the need for improved corrosion resistance, the Clean Air Act of 1970 and the later revisions also had a major impact. The most notable development was that of the cathodic electrodeposition (ELPO) priming process, which has become the dominant method of priming cars, trucks, and components throughout the world today.

In 1976, PPG Industries introduced the cathodic electrodeposition (ELPO) primer process. Opposite to the anodic process, the body or component is the cathode. The cathodic ELPO primer provided

superior corrosion resistance than that of anodic primer on both the exterior surfaces and the interior cavity areas. Today, nearly 100% of the cars and trucks manufactured in the world use the cathodic ELPO primer process.

Just as quickly as ELPO primer was adopted, many paint lines in the industry are 1) converting from conventional (0.6 mil) primer to high build (1.2 - 1.4 mil) primer for improved corrosion resistance and hiding characteristics, 2) color matching the primer surfacer to the topcoat to reduce topcoat coating thickness, 3) converting to ELPO primers with better throw power for cavity coverage, 4) using powder paints which reduce environmental concerns and offer more efficient paint utilization, and 5) investigating the use of coil coat pre-primed steel that offers the possibility of eliminating the entire post-assembly prime process.

This list is not all-inclusive, however, it shows some of the trends in the industry to better improve customer satisfaction and reduce costs.

Design Improvements^{3,11}

Along with new innovations in materials and processing, product designs were studied and recommendations were made to reduce the product susceptibility to the different types of corrosion. Simple logic would indicate that design has a key role in the corrosion resistance of a vehicle or component, but it wasn't always practiced. Thus, the key factor in improving the design for corrosion resistance was the recognition by the design community that design has a great affect on corrosion resistance, and that not all problems can be solved simply by materials and/or processing. The creation of departments within the various automakers for corrosion performance and the availability of corrosion "experts" to each new vehicle program to provide the design guidance has undoubtedly had a major influence. Face lifts wherein the exterior body panels are modified to give a new appearance oftentimes permit modification to ease a corrosion concern, however, only in the case of a complete re-design or new program is it usually possible to incorporate major design innovations. The following design concepts and innovations have been discussed in various references including SAE paper No. 770292 and apply to most engineering applications to reduce or eliminate corrosion.

- Place cross body reinforcements inside the body on top of the floorpan rather than on the underside.
- Shingle all undervehicle joints rearward to prevent poultice and moisture intrusion directly into the joint.
- Provide necessary access holes to body panels and structural members to allow complete pretreatment and primer coverage.
- Avoid "nose over" hood configurations which have more corrosion stone chip susceptibility.
- Avoid severe tuck-under areas to prevent lower body stone chipping or use moldings or anti-chip material to reduce stone chipping.
- Provide adequate clearance between inner and outer panels for interior anti-corrosion material application.
- Design door panels to be properly shingled or provide other design considerations to reduce stone chipping and subsequent corrosion.
- Provide adequate access holes for fixtured wax applications, if necessary.
- Avoid louvers in hoods
- Avoid poultice entrapment areas (shelves) in rear lower fender and other areas.
- Eliminate unnecessary holes in exterior body panels by adhesively bonding all ornamentation using various isolation techniques, or fabricate holes and install attachment studs in the body shop prior to paint.
- Isolate stainless steel, magnesium, and aluminum parts to prevent galvanic corrosion.
- Use full stamped door panels to eliminate corrosion at upper frame and lower door panel joints.
- Locate electrical parts inside the vehicle, where possible, or provide proper sealing, shielding and/or drainage.

Engineering design based on the application of sound corrosion principles is commendable, however, it must be determined whether the proposed recommendations are feasible, that they can be achieved with existing facilities and operation, and that they will indeed satisfy the engineering requirements. Thus, the design community must work closely as a team with manufacturing and materials personnel. This intensive upfront planning and design involvement will provide the best corrosion performance and customer satisfaction at the least product cost.

Other Vehicle Advancements

As in the body area, many other advancements have been made to improve the total vehicle corrosion performance. Following is a partial list of improvements in the powertrain, chassis/suspension, electrical and body areas.

- Most undervehicle and underhood systems, components, and fasteners are painted, plated and/or waxed for improved cosmetic corrosion resistance and functional performance.
- Many vehicles have implemented undervehicle splash shields to reduce the underbody and underhood corrosion and splash environment and to provide better aesthetic appearance.
- Bimetal and stainless steel encapsulated trim moldings and better trim and decorative part attachment techniques have been implemented.
- Electrical improvements include isolation from the environment (i.e., located in passenger compartment or in less severe locations), better sealing and coatings on control boxes, weatherpac connectors, etc.
- Most exhaust systems use various types of stainless steel and aluminized stainless steel for improved service life.
- Some chassis/suspension systems use aluminum.
- Many vehicle lines use plastic materials and aluminum for major exterior body panels.
- Most door hardware and other body components (e.g., door joint switches, park brake cable systems, bumpers) are either coated or made of corrosion resistant material for improved cosmetic corrosion and functional performance.
- Brake and fuel pipes and fuel tanks (internal and external) have corrosion resistant coatings.

Systems Approach To Corrosion Avoidance

World class performance goals and product costs of present and future vehicle programs and customer expectations are directing further development of the systems approach when optimizing overall corrosion performance. As we've indicated, in the past decade, tremendous advancements have been made in the areas of design, materials, and processing to improve corrosion avoidance; the next decade will offer even greater challenges in these areas with major emphasis in the design area. These challenges will demonstrate the utmost importance to maintain a coordinated and balanced effort between design, materials, and processing. Even though there will be increased pressure to reduce product cost and environmental impact, corrosion avoidance and product value must continue to improve to meet growing customer expectations.

Summary

In summary, the automotive industry, as a whole, has greatly improved the overall corrosion performance of cars and trucks in the last decade. Industry trends indicate that the next decade will be just as exciting and challenging with a common objective of eliminating corrosion as a customer concern while decreasing product cost. Research and advancements will continue in the materials (i.e., pre-coated steel, pretreatment, primer, topcoat), processing, and design areas with an emphasis on a systems approach to total vehicle corrosion avoidance.

REFERENCES

1. B. Bertram, "Salt Institute Statistical Report Analysis," 1990.
2. R. Baboian, "Automotive Corrosion by Deicing Salts," proceedings from NACE Corrosion Conference, March 1981.
3. L. C. Rowe, "The Application of Corrosion Principles to Automotive Engineering Design," proceedings from NACE Corrosion Conference, March 1981.
4. M. G. Fontana, Corrosion Engineering, McGraw-Hill, 1986.
5. G. Mascher, "Prospects of Zinc-Coated Steel in the European Automotive Industry," proceedings of the International Conference on Zinc and Zinc Alloy Coated Sheet sponsored by the Iron and Steel Institute of Japan (GALVATECH), September 1989.
6. A. M. Kalson, Jr., "Coated Steels Sheets in North America, An Automotive Perspective," proceedings of the International Conference on Zinc and Zinc Alloy Coated Sheet sponsored by the Iron and Steel Institute of Japan (GALVATECH), September 1989.
7. American Iron and Steel Institute, "Automotive Steels," displayed at the 1988 and 1989 Society of Automotive Engineers International Exposition.
8. G. J. Cormier, "Effective Cleaning of Zinc and Aluminum Surface," SAE paper 89255, presented at 1989 Automotive Corrosion and Prevention Conference, December 1989.
9. F. M. Loop, "High Film Build Cathodic Electrodeposition for the Automotive Industry," PPG Industries.
10. "Topcoat Technology Training," PPG Industries, February 1989 (internal training manual; for more information contact PPG Industries).
11. "Prevention of Corrosion of Motor Vehicle Body and Chassis Components" - SAE HS J447, June 1981.
12. H. E. Townsend, "Accelerated Corrosion Testing: A Cooperative Effort by the Automotive and Steel Industries," proceedings of the World Materials Congress, September 1988 (Corrosion - Resistant Automotive Sheet Steels).
13. A. W. Bryant, W. C. Oldenberg, "1985 Body Corrosion Field Survey - 5 and 6 Year Old Vehicles," SAE 862025, SAE Automotive Corrosion and Prevention Conference, December 1986.
14. A. W. Bryant, L. M. Thompson, W. C. Oldenberg, G. Hook, J. Schroeder, "U.S. Automotive Corrosion Trends at 5 and 6 Years", SAE 892578, SAE Automotive Corrosion and Prevention Conference, December 1989.

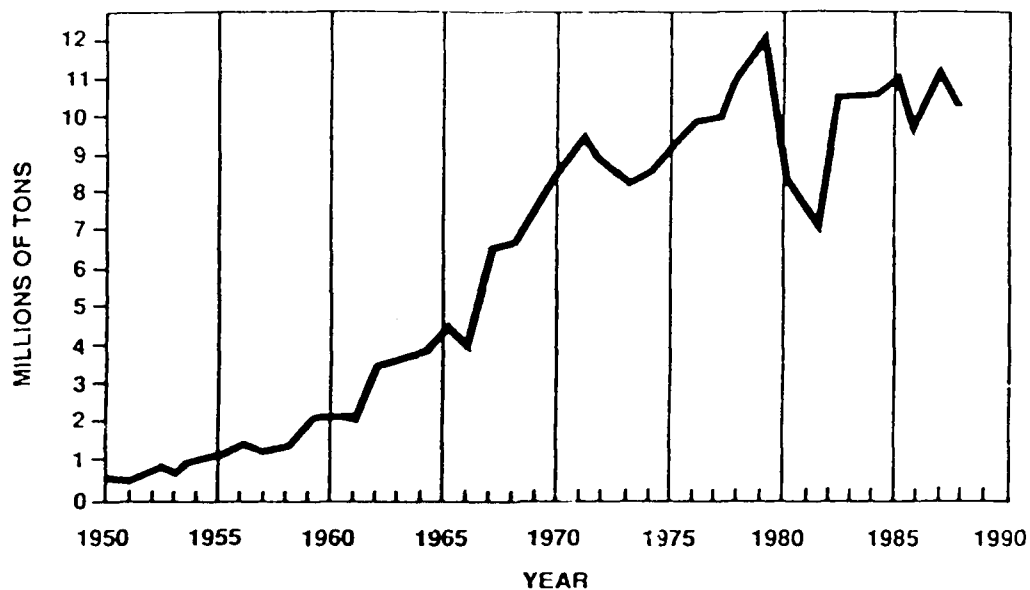


FIGURE 1 - DE-ICING SALT USAGE IN THE UNITED STATES

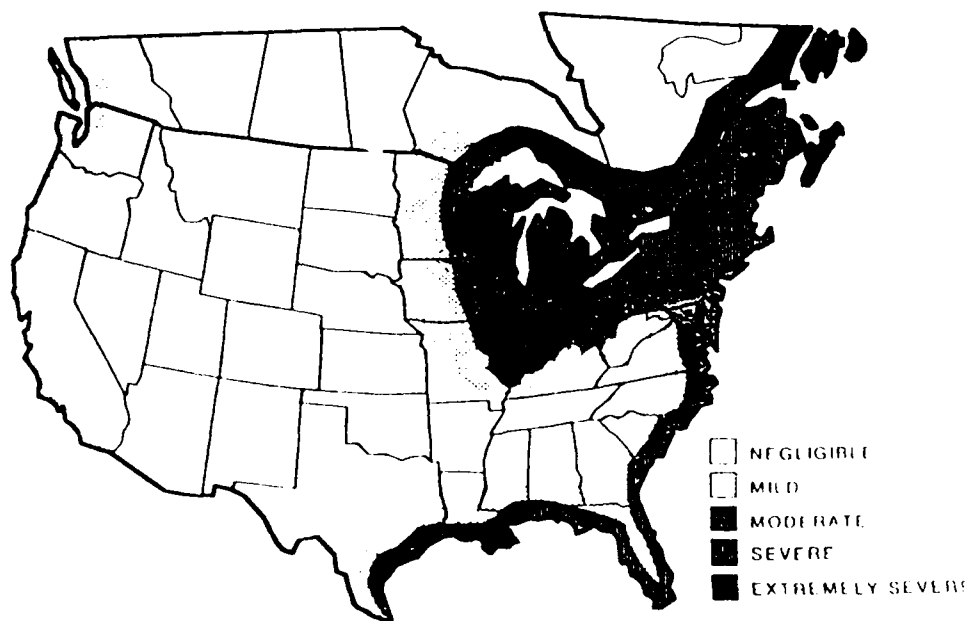


FIGURE 2 - VEHICLE CORROSION ENVIRONMENT
IN CANADA AND THE UNITED STATES

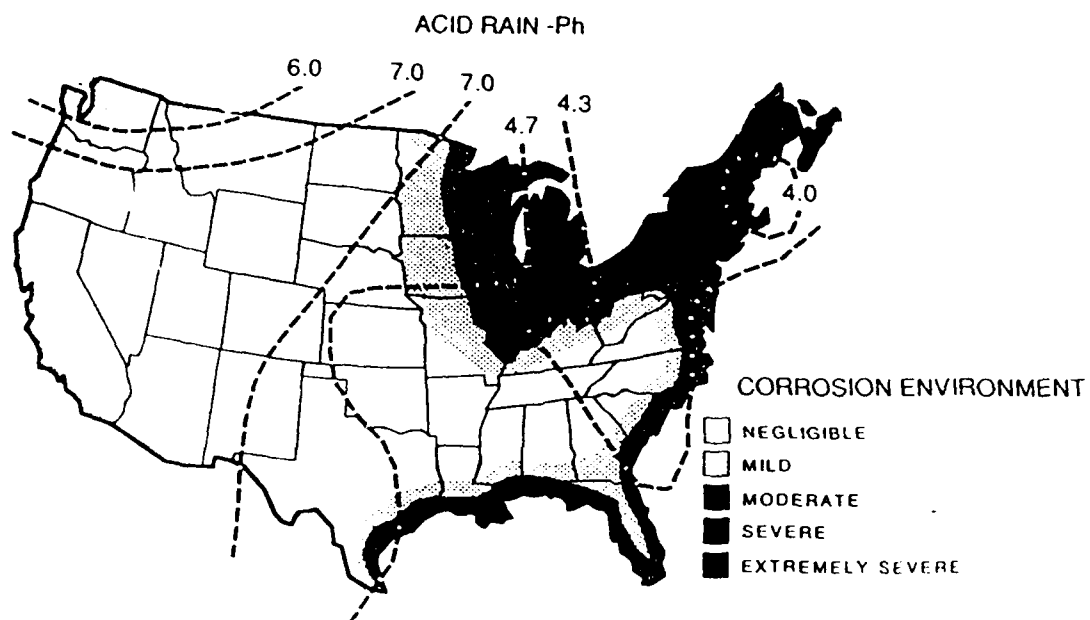


FIGURE 3 - ACIDITY OF PRECIPITATION ALONG WITH CORROSIVE AUTOMOTIVE ENVIRONMENTS IN THE UNITED STATES

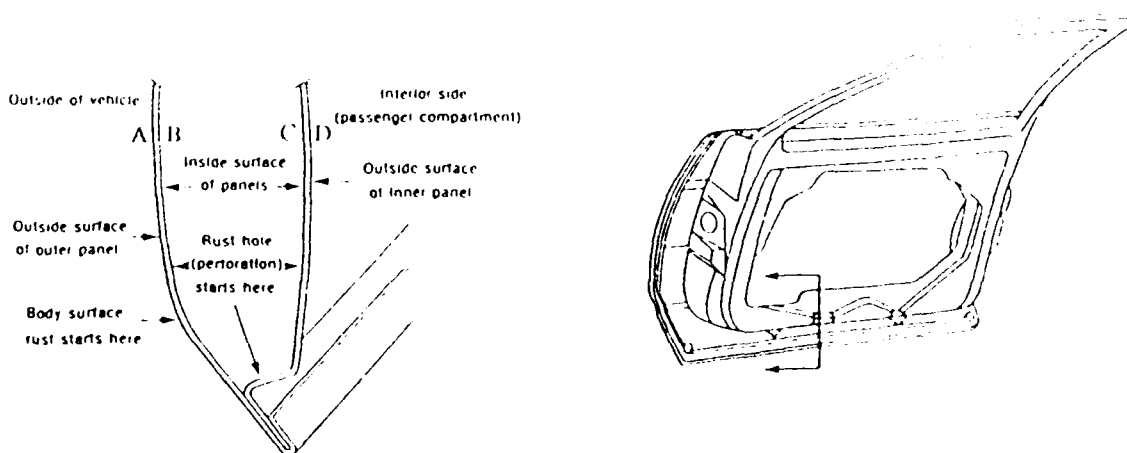


FIGURE 4 - CROSS SECTION OF A DOOR WITH TWO PANELS (INNER PANEL & OUTER PANEL)

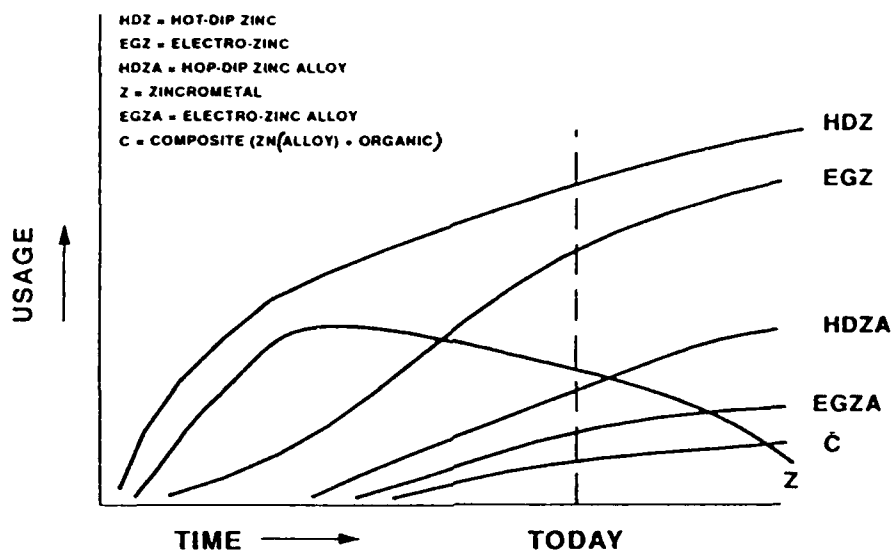


FIGURE 5 - AUTO BODY ZINC BASED PRE-COATS
USAGE TRENDS

TABLE 1⁶

COATED SHEET STEEL USAGE

NORTH AMERICAN VEHICLE MANUFACTURERS

TRENDS INTO THE '90s

MANUFACTURER	MATERIALS	EXTERIOR BODY PANELS	UNDERBODY/STRUCTURAL PANELS
A	Major - minor -	GA 50/50 EG 100/100	GA 50/50 HD 100/100
B	Major - minor -	EG 60/60	EG 60/60 HD 100/100
C	Major - minor -	EG 60/60	HD 60/60 HD 100/100
D	Major - minor -	GA 50/50	GA 50/50
E	Major - minor -	DGA 45/45	GA 45/45
F	Major - minor -	ZNO 30/30	ZNO 30/30
G	Major - minor -	ZN 30/30	ZN 30/30
H	Major - minor -	DGA 45/45	GA 45/45
I	Major minor -	DGA 45/45	GA 45/45

Key: GA - ZnFe (Galvannealed - Hot Dip or Electro)
 EG - Electrogalvanized
 HD - Hot-Dip Galvanized
 ZN - Electro ZnNi Alloy
 DGA - Double Layer ZnFe
 ZNO - ZnNi Alloy + Organic
 HDH - Hot-Dip Galvanized/Alloy

APPENDIX 1

<u>Timing (approximate)</u>	<u>Improvement</u>
1963-65	Incorporated two-sided hot-dip galvanized steel rocker panels and wheelhouses.
1968	Incorporated two-sided hot-dip galvanized steel tailgates.
1971	Incorporated anodic electrodeposition primer
1975-85	Incorporated more one-sided pre-coated steel products (i.e., Zincrometal*, one-sided galvanized steel) on fenders, hoods, doors, decklids.
1976	Incorporated immersion cathodic electrodeposition (ELPO) primer to improve perforation corrosion resistance. Most vehicle manufacturers had fully implemented this process in their assembly plant by 1985.
1976	Started to incorporate anti-chip lower body coatings.
1977	Incorporated one-sided electrogalvanized quarter panels.
1978	Canadian government issued "The Canadian Anti-corrosion Code for Motor Vehicles," which required vehicle manufacturers to warranty their vehicle against corrosion.
1980	Incorporated two-sided pre-coated steels for structural members (i.e., engine compartment rails, etc.) on new front wheel drive vehicles.
1980	Industry provided a 3 year/36,000 mile rust-through corrosion warranty. The Canadian warranty may have been different due to the Canadian Code for Rust Protection.
1982	Incorporated small crystal-size phosphate to obtain improved corrosion resistance.
1985	Improved spray phosphate systems and started to implement immersion phosphate systems to improve coverage in body cavity areas for improved perforation resistance.
1985	Incorporated more two-sided pre-coated steel products on hood, door and decklid inners. Also, two-sided pre-coated steel products were being phased into floorpans.
1985/86	Many new vehicle programs incorporated two-sided galvanized steel on all major body inner/outer panels (except roof) and all structural members.
1985/1986	Started to use weatherpac electrical connectors and stainless steel exhaust systems.

- 1987 Domestic manufacturers warranty coverage is increased.
- 1990 Most manufacturers incorporated two-sided pre-coated products to resist exterior cosmetic and interior rust-through corrosion.
- 1994-95 Most manufacturers will have two-sided pre-coated steel products (i.e., two-sided galvanized, zinc-iron, zinc-nickel or composite steels) on exterior body panels to resist exterior surface rust and corrosion rust-through corrosion.

In addition to all the material and processing changes that have occurred, many system and component part design improvements have also been incorporated into the car/truck designs starting in the 1980s timeframe to improve cosmetic, perforation and functional corrosion performance.

Electrodeposition of Zn-Fe Alloy at High Current Densities

Lu Yanping

University of Science and Technology Beijing

Dept. of Corrosion Engg.

Beijing 100083, CHINA

Wu Jixun

University of Science and Technology Beijing

Dept. of Corrosion Engg.

Beijing 100083, CHINA

Abstract

In order to electroplate the Zn-Fe alloy with high corrosion resistance onto the steel sheet, this paper discusses the plating process of Zn-Fe alloy coating at high current densities. The microstructure, phase composition, microhardness, adhesion, stable potential and corrosion resistance of electrodeposited Zn-Fe alloy are also studied by metallographic microscope, X-ray diffraction instrument, mossbauer spectrometer, microhardness tester, bending test, electrochemical determination, salt spray corrosion test and corrosion weight loss method. The results show that using electroplating a good quality, atmospheric corrosion resistance Zn-Fe alloy containing 16-17 wt% Fe can be prepared from the bath consisting of metal sulphate.

Key terms: electrodeposition, Zn-Fe alloy, current density, corrosion resistance

1. Introduction

As the rapid development of industry, environment pollution and atmosphere corrosion getting more seriously, higher and higher anti-corrosion standard and service life has been put forward for the automobile industry^[1]. As a result, various new type surface treatment steel sheet with high corrosion resistance are urgently required for the automobile industry.

In this work, the electrodeposition technology and the performance for electroplating Zn-Fe alloy on steel sheet of type 08F mild steel have been investigated, so as to determine the technological parameters for obtaining Zn-Fe alloy deposit containing 16-20 wt% Fe and the relationship between the deposit composition, structure and its performance in order to provide useful data for the industrial production.

2. Technology of Electrodepositing Zn-Fe Alloy

2.1 Composition and its function in the bath

In this work^[2], the plating bath with metal sulphate system was chosen. Composition of the bath is shown in Table 1.

Table 1. Composition of the plating bath

Composition	content, g/l	composition	content, g/l
ZnSO ₄ · 7H ₂ O	57-145	C ₆ H ₈ O ₇ · H ₂ O	0.5-1.0
FeSO ₄ · 7H ₂ O	137-224	Al ₂ (SO ₄) ₃ · 18H ₂ O	15-35
Na ₂ SO ₄	42-84	wetting agent	0.05-0.10

(1) Main salt: Zn and Fe ions in the bath are provided by ZnSO₄ and FeSO₄. When current density is in the range of 10-35A/dm², and the content of zinc sulphate (ZnSO₄ · 7H₂O) in the bath is 115g/l, and content of iron sulphate (FeSO₄ · 7H₂O) is 169g/l, the deposit of Zn-Fe alloy containing 12-20 wt% Fe can be obtained. Keeping the overall concentration of metal ions unchanged, when the content of heptahydrated iron sulphate is over 169g/l Fe content in the deposit increases linearly.

(2) Conducting salt: sodium sulphate is often used. It can increase the conductance of solution, so as to save electricity and increase the dispersion effect of plating bath. The addition quantity is about 55-75g/l.

(3) Buffer: Aluminium sulphate have good buffering effect. It makes the Ph value of plating bath stable during the electrodeposition process and increases deep electroplating property. the addition quantity is 20g/l.

(4) Stabilizing agent: In fact citric acid is the complexing agent of Fe²⁺. Its effect in plating bath is to inhibit the production of Fe³⁺. If it is not added to the plating bath, the undissolved products will be easily produced (Fe (OH)₃). That will influence the composition and quality of electroplating coating. Its addition quantity is about 0.5g/l.

(5) Wetting agent: The "HAIUO" detergent can decrease the surface tension, wet the surface of plating parts, and improve the ability for uniform electrodeposition and obtain uniform lustre deposit. The addition quantity is about 0.05-0.10 g/l. In this case, the content of "HAION" detergent is over 0.10 g/l and piebald surface was observed in deposit obtained.

2.2 Selection of operating conditions for electroplating

(1) Current density: Higher current density can be used. The Zn-Fe alloy electrodeposition coating containing 12-20 wt% Fe can be obtained when selected current density changing from 10 to 35 A/dm². If the current density is below 20 A/dm², the Fe content in the deposits obtained increases with the increase of current density, while when current density changes from 20 to 35 A/dm², Fe content in the deposits decreases, that shows the characteristic of abnormal codeposition. Considering systematically, it is better to select the current density region from 20 to 30 A/dm². in this case, the electrodeposition rate is in the region from 3.06×10^{-3} to 4.06×10^{-3} g/cm². min.

(2) pH value in the bath: The pH of plating bath can change from 1.5 to 2.5, and the optimum pH is about 1.5. A superhigh pH of the plating bath can lead to the increase of Fe³⁺ content, worse quality of the plating and decrease of the cathodic current efficiency. In general, the pH of plating bath does not

decrease naturally. However, the pH should not be controlled a overflow value, since a too low pH can lead to production of a great dal of hydrogen gas, so to decrease cathodic current efficiency. In this work, when pH value is in the range of 1.5-2.5, Zn-Fe alloy deposit containing 12-20 wt% Fe can always be obtained.

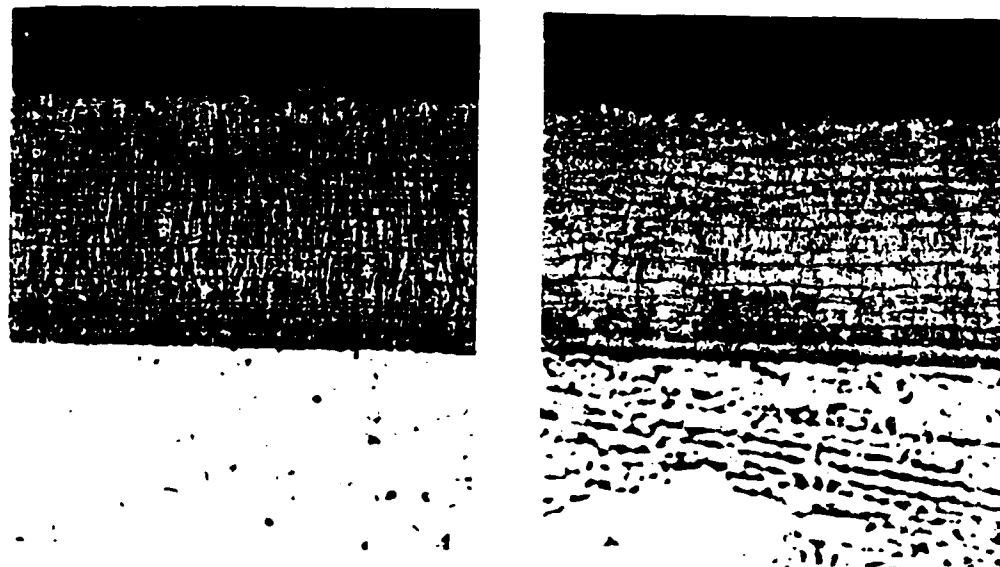
(3) Temperature: The operation temperature of plating bath is in the range of 55-60°C. In this case, the solubility of each component in plating bath and conductivity of the bath increases. As a result, higher current density (30 a/km²) can be adopted, that increases the electrodeposition rate. A superhigh temperature can lead to increase of energy consumption, inconvenient operation, and increase of the decomposition products of the organic additives in the bath, while a overflow temperature can lead to the decrease of electrodeposition rate and the uniformity of plating. the effect of temperature on Fe content in the deposit is small.

(4) Stirring: For the commonly used plating bath, properly stirring can improve the ability for uniform electrodeposition. For the bath of electroplating Zn-Fe alloy, however, stirring can make Fe²⁺ easily oxidized to Fe³⁺, so to make the appearance and tenacity of the deposit get worse, and decrease the current efficiency of plating bath. Therefore, in usual cases, stirring either by compressed air or by mechanical can't be used, but the way with moving cathode can be adopted. The moving relocity remain to be further studied.

3. Structure Characteristics of Zn-Fe Alloy Deposits

3. 1 Metallographic structure of the deposit

the criss section of specimen with electrodeposit was etched in aloohol solution containing 5% nitric acid, then exanined using XJL-01 thpe metallographic microscopy. It can be seen clearly that the etched cross section of electrodeposited Zn-Fe alloy coatings is the banded structure, as shown in fig. 1.



a) Zn-18Fe (15 A/dm²)

b) Zn-16Fe (30 A/dm²)

Fig. 1 Metallographic structure of Zn-Fe alloy deposit $\times 650$

According to F. A. Lowenheim⁽³⁾, the occurrence of banded structure is due to the faster consumption of the metal ions (Fe^{2+}) with relative potential under high current density, which lead to an increase of the concentration of the metal ions with relatively negative potential so it will deposited more, till its concentration decreases again. Therefore, the two components often periodically deposit according to certain proportion, that lead to the formation of banded structure. and with the increase of current density, this tendency gets more notably.

Under microscopy examination, it is also found that each layer is the corresponding grain layer. And this grain layer is a kind of structure with fiber or cylinder formed along electrical field direction, its structure is compact and no crack exists. Under low current density, however, since the preferential grain growth perpendicular to substrate surface, the obtained deposit structure (Fin. 1, a) shows a stronger fibre tendency compared with that with high current density (Fig. 1, b). This kind of the deposit morphology appears "honeycomb" shape, it is thin and not compact, while the deposit obtained under high current density appears continuous and fine ridge structure, its corrosion resistance increases notably, since with the increase of the cathodic current density the grain formation velocity increases.

3. 2 Phase composition of the deposit

from the X-ray diffraction results of the deposit (Table. 2), it is seen that the phase composition in Zn-Fe alloy deposit is mainly composed of η phase and δ_1 phase, secondly, of γ , ϵ phase and α -Fe with extremely small quantity. η phase is the continuous solid solution of zinc, in which the Fe content is not higher than 0.03 wt%, and η phase has hexagonal close packed lattice. δ_1 phase is close to FeZn_7 . Zn content in δ_1 phase is 88.6-93.0 wt%. δ_1 phase has also hexagonal lattice. It is very hard, but rather ductility. η phase and δ_1 phase are the internal factor for increasing the corrosion resistance of Zn-Fe alloy electrodeposit.

The study shows that the quantity of η phase and δ_1 phase is closely connected with the composition in the deposit. With the increase of Fe content in the deposit, the quantity of η phase decreases, while the quantity of δ_1 phase increases. Therefore, controlling the electrodeposit composition will be of vital importance for improving the property of electrodeposition coating.

Table. 2 X-ray diffraction analysis data of Zn-17Fe alloy deposit

lattice space $d, \text{\AA}$	corresponding phase	diffraction data ref. (4)			ASTM	
		η	δ_1	γ	ϵ	α -Fe
2.47 (9)	η	2.47				
2.37 (6)	δ_1		2.36			
2.20 (4)	γ			2.19		
2.18 (9)	δ_1		2.17			
2.14 (22)	δ_1		2.14			
2.10 (100)	η	2.09				
2.03 (2)	α -Fe					2.03
1.89 (2)	ϵ				1.90	
1.62 (2)	δ_1		1.63			
1.38 (6)	δ_1		1.39			
1.25 (2)	γ			1.25		
1.24 (3)	η	1.24				
1.17 (17)		1.18	1.18	1.18		1.17
1.16 (3)	η	1.15				

In order to further determine the local structure in the deposit, inner conversion electro mössbauer spectroscopy and X-ray back scattering mössbauer spectroscopy measurements were applied to the deposit. The analysis results show that the phase composition from surface to inner part of the deposit in $\delta_1 \rightarrow \gamma \rightarrow \delta_1 \rightarrow \epsilon + \delta_1 \rightarrow \gamma \rightarrow \delta_1$. Fe content in the deposit has little effect on the structure of electrodeposit, only the relative thickness of phase layer has some changes^[3]. This results strongly support the existance of the banded structure in the deposit.

4. Properties of Zn-Fe Alloy Deposits

4.1 Microhardness of the deposit

The hardness of Zn-Fe alloy deposit is directly related to Fe content. Table 3 shows the average value of the microhardness of Zn-Fe alloy deposit with a thickness of 30-35 μ m.

Table. 3 Microhardness value of Zn-Fe alloy deposit (50g)

NO	Fe content, wt%	hardness value (Hm), kg/mm ²					
		1	2	3	4	5	average
1	16.69	76	85	82	79	83	81
2	18.24	89	93	82	96	95	91
3	20.22	107	112	109	101	111	108

From Table 3, it is seen that the microhardness of the deposit surface increases with the increase of Fe content in the deposit. This is probaliy because more δ_1 phase existing in the deposit with higher Fe content than that with lower Fe content.

4.2 Adhesion of the deposit

The bending experiment was adopted to examine the adhesionof the deposit. When specimin of electrodeposited Zn-Fe alloy coating is survied 180° bend, the edge bended specimen is examined through bare eyes. If splitting, falling or large cracking occur in the cross section of electrodeposited coating, the adhesion is not pass. Table 4 lists the bending experiment results for Zn-Fe alloy deposit.

Table 4. The bending experiment results of Zn-Fe alloy deposit

NO	Thickness of deposit, mm	Fe content in deposit, wt%	90°bend	180°bend
1	0.025	17.13	cracking	unsplitting
2	0.028	16.78	cracking	unsplitting
3	0.053	16.69	cuacking	splitting
4	0.050	18.24	cracking	splitting
5	0.051	20.21	cuacking	falling

The results show that all specimens produce cracks after bended. Specimen of alloy deposit above 50 μ m

thick and 16-20 wt% Fe content produces splitting after bended to broken. This shows that the adhesion of the deposit is worse and practical use value. While no any spitting and falling were observed for the specimen with the deposit of 25.2 μ m and 28.4 μ m thick, 16-17 wt% Fe content. This shows its good adhesion. Therefore, the adhesion of Zn-Fe alloy deposit is related to not only deposit composition but also to the thickness of the deposit. In this work, to obtain the deposit with good adhesion, the thickness of the deposit is 25-30 μ m, Fe content in the deposit is 16-17 wt%.

4. 3 Stable potential of deposit

In order to predicate the electrochemical character of Zn-Fe alloy deposit in atmospheric environment, the stable potential for the specimen in 5% NaCl aqueous solution was measured using M351 corrosion measurement system. The results measured are listed in talbe 5.

Tbale 5. Stable potential of Zn-Fe alloy deposit (298k)

NO	Fe content, wt%	Potential valur, V (SCE)
1	0.01 (Pure zinc)	-1.058
2	16.19	-1.037
3	18.06	-1.028
4	20.21	-1.009
5	08F	-0.640

From Talbe 5, it is seen that the electrode potential of Zn-Fe alloy deposit with 16-20 wt% Fe content is close to that of pure zinc, but more negative that 08F mild steel, so this kind of the deposit can provide electrochemical protection to mild steel and decrease the corrosion rate of mild steel. It is also shown that the potential of Zn-Fe alloy deposits is a little positive than pure zinc and more towards more positive direction with the increase of Fe content in the deposit. So the corrosion rate of Zn-Fe alloy deposit is smaller than that of pure zinc, this is beneficial to the painting ability of the deposit.

4. 4 Corrosion resistance of the deposit

The corrosion resistance of the deposit is studed using YW65-1 type salt spray tester. The test factors are as follows; 5% NaCl aqueous solution, pH is 6.5, temperature is $35 \pm 1^\circ\text{C}$. The spraying way is an hour spraying 15 minutes and stopping 45 minutes, in a day as a period, spraying test continueing 8 hours, then stopping 16 hours. The expreimental results are listed in Talbe 6.

Table 6. Salt spray corrosion test

Observation or measurement		Zn-Fe alloy deposit			08F mild steel
		16% Fe	18% Fe	20% Fe	
Appearance change of the sample	24h.	irregular white rust spots			much brown rust specks
	48h.	little white rust specks	more white rust		brown rust layer
	72h.	uniform thin white rust layer			thick rust layer
	144h.	uniform paste white rust			extremely attacked, loose rust layer
Corrosion rate, mm/a		0.57	0.67	0.75	0.45

From Table 6, it is seen clearly that after 144 hours salt spray, 08F mild steel was rusted seriously, and thick and loose yellow rust produced. While for the mild steel with Zn-Fe alloy deposit containing 16-20 wt% Fe, only some white corrosion products produced on the surface of plating coating, but steel substrate is not corroded. This shows that the deposit has the effect of cathodic protection on steel sheet (see Table 5). In this case, the stable potential of the deposit does not get more negative. on the contrary, it moves towards positive direction ($-0.998 \sim -1.011$ V vs. SCE). So as anodic coating, this kind of Zn-Fe alloy deposit is effective for prevent atmospheric corrosion.

It is also found that Fe content has obvious effect on the corrosion resistance of the deposit. When Fe content is increased from 16 wt% to 20 wt%, the corrosion rate is increased from 0.57mm/a to 0.75 mm/a. This is because that during the Zn-Fe alloy electrodeposition process, it is difficult to obtain holeless deposit. if Fe content increases (or more accurately, the quantity of δ_1 phase increases) the Zn/ δ_1 phase galvanic corrosion effect increases, so to decrease the service life of the deposit. Among them, corrosion rate of Zn-Fe alloy deposit containing about 16 wt% Fe has least.

5. Conclusions

(1) Using metal sulphate system plating bath, Zn-Fe alloy electrodeposit containing 16-20 wt% Fe was obtained.

(2) The composition and structure of Zn-Fe alloy deposit mainly depend on the Fe^{2+}/Zn^{2+} ratio and the cathodic current density.

(3) Increasing Fe content in the deposit will make the quantity of δ_1 phase in the deposit and the surface hardness increase, that lead to decrease of adhesion and corrosion resistance.

(4) It is completely feasible to use the Zn-Fe alloy deposit containing 16-20 wt% Fe as the anti-atmosphere corrosion coating of mild steel sheet. Among them, Zn-Fe alloy deposit with 16-17 wt% Fe content and a thickness about 30 μ m has the best adhesion and corrosion resistance.

References

1. H. Takeshi, SAE 885043 (1988)
2. F. A. Lowenheim "Modern Electroplating". Third Edition, A Wiley-Interscience Publication,

(1974)

3. Lu Yanping et al, Plating and Finishing (Chinese) 93 (1987) P. 21

4. H. Tomihiro et al, Trans. ISIJ, 11 (1983) P. 956

5. J-X Wu, Y-P Lu et al, Proc. International conferece on Znic and Znic Alloy Coated Steel Sheet (Tokyo, Japan, Sept. 5-7 1989) P. 619

Hydrothermal Properties of Protective Polymer Coatings on Steel

Richard D. Granata
Zettlemoyer Center for Surface Studies
7 Asa Drive
Bethlehem, PA 18015

Kevin J. Kovaleski
Zettlemoyer Center for Surface Studies
and Department of Chemistry
Lehigh University
6 East Packer Avenue
Bethlehem, PA 18015

Abstract

Large impedance changes were observed when measurements were made of protective polymeric coatings treated hydrothermally (heated water) at 60°C versus ambient laboratory conditions using electrochemical impedance spectroscopy (EIS). These data were compared to condensing humidity and adhesion tests. A two-coefficient equation ($\text{Rating} = A_1X_1 + A_2X_2$) yielded 96% correlation. Good agreement was obtained using this relationship to predict condensing humidity performance of 4 coatings systems. A chemical model suggests that polymer properties can be selected to optimize hydrothermal properties for specific service conditions. EIS data can be rapidly generated and correlated to long-term or concurrently generated data for predicting new coatings performance.

Key terms: polymer coating, degradation, mechanism, steel, corrosion, hydrothermal, blistering, electrochemical impedance, accelerated testing, epoxy coating, condensing humidity

Introduction

Polymeric coatings are commonly evaluated using accelerated laboratory tests: salt fog or spray (ASTM B117, American Society for Testing and Materials, Philadelphia, PA), modified salt exposure tests (e.g. salt fog with added SO₂, ASTM G85), and various cyclic exposure tests (ASTM D2246, D2933 or G89). Humidity exposure (ASTM D870) and physical resistance tests (adhesion, ASTM D2197 and D3359; impact resistance, ASTM D256; etc.) are widely used as preliminary tests. However, none of the laboratory corrosion tests is entirely satisfactory, despite their long and general use. Standard laboratory methods to establish comparative rankings of the corrosion performance of different materials are especially susceptible to error, and samples evaluated under such tests frequently show substantial differences from those exposed to the environment¹.

Polymer coatings degradation mechanisms associated with corrosion processes have been studied extensively in our laboratory²⁻⁹. Emphasis has been placed upon special adaptations of analytical techniques for investigating the coating/metal interface. Auger, X-ray photoelectron, Mössbauer, NMR, FTIR, dielectric, vibrational and positron annihilation lifetime spectroscopies have been used in studies of the coatings and their interphases with metal substrates. Electrical and electrochemical techniques have been useful evaluation tools for protective organic coatings^{10,11}. Resistance and impedance data determined for a variety of exposure conditions have provided important information on protective organic coatings properties. Coating porosity, water uptake and permeability to ions can be studied electrochemically.

Coatings investigations using electrochemical methods are usually conducted under ambient laboratory conditions (15-25°C) as a function of immersion time. Effects of water at constant temperature on coatings performance is becoming well characterized. However, many practical coatings applications involve service at elevated temperatures which is reflected by the numerous test methods requiring 38-74°C or higher¹². Accelerated cyclic test procedures often use elevated temperature in at least one stage⁶. Coatings must withstand heat sterilization procedures in the food packaging industry or accelerated test conditions of 85°C/85% RH (relative humidity) and 121°C/2 atm steam in the electronics industry⁷. A better understanding of coatings' protective behaviors subjected to elevated temperature is warranted. This paper presents progress in developing a useful mechanism describing the hydrothermal properties on protective organic coatings for steel. Also, a procedure is demonstrated which may be applicable to developing useful correlations between short-term EIS measurements and long-term service conditions or tests.

Experimental Methods

Electrochemical impedance spectroscopy^{2,5,7,13} (EIS) and positron annihilation lifetime spectroscopy^{8,9,14} (PALS) are the focus of recent and on-going work in our laboratory on protective polymer coatings characterization. EIS studies can readily determine the presence and extent of coatings defects by electrical conduction through the coating^{4,5,15-18}. However, some of the more intriguing findings are those in which no physical defect can be readily identified^{19,20}. In the absence of defects, the mechanism of coatings protection or degradative failure is not easily understood. Increasing emphasis is being placed upon cyclic environmental exposures used as evaluation methods^{6,21}. Thermal effects are important in studies of organic protective coatings, particularly with respect to materials transport into coatings. PALS provides the ability to evaluate coatings properties' changes nondestructively, in situ and non-invasively^{9,22}. Responses to water or solvent ingress and temperature-dependent changes can be readily monitored²³. The PALS technique is described in another paper of this proceedings¹⁴. The majority of this paper concerns EIS methods with PALS data used in the model development.

Specimen preparation

Epoxy. Specimens were prepared from 10 x 15 x 0.05 cm SAE-1010 steel panels. The panels were wet ground with 240 grit SiC paper, rinsed with ethanol and dried in warm air with a blow-drier. Table 1 describes the components of the coatings. The coatings formulations and cure conditions for the EIS studies are given in Table 2. Each formulation contained 0.06-0.09% by weight surfactant (last item, Table 1) to improve cured film properties. Formulations were applied by draw bar at a thickness of 100 μm wet. After curing, the panels were cut into 5 cm squares. Final cured thicknesses ranged from 54 to 66 μm . An additional set of coatings was prepared based on the E1 system using resin-hardener ratios of 3:2, 1:1 and 2:3. The non-stoichiometric mixtures were prepared for evaluation of resin or hardener excess on hydrothermal behavior.

Polybutadiene. Substrates for polybutadiene specimens were prepared in the same manner, but were cut into 5 cm squares before applying the coating. Polybutadiene was applied by spin-coating²⁴ and cured by baking at 195°C for 30 min. Cured-film thickness was 30 μm .

Polyester Baking Enamel. A melamine-type polyester enamel coating was applied by spin-coating. The enamel was baked at 190°C for 20 min and equilibrated at RT and 50% RH for 1 d before testing. Cured-film thickness was 60 μm .

Urethane. A general-purpose, two-part urethane was applied by spin-coating and cured under ambient conditions of 22°C and 50% RH for 7 d before testing. Cured-film thickness was 40 μm .

Polyimide. Polyimide samples were prepared in a similar manner as the polybutadiene samples. The polymer was an imide of pyromellitic dianhydride (PMDA) and 4,4'-oxydianiline (ODA). Polyimide was cured 12 min at 85°C followed by 20 min at 200°C, giving a final film thickness of 10 μm .

EIS Method

Data were obtained from a system consisting of a PARC Model 173/179 potentiostat-electrochemical controller (EG&G Princeton Applied Research Corp., Princeton, NJ) with a computer-controlled Solartron 1250 Frequency Response Analyzer (Schlumberger, Elmsford, NY). The impedance spectra were determined from 65.5 kHz to 3.1 mHz. The input amplitude was 15 mV above 100 mHz and 50 mV below 100 mHz. A diagram of the impedance measurement system is shown in Figure 1.

The electrochemical cell consisted of a glass cylinder clamped and o-ring sealed to the specimen surface. The seal exposed 8.8 cm^2 of specimen surface to the distilled water test medium ("electrolyte"). Distilled water provided adequate conductivity for these studies relative to the highly resistive coatings. The reference electrode was Ag/AgCl, and a high density graphite rod served as the counter electrode. Spectra obtained for polymer coated specimens were evaluated using equivalent circuit models shown in Figure 2. The evaluations were carried out using non-linear least squares analyses²⁵. The results of the analyses indicated that Model 1 was usually more satisfactory than Model 2 for short-term hot water exposures; a single inflection was observed in $\log |Z|$ versus $\log f$ plots and is indicative of one time constant (a parallel RC pair). Model 1 was satisfactory in cases of a single inflection in $\log |Z|$ versus $\log f$ plots obtained on defect-free coatings, whereas Model 2 was useful in more complex cases involving coatings defects. Typical coating degradation with defect development versus exposure time as monitored with EIS is shown in Figure 3: The initial spectrum transforms to impedance behavior consistent with Model 2 in which an irreversible defect forms due to corrosion processes.

Hydrothermal Method. Defect-free coatings yielded impedance spectra similar to those shown in Figure 4 when subjected to hydrothermal measurement sequences. The hydrothermal studies were conducted on a separate specimen for each sequence, beginning and ending at RT (RT = 22°C), through one of three elevated temperatures (40, 60 or 80°C). The typical sequence is shown in Figure 5 and consisted of: (1) Impedance spectrum taken at RT in water (this procedural step was designated, RT1); (2) Specimen incubated in water at the test temperature for 1.5 h and the impedance spectrum taken at the elevated temperature (this step was designated by the temperature used, e.g. 60°C); (3) Specimen equilibrated in water at RT for 1.5 h and a spectrum recorded (designated RT2); and (4) Specimens equilibrated at ambient laboratory conditions (22°C and 50% RH) for 1 week before a final spectrum was begun immediately after filling with electrolyte (final step designated RT3).

Additional impedance measurements were made using powdered graphite as the conductive phase between the specimen and counter electrodes to determine the response to temperature in the absence of an electrolyte or water. The ratio of the capacitance at 60°C to that at RT is defined as the dielectric temperature ratio (DTR). Results from these measurements will be reported as DTR values.

Differential Scanning Calorimetry (DSC) Method

A Mettler DSC 30 with TC10A TA processor (Mettler Instrument Co., Hightstown, NJ) was used to determine glass transition temperature range for each of the coatings. Each coating was carefully removed from the metal substrate and placed in a tared analysis pan. The sample weight was determined and entered into the instrument for use in calculations.

Polymers undergo significant changes in physical properties at their glass transition temperature. Therefore, the coating glass transition temperature was evaluated as a possible explanation for large

differences in hydrothermal properties. For glass transition determination, the sample was cooled to -150°C for 2 min followed by measurement while heating 10°C/min to 250°C. The DSC data were analyzed with the integral processor to obtain the results.

Condensing Humidity Exposure Method

Panels were subjected to condensing humidity at 40°C following ASTM Standard Method D4585. A benchtop unit was assembled using a constant temperature water bath and acrylic sheet housing to hold the test panels and to confine the moisture within the chamber. Sets of sixteen panels were evaluated. Panel dimensions were 6 x 15 x 0.05 cm. The panel edges were protected with plastic tape. The test panels were evaluated after 72 h in the chamber. The specimens were removed, dried and representative micrographs were made (50X) using a light microscope. The photographs were evaluated with a LECO Model 2001 Image Analysis System (LECO, St. Joseph, MI) to determine the percentage area underfilm rusting, and then rated (0-10; 10 = best) using ASTM Standard Method D610.

Karl Fischer Water Determination

Adsorbed water under non-immersed conditions was considered for explaining the differences in hydrothermal response. Free films were equilibrated in constant humidity chambers (0.1, 39 and 100% RH) for one week. Water content was determined in the free films by use of the Karl Fischer titration method: An Aquatest IV (Photovolt Corp., New York, NY) was titrated to zero without sample; the weighed, free film sample was introduced into the vigorously stirred titration chamber and was titrated repetitively to zero until no significant readings were obtained; water content was the sum of the readings. The Karl Fischer solvent system extracted water from the coating during the titration procedure. The procedure used was recommended by the manufacturer for this type sample.

Statistical Methods

Analyses of the data were performed using matrix correlation and multiple linear regression programs²⁶. Data and calculated results were correlated to ASTM D610 results.

Results

EIS

Hydrothermal effects typically observed with the epoxy polymer matrices are presented in Figure 6 as the average results for three replicates. The sensitivity limit for the measurement system with 8.8 cm² specimen area is approximately 10¹¹ ohm·cm². Consequently, the low frequency impedance may be higher than this sensitivity limit which should be considered a minimum value in cases where this value is obtained. The 60°C log |Z| values show changes of 1-5 log units versus the RT values. The urethane coating showed the largest change and failed to return to its initial value upon equilibration at RT. Permanent degradation of the urethane coating occurred at 60°C during the short exposure period. The epoxy, polybutadiene and polyester exhibited smaller changes than the urethane, and no permanent changes to these coatings were observed due to the single, short duration thermal exposure. These results are a summary of the general impedance responses obtained for polymeric coatings subjected to transitory hydrothermal conditions (exposures to heat and aqueous media). Figure 7 presents an example of a cyclic exposure test used in the automotive industry⁶. Note the similarities between the individual phases of the exposure cycle (Figure 7) to the hydrothermal EIS measurement conditions (Figure 5). Similar impedance changes may occur during cyclic, accelerated exposure tests. Figures 8-10 are plots of responses of fifteen epoxy coatings to thermal transitions during water exposure. Four additional coatings were subsequently evaluated to test predictions based on the results of the first set (15 coatings). Those results are presented in Figure 11.

Table 3 lists the water uptake values calculated from EIS results obtained for coating system E1 with stoichiometric and nonstoichiometric mix ratios. Water uptake was calculated using a modified Brasher formula²⁷,

$$\text{WATER UPTAKE } (\%)_{60^{\circ}\text{C}} = \frac{\text{Log} \left(\frac{C_{c,60^{\circ}\text{C}}}{C_{c,RT1}} \right) - \text{Log}(DTR)}{\text{Log } 67} \quad (1)$$

where $C_{c,60^{\circ}\text{C}}$ and $C_{c,RT1}$ are the coatings capacitances obtained for 60°C and RT1 measurements, DTR is the dielectric temperature ratio and 67 is the dielectric constant of water at 60°C.

Condensing Humidity

The fifteen epoxy coatings of Figures 8-10 and the four epoxy coatings of Figure 11 were subjected to condensing humidity for 72 h using a water temperature of 40°C. The exposure results for the sets of 15 and 4 coatings are presented graphically in Figures 12 and 13, respectively, as digitized images of the samples' micrographs with label and ASTM D610 rating for each specimen. These ratings were correlated with each of the coatings properties measurements.

Differential Scanning Calorimetry

Table 4 shows glass transition temperatures, T_g and low frequency, logarithm impedance values at 60°C obtained for several coatings. The intent of these data is to illustrate the independence of T_g and hydrothermal effects: Coatings, PBD, PE and PI, were determined to have high, moderate and low T_g values but very similar impedance values. Thus, no relationship appears to exist between T_g and hydrothermal effects.

Karl Fisher Determination

Table 5 lists data for water in epoxy films obtained by the Karl Fischer method. Individual samples were equilibrated at each relative humidity for one week before analyses. These data provide independent evidence of the range of water interactions observed for these coatings versus the empirical Brasher formula (capacitance data). The fifteen coatings of the same types in Figures 8-10 were equilibrated one week at 75% RH before analyses. The data were used in the statistical methods.

Discussion

Generally, high $\log |Z|$ values at low frequency are indicative of low conductivity, protective coatings. Comparison of impedance values in Figures 8-10 suggest: 1) The cured polymer structure has a stronger influence on impedance than the presence of hydrophilic (\sim I) or hydrophobic (\sim O) solvents. Epoxy systems E1 and E2 exhibited relatively small changes in $\log |Z|$ values at low frequencies on increasing temperature. This statement is true for those systems with and without solvent. 2) Hydrophobic solvents promote lower conductivity coatings versus hydrophilic solvents. This finding suggests that residual hydrophobic solvent will enhance the water resistance of coatings containing solvents. Low transmission rates for water may appear to be a desirable protective coating property for slow degradative processes, but could be undesirable if water which slowly penetrated the coating needed to be rapidly released. 3) The absence of solvents in the epoxy formulations does not appear to adversely affect the water resistance.

The impedance results for the four additional coatings plotted in Figure 11 are generally high values relative to initial set of fifteen coatings. Coating E9-I exhibits highest low frequency impedance values at RT of all coatings in this study. Also, the coating has an appreciable hydrothermal response at 60°C.

One hypothesis is that this behavior represents ideal behavior in which very high resistance to charge transport occurs at low temperatures, resistance decreasing significantly with increasing temperature while maintaining high resistance relative to other coatings. The coating can strongly resist ingress of water at low temperatures and permit egress of water with increasing temperature. This hypothesis is supported by the condensing humidity test results.

Figure 12 presents results of the condensing humidity tests (ASTM D610) performed on the first set of coatings. The results are qualitatively in agreement with expectations for these polymer systems. Correlation of the EIS data was desired to enable predictive capabilities based upon the relatively short EIS test procedure. In this study, all EIS data were acquired before any other performance test was performed. After obtaining the EIS data, the condensing humidity test (ASTM Standard Method D4585) was selected, performed on similarly prepared specimens and evaluated using ASTM Standard Method D610. Although the EIS test cycle was one week versus 72 h for condensing humidity test, equilibration at RT3 may occur in a considerably shorter time period, for example, 3 h. More importantly, the method described here can be applied to service data or long-term test procedures. In those cases, one week would be relatively short compared to years of exposure or service time.

Matrix correlation and multiple linear regression procedures were used to establish a useful relationship of condensing humidity to EIS test results. Table 6 lists and defines the parameters used in these statistical procedures. Table 7 lists the data and calculated values described in Table 6. All parameters and the correlation process are described in detail elsewhere²⁸. Parameters were reduced to two by statistical criteria using the matrix correlation procedure. The most significant parameters were TAUDTR and TAURT3. The two parameters accounted for 96% of the observed variations. The TAUDTR parameter combines coating resistivity and capacitance and applies a correction factor related to dry polymer mobility as a function of temperature. In this manner a measurement is obtained characterizing the polymer's role in pore resistance or capacitance changes. The TAURT3 parameter provides a measure of permanent changes which may have occurred in the coating as a result of ingress and egress of water during hydrothermal response. (Effects of mobile phases other than water may be evaluated by experiments analogous to these hydrothermal measurements.) Multiple linear regression procedures were used to obtain an equation for predicting the performance of similar coatings based upon the two most significant parameters. The equation is:

$$\text{Predicted Rating}_{\text{ASTM D 610}} = A_1 \times \text{TAUDTR} + A_2 \times \text{TAURT3} \quad , \quad (2)$$

where TAUDTR and TAURT3 are defined in Table 6, and A_1 and A_2 are coefficients obtained by multiple linear regression analysis.

Equ. 2 was tested as follows: Four additional epoxy coatings materials were selected, E7, E9-I, E10 and E11, impedance measurements acquired and the values of TAUDTR and TAURT3 were used to calculate predicted ASTM D610 ratings. Coated panels were prepared with these epoxy materials and subjected to condensing humidity for the same time as the first set of coated panels. The predicted (Eqn. 2) and actual ratings (Fig. 13) are given in Table 8. Comparison of predicted to actual values indicates an excellent agreement in three of the cases and very good agreement in the fourth case, E10. Also, the prediction for coating E9-I was greater than the maximum rating of 10 which suggests that the coating is better than all coatings used to obtain the initial relationship. This prediction is possible since the parameters do not have a maximum limit. Thus, it may be possible to develop a coating appraisal system based upon long periods of exposure times and short-term impedance measurements. The appraisal system based on hydrothermal impedance measurements enables ranking and prediction of coatings

performance. Correlation of the results to the performance test of choice or existing service data can be used to modify coatings properties with reduced dependence on long-term tests. Results correlation to appropriate or required performance tests can be used to estimate coating lifetime with minimized long-term evaluation. Service life tests can be reserved for coatings with superior lifetime estimates.

A schematic model describing water/polymer/solvent interactions for the hydrothermal effect is given in Figure 14. The model is based upon several observations. Table 3 suggests the unreacted coating components having hydrophilic moieties enhance water uptake or polymer/water interactions. Table 5 data and the results of statistical procedures demonstrate that the polymer structure has a strong influence on water uptake and protective coating performance. Also, coatings having excellent protective properties are not inert to water but actually benefit from the presence of small water concentrations. These coatings may "swell" very slightly and plug conductive pathways. The two dimensional model in Figure 14 attempts to accommodate these concepts by showing polymer response to water ingress. Conformational changes occur affecting the conductive properties of the coating. The changes may be beneficial or detrimental depending upon the cured film structure, the ratio of hydrophobic/hydrophilic components, and the difference between hydrophobic and hydrophilic properties. The hydrophobic/hydrophilic properties can be estimated by calculations based upon polymer structure²⁸. Polymer structures may be selected to optimize hydrothermal properties for specific service conditions.

Summary

This paper presents the initial explanation of the hydrothermal properties of protective organic coatings based upon EIS observations. The hydrothermal properties described here are primarily due to polymer/water interactions accelerated by thermal processes and are readily measured by EIS. Summary statements are as follows:

1. Impedance measurements made as a function of temperature enable better discernment of coating property differences.
2. Both capacitive and resistive properties change dramatically with exposure to water at elevated temperature: Resistive properties exhibit larger changes.
3. Combined RC factors obtained at elevated temperature may provide useful criteria for ranking coatings.
4. A rating procedure has been described ($\text{Rating} = A_1X_1 + A_2X_2$), and predictions of performance in condensing humidity tests based on this equation were very good.
5. Information on the role of water and temperature factors in coatings degradation processes can be monitored using procedures based upon hydrothermal impedance studies.
6. Solvents may be detrimental to coating performance by providing channels for water ingress or by blocking channels for water egress.
7. Information derived from hydrothermal studies is useful in development of more detailed models for protection by coatings.

Acknowledgement

The authors are grateful for the support provided by the Office of Naval Research, Grant No. N00014-90-J-1229.

References

1. R.A. Dickie and F.L. Floyd, "Polymeric Materials for Corrosion Control," R.A. Dickie and F.L. Floyd, eds., ACS Symposium Series 322, (Washington, DC: American Chemical Society, 1986), p. 5.
2. H. Leidheiser, Jr. and R.D. Granata, IBM Journal of Research and Development, 32 5 (1988): p. 582.
3. R.D. Granata, M.A. De Crosta, J.F. McIntyre, and H. Leidheiser, Jr., Industrial Engineering and Chemical Product Research and Development, 26 (1987): p. 427.
4. J.M. Atkinson, R.D. Granata, H. Leidheiser, Jr., and D.G. McBride, IBM Journal of Research and Development 29 1 (1985): p. 27.
5. R.D. Granata, P. Deck and H. Leidheiser, Jr., Journal of Coatings Technology, 60 763 (1988): p. 41.
6. H.E. Townsend, R.D. Granata, D.C. McCune, W.A. Schumacher, R.J. Neville, Proceedings of the Fifth Automotive Corrosion and Prevention Conference and Exposition, Dearborn, MI, October 21-23, 1991, SAE Technical Paper Series, paper no. 912275 (Warrendale, PA: SAE International, 1991).
7. R.D. Granata, K.W. Tiedge and H.L. Vedage, Second International Symposium on Corrosion and Reliability of Electronic Materials and Devices, The Electrochemical Society Meeting, Toronto, CANADA, October 11-16, 1992, accepted.
8. R.D. Granata, M. Moussavi-Madani and R.C. MacQueen, CHEMTECH, December (1992): p. 724.
9. R.C. MacQueen and R.D. Granata, Journal of Polymer Science, accepted for publication.
10. H. Leidheiser, Jr., Progress in Organic Coatings 7 (1979): p.79.
11. H. Leidheiser, Jr., Journal of Coatings Technology 63 802 (1991): p.20.
12. "Annual Book of ASTM Standards," American Society for Testing and Materials, (Philadelphia, PA: American Society for Testing and Materials, 1990): ASTM Designations; D 870 - Water Immersion Test of Organic Coatings on Steel (38°C or other), D 1735 - Water Fog Testing of Organic Coatings (38°C), D 2246 - Finishes on Primed Metallic Substrates for Humidity-Thermal Cycle Cracking (38°C), D 2247 - Coated Metal Specimens at 100% RH (38°C), D 2248 - Detergent Resistance of Organic Finishes (74°C) and G 42 - Cathodic Disbonding of Pipeline Coatings Subjected to Elevated or Cyclic Temperatures (60°C).
13. R.D. Granata and K.J. Kovalski, in "Electrochemical Impedance: Analysis and Interpretation, ASTM STP 1188," J.R. Scully, D.C. Silverman and M.W. Kendig, eds., (Philadelphia, PA: American Society for Testing and Materials, 1993), p. 450.
14. R.D. Granata, R.C. MacQueen and K.J. Kovalski, This proceedings.
15. M.W. Kendig and J. Scully, Corrosion 46 1 (1990): p.22.
16. H.P. Hack and J.R. Scully, Journal of the Electrochemical Society 138 1 (1991): p.33.
17. S. Haruyama, M. Asari and T. Tsuru, in "Corrosion Protection by Organic Coatings," M.W. Kendig and H. Leidheiser, Jr., Eds., The Electrochemical Society, Proceedings Volume 87-2, (1987): p.197.
18. H. Leidheiser, Jr., D.J. Mills and Wayne Bilder, in "Corrosion Protection by Organic Coatings," M.W. Kendig and H. Leidheiser, Jr., Eds., The Electrochemical Society, Proceedings Volume 87-2, (1987): p.23.
19. J.E.O. Mayne and D.J. Mills, Journal of the Oil and Colour Chemists' Association 58 (1975): p.155.
20. H. Leidheiser, Jr., R.D. Granata and R. Turoscy, Corrosion 43 5 (1987): p.296.
21. B.S. Skerry, Journal of Coatings Technology 60 765 (1988): p.97.
22. Cs. Szeles, K. Suveg, A. Vértés, M.L. White, and H. Leidheiser, Jr, Journal of Coatings Technology 60 758 (1988): p.47.
23. R.C. MacQueen, PhD Dissertation, Lehigh University, October, 1992.
24. T.C. Patton, "Paint Flow and Pigment Dispersion," 2nd ed., (New York: John Wiley & Sons, 1979), p. 584.
25. J.R. Macdonald, "LEVM/OLSON Complex Non-Linear Least Squares Fitting Program," Dept. of Physics and Astronomy, University of North Carolina, Chapel Hill, NC 27599-3255 (1988).
26. D.P. Doane, "Exploring Statistics with the IBM PC," Addison-Wesley Pub. Co., New York (1988).
27. D.M. Brasher and A.H. Kingsbury, Journal of Applied Chemistry 4 (1954): p.62.
28. K.J. Kovalski, PhD Dissertation, Lehigh University, expected October, 1993.

Table 1. Epoxy Coating Components

Material	Equivalent Weight (g/eq)	Description	Solvent	Solubility in H ₂ O
Resin-1	172-176	diglycidyl ether of bisphenol A (DGEBA)	none	none
Resin-2	175-205	polyglycol diepoxide	none	slight
Resin-3	172-179	novolac epoxy	none	< 1 %
TETA	24.4	triethylenetetramine	none	complete
Hardener-1	116	polyamide resin	none	0.5 %
Surfactant - polyether modified dimethyl-polysiloxane copolymer	---	monophenyl glycol, 12.5 % solution	xylene	----

Table 2. Epoxy Coatings Systems for Impedance Measurements

POLYMER SYSTEM	CODE		
	NO SOLVENT	HYDROPHOBIC SOLVENT*	HYDROPHILIC SOLVENT*
Resin-1 TETA	E1	E1-O	E1-I
Resin-1 Hardener-1	E2	E2-O	E2-I
Resin-2 Hardener-1	E4	E4-O	E4-I
Resin-1:Resin-2 (1:1) TETA	E5	E5-O	E5-I
Resin-1:Resin-2 (1:1) Hardener-1	E6	E6-O	E6-I
Resin-1:Resin-2 (8:2) TETA	E7	---	---
Resin-3 Hardener-1	---	---	E9-I
Resin-1:Resin-2 (7:3) TETA	E10	---	---
Resin-1:Resin-2 (6:4) TETA	E11	---	---

15 Systems: Solventless, Hydrophobic or Hydrophilic
(* 5 % solvent before oven cure)

4 Systems: Added for proof of ranking prediction
(E7, E9-I, E10 & E11)

All Systems: Cured 2 h at 100°C

Table 3. Water Uptake by EIS for E1 System versus Resin:Hardener Ratio.

Epoxy:Hardener Ratio (equivalents)	3:2	1:1	2:3
Water uptake (volume %)	5.45 ± 0.15	2.47 ± 1.48	8.43 ± 0.02

Table 4. Glass Transition Temperatures and Low Frequency Impedance

Coating	T _g (midrange, °C)	Log f at 0.003 Hz (60°C)
E1	112	8.8
E2	65	8.9
E4	0	6.6
PBD	-36	9.9
PE	37	9.1
PI	220	9.3

Table 5. Water Present in Epoxy Films Determined by Karl Fischer Method

Film	Water Content in PPM of Films Equilibrated in Air		
	0.1% RH	39% RH	100% RH
E1	< 1	< 1	540 ± 20
E2	8.0 ± 0.2	68 ± 7	800 ± 8
E4	31.0 ± 0.3	220 ± 4	10800 ± 110

Table 6. Data and Calculated Results Used in Statistical Analysis

Parameter Name	Description
ASTM	ASTM D610 rating for 72 h in condensing humidity.
POSINT	Positron annihilation intensity (I_3)
POSFV	Positron annihilation free volume ($I_3\tau_3$)
TAUDTR	Time constant defined: $R_{po}(60^\circ\text{C}) \times C_c(60^\circ\text{C})/\text{DTR}$. DTR is the dielectric temperature ratio, $C_c(60^\circ\text{C})/C_c(\text{RT1})$, for dry polymer substituting powdered graphite for the aqueous medium.
LOG-R-	Logarithm of R_{po} at 60°C .
TAU60	Time constant defined: $R_{po} \times C_c$ at 60°C .
LOGRC60	$\log R_{po} - \log C_c$ at 60°C .
LOGRCDTR	$\log R_{po} - \log C_c/\text{DTR}$ at 60°C .
WURT2	Water uptake at RT2 with respect to RT1 (Brasher formula).
C0	Initial capacitance at RT1.
CRT2	Capacitance value at RT2
LOGRCRT2	$\log R_{po} - \log C_c$ at RT2.
LOGRCRT3	$\log R_{po} - \log C_c$ at RT3.
TAURT2	Time constant defined: $R_{po} \times C_c$ at RT2.
CRT3	Capacitance value at RT3.
WURT3	Water uptake at RT3 with respect to RT1 (Brasher formula).
C60	Capacitance value at 60°C .
C60DTR	Capacitance value at 60°C divided by DTR.
WU60	Water uptake for 60°C using the modified Brasher formula: $\text{WU} = [\log (C_{60^\circ\text{C}}/C_{\text{RT1}}) - \log (\text{DTR})] / \log 67$
PRF	Performance rating factor, $R_{po} \times C_c \times 10^A \times 1000$ at 60°C , where A is numerical adhesion rating (0-5, 5 best) ASTM D 3359.
TAURT3	Time constant defined: $R_{po} \times C_c$ at RT3.
C60-CO	Ratio of capacitance at 60°C to capacitance at RT1.
KF	Water in free film (ppm).
POSTAU	Positron annihilation lifetime (τ_3)

Table 7. Calculated Values for Parameters Defined in Table 6 (Part A).

Coating System (ASTM D610)	C ₀	C _{60°C}	C _{RT2}	C _{RT3}	LOG-R- Ω·cm ² /μm
	nF/cm ₂ · μm				
1. E1(10)	4.67 ± 0.51	5.32 ± 0.63	5.23 ± 0.96	5.20 ± 0.97	7.5 ± 0.8
2. E2(10)	4.04 ± 0.87	5.40 ± 0.87	4.82 ± 1.18	4.20 ± 0.69	7.6 ± 0.4
3. E4(1)	10.2 ± 1.1	62.2 ± 4.6	24.5 ± 1.9	23.0 ± 1.7	2.4 ± 0.2
4. E5(1)	7.22 ± 0.58	20.0 ± 1.4	11.4 ± 0.7	9.07 ± 0.54	5.3 ± 0.3
5. E6(3)	7.13 ± 0.50	17.4 ± 1.6	7.88 ± 0.34	7.54 ± 0.81	5.7 ± 0.3
6. E1X8(10)	6.37 ± 0.74	7.81 ± 0.69	6.87 ± 0.65	6.61 ± 0.60	7.8 ± 0.4
7. E2X8(10)	5.64 ± 0.59	7.35 ± 0.62	6.00 ± 0.52	5.97 ± 0.55	7.9 ± 0.3
8. E4X8(1)	10.9 ± 1.0	722 ± 94	22.5 ± 2.8	18.6 ± 1.7	2.2 ± 0.1
9. E5X8(1)	8.32 ± 1.31	21.7 ± 1.5	11.7 ± 1.0	7.62 ± 0.55	5.1 ± 0.4
10. E6X8(2)	6.75 ± 0.98	20.7 ± 1.1	9.26 ± 1.07	7.72 ± 0.98	4.9 ± 0.3
11. E1CEL(10)	7.32 ± 0.91	8.27 ± 0.64	7.58 ± 0.65	7.49 ± 0.64	7.8 ± 0.4
12. E2CEL(10)	6.43 ± 0.92	8.49 ± 0.89	6.79 ± 0.68	6.31 ± 0.63	7.8 ± 0.4
13. E4CEL(2)	11.1 ± 1.1	2300 ± 300	24.1 ± 2.4	28.6 ± 1.3	2.4 ± 0.1
14. E5CEL(1)	8.48 ± 1.93	86.6 ± 15.2	13.4 ± 2.0	9.81 ± 1.54	3.6 ± 0.5
15. E6CEL(3)	6.21 ± 0.79	17.0 ± 0.9	9.14 ± 1.00	8.99 ± 0.60	4.5 ± 0.2

Table 7. Continued (Part B).

Coating System (ASTM D610)	DTR	C_{60DTR} $\text{nF}/\text{cm}^2 \cdot \mu\text{m}$	WU60 [v%]	TAUDTR [ms]	LOGRCTR $\Omega \text{F}^{-1} \text{cm}^4 \mu\text{m}^{-2}$
1. E1(10)	1.02 ± 0.01	5.22 ± 0.62	2.60 ± 1.58	170 ± 26	15.8 ± 1.3
2. E2(10)	1.17 ± 0.01	4.62 ± 0.74	3.30 ± 1.55	184 ± 34	15.9 ± 1.4
3. E4(1)	2.26 ± 0.01	27.5 ± 2.0	21.8 ± 1.2	0.0069 ± 0.0008	10.0 ± 0.6
4. E5(1)	1.67 ± 0.22	12.0 ± 1.8	12.0 ± 1.4	2.4 ± 0.4	13.2 ± 1.2
5. E6(3)	1.33 ± 0.21	13.1 ± 2.4	14.3 ± 2.8	6.6 ± 1.3	13.6 ± 1.5
6. E1X8(10)	1.10 ± 0.01	7.10 ± 0.63	2.05 ± 0.81	450 ± 46	15.9 ± 0.8
7. E2X8(10)	1.23 ± 0.01	5.98 ± 0.51	1.34 ± 1.03	480 ± 44	16.1 ± 0.8
8. E4X8(1)	1.95 ± 0.10	370 ± 52	80.5 ± 15.6	0.059 ± 0.009	8.6 ± 0.9
9. E5X8(1)	1.57 ± 0.01	13.8 ± 1.0	12.1 ± 3.4	1.7 ± 0.2	13.0 ± 0.7
10. E6X8(2)	2.91 ± 0.37	7.11 ± 0.98	1.25 ± 4.36	0.56 ± 0.04	13.0 ± 1.2
11. E1CEL(10)	1.11 ± 0.01	7.45 ± 0.58	1.39 ± 0.96	470 ± 44	15.9 ± 0.7
12. E2CEL(10)	1.31 ± 0.01	6.48 ± 0.68	0.17 ± 0.19	410 ± 48	16.0 ± 0.9
13. E4CEL(2)	1.72 ± 0.05	1340 ± 179	97.6 ± 35.1	0.34 ± 0.05	8.3 ± 0.8
14. E5CEL(1)	1.53 ± 0.10	56.6 ± 10.6	41.2 ± 20.0	0.23 ± 0.05	10.8 ± 1.4
15. E6CEL(3)	3.82 ± 0.39	4.45 ± 0.51	-7.86 ± 4.75	0.14 ± 0.02	12.9 ± 1.0

Table 7. Continued (Part C).

Coating System (ASTM D610)	C60-CO	WURT2 [v%]	WURT3 [v%]	TAU60 [ms]	LOGRC60 $\Omega F^{-1} cm^4 \mu m^{-2}$
1. E1(10)	1.14 ± 0.18	2.12 ± 0.72	2.00 ± 0.50	170 ± 30	15.8 ± 1.3
2. E2(10)	1.34 ± 0.36	2.58 ± 0.13	0.94 ± 0.10	210 ± 50	15.9 ± 1.4
3. E4(1)	6.12 ± 0.80	17.5 ± 1.3	16.0 ± 1.0	0.016 ± 0.002	9.6 ± 0.6
4. E5(1)	2.77 ± 0.30	9.24 ± 0.48	4.90 ± 1.27	4.0 ± 0.3	13.0 ± 0.6
5. E6(3)	2.44 ± 0.28	1.83 ± 1.14	1.73 ± 0.34	8.7 ± 0.9	13.5 ± 0.8
6. E1X8(10)	1.23 ± 0.18	0.41 ± 0.18	0.69 ± 0.69	490 ± 50	15.9 ± 0.8
7. E2X8(10)	1.30 ± 0.18	0.85 ± 0.21	0.96 ± 0.27	580 ± 54	16.0 ± 0.7
8. E4X8(1)	66.2 ± 10.5	15.8 ± 3.2	12.1 ± 1.4	0.11 ± 0.02	8.3 ± 0.8
9. E5X8(1)	2.61 ± 0.45	7.62 ± 1.38	0.00 ± 0.00	2.7 ± 0.3	12.8 ± 0.7
10. E6X8(2)	3.07 ± 0.47	7.00 ± 0.95	3.01 ± 0.85	1.6 ± 0.1	12.6 ± 0.5
11. E1CEL(10)	1.13 ± 0.17	0.56 ± 0.39	1.42 ± 1.14	520 ± 48	15.9 ± 0.7
12. E2CEL(10)	1.32 ± 0.23	0.36 ± 0.14	0.63 ± 0.12	540 ± 70	15.9 ± 0.9
13. E4CEL(2)	207 ± 33	16.2 ± 3.2	21.7 ± 1.9	0.58 ± 0.08	8.0 ± 0.7
14. E5CEL(1)	10.2 ± 2.9	10.3 ± 2.3	3.30 ± 1.63	0.34 ± 0.08	10.7 ± 1.3
15. E6CEL(3)	2.74 ± 0.38	7.53 ± 3.38	8.48 ± 1.47	0.54 ± 0.04	12.3 ± 0.5

Table 7. Continued (Part D).

Coating System (ASTM D610)	TAURT2 [ms]	TAURT3 [ms]	LOGRCRT2	LOGRCRT3	KF ppm
			$\Omega F^{-1} \text{cm}^4 \mu\text{m}^{-2}$		
1. E1(10)	1700 ± 350	2100 ± 440	16.8 ± 1.8	16.9 ± 1.8	36.0 ± 0.7
2. E2(10)	3000 ± 840	2700 ± 550	17.1 ± 2.3	17.2 ± 1.8	7.0 ± 0.1
3. E4(1)	0.019 ± 0.002	2.9 ± 0.3	10.5 ± 0.6	12.7 ± 0.6	189 ± 4
4. E5(1)	720 ± 64	360 ± 32	15.7 ± 0.7	15.6 ± 0.7	50.0 ± 1.0
5. E6(3)	630 ± 36	600 ± 68	16.0 ± 0.5	15.9 ± 0.9	16.0 ± 0.3
6. E1X8(10)	550 ± 59	420 ± 43	16.1 ± 0.9	16.0 ± 0.8	14.0 ± 0.3
7. E2X8(10)	380 ± 34	470 ± 45	16.0 ± 0.7	16.1 ± 0.8	7.0 ± 0.1
8. E4X8(1)	0.014 ± 0.002	0.12 ± 0.01	10.4 ± 1.0	11.5 ± 0.7	608 ± 12
9. E5X8(1)	740 ± 79	480 ± 46	15.7 ± 0.8	15.9 ± 0.8	34.0 ± 0.7
10. E6X8(2)	580 ± 74	150 ± 21	15.8 ± 1.0	15.4 ± 1.1	28.0 ± 0.6
11. E1CEL(10)	600 ± 60	470 ± 47	16.0 ± 0.8	15.9 ± 0.8	11.0 ± 0.2
12. E2CEL(10)	430 ± 51	630 ± 70	16.0 ± 1.0	16.2 ± 0.9	23.0 ± 0.5
13. E4CEL(2)	0.019 ± 0.002	0.36 ± 0.02	10.5 ± 0.8	11.6 ± 0.3	869 ± 17
14. E5CEL(1)	6.7 ± 1.4	620 ± 130	13.6 ± 1.4	15.8 ± 1.7	246 ± 5
15. E6CEL(3)	360 ± 42	180 ± 15	15.6 ± 0.9	15.3 ± 0.7	43.0 ± 0.9

Table 7. Continued (Part E).

Coating System (ASTM D610)	POSFV [ns]	POSINT [%]	POSTAU [ps]
1. E1(10)	36.5 ± 0.6	22.1 ± 0.3	1656 ± 14
2. E2(10)	39.6 ± 0.5	20.6 ± 0.2	1926 ± 16
3. E4(1)	28.5 ± 0.5	13.6 ± 0.2	2097 ± 23
4. E5(1)	27.3 ± 0.6	16.4 ± 0.3	1667 ± 19
5. E6(3)	31.9 ± 0.5	16.3 ± 0.2	1953 ± 18
6. E1X8(10)	39.0 ± 0.6	21.6 ± 0.3	1805 ± 15
7. E2X8(10)	41.7 ± 0.5	20.5 ± 0.2	2033 ± 17
8. E4X8(1)	30.8 ± 0.6	13.6 ± 0.2	2270 ± 24
9. E5X8(1)	30.0 ± 0.5	16.2 ± 0.2	1845 ± 19
10. E6X8(2)	35.4 ± 0.6	16.0 ± 0.2	2213 ± 22
11. E1CEL(10)	36.8 ± 0.6	20.8 ± 0.3	1769 ± 16
12. E2CEL(10)	39.7 ± 0.5	20.2 ± 0.2	1963 ± 16
13. E4CEL(2)	28.9 ± 0.5	13.2 ± 0.2	2192 ± 23
14. E5CEL(1)	26.8 ± 0.6	15.1 ± 0.3	1775 ± 21
15. E6CEL(3)	32.6 ± 0.5	15.5 ± 0.2	2100 ± 21

Table 8. Performance Predictions Based on Equation (2)

Epoxy Coating	Predicted Rating	Actual Rating
E7	6.5	6
E9-I	10.4	10
E10	5.6	4
E11	2.3	2

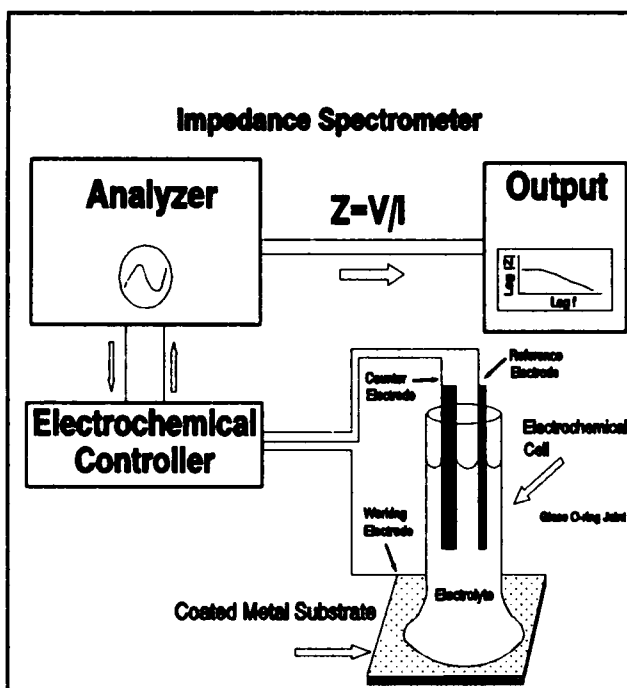
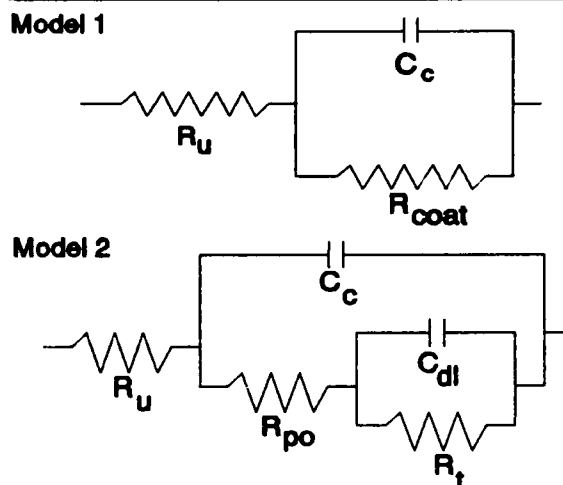


Figure 1. EIS instrumentation.



- R_u - Uncompensated solution resistance
- C_c - Intact coating capacitance
- R_{coat} - Intact coating resistance
- R_{po} - Pore resistance of the coating
- C_{dl} - Double-layer capacitance of the metal/solution interface
- R_t - Charge transfer resistance of the metal/solution interface

Figure 2. Equivalent circuit models.

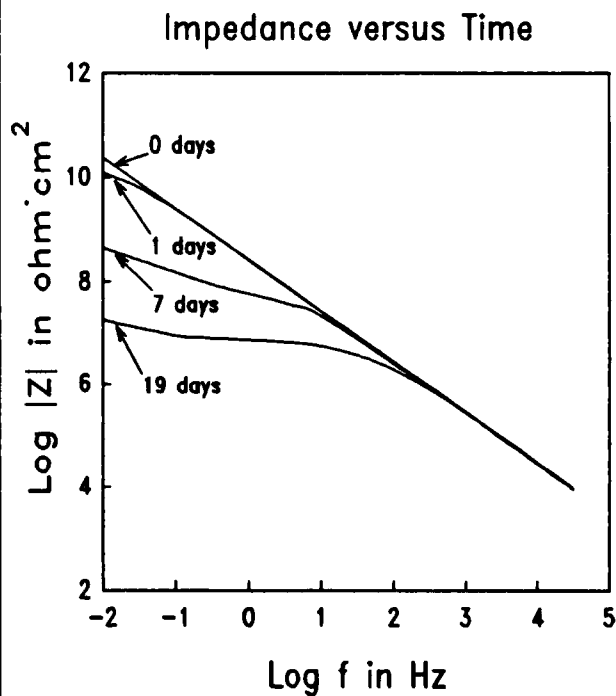


Figure 3. Impedance versus time for polybutadiene. Irreversible coating changes.

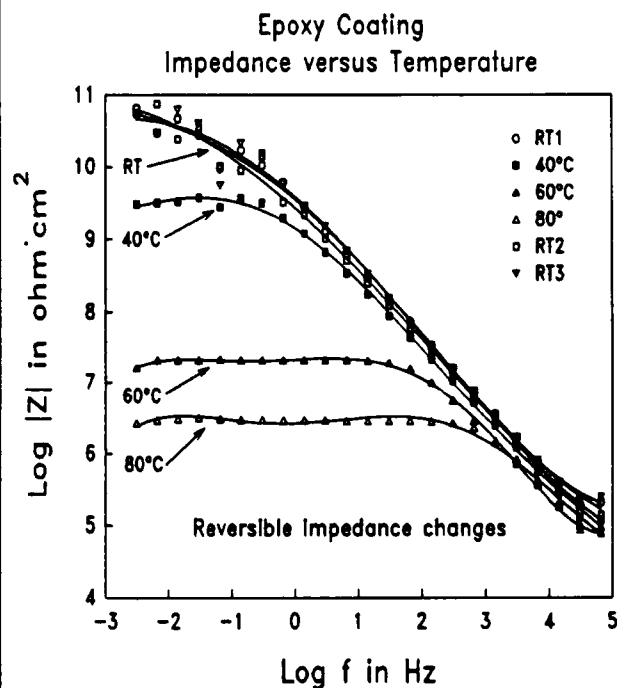


Figure 4. Large hydrothermal impedance change (reversible) at low frequency.

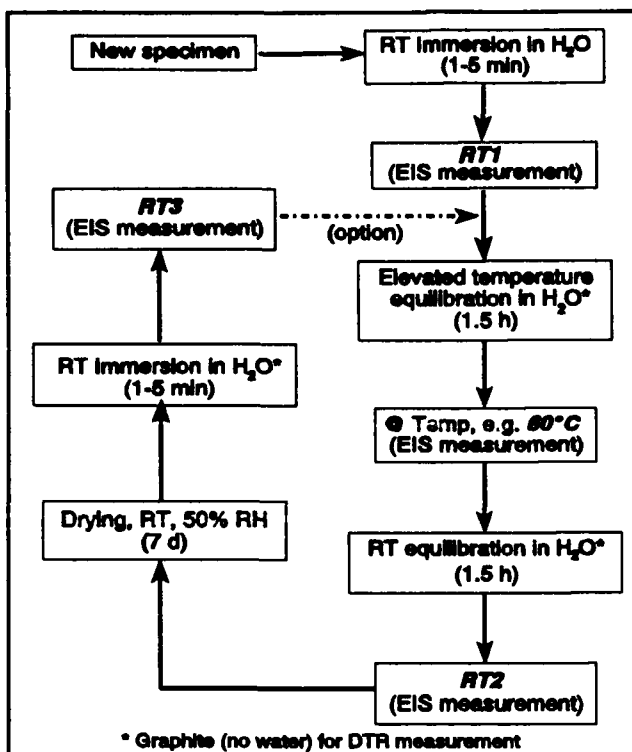


Figure 5. EIS measurement of hydrothermal effect on polymer coated metal specimens.

Low Frequency Impedance Data for a Two-Part Epoxy, a Two-Part Urethane, Polybutadiene, and a Polyester Baking Enamel

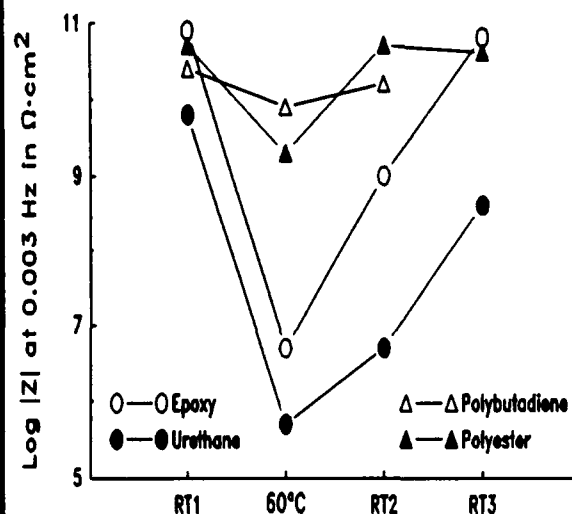


Figure 6. Coatings exhibiting large and small hydrothermal impedance changes at low f .

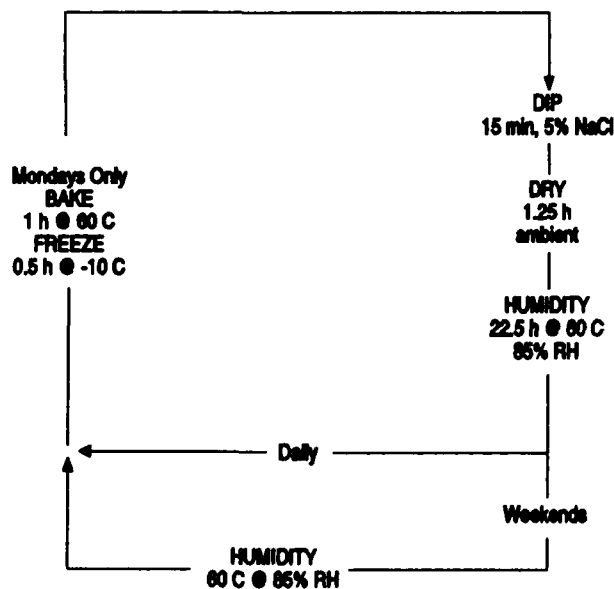


Figure 7. Cyclic exposure test includes thermal, aqueous exposure and drying conditions.

R_{po} VERSUS CONDITIONS, 5 EPOXIES/SOLVENTLESS

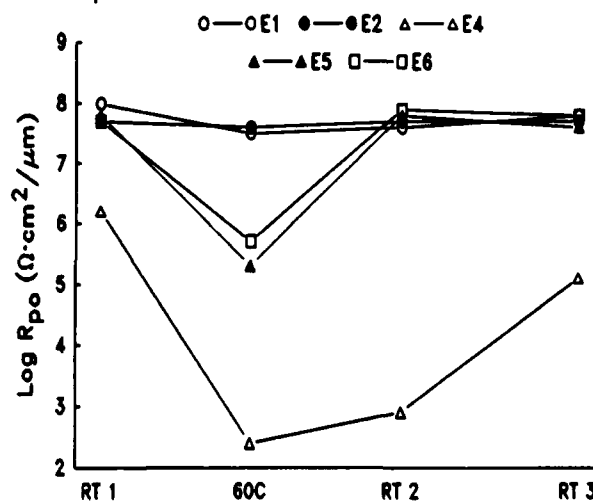


Figure 8. Hydrothermal impedance behavior of 5 solventless epoxy coatings: Room temperature-60°C transitions.

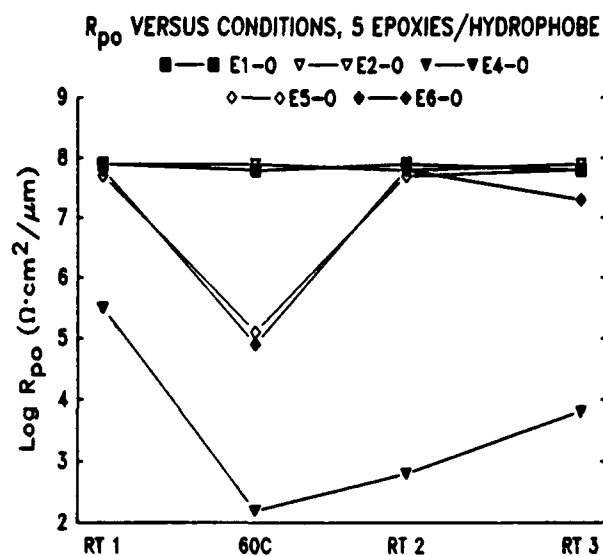


Figure 9. Hydrothermal impedance behavior of 5 epoxy coatings with hydrophobic solvent: Room temperature-60°C transitions.

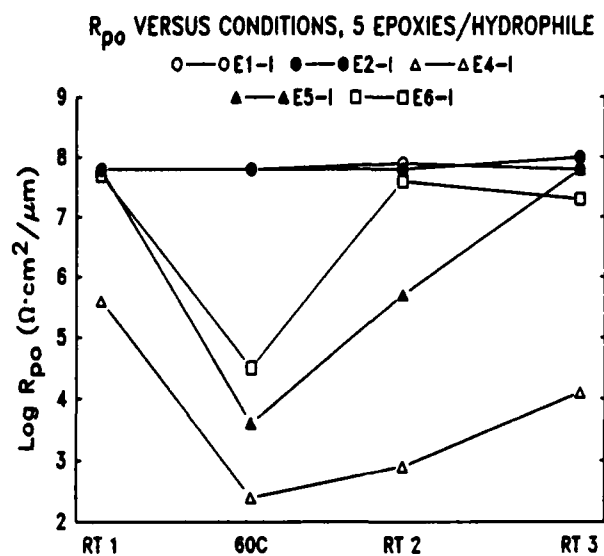


Figure 10. Hydrothermal impedance behavior of 5 epoxy coatings with hydrophilic solvent: Room temperature-60°C transitions.

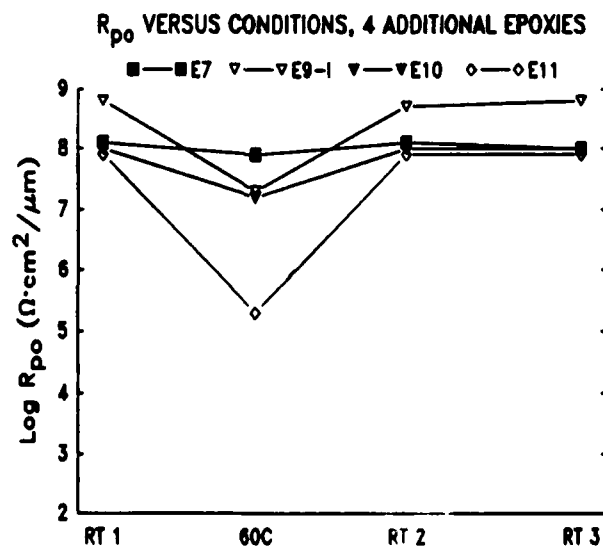
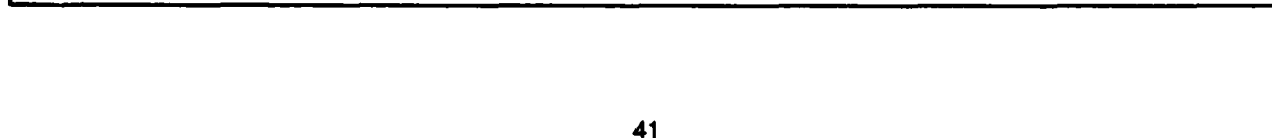
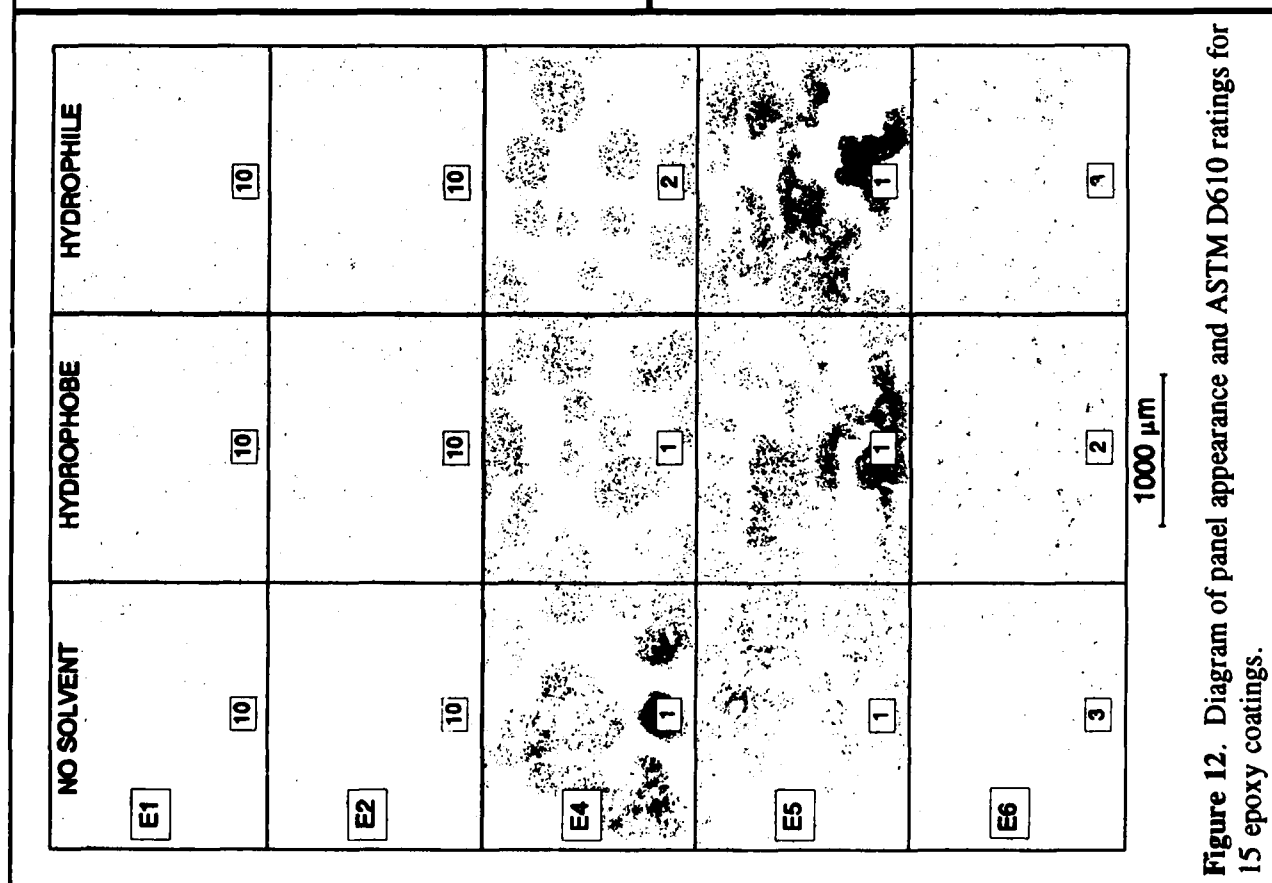
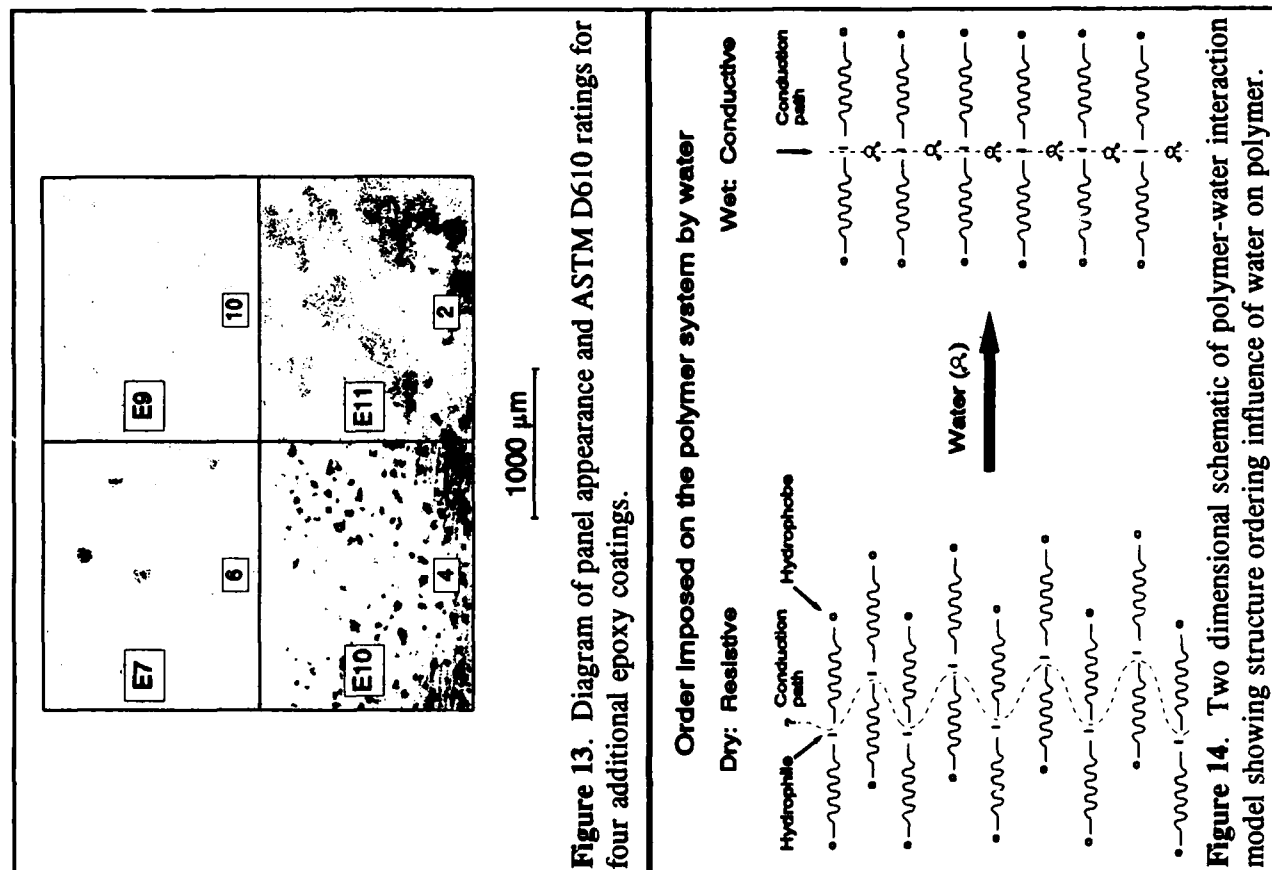


Figure 11. Hydrothermal impedance behavior of four additional epoxy coating systems: Room temperature - 60°C transitions.



Corrosion Behavior of Oxide Coated Cold-rolled and Electrogalvanized Sheet Steel

W.B. Nowak
Dept. of Mechanical Engineering
Northeastern University
360 Huntington Ave., Boston, MA 02115

H.E. Townsend
Homer Research Laboratories
Bethlehem Steel Corporation
Bethlehem, PA 18016

L. Li
Dept. of Mechanical Engineering
Northeastern University
360 Huntington Ave., Boston, MA 02115

Abstract

We studied the effects of sputtered oxide films on the corrosion and electrochemical behavior of cold-rolled (CRS) and electrogalvanized (EG) steel sheet. Films of Al_2O_3 , TiO_2 , Ta_2O_5 , and Cr_2O_3 were applied by off-axis dc magnetron sputter deposition. The films (deposited at 5 mTorr (0.667Pa), substrate temperature at about 50°C , and self-bias of -30 to -60 volts) were 1.2 to 4.0 micrometers thick and possessed an amorphous structure. The coated samples exhibit voltage-current behaviors similar to those of their substrates during polarization tests (at room temperature and 10 mV/min. scan rate) in aerated neutral 3.5% sodium chloride solution. Open-circuit potential (E_c) vs time was measured on coated CRS and EG samples for 24 hours continuously immersed in the solution. E_c V(SCE) changed rapidly during the first two hours then gradually approached the substrate rest potential over the 24 hours. Pores were found in oxide films by scanning electron microscope examination of cross section and surface morphologies. Corrosion behaviors of painted, oxide-coated CRS and EG samples were determined by measurement of scribe creep in cyclic corrosion tests involving repeated exposure to alternating periods of wetness, drying, and salt water. These results are compared to those for both uncoated and conventionally phosphated substrates.

Key terms: steel, electrogalvanized, sputter, oxide film, cyclic corrosion, polarization test

Introduction

Many engineering materials are used as a composite system (i.e. coating plus substrate) which has a performance that cannot be achieved by either the coating or substrate alone. Coated cold-rolled sheet steel has been widely used in the automobile industry for the manufacture of corrosion-resistant automobile bodies. The coatings currently used to protect steel autobody panels are hot-dip galvanized and galvaneal, electroplated zinc, zinc-nickel and zinc-iron, and composite organic/zinc nickel[1].

A galvanic coating provides corrosion protection via its sacrificial action and sometimes via its thin oxide surface film, or its own barrier action. Air-formed oxide films on metal and alloy surfaces are very thin, typically a few nanometers in thickness, which limits their life time especially in the environments where chloride ions exist. It is recognized that a homogeneous amorphous passive layer shows extraordinary protection. Research on synthetic oxide passive layers applied directly onto substrates has been reported by several authors. Townsend, Cleary, and Allegra [2] have investigated the use of oxide films (Al_2O_3 , Cr_2O_3 , TiO_2) and multilayer oxide composites (Al_2O_3 over or under Cr_2O_3), about 300 nm per layer, sputter-deposited onto cold rolled steel as corrosion barriers to saline solutions. Ishikawa and Sugimoto [3, 4] have studied the corrosion resistance (time trace of open circuit potential) of oxide multilayer films, such as, $\text{Ta}_2\text{O}_5/\text{Ta}_2\text{O}_5$, $\text{Ta}_2\text{O}_5/\text{Al}_2\text{O}_3$, $\text{Ta}_2\text{O}_5/\text{Cr}_2\text{O}_3/\text{Al}_2\text{O}_3$, and $\text{Cr}_2\text{O}_3/\text{Al}_2\text{O}_3/\text{Cr}_2\text{O}_3/\text{Al}_2\text{O}_3$ deposited by MOCVD onto iron substrates with each layer's thickness about 100nm. All of the above research shows evidence that thicker films provide longer life times. The work presented here concerns sputter deposited, relatively thicker (330-4000nm), passive oxide films onto cold-rolled (CRS) and electrogalvanized (EG)¹ sheet steel substrates, their structure, composition, corrosion resistance, and electrochemical behavior.

The use of physical vapor deposition methods to fabricate corrosion resistant coatings is still in its early stages. Since it is a dry coating process without deleterious environmental waste components, PVD methods are increasingly used in the coating industry.

Experimental Details

We have used reactive dc magnetron sputter deposition to prepare tantalum, titanium, chromium and aluminum oxide films on cold-rolled and electrogalvanized sheet steel substrates. The vapor source used for this work was an A300 2-inch diameter (50mm) planar magnetron sputter gun installed in a bell jar vacuum system. The construction of this source permits variation of the magnetic field configuration. It was used with all its permanent magnets in place, thus giving an "unbalanced" source[5]. Both an oxide target with an rf power supply and a metal target with a dc or rf power supply were investigated. The metal target and dc supply were chosen for the work reported here because of the considerably faster deposition rates.

Base pressure of the vacuum system was 10^{-5} Torr (1.33 mPa) and the total working pressure, argon plus oxygen, was 5 to 20 mTorr (0.667-2.667 Pa). Substrates (CRS and EG coupons, 1.59cm diameter and 2.54×2.54 cm square, respectively) were ultrasonically degreased in Alconox and acetone and were sputter cleaned in-situ by an argon glow discharge at -800 to -1000 V for 15 min. The metal target was presputtered for 30 min. before deposition. Off-axis sputter deposition was used to avoid film loss by resputtering due to energetic negative ions. Substrates (electrically isolated) were self biased negatively between 30 and 60 volts, and attained a temperature of about 50°C during deposition. The working distance between substrate and target is about 3-5cm vertically. A simplified diagram of the deposition setup is given in Fig. 1.

Film thicknesses were measured with a DekTak II profilometer on masked coverglass test coupons which were coated in the same batch. Auger electron spectroscopy (AES), depth

¹EG is a trademark of Bethlehem Steel Corporation.

profiling and X-ray photoelectron spectroscopy (XPS) analyses were performed on oxide-film-coated CRS and EG samples to find the stoichiometry and chemical states. Surface and cross section morphologies of the oxide films were examined in a scanning electron microscope (SEM). X-ray diffraction scans were taken from selected samples to determine qualitatively the crystallization condition of the as-deposited oxide film.

A laboratory environmental test was applied to CRS and EG samples coated with Ta_2O_5 , TiO_2 , Cr_2O_3 , and Al_2O_3 oxide films along with uncoated and conventionally phosphated samples. These samples were painted with spray applied primer (Taylor Made Products, TP-51 Grey) and a spray applied topcoat (Plastikote 1023 Antique White). The painted samples (2.54×2.54 cm) were scribed with a carbide pencil to expose the steel substrates and placed in a Liebsch automatic test cabinet. Two test conditions were used: Mazda and GM 9540-P (Cycle B). Eight cycles of Mazda were used, each cycle comprises: 6h of ASTM B117 salt spray; 3h of drying in 20-30% RH at 50°C ; 14h of humid exposure at 95% RH at 50°C ; and 1h drying in ambient air. Each cycle of the GM test comprises: 8h during which 4, 15-min intervals of salt spray are alternated with drying at 25°C , and $< 50\% \text{RH}$; 8h at 49°C 100%RH(FOG) and 8h at 60°C , $< 20\% \text{RH}$. CRS-substrate samples were taken out after 39 GM cycles as extensively rusted, but EG-substrate samples went through 72 GM cycles. Following exposure, loose paint next to the scribe mark was removed by scraping with a dull metal blade and taping with 3M 610 adhesive tape. Total extent (on both sides of the scribe) of delaminated paint was estimated to the nearest mm. The replicates of each condition varied from 2 to 7 (Table 1 and 2).

Open circuit (or rest) potential, potentiodynamic polarization and polarization resistance were measured on oxide-coated CRS and EG samples which were compared with uncoated ones. All the tests were performed in aerated neutral 3.5% sodium chloride solution. Test surface area of the sample was 1 cm^2 with the remaining surface covered with Amercoat 90 epoxy (Ameron, Brea, CA). Each sample was immersed in the solution for one hour to stabilize the rest potential, E_c , before potentiodynamic scanning (scan rate 10 mV/min). All potentials were measured vs a saturated calomel electrode. Polarization resistance was evaluated by measuring the voltage-current behavior near E_c using the potentiodynamic method[9]. The instruments used for these experiments were Model 173 Potentiostat/ Galvanostat with Model 376 Logarithmic Current Converter. The corrosion cell used for the electrochemical measurements was an one-liter, multi-necked, flat-bottomed flask.

Experimental Results and Discussion

Film Deposition

The following oxide films and oxide film composites were applied to CRS and EG substrates: Al_2O_3 , Ta_2O_5 , Cr_2O_3 , TiO_2 , $\text{Al}_2\text{O}_3/\text{Al}_2\text{O}_3$, $\text{Al}_2\text{O}_3/\text{Ta}_2\text{O}_5$, $\text{Al}_2\text{O}_3/\text{Cr}_2\text{O}_3$, $\text{Al}_2\text{O}_3/\text{TiO}_2$ (top/bottom). Factors that determine the sputter deposition rates are: power density in the erosion area, size of the erosion area, source to substrate distance, source material, working pressure, and the partial pressure of reactive gas (oxygen in this work). The lower the oxygen partial pressure, the higher the deposition rate. However, the oxygen pressure also controls the stoichiometry of the oxide film, and runs were performed to determine the lowest pressure with full stoichiometry by AES depth profiling of as-deposited films at different oxygen partial pressures. The relatively low deposition rates are due to the formation of a thin oxide film on the metal target surface during sputtering.

Film Characterization

AES surface spectra showed some substrate signals from thin aluminum oxide films: the signals diminished as film thickness increased, as reported by other researchers[2]. No substrate signal was detected when film thickness was above 330nm. Because the films were deposited onto as-received CRS and EG substrates which had surface roughnesses of about 3000nm peak to peak, the film has to reach a certain thickness to cover a rough surface even though there is some conformality. In very thin films, the uncovered surface may contribute to the substrate detection. Chemical states of Al^{3+} , Cr^{3+} , Ta^{5+} , and Ti^{4+}

were detected by XPS analyses in the deposited oxide films. X-ray diffraction spectra of sputter deposited oxide films show an amorphous structure which is typical of low substrate temperature deposition at low bias. Although AES spectra showed no substrate signal for thicker films, micron pores and fissures caused by processing and substrate inhomogeneities may exist. SEM pictures (Figs. 2 and 3) show that pores existed in Ta₂O₅ films deposited on glass, and that fissures formed in the films deposited on CRS and EG.

Corrosion Testing

Simulated environmental corrosion test results are summarized in Tables 1 and 2. In the Mazda cyclic corrosion test, Ta₂O₅ coated CRS had better corrosion resistance than nontreated and phosphated CRS; Ta₂O₅ coated EG were better than nontreated EG but not as good as phosphated EG. In the GM corrosion test, TiO₂, Cr₂O₃ and Al₂O₃ coated CRS were better than nontreated but not as good as zinc phosphated; TiO₂, Cr₂O₃ and Al₂O₃ coated EG samples showed no improvement over nontreated EG samples.

Immersion Tests and Mixed Potential

Continuous open circuit potential 24 hour recording of Al₂O₃, Ta₂O₅, TiO₂ and Cr₂O₃ coated CRS and EG samples in aerated, neutral, 3.5% NaCl aqueous solution at room temperature revealed the following results:

- All the samples' rest potentials decayed from a noble value toward the rest potential of their corresponding substrates.
- The magnitude of rest potential decay on coated EG samples was smaller than on coated CRS samples.
- No rust was seen on coated EG samples after 24 hours, but rust formed on coated CRS samples.
- White corrosion products formed on coated EG sample surfaces but were not found on coated CRS sample surfaces.

Tables 3 and 4 list some rest potential data picked from the immersion tests. The data during the first 10 hours immersion of a Ta₂O₅ coated CRS sample were plotted on a $\log(-E_c)$ vs \log time graph as shown in Fig. 4. Two regions are evident. Up to about 1.5 hours, the variation of E_c with time may be represented by:

$$E_c = -0.28t^{0.072} \quad (1)$$

after 1.5 hours, the variation is:

$$E_c = -0.28t^{0.047} \quad (2)$$

E_c in V(SCE), t in hours.

The change in the decay rate may reflect the evolution of the chemical composition of the oxide film while in the solution. The rest potentials of samples coated with single and double oxide films after 1 hour immersion are summarized in Table 5. The approximate correspondence of rest potential of oxide-coated samples with the value of their substrate material was consistent with the existence of micron pores and fissures in the film. It is these pores and fissures that make the sample surface complex, large oxide area plus small exposed substrate area. The chemical inhomogeneities on the electrode surface result in more than one redox reaction, and a mixed potential is formed. When more than one reaction is expected to occur, the prevailing reaction in determining the potential is that with the largest exchange current density[7]. The value of the mixed potential lies between the two equilibrium potentials, and it depends essentially upon the position of the partial current-voltage curves[8].

Polarization Tests

No initial passive state was found in all the electrochemical tests. The potentiodynamic anodic polarization behavior of oxide-coated CRS and EG samples are given in Figs. 5 to 7. On coated CRS samples, current kept increasing as voltage was scanned anodically. However, on bare and oxide coated EG samples there were regions of decreasing current between -0.9 to -0.7 V(SCE). After the current turning point, the electroplated zinc coating was almost gone and a very thin zinc film remained, with cracked and discontinuous oxide film on top of the zinc for the oxide-coated samples. Long cracks and white corrosion products were observed on dried polarization tested samples under SEM observation. The remaining thin zinc film (which was not continuous) on bare samples was visually obvious. It is believed that such a thin zinc film was left on substrates under the oxide film as evidenced by the similar anodic polarization behavior of bare and coated EG samples. However, quantitative measurement is not feasible due to the roughness of the surface and the oxide film. The electrons consumed between the test points A and B (Fig. 5) can be calculated as roughly 14.4 C. The proportionally reacted zinc, calculated using Faraday's law, was 0.00488 g which equals 6.84 μm of zinc coating on 1 cm^2 . The EG samples had 40 g/m^2 , equal to 5.61 μm , of zinc coating. This calculation shows that at the current decay point B the zinc coating was almost gone. The discrepancy was due to crevice corrosion and assumptions in the coulomb calculation. After most of the zinc coating dissolved into the solution, the remaining zinc reacted with iron and possibly oxygen to form a protective thin film.

Linear current-voltage curves measured near the rest potential (Figs. 8 to 11) were used to derive the polarization resistances (R_p) according to the function[9]:

$$R_p = \frac{\Delta E}{\Delta i_{app}} = \frac{B}{i_{corr}} \quad (3)$$

where:

ΔE — overvoltage

Δi_{app} — applied current density

B — proportionality constant

i_{corr} — corrosion rate

Polarization resistance, defined as the slope of the polarization curve at the origin, is independent of the degree of linearity. The samples were linearly polarized to overvoltages between -50 and 50 mV to observe system behaviors. Each sample was first anodically polarized to 50 mV or full current scale, scanned back immediately, then scanned cathodically. Polarization resistance was calculated using the slope of the anodic curve up to 10 mV. Table 6 lists the polarization resistances of CRS and EG substrates, both bare and coated with single and double oxide films. Polarization resistances increased on oxide coated samples except for the sample of $\text{Al}_2\text{O}_3/\text{EG}$. At the same coating conditions, the CRS substrates have a higher R_p than the EG substrates. Al_2O_3 , Ta_2O_5 , and TiO_2 coated samples have higher R_p than Cr_2O_3 coated ones. Al_2O_3 , Ta_2O_5 and TiO_2 are n-type semiconductors while Cr_2O_3 is p-type. The energy gaps and different junctions such as n-n, n-p, and p-n on the surface and interface will contribute to the polarization resistance.

Using the concept of a passive surface layer to protect metal from corrosion, one may interpret the decreased corrosion rate to the reduced transport rate of reactant species through the layer. An alternate viewpoint is that the barrier layer serves as a resistor to drop a large part of the applied voltage, thus lowering the electric field at the interface, with a consequent decrease in the corrosion rate[10]. Increasing film thickness and using alternating layers both reduce the number and size of defects through the film and further reduce the transport rate. This may be one of the reasons that samples coated with double oxide films had higher R_p and higher anodic polarization tafel slope than that of uncoated and single oxide film coated ones in potentiodynamic tests. A synthetic oxide film prevents its metal substrate from

corrosion mainly through its barrier action. The barrier property which determines the corrosion resistance strongly depends on its structure (defects, stress).

Synthetic Oxide Film Breakdown on EG and CRS

The ionic transport in passive layers has been investigated by many people, and the general results and models are discussed and summarized by Fromhold[10]. When an oxide film is placed into an aqueous solution, OH^- and H_2O will be adsorbed on its surface immediately forming a hydrated interface. Meanwhile, the solution will reach the covered metal through film defects which were formed by growth, substrate roughness and film stress. Aggressive anions like Cl^- are adsorbed on the hydrated oxide film and react with the film to form soluble halide complexes[11, 12]. Cl^- can also penetrate the defects to react with substrate metal.

In immersion and polarization tests, oxide coated EG samples corroded first at film defects (pores and fissures). The corrosion quickly penetrated through the coating. As the CRS substrate was under cathodic protection by the zinc coating, corrosion is prevented from going deeply, but expands laterally. This is similar to 2-D pit growth in thin films[13]. However, oxide coated CRS corroded in a different way. Rust first formed on defects. As the corrosion went deep into the substrate, the film around the defects was thinned and rust expanded out. This behaves as 3-D pit growth in bulk materials. On coated EG samples zinc dissolved into solution through pores and fissures, piling up corrosion products and leaving a poorly adherent oxide film. The loss of adherence did not occur on coated CRS samples.

In the GM test, the corrosion systems were paint/oxide/Zn/CRS for coated EG samples, and paint/oxide/CRS for coated CRS samples (top/middle/bottom). For the EG samples, the Zn layer corroded first, and coating adherence was lost via crevice corrosion and cathodic delamination[14]. This may be the reason that oxide-coated EG samples show no improvement over non-coated ones. However, for CRS samples, the oxide coating may act as a barrier to lateral corrosion, reducing the rust expanding rate, and increasing the scribe creep resistance.

CONCLUSIONS

1. Application of stoichiometric oxide films to cold rolled and electrogalvanized steel substrates tends to increase both polarization resistance and corrosion potential in aerated neutral 3.5% NaCl solution.
2. These effects are greater for thicker films and for some multilayer films, probably because of reduced film porosity and better barrier properties.
3. In the case of cold rolled substrates, resistance to paint delamination in a cyclic corrosion test is significantly improved by the application of the oxide films. In the best case, the degree of improvement exceeds that provided by conventional zinc phosphate. This suggests that the barrier properties of the oxide films are important in the delamination of paint from cold rolled steel.
4. With electrogalvanized substrates, the oxide films provide much less improvement in resistance to paint delamination in a cyclic corrosion test. This suggests that barrier properties of the surface oxides are of lesser importance in the delamination of paint from electrogalvanized steel.

ACKNOWLEDGMENT

The authors want to thank D. H. VanBilliard at Bethlehem Steel Corporation for the AES and XPS analysis of all the samples; J. Surette, J. Doughty, S. Mich, and J. Hinds at Northeastern University for their technical assistance. This work was supported by the Bethlehem Steel Corporation.

References

- [1] H. E. Townsend, "Coated Steel Sheets for Corrosion-Resistant Automobiles," CORROSION/91, paper no.416(Cincinnati, Ohio: National Association of Corrosion Engineers, 1991).
- [2] H. E. Townsend, H. J. Cleary, and L. Allegra, Corrosion, 37 7(1981): p.384.
- [3] M. Ishikawa and K. Sugimoto, J. Japan Inst. Metals, 51 11(1987): p.1054.
- [4] K. Sugimoto, Corrosion Engineering, 38 (1989): p.223.
- [5] B. Window and G. L. Harding, J. Vac. Sci. Technol. A 10(5), 9/10(1992): p.3300.
- [6] D. Briggs and M. P. Seah, Practical Surface Analysis, (Wiley, New York, 1990): p.169. December 1, 1992.
- [7] N. Sato, "The Passivity of Metals and Passivating Films," Passivity of Metals, edited by R. P. Frankenthal and J. Kruger, (The Electrochemical Society, Inc., Princeton, NJ, 1978): p.29.
- [8] K. J. Vetter, Electrochemical Kinetics Theoretical and Experimental Aspects, (Academic Press, New York, NY, 1967): p.733.
- [9] D. A. Jones, Principles and Prevention of Corrosion, (Macmillan Publishing Company, New York, 1992): p. 151.
- [10] A. T. Fromhold, Jr., "Ion Transport in Passive Layers," Passivity of Metals, edited by R. P. Frankenthal and J. Kruger, (The Electrochemical Society, Inc., Princeton, NJ, 1978): p.59.
- [11] T. H. Nguyen and R. T. Foley, J. Electrochem. Soc., 126 11(1979): p.1855.
- [12] K. Hayashi and Y. Miyoshi, Tetsu-To-Hagane, 78 4(1992): p.601.
- [13] G. S. Frankel, Corrosion Science, 30 12(1990): p.1203.
- [14] H. Leidheiser, JR. "Coatings," Corrosion Mechanisms, edited by F. Mansfeld, (Marcel Dekker, Inc., New York, NY, 1987): p.165.

Table 1: Mazda cyclic corrosion test results (8 cycles).

Substrate	Pretreatment	Creep Ave (mm)	Creep (max-min) (mm)	No. of Samples
CRS	Ta ₂ O ₅	6	10-3	6
CRS	none	>15	>15	3
CRS	Zinc Phosphate	14	>15-11	3
EG	Ta ₂ O ₅	7	>15-3	6
EG	none	>15	>15	3
EG	Zinc Phosphate	3	4-1	3

Table 2: GM cyclic corrosion test results (39 cycles for CRS and 72 cycles for EG).

Substrate	Pretreatment	Creep Avg (mm)	Creep (Max-Min) (mm)	No. of Samples
CRS	none	12	13-11	3
CRS	Zinc Phosphate	3	3-2	4
CRS	TiO ₂	7	21-2	4
CRS	Cr ₂ O ₃	7	17-2	5
CRS	Al ₂ O ₃	4	4-3	2
EG	none	3	3	3
EG	Zinc Phosphate	2	2	3
EG	TiO ₂	3	4-3	3
EG	Cr ₂ O ₃	4	6-3	7
EG	Al ₂ O ₃	3	3	2

Table 3: Selected rest potential E_c of single oxide coated EG samples during 24 hrs immersion.

Oxide Film	E _c (V)					
	Initial	1 (hr)	2 (hr)	3 (hr)	10 (hr)	24 (hr)
none	-1.017	-1.035	-1.039	-1.043	-1.049	-1.058
AlO	-1.008	-1.020	-1.020	-1.020	-1.022	-1.035
TaO	-1.021	-1.028	-1.038	-1.038	-1.040	-1.042
TiO	-0.967	-0.990	-0.998	-1.002	-1.015	-1.012
CrO	-0.938	-0.963	-0.970	-0.982	-1.012	-1.024

Note:

AlO=Al₂O₃, TaO=Ta₂O₅, CrO=Cr₂O₃, TiO=TiO₂

All the rest potentials (E_c) are vs SCE.

Table 4: Selected rest potential E_c of single oxide film coated CRS samples during 24 hrs immersion.

Oxide Film	E_c (V)					
	Initial	1 (hr)	2 (hr)	3 (hr)	10 (hr)	24 (hr)
none	-0.441	-0.533	-0.689	-0.695	-0.680	-0.672
AlO	-0.720	-0.555	-0.568	-0.580	-0.596	-0.613
TaO	-0.457	-0.520	-0.538	-0.545	-0.562	-0.583
TiO	-0.310	-0.492	-0.508	-0.518	-0.558	-0.593
CrO	0.543	0.460	0.432	0.100	-0.550	-0.564

Table 5: The rest potential E_c of bare substrate, single and double oxide film coated samples after 1 hr immersion (top/bottom).

Substrate	Oxide Film	E_c (V)	Oxide Film	E_c (V)
EG	none	-1.043	none	-1.043
EG	AlO/AlO	-0.988	AlO	-1.009
EG	AlO/TaO	-1.017	TaO	-1.017
EG	AlO/CrO	-0.967	CrO	-0.988
EG	AlO/TiO	-0.972	TiO	-0.980
CRS	none	-0.685	none	-0.685
CRS	AlO/AlO	-0.537	AlO	-0.520
CRS	AlO/TaO	-0.550	TaO	-0.531
CRS	AlO/CrO	-0.479	CrO	-0.460
CRS	AlO/TiO	-0.493	TiO	-0.499

Table 6: Polarization resistances of bare substrate, single and double oxide film coated samples (top/bottom).

Substrate	Oxide Film	R_p (Ω)	Oxide Film	R_p (Ω)
EG	none	2.22E2	none	2.22E2
EG	AlO/AlO	3.30E3	AlO	1.85E2
EG	AlO/TaO	1.00E5	TaO	2.86E4
EG	AlO/CrO	1.20E3	CrO	8.00E2
EG	AlO/TiO	1.50E3	TiO	2.50E3
CRS	none	1.54E2	none	1.54E2
CRS	AlO/AlO	1.00E5	AlO	2.68E4
CRS	AlO/TaO	6.10E4	TaO	2.50E4
CRS	AlO/CrO	2.40E4	CrO	2.22E3
CRS	AlO/TiO	3.30E4	TiO	6.67E3

Note: (in Table 4-6)

AlO=Al₂O₃, TaO=Ta₂O₅, CrO=Cr₂O₃, TiO=TiO₂

All the rest potentials (E_c) are vs SCE.

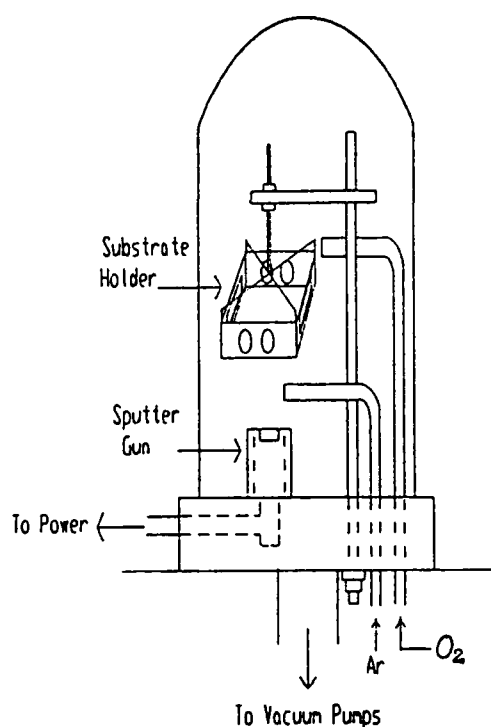


Figure 1: Schematic diagram of off-axis sputter deposition.

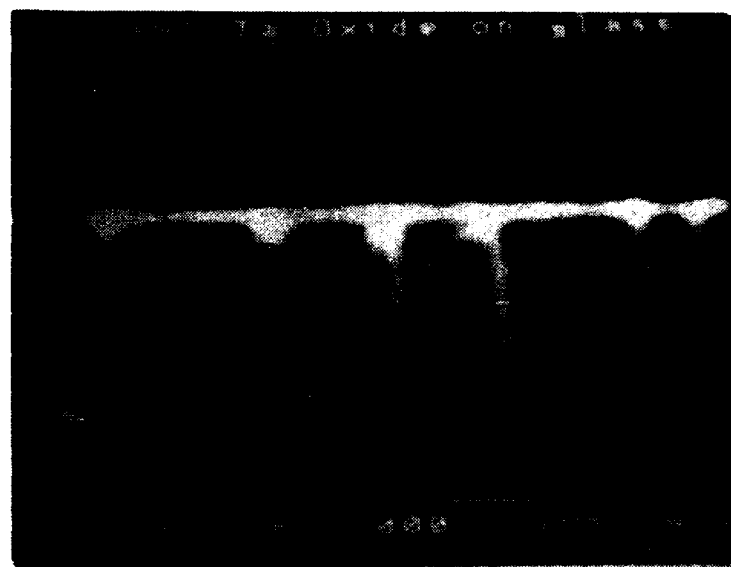
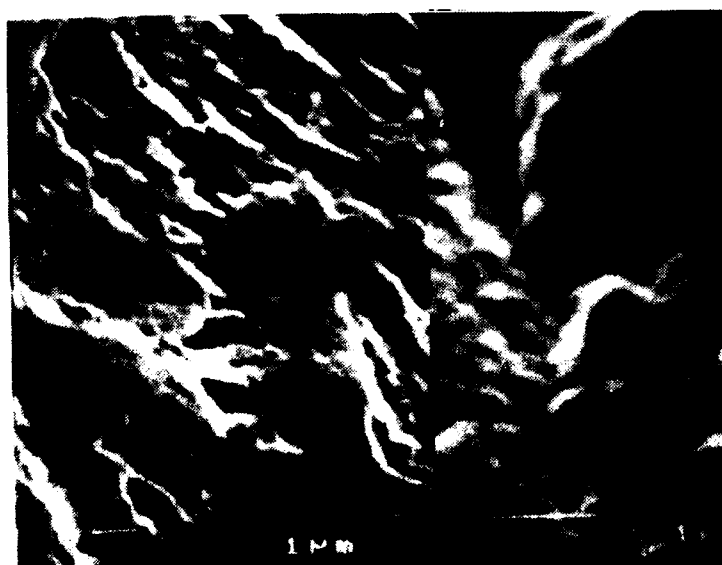


Figure 2: SEM photomicrograph of Ta_2O_5 film cross-section on glass.



(a)



(b)

Figure 3: (a) SEM photomicrograph of Ta_2O_5 film morphology on EG. (b) SEM photomicrograph of Ta_2O_5 film morphology on CRS.

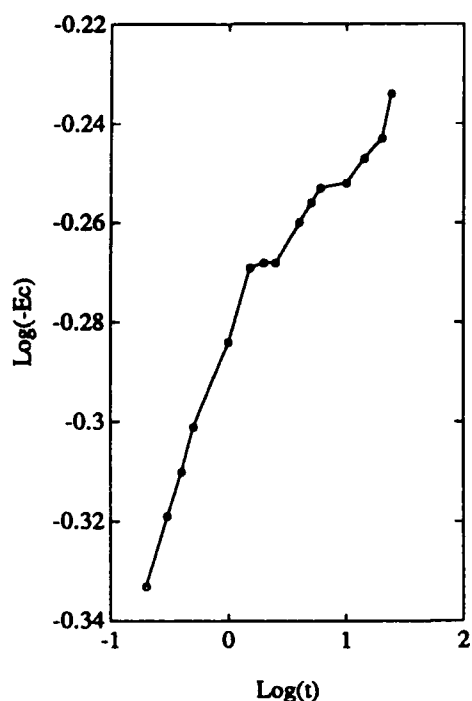


Figure 4: Rest potential E_c (V_{SCE}) vs time (hr) of Ta_2O_5 coated CRS samples.

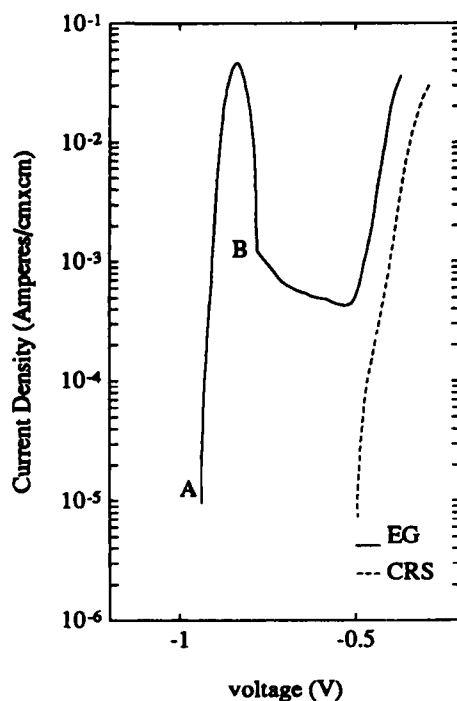


Figure 5: Potentiodynamic anodic polarization curves of CRS and EG substrates.

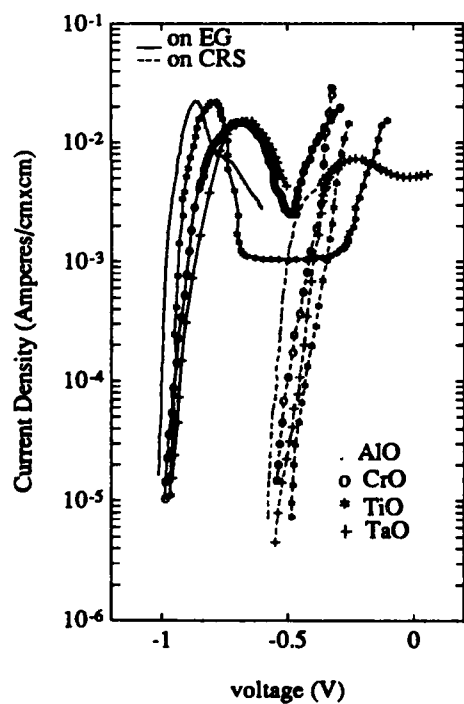


Figure 6: Potentiodynamic anodic polarization curves of single oxide coated CRS and EG samples.

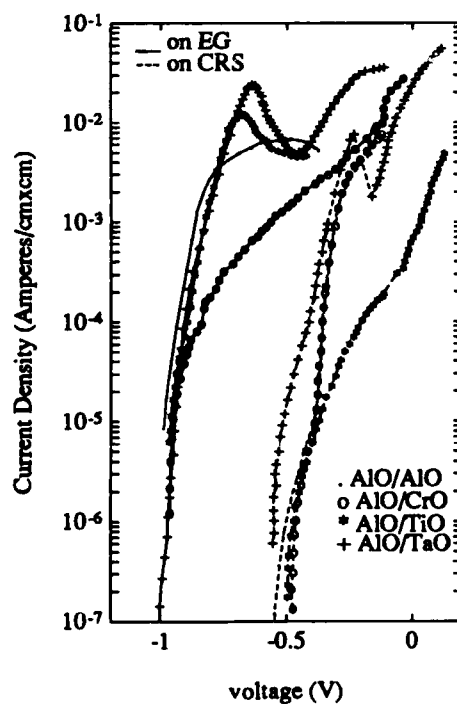


Figure 7: Potentiodynamic anodic polarization curves of double oxide coated CRS and EG samples.

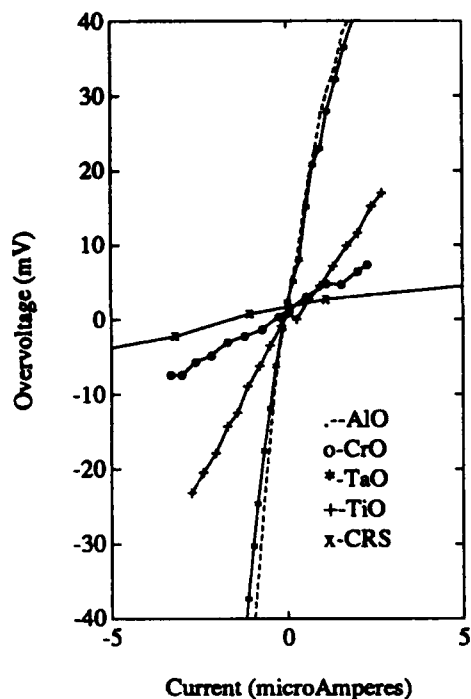


Figure 8: Potentiodynamic polarization curves of CRS and single oxide coated CRS samples near E_c .

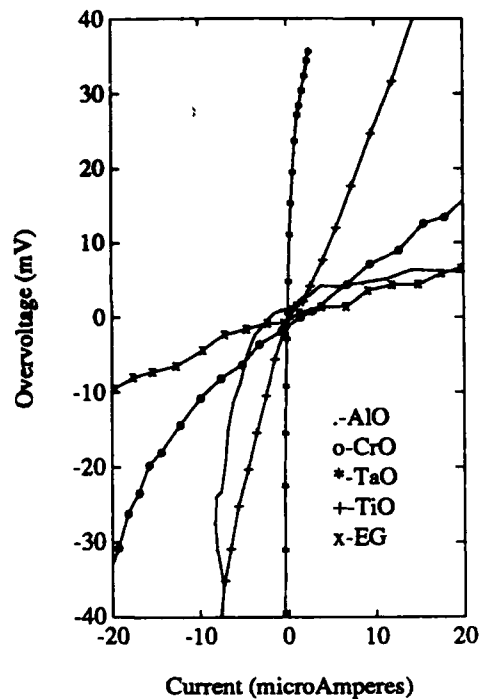


Figure 9: Potentiodynamic polarization curves of EG and single oxide coated EG samples near E_c .

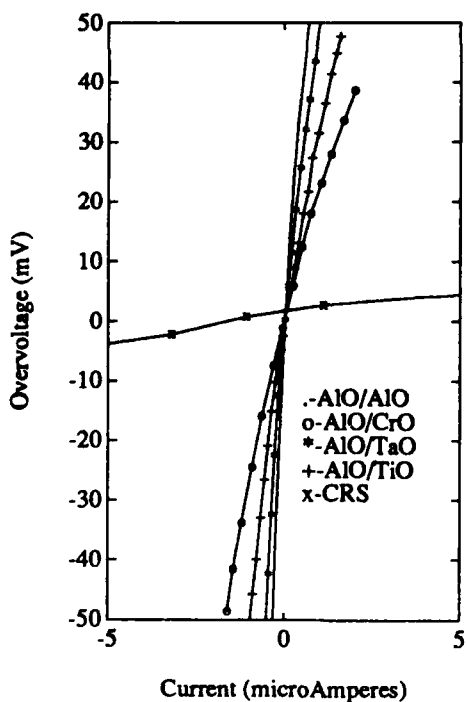


Figure 10: Potentiodynamic polarization curves of CRS and double oxide coated CRS samples near E_c .

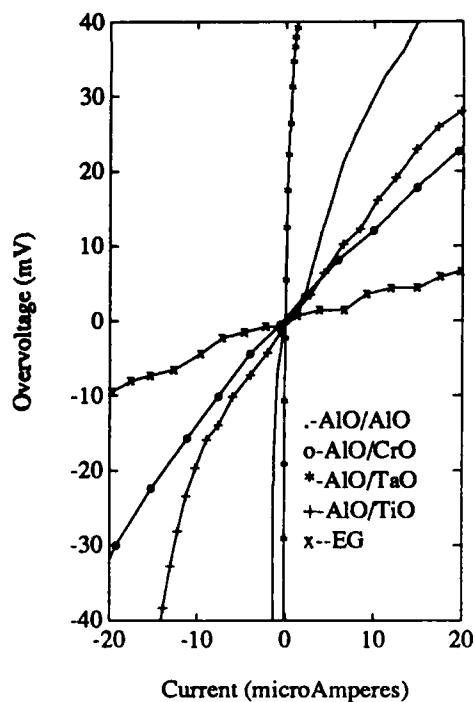


Figure 11: Potentiodynamic polarization curves of EG and double oxide coated EG samples near E_c .

Corrosion Behavior of Oxide Coated Cold-Rolled and Electrogalvanized Sheet Steel*

W. Nowak

*** Paper not available at time of printing.**

Study of Enamelling Properties on the Hot-Rolled Ti-Containing Steel Sheets

Xu Xiaolian

Institute of Iron and Steel Research

Post Code: 114001

Anshan Liaoning China

Zhao Keping

Institute of Iron and Steel Research

Post Code: 114001

Anshan Liaoning China

Liu Ri

Institute of Iron and Steel Research

Post Code: 114001

Anshan Liaoning China

Abstract

In present work the electrochemical hydrogen permeation technique and the fishscaling technique of enamelled steel sheets were used to study fishscale resistance of the enamelled hot-rolled steel. The results showed that the hot-rolled Ti-containing steel sheets have smaller hydrogen diffusivity, therefore, better fishscale resistance than A_2 and 10^4 . In addition, the enamel on the Ti-containing steel sheets has lower porosity and better adherence. Thus, the Ti-containing steel is a good enamelling material.

Key Words: enamelling property, Ti-containing steel, fishscale

Introduction

Fishscale is one of the major defects on enamelled products. It is essentially caused by entrance of hydrogen in steel at pickling and/or firing. It will be controlled by combination of processing and composition modification. It is possible that steel with small amounts of alloy elements help prevent fishscale. Recently, Japanese and European steel producers are already supplying this type of products ⁽¹⁾. Because the cold-rolled steel sheets have better fishscale resistance, the previous works mainly concentrated on the cold-rolled steel sheets ⁽²⁻⁴⁾. Due to the thickness limitation and high price of cold-rolled steel sheets, it is necessary to develop enamelled hot-rolled steel sheet with good fishscale resistance, low porosity and good adherence.

The present work attempts to study hot-rolled steel sheet with good enamelling property and to find out the effect of Ti-content, processing etc. on fishscale resistance, enamel porosity and adherence. In this paper, the experimental methods will be discussed.

Experimental

Because the fishscale is related to hydrogen diffusion in steel, the electrochemical hydrogen permeation technique was used to measure hydrogen diffusivity in various steels. These results were compared with the forced fishscaling results.

The chemical compositions of the steel sheets used in this study are listed in Table 1.

The specimens for hydrogen diffusion were cut from hot-rolled steel sheets of 3mm thickness. The final temperature was about 800°C and the rolling temperature was 650-700°C, but No. 5 was rapidly cooled at about 2 times rate. The specimens size was 30×30×2.5mm. The specimens were first ground mechanically and then electropolished in a solution containing 1000ml H₃PO₄+140g CrO₃+50ml distilled water at 70 °C for 10 minutes with a current density of 0.5A/cm². They were then cleaned with tap water and dried. Finally they were degreased with acetone. By using electrochemical hydrogen permeation technique developed by Devanathan and Stachurski^[8], hydrogen diffusivity has been measured. One side of the specimen was coated with a Ni-layer of about 0.1µm thickness. Then the specimens were mounted between the two half cells giving 1cm area of exposure. The hydrogen inlet half cell in cathodic compartment, filled with 0.2 mol NaOH+0.6mol Na₂S, was controlled by a galvanostatic circuit with a current density of 10 mA/cm². The anodic surface was exposed to an electrolyte of 0.2 mol NaOH and polarized at+ 0.2V over corrosion potential by a potentiostat. All chemicals were analytically pure. The experiments at each condition were run three times and the average value was taken.

In order to ascertain the fishscale resistance of the used steels, the specimens of 150×100×2.5mm were used. They were pickled in 10% HCl for 8 minutes and dried. On one side of specimens the ground enamel was coated and fired at 880°C for 8 minutes, and then finish enamel was applied and fired at 850°C for 5 minutes, so the specimens can be mounted in the fishscaling electrolytic cell (shown in Fig.1), filled with a forced solution, as the cathodical electrode with the uncoated side towards the forced fishscaling solution. The cell was controlled by a galvanostatic circuit with a current density of 0.12A/cm². The first fishscaling point was recorded^[9].

With a normal metallographic microscope the porosity on the enamelled specimens was observed. With a electron scanning microscope and a electron microprobe analyzer the transition layer between metal and enamel was measured.

Results

1. Fishscaling tests on enamelled steel sheets

For all the enamelled specimens of A_2 and 10^* , the natural fishscaling occurred within one hour after firing on ground enamel as shown in Figure 2. When the finish enamel was still coated, in the 75% specimens on A_2 the natural fishscaling occurred within 24 hours after firing of the finish enamel as shown in Figure 3, but 10^* had no longer natural fishscaling after firing of the finish enamel. This showed that 10^* steel has better fishscale resistance than A_2 .

For the Ti-containing steel, the 50% specimens of No. 3 had a small amount of fishscaling after firing of ground enamel. Its appearance is analogous to Figure 2. It showed that its fishscale resistance is unsufficient. For other steels no natural fishscaling occurred. In order to compare the fishscale resistance of the various Ti-containing steels, fishscaling tests were carried out in the laboratory. The results are shown in Table 2. As can be seen from this Table the material containing 0.06% Ti has already relatively high fishscale resistance, no natural fishscaling occurred. Fishscale resistance increases with increasing of Ti content. Figure 4 shows the appearance of forced fishscaling of a Ti-containing steel. The appearance is similar to fishscaling of A_2 in Figure 3. This also demonstrated that hydrogen is a reason of fishscaling.

2. Hydrogen permeation tests

Hydrogen diffusivities of all kinds of specimens measured at 20°C , are given in Table 3. From the Table 3 it is derived that at the hot rolled state the hydrogen diffusivity of the Ti-containing steel is much smaller than that in A_2 or 10^* mild steel. The hydrogen diffusivity of Ti-containing steel (No. 4 and No. 5) is about $1/2 \sim 1/3$ and $1/5 \sim 1/7$ of A_2 or 10^* steel, respectively. Hydrogen diffusivity decreases with increasing of Ti-content. From Table 3 it can be derived that the hydrogen diffusivity of No. 5 is still smaller than that of specimens containing more Ti steel. This indicated effect of rolling process (cooling rate) on hydrogen diffusivity.

3. Effect of Ti of porosity of enamel surface

Figure 5 a and b are examples of large surface bubble structures of A_2 steel after firing of ground enamel and finish enamel, respectively, which will lead to reduction in corrosion resistance, while c and d are examples of small surface bubble structures of Ti-containing steel.

4. Effect of Ti on enamelling adherence

Good adherence is achieved when the enamel at the interface is saturated with the oxide of the base metal and the scale formed during firing on the steel surface is dissolved completely in the molten enamel. This is not dependent on the average analysis of the steel, but on the surface activity. For the Ti-containing steel Ti has surface enrichment tendency⁽²⁾. Furthermore, using electron microprobe analyzer, the Si and Ti

surface enrichment was also found as shown in Figure 6. Under identical conditions, the average thickness of transition layer between metal and enamel for A_3 , 10 $^{\circ}$ and Ti-steel (No. 4) was measured to be 21.0 μ m, 22.1 μ m and 35.2 μ m, respectively using a electron scanning microscope. The transition layer will provide good adherence. With test a good adherence of Ti-containing steel was also demonstrated.

Discussions

1. The test methods

As can be seen from Table 2 and 3, fishscaling time becomes longer and hydrogen diffusivity becomes smaller with increasing of Ti in steel. these two tendencies are consistent. The results of the fishscaling tests can synthetically give the fishscale behavior for the system of steel sheets and porcelain enamel. The advantage of this method is that the fishscaling, caused by any aspect, can be observed. The difference between Fig. 2 and 3 is caused by firing process and/or enamel thickness. This is a convenient method for enamel plants, but it is sometimes difficult to distinguish the fishscale cause. On other hand, the fishscale behavior can be measured only after firing of enamel.

For the hydrogen permeation technique the values measured at room temperature can be used to describe the fishscale behavior of materials after undergoing of temperature change. This is a convenient method for steel sheets production plants. Using this technique effect of the certain factors in regard to materials of fishscale behavior may be compared. However it can not be used to describe the fishscale behavior caused by porcelain enamel.

2. Effect of Ti on steel on fishscale resistance

The results showed that increasing Ti in steel plays a significant role for increasing of fishscale resistance. Ti in steel reduces the hydrogen diffusion rate, thus reducing the hydrogen evolution amount from steel. The small amount of hydrogen of slow release can not introduce fishscaling of enamel.

It was measured and calculated that in the range from 20 ~ 90 $^{\circ}$ C the activation energy of hydrogen diffusion and the hydrogen trapping energy in Ti-containing steel are much larger than that in A_3 and 10 $^{\circ}$ steels⁽⁸⁾. Thus Ti-containing steel has a smaller diffusivity of hydrogen.

Because Ti in steel has a great affinity to C and N, it has been shown by analysis that Ti in steel exists mainly as carbide⁽⁹⁾, a small amount of Ti in steel can exist also in nitride, sulfide and atomic state. TiC in steel is the strongest hydrogen trap, especially if distributed as a dispersed phase⁽⁹⁾. By using electron scanning microscope, it was observed that the carbide in No. 5 is much smaller than that in other specimens. This can explain the cause of low hydrogen diffusivity in No. 5.

3. Effect of Ti in steel on enamel porosity

Because Ti in steel can strongly 'fix' C and N, this leads to a reduction tendency of CO-forming in firing and to a reduction tendency of nitrogen evolution by aging. This decreases porosity of enamel. On the other hand, the formed carbide, nitride and sulfide of Ti are also strong traps for hydrogen and can catch a part of hydrogen, i. e. they can decrease hydrogen evolution amount, especially slow down the hydrogen diffusion rate. Thus Ti in steel may reduce both hydrogen damage and surface porosity of enamel.

It was observed from Fig. 5 that enamel on Ti-containing steel has a smaller bubble structure than that on A₂. This type structure will provide good corrosion resistance.

Conclusion

The forced fishscaling technique and the electrochemical hydrogen permeation technique can be used to study the fishscale resistance of a system of steel sheets and enamel or of steel sheets used for enamelling.

Ti in steel, specially in a dispersed phase, decreases the hydrogen diffusivity. It increases fishscale resistance of a system on metal and enamel. In addition, it decreases porosity on the enamel.

Furthermore Ti in steel stimulates the adherence of enamel on steel sheets.

The hot-rolled Ti-containing steel sheets have a good enamelling behavior.

References

1. K. G. Brickner, International Enamelist, 37(1987) (2) 2.
2. Feng Zhimin, Fu Yulan and Zhao Keping, Acta Met. Sinica, 22(1986) B189.
3. Takechi, Kokai Tokkyo Koho, 51-126912.
4. Yoshida. Toshiaki, Kokai Tokkyo Koho, 56-248.
5. M. A. V. Devanathan and Z. Stachurski, Proc. Roy. Soc., London, 270 (1962) 90.
6. Hans, Hadwiger, Email, 105 Jahrg., Sprechsaal, 1047.
7. Zhao Keping and Xu Xiaolian, 7th APCCC, Beijing, Aug. 19-23, 1991.
8. Zhao Keping, Fu Yulan and Xu Xiaolian, 4th International Congress of Materials and Hydrogen, May 9-13, 1988. Beijing, P637.
9. G.M. Pressouyre, Met. Trans., 10A(1979) 1571.

Table 1. Chemical Composition of Specimens Used

No.	Kind of Steel	Chemical Composition (wt %)					
		C	Si	Mn	P	S	Ti
1.	A ₃	0.11	0.18	0.43	0.008	0.031	-
2.	10 [#]	0.09	0.20	0.43	0.008	0.030	-
3.	Ti-Steel	0.03	0.16	0.30	0.009	0.014	0.03
4.	Ti-Steel	0.06	0.02	0.24	0.009	0.017	0.06
5.	Ti-Steel	0.07	0.02	0.28	0.009	0.020	0.12
6.	Ti-Steel	0.05	0.05	0.24	0.011	0.020	0.18

Table 2. Fishscaling Time of Specimens

No.	Kind of Steel	Ti-Content (%)	Fichscaling Time (min.)
1.	A ₃	-	Natural Fishscaling of 100% Specimens
2.	10 [#]	-	Natural Fishscaling of 100% Specimens
3.	Ti-Steel	0.03	Natural Fishscaling of 50% Specimens For non-fishscaling, 23 min.
4.	Ti-Steel	0.06	57
5.	Ti-Steel	0.12	75
6.	Ti-Steel	0.18	88

Table 3. Hydrogen Diffusivity D of Various Specimens (25±1°C)

No.	Kind of Steel	Ti-content (%)	$D \times 10^{-10} \text{ (m}^2/\text{s)}$
1.	A ₃	-	13.54
2.	10 [#]	-	9.83
3.	Ti-Steel	0.03	7.80
4.	Ti-Steel	0.06	4.55
5.	Ti-Steel	0.12	2.05
6.	Ti-Steel	0.18	2.40

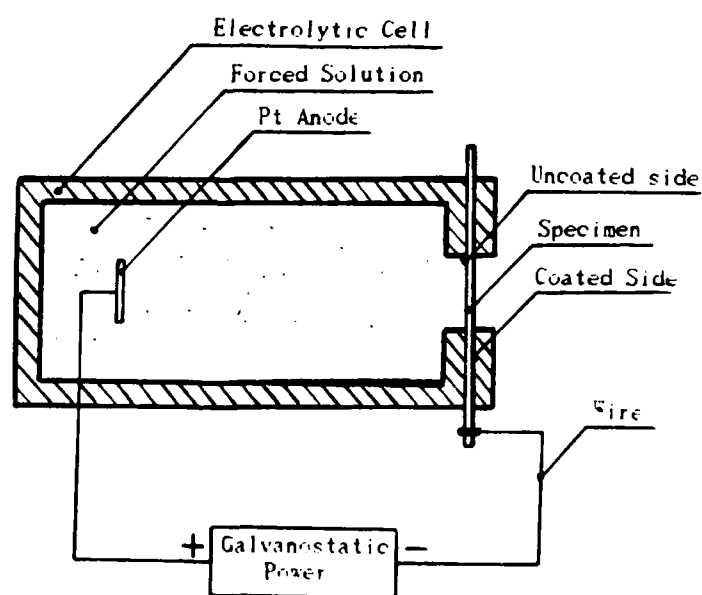


Fig. 1 Fishscaling Device Sketch



Fig. 2 Appearance of Natural Fishscaling of A₃ after Firing of Ground Enamel



Fig. 3 Appearance of Natural Fishscaling of A₃ after Firing of Finish Enamel



Fig. 4 Appearance of Forced Fishscaling of Ti-Containing Steel

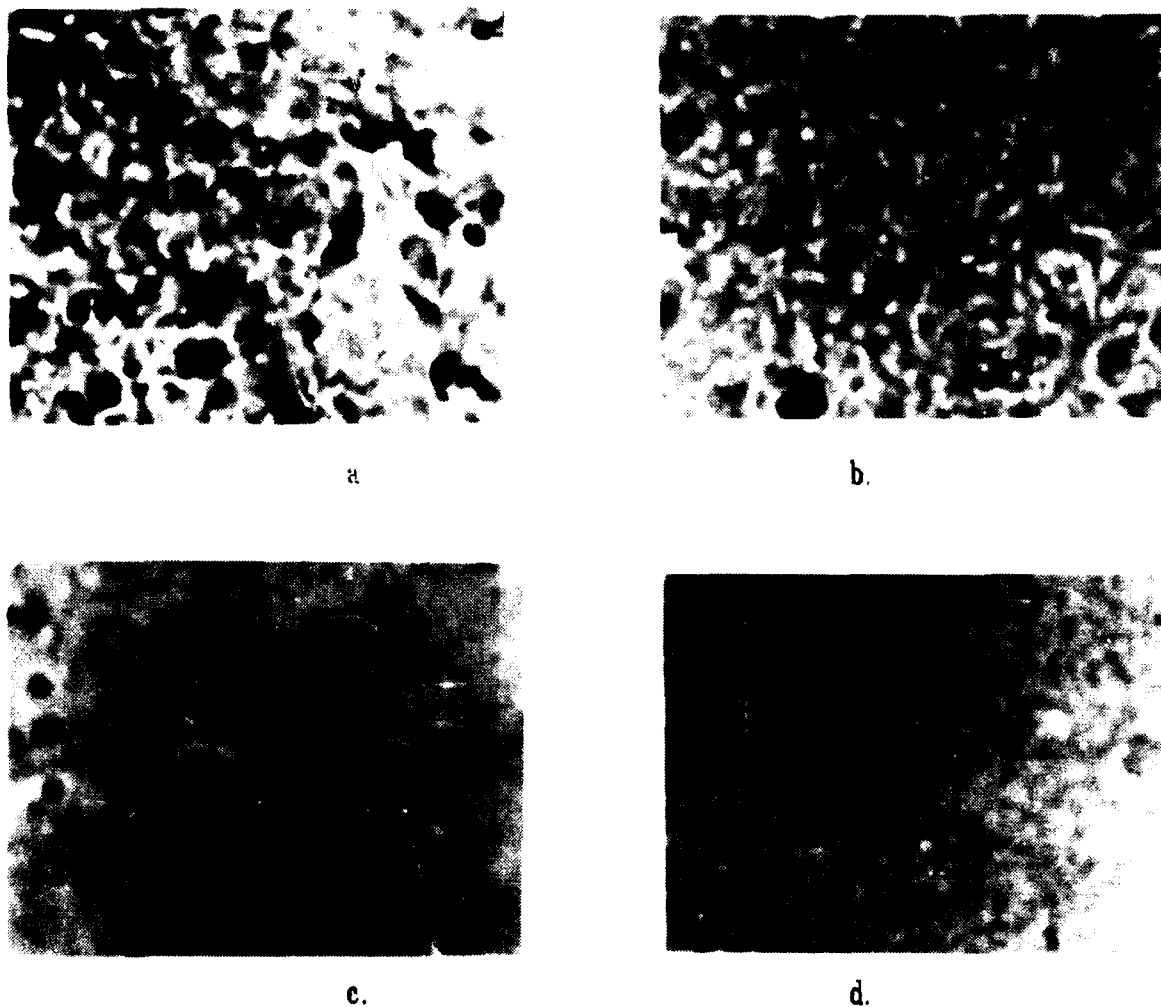


Fig. 5 Enamel Surface Bubble Appearance on A₃ and Ti-Steel
 a. A3 Enamelled once b. A3 Enamelled twice
 c. Ti-Steel, Enamelled once d. Ti-Steel, Enamelled twice

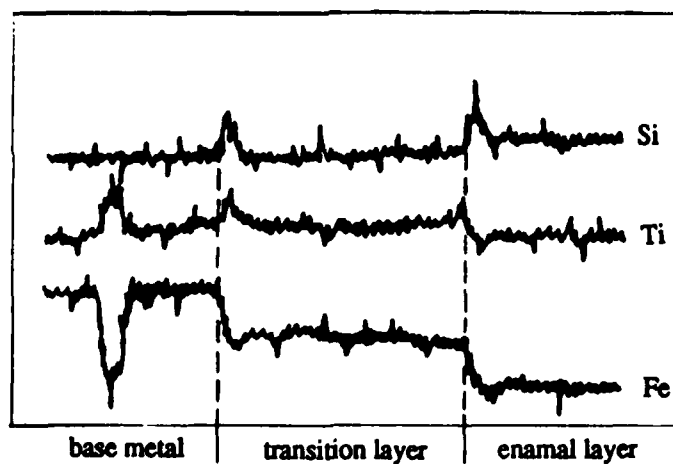


Fig. 6 Composition Change of Fe, Ti and Si in Transition Layer

**Study of Anticorrosion Properties of Metal Arc -
Sprayed Coatings on Carbon Steel for Use in Petroleum Products**

Alec Groysman
Oil Refineries Ltd.
PO Box 4
31000 Haifa Israel

Vladimir Belashchenko
Metalspray USA, Inc.
11615 Busy street
Richmond, VA 23236, USA

Abstract

An investigation of the protective properties of different metal arc - sprayed coatings (aluminum, stainless steel, bronze) on carbon steel in petroleum products and two - phase water - hydrocarbon systems has been carried out in laboratory and field conditions. Parameters of the arc - sprayed process have been optimized to increase anticorrosion properties and bond strength of coatings. Electrochemical methods and special solutions for accelerated tests have been applied. Also protective properties of combined aluminum - sealer petroleum-, water-, and atmosphere - resistant coatings have been examined for the petroleum storage tanks. It has been shown that aluminum coatings provide the best protective properties in the petroleum products and water - hydrocarbon systems. The estimated durability of aluminum coatings (as sprayed) is about 15-20 years and for the case of combined aluminum - sealer coatings durability is 25-30 years. All petroleum - resistant coatings studied do not influence the quality of petroleum products when stored for 12 months.

Key terms: petroleum products, arc - sprayed coatings, anticorrosion properties, combined aluminum - sealer coatings.

Introduction

The pure petroleum products (gasoline, kerosene, diesel oil, jet fuel, and lubricants) are not corrosively aggressive to steel and other alloys. However, oxygen and hydrogen sulfide can dissolve well in petroleum products. In addition, water is present in petroleum products. These corrosively aggressive substances result in corrosion of storage tanks, pipes and other structures which are in a contact with petroleum products.

Zinc and aluminum arc - sprayed coatings (ASC) are recommended for anticorrosion protection of steel and other alloys in contact with petroleum products, atmosphere, fresh and sea water [1-3]. However, zinc coatings are dissolved under hot water and hydrogen sulfide influence. What is more, toxic zinc aerosol is formed when the arc - spray process is used. Therefore, aluminum was chosen as a basic material for the experiments performed. Besides, we did not find information about the efficiency of combined metallizing - sealer coatings (MSC) for the protection of steel structures in contact with petroleum products.

The goals of this work were:

- i) Tests of the protective properties of arc - sprayed coatings (ASC) and combined metallizing - sealer coatings (MSC) in contact with petroleum products and water - hydrocarbon systems in laboratory and field conditions.
- ii) Optimization of arc - spray process parameters to get the best anticorrosion properties and bond strength of coatings.
- iii) Investigation of the coating influence on the quality of petroleum products in contact with the coatings.

I. Anticorrosion properties of ASC and combined MSC.

A. Electrochemical investigation of anticorrosion properties of ASC.

Electrochemical properties of aluminum, stainless steels (13Cr & 18Cr10Ni), and bronze (90%Cu 10%Sn) coatings have been studied. The thickness of aluminum coatings varied from 0.1 to 0.5 mm, the thickness of other coatings was 0.3 mm. Samples to be studied were steel plates

(50x50x3 mm). Electrode potentials of ASC were measured in relation to Ag-AgCl reference electrode in 0.5 N NaCl solution and waste water from petroleum storage tanks (Figures 1, 2). The nature of the coatings and their thickness influence the dependence between the electrode potential (E) and exposure time (t) in electrolyte solutions. The largest changes of E are observed for the first 2-3 hours. Stationary electrode potentials (E_{st}) of aluminum coatings are stabilized after 24 hours of exposure in the aggressive solutions. The E values of thin (0.1 mm) aluminum coatings on steel are between E of aluminum and E of a carbon steel. This fact can be explained by a through porosity of the coatings. As the coating thickness (h) increases, a sharp increase of E_{st} was observed in the vicinity of $h=0.2$ mm. From the "critical" thickness (h') E_{st} for the coatings is practically equal to E_{st} for aluminum and does not decrease with increasing h. It means that from $h=h'$ the aluminum coatings investigated practically do not have through porosity. The two electrolyte solutions mentioned are more corrosive to aluminum and carbon steel than petroleum products. Therefore $h'=0.2$ mm could be considered as an optimal thickness for the particular case.

The E values of coatings from SS13Cr, SS18Cr10Ni and bronze on steel are more positive than E of steel (Fig.2). These three types of coatings are cathodic. Thus they are only insulating steel from an aggressive environment, i.e. protecting steel as a barrier. These data are confirmed by visual examination. Rust points and spots appeared on metallizing coatings of SS13Cr, SS18Cr10Ni and bronze after several days of exposure in the aggressive environment.

B. Accelerated tests of ASC and combined MSC.

Accelerated tests of different coatings were performed in an aggressive environment for 3 months. The corrosive environment for ASC and combined MSC was a mixture of a petroleum product (gasoline, kerosene, diesel or industrial oil) and 0.5 N NaCl solution saturated with hydrogen sulfide. After exposure the samples with the coatings were washed in gasoline and dried (except combined MSC) at 120°C to constant mass. The corrosion products were removed from the samples by means of a water jet. The corrosion resistance of coatings was estimated

gravimetrically and visually after 1, 2 and 3 months of tests and after a steam treatment for 24 hours. The steam treatment imitated the process of tanks and vessels being cleaned from petroleum sludge.

The accelerated tests showed the following.

i) Aluminum coatings have very good corrosion resistance in all petroleum products tested (gasoline, diesel oil and kerosene) and two phase water - hydrocarbon systems. Aluminum coatings have practically no changes after steam treatment.

ii) Some types of stainless steel coatings sometimes have corrosion resistance better or comparable with aluminum coating in particular types of petroleum products: SS18Cr10Ni+Al - in gasoline; SS18Cr10Ni and SS13Cr in kerosene.

iii) Rust spots appeared on the stainless steel and bronze coatings after steam treatment. It means that these coating compositions are not resistant to steam treatment.

Thus, it is possible to conclude that aluminum coatings are most attractive as anticorrosion coatings in the environments investigated. At the same time it is necessary to stress that corrosion losses for the case of a monolithic aluminum are significantly less than for the case of aluminum coatings. For example, during 3 months corrosion losses were 0.23-0.28 g/m² and 2.45-5.92 g/m² respectively. This fact shows that to improve anticorrosion properties it is necessary to decrease porosity.

One of the possible approaches to decrease porosity is the application of coatings sealers. Copolymer chlorvinyl and vinylacetate paint (with aluminum or carbon dust fillings) as the sealer has been used. Accelerated tests of combined MSC have been done in the same aggressive environment as in the case of ASC. Anticorrosion properties of combined MSC have been determined visually. After three months of accelerated tests including steam treatment only aluminum - sealer (with carbon fillings) had no changes. Rust points and spots appeared on the stainless steel and bronze combined MSC after steam treatment. Corrosion resistance of examined combined MSC is higher than that of ASC.

C. Field tests.

Field tests of the aluminum ASC and aluminum - sealer coatings sprayed on plate samples and on the models of reservoirs have been carried out for more than 6 years. Copolymer chlorvinyl and vinylacetate with a carbon or aluminum dust fillings were used as a sealer. After 6 years of test there were no defects on the aluminum coatings (as sprayed) in gasoline, but there were some rust spots in kerosene. The reason of the rust was probably porosity of the coatings. As the result of the sealers applications, porosity of the coatings was decreased and coatings protective ability was improved. MSC had no defects after six - year field tests in gasoline, kerosene and diesel oil. There were some defects in the case of industrial oil. It is necessary to stress that these results sometimes are not correlated with the accelerated laboratory tests of ASC and MSC, but field tests give a prognosis of the duration of the anticorrosion coatings.

2. Spraying technology and coatings anticorrosion properties.

Coatings properties depend mainly on design of the arc spray head or spray nozzle system (NS) and the process performance. Presently two types of nozzle systems ("open" and "closed") are widely used to spray different kind of coatings [4,5]. We tested both of them to make the correct choice for the particular case of the anticorrosion protection of a carbon steel in petroleum products. In general, different nozzle systems are providing customers with different spray pattern and particles size distributions. For example, for stand-off 100-120 mm and aluminum wire with diameter 2 mm for "closed" and "open" nozzle systems, which we used in this project, standard deviation of spray pattern distribution (σ_p) and average particles size (d) were: for "closed" NS $\sigma_p = 11-13$ mm, $d = 40-80$ μ m; for "open" NS $\sigma_p = 7-8$ mm, $d = 50-100$ μ m. Because of the smaller value of σ_p and bigger d for the case of the "open" NS it is possible to expect better values of coatings bond strength. At the same time the smaller size particles for "closed" NS allowed us to expect a lower level of coatings porosity and better

corrosion resistance.

For the spraying performance optimization we used a stochastic approach [6]. In accordance with this approach for every particular NS and spraying material there should be an optimal range for the nondimensional parameter $B = WdK \cdot \rho_p \cdot \delta_p / G$, where G is the deposition rate, ρ_p is the density of the spraying material, $K = 5h/d$; h is a mean particle thickness after solidification; W is the spray head velocity. In the optimal range of B it is possible to expect maximum coatings bond strength and structure homogeneity, i.e the best corrosion resistance. Spray regimes of aluminum are in the table. The thickness of aluminum coatings was 0.22 ± 0.02 mm in all cases. Anticorrosion properties of recieved aluminum coatings (see table) have been studied on the basis of kinetics of dissolution of aluminum coatings in gasoline in static conditions for 1-10 months, in water solutions in dynamic conditions for 6 hours and in static conditions for 22 days. Concentration of aluminum in gasoline has been determined by means of atomic absorption method, in water solution - spectrophotometric method. Corrosion resistance of aluminum wire (used for drifting ASC) was examined for compare in the same conditions. Study of corrosion resistance of aluminum coatings drifted on steel by means of 8 technological regimes (see table), shows the low aluminum concentration in gasoline ($1.3 \cdot 10^{-4}$ g/100 ml gasoline) throughout 10 months of experiment. These data agree with the results of long term (over 6 years) field test of aluminum coatings on the reservoir models with gasoline.

Corrosivity of petroleum products is defined by contents of aggressive substituents, mainly because of water, dissolved salts and gases. Thus metallizing coatings are more vulnerable to water solution (wastes) frequently present in petroleum storage tanks. Therefore corrosion resistance of aluminum coatings was determined in water solution modeling wastes in storage tanks.

Kinetic curves of dissolution of aluminum coatings in dynamic conditions show the least mass loss for coatings, sprayed by means of "closed" nozzle system in regimes 2 and 3 (Fig.3). For the "open" nozzle system the best result is at the regime of 6. However, corrosion resistance of these coatings is less than of the coatings sprayed by means of "closed" nozzle system. These data are confirmed with the

results of dissolution of aluminum coatings in static conditions (Fig.4). Comparison of data for mass loss (corrosion) of stationary region for more than 4 hours and adherence of aluminum ASC as function of B - parameter shows that the optimal spraying range $1.0 < B < 1.5$ (Fig.5).

Kinetic curves of dissolution of aluminum coatings in static conditions allow to estimate the durability of these coatings - about 15-20 years. The durability of combined MSC is longer 1.5-2 times than only aluminum ASC. We estimate approximately 25-30 years as the durability of combined coatings. That is, combined MSC can protect the storage tanks and other structures in contact with petroleum products for full economical life (whole service time) of these structures.

III. Influence of the aluminum ASC and combined MSC on the quality of petroleum products.

It is important that the anticorrosion coatings of the petroleum storage tanks do not have an influence on the physico-chemical properties (i.e. quality) of the petroleum products even after a long-term storage period in tanks in contact with the applied anticorrosion coatings. We have determined the physico-chemical properties of gasoline, kerosene, diesel oil according to standards for these petroleum products after 1, 3, 6, 9 and 12 months of contact with anticorrosion coatings. For comparison we have determined the quality of petroleum products that have not been in contact with these coatings. After 1-3 months of contact of aluminum ASC with petroleum products the quantity of suspended solids in the petroleum products increases. The aluminum particles, coupling poorly with one another, pass into the petroleum product and make the quality of the latter worse. After shot (or sand - quartz) blasting of aluminum ASC surfaces the aluminum particles do not pass into petroleum products and the quality of the latter does not change for 12 months of contact with aluminum ASC. This fact points out the necessity of shot (or sand - quartz) blasting of aluminum ASC for the purpose of removing the poor coupling particles from the aluminum surface. We have determined that examined combined MSC (copolymer chlorvinyl and vinylacetate with

aluminum and carbon dust fillings) do not influence the quality of petroleum products when the latter are stored for 12 months.

These results allow recommending the aluminum ASC and combined MSC (chlorvinyl and vinylacetate copolymer with aluminum and carbon powder as fillings) for long-term anticorrosion protection of storage tanks and other structures in contact with petroleum products.

SUMMARY

1. Aluminum arc-sprayed coatings and combined metallizing-sealer coatings have been examined and recommended for the anticorrosion protection for the whole service time of structures contacted with petroleum products. The sealer (paint) is copolymer chlorvinyl and vinylacetate with carbon or aluminum dust fillings.

2. Optimal thickness 0.2 mm of aluminum ASC is recommended. The predicted durability of aluminum ASC is about 15-20 years, of combined MSC - 25-30 years.

3. High protective properties of aluminum ASC are reached by means of "closed" nozzle system of metallizing apparatus. The optimal B-parameter is $1.0 < B < 1.5$.

4. Aluminum ASC and combined MSC do not influence the quality of petroleum products when the latter are stored for 12 months.

REFERENCES

1. L.L.Shrier, Corrosion, (London: Butterworths, 1979), p.632.
2. C.A.Robiette, Anticorrosion Methods and Materials, 29, 8 (1982): p.12.
3. H.E.Townsend, C.F.Meitzner, Materials Performance, 22, 1, (1983):p.54.
4. R.Kreinbuchl, DVS-Ber., 47 (1977): s.32.
5. Ott Walter, Machinemarkt, 85, 97 (1979): s.20.
6. V.E.Belashchenko and Yu.B.Chernyak, Proceedings of the International Thermal Spray Conference (Orlando, USA, 1992), p.433.

Table.

Technological regimes of aluminum arc spray on steel

Number of regime	Type of nozzle system	Expenditure of air, m ³ /hour	Spray head velocity W, m/s	Deposition rate G, kg/hour
1	C	110	0.6	4.5
2	C	110	1.4	4.5
3	C	110	2.2	4.5
4	C	110	1.4	12
5	O	90	0.8	4.5
6	O	90	1.6	4.5
7	O	90	2.4	4.5
8	O	90	1.6	12

C = "closed" nozzle system; O = "open" nozzle system.

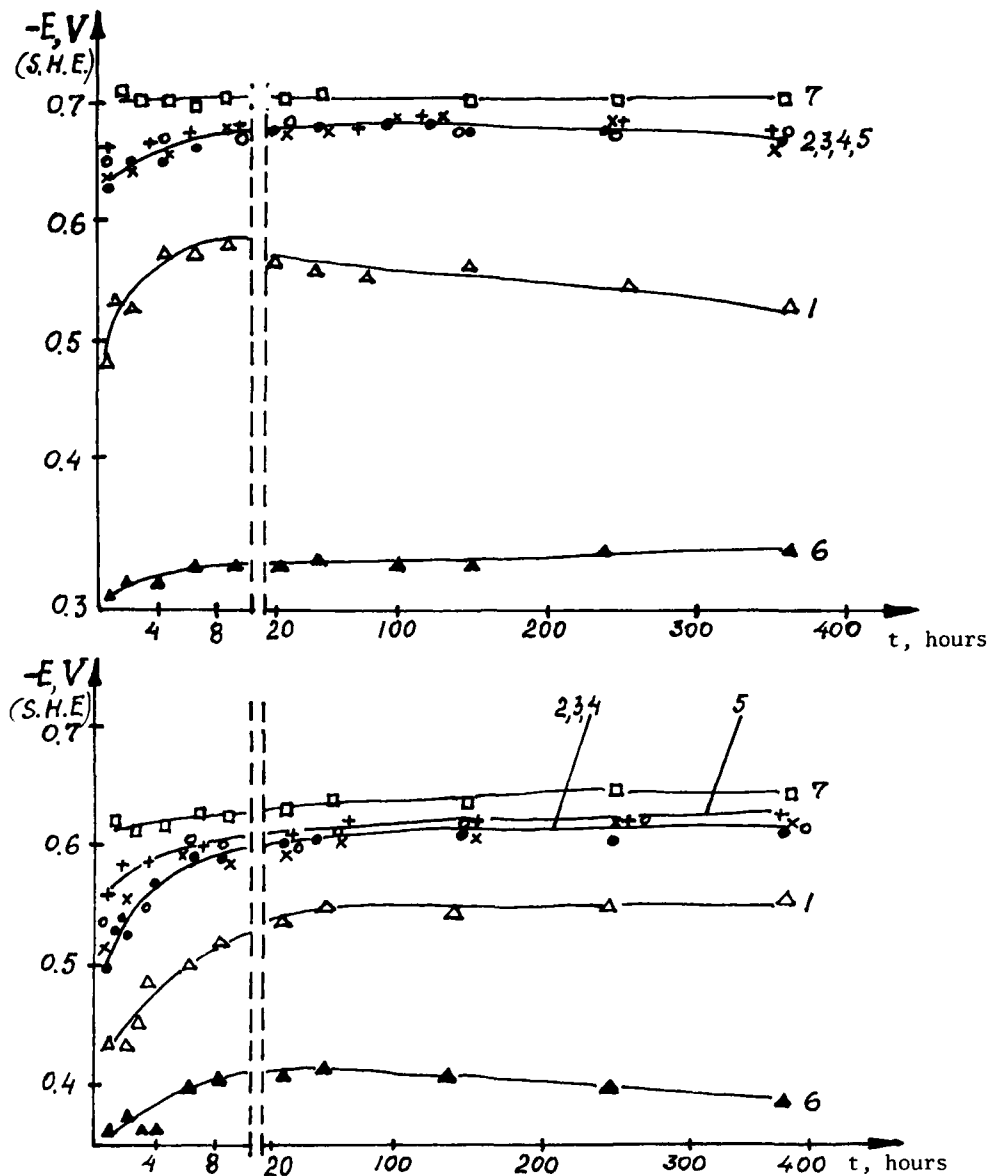


Figure 1.

Electrode potential of ASC of different thickness on steel in 0.5 N NaCl (a) and waste water (b) vs exposure time:

1 - 0.1 mm (\triangle); 2 - 0.2 mm (\bullet); 3 - 0.3 mm (\times); 4 - 0.4 mm (\circ); 5 - 0.5 mm ($+$); 6 - carbon steel (\blacktriangle); 7 - aluminum film (\square).

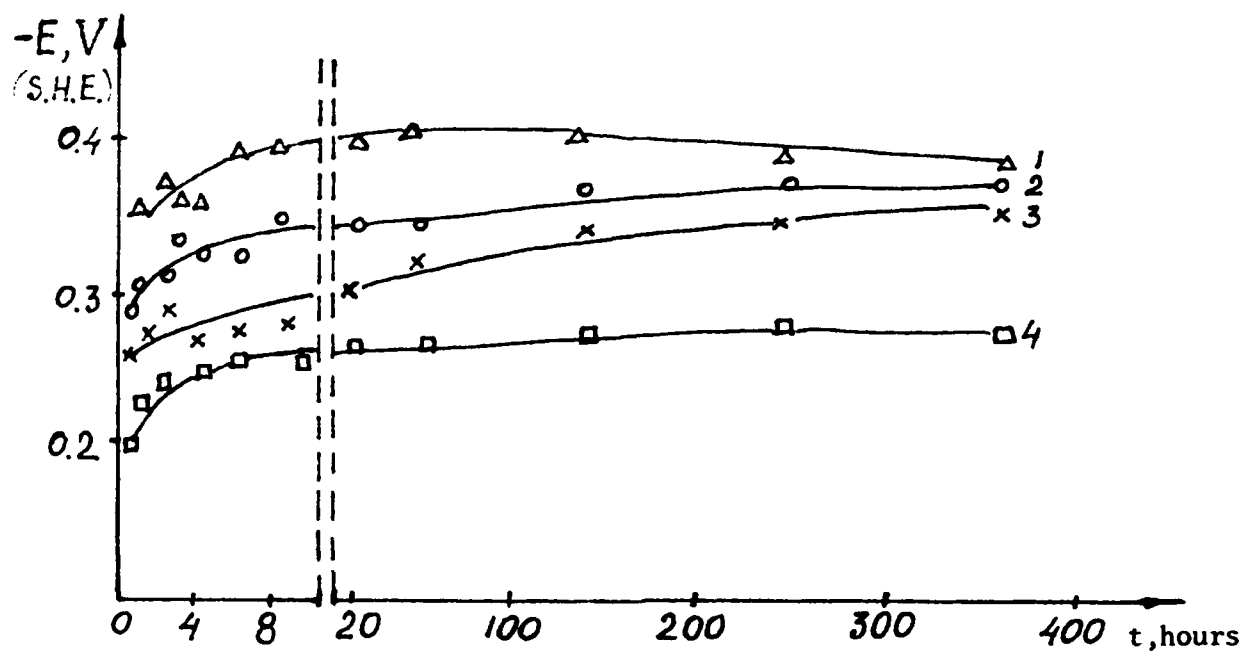


Figure 2.

Electrode potential of ASC on carbon steel in waste water
vs exposure time; 1 - carbon steel; 2- ASC SS13Cr;
3 - ASC SS18Cr10Ni; 4 - ASC Bronze. $d=0.3$ mm.

25 C.

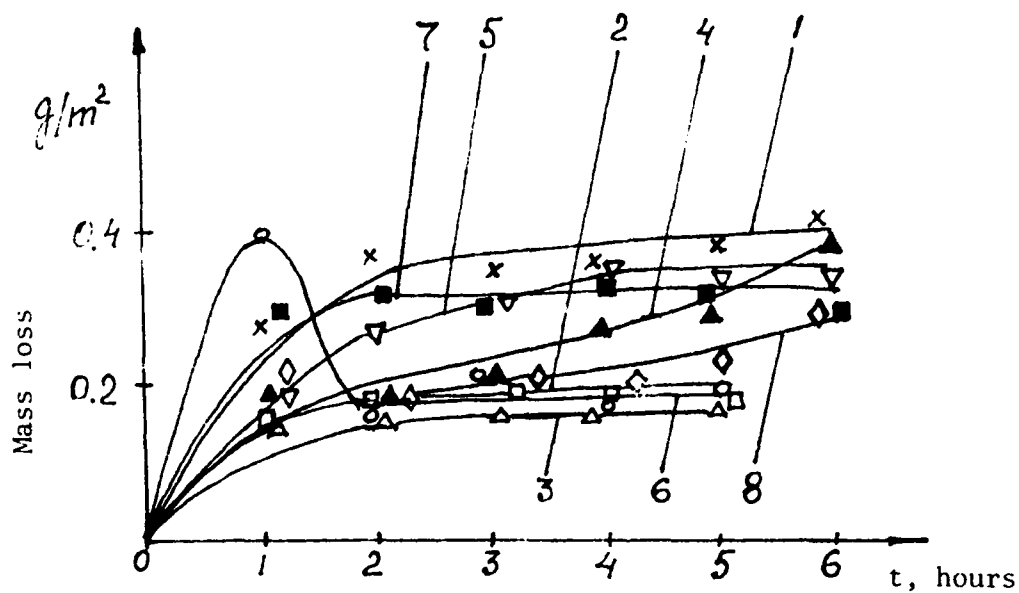


Figure 3.

Mass loss of aluminum ASC in distilled water vs exposure time.
Dynamic conditions, 25 C.

(Curve numbers correspond to the numbers of the
technological spray regime - see table).

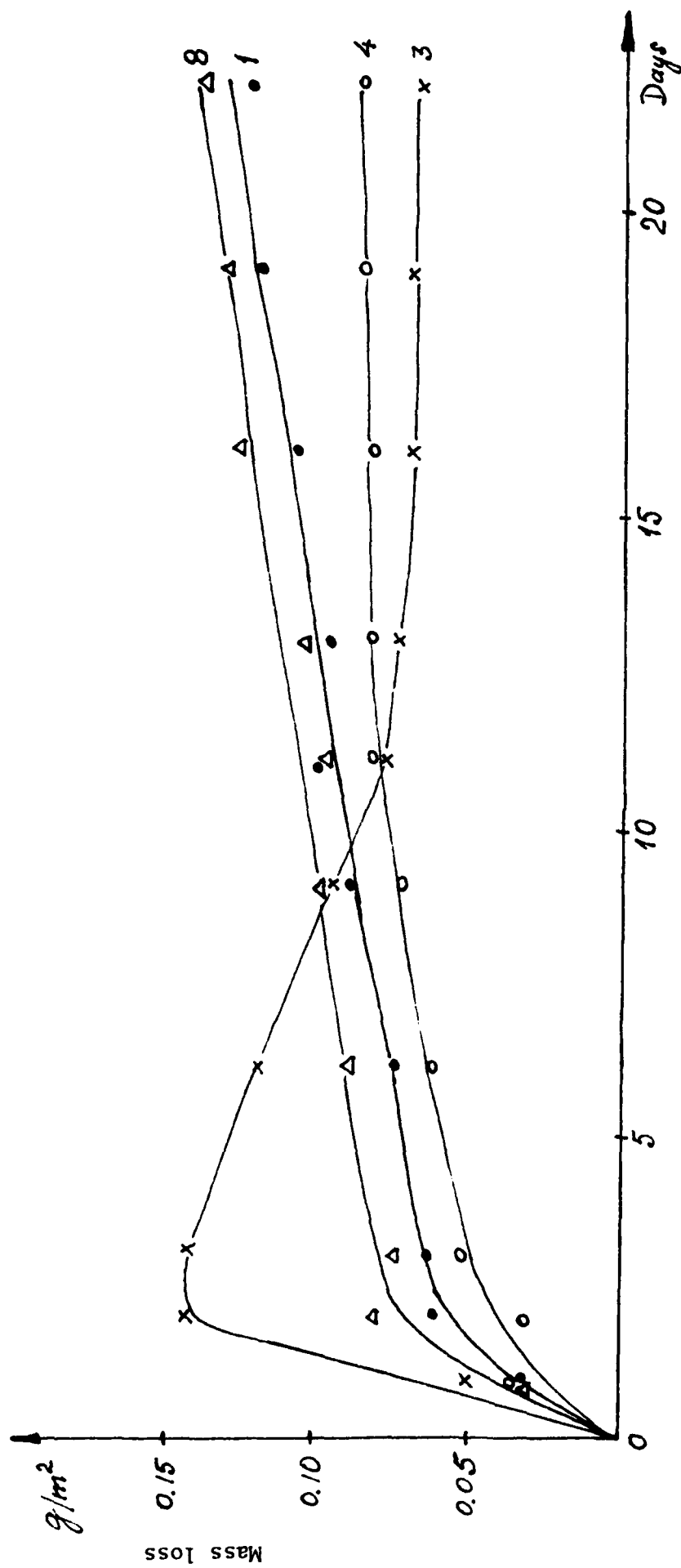


Figure 4.

Mass loss of aluminum ASC in distilled water vs exposure time.

Static conditions, 25 C.

(Curve numbers correspond to the numbers of the technological spray regime - see table).

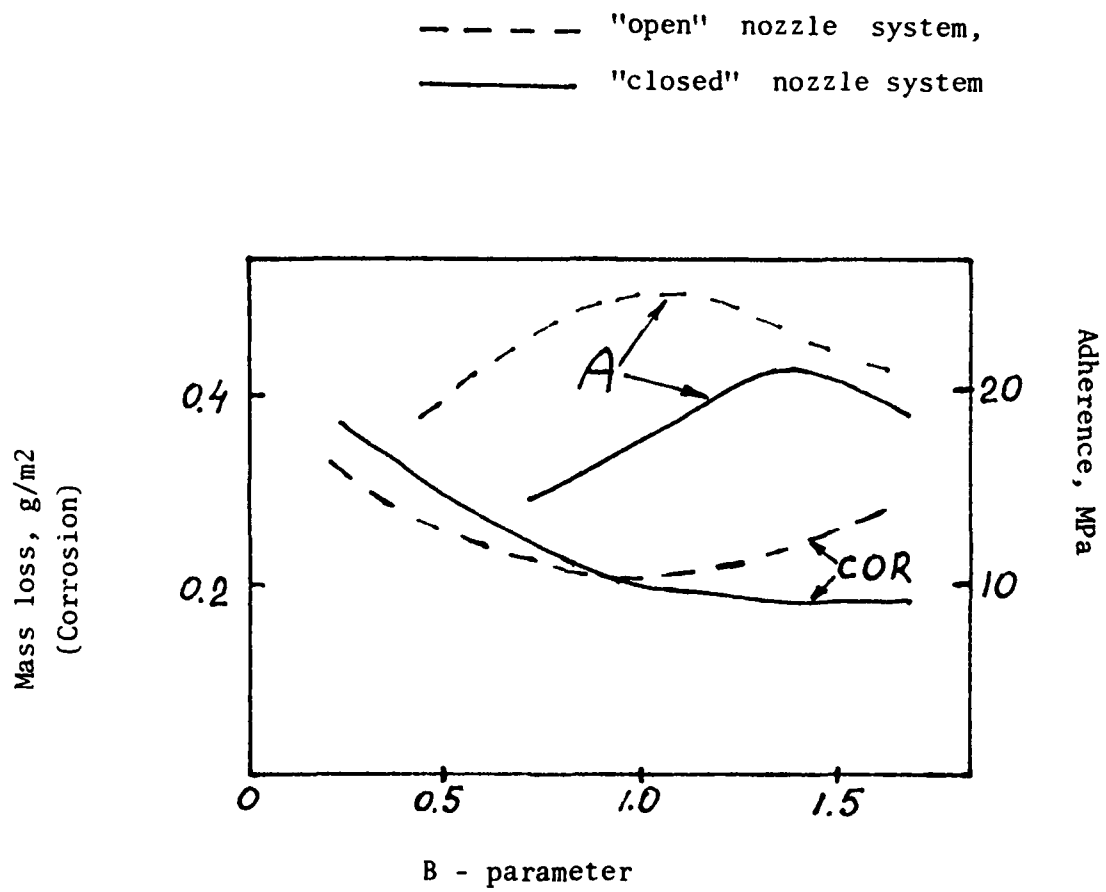


Figure 5.

A Discussion on the Role of Cations in Enhancing Internally Coated Metal Container Corrosion Failure.

W. S. Tait
S. C. Johnson & Son, Inc.
1525 Howe St.
Racine WI 53403-5011

K. A. Handrich
S. C. Johnson & Son, Inc.
1525 Howe St.
Racine WI 53403-5011

Abstract

Time prior to 30% failure (T_{30}) of internally coated metal containers increased as the solution cation was changed from $\text{Ca}^{+2} \rightarrow \text{K}^{+} \rightarrow \text{Na}^{+} \rightarrow \text{Li}^{+} \rightarrow$ deionized water, for salt concentrations from 0 to 0.1M. This trend is similar to that reported by Leidheiser et. al. for coated steel cathodic delamination rates. Pore resistance values obtained with electrochemical impedance spectroscopy also followed the trend observed for T_{30} times. However, potassium salt caused earlier failure than the calcium salt when the salt concentration was 2M. The relationship between mean activity coefficients and T_{30} times help resolve the seeming inconsistency between 2M and lower concentration data.

The correlation between trends observed for pore resistance and T_{30} times suggest that the polymer coating degradation mechanism proposed by Leidheiser et. al. is also operative when the coated metal is at rest potential. However, our data suggests that coating morphological changes occur at salt concentrations below the 0.5M level originally hypothesized.

It is speculated that cation water sheath structure may determine how effectively a cation alters coating morphology. However, lack of general agreement on the number of water molecules in a cation water sheath and information on group II cation water sheath structure prevents formulation of a more rigorous hypothesis on this relationship. It is also speculated that the thermodynamic state of a cation in a coating may be similar to cation thermodynamic state of the bulk electrolyte.

Key terms: mean activity coefficient, cation, coated metal, metal containers, internally coated containers, cathodic delamination, rest potential

Introduction

Leidheiser and Wang[1] discussed the effect of group I metal cations on delamination of polybutadiene and epoxy-polyamide coated steel, when subjected to an applied cathodic voltage. They observed that coated metal delamination rates in salt solutions increased as solution cations were changed from $\text{Li}^+ \rightarrow \text{Na}^+ \rightarrow \text{K}^+ \rightarrow \text{Cs}^+$. They concluded that delamination was controlled by diffusion of cations through the coating to maintain charge neutrality. They also observed that a rough parallelism existed between delamination rates and diffusion coefficients for group I cations. Halide ions were shown to have no effect on coating delamination.

In a later paper, Leidheiser, Granata, and Turoscy[2] hypothesized that 0.5M sodium ion concentrations caused morphological changes in polybutadiene coated steel, leading to defects that served as charge transport pathways. They concluded that these pathways promoted coating cathodic delamination. It was also concluded that cation ion concentrations <0.5M did not cause coating morphological changes.

Results from their work led us to speculate that different cations would also produce different corrosion rates for internally coated metal containers at rest potential.

Experimental

Commercial internally coated, tinplated steel aerosol containers were filled with 18 Mohm deionized water, or 1 of 4 inorganic salt solutions (LiCl , NaCl , KCl , and CaCl_2) prepared with 400 Kohm deionized water. Cation concentrations of 0.05M, 0.075M, 0.1M and 2M were used in these studies.

Filled containers were pressurized to 40 psig with liquefied petroleum gas. One hundred (100) containers were filled for each variable in the deionized water through 0.1M salt concentration studies, and 50 containers were filled with each variable for the 2M salt concentration studies. Filled containers were stored at 21.1°C (70°F) and periodically visually inspected for perforation.

Container corrosion rates for each solution variable were quantified with the time at which 30% of test containers (T_{30}) for a given solution variable perforated from corrosion. Time to reach a given percent failure is the typical statistical parameter used for characterizing population lifetimes[3], and was used here because all containers in a given population (salt variable) do not fail simultaneously[4].

Container internal coatings were thermally cured 5μ thick epoxy resin coatings used for commercial aerosol containers. A complete description of coated containers used for this research was presented in a previous publication[5].

Electrochemical impedance spectroscopy (EIS) measurements were also conducted on container samples after 20 and 100 days exposure. The EIS test cell and measurement parameters used for this research were described in a previous publication[6].

Results

Figure 1 contains a typical graph of cumulative percent container failures. It can be seen in Figure 1 that the cumulative percent failure (e.g. percent failures at 60 days) increases from deionized water \rightarrow Li⁺ \rightarrow Na⁺ \rightarrow K⁺ \rightarrow Ca²⁺. The Kruskal Wallis statistical test[7] indicated that all curves were independent of each other at the 95% confidence level.

Failure data from all studies are summarized in Table 1. The time at which 30% of the containers failed from corrosion, T₃₀, is used to characterize each container-solution variable. T₃₀ times increased in all studies as the solution cation was changed from Ca²⁺ \rightarrow K⁺ \rightarrow Na⁺ \rightarrow Li⁺ \rightarrow deionized water, with the exception of 2M calcium and potassium solutions.

This trend can be seen more clearly in Figure 2, where 0.05M through 0.1M data are charted for each cation. It can also be seen in Figure 2 that increasing cation concentration from 0.05M to 0.1M had little or no effect on the magnitude of T₃₀ times. The trend in T₃₀ times for the group I cations inversely follows the trend observed by Leidheiser et. al. for cathodic delamination rates.

The 2M potassium solution T₃₀ time in Table 1 is lower than the corresponding value for 2M calcium solution. These values appear to contradict data from lower concentrations. However, it will be proposed in the next section that the 2M data are consistent with lower concentration data, when T₃₀ times are considered in terms of salt mean activity coefficients.

Pore resistance values also followed the trend observed for T₃₀ times, as can be seen in Figure 3. Pore resistance values indicate how readily electrolyte moves through a coating.

Discussion

The relationship observed by Leidheiser et. al. for cathodic delamination rates correlates with that observed for container T₃₀ failure times. It is reasonable to suggest that (because of the similarity between the 2 different studies) the cation coating degradation mechanism may be the same for cathodic delamination and coated metal corrosion at rest potential.

It can be seen by comparing Figures 2 and 3 that coating pore resistances and T₃₀ times followed the same trend. This observation leads to the hypothesis that coating degradation is the precursor of metallic corrosion, as opposed to corrosion occurring in pre-existing coating pores.

This hypothesis is strengthened by further observations that: a) deionized water does not produce visible corrosion for at least 100 days, but metallic corrosion is observed at scratches through coatings within several hours after submerging in deionized water, b) visible corrosion of coated container samples exposed to salt solutions does not appear until 6 to 20 days after initial exposure, and c) pores were not observed in coatings used for this study. It has also been our experience that visible corrosion is also observed at scratches through coatings within hours after submersion in salt solutions.

All of the data and observations presented so far lend credence to the Leidheiser et. al. hypothesis that cations cause morphological changes in coatings which create charge transfer pathways through the coatings. However, the work presented here also suggests that morphological changes occur at concentrations below 0.5M.

The 2M T_{30} time for potassium is less than that for calcium; an apparent contradiction to the trend noted for lower concentrations. In addition, the qualitative relationship between diffusion coefficients and cathodic delamination for group I cations, discussed by Leidheiser et. al., does not hold for T_{30} times when the calcium coefficient (a group II cation) are included with group I coefficients. The lack of an apparent relationship is made clear by comparing T_{30} data in Table 1, with diffusion coefficient data in Table 2[8]. The diffusion coefficient for calcium ions is less than that for lithium, yet the calcium ion variable failed at the earliest times. The relationship between mean activity coefficients and T_{30} times help resolve both of these apparent contradictions.

Figure 4 contains a graph of activity coefficients as a function of concentration, produced from data published by Harned and Owen[9]. Mean activity coefficient data are only available to 0.1M, thus curves were extrapolated to 0 concentration by assuming the activity coefficient of pure water (an infinitely dilute salt solution) was equal to 1[10].

It can be seen in Figure 4 that at concentrations below approximately 1.2M, the mean activity coefficient increases in the order of $\text{Ca}^{+2} \rightarrow \text{K}^{+} \rightarrow \text{Na}^{+} \rightarrow \text{Li}^{+}$. It appears from a comparison between Figure 4 and T_{30} times (Table 1), that smaller activity coefficient values result in lower T_{30} times. Indeed, the activity coefficient for 2M potassium is smaller than the corresponding 2M calcium coefficient, and the potassium T_{30} time is also less than that for calcium.

The relationship between activity coefficients and T_{30} times is more apparent in Figure 5, which contains a graph of T_{30} times as a function of mean activity coefficients. An activity coefficient of 0.9999 was assumed for 18 Mohm deionized water (activity coefficient for pure water is 1). Activity

coefficients for concentrations below 0.1M were extrapolated assuming a linear relationship between activity coefficient and concentration between 0 and 0.1M. The 2M data for potassium and calcium are included in this graph. The continuity of the data for all concentrations indicate that 2M and lower concentration T_{30} times are consistent. Consequently, activity coefficients provide a means for examining the relationship between T_{30} times for group I and II cations.

Solvated cation structure in a coating probably determines how effectively it alters coating morphology, thereby creating charge transport pathways. Anodes and cathodes can only be separated when electrical neutrality of the metal surface is maintained by motion of cations to cathodic sites (and anions to the anodic sites) through the coating, or along the coating-metal interface. Separation of anodes and cathodes leads to pitting corrosion and more rapid general corrosion.

It is generally accepted that cations in solution are surrounded by a sheath of water molecules[11,12]. How a water sheath is bound to its cation is believed to be a function of cation size[13,14,15]. Small cations such as Li^+ are believed to have compact, tightly bound water sheaths, whereas larger cations such as Cs^+ are believed to have diffuse, loosely bound water sheaths. Water molecules in diffuse water sheaths are also believed to be free to move independently of the cation[15].

We hesitate to formulate an exact hypothesis on the relation between cation water sheath structure and coated metal corrosion because there is lack of general agreement on the exact number of water molecules in cation water sheaths[16], and corresponding information on group II cation water sheath structure is incomplete. However, cation water sheath structure may help to explain why calcium is more effective in promoting coated container corrosion than group I cations at concentrations $\leq 0.1\text{M}$. Consequently, it is hypothesized that cations migrate into coatings with their water sheaths intact and water molecules associated with larger cations are more free to move independently of the cation, providing water for metallic corrosion. Mossbauer spectroscopy studies demonstrated that Co^{+2} cations are present in polybutadiene coatings with their corresponding water sheaths[17].

In addition to activity coefficients, T_{30} and pore resistance data follow the same trends observed for other bulk electrolyte properties such as partial molal heat capacity[15], dielectric relaxation[13], viscosity[14], and heats of hydration[18]. The similarity between trends in coated metal corrosion data and bulk electrolyte properties suggest that electrolyte in the polymer coating has the same properties as the bulk electrolyte.

Summary

It appears from cathodic delamination studies, research on the structure of water around ions, and results reported here on coated container failure rates that the following conclusions can be drawn:

1. Cations migrate into coatings and change their morphology, thereby creating charge transport pathways. However, morphological changes in coatings occur at salt concentrations below the 0.5M level originally hypothesized by Leidheiser et. al.
2. Salt mean activity coefficients provide a means for comparing T_{30} times from group I and group II cations.
3. The structure of cation water sheath may determine how effectively a cation alters coating morphology. Lack of general agreement on exact water sheath structure prevents formulation of an exact hypothesis on this relationship.
4. The thermodynamic state of a cation in a coating may be similar to cation thermodynamic state in the bulk electrolyte.

References

- 1) H. Leidheiser, Jr. and W. Wang, Corrosion Control by Organic Coatings, edited by H. Leidheiser Jr., p. 70, NACE, Houston TX (9181)
- 2) H. Leidheiser, R. D. Granata, and R. Turoscy, Corrosion, 43(5), p. 296 (1987)
- 3) W. Nelson, Accelerated Testing, pp. 12 - 15, John Wiley & Sons, NY (1990)
- 4) W. S. Tait, K. A. Handrich, S. W. Tait, and J. W. Martin, STP1188, edited by J. C. Scully, D. C. Silverman, and M. W. Kendig, American Society for Testing and Materials, PA (in press)
- 5) W. S. Tait Electrochem. Soc. Proc., 87-2, p. 229 (1987)
- 6) W. S. Tait and J. A. Maier, J. Coat. Technol., 62(781) pp. 41 - 44 (1990)
- 7) S. Siegel and N. J. Castellan Jr., Nonparametric Statistics, pp. 206 - 216, McGraw-Hill Book Co., NY (1988)
- 8) Handbook of Chemistry and Physics, 50th edition, p. F47, The Chemical Rubber Co., Cleveland OH (1969)
- 9) H. S. Harned and B. B. Owen, The Physical Chemistry of Electrolytic Solutions, pp. 562 and 567, Reinhold Publishing Corporation, NY (1950)

- 10) F. Daniels and R. A. Alberty, Physical Chemistry, third edition, p. 144, John Wiley & Sons, Inc., NY (1966)
- 11) J. Burgess, Metal Ions in Solution, pp. 19 - 23, John Wiley & Sons, NY (1978)
- 12) J. O'M Bockris and A. K. N. Reddy, Modern Electrochemistry, Volume 1, Plenum Press, NY (1977)
- 13) H. S. Frank and W-Y Wen, Disc. Farad. Soc., 24, pp. 133 -n 140 (1957)
- 14) J. D. Bernal and R. H. Fowler, J. Chem. Phys., 1(8), pp. 515 - 548 (1933)
- 15) E. Wicke, Angew. Chem., 5(1), pp. 106 - 122 (1966)
- 16) J. Burgess, Ions in Solution, pp. 28, 33 - 35, John Wiley & Sons, NY (1988)
- 17) H. Leidheiser, Jr., A. Vertes, and I. Czako-Nagy, J. Electrochem. Soc., 134(6), pp. 1470 - 1472, (1987)
- 18) J. O'M Bockris and A. K. N. Reddy, op. cit., p. 96

Table 1: Container Failure Data

<u>Solution</u>	<u>T₃₀ Times</u>			
	<u>0.05 Molar</u>	<u>0.075 Molar</u>	<u>0.1 Molar</u>	<u>2 Molar</u>
CaCl ₂	47 days	49 days	44 days	58 days
KCl	54 days	56 days	50 days	47 days
NaCl	60 days	57 days	53 days	
LiCl	62 days	60 days	57 days	
DI Water	204 days	204 days	204 days	204 days

Table 2: Diffusion constants (10^{-5} cm²/sec)

<u>Salt</u>	<u>0.01M Concentration</u>	<u>0.1M Concentration</u>
LiCl	1.312	1.269
NaCl	1.545	1.483
KCl	1.917	1.844
CaCl ₂	1.188	1.110

Figure 1: Typical Cumulative Percent Failure Data as a Function of Time

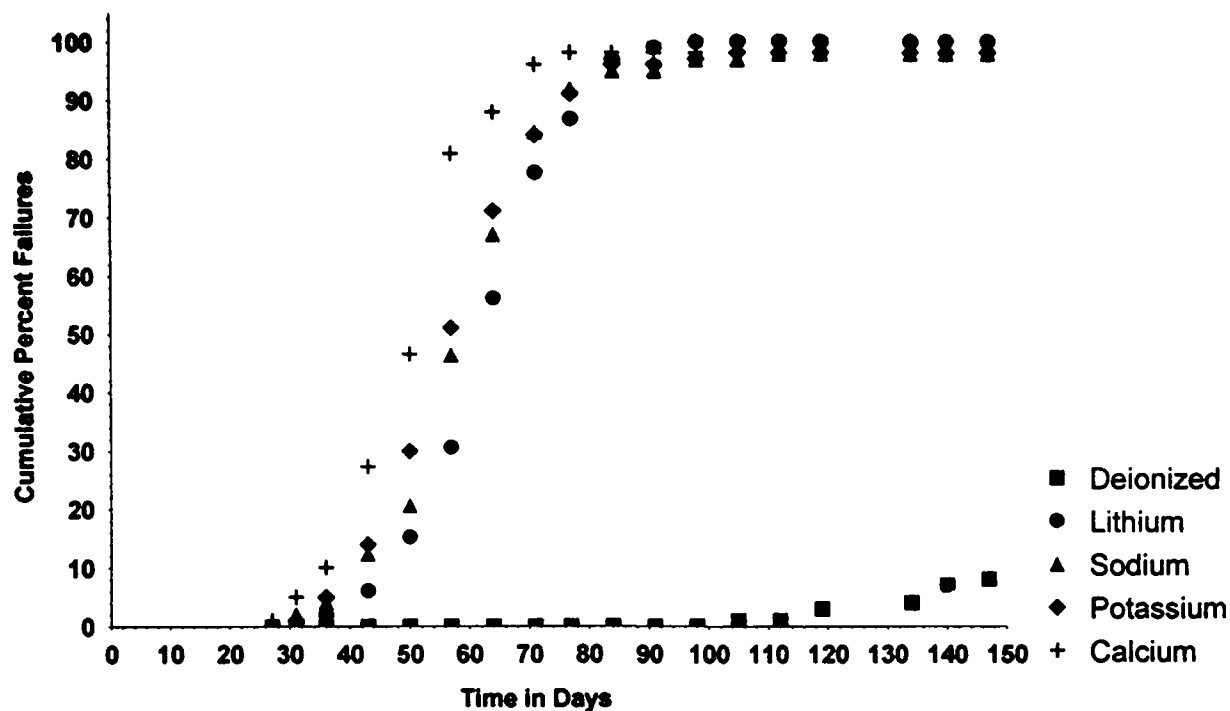


Figure 2: Days to 30% Failure

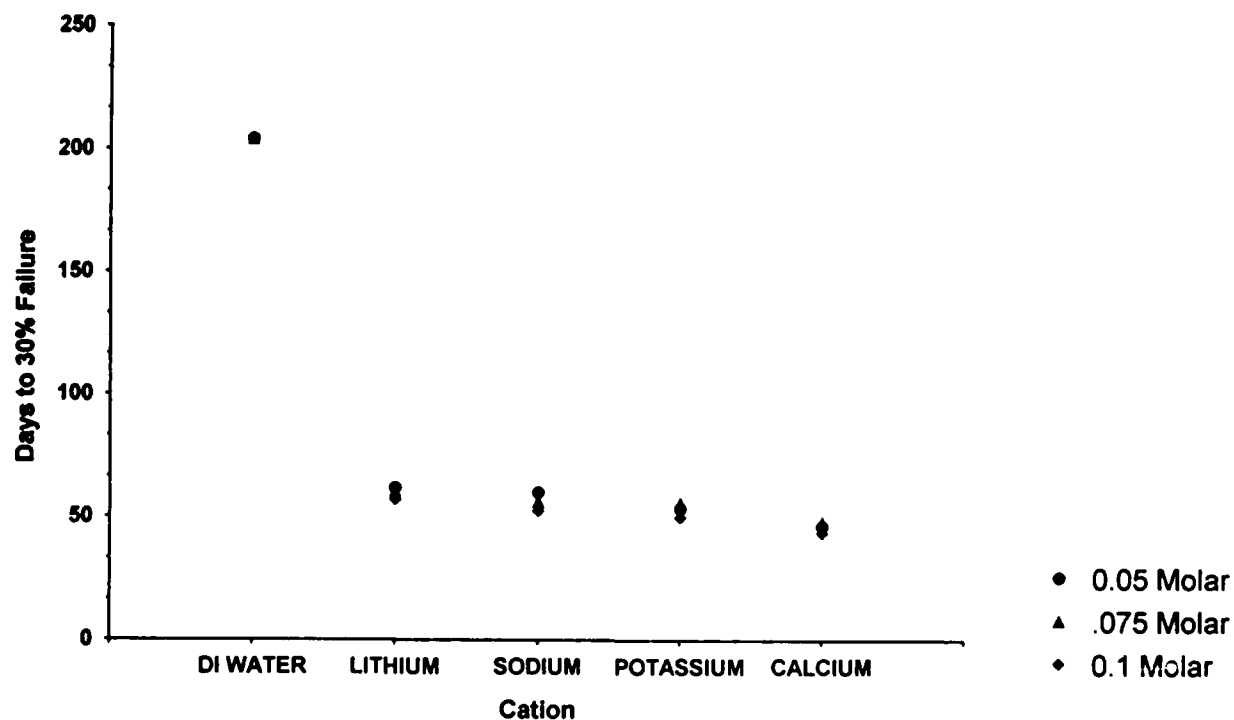


Figure 3: Pore Resistance Values for Different Cations

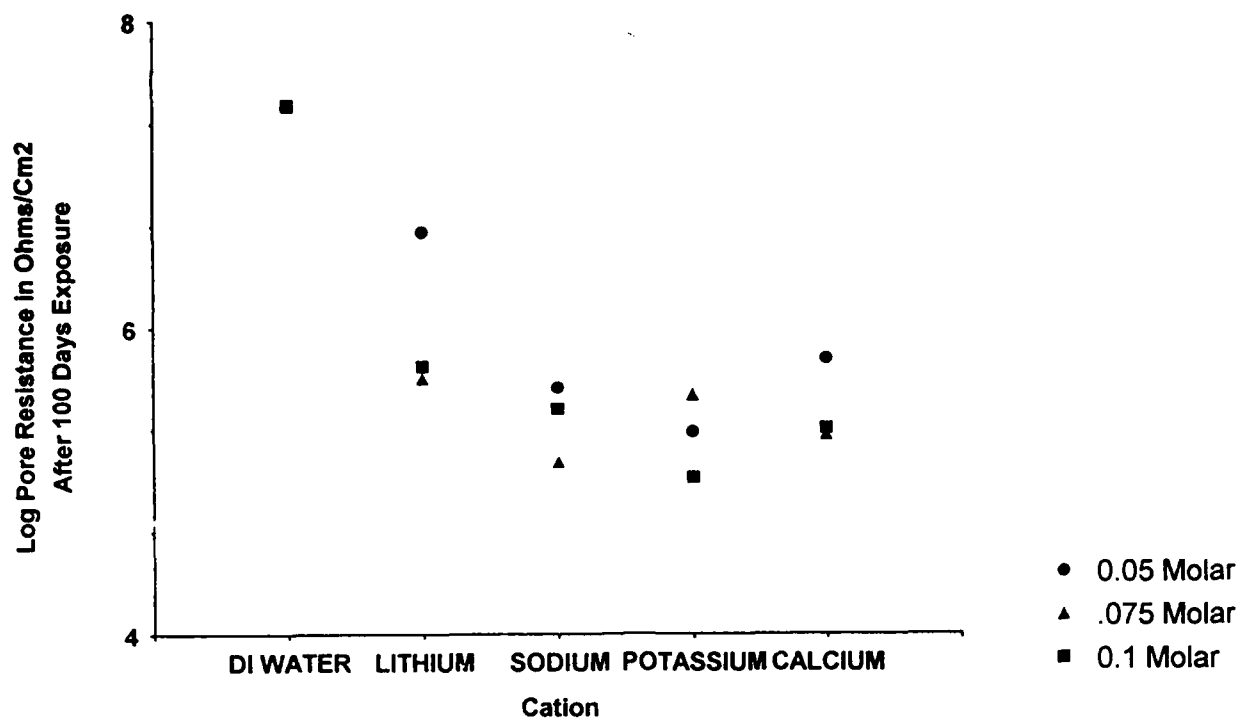


Figure 4: Mean Activity Coefficients as a Function of Concentration

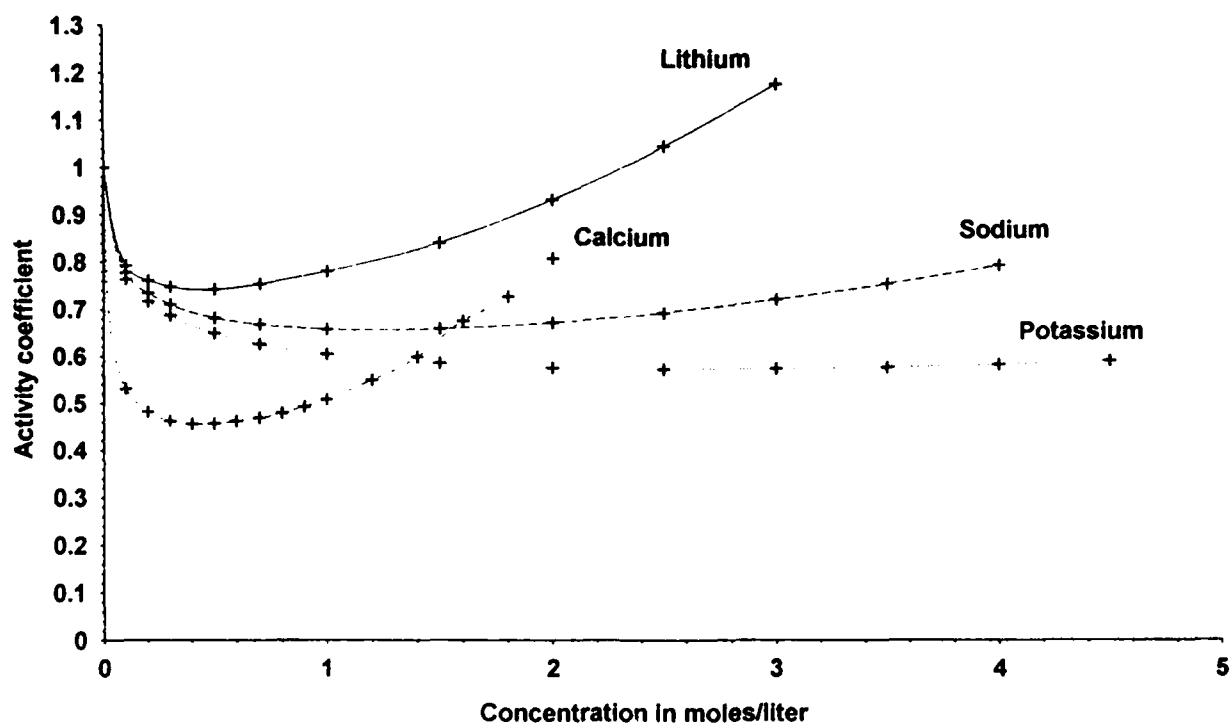
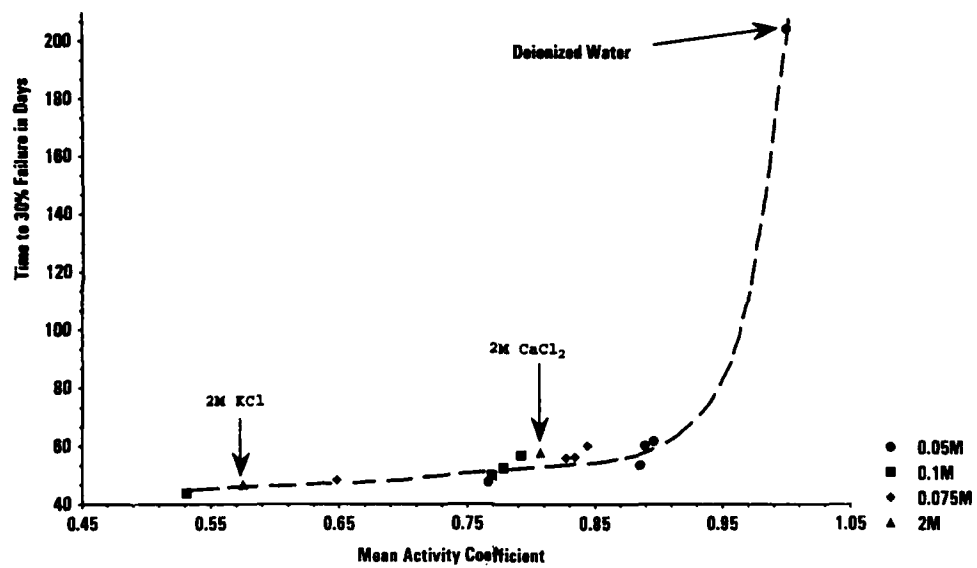


Figure 5: Failure Times as a Function of Activity Coefficients



The detrimental effect of water-soluble contaminants at the steel/paint interface. Panoramic view of the authors' research on the subject

Manuel Morcillo
Centro Nacional de Investigaciones Metalúrgicas
Gregorio del Amo, 8
28040-Madrid Spain

Abstract

It is well known the detrimental effect of water-soluble contaminants at the steel/paint interface. The presence of hydrosoluble species at the steel/paint interface promotes osmotic blistering of the coating and underfilm corrosion of the steel. Both processes drive to the deterioration of the paint system in very short periods of time. Painting of rusty steel is prone to suffer this problem.

Although it is a long-standing problem numerous questions are yet missing. In this paper attempts are done to answer some of these questions. The research is conducted in outdoor exposure tests with real paint systems and in laboratory studies with model paint films. The author presents in the paper a review of the different researches carried out with his co-workers in the last five years.

Key terms: water-soluble contaminants, osmotic blistering, underfilm corrosion, metal-paint interface.

Introduction

The presence of water-soluble contaminants within the corrosion products is an accelerating factor of the process of metallic corrosion. They have also a negative effect on the behaviour of organic coatings applied over contaminated substrates.

The presence of hydrosoluble species, e.g. chlorides and sulphates, at the metal/paint interface promotes osmotic blistering of the coating and underfilm metallic corrosion. Both processes can drive to the deterioration of the paint system in a very short period of time. Painting of rusty steel is prone to suffer this problem¹.

Although it is a long-standing problem numerous questions are yet missing. We report here some of them: What chemical substances or combinations of them are specially detrimental? Are there

critical concentration levels for these corrosion-stimulating substances that, once exceeded, produce a significant deteriorating effect on the coating? Are these critical concentration levels expected to be found within the corrosion products? How do different paint systems behave in these situations? What roles do the metallic substrate, the thickness of the coating and the exposure conditions play?

In this paper attempts are done to answer some of these questions. The research has been conducted in outdoor exposure tests with real paint systems and in the laboratory with model paint films. The author presents in the paper a review of the different researches carried out with his co-workers in the last five years.

The premature failure of typical paint systems applied over contaminated steel

Hot rolled mild steel plates, 3 mm thick, with intact millscale (grade A of the Swedish standard SIS 055900) was used for preparing 12.5 x 25 cm specimens. Then they were shot blasted (S-280) until the ASa3 cleaning grade was achieved. The presence of water-soluble contaminants at the steel/paint interface was simulated by placing onto the specimens variable quantities of $\text{FeSO}_4 \cdot 7\text{H}_2\text{O}$ and NaCl , in amounts equivalent to the contamination levels shown in Table 1. Once dried, diverse commercial paint systems with different dry film thicknesses were applied by air spraying and outdoor exposed in atmospheres of different aggressivity^{2,3}.

Table 2 shows a synthesis of the results obtained corresponding to samples contaminated with NaCl , 500 mg/m². No blistering was apparent on the control panels where paint systems were applied over uncontaminated blasted steel. However, deterioration occurred whenever the level of NaCl at the interface was of 500 mg/m². In the case of FeSO_4 , the critical level was of 2500 mg/m².

The deterioration of the paint coating initially takes the form of a fine blistering on the whole surface of the specimen. In some systems the deterioration had already appeared within the first six months of exposure but in others takes longer (1-2 years). However, in 3-4 years of exposure to the atmosphere, the deterioration appeared in all the atmospheres and in practically all of the paint systems and coating thicknesses taken into consideration. Then, the deterioration process progressed more slowly. An exception to this behaviour is found in those systems with a zinc silicate primer, in which blistering did not take place, at least during the 8 years of exposure to the atmosphere. This was presumably due to the formation of insoluble zinc products⁴.

This research, still underway, meant a starting point to carry out laboratory researches in order to shed some light on the mechanisms involved in such a described behaviour.

Expected levels for soluble salts in contaminated rusty steel

Firstable, it was important to know whether those critical contamination levels ($300 \text{ mg Cl}^-/\text{m}^2$ and $1580 \text{ mg SO}_4^{=}/\text{m}^2$) could be expected to be found in the adherent rust layer formed on steel during atmospheric exposure.

Thus, a set of panels that had been outdoors exposed during 1 year at 39 test sites covering a wide range of atmospheric conditions, once the non-adherent rust layer was removed, were analyzed for soluble chlorides and sulphates⁵. The graphs in Fig. 1 show the results obtained.

From Fig. 1 is deduced that the critical chloride level can already be found in light marine atmospheres, ISO categorie S1 (Cl^- deposition rate $> 3 \text{ mg Cl}^-/\text{m}^2$). In the case of sulphates the critical level is only found in heavy industrial atmospheres, ISO categorie P3 (SO_2 deposition rate $> 200 \text{ mg SO}_4^{=}/\text{m}^2$), although a cause of the seasonal effect of SO_2 high sulphate concentration can also be found in the rust formed during the winter months in urban atmospheres^{6,7}. Another aspect to be considered is the non-uniform sulphate distribution on the metallic substrate, so, in certain areas, the local accumulation of contaminant can exceeds the critical level to promote a premature failure of the coating⁸.

The underfilm corrosion process at contaminated steel/paint interfaces

Specimens, $5 \times 5 \text{ cm}$, were prepared from a flat mild steel plate 0.5 mm thick. Then they were completely degreased with trichloroethylene. Subsequently, on one side of the specimen different concentrations of contaminants FeSO_4 and NaCl were applied, as well as combinations thereof. Then, by means of a wire-wound rod a peelable (strippable) varnish film was applied to a dry film thickness of $8 \mu\text{m}$. The specimens were subsequently placed in a chamber where they were subjected to an aerosol of distilled water. Table 3 shows some of the results obtained⁹.

Free films of the varnish used showed permeation rates for water vapour and oxygen (under aqueous film) of 1.2×10^{-2} and $0,85 \times 10^{-3} \text{ g.cm}^{-2}.\text{d}^{-1}$ respectively. Taking into account that for the dissolution of one gram of iron, to form FeOOH , similar amounts of oxygen (0.43 g) and water (0.48 g) are needed, it is reasonable to think that the permeation rate of oxygen -ten times lower- be the controlling step of the corrosion process under the varnish film. However, on this assumption and according to the above mentioned value of oxygen permeation rate one would expect an underfilm corrosion of $197.6 \text{ mg/dm}^2.\text{day}$ after 485 hours of exposure in the humidity condensation chamber, instead of the absence of corrosion (at least not measurable with the gravimetric technique employed) for uncontaminated interfaces. Therefore, it may be concluded that the controlling factor for the underfilm corrosion process on uncontaminated surfaces is not the arrival of oxygen to the steel/varnish interface but the

ionic conduction resulting from the saline deposit in the interface; low concentrations of contaminant are enough to promote significant underfilm corrosion of steel after very few hours of testing (Table 3). In the case of highly contaminated surfaces, the ionic conduction is no longer controlling the underfilm corrosion which is now governed by the diffusion of oxygen through the varnish film. The following conjectures support this idea: (a) the above mentioned lesser permeation rate for oxygen, and mainly because of the entrance of water by osmotic processes through the varnish film caused by the existence of soluble substances at the steel/varnish interface, and (b) the agreement between the consumption of oxygen derived from underfilm corrosion data (when the varnish film is still in good condition) and transport of oxygen through free films of varnish. For example, underfilm corrosion data of steel after 26 hours of exposure in the humidity condensation chamber were $0.70 \times 10^{-3} \text{ g.cm}^{-2}\text{d}^{-1}$ and $1.34 \times 10^{-3} \text{ g.cm}^{-2}\text{d}^{-1}$ for an interfacial contamination of 500mg/m^2 of NaCl and FeSO_4 , respectively (Table 3). From these values the estimated consumption of oxygen is 0.28×10^{-3} and $0.53 \times 10^{-3} \text{ g.cm}^{-2}\text{d}^{-1}$ respectively, figures in consonance with the permeation rate of oxygen ($0.85 \times 10^{-3} \text{ g.cm}^{-2}\text{d}^{-1}$) through the varnish film.

The accumulation of water at the steel/varnish interface as a result of the osmotic process, and of rust from the underfilm corrosion process promotes blistering of the coating once the pressure that both products exert exceeds the adhesion strength of the varnish film to the metallic support.

The joint action of chlorides and sulphates

Also of interest is to ascertain the effect produced by both contaminants acting jointly, since this circumstance occurs often in practice (e.g. industrial zones near the coast). Fig. 2 shows in a tridimensional diagram the influence of the contaminants FeSO_4 and NaCl , and combinations thereof, on underfilm corrosion of steel.

For a determined level of one of the contaminants, the incorporation of the second contaminant promotes an increase in the corrosion of the underlying steel. One must consider questions such as: Is there any additivity of effects? Is there any synergic or inhibiting effect? In order to answer these questions, Table 4 shows the values of the relation (R),

$$R = \frac{\text{corrosion for a determined combination of contaminants}}{\text{Sum of the individual corrosions of each of the contaminants acting independently}}$$

As can be seen in Table 4, the value of R stays very close to the unity, suggesting a quasi-additive effect.

The effect of the presence of rust

In agreement with Bayliss⁴, the problem with all these experiments on seeded panels is that the contamination is in a different form and situation than occurs in practice. For example, ferrous chloride contamination is likely to be at the bottom of a corrosion pit and encapsulated in rust and not uniformly spread over the steel surface.

In order to get a better approach of the situation occurring in practice, where the saline contaminant is located in the rust layer formed on the steel, the following experiment was performed in the laboratory¹⁰.

Cold-rolled pre-weighed steel specimens were exposed to wet-dry cycles (using distilled water sprays), building up a rust layer of approximately 1 g/cm². After a light brushing to remove the not firmly adhered rust, variable amounts of NaCl and FeSO₄·7H₂O solutions were added. The samples were then coated with clear coatings of alkyd-melamine and chlorinated rubber to a dry film thickness of 30 μm. After a certain period of curing the painted specimens were runned during 500 hrs in a condensing humidity test. Simultaneously, uncontaminated and unrusted painted specimens were exposed as controls. On removing the specimens from the chamber the coating was eliminated by immersion in methylene chloride. Subsequently, the rust formed on the steel surface was removed by immersion in a bath of inhibited hydrochloric acid and steel corrosion rate calculated by the weight loss technique. Fig. 3 shows the results obtained

There are several important features in the figure 3:

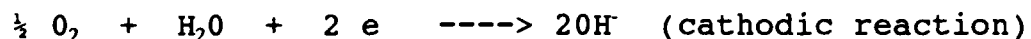
- a) the significant corrosion of uncontaminated rusted specimens which contrasts with the absence of corrosion (not detectable at least with the gravimetric technique employed) in uncontaminated and non-rusted specimens. The rust in that case supplies the cathodic reaction of the corrosion process underneath the paint film as has been postulated by some others researchers¹¹,
- b) the corrosion of steel is strongly dependent on the type of varnish applied and the level of saline contamination at the interface. The latter confirms again results exposed earlier, and
- c) no great dependence can be deduced on the type of contaminant employed and ever less on the presence of rust at the contaminated interface.

The roles of the type and the thickness of the coating and the kind of interfacial contamination

Once described the deterioration mechanism for which the organic coating fails as a consequence of interfacial contamination, it is important to ascertain the roles of the different variables involved: a) the paint coating, b) its thickness, and c) the contaminant solution.

Samples of 5.0 x 4.6 cm were prepared from cold rolled mild steel plates, 1 mm thick. Once degreased and weighted they were contaminated with diverse chloride and sulphate solutions. Then, vinyl and polyurethane films (15, 40 and 80 μm of DFT) were applied. The samples were exposed during 600 hrs in a humidity condensation chamber. After that time the varnish film was removed and the underfilm corrosion rate calculated by the weight loss technique. Table 5 shows the results obtained^{12,13}.

Underfilm corrosion process obeys to a mechanism of electrochemical nature where the following reactions take place



For the cathodic reaction oxygen and water must penetrate through the paint film to reach the metal/paint interface.

Accordingly to the data reported in Table 5 underfilm corrosion is mainly influenced by the type and the thickness of the varnish film. The contaminant solution exerts only a very slight effect (see average figures in Table 5). The entrance of water molecules through the coating is facilitated by the osmotic pressure, due to the presence of interfacial water-soluble salt. It is the oxygen permeation, depending on the type and the thickness of the film (Table 6), the controlling factor of the corrosion process. The minor role exerted by the interfacial contaminant solution is in agreement with the conductivity measurements of the interfacial solutions (Table 7); the ionic conductivities are similar for the different water-soluble salts employed.

The effect of the metallic substrate

Although most of the research has been conducted on mild steel, it is interesting to show some of the results obtained with hot-dip galvanized (HDG) steel as substrate for paint coating. There is increasing concern about the painting of weathered HDG-steel.

A series of fresh HDG steel were weathered in the laboratory through exposure in salt fog and moist sulphur dioxide chambers. They were subsequently light wire brushed before the application of adequate commercial paint systems for HDG steel. Afterwards, they were outdoors exposed in urban (4 years) and marine (2 years) atmospheres. Table 8 shows some of the results obtained^{14,15}.

The weathering in the salt fog or moist sulphur dioxide chambers produce a highly negative effect on the subsequent behaviour of the paint systems. In particular, the latter frequently promotes severe film delaminations of the paint films. The less detrimental effect of chloride contamination on the zinc substrate could be explained as it was commented before, a cause of the formation of more insoluble corrosion products by the chemical reaction of zinc with the chloride solution¹⁶.

The critical threshold of contamination

We should like to end talking about critical levels of water-soluble salts for this deterioration process, the same concept used as introductory remark in the paper. Are there critical thresholds of contamination which once exceed the premature failure of the paint coating occurs?

With real paint systems, 100 μm DFT, critical levels of chloride (300 mg/m^2) and sulphate (1580 mg/m^2) promote severe degradation of the paint coatings in atmospheric exposure. However, with model varnish films of a lower DFT, e.g. 8 μm , a small amount of contaminant (5 $\text{mg Cl}^-/\text{m}^2$) was enough as well to produce a fast blistering and significant underfilm corrosion. So, the concept of critical threshold of interfacial contamination is directly connected with the thickness of the paint film.

More than talking about critical levels the possibilities for the oxygen to reach the interfacial region could be explored; oxygen transfer through the paint film is the real controlling factor of this degradation process and in this sense the nature of the coating and its thickness certainly play very important roles.

Conclusions

The presence of water-soluble salts at the interface metal/paint can produce a premature failure of the paint system promoting a fast severe blistering and significant underfilm corrosion. The former is a consequence of the osmotic pressure and the latter depends upon the corrosion-stimulating nature of the salts. The first process is directly related with the entrance of water molecules through the paint film, whilst the oxygen transfer is the controlling factor of the second. Both, water and oxygen permeation, are extremely dependent of the nature and the thickness of the paint system. Other variables (metal substrate, contaminant nature, surface concentration of contaminant, presence of rust and exposure conditions) although play an important but minor role.

Acknowledgements

The author of this paper wants to thank Prof. S. Feliu for its valuable advises along this research. Special recognition is due to the following co-workers who contributed very substantially to this project: J. Simancas, L.S. Hernández, S. Flores, F.J. Rodríguez, J.M. Bastidas, J.C. Galván, J.L. Ruiz, S. Feliu Jr. and S. Giménez.

This work was also made possible thanks to the contribution of the following laboratory assistants: M.F. Luque, M.A. Castadot, R. Osterman and M. Cutierrez.

References

1. M. Morcillo, S. Feliu, J.C. Galván and J.M. Bastidas, *Journal of Protective Coatings and Linings*, 4 9 (1987): p. 38.
2. M. Morcillo, S. Feliu, J.C. Galván and J.M. Bastidas, *Journal of Oil and Colour Chemists' Association*, 71 1 (1988): p. 11.
3. J. Simancas, Ph Doctoral Thesis. Univ. Complutense de Madrid (1991).
4. D.A. Bayliss and K.A. Chandler, *Steel Corrosion Control*, (Elsevier Science Publishers BU, 1991) p. 28.
5. S. Flores, F. Räuchle and M. Morcillo, *Proc. 4º Congreso Iberoamericano de Corrosión y Protección*. Vol. I, AAC, Mar del Plata (1992): p. 41
6. J.E.O. Mayne, *Journal of Applied Chemistry*, 9 (1959): p. 673.
7. K.A. Chandler and J.E. Stanners, *Proc. 2nd Int. Congr. Metall. Corros.*, New York (1963): p. 325.
8. H. Schwartz, *Werkstoffe und Korrosion*, 16 (1965): p. 93.
9. M. Morcillo, J.S. Hernández, J. Simancas, S. Feliu Jr. and S. Gimenez. *Journal of the Oil and Colour Chemists' Association*, 73 1 (1990): p. 24.
10. M. Morcillo, S. Feliu and J. Simancas, *Farbe und Lack*, 95 105 (1989): p. 726.
11. K. Hoffmann and M. Stratmann. *Proceedings of the 11th Inter. Corrosion Congress*. Florence, Vol. II, p. 2.293-2.230.
12. F.J. Rodriguez, J. Simancas and M. Morcillo. *Proc. 4º Congreso Iberoamericano de Corrosión y Protección*, Vol. II, AAC, Mar del Plata, (1992, p. 501.
13. F.J. Rodríguez, J.C. Galván and M. Morcillo, *Proc. 10th European Corrosion Congress*. Barcelona (1993)(in press).
14. M. Morcillo, J.L. Ruiz, J. Simancas and L.S. Hernández, *Journal of Protective Coatings and Linings*, 6 11 (1989): p. 81.
15. J.L. Ruiz, L.S. Hernández, J. Simancas and M. Morcillo, *Proc. 1^{er} Congreso Nacional de Tratamientos de Superficies*. AIMME. Valencia (1992).
16. E.V. Schmid, *Exterior durability of organic coatings*, (FMJ International Publications Ltd., Redhill, 1988 p. 39.

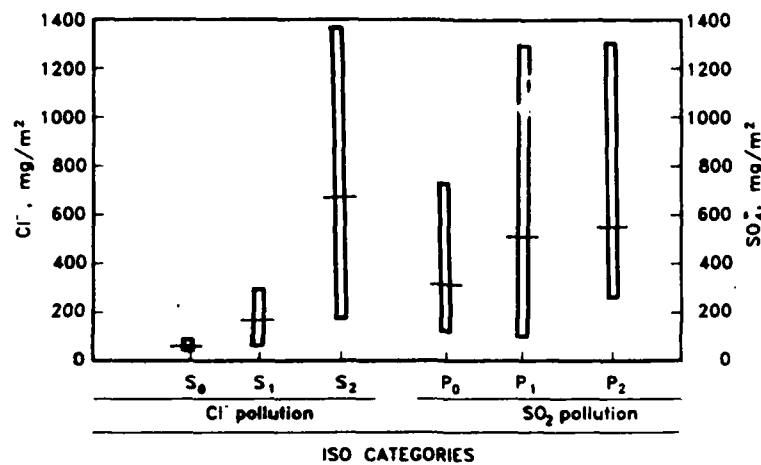


Fig. 1.- Levels of chlorides and sulphates found in the adherent rust layer formed during one year in atmospheres of different categories according to ISO 9223.

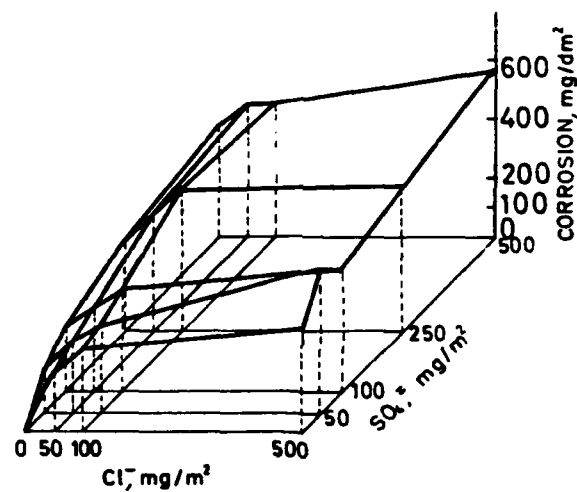


Fig. 2.- Tridimensional diagram showing the influence of the contaminants FeSO_4 and NaCl , and combinations thereof, on the underfilm corrosion of steel.

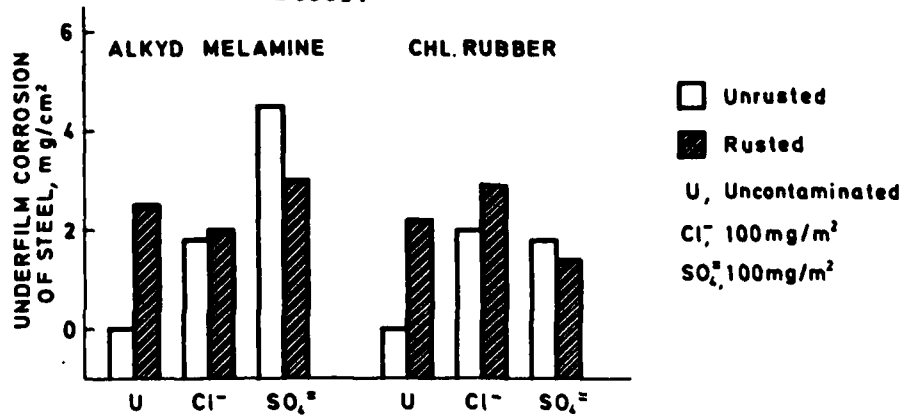


Fig. 3.- Underfilm corrosion rates of steel coated with a varnish film applied on uncontaminated and contaminated unrusted and rusted steel.

Table 1 Saline contamination levels, mg/m²

NaCl	FeSO ₄
20	150
100	250
500	500
	1000
	2500

Table 2.- Rating of paint systems applied over blasted steel contaminated with NaCl, 500 mg/m², and outdoor exposed in atmospheres of medium (C2) and severe (C4) corrosivity³

Paint System	DFT (μm)	4 years of exposure ²				8 years of exposure ³			
		Blistering		Rusting		Blistering		Rusting	
		C2	C4	C2	C4	C2	C4	C2	C4
Alkyd	80-100	8M	6MD	10	9	8D	6MD	7	8
Polyurethane	120	4D	4D	10	10	2MD	--	2	--
Zinc Silicate/ Vinyl	90-100	10	10	10	10	10	10	10	10

Blistering: ASTM D714

Rusting: ASTM D610

Table 3.- Underfilm corrosion of steel (mg/dm²). Uncontaminated and contaminated steel coated with a varnish film, 8 μm DFT, and exposed in a humidity condensation chamber².

Cl ⁻ , mg/m ²	SO ₄ ⁼ , mg/m ²											
	0			50			100			500		
	A	B	C	A	B	C	A	B	C	A	B	C
0	N.D.	N.D.	N.D.	42	108	147	70	151	228	134	307	405
5	14	47	80	50	144	209	68	204	320	100	298	390
20	29	110	137	56	121	271	69	211	331	108	270	417
100	32	208	291	51	180	310	82	253	357	114	320	473
500	70	203	366	104	307	526	94	353	453	179	413	600

A: 26 hours

B: 185 hours

C: 485 hours

N.D.: Underfilm corrosion of steel is not observed, nor is it detected with the gravimetric technique employed

Table 4. R values for different combinations of chlorides and sulphates after 485 hours of exposure in a humidity condensation chamber⁹

Cl ⁻ , mg/m ²	SO ₄ ⁼ , mg/m ²	
	50	100
5	0.9	1.0
20	1.0	0.9
100	0.7	0.7

Table 5. Underfilm corrosion rates (mg/cm².d) of steel coated with varnish films of different dry film thickness (DFT) applied over substrates contaminated (100 mg/m²) with diverse salt solutions^{12,13}.

Contaminant	DFT (μm)	Vinyl	Polyurethane
NaCl	15	0.066	0.015
	40	0.053	0.013
	80	0.041	0.025
	Ave.	0.053	Ave. 0.018
NH ₄ Cl	15	0.067	0.026
	40	0.035	0.015
	80	0.029	0.017
	Ave.	0.044	Ave. 0.019
CaCl ₂	15	0.045	0.022
	40	0.034	0.022
	80	0.033	0.018
	Ave.	0.037	Ave. 0.018
Na ₂ SO ₄	15	0.059	0.015
	40	0.042	0.017
	80	0.043	0.020
	Ave.	0.048	Ave. 0.017
(NH ₄) ₂ SO ₄	15	0.056	0.013
	40	0.028	0.015
	80	0.027	0.017
	Ave.	0.037	Ave. 0.015

Table 6. Oxygen permeation values through different paint films^{12,13}.

Varnish	DFT (μm)	Oxygen permeation ($\text{g O}_2 \cdot \text{cm}^{-2} \cdot \text{d}^{-1}$)
Vinyl	10	4.76×10^{-4}
	50	1.67×10^{-5}
	100	0.95×10^{-5}
Polyurethane	20	3.89×10^{-4}
	50	0.88×10^{-5}
	100	0.82×10^{-5}

Table 7. Conductivity measurements of diverse saline solutions 0.06 M^{12,13}.

Saline solution	Conductivity (mS/cm)
NaCl	6.40
NH_4Cl	7.97
CaCl_2	6.31
Na_2SO_4	8.95
$(\text{NH}_4)\text{SO}_4$	11.76

Table 8. Outdoor performance of paint systems applied over contaminated hot-dip galvanized (HDG) steel^{14,15}.

Paint System	HGD, Salt fog weathered		HDG, Moist sulphur dioxide weathered	
	Outdoor Exposure		Outdoor exposure	
	Urban	Marine	Urban	Marine
1	X	X	X	0
2	X	X	X	X
3	X	X	●	X
4	0	X	X	X
8	X	X	●	X
0	Good condition		X	Bad condition
			●	Fully delaminated

Anticorrosive Coatings Based on Phase Decomposed Polymer Blends

Vladimir Verkholtantsev
Tambour Ltd
Paint and Chemical Industries
PO Box 2238
24121 Akko Israel

Mati Flavian
Tambour Ltd
Paint and Chemical Industries
PO Box 2238
24121 Akko Israel

Abstract

Heterophase self-stratifying organic coatings (HSSC), that obtain their specific structure during a film forming process due to phase separation of incompatible polymer blends, were recently offered for several applications and particularly for weather/anticorrosive coatings that are applied in one coat.

HSSC combines heterogenous structure of the polymer matrix that provides improved mechanical properties and lower permeability with self-stratification yields increased adhesion and top surface coating properties with protection thanks to the anticorrosive pigments and insulation function of conventional coating.

In particular, the selected epoxy/thermoplastic partially miscible resin blends provide phase heterophasity on evaporation of the common solvent and during the curing process. The enrichment of the coating's top part with acrylic, vinyl and other thermoplastic resins, and of the lower part with epoxy resin (ambient cure) resulting from self-stratification, provide the anticorrosive coating with better weather resistance and higher adhesion durability.

Key terms: Anticorrosive coatings, self-stratifying coatings, incompatible polymer blends, heterophase polymer structure.

Introduction

All conventional outdoor anticorrosive coatings exploit the same type of coating structure, namely a primer coat that consists of anticorrosive pigment which is incorporated into a homophase polymer matrix that provides adhesion to the substrate, and a top coat which is usually free from anticorrosive ingredients that have mainly insulation and weather protection functions.

Since the 70's, and especially during the last decade, a number of serious theories predicted, with practical confirmation, that the use of heterophase film forming systems with a special controlled polymer structure could provide significant enhancement of mechanical and protective functions of organic coatings, comparing with the regular homophase polymer binders.

Of particular interest is the approach to the polymer structure in organic coatings, that was proposed by Funke [1, 2], who suggested improvement in coating properties due to the controlled heterogeneity and self-stratification during the film forming process. This idea, then, was applied to powder coatings, where self-stratification of incompatible polymer blends could be realized easily during the stoving stage of the film forming process [3].

However, the analysis of some results led us to the conclusion that essential reinforcing and increasing of coating durability may be achieved not by copying the multilayer structure of traditional coatings, but preferably by the forming of certain microheterogeneity of the polymer matrix. This does not exclude the possibility of improving coating properties by nonuniformity through the coating thickness. It was found that the controlled heterogeneity of the polymer film former, as well as nonhomogeneity-in-layer, can be obtained by using phase separation during film forming process on a combination of an incompatible polymer blend with at least two solvents of different volatility and affinity to both polymers. For instance, the initial film forming system can be formulated by the dissolution of a curable oligomer/thermoplastic partly miscible polymer blend in a mixed common solvent (two or more individual solvents). Due to solvent evaporation on application, such a solution transfers into a two-phase state, that is, it undergoes phase separation on the substrate, forming microheterophase or, under certain conditions, nonhomogeneous-in-layer coatings. The second "driving force" of phase separation is the curing process. Some basics and specific features of these processes were described in review papers [4, 5].

Since 1989, the Paint Research Association started the Self-Stratifying Coatings Project [6]. The thermodynamic approach to the self-stratifying system was described recently in the work [7], and a serious attempt to extend the self-stratification concept to water borne (dispersion type) coating compositions was reported in the publication [8]. According to data presented in article [9], stratification and heterogeneity in block copolymer binders appear to be useful in automotive and water borne plastic coatings.

The recent results obtained by us, in the development of the self-stratification concept in anticorrosive coatings, are cited in this paper.

I. Heterophase and Stratified Polymer Film Structure

A. Concept

First of all, the reported approach to anticorrosive coatings is a structural concept.

The heterophase coating matrix (coherent phase) may be formed from a heterophase composition, consisting of an incompatible polymer mixture. This way is not convenient due to the kinetical instability of the composition, which will also result in lack of reliability in controlling the polymer structure and associated coating properties.

The other approach, that promises to provide more technical opportunities, is to form heterophase film structure from initially homophase incompatible but partially miscible polymer blend, that provides homophasy by the incorporation of a common, usually multi-component, solvent. In this case, the heterophase polymer structure can be formed under more or less controlled and reproducible conditions during the film forming process. In Table 1 the main features of these approaches are compared, with emphasis on the fact that phase decomposition on film formation provides fine heterophase (microheterophase) structure and interphase durability. Since the paint composition and process condition are controlled, the film formation through the phase decomposition provides:

- enrichment of coherent and incoherent phases of two-phase polymer matrix with selected polymer component.
- tendency to self-stratification, while development of the process depends on a few factors such as (a) mechanism of phase separation (either nucleation and particles growth or spinodal decomposition occur), (b) volatility of solvents and (c) velocity of the curing process.
- formation of the isolated clear polymer layer either on the top or in the adhesion interphase of the coating [10].

B. Coating Composition and Methodics

Since incompatible polymer blends may be only used in HSSC, the polymer / polymer compatibility, its prediction and evaluation is of the first concern. Most commercial polymers for plastics, rubber, fibers etc. are incompatible. Numerous researches were carried out in order to provide homophasy of their mixtures, since improvement in properties by blending (a simplified version of physical modification of polymers) can be very easily performed.

On the other hand, certain efforts must be applied to select incompatible couples of film forming resins, with each partner having the desirable properties. Conventional film forming resins use to be relatively low molecular weight oligomers (MW mainly between 600 and $3 \cdot 10^3$), designed especially to be compatible with other film forming resins and to provide easy mutual modification. Higher molecular weight and lower compatible commercial polymers such as PVC, acrylic, polyurethane, polyamide resins etc. can hardly be utilized in coating composition because of their poor film forming properties and their demand for higher solvent consumption to reduce viscosity on coating application. So, only a limited number of commercial film forming resins can be used to obtain distinctly separated polymer blends.

In our previous works [4,5,10] the following resin combinations were presented as valuable for HSSC:

Thermoset Resins

Epoxy
"
"
"
"
Polyester
"
Alkyd/Amino Resin
Combination

Thermoplastic Resins

Vinyl
Perchlorovinyl
Chlorinated Rubber
Polysiloxane
Acrylic
Polysiloxane
Acrylic

Acrylic

For the present study, a number of low and middle molecular weight epoxy resin grades as providing ambient cure and anticorrosive coating properties, were combined with vinyl, acrylic and siloxane commercial resins: Chlorinated Polyethylene (BASF), VROH (Union Carbide), Chlorinated Vinyl Resin (PCVR), Silicone Resin SR 82, (Gen. Electric) etc. Phase diagrams (Fig. 1) which are necessary for the prediction of coating structure, were built using experimental data (for the methodics - see our previous work [4]).

It could be mentioned that any phase diagram reflects a phase composition of equilibrium state in a "closed" system, i.e. in the absence of heat or mass exchange, and strictly speaking, can not be applied to a paint layer that yields a film on a substrate. Nevertheless, the information provided by the phase diagram helps in the prediction of composition, quantity and polymer/polymer ratio in separated phases.

The basic components of practical self-stratifying anticorrosive coating composition are listed below:

<u>No.</u>	<u>Component</u>	<u>Function</u>	<u>Content (appr.), wt</u>
1	Epoxy Resin	Anticorrosive (Thermoset)	20
2	Thermoplastic Resin	Weather Resistance	8
3	Structure Modifier	Stratifier	5
4	Functional Pigments	Anticorrosive	15
5	Neutral Pigments	Weather Resistance	15
6	Solvent Blend	Application	30
7	Hardener	Curing Process	7
			<hr/> 100

II Film Forming Process

The process of forming HSSC structure can be illustrated by the simplest model composition comprising two incompatible polymers and two solvents distinguished by volatility and thermodynamic affinity to each polymer.

A. Phase Separation

A suitable example is supplied by the systems of solid ER + PCVR + acetone + xylene. The experimental phase diagram for this system is shown in Figure 1-a. The parabolic surface limits the space inside the pyramid, corresponding to the two-phase state, that is, the space of phase decomposition.

Let us select the "point of composition" A which reflects the initial composition of a four-component solution in one-phase region. Naturally, this point should be situated on the line connecting points P and S, which express the initial ratio between polymers and solvents correspondingly. When solvents evaporate from the liquid film forming layer, their absolute and relative contents change and the point of composition moves in the direction of point P. At a specific moment, it would cross the spinodal border surface. Theoretically, from this moment the system will undergo the phase separation, forming a two-phase liquid system. In practice, the phase separation begins after a certain delay due to inclination of the polymer system to relax. Moreover, the cross-point A' should be situated not on the line PS, but certainly outside because of the difference in volatility of solvents. Due to the higher volatility of acetone, point A' must correspond to the solvent composition with relatively higher xylene content that it had in the initial point A. The composition of each separated phase can be determined by the location of point A on the border surface and tracing from A' to point P, where, theoretically, the system should consist only of nonvolatile components and be separated into two phases of composition corresponding to points C' and C". This should occur if both phases remain liquid, that is, in the absence of any kinetic restrictions. Real polymer systems should "solidify" when the average composition related to point B (very high polymers content), and the composition of the separate solid phases will correspond to points B' and B". Then, on losing the residual amount of solvent, and due to the development of chemical reactions of curing between epoxy resin and hardener, each phase undergoes the "secondary" phase separation, moving to points C' and C". Strictly speaking, they cannot be completely separated during film formation, and the final step of phase separation should be expected during the coating service as a result of post-cure reactions. Moreover, we assume that epoxy hardener is also present in the composition, in an amount that does not change significantly any equilibrium ratio.

B. Self-Stratification

Phase separation in polymer blend solution is a process which needs driving forces for displacement of separated phases to form a nonhomogeneous-in-layer structure and, in extreme, for the direction of the evolving phase either to the top or to the adhesion side. Since the film forming system is heterophase, any concentration gradients are ineffective with the exception, perhaps, of solvent concentration gradient which might be capable to provide transportation of particles (solvophoresis [11]).

Generally, a few types of driving forces could be applied to the process and cause separation into layers:

- interfacial surface tension. This driving force may (a) direct one of the coexisting phases to the substrate (selective wetting), (b) provide separation of the capillar system into layers (when a typical for spinodal decomposition structure forms) according to Marangony's effect [5].
- difference in composition when both phases, with different solvent content, have to rearrange their structure during contraction on solvent evaporation process.
- kinetic causes such as the increase in surface viscosity of the applied liquid layer due to extensive evaporation of solvents.
- gravity and probably other external forces. According to the calculation and experimental data reported in [4], the gravity should be considered as a weak parameter for structure control as compared to the wetting of substrate and capillar forces.

The resultant efficiency of stratification depends on the relative contribution of the driving forces and kinetical restrictions that arise from increasing viscosity (until fixation of polymer structure) on solvent evaporation and chemical reactions on curing.

From the above discussion we may conclude that the heterophase and self-stratified polymer structure must show sensitivity to the main technological parameters, such as characteristics of solvents, application and curing conditions.

III. Film Structure

Parameters of heterophase coating structure can be identified in cross sections by means of a scanning electron microscope (SEM). It is convenient to apply the coating to the substrate where it could be easily splitted separately or together (if a brittle substrate-like glass panel is used) on cooling under liquid nitrogen [5]. Figure 2 represents two typical examples (SEM JSM 5300). The whitter coherent phase epoxy/vinyl film (fig. 2-a and 2-b) is enriched with vinyl resin, while the particles of the incoherent phase consist mainly of epoxy resin. Self-stratified coating (fig. 2-c) includes a heterophase main layer (filled with pigments) and a clear top layer of 7-10 μ m thickness.

Reliable information about phase composition can be obtained from the affiliation of SEM with X-rays analysis. Completely stratified (double layer) polymer structure in epoxy/perchlorovinyl blended film (fig. 3) was formed by the heating of slowly curing coating at 100°C. Higher absorption of the upper layer in Cl spectral line indicates the fact that this layer is enriched with perchlorovinyl resin. Its top position corresponds to prevail of Marangony's effect over gravity on the stratifying process.

SEM + EDS analysis of HSSC (Table 2) is capable of registering the difference in polymer composition between both sides (surfaces) of the delaminated films. Unfortunately, this precision methodic cannot provide information about polymer distribution through the film thickness.

Depending on epoxy/thermoplastic ratio, as well as on some technology conditions, the phase separation process on film formation may be directed toward:

- either epoxy or thermoplastic resin enriched phase isolated from the solution of the polymer blend, and
- either nucleation and particle growth or spinodal mechanism of phase decomposition occurs with correspondent difference in film structure.

The ability to control these two main factors of the phase decomposition process, and the consideration of some other characteristics such as solvent evaporation rate, volatility ratio, selective wetting of substrate by higher or lower polar liquid phase (all contributing parameters discussed in works [4,5]), can provide a predictable type of heterophase polymer structure (fig. 4):

- heterophase and uniform-in-layer (S1 and N1);
- heterophase and self-stratified to the top (S2), or to the lower (S3) part of the coating;
- nonhomogeneous-in-layer (N2);
- sandwich structure (very seldom - usually in additional heating after solvent evaporation);
- double-layered (completely stratified) film on heating of most presented types before being cured.

Depending on the field of coating application, a certain type of film structure may be preferred. According to our knowledge, structural types S2, N2 and N3 should be recommended for the anticorrosive industrial coatings, while S2 - for the weather/anticorrosive coatings.

IV. Anticorrosive Properties

Heterophase and self-stratifying coatings were offered for anticorrosive use almost a decade ago [12]. During this period, a number of studies were carried out to determine their technical opportunities in this field. Most of them have shown a distinctive advantage to HSSC, applied in one coat of 60-120 μ m dry film thickness, as compared to 2-3 coats of primer + top traditional anticorrosive coatings even when the latter were applied in higher (200-300 μ m) thickness. Besides material and trade savings, they can be so composed to be available as anticorrosive/weather resistant coatings (epoxy/vinyl, epoxy/ acrylic and epoxy/siloxane versions).

Results, presented in Table 3, give evidence in favor of self-stratifying epoxy/vinyl coatings (30-40 μ m thickness) that have been tested against two "standard" compositions: one-coat high-built (110 μ m) and 2 coats primer + top coat system (300 μ m thickness). Here and earlier [5, 10, 12], the reported fact that HSSC exhibits outstanding anticorrosive properties deserves some explanation.

Depending on the coating composition, film structure and nature of substrate, a number of factors can contribute to the anticorrosive functions of HSSC (besides surface pre-treatment):

- anticorrosive pigments (oxidizing pigments inhibitors - passivators, phosphate-type pigments that provide inhibition in aerated media and form the phosphate surface capable of inhibiting the acid corrosion etc).
- the presence of amines in film forming composition such as epoxy hardeners; their absorption on metal substrate provides a barrier inhibition.
- insulative function of the coating.
- free energy of polymer/metal adhesion which has to be exceeded to allow the formation of rust as a new phase. Higher magnitude of free energy of interphase may be provided when the more adhesion-reliable resin (epoxy) concentrates in the lower part of the coating, in the self-stratification process.

Moreover, when properly formulated, HSSC can exhibit self-healing ability regarding erosion and corrosion-caused coating microdefects (phase separation associated with post-cure reactions between epoxy resin and hardener). All these features make HSSC available for the long term corrosion protection.

V. Application to Rusty Steel Substrates

Most coatings offered for the long term corrosion protection demand well prepared metal surfaces. Rust, contaminations and moisture should be removed prior to application. There are many practical situations, however, where it is either technically impossible or economically undesirable to achieve surface preparation to bright metal finish. Hence, there is considerable interest in coatings which are tolerant to contaminated or corroded substrates, or that can be effective when applied to old, heavily corroded metal substrate from which only the weak-coupled rust has been removed [13].

The data provided in Table 4 exhibits a certain extension in lifetime service for the specially formulated HSSC applied to pre-rusted steel panels, as compared to the coatings tested on the mild steel panels. These results correlate with good service behaviour of the same compositions in natural outdoor exposition (application to old and corroded steel constructions after partially removing the rust by hand and washing out the remaining rust with water).

We may suggest that HSSC allows for some improvement in the rusted steel protection due to its ability to wet the remaining rust with the separated liquid phase, enriched with solvent and epoxy resin. In this case, all rust particles are completely covered and binded with cured resin. This new rust + resin layer, being a part of HSSC, contributes to corrosion protection by the inactivation of rust as well as by additional insulation from moisture and oxygen.

VI. Development of the concept

In order to provide distinct phase separation and self-stratification, about 25-35% of solvent has to be introduced into the ambient cure epoxy/thermoplastic coating composition, which enable them to be applied with conventional equipment. Low, or even zero-VOC coatings compositions based on lower molecular weight curable resins, particularly similar to those earlier described in the paper [14], may be developed to meet the most severe environmental legislations. Papers [4, 8, 15] reported about heterogeneous water-based coatings, based either on mixed emulsions or on synthetic latices consisting of heterogeneous particles. One can suggest that the water/solvent-based hybrid film forming systems, particularly "emulsion-in-solution" systems, may be of interest in connection with HSSC [16].

Conclusion

Coating compositions that consist of two incompatible polymers, and particularly thermoset/thermoplastic combinations (comprising of epoxy as the thermoset resin) and a minimum of two solvents, enable coatings to be obtained according to the conventional technology, possessing microheterophase and self-stratifying polymer matrix structure due to the phase decomposition during film formation as a result of solvent evaporation and chemical reactions on the curing process.

Being controlled, the heterophase polymer structure and self-stratification offer some new opportunities in coating performance and positively incorporated into anticorrosive properties. Formulated for higher phase separation, coating compositions allow immediate application to rusty steel surface and provide reliable corrosion protection.

It is recommended to apply anticorrosive coatings, based on phase decomposed binders, in one coat, thus revealing that their protective properties are equivalent to those of multi-layer coatings of even greater thickness.

References

1. W. Funke, Journa. Oil and Colour, Chem. Assoc., 59 (1976): p. 506.
2. W. Funke, Ind.-Lackier Betrieb, 44, 8 (1976): p. 305.
3. H. Murashe, W. Funke, 15th FATIPEC, 1980, Congress Book II, p. 387.
4. V. Verkholtantsev, Progr. Org. Coat., 13 (1985): p. 71.
5. V. Verkholtantsev, Progr. Org. Coat., 18 (1990): p. 43.
6. C. Carr, Journ. Oil and Colour, Chem Assoc., 73 (1990): p. 403.
7. T.A. Misev, Journ. Coat. Technol., 63, 795 (1991): p. 23.
8. A. Hofland, 21th FATIPEC, 1992, Congress Book II, p. 207.
9. Th. Mezger, Progr. Org. Coat., 20 (1992): p. 353.
10. V. Verkholtantsev, Journ. Coat. Technol., 64, 809 (1992): p. 51.
11. M. Kosmulski, E. Matijevic, Journ. Colloid and Interface Sci., 150, 1 (1992): p. 291.
12. V. Krilova, I. Kainova, V. Verkholtantsev, Lakokras. Mater. Ikh Primen, 4 (1984): p. 32.
13. N.L. Thomas, "Journ. Oil and Colour, Chem Assoc., 3 (1991): p. 83.
14. Yu. Shleomenson, Lakokras. Mater. Ikh Primen., 2 (1979): p. 8.
15. r. Arnoldus, R.L. Adolphs, W.M.W Zom, Polymers Paint Colour Journal, 181 (1991): p. 405; 20th FATIPEC 1990, Congress Book, p. 81.
16. V. Verkholtantsev, Lakokras. Mater. Ikh Primen., 4 (1990): p. 13.

Table 1 - Comparison of two approaches to obtain heterophase polymer structure from incompatible polymer blend

Features	Mixed Blend	Phase Decomposed Blend
Process	Forced	Spontaneous
Phase Structure	Rough	Fine
Specific Interphase Surface (order), m^2/m^3	0.1-1	1 - 100
Durability of Interphase Surface	Lower	Higher

Table 2 - SEM + EDS analysis of both surfaces of epoxy/vinyl and epoxy/siloxane self-stratified clear films (film thickness 80 μm , applied to the glass panels by spraying and delaminated under liquid nitrogen)

Composition	Side	Cl or Si Content (%)		
		x 150	x 2000	Average Calculated Value
ER/Vinyl Resin	Air	-	1.51	1.25
	Substrate	-	1.21	
ER/Siloxane Resin	Air	1.26	1.27	0.95
	Substrate	0.81	0.86	

Table 3. Anticorrosive properties of self-stratifying coatings (1, 2) tested comparatively against conventional (3, 4) anticorrosive compositions (standard mild steel panels, application by spray with cross-cut, humidity test ASTM 2247-68, 2500 hrs).

No.	Composition	Coats	Total Film Thickness, microns	Test Results			
				Film		Substrate	
				Blisters	Creep, mm	Adhesion Retention, Score	Undercoat Corrosion
1	Epoxy/Vinyl (I)	1	90	No	No	+	Clear
		1	40	No	2	+	Clear
2	Epoxy/Vinyl (II)	1	30	No	2	+	Clear
3	Epoxy HB	1	110	No	-	+	Dark Corrosion 80%
4	Epoxy Primer + Epoxy Top Coat	2	300	Fine	7	+	Dark Corrosion 80%

Table 4. Anticorrosive properties of self-stratifying coatings tested comparatively against conventional 2 coats system on mild and pre-rusted steel panels (c. 30 g rust/m²)

Coatings	Application	Test Results (days, no change)			
		Salt-Spray Test ASTM B177-85		Humidity Test ASTM 2247-68	
		Mild	Pre-rusted	Mild	Pre-rusted
Epoxy/Vinyl (III)	1 coat 100 µm	30	40	60	80
Epoxy/Siloxane	1 coat 100 µm	40	60	70	80
Epoxy Primer + Top	2 coats 300 µm	30	20	60	40

Fig. 1. Phase diagrams of four-component polymer systems:

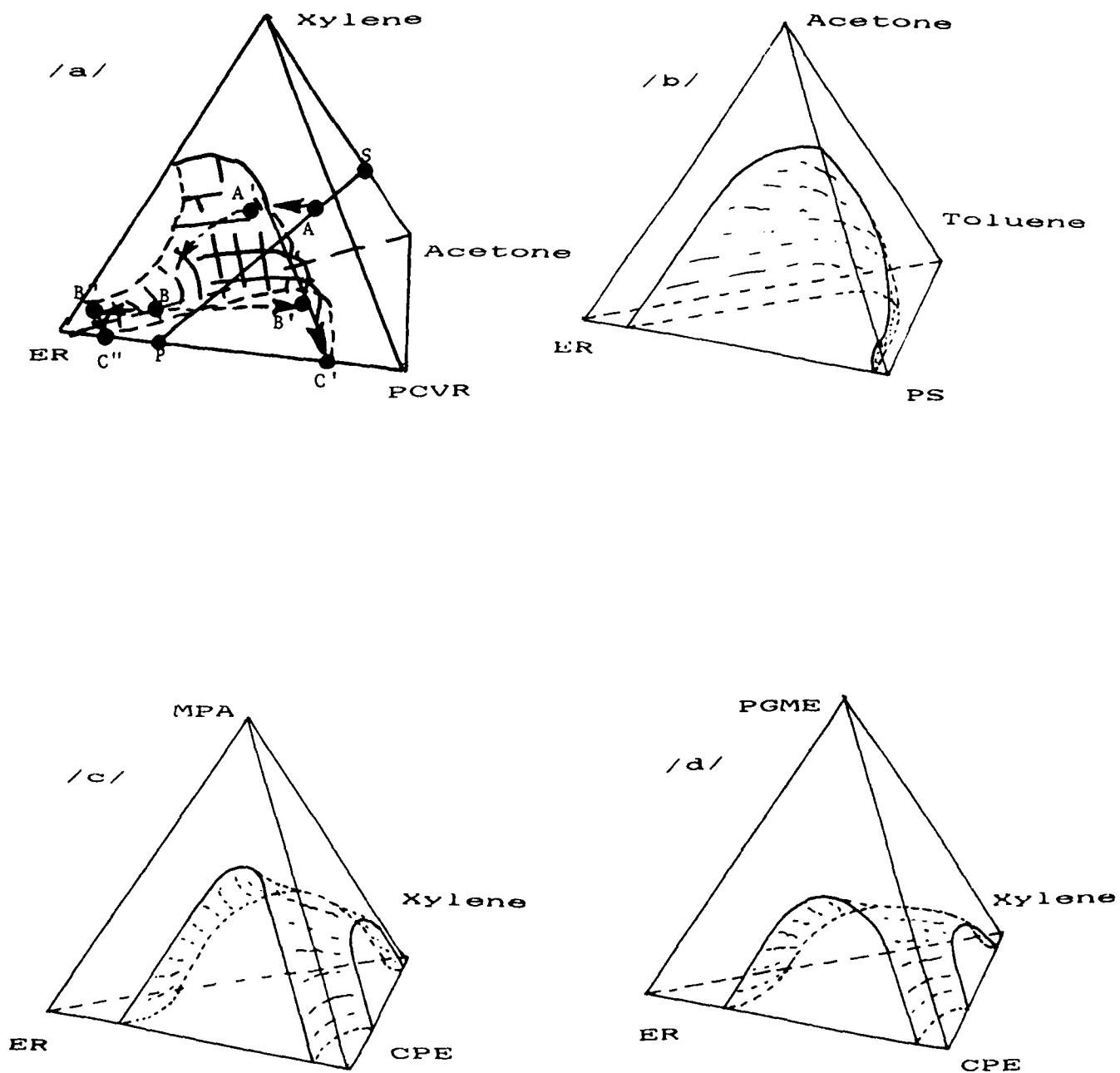




Fig. 2 SEM micrographs of film cross sections: Heterophase ER/VR [a-magn. 500, b-magn. 3000] and selfstratified ER/SR heterophase matrix and filled with clear homophase top layer [c].

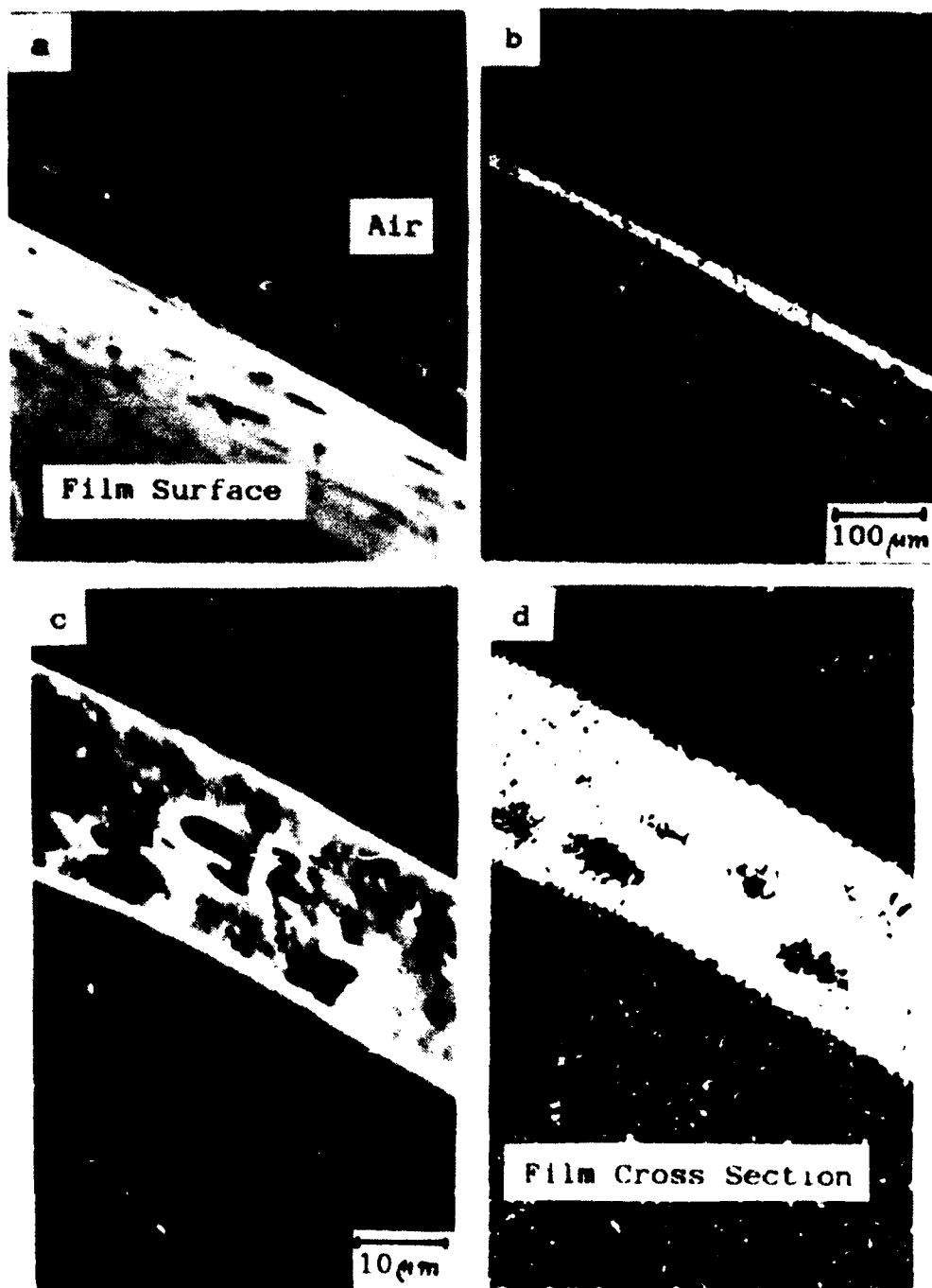


Fig. 3 SEM micrographs in regular [a,c] and Cl-absorbing spectral line [b,d] of film cross sections [ER/PCVR, 90/10 by wt]: a,b - magn. 120, c,d - magn. 1500.

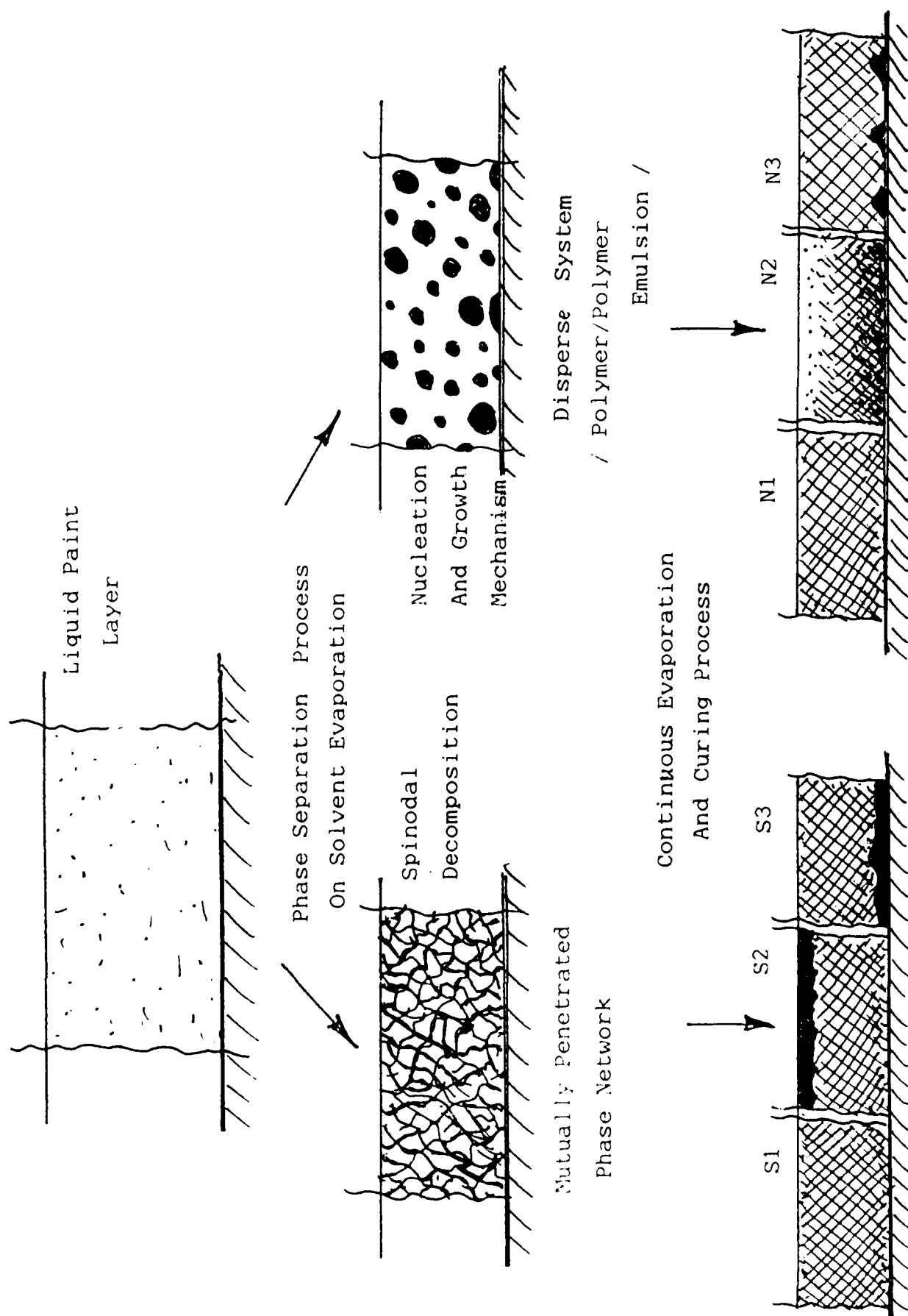


Fig. 4 Heterophase and Selfstratified Film Structure /Schematic Representation/

Application of Electrochemical Impedance Spectroscopy to Study the Efficiency of Anti-corrosive Pigments in an Epoxy Resin.

Ahamed Amiradin
Swedish Corrosion Institute
Roslagsvägen 101 Hus 25
S-104 05 Stockholm
Sweden

Corrine Barreau
Institut de Recherche de la Siderurgie Francaise
185 rue President Roosevelt
F-781 05 Saint Germain en Laye
France

Dominique Thierry
Swedish Corrosion Institute
Roslagsvägen 101 Hus 25
S-104 05 Stockholm
Sweden

Abstract

The anti-corrosive properties of seven different pigments used in an epoxy-polyamide resin applied on a steel surface have been studied by means of Electrochemical Impedance Spectroscopy (EIS). The experimental conditions were total immersion in 3% NaCl and outdoor exposure. The onset of delamination and corrosion beneath the organic coating were determined in all cases. The results of EIS were complemented by adhesion tests. The results indicate that EIS is an efficient method to classify different pigments vis-a-vis their anti-corrosive properties. In particular, a very good correlation was observed between the breakpoint frequency and the disbonded area. From the results, it also appears that zinc phosphate performed as well as zinc chromate except in a marine environment where the former performed poorly. All the other 5 pigments put up a distinctly inferior performance to that of zinc chromate irrespective of the exposure conditions.

Key terms: Electrochemical Impedance Spectroscopy, anti-corrosive pigments, epoxy-polyamide, breakpoint frequency.

Introduction

Organic coatings have been used for a long time to protect metals against corrosion. The primary effect of an organic coating is to act as a barrier against water, oxygen and aggressive ions. However, all organic coatings are more or less permeable to these species and their presence at the metal-coating interface may lead to a loss of adhesion followed by corrosion and/or delamination. Therefore, as a second line of defence, anti-corrosive pigments are incorporated into the paint coating. These pigments may protect by either a physico-chemical or an electrochemical mechanism¹. Pigments which protect by physicochemical mechanisms generally have a lamellar, flaky or plate like shape. This shape greatly increases the length of the diffusional pathways for oxygen and water and decreases their permeability². Examples of such pigments are micaceous iron oxide and aluminum flakes. Pigments which protect by electrochemical mechanisms are inhibitors which are sparingly soluble in water. They continuously dissolve in the water entering the coating from the atmosphere so that only an inhibitive solution reaches the coating-metal

interface. Examples of this type of pigment are red lead and zinc chromate which are both, however, toxic.

During the last decade, serious attempts have been made to find non-toxic anti-corrosive pigments that can replace zinc chromate and red lead whose applications are subject to legislative limitations. A large number of new pigments have recently been proposed as possible substitutes for zinc chromate. These substitutes may be classified into 5 groups: phosphates, borates, complex silicates, organic salts and basic ion-exchange pigments³. Despite the large body of literature available on this subject, the protective value and the protective mechanisms of paints based on the new pigments are still a matter of discussion.

Many electrochemical investigations of the corrosion of polymer-coated metals are performed by means of Electrochemical Impedance Spectroscopy. DC methods are rarely used because of the high resistance of the polymer coating.

There is almost an unanimity of opinion that the polymer-coated metal is represented by the simple equivalent circuit presented in Fig 1 where R_u is the uncompensated resistance between the coated metal and the tip of the reference electrode, C_c represents the capacitance arising from the paint coating, R_c is the resistance ("pore resistance") due to the paint coating and Z_m represents the general impedance of the metal-electrolyte system when the water in the environment penetrates the coating and reaches the metal. This term includes the double-layer capacitance, C_d , of the metal-electrolyte interface. Many authors, however, differ with respect to the actual composition of Z_m probably due to different surface treatments⁴, electrolyte concentrations⁵ etc.

According to Haruyama et al⁶, all elements in the equivalent circuit, with the sole exception of the coating capacitance, may be used as parameters to evaluate coating disbonding. This is summarized in equations 1-4.

$$C_c = C_c^0 \cdot A \quad (1)$$

$$C_d = C_d^0 \cdot A_d \quad (2)$$

$$C_c = (\epsilon \cdot \epsilon_0 \cdot A) / l \quad (3)$$

$$R_c = R_c^0 / A_d \quad (4)$$

where C_c^0 , C_d^0 and R_c^0 are the area-specific values, ϵ_0 is a constant, ϵ is the relative dielectric constant, l is the thickness of the paint coating, A is the total area of the specimen and A_d is the total delaminated area. It is important to note that this treatment assumes that the specific coating resistance and the coating thickness stay more or less constant while delamination and corrosion proceed under the coating. It is also assumed that changes in the coating capacitance are due only to an increase in the value of the dielectric constant of the organic coating caused by the penetration of water (Eq 3). This last assumption is probably not valid, as changes in the coating capacitance have been observed due to the initiation of the delamination process⁷.

In addition to the passive elements in the equivalent circuit, the frequency ("breakpoint frequency") at which the phase angle falls to 45 degrees in the high frequency range (i.e. when the resistive and reactive impedances are equal) has been used as a direct measure of the delaminated area. The breakpoint frequency, f_b , is derived from Haruyama's treatment (Equation 5) and therefore suffers from the same limitations (i.e constant

coating capacitance, thickness and specific coating resistance) during the delamination and corrosion processes.

$$f_b = A_d / (2 \cdot \pi \cdot \epsilon \cdot \epsilon_0 \cdot \rho \cdot A) \quad (5)$$

where ρ is the specific resistance of the solution. It should be noticed that f_b depends only on the coating parameters. The exact physical meaning of the breakpoint frequency is not, however, clear even though a good correlation is generally obtained with the delaminated area⁸.

In the present study, the behaviours of six non-toxic inhibitive pigments drawn from all the five groups described above, are compared with that of the standard zinc chromate. All seven pigments were incorporated into the same epoxy-polyamide binder and exposed to 3% NaCl solution, to a marine atmosphere and to an industrial atmosphere. The results of EIS have been complemented with other techniques such as image analysis using microscopic examination and adhesion measurements. The present study is part of a large investigation undertaken with the aim of optimising the use of EIS to study the degradation of coated metal. Previous results have been presented elsewhere^{5,9,10}.

Experimental

A. Sample Preparation

All anti-corrosive pigments used in the present work are commercial and they are listed in Table 1. The anti-corrosive pigments were added to an epoxy-polyamide resin in the proportions recommended by the manufacturers. The Pigment Volume Concentration was adjusted to 21% by adding TiO_2 to the formulations. Cold rolled steel was phosphated and chromate-rinsed before painting. The dry film thickness was 20 μm .

B. Exposure Conditions

The painted panels were exposed to 3% NaCl solution. The EIS data were obtained using a conventional three-electrode electrochemical cell. The exposed area was 10 cm^2 . Six panels of each paint were used in the study. The exposure was continued until the paints visibly broke down as shown by blistering and/or rusting. In addition, panels were exposed under atmospheric conditions at Biarritz (Southern France) corresponding to a marine environment and Rouen (Northern France) corresponding to an industrial environment.

C. Impedance Measurements

The experimental set-up has been described in detail elsewhere⁵. The spectra were interpreted by a Non-linear Least Squares (NLLS) method using software developed in the University of Twente, The Netherlands¹¹. This software uses Nyquist plots to obtain the approximate values of the passive elements in the equivalent circuit which are then fitted using a NLLS procedure. The quality of the fit is given by the chi-square and the frequency error distribution (i.e. the residuals of the imaginary and real parts as a function of the frequency). The lower the value of chi-square, the better is the fit. The frequency error distribution for a good fit is less than 2% at all frequencies and the curve should not show any pronounced periodicity. One advantage of this software is that Constant Phase Elements (CPE) may be used instead of capacitances and diffusion elements, which may give valuable information concerning the heterogeneities in the coating.

D. Visual Observations

After exposure, the panels were removed, washed with deionized water and dried. The type and extent of degradation were assessed visually and by means of an image analyzer.

E. Adhesion Measurements

The adhesion of the paint after exposure to 3% NaCl was tested according to ASTM Standard D-3359¹².

Results and Discussion

A. Immersion Studies

1. Equivalent Circuit. The Nyquist Impedance Spectra showed three successive patterns with increasing periods of exposure. Initially, a capacitive behaviour (Fig 2a), later one semi-circle (Fig 2b) and finally two semi-circles (Fig 2c).

When the spectrum shown in Fig 2c was analyzed using the NLLS fit program, it was found that equally good fits were obtained with quite a few equivalent circuits. It was, therefore, decided to propose an equivalent circuit which satisfied both the following criteria:

1. The circuit should be physically meaningful.
2. The circuit should give a reasonably good fit to the data, but it need not mathematically be the best.

The model shown in Fig 3 satisfies both these criteria. Comparison of Fig 3 with Fig 1 shows that Z_m constitutes the double-layer capacitance C_d in parallel with the charge-transfer resistances (R_1 and R_2) and the mass-transfer impedances (Z_1 and Z_2) of the anodic and cathodic reactions.

This circuit also closely resembles the equivalent circuit proposed by Bonnel et al¹³ for uncoated steel in 3% NaCl solutions. However, in the present work, the Coating Capacitance, C_c , has been replaced with a CPE, Q_c , the admittance of which is given by

$$Y = Y_0(j\omega)^n \quad (6)$$

where the coefficient Y_0 is a simple explicit function coupling solution resistance to capacitance and n is a measure of the surface roughness¹⁴. It is a common observation in EIS of polymer-coated metals that the semi-circles are often depressed beneath the real axis. As observed recently by Frechete et al¹⁵, depressed semi-circles are better analyzed with CPE rather than the conventional capacitance. Figures 4a and 4b shows the frequency error distribution in fitting the data with Q_c and C_c respectively. As can be seen, the frequency error and chi-square value are much higher when C_c is used instead of Q_c . However, the double-layer capacitance, C_d , was retained as such because it did not affect the fit in a similar way.

It should be noted that although visual observation of the spectrum in Fig 2c indicates only two time-constants, the proposed equivalent circuit has four. The frequency errors and the chi-square values obtained when the data was fitted to the circuits commonly used for polymer coated metals having three and two time constants are shown in Fig 4c and 4d respectively. Comparison with Fig 4a indicates that the best fit is obtained with the circuit given in

Fig 3. Walter¹⁶ observes that two time-constants appear as two distinct semi-circles in the Nyquist spectra only if one time constant is more than 20 times the magnitude of the other and if the resistance in the first time-constant is more than 5 times that of the resistance in the second. Thus, the number of time constants should be determined by data analysis rather than by visual observation as is traditionally done in EIS.

It should also be noted that some of the passive elements may not be found at the

beginning of the exposure. This is illustrated in Figure 5 for zinc chromate. During the first 30 days of exposure, the anodic branch of the equivalent circuit is not observed. The formation of a rust spot on the sample is preceded by a large decrease in cathodic charge-transfer resistance probably due to the formation of a blister resulting in an increase in the delaminated area. When the blister ruptures, rust is visually observed on the sample. This coincides with the first observation of the anodic branch in the equivalent circuit indicating that this resistance is closely related to the presence of corrosion products on the samples. Similar observations were made on all panels showing rust spots.

2. Comparison of Paint Behaviour. All samples were analyzed according to the equivalent circuit proposed in Fig 3. The data presented in this section generally represent the mean values of six specimens. The variation between replicates was generally within $\pm 20\%$. However, wide variations occur in a few cases due to the heterogeneity of the paint coating. These values were rejected.

The time dependence of the dielectric parameters Y_0 and n of Q_c as well as that of R_c and C_d are given in Fig 6. The time-dependence of f_b is given in Fig 7.

From a performance point of view, the behaviour of the seven paints falls into two distinct types. The first type of behaviour was shown by five paints - P2, P3, P4, P5 and P6, for which Y_0 , C_d , and f_b continuously increased from the beginning with corresponding decreases in the values of R_c and n . Blistering and rusting set in very early and the exposure was continued for only a month or so with only P6 lasting for two months. Delamination at the end of the exposure period, measured by the image analyzer, was about 1 to 5% of the exposed area and the adhesion at the end of the exposure was generally very low (Table 2). It is obvious that the rate of corrosion in these five paints is controlled by the rate of delamination, a phenomenon also observed by Walter¹⁷.

It should be noted that the gradual increase of the Y_0 value of Q_c with time is in sharp contrast with the usual time-dependent behaviour of C_c which reaches a steady-state value after some time¹⁸. The observed changes in the Y_0 value with time are probably related to the formation and rupture of blisters as observed by Van Westing⁷.

Such rapid changes in the passive elements and breakpoint frequency were not observed with paints coated with zinc chromate (P1) or zinc phosphate (P7). At the end of 100 days of exposure, the delamination was only 0.03 to 0.07% of the exposed area. The adhesion was also good (Table 2).

3. Determination of the disbonded area. Fig 8 shows the end-of-exposure values of f_b and C_d plotted as a function of A_d measured by the image analyzer. The data represent the mean values of six specimens for each paint system. A very good correlation is observed between f_b and A_d . This is consistent with other reports. A good correlation between C_d and A_d is also obtained for the five paints which exhibited a high delamination. However, there was no correlation between C_d and A_d in the case of P1 and P7 and the magnitude of C_d was about 1-2 decades lower than the magnitude obtained by extrapolation of the line shown in Fig 8. A possible explanation of this could be related to the formation of a protective film of corrosion products on the steel substrate leading to a large decrease in C_d for these systems.

Taking into account only f_b for all seven paints and the time taken to reach a value of 50 kHz (the maximum measurable value under the present experimental set up), the paints may be ranked vis-a-vis their corrosion protection properties on steel in the following decreasing order of efficiency

P7,P1 >> P6 >> P2,P3,P4,P5

It should be noted that zinc phosphate performs slightly better than zinc chromate in 3% NaCl.

B. Atmospheric Exposures

Table 3 gives f_0 of the seven paints as a function of exposure time in Biarritz marine test station. It is evident that zinc chromate is far superior to all other paints and that the phosphate-based paints including P7 perform poorly. In this case, the paints may be ranked in the following order of decreasing efficiency

P1 >> P3,P6,P7 > P2,P5

Table 4 gives f_0 as a function of exposure time at the Rouen industrial test station. Here, the phosphate-based paints performed as well as zinc chromate. The performance of all other paints is significantly lower than that of P1, P6 and P7. Their ranking is the same as that in the immersion studies.

C. Comparison of Immersion Studies and Atmospheric Exposure

The preceding discussion has clearly shown that zinc chromate performs very well under all exposure conditions used in the present study. However, the phosphate-based paints (P6 and P7) behaved differently in different environments, performing well in both 3% NaCl solution and an industrial atmosphere but not at a marine test site. A possible explanation is related to the pH of the electrolyte or rain water in the environment. At Rouen industrial station, the rain water has a pH of 3-4 due to the high level of pollutants, like SO_2 , present in the atmosphere. The pH of the 3% NaCl solution is 5.2. In Biarritz, the rain water has a pH between 6.8 and 7.5. It is well known that the limitation of zinc phosphate as an inhibitive pigment is its poor solubility¹⁹ which however increases with the pH of the electrolyte²⁰ so that it is quite effective in industrial atmospheres even in an alkyd binder²¹. Thus, at the marine test station, the pH of the environment is probably too high for the phosphate-based pigments to dissolve and function as an inhibitor. Under these conditions, the phosphate-based paints function only as an inert pigment. At the lower pH encountered at the industrial test site, the phosphates dissolve and thereby function as efficient inhibitors. In the case of 3% NaCl solution, the total amount of zinc phosphate leaching from the paint and reaching the metal-coating interface is also augmented by the continuous presence of the electrolyte compared to actual atmospheres which are characterized by alternate wet and dry periods. Thus it is important to select a laboratory exposure condition relevant to the actual atmosphere.

The observation that zinc chromate is slightly inferior to zinc phosphate under total immersion conditions can also be explained by the continuous presence of water which, in the case of the chromate, acts in exactly the opposite way, decreasing its efficiency. Too much water is deleterious to its protective properties because the coating formed then serves as a semipermeable membrane between water and a saturated solution of zinc chromate leading to osmotic blistering²².

The other four paints (P2, P3, P4, P5) behaved poorly under all three exposure conditions due either to bad adhesion or to poor inhibiting properties.

Finally, it is interesting to note that the rate of degradation for all paints was much higher in Biarritz than in Rouen. This is probably due to the differences in chloride deposition and the daily duration of sunlight between the two stations. As epoxy-

polyamide resins are well known to be very sensitive to photodegradation due to UV radiation, the more sunshine, the more degradation. Biarritz, being in the South-West of France enjoys more hours of sunlight than Rouen which is in the North of France.

Conclusions

- * Proposed equivalent circuits in EIS should be both physically meaningful AND should give a reasonably good fit with experimental data.
- * The number of time constants in a spectrum should be confirmed by NLLS fit and not be merely based on visual observations.
- * The coating capacitance should be replaced with a Constant Phase Element in order to obtain more realistic results.
- * The breakpoint frequency, regardless of the validity of its theoretical basis, is a good approximation of the delaminated area.
- * Zinc chromate shows good inhibiting action under all the exposure conditions used.
- * Phosphate-based pigments, especially zinc phosphate, behave as well as or even slightly better than the Chromate in 3% NaCl and at an industrial test site because they dissolve and act as inhibitors. However, this was not so in the marine test site because of their poor solubility in neutral solutions and the low time-of-wetness so that they remain insoluble, functioning only as inert pigments.

Acknowledgements

The authors thank Sollac (France), the Swedish National Board for Industrial and Technical Development (NUTEK) and the International Program for Chemical Sciences (IPICS), Uppsala University, Sweden, for financial support.

References

1. W.Funke in Polymeric Materials for Corrosion Control, Ed: R.A.Dickie and F.L.Floyd, American Chemical Society, (1986) p 222.
2. B.Bieganska, M.Zubielawiez and E.Smieszek, Prog. Org. Coatings, **16** (1988) p 219.
3. B.P.H.Goldie and D.G.Othen in Chemical Inhibitors for Corrosion Control, Ed: B.G.Clubley, Royal Society of Chemistry, **71**, (1990) p 121.
4. F.Mansfeld, M.W.Kendig and S.Tsai, Corrosion, **38** 9 (1982) p 478.
5. A.Amirudin and D.Thierry, Br. Corr. J., **26** 3 (1991) p 195.
6. S.Haruyama, M.Asari and T.Tsuru., Proc. Symp. Corr. Prot. by Org. Coat. Ed: M.W.Kendig and H.Leidheiser, Electrochemical Society, (1987) p 197.
7. E.Van Westing, Ph.D thesis, Delft University of Technology (1992).
8. H.P.Hack and J.R.Scully, J. Electrochem. Soc., **138** 1 (1991) p 33.
9. A.Amirudin, C.Barreau, D.Massinon and D.Thierry, Mat. Sci. Forum, **111-112** (1992) p 291.
10. A.Amirudin, C.Barreau, D.Massinon and D.Thierry, Proc. 2nd Int. Conf. on Zinc and Zinc Alloy Coated Steel Sheet (1992) p 549.
11. B.Boukamp, Ext. Abst., 1st Int. Symp. on EIS, Bombannes, France (1989) p C1.11.
12. American Society for Testing and Materials ASTM Standard D 3359-87, Vol 06.01 (1988) 515.
13. A.Bonnel et al, J. Electrochem Soc., **130** (1983) p 753.
14. Nyikos et al, Electrochimica Acta, **30**, (1985) p 1533.
15. E.Frechette, C.Compere and E.Ghali, Corros.Sci, **33** (1992) p 1067.

16. G.W.Walter, J. Electroanal. Chem, **118**, (1981) p 259.
17. G.W.Walter, Corros. Sci., **32**, (1991) p 1059.
18. G.W.Walter, Corros. Sci., **32**, (1991) p 1041.
19. S.Turgoose, in Chemical Inhibitors for Corrosion Control, Ed: B.G.Clubley, Royal Society of Chemistry, **71**, (1990) p 72.
20. J.A.Burkill and J.E.O.Mayne, JOCCA, **71** 9 (1988) p 273.
21. F.de L. Fragat and J.E.Dopico, JOCCA, **74** (1991) p 92.
22. M.Svoboda and J.Mleziva, Prog. Org. Coat., **12** (1984) p 251.

Table 1. List of investigated pigments

Ref no	Pigment	Group
P1	Zinc chromate	—
P2	Barium metaborate	Borate
P3	Calcium silicate	Basic
P4	Amino carboxylate	Organic
P5	Calcium, Barium phosphosilicate	Complex silicate
P6	Aluminium triphosphate	Phosphate
P7	Zinc phosphate	Phosphate

Table 2. Adhesion and visual delamination/corrosion at the end of exposure

Ref no	No of days exposed	Grade of adhesion	Percent delamination and corrosion
P1	100	5B	0.76
P2	28	1B	4
P3	34	5B	1.74
P4	24	3B	4
P5	32	3B	5.44
P6	56	4B	1
P7	100	5B	0.3

Table 3. Variation of f_b as a function of the exposure time in Biarritz marine test station

Ref no	f_b , Hz $t = 0$	f_b , Hz $t = 6$ months	f_b , Hz $t = 12$ months
P1	2	15	170
P2	4	485	6200
P3	3	190	10000
P4	3	1400	>30000
P5	3	130	5000
P6	3	160	>30000
P7	3	50	1100

Table 4. Variation of f_b as a function of the exposure time for all paints exposed in Rouen industrial test station

Pigment	f_b , Hz $t = 0$	f_b , Hz $t = 6$ months	f_b , Hz $t = 9$ months
P1	2	4	4
P2	4	80	160
P3	3	15	30
P4	3	20	30
P5	3	20	40
P6	3	5	15
P7	10	10	10

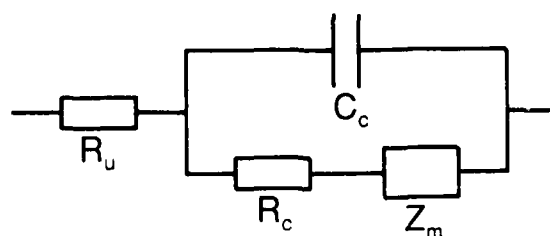


Figure 1. General equivalent circuit for a polymer-coated metal.

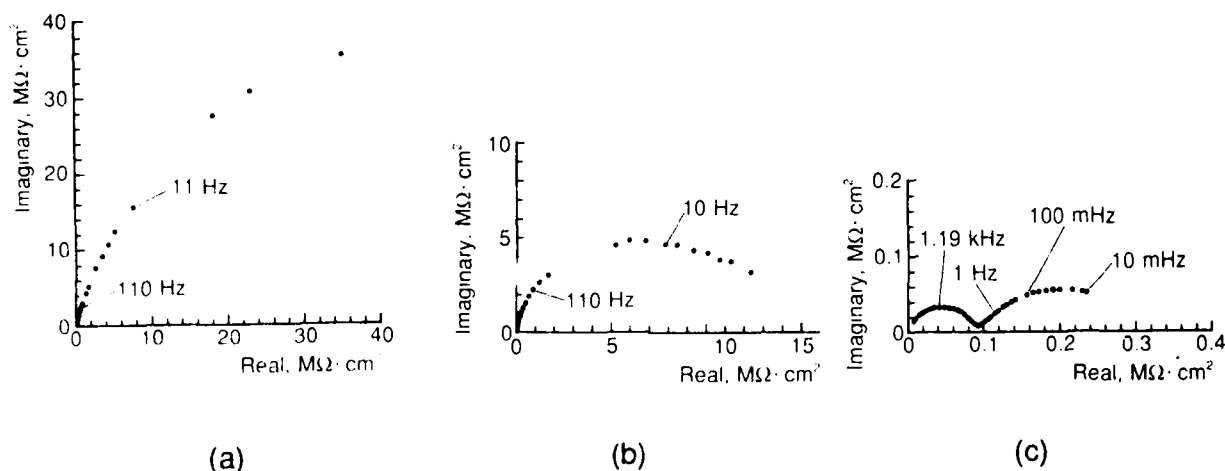


Figure 2. Nyquist plots (a) 2 days, (b) 8 days, (c) 56 days.

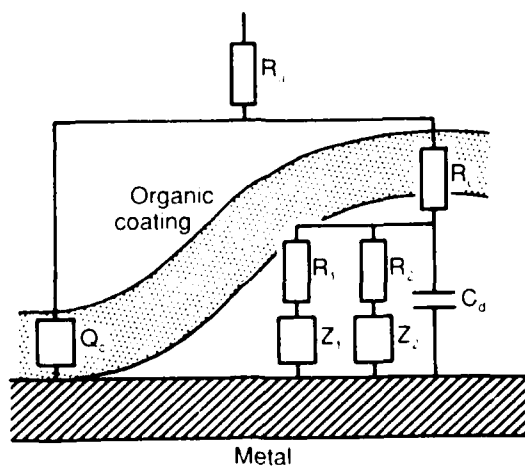


Figure 3. Proposed equivalent circuit for the present work. R_1 and R_2 are the charge-transfer resistances and Z_1 and Z_2 the mass-transfer impedances.

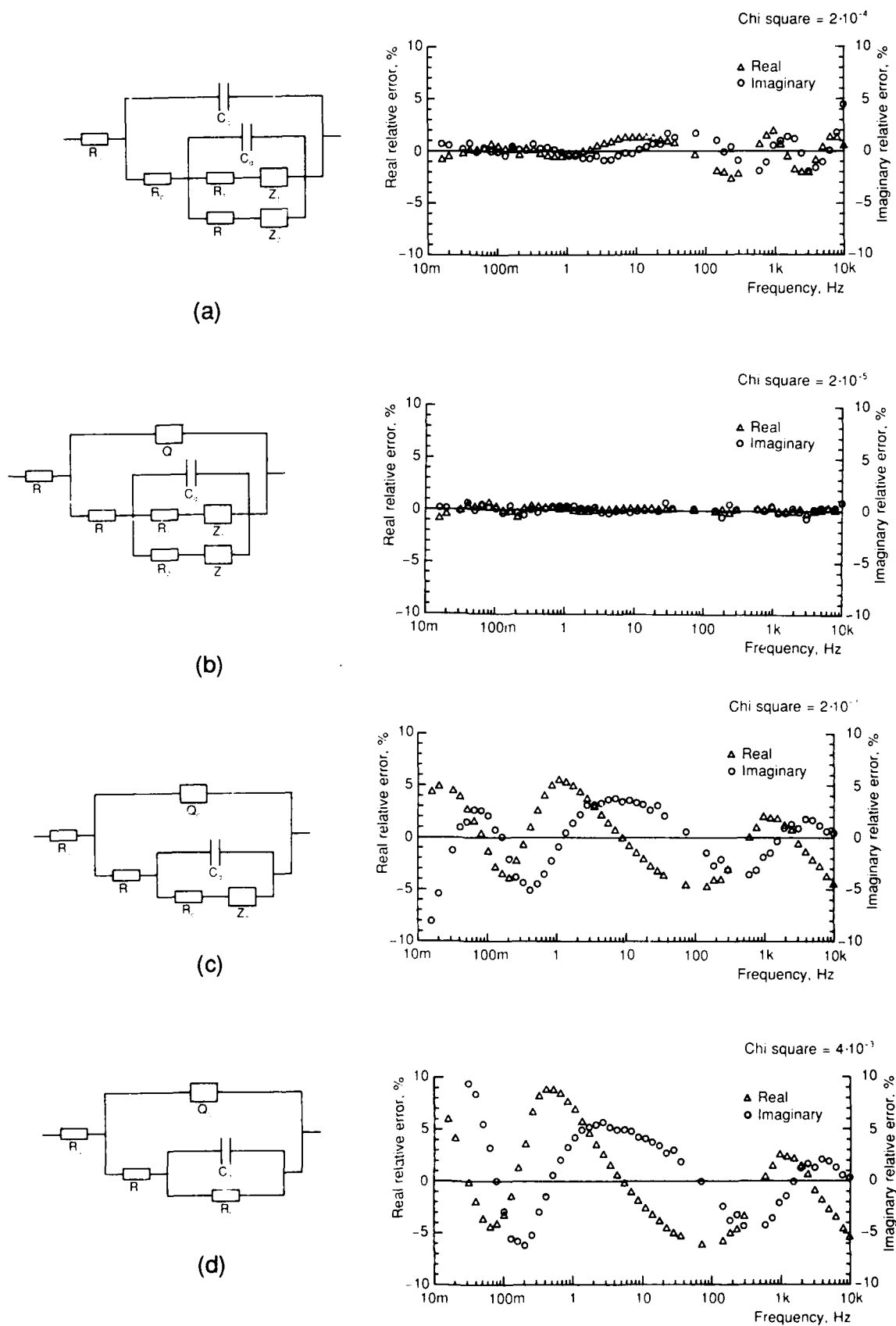


Figure 4. Frequency error distribution for proposed circuit with (a) capacitance, (b) CPE, and for the conventional circuit with (c) 3 time constants — Z being equal to a Warburg diffusion element — and (d) 2 time constants.

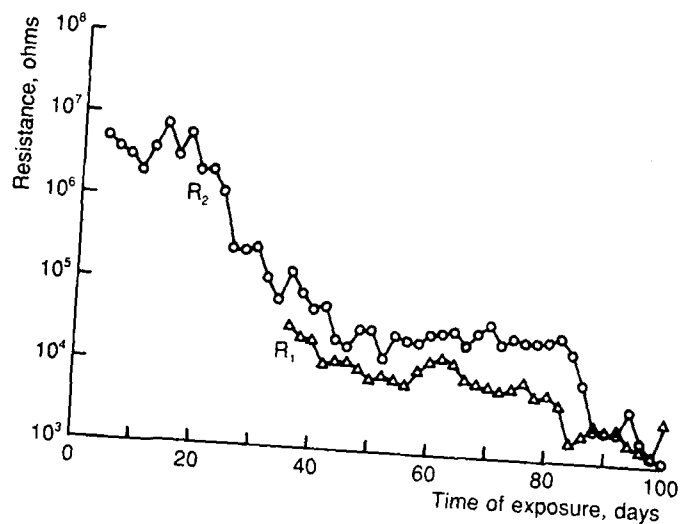
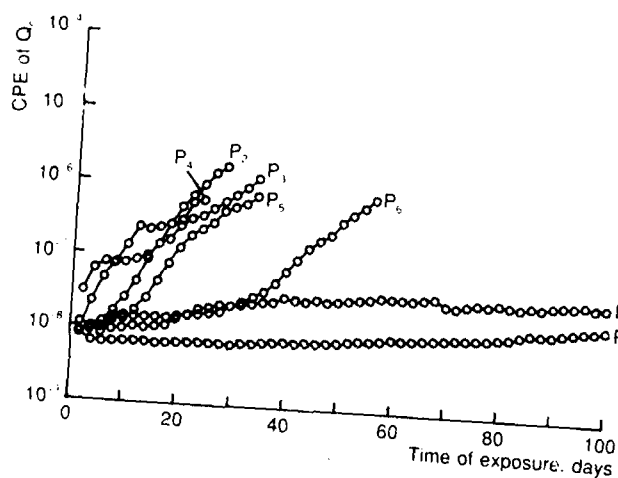
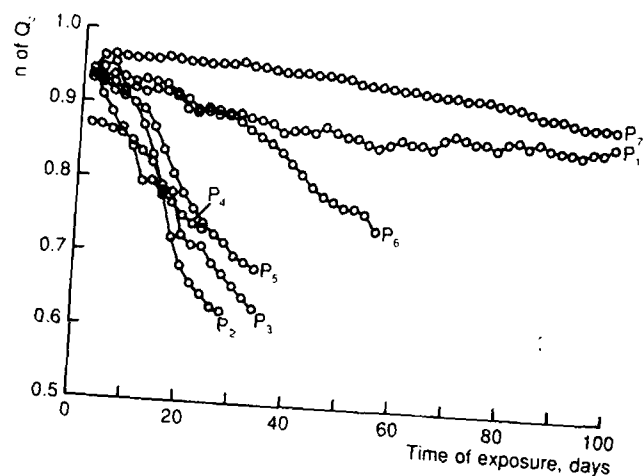


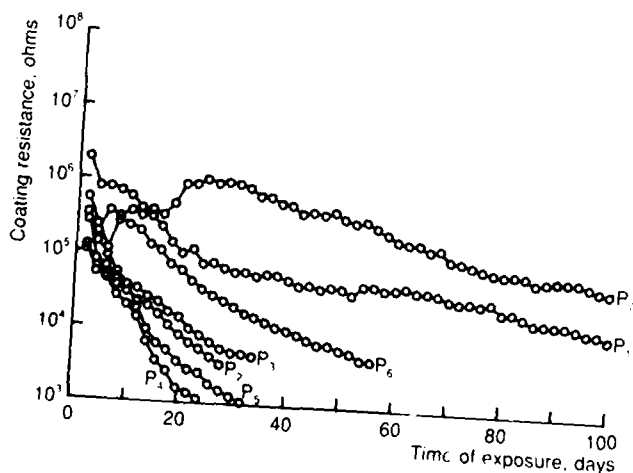
Figure 5. Time-dependence of R_1 and R_2 in the case of zinc chromate.



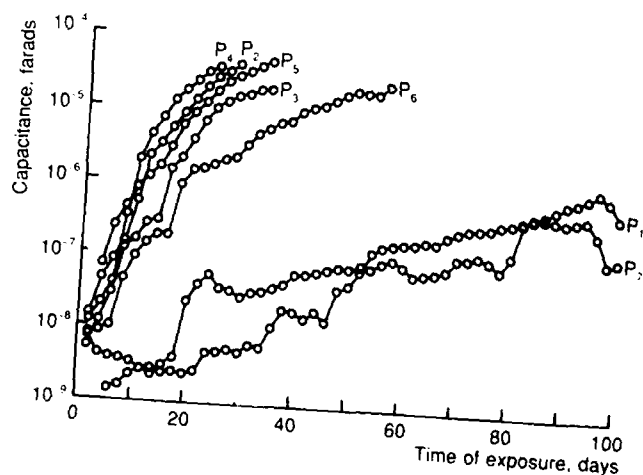
(a)



(b)



(c)



(d)

Figure 6. Time-dependence of (a) Q_c , (b) n , (c) R_c , and (d) C_d .

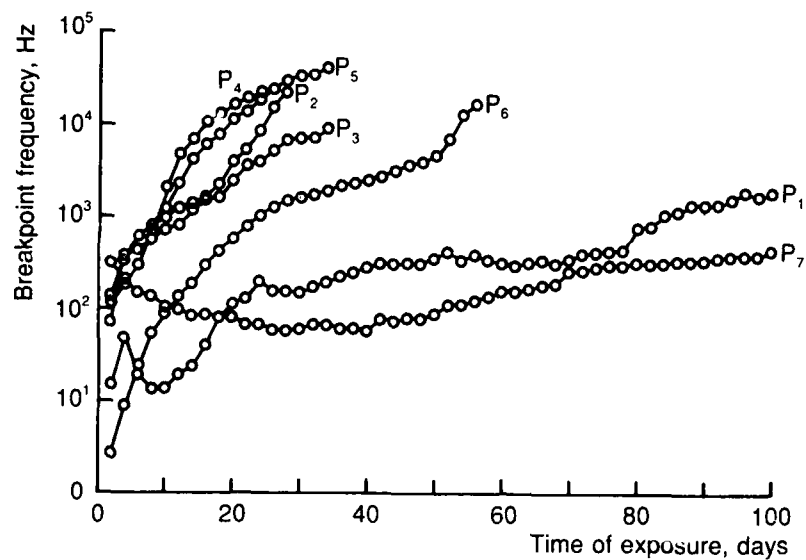


Figure 7. Time-dependence of f_b .

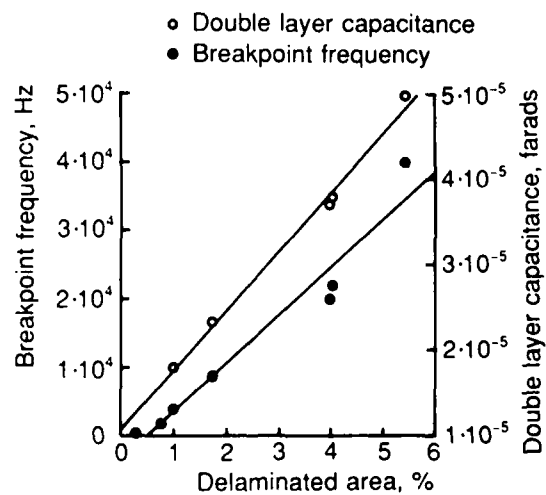


Figure 8. The end-of-exposure values of f_b and C_d as a function of A_d measured by the image analyzer.

Determination of the Protective Properties of Polymer Coatings from High-Frequency Impedance Data

F. Mansfeld and C.H. Tsai

Corrosion and Environmental Effects Laboratory (CEEL)

Department of Materials Science and Engineering

University of Southern California

Los Angeles, CA 90089-0241, USA

Abstract

A theoretical analysis of the impedance of polymer coated steel has been performed with the goal of identifying parameters which can be used in the assessment of coating performance in a short measurement time without rigorous analysis of EIS-data. The results of this analysis applied to nine different coating systems suggest that the breakpoint frequency f_b , the frequency f_{min} of the phase angle minimum Φ_{min} observed at high frequencies, and the ratio of the impedance recorded at two frequencies can be used for this purpose. The analysis also shows that f_b and f_{min} depend both on the delaminated area A_d and the coating resistivity ρ , while Φ_{min} and the ratio f_b/f_{min} depend only on A_d . Recording of f_b , f_{min} and Φ_{min} allows to determine coating damage and is therefore recommended for the design of a commercial device for field testing of the remaining lifetime of protective coatings. The amount of water uptake of the coating determined from the coating capacitance in the first days of exposure agreed well with the visually observed coating damage after exposure to 0.5 N NaCl for one year.

Key terms: protective coatings, impedance spectroscopy, delamination, field testing, water uptake, exposure tests

Introduction

Electrochemical impedance spectroscopy (EIS) has been shown to be a powerful technique in the evaluation of the performance and degradation processes of commonly used coating systems [1-3]. The general approach includes recording of the impedance spectra in a wide frequency range (10^5 - 10^{-3} Hz) as a function of the exposure time to the corrosive environment and analysis of the EIS-data based on an equivalent circuit model. The performance of the coating

is evaluated according to the magnitudes of the parameters in the equivalent circuit and their changes with exposure time. This procedure is usually time consuming and requires appropriate software to analyze the EIS-data. One objective of the present study is to develop an approach for evaluating coating performance in a short time without quantitative analysis of the EIS-data. The results of this approach are proposed as basis of a device for the determination of coating properties in field studies which can be used in decisions concerning removal of paint systems without remaining useful lifetime and application of fresh protective coatings.

Earlier theoretical studies [4] of the changes of the impedance spectra of a polymer coated metal during exposure to a corrosive environment have been expanded [5,6] using the model shown in Fig. 1, where C_c is the coating capacitance, R_{po} the coating resistance ("pore resistance") [1-3], C_{dl} the capacitance at the area under the coating where corrosion occurs, and R_p is the corresponding polarization resistance. R_Ω is related to the electrolyte resistance, the ohmic resistance in electrical leads, etc. When a coating is undamaged and still protective, the impedance spectrum in a Bode-plot shows only one time constant with a wide linear capacitive region in which the slope equals -1 and the phase angle is close to 90 degrees. As the coating degrades due to the penetration of electrolyte into the coating and the occurrence of delamination and corrosion at the coating/metal interface, the impedance spectrum exhibits two time constants. The first time constant at higher frequencies is associated with the properties of the coating, while the second one at lower frequencies is related to the degree of delamination and/or corrosion. Since the ionic current through the degraded coating is concentrated at the delaminated area, the magnitudes of R_{po} , C_{dl} , and R_p should be related to this area as suggested by Haruyama et al. [7], who suggested that the decrease of R_{po} and R_p and the increase of C_{dl} with exposure time are due to an increase of the delaminated area A_d according to:

$$R_{po} = R_{po}^0 / A_d, \quad (1)$$

$$R_p = R_p^0 / A_d \quad (2)$$

$$C_{dl} = C_{dl}^0 A_d, \quad (3)$$

$$\text{where } R_{po}^0 = \rho \cdot d \text{ (ohm.cm}^2\text{)}. \quad (4)$$

R_p^o (ohm.cm²) and C_{dl}^o (μF/cm²) are characteristic values for the corrosion reaction at the coating/metal interface, which are assumed not to change with coating degradation, d is coating thickness and ρ is the coating resistivity. The experimental value of the coating capacitance C_c (μF) depends on the total sample area A , the thickness of the coating d and its dielectric constant ϵ :

$$C_c = (\epsilon\epsilon_0/d)A = C_c^o A, \quad (5)$$

Haruyama et al. [7] have suggested that the extent of delamination can be determined experimentally from the breakpoint frequency f_b , which is the frequency at the phase angle $\Phi = 45^\circ$ in the capacitive region (Fig. 2):

$$\begin{aligned} f_b &= 1/2\pi R_{po} C_c = (1/2\pi R_{po}^o C_c^o)(A_d/A) \\ &= (2\pi\epsilon\epsilon_0\rho)^{-1}(A_d/A) = f_b^o D, \end{aligned} \quad (6)$$

where $D = A_d/A = f_b/f_b^o$ is the delamination ratio and

$$f_b^o = 1/2\pi\epsilon\epsilon_0\rho \quad (7)$$

is a characteristic frequency which depends only on the coating parameters ϵ and ρ and is independent of coating thickness d . In Haruyama's approach [7] it is assumed that ρ and ϵ do not change with exposure time. The results obtained by Mansfeld and Tsai [6] for coating systems used by the U.S. Navy show that this assumption is oversimplified since ϵ increases due to water uptake and ρ decreases as conductive paths and defects develop in the coating. In Eq. 7, f_b^o is therefore not a constant value, but is likely to change with exposure time as ϵ increases and ρ decreases. In addition to f_b , Mansfeld and Tsai [4 - 6] have suggested that the minimum of the phase angle Φ_{min} and its frequency f_{min} can be used to characterize the extent of delamination (Fig. 2). Using the equivalent circuit in Fig.1 and certain simplifying assumptions, they have shown that the following relationships apply:

$$R_{po} = \rho d/A_d = \rho d/DA \quad (8)$$

$$f_b = k_b^o D/\rho \quad (9 \text{ a})$$

$$k_b^0 = (2\pi\epsilon\epsilon_0)^{-1} \quad (9 \text{ b})$$

$$f_{\min} = a_1(D)^{1/2}\rho^{-1} \quad (10 \text{ a})$$

$$a_1 = (2\pi d)^{-1}(C_c^0 C_{dl}^0)^{-1/2} \quad (10 \text{ b})$$

$$\tan \Phi_{\min} = a_2(D)^{-1/2} \quad (11 \text{ a})$$

$$a_2 = 2 (C_c^0 / C_{dl}^0)^{1/2} \quad (11 \text{ b})$$

$$f_b/f_{\min} = K_b^0 (a_1)^{-1}(D)^{1/2} \quad (12 \text{ a})$$

$$= (C_{dl}^0 / C_c^0)^{1/2}(D)^{1/2}. \quad (12 \text{ b})$$

In order to decide whether an observed increase of f_b is due to changes in D , ρ or both, Mansfeld and Tsai [5,6] have proposed the use of the ratio f_b/f_{\min} (Eq.12), which is independent of the coating resistivity ρ . Since Φ_{\min} is also independent of ρ (Eq.11), this parameter can be used for the same purpose. This approach has been used in the present study for the analysis of the corrosion behavior of steel coated with various paint systems used by the U.S. Navy.

Another approach to determine coating damage uses the measurement of the impedance at two frequencies [8]. If these frequencies are located in the capacitive region, where the slope of the $\log |Z| - \log f$ curve has a value of -1, then the ratio of the two measured impedance data is the same as the ratio of the frequencies. With increasing coating damage, this ratio R decreases due to the decrease of coating resistance R_{po} . In Fig. 3 the ratios R_1 and R_2 are plotted as a function of D , where R_1 and R_2 are defined as:

$$R_1 = \log (Z_{100}/Z_{10000}) \quad (13)$$

$$R_2 = \log (Z_1/Z_{100}), \quad (14)$$

with Z_i being the impedance for the frequency f_i . For a perfect coating, for which the impedance is capacitive in the entire measured frequency region, $R_1 = R_2 = 2$. If a contribution from R_{po} appears in the frequency range in which R_1 or R_2 are determined, R_1 and/or R_2 will decrease with decreasing R_{po} . R_1 , which is determined at the higher frequencies, is independent of the coating thickness d and is most sensitive to coating damage for values of D between 0.1 and 10%. R_2 depends slightly on d for thin coatings and is most useful for

D-values smaller than 0.1%. R_2 is therefore more applicable in the very early stages of coating degradation [8].

Since the parameters f_b , f_{min} , Φ_{min} , R_1 and R_2 are determined in the high-frequency region, their measurement time is very short. If calibration curves such as those shown in Fig. 3 can be established, rigorous analysis of the impedance spectrum for the determination of coating performance will not be necessary.

Experimental Approach

Materials

Nine coating systems (Table 1), in the as-received condition and after two years atmospheric exposure in Cape Canaveral, Florida, were used in this study. The coating systems were prepared by the Naval Civil Engineering Laboratory (NCEL) in Port Hueneme, CA according to Steel Structures Painting Council Paint Specification and Navy coating application standards. In most systems a primer is covered by two layers of a topcoat. These coatings were numbered CR# 1-9. For CR #1 and 2 a Zn-chromate alkyd primer was used, for CR #3 and 4 a zinc oxide-iron oxide alkyd primer was used, coatings #5 and 6 had a organic zinc-rich primer, CR#7 and 9 were covered with an epoxy polyamide primer and for CR#8 a latex primer was used. The second and third coating layers consisted of enamel alkyd or enamel silicon alkyd for CR #1-4 and of epoxy polyamide, latex or polyurethane for CR #5-9. CR #8 was an all-latex system (Table 1). This coating was so porous that the impedance spectra were mainly those of the steel. Therefore CR #8 was eliminated from this study.

Measurement of EIS-data

The coated steel samples with an exposed coating area of 20 cm² were exposed in an electrochemical cell with a stainless steel 316 plate (15 cm²) and a saturated calomel electrode (SCE) as counter (CE) and reference electrode (REF), respectively. A platinum wire was coupled capacitatively through a 200 pF capacitor with the reference electrode in order to eliminate phase shift which occurs in the highest frequencies range due to phase shift from the reference electrode. The EIS-data were obtained using a Solartron model 1286 potentiostat and a Solartron model 1250 frequency response analyzer (FRA), which were controlled by an XT computer. Details of

the optimized approach for collecting impedance spectra for polymer coated metals have been given elsewhere [6,8].

In the first part of the EIS experiments for polymer coated steel, an as-received sample for the coating systems CR #1, 2, 5, 6, 8 and 9 was exposed to 0.5 N NaCl (open to air). In the second part, EIS-data were determined for coating systems which had been exposed outdoors at the NCEL Marine Atmospheric Test Site in Cape Canaveral, Florida for more than two years (CR #1 - 7 and 9). The EIS-data were determined at E_{corr} for both types of samples as a function of exposure time. If there was no stable E_{corr} for very protective coating systems such as CR #6 and CR #9, a potential which is equal to E_{corr} for bare steel exposed to the same corrosive environment was applied, i.e. -600 mV vs SCE. The data were analyzed with the COATFIT software program [9] developed at CEEL, which is based on the model in Fig. 1. In addition parameters such as f_b , f_{min} , Φ_{min} , R_1 and R_2 were determined for each exposure time.

Results and Discussion

Effects of Chloride-Containing Media

Fig. 4 shows typical impedance spectra for CR #2 (alkyd primer with enamel silicon alkyd topcoat) after 43, 90 and 162 days exposure to 0.5 N NaCl. The impedance spectra changed with increasing exposure time from the capacitive nature typical for an intact coating to spectra exhibiting two time constant. At intermediate frequencies the spectra are dominated by the pore resistance R_{po} (Fig. 4). The breakpoint frequency f_b and the frequency f_{min} of the minimum phase angle Φ_{min} , which can be observed after about 90 days, shift to higher frequencies, while Φ_{min} decreases.

The results of the fit of the experimental EIS-data to the model in Fig. 1 are shown in Fig. 5 for the coating systems CR #1, 2, 5, 6 and 9. The initial coating capacitance C_c is the lowest for CR #9, which apparently has the thickest coating layer (Fig. 5 a). Coatings CR #1, 2 and 5 seem to have the same thickness. The coating composition and thickness were unknown to the investigators at the time of the test. The increase of C_c in the first days of exposure is due to water uptake by the coating [10]. Degradation of the coating during exposure for one year was indicated for CR #1, 2 and 5. Fig. 5 b shows that the pore resistance R_{po} decreased the most for coating CR

#2. At the end of exposure R_{po} was the lowest for CR #2 followed by CR #1 and #5. A continuous increase of the double layer capacitance C_{dl} (Fig. 5 c) can be considered as evidence that the area at which delamination and/or corrosion occur is increasing. This increase occurred first and was the largest for CR #2, which indicates that this coating system provides the least corrosion protection. It will be noted that C_{dl} reaches values as high as several mF (Fig. 5 c), which cannot be related to the double layer capacitance at the metal/coating interface. As will be discussed below, for CR #2 a large open blister was observed and the experimental values of C_{dl} and R_p (Fig. 5 d) are related primarily to this blister. The decrease of R_p , which suggests an increase of the delaminated area at the metal/coating interface [Eq.2], is the largest for CR #2 followed by CR #1 and 5 (Fig. 5 d). This analysis of EIS-data for the five coating systems shows qualitatively that the coatings CR # 1, 2 and 5 suffer degradation and occurrence of corrosion at the metal/coating interface during exposure to NaCl for one year, while the coatings CR # 6 and 9 remain more or less unchanged.

The coating capacitance C_c increases with increasing water uptake. C_c is quite sensitive to water uptake since the dielectric constant of water is more than 20 times larger than that of coating. Therefore the volume fraction v of electrolyte absorbed by the coating can be determined from the experimental values of C_c [11,12] :

$$v = \log \{C_c(t)/C_c(0)\} / \log 80, \quad (15)$$

where $C_c(t)$ is coating capacitance at a given time t and $C_c(0)$ is the initial coating capacitance. After exposure for 10 days, the volume fraction of water uptake decreased in the order CR# 2 > 1 > 6 > 5 > 9.

Touhsaent and Leidheiser [12] have suggested that the rate of change of coating capacitance, dC_c/dt , measured at early times can be used to predict the lifetime of organic coatings. Table 2 summarizes the specific coating capacitance C_c^0 obtained at $t = 2$ h (Fig. 5 a and Eq. 5), the rates of changes of the coating capacitance dC_c/dt , the rate of water uptake dv/dt in the first 10 days calculated according to Eq. 13, and the percentage of rusted area A_r at 365 days determined according to ASTM D 610 for these coating systems. It can be seen that dv/dt and dC_c/dt determined at the initial times of exposure correlate well with A_r after much longer exposure times (365 days). One exception is CR #5, which shows smaller values of dv/dt and dC_c/dt than CR #6, but a higher A_r . This is probably due to the

thinner coating for CR #5, which provides less protection. The data in Table 2 can be used to rank the different coating systems in terms of properties which are expected to be related to corrosion protection provided by these coatings. For both dv/dt and dC_c/dt CR #2 is ranked first. The same coating system also is the thinnest based on the highest value of C^o_c . The same ranking is obtained for visual observation according to which CR #2 has the largest corroded area A_r , while $A_r = 0$ for CR #6 and 9. This result suggests that there is a correlation between water uptake, coating thickness and rusted area. By summing up the individual rankings as ΣR , one arrives at the final ranking R_T of the five coatings systems in the order of increasing corrosion protection $2 < 1 < 5 < 6 < 9$.

As discussed above, certain parameters, which are related to coating deterioration, can be determined directly from the spectra without a fit to the model in Fig.1. Fig. 6 shows the time dependence of f_b , f_{min} , Φ_{min} and f_b/f_{min} . The breakpoint frequency f_b (Fig. 6 a) shows the same time dependence as R_{po} (Fig. 5 b) with f_b increasing by a factor of about 10^4 for CR #2 and showing smaller increases for CR #1 and 5. Values for f_{min} and Φ_{min} could only be detected for CR # 1,2 and 5 (Fig. 6 b and c). For CR #2 f_{min} increased after about 100 d, for CR #1 f_{min} and Φ_{min} were first detected after 245 d and for CR #5 these parameters could first be recorded after 300 d. These results agree with the finding that CR #2 is the least protective coating followed by CR #1 and CR #5 (Table 2).

An important result concerning the mechanism of coating degradation can be obtained by a comparison of the numerical values of f_{min} (Fig. 6 b) and Φ_{min} (Fig. 6 c). The question is whether changes of these parameters with exposure time are due to change of delamination ratio D with ρ remaining constant as Haruyama et al have suggested [6], due to changes of ρ at constant D or both. To answer this question it is necessary to expand the analysis given elsewhere [5], in which only the dependence of the parameters which can be obtained from EIS-data on coating thickness d , delaminated area A_d and delamination ratio D was considered [6a]. As already mentioned above, changes due to the decrease of the coating resistance ρ have also to be taken into account in the analysis of the degradation of polymer coatings.

Eq. 8-12 show that both R_{po} and f_b depend on the ratio ρ/D . On the other hand, f_b/f_{min} and Φ_{min} depend only on D . The result that Φ_{min} (Fig. 6 c) and f_b/f_{min} (Fig. 6 d) were independent of exposure time for CR #1 and CR #5 after 210 d suggests that the delamination ratio D remained constant. Therefore one can conclude that the observed decrease of R_{po} (Fig. 5 b) and the increase of f_b (Fig. 6 a) for CR #1 and CR #5 are due to a decrease of the coating resistivity ρ . The increase of f_b/f_{min} with time at constant $\tan \Phi_{min}$ for CR #2 after 160 days seems contradictory to what Eq. 11 and 12 predict. However, examination of CR #2 indicated that a large broken blister (8 mm in diameter) filled with corrosion products was formed during that period of time. The direct exposure of the bare steel surface to the corrosive environment is expected to necessitate a change from the model in Fig. 1 to a model which includes a contribution from this large, actively corroding area.

The most likely sequence of events will be illustrated for CR # 2. In the first three months of exposure the coating resistivity ρ decreased and a very small delaminated area A_d developed (Fig. 5 and 6). The large increases of f_b (Fig. 6 b) and the large decrease of R_{po} (Fig. 6 b) are due to the decrease of ρ , while the increase of C_{dl} (Fig. 6 c) is due to the increase of A_d . After this time ρ remained more or less constant and any further changes of the impedance spectra between 100 and 300 d are due to further increases of A_d as indicated by the increase of the ratio f_b/f_{min} (Fig. 6 d).

Inspection of the time dependence of the ratios R_1 and R_2 confirms that coating degradation was the largest for CR #2 followed by CR #1 and #5 (Fig. 7). It will be noted that for CR #1, 2 and 5 R_2 was much less than the value 2 for a perfect coating even at the beginning of the exposure. For CR #5, the initial R_2 - values were only about half of the theoretical value. Apparently, for these alkyd-based coatings some conducting paths were already existing in the as-received coating or were formed immediately after immersion.

Effects of Atmospheric Exposure

The samples which had been exposed to the atmosphere for two years in Florida were also exposed in 0.5 N NaCl. In examining the results of the analysis of the EIS-data for these samples one finds a very large initial increase of C_c for CR #2, which is due to water uptake of the coating (Fig. 8 a). For the same coating without outdoor

exposure a much smaller water uptake was observed (Fig. 5 a). Table 3 provides a summary of the parameters which were used in Table 2 for the previously exposed samples after exposure to 0.5 N NaCl for 55 days. A comparison of the data in Tables 2 and 3 indicates that previous atmospheric exposure increases the rate of water uptake of these coating systems independent of coating thickness except for CR #1 (alkyd/enamel alkyd), which did not show an increased rate of water uptake. The final ranking R_T in terms of increasing corrosion protection results in the sequence CR #2 < 3 < 4 < 1 < 6 < 5 < 7 < 9. According to the results in Tables 2 and 3 the alkyd systems provide less corrosion protection than the coatings with a zinc-rich primer and the coatings with an epoxy polyamide primer and the same or a latex topcoat.

A decrease of R_p (Fig. 8 b) and an increase of f_b (Fig. 8 c) were only observed for CR #2 in the exposure time of 55 d. A comparison of the changes of f_b , f_{min} , $\tan \Phi_{min}$ and f_b/f_{min} for CR #2 in Fig. 9 suggests that both D and ρ changed during testing in NaCl. The continuous decrease of R_{po} suggests that ρ/D decreased continuously with exposure time (Eq. 8), while the decrease with time of Φ_{min} and the increase of f_b/f_{min} , which are independent of ρ (Eq. 11 and 12), indicate that rapid delamination occurred for CR #2 during exposure to 0.5 N NaCl. The observed time dependence of R_1 and R_2 (Fig. 10) confirms that rapid coating degradation occurred for CR #2 with both R_1 and R_2 showing a continuous decrease with time. For CR #5 R_2 showed a continuous decrease with exposure time, while the initial value of R_2 for CR #5 was close to 1. For CR # 6 and 9 R_2 had values which are indicative of undamaged protective coatings. The high values of R_p ($> 10^7 \Omega$) (Fig. 8 b) and the low values of $f_b < 10$ Hz (Fig. 8 c) for the rest of the coating systems suggest that these systems are still protective during this short test period in 0.5 N NaCl despite previous atmospheric exposure.

Conclusions

The usefulness of the EIS technique for studying coating degradation processes has been demonstrated. The rate of water uptake determined in the early stage of exposure from the rate of changes in coating capacitance C_c can be used as an indicator for the long term performance of the coating. EIS is a very sensitive tool for the detection of local defects within the coating due to the formation of

conductive paths characterized by R_{po} . The corrosion processes at the metal/coating interface can be evaluated in the low-frequency range by the polarization resistance R_p and the double layer capacitance C_{dl} .

A theoretical analysis of the impedance of polymer coated steel has been performed. The results of this analysis have been applied to experimental EIS-data for nine different coating systems in the as-received condition and after outdoor exposure. The breakpoint frequency f_b , the frequency f_{min} of the phase angle minimum Φ_{min} and the ratios R_1 and R_2 have been found useful for qualitative determination of coating performance without rigorous analysis of EIS-data. Since these parameters are determined at relative high frequencies, the measurement time is greatly reduced. It is suggested that this approach can be used in the design of a commercial device for field testing of protective coatings.

In considering the use of the breakpoint frequency for the assessment of coating performance, one has to consider that ϵ , ρ and D are likely to change with exposure time. Whether the increase of f_b or the decrease of R_{po} with exposure time are due to changes of ρ , D or the ratio ρ/D can be verified from the time dependence of Φ_{min} or f_b/f_{min} which depend only on the delamination ratio D .

Acknowledgement

This work has been funded by the Naval Civil Engineering Laboratory, Port Hueneme, CA under Contract No. N00014-88-K0034.

References

1. F. Mansfeld, M. W. Kendig, and S. Tsai, Corrosion **38**, 478 (1982).
2. M. W. Kendig, F. Mansfeld and S. Tsai, Corr. Sci. **23**, 317 (1983).
3. F. Mansfeld and M. W. Kendig, ASTM, STP **866**, 122 (1985).
4. F. Mansfeld and C. H. Tsai, Corrosion **47**, 958 (1991).

5. F. Mansfeld, C. H. Tsai and H. Shih, in Proc. Symp. "Advances in Corrosion Protection by Organic Coatings", The Electrochem. Soc., Proc. Vol. 89-13, p. 228 (1989)
6. C.H. Tsai and F. Mansfeld, "Determination of Coating Deterioration with EIS. II. Development of a Method for Field Testing of Protective Coatings", submitted to Corrosion
7. S. Haruyama, M. Asari and T. Tsuru, in Proc. Symp. "Corrosion Protection by Organic Coatings", The Electrochem. Soc., Proc. Vol. 87-2, 197 (1987).
8. C. H. Tsai, PhD thesis, USC, August 1992.
9. F. Mansfeld, C.H. Tsai, and H. Shih, ASTM STP 1154, 186 (1992).
10. F. Mansfeld, M. W. Kendig, and S. Tsai, Corrosion 38, 570 (1982).
11. D. M. Brasher and A. H. Kingsbury, J. Appl. Chem. 4, 62 (1954).
12. R. Touhasaent and H. Leidheiser, Corrosion 28, 435 (1972).

Table 1. Coating systems - components and coating application codes.

Code/Coat	Primer Coat	Second Coat	Top Coat
CR1	Alkyd ^a	Enamel Alkyd ^b	Enamel Alkyd ^b
CR2	Alkyd ^a	Enamel Si-Alkyd ^c	Enamel Si-Alkyd ^c
CR3	Alkyd ^d	Enamel Alkyd ^b	Enamel Alkyd ^b
CR4	Alkyd ^d	Enamel Si-Alkyd ^c	Enamel Si-Alkyd ^c
CR5	Zinc-rich Primer ^e	Epoxy Polyamide ^f	Polyurethane ^g
CR6	Zinc-rich Primer ^e	Epoxy Polyamide ^f	Latex ^h
CR7	Epoxy Polyamide ^f	Epoxy Polyamide ^j	Latex ^h
CR8	Latex ⁱ	Latex ^h	Latex ^h
CR9	Epoxy Polyamide ^f	Epoxy Polyamide ^j	Epoxy Polyamide ^k

a. TT-P-645

d. SSPC-25

g. MIL-C-85285

j. MIL-P-24441

b. TT-E-489

e. SSPC-20, type2

h. MIL-P-28578

k. MIL-P-24441(white)

c. TT-E-490

f. MIL-P-24441(green)

i. MIL-P-28577

Table 2. Rates of Water Uptake and Change of Capacitance in the first 10 days, Specific Coating Capacitance C_o^c and Percentage of rusted area at 365d for as-receive samples.

sample	dv/dt ^a	rank	dC/dt ^b	rank	C_o^c	rusted area ^d	rank
CR1	1.23	2	1.90	2	2.66	0.92	2
CR2	1.46	1	2.49	1	2.80	3.81	1
CR5	0.32	4	0.41	4	2.70	0.02	3
CR6	0.90	3	0.60	3	1.24	0.00	4
CR9	0.13	5	0.036	5	0.62	0.00	4

a. in volume %/day

b. in 10^{-10} F/day

c. in 10^{-9} F (at $t = 2h$)

d. in % (ASTM-D610 rating, 10 = 0%, 9 = 0.03%, 5 = 3%, 2 = 33%)

Table 3. Rates of Water Uptake, Change of Capacitance in the first 10 days, Specific Coating Capacitance C_o^c and Percentage of rusted area at the end of test (55d) for samples after atmospheric exposure.

sample	dv/dt ^a	rank	dC _o /dt ^b	rank	C_o^c	rust area ^d	rank
CR1	0.73	6	1.45	3	3.50	< 0.01 ^e	5
CR2	4.31	1	24.0	1	4.26	3.2	1
CR3	1.71	2	1.5	2	2.60	0.04	2
CR4	0.98	4	1.3	4	2.10	0.035	3
CR5	0.70	7	0.67	6	1.90	0.02	4
CR6	1.62	3	1.2	5	1.20	< 0.01	5
CR7	0.75	5	0.37	7	0.97	0.00	7
CR9	0.67	8	0.034	8	0.55	0.00	7

a. in volume %/day

b. in 10^{-10} F/day

c. in 10^{-9} F (at $t = 2h$)

d. in % (ASTM-D610 rating, 10 = 0%, 9 = 0.03%, 5 = 3%, 2 = 33%)

e. with 10% area covered with small blisters of about 1mm in diameter

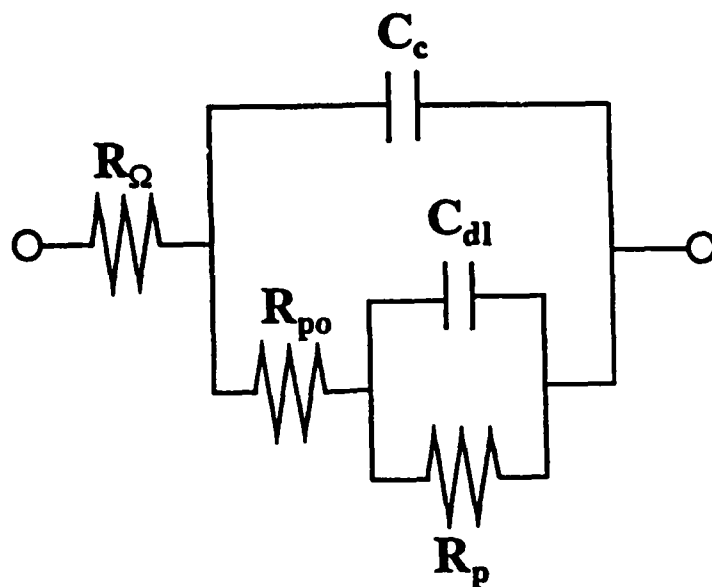


Fig. 1. Equivalent circuit for the impedance behavior of a polymer coated metal.

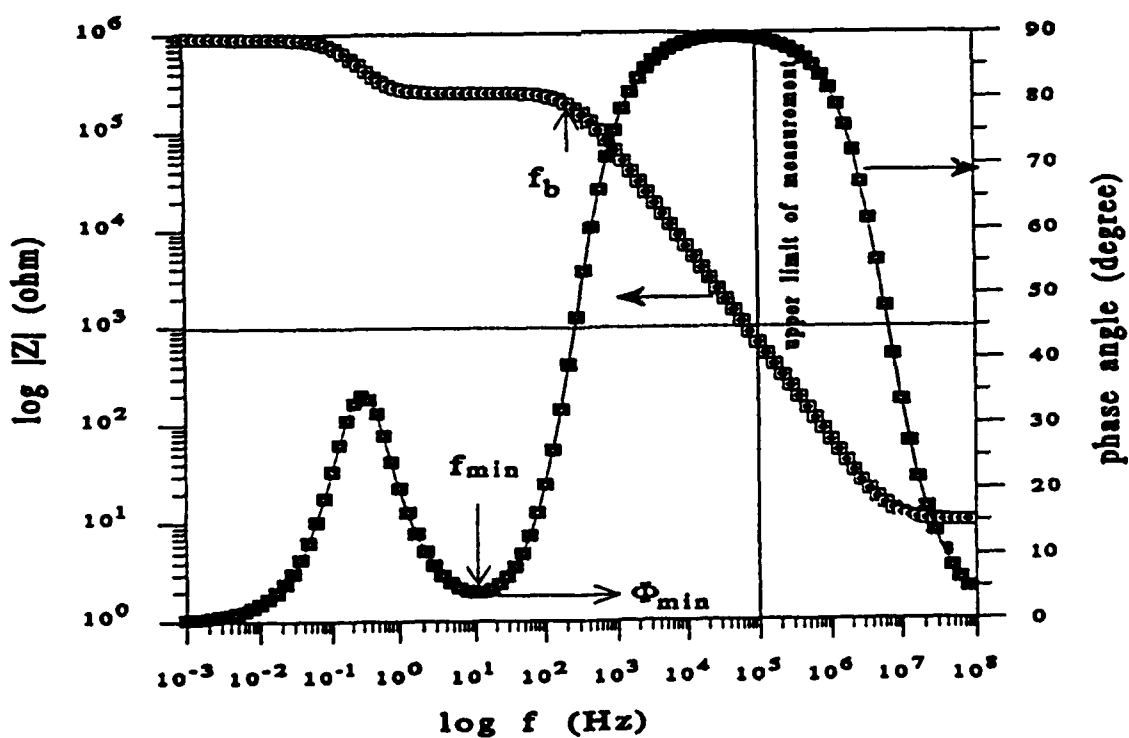


Fig. 2. Bode-plot for degraded coated steel showing the breakpoint frequency f_b , the phase angle minimum Φ_{min} and its frequency f_{min} .

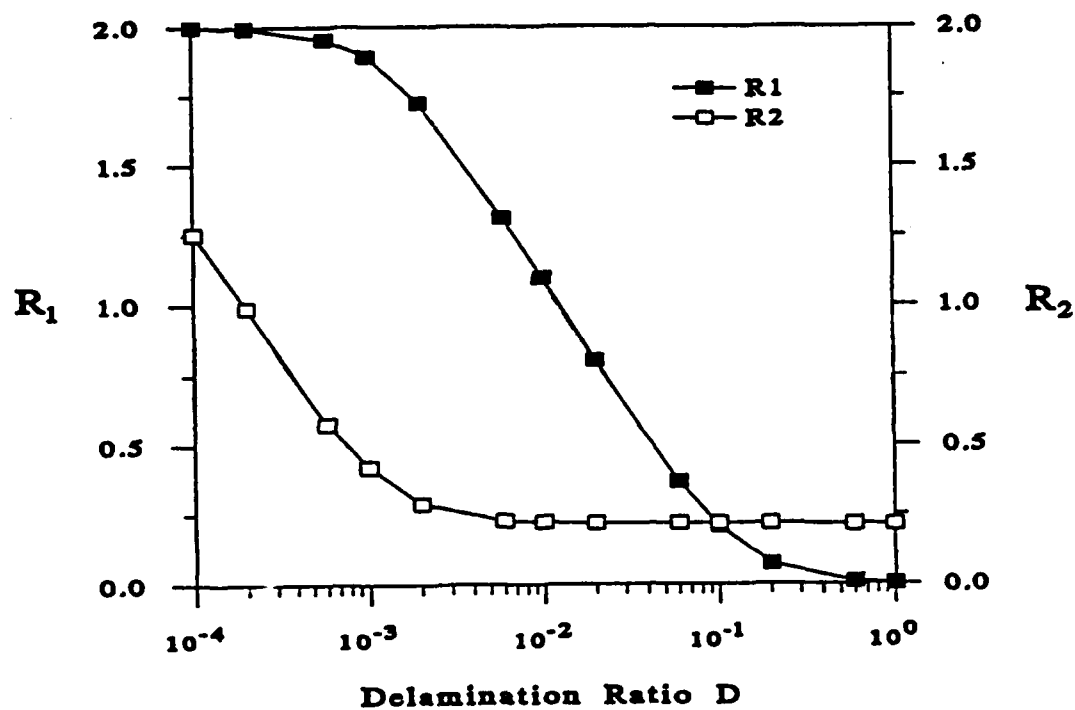


Fig. 3. Theoretical plots of R_1 and R_2 versus delamination ratio D for

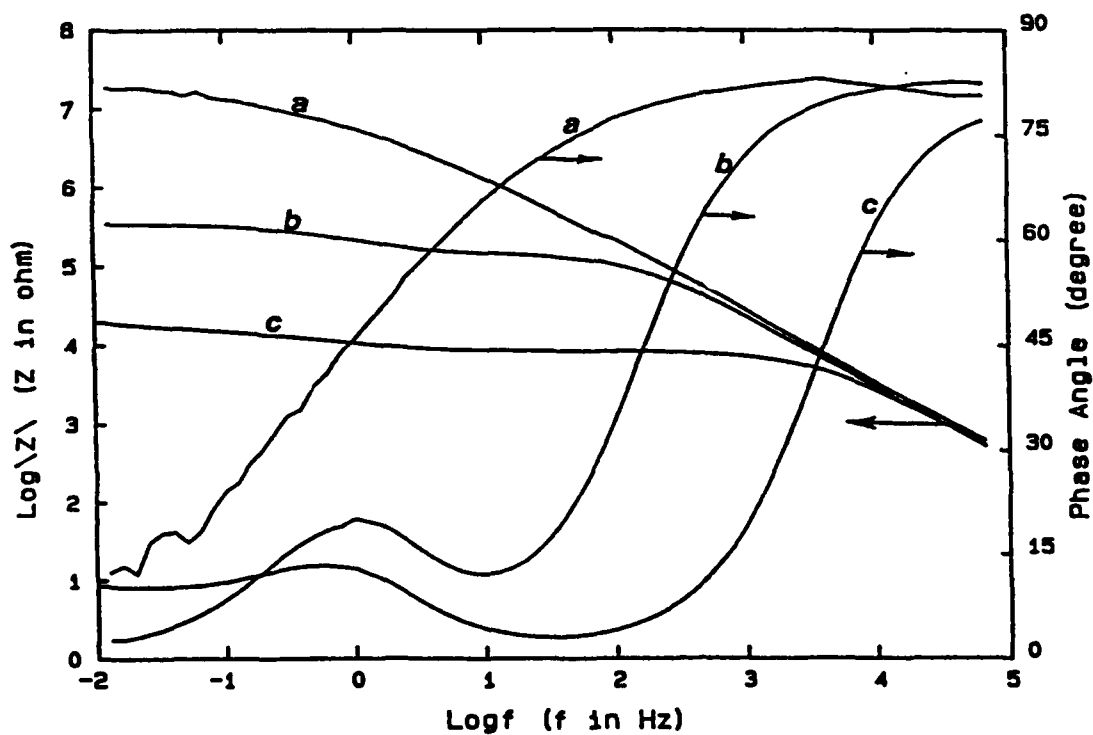


Fig. 4. Impedance spectra for CR #2 after exposure to 0.5 N NaCl for 43 (a), 90 (b) and 162 days (c).

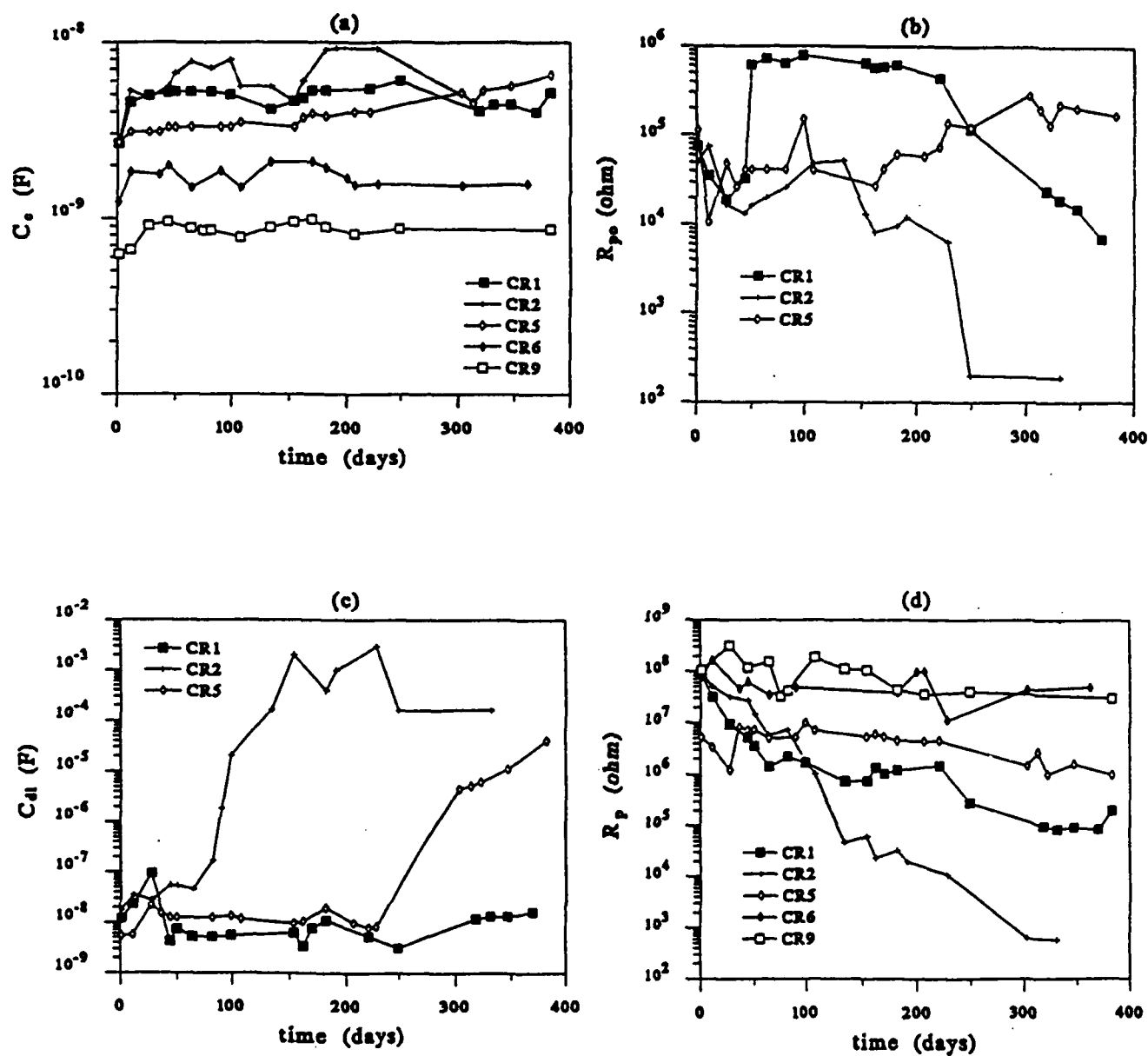


Fig. 5. Analysis of EIS - data for coating CR #1, 2, 5, 6, and 9 as a function of exposure time; (a) C_o , (b) R_{po} , (c) C_{dl} , and (d) R_p .

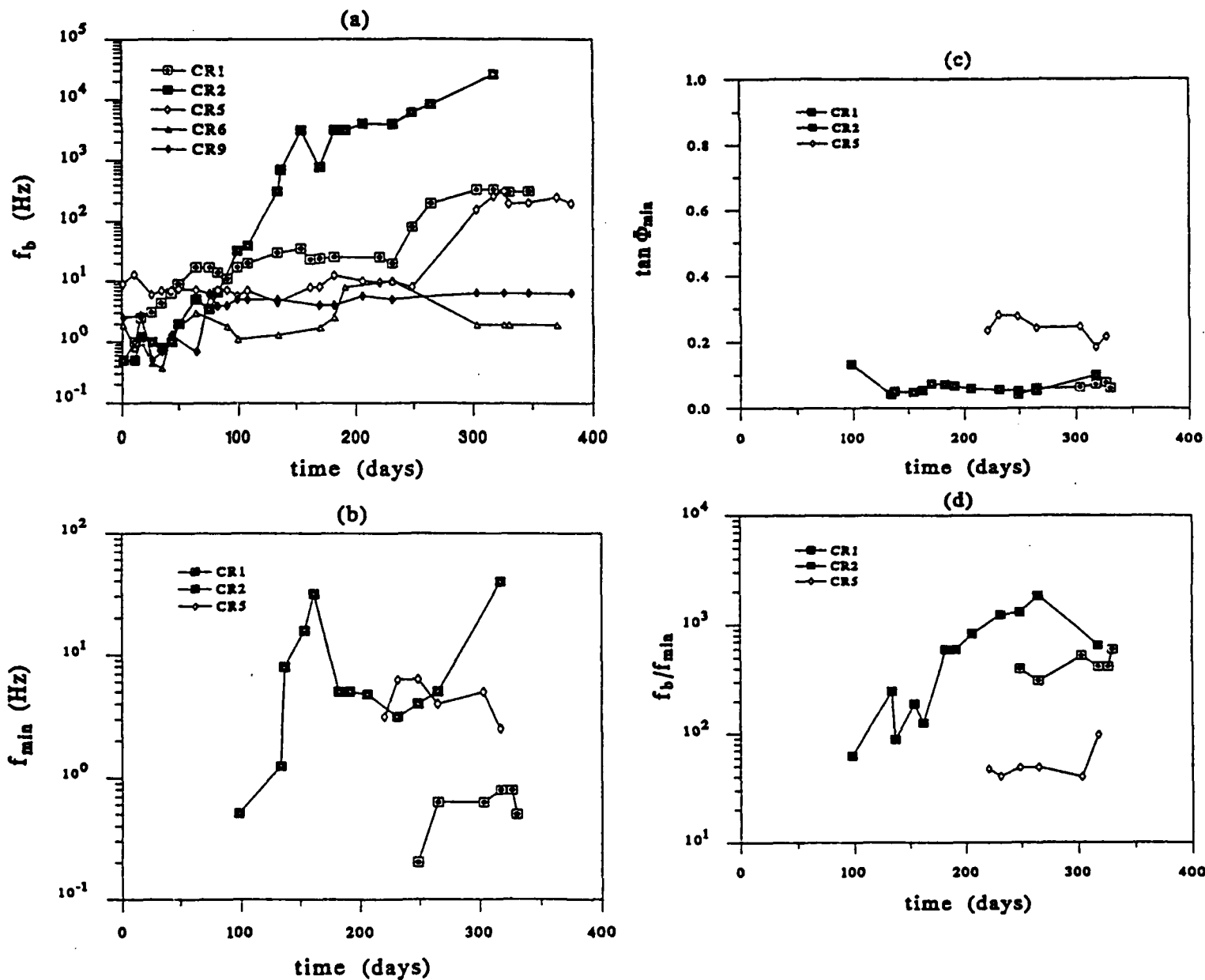


Fig. 6. Time dependence of the parameters (a) f_b , (b) f_{min} , (c) $\tan \Phi_{min}$ and (d) f_b/f_{min} .

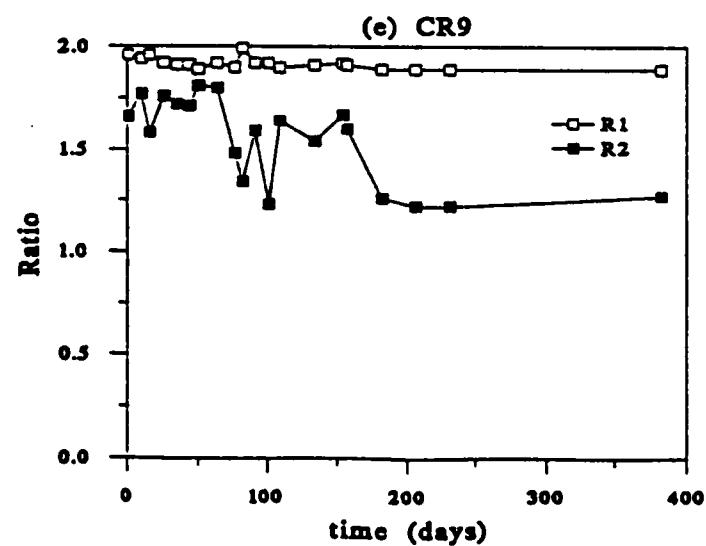
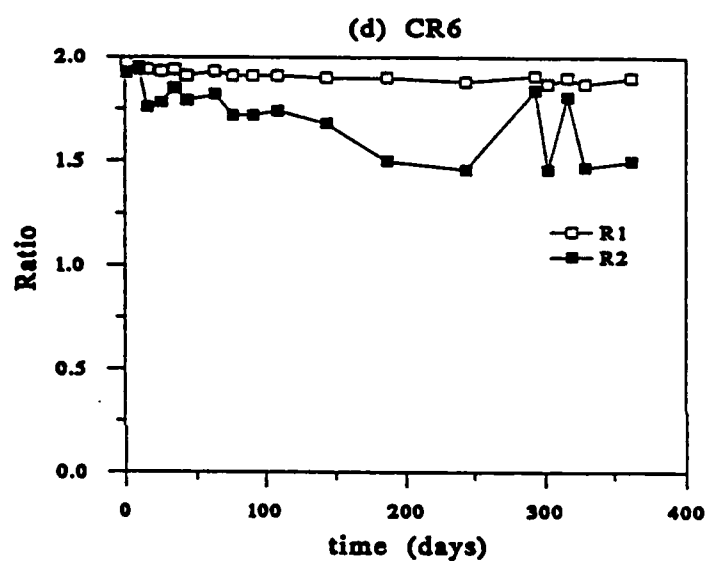
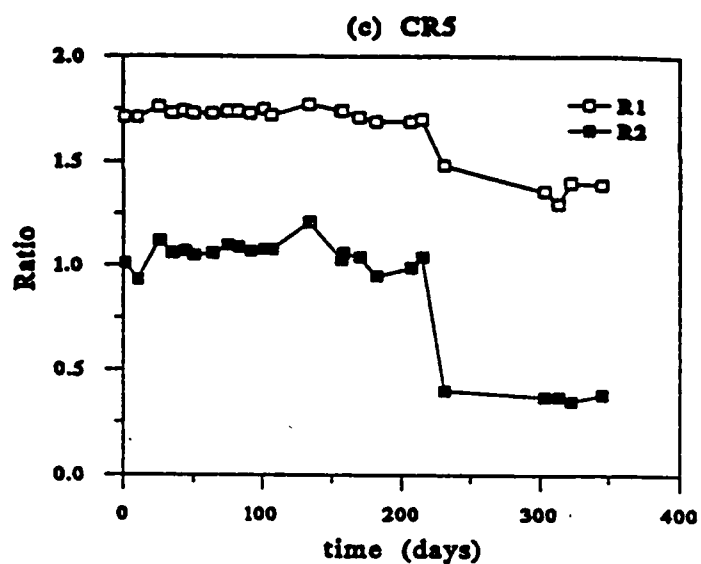
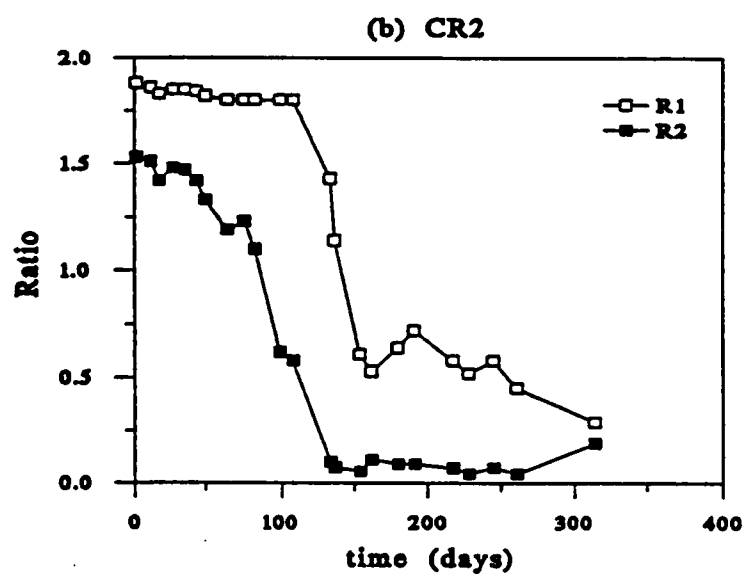
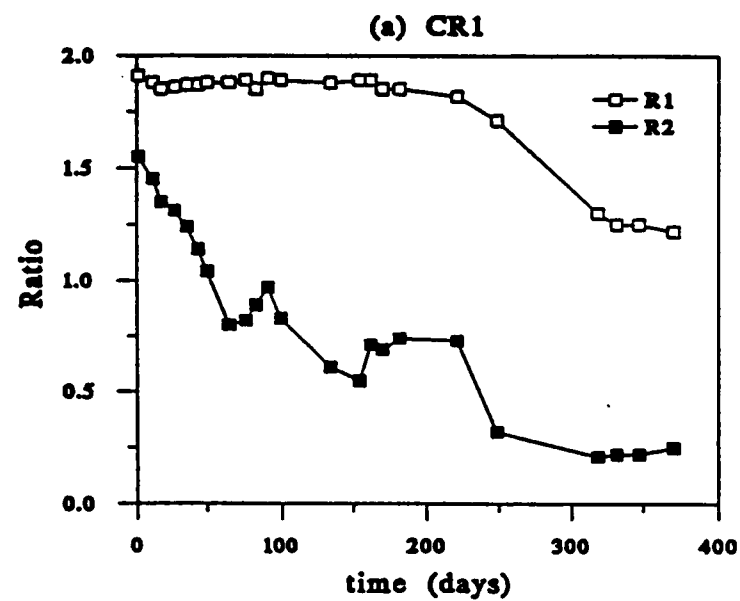


Fig. 7. Time dependence of R1 and R2 for (a) CR#1, (b) CR#2, (c) CR#5, (d) CR#6, and (e) CR#9 during testing in 0.5 N NaCl after atmospheric exposure.

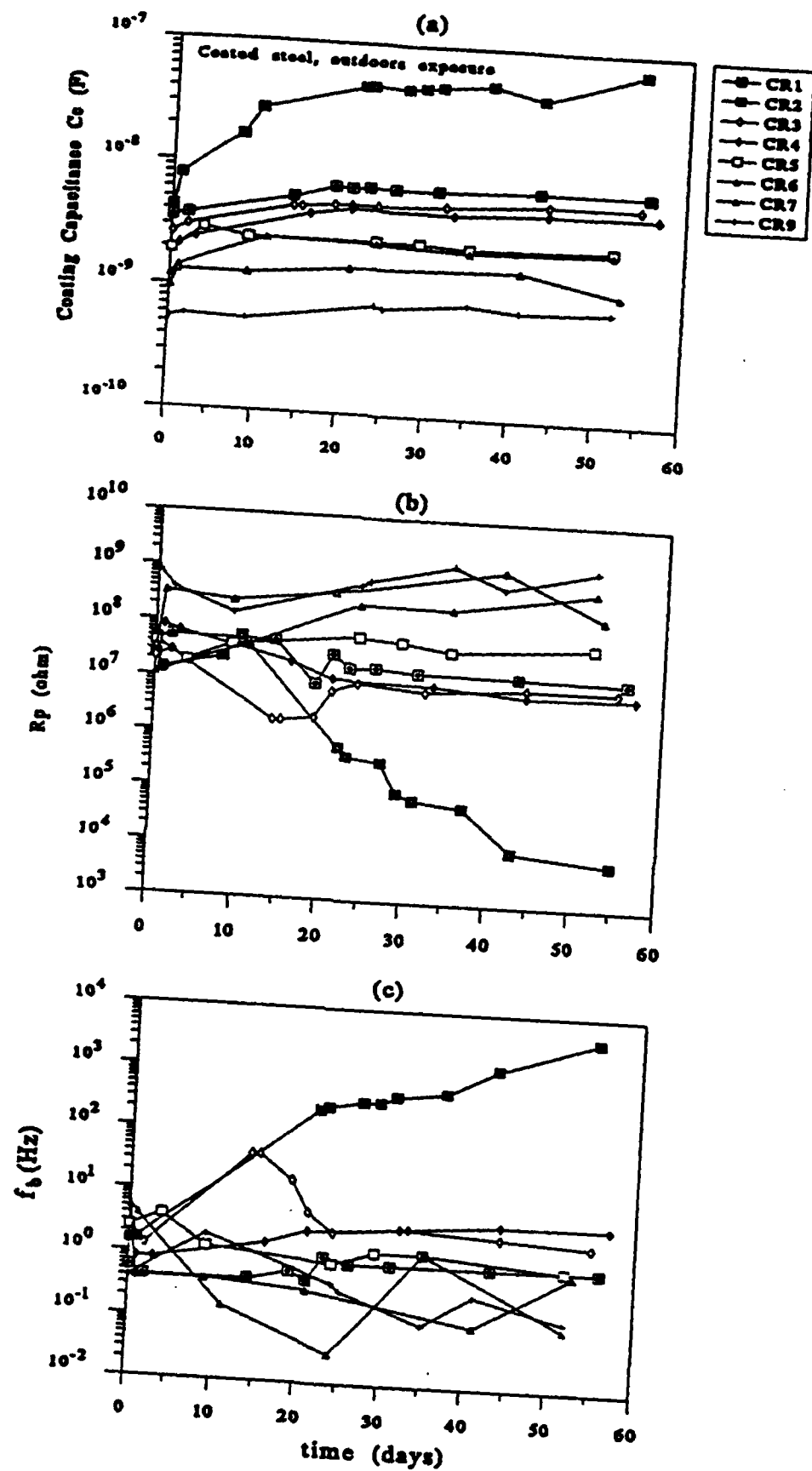


Fig. 8. Time dependence of (a) coating capacitance C_c , (b) polarization resistance R_p and (c) breakpoint frequency f_b during exposure to 0.5 N NaCl for coated steel samples after atmospheric exposure.

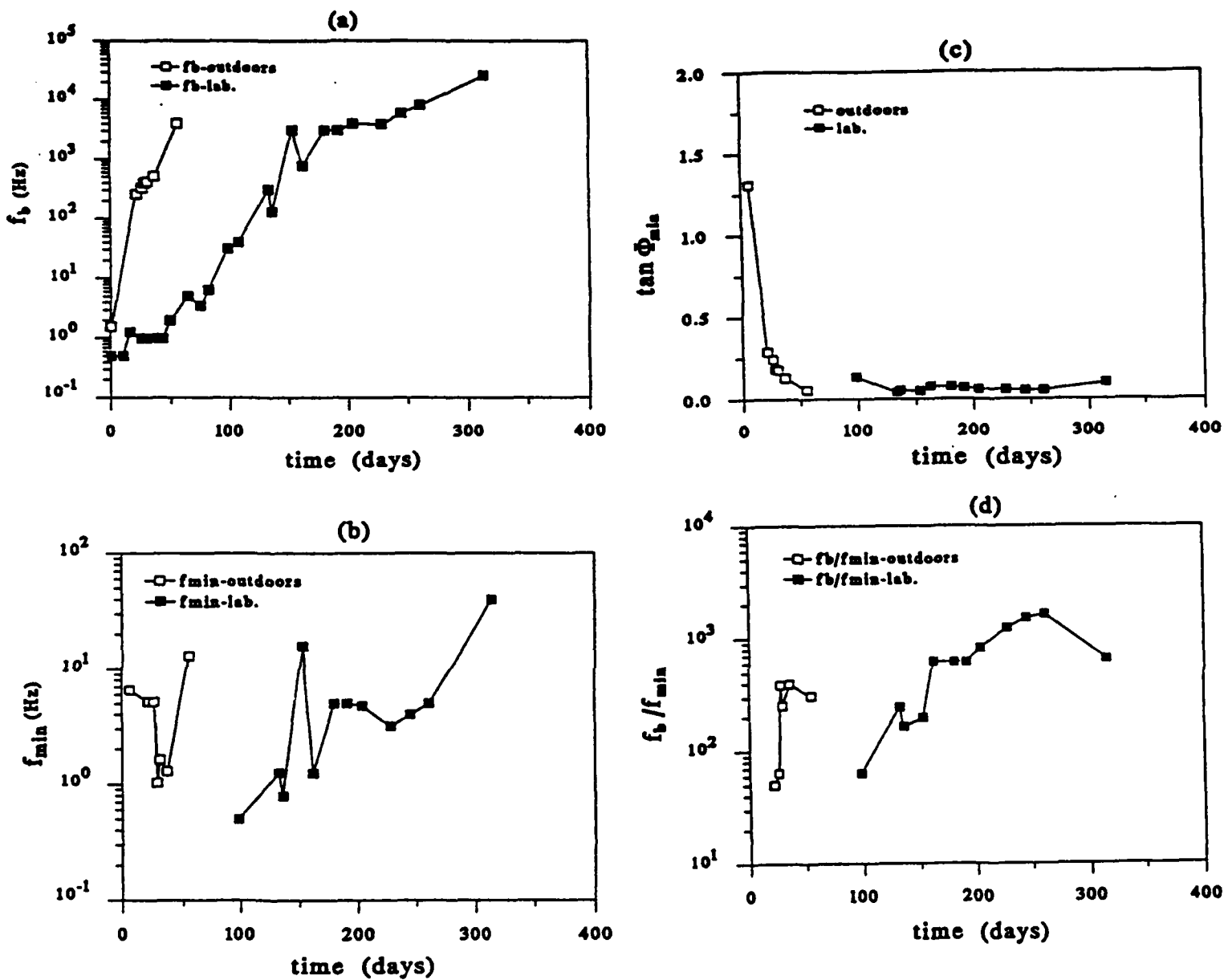


Fig. 9. Time dependence of f_b , f_{min} , $\tan \Phi_{min}$ and f_b/f_{min} for CR #2 after atmospheric exposure.

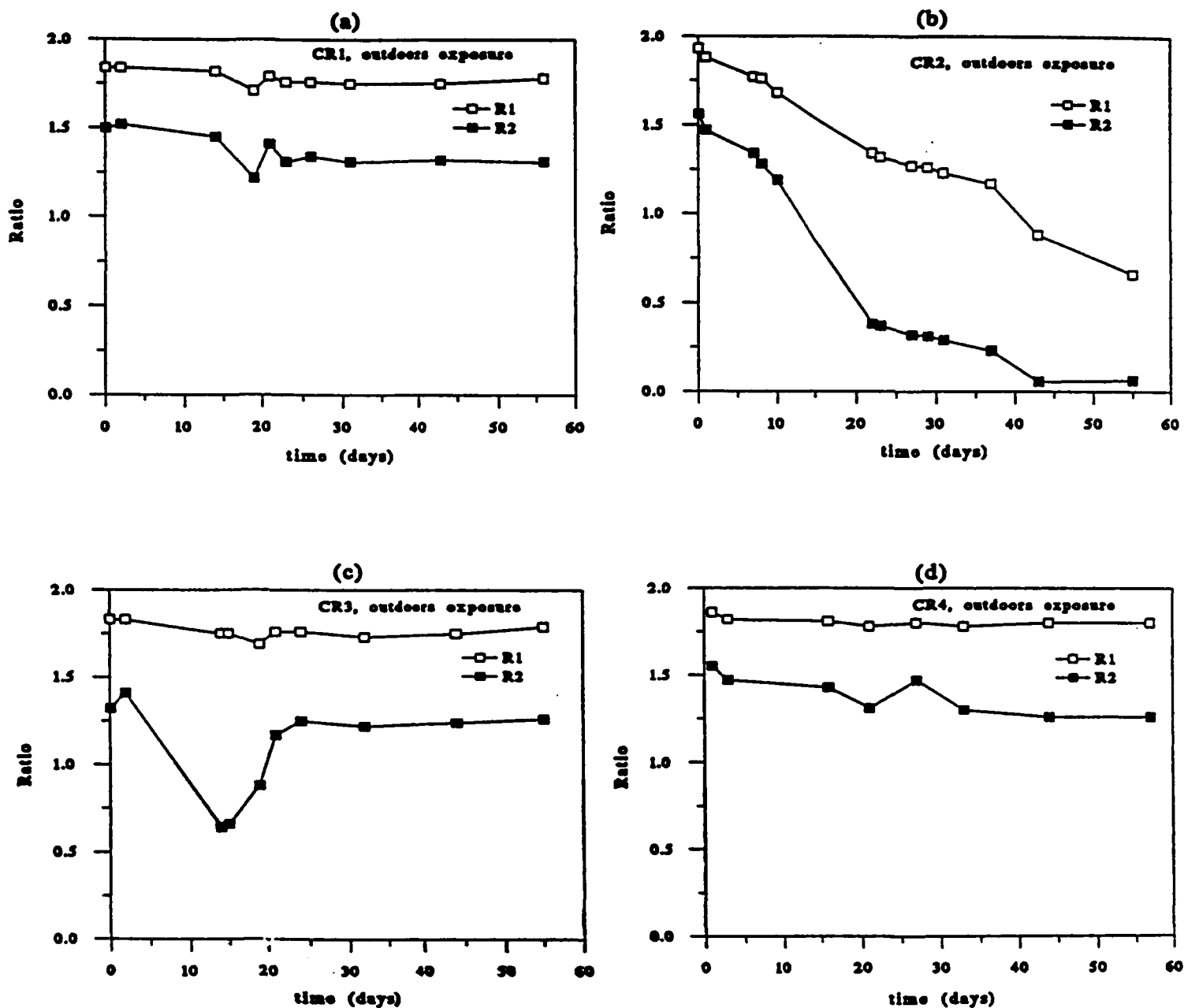
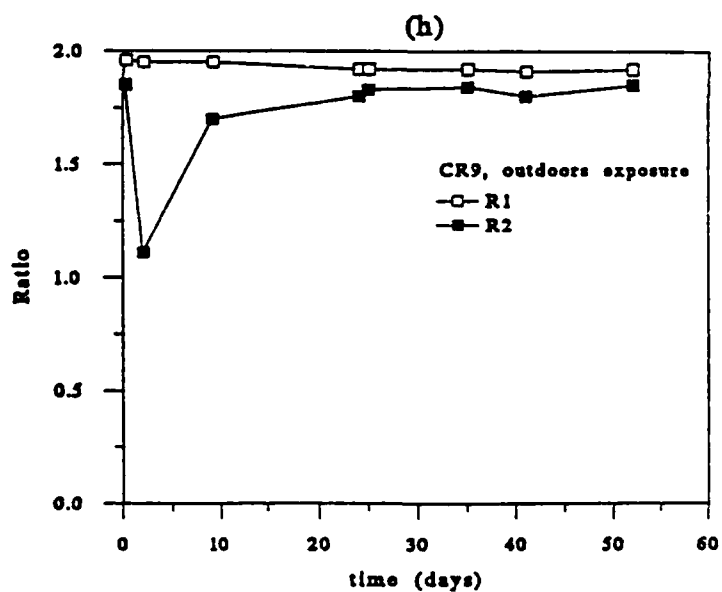
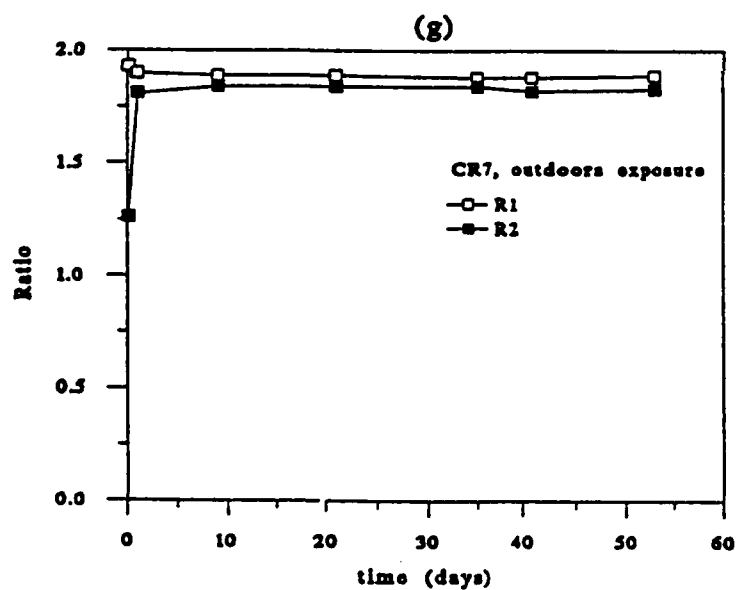
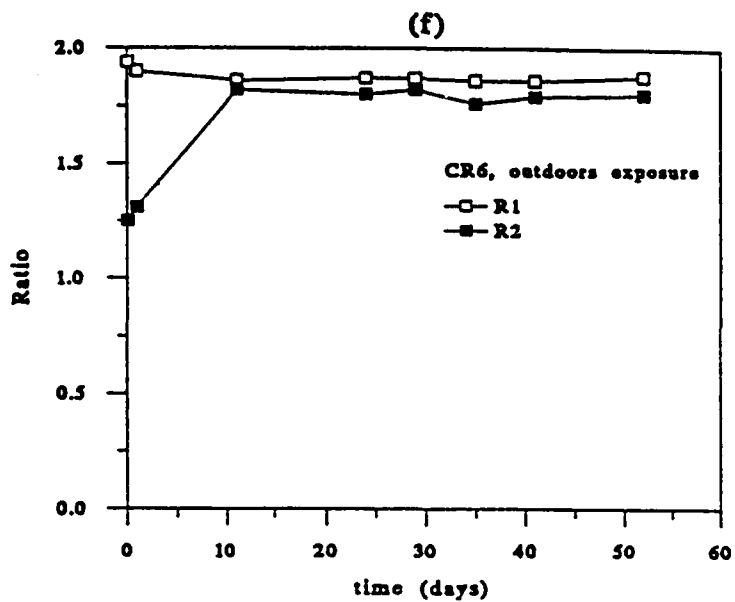
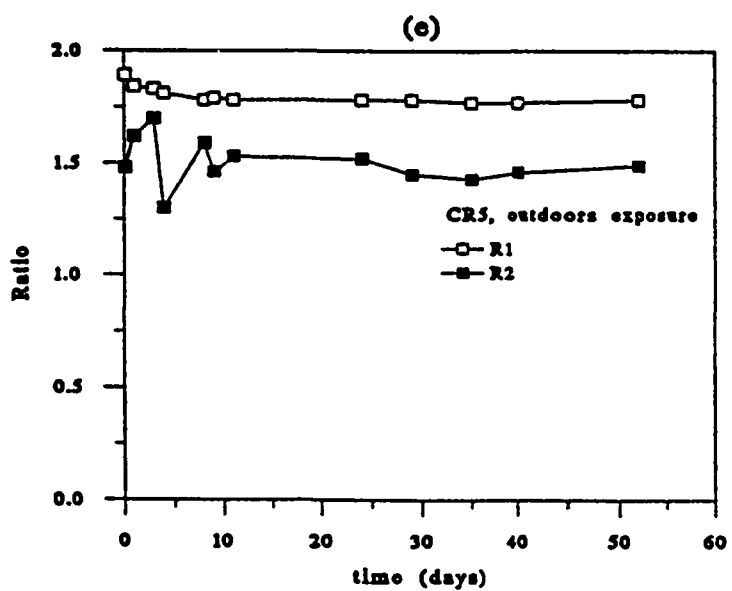


Fig. 10. Time dependence of R_1 and R_2 during exposure to 0.5 N NaCl for coated steel samples after atmospheric exposure.



Long-Term Electrochemical Characterizations of MIL-P-24441 Epoxy Coated Steel Using Electrochemical Impedance Spectroscopy (EIS)

J.N. Murray

Carderock Division, Naval Surface Warfare Center (CDNSWC)
Marine Corrosion Branch, Code 613
Annapolis, MD 21402

H.P. Hack

Carderock Division, Naval Surface Warfare Center (CDNSWC)
Marine Corrosion Branch, Code 613
Annapolis, MD 21402

Abstract

Several types of MIL-P-24441 epoxy coatings on steel substrates have been exposed continuously to substitute ocean water for periods up to three years. The samples have been evaluated visually and electrochemically via Electrochemical Impedance Spectroscopy (EIS). The summarized test data were analyzed and a comparison of the values to those suggested in the literature are presented.

Key terms: Epoxy coatings, EIS, Electrochemical Impedance Spectroscopy, blister rates, sea water immersion

Introduction

The use of EIS as a means for characterizing the status of organic coatings designed for immersion applications has been pursued at CDNSWC starting in about 1985. The program has been multi-purposed and the basic three goals were/are; a) to determine which EIS parameter (if any) could be used to predict rapidly the useful life of a coating system in a sea immersion environment, b) to establish a statistically valid, electrochemical data base characterizing the general behavior of organic coating systems in immersion conditions over long test periods and c) to attempt to refine existing electrical analog models to assist in understanding the epoxy coating degradation mechanisms.

Experimental

The organic coating systems reported herein were either commercially purchased MIL-P-24441, Type I or Type II polyamide/epoxy coatings applied at CDNSWC and the paint shop at the Mare Island Naval Ship Yard or transparent (unfilled) coatings prepared at CDNSWC from the organic components obtained from the qualified suppliers listed within the MIL-P-24441 document. Both sprayed and dipped coated steel substrate samples were initially cured for a minimum of one week in laboratory room ambient conditions and subsequently placed in a molecular sieve desiccated

dry box for a minimum of 30 days to complete the removal of the solvents and absorbed water. For samples intended for total immersion in ASTM-D-1141 substitute ocean water, all sample edges were thickly masked with a commercial epoxy and cured at laboratory ambient conditions to attempt to preclude edge penetration. This approach was later changed to the use of permanently mounted, O-ring seal type cells tested previously (H. Leidheiser, Lehigh University). Both 13.1 cm² active area acrylic cells and glass plumbing joints with a defined area of 31.2 cm² were used.

EIS data were accumulated over a frequency range of 5×10^{-3} to 10^5 Hz. Two distinct EIS systems have been utilized. An input signal of 10 mV was utilized with the initial system whereas a 5 mV value was utilized with the second unit. A higher input signal of 60 mV had been shown acceptable for 150 μ m thick epoxy coatings but a 10 mV input signal had also been indicated to accelerate blistering propagation of thin (50 μ m) alkyd coatings.

The results described in this paper are for coatings left at the native E_{corr} potentials between EIS runs. The sample potentials, normally slightly positive (vs Ag/AgCl reference electrode), were preset at -0.6 V for 60 seconds prior to and during the EIS runs to minimize the phase shift noise observed in the lower frequency ranges. EIS spectra were obtained at 0.1, 0.5, 1, 2.5, 5 and 8 hours exposure, then 1, 2, 3, 4 days, 1, 2, 3, 4, 6, 8, 10 and 13 weeks and approximately monthly thereafter. EIS parameters were calculated using the assumptions of the nested, 2 resistor-capacitor (R-C) network model. This model was apparently¹ first introduced by Mikhailovskii et al in 1965² and has become widely accepted starting in the mid-1970's. The parameters of interest included the coating capacitance (C_{coat}), the maximum impedance at low frequency (Z_{max}), the low and high breakpoint frequencies (f_{lo} , f_{hi}), the coating pore resistance (R_{pore}), the polarization resistance of the corroding substrate (R_p) and the sample corrosion potential.

Results and Discussion

In general, the MIL-P-24441, Type I sprayed coatings which have had only 13 cm² of exposed area via permanently clamped cells have not shown any blistering in the approximately three years of continuous exposure. The two, three and four layer transparent coated samples in 31 cm² test cells have developed small blisters and typical blister development data are summarized in Figure 1. The linear relationship between blister area and exposure time is as expected from diffusional considerations. The blisters tend to be blue-black in color and rarely exceed 0.3 cm diameter. Possibly the filled coatings have accumulated fluid between the coating and the metal surface in the three years exposure but the higher tensile strength of the composite coating probably prevents the physical yielding of the coating surface.

EIS and blister data published previously³ from MIL-P-24441, Type II coatings were from 100 cm² samples completely immersed between

EIS runs. The edges of the Type II samples were coated with an adhesive type epoxy to minimize fluid penetration through the edges. The superior blister resistance performance of the Type I coating samples disclosed in this paper is probably attributed to both the superior formulation and the cell approach which precludes fluid penetration from edges.

The initial coating capacitance increases exponentially with time as water absorption proceeds from the moment of initial exposure to the ASTM-D-1141 electrolyte. Typical data from six sprayed MIL-P-24441, Type I coatings are presented in Figure 2 out to approximately three years continuous exposure. A calculated initial dielectric constant for the transparent epoxy polymer coating of 3.8 (1.0 hour exposure, about 0.01 w/o H₂O) was in reasonable agreement with the published value of 3.62⁴. The equivalent dielectric constant for the filled and pigmented MIL-P-24441 Type I coating was 7.9 matching that calculated for an epoxy matrix with approximately 25 v/o inorganic filler and pigments. Water absorption was shown to saturate at approximately one year with the 100 μ m thick transparent coatings and as seen in Figure 2, at approximately 2.5 years with the 150 μ m thick MIL-P-24441 coatings. Because of the continuing water absorption process, the coating capacitance, calculated from impedance measurements in the 5,000 to 100,000 Hz range can be used for only approximating aged coating thickness calculations. C_{coat} by itself appears to be of limited use for predicting blistering or pore rusting onset times with these epoxy coatings.

Perhaps the most useful EIS parameter found was Z_{max} . The studies confirmed most of the original claims by Bacon et al.⁵ for the use of d-c resistance values to characterize organic coatings except the maximum impedance values for these thicker, superior epoxy coatings are considerably higher, i.e., 10^9 to $10^{11} \Omega \cdot \text{cm}^2$. The majority of the data obtained with commercially available EIS equipment were near or at the measurement limitations of $1.4 \times 10^{10} \Omega$ for the 5 mV input signal. With an earlier cell size of 13.1 cm^2 , the highest measurements were limited to $10^{11} \Omega \cdot \text{cm}^2$. Recent measurements with a breadboarded advanced EIS unit using a 31.2 cm^2 sample area have indicated freshly exposed epoxy coatings have impedances of about $10^{11} \Omega \cdot \text{cm}^2$. Typical long-term exposure data from the sprayed 6 samples are presented in Figure 3 and show a spread of from 1 to $5 \times 10^{10} \Omega \cdot \text{cm}^2$ with time dependent, cyclic wanderings around a mean value. The data reinforce the concept of sub-micron pores through the coating being created and subsequently "repaired" by perhaps substrate corrosion products resealing at least part of the coating pores which allow the environment transport through the coating.

The six spray coated samples and transparent samples which have not developed blisters do not exhibit the high frequency breakpoint suggested by Haruyama⁶ as being proportional to the disbanded coating area. As previously published⁷, there is a second low frequency breakpoint which can also be shown to be proportional to the disbanded area. The f_{10} values for the six MIL-P-24441 samples

have remained approximately stable in a range of 0.5 to 3 Hz for the three years of exposure. Using a coefficient of 1000 Hz/% disbonded area, the frequency range would correspond to 0.0005 to 0.003% disbonded area. This could involve approximately 2000, 1 μ m diameter pores per cm² or a higher multiple of smaller diameter pores, not unrealistic for these high integrity epoxy coatings.

The only epoxy coating systems which have developed R_{pore} characteristics are those of singly applied, transparent layers or very thin double layers applied over high profile grit blasted surfaces. In these two classes two types of blisters developed and, as also noted by Haruyama⁶, the majority being black or blue-black blisters as discussed earlier with additionally a minority being rust colored. For these cases, the 2 R-C network model was found quite appropriate for analysis of the EIS data. The f_{hi} values and the corresponding blister area data from eight single layer transparent epoxy samples are presented in Figure 4. The scatter is excessive for these samples but an approximate coefficient of 50,000 Hz/% blister area can be calculated. Interestingly, this is relatively close to the value determined in the analysis published earlier.

All EIS parameters from the nested R-C model can be used to indicate the amount of disbonded area which for most of these studies is between 0.01 and 0.5%. Several authors have recently published valid objections to the break-point frequency model as not being sufficiently realistic for the case of blister areas being significantly larger than the pore area within the coating blister mantle⁸. The findings here indicate agreement with these general objections but also side with Haruyama's initial claim that f_{hi} remains proportional to the disbonded area, perhaps a common 5% factor applying to these MIL-P-24441 coating systems.

The use of Z_{max} to characterize an existing coating does require approximately 1 hour if the value is to be measured at 5×10^{-3} Hz. Very early work studying the electrochemical characteristics of coated metal surfaces had found a correlation between the potential of the sample and weight gain, visual appearance of blistering and coating resistance with certain coating systems but not with others⁹. Recently, in an attempt to find a faster coating screening measurement, a correlation has been observed between the measured epoxy coating "corrosion" potential and Z_{max} . The impedance of the voltmeter must be significantly higher than 10^{10} Ω to minimize undue polarization of the sample area. Samples with impedances in the range above 10^{10} $\Omega \cdot \text{cm}^2$ have potentials between 0 to +200 mV (vs SCE). Samples with low frequency impedance values in the range of 10^8 to 10^9 $\Omega \cdot \text{cm}^2$ have potentials in the -300 to 0 mV range. Where samples are degraded and rust is evident in the sample area, the potentials are in the -700 to -600 mV range. The attempt to correlate the measured potential and the onset of blistering is currently underway.

Summary

Although there have been some difficulties in establishing valid, low frequency Z_{\max} values, the use of EIS has been instrumental in characterizing the behavior of relatively thick, high performance epoxy coating systems on steel substrates. The EIS data base for three coating systems has been extended up to 3.5 years for laboratory conditions with Z_{\max} apparently providing the superior parameter to define the coating status. Several other EIS parameters have been offered as being superior in that measurement times for Z_{\max} at 10^{-3} Hz are perhaps unnecessarily long. The possible use of the sample "corrosion" potential appears to provide a rapid preliminary assessment for the MIL-P-24441 epoxy coatings which would be used to define the necessity of a more detailed, full EIS spectra for objective decisions as to the acceptability of the coating system.

References

1. Walter, G.W., Corr. Sci., 26 9, (1986): p. 681.
2. Mikhailovskii, Y.N., V.V. Leonov and N.D. Tomashov, Korr. Met. & Spanov, Brit. Lend. Lib. Translat. 202, (1965).
3. Scully, J.R., J. Electrochem. Soc., 136 4 (1989): p. 979.
4. Hdbk. Chem. & Physics, 45th.edit., CRP, Inc. (1964): p. E-35.
5. Bacon, R.C., J.J. Smith and F.M. Rugg, Ind. Eng. Chem., 40 (1948): p. 161.
6. Haruyama, S., M. Asari and T. Tsuru, Proc. Vol. 87-2, Electrochem. Soc. (1987): p. 197.
7. Hack, H.P. and J.R. Scully, J. Electrochem. Soc., 138 1 (1991): p. 33.
8. Kendig, M.W., S. Jeanjaquet and J. Lumsden, ASTM STP 1188 (American Society for Testing and Materials, Philadelphia, PA 19103, 1993) p. 407.
9. Wolstenholme, J., Corr. Sci., 13 (1973): p. 521.

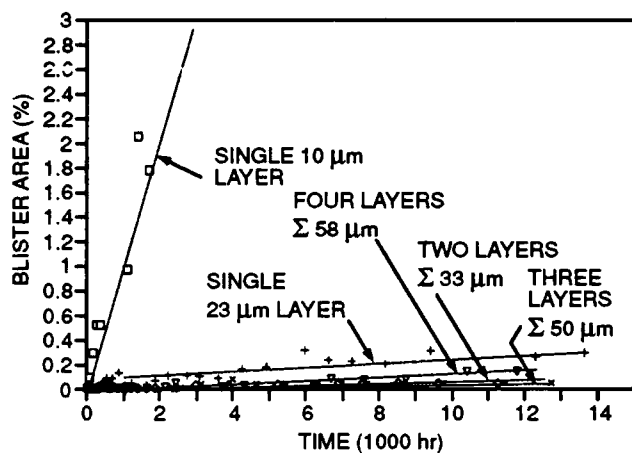


FIG. 1. SUMMARY OF BLISTER DEVELOPMENT DATA, TRANSPARENT EPOXY COATINGS

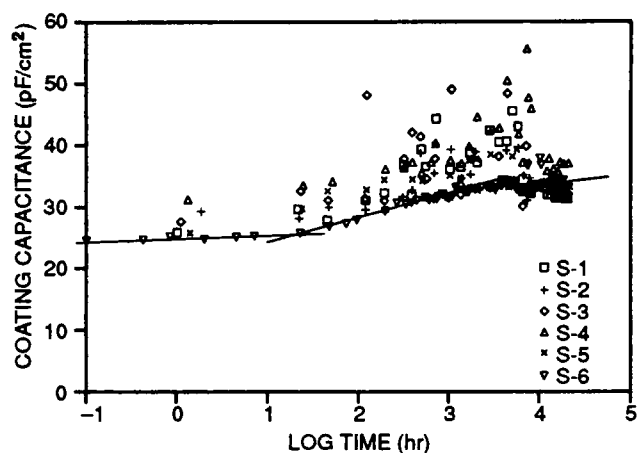


FIG. 2. TYPICAL LONG-TERM COATING CAPACITANCE DATA MIL-P-24441, TYPE I, F-150, F-151, F-154 EPOXY SYSTEM

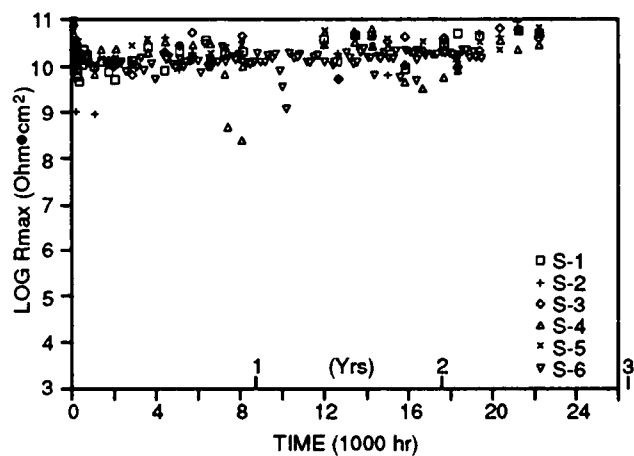


FIG. 3. TYPICAL LONG-TERM MAXIMUM IMPEDANCE DATA MIL-P-24441, TYPE I, F-150, F-151, F-154 EPOXY SYSTEM

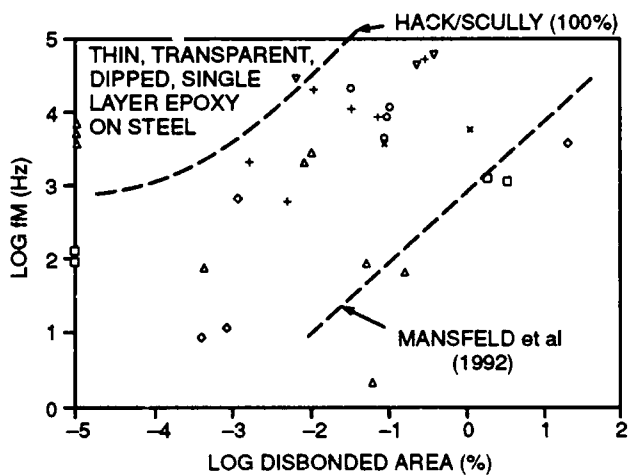


FIG. 4. BLISTER AREA AND BREAKPOINT FREQUENCY (f_b) CORRELATION, TRANSPARENT EPOXY COATINGS

ELECTROCHEMICAL METHODS TO MONITOR DEGRADATION OF ORGANIC AND METALLIC COATINGS

T. C. Simpson
Bethlehem Steel Corporation
Homer Research Laboratories
Bethlehem, PA 18016

Abstract

Electrochemical methods are ideally suited to the monitoring of coating degradation. In recent years, electrochemical techniques have been used in a wide variety of applications to aid in mechanistic and kinetic evaluations of organic and metallic coatings. This manuscript describes three applications of electrochemical methods to the study of the degradation of organic and metallic coatings. These applications include an in-situ electrochemical monitor, an electrochemically monitored etching method, and electrochemical impedance spectroscopy (EIS) for the evaluation of defects in organic coatings and chemical pretreatments on coated steel products. Discussion of these applications will highlight the particular advantage of each in evaluating coating degradation.

Key terms: atmospheric monitoring, electrochemical, EIS, Galvalume, galvanneal, phosphate

I. Introduction

Electrochemical methods have been used by numerous investigators in recent years for the estimation of corrosion performance of organic and metallic coatings. Information obtained through electrochemical monitoring of these systems often provides an invaluable aid by supplementing information collected using other physical, chemical, or mechanical methods. This manuscript reviews recent efforts in three application areas for electrochemical methods. The first area is the use of an electrochemical monitor for in-situ detection of organic coating degradation. The second is the use of electrochemical monitoring in combination with chemical etching of coatings and short term field exposure for the prediction of field service lives. The third is the use of electrochemical impedance spectroscopy (EIS) to detect phosphate coating and organic coating degradation.

II. In-Situ Monitoring of Coating Degradation

One difficult problem in monitoring coating degradation is making measurements of a material in its exposure environment. In most cases the material must be removed from its original exposure environment and/or altered in some way prior to making the measurement. An atmospheric electrochemical monitor (ATMEIS) has been developed that enables completely in-situ monitoring of organic coating degradation during exposure in an atmospheric corrosion chamber.

A.) Design of ATMEIS

The ATMEIS, capable of in-situ detection of organic coating degradation, was developed in 1989 at Johns Hopkins University (1-4). The monitor consists of a painted steel coupon upon

which a gold electrode (covering less than 10% of the front surface of the sample coupon) is electron-beam deposited. The impedance of the substrate/coating system is determined in a two-electrode measurement using the steel substrate and the electron beam-deposited electrode. The monitor can be used, therefore, in the absence of a remote reference or counter electrode. This monitor was developed to assess the degradation of organic coatings in atmospheric exposures simulating acid deposition.

The monitor relies on the assumption that the impedance of the interface of the deposited electrode lying on the surface of the coating is low relative to the impedance of the coating and the steel-coating interface. This assumption has been verified (2). This enables a two-electrode measurement rather than a conventional three-electrode measurement to be completed. The two-electrode approach is valid because placement of the deposited electrode at the surface of the coating enables its entire interface with the coating to be wetted and utilized, resulting in a low interfacial impedance relative to the coating or the steel-coating interface. The primary value of the monitor is that it has the potential of being used for completely in-situ monitoring of atmospheric or vapor phase coating deterioration on a real-time basis and/or on real structures. Such a method is otherwise unavailable.

B.) Testing of ATMEIS

Data collection using the ATMEIS monitor has been verified in immersion exposures to ensure that 1) The EIS data collected with the monitor electrode are nominally identical to those collected using conventional electrodes and 2) The presence of the monitor does not have any adverse effects on the normal degradation of the paint system. The results of these verifications were reported elsewhere (1-3).

The monitor has also been used to collect EIS data during exposure of samples in an atmospheric exposure chamber. Figure 1 shows EIS data collected using the ATMEIS as a function of atmospheric exposure time to 1 ppm sulfur dioxide, 95% RH. The quality of the EIS data, as well as the expected decrease in low frequency impedance with exposure time, demonstrate the feasibility of the monitor for studying and evaluating coating degradation in atmospheric exposures. Figure 2 compares near d-c impedance values as a function of exposure time for ATMEIS specimens during the sulfur dioxide experiment with tensile adhesion strength measurement for a series of conventional specimens (samples that do not contain the ATMEIS monitor, but are otherwise nominally identical) exposed during the same chamber run. Decreases in the near d-c impedance correspond well to changes in the mechanical properties. ATMEIS data are given for two different samples and tensile adhesion values are averages of at least three specimens. Locus of failure in the tensile specimens occurs initially within the paint system, but shifts to the metal/primer interface at later exposure times. Visual examination of the failure surface indicates that this failure is associated with corrosion at the metal/primer interface. Thus, EIS is detecting corrosion at the interface.

III. Prediction of atmospheric corrosion performance

An additional problem that often occurs in monitoring coating degradation is estimation of effects of process/composition changes on long-term corrosion behavior. Coatings with service lives on the order of 20+ years typically require field exposures on the order of years to estimate effects of process and/or composition changes. Exposures of this length are often impractical and would significantly impede product development. For this reason, it is

desirable to use accelerated methods to estimate long-term corrosion behavior. The method we have developed is an electrochemically monitored etching method that enables estimation of long-term corrosion behavior of aluminum/zinc and related alloy coatings on steel. The method has been used in combination with a short-term field exposure.

A.) Description of Electrochemically monitored etch method

The electrochemically monitored etch method involves selective etching of active phases within aluminum/zinc alloy coatings prior to field exposure. The method was first investigated using the aluminum/zinc coating Galvalume. Galvalume is a coating of widespread use in the metal building industry in both the painted and unpainted condition. This coating was originally developed by Bethlehem Steel in the early 1960's (5). Galvalume is a thin (20-25 μ m) metallic alloy coating applied over steel in a continuous hot-dip process. The composition of Galvalume is 55% Al, 1.6% Si, and the balance Zn (5). Galvalume coatings have gained widespread use largely because of their excellent corrosion performance leading to long field service lives (20+ years) (6-8). Initial results using this method on Galvalume were quite encouraging. The method resulted in dissolution of the same active phases as typically occurs during field exposure (9). For this reason, the method was extended to use for the possible screening of new coating compositions.

Galvalume and related aluminum/zinc alloy coatings (of varying compositions) have been tested using this electrochemically monitored etching method (9). The electrochemically monitored etching method consists of continuous electrochemical potential monitoring of flat, unpainted, specimens during an exposure to an aqueous 0.5 M H₂SO₄ solution. During this time chemically active phases of these coatings are selectively removed. As these phases are removed, the electrochemical potential shifts to indicate this removal. Initial evaluations involved immersion of flat specimens in the acid solution until the electrochemical potential reached a specific value. A schematic of a typical electrochemical etching curve for NCT (non-chem treated) Galvalume in 0.5 M H₂SO₄ is shown in Figure 3. Regions of these curves are marked to indicate our prediction of the primary dissolution taking place within that potential region. These predictions are based on electrochemical potential measurements for pure Al, Zn, Mg and for steel in the etching solution. Figure 4 shows an electron microprobe image of a Galvalume coating after 15 and 30 minutes of etching. Note that the interdendritic zinc rich regions are selectively leached during the etching process. The etching process is reproducible and is uniform over the entire sample surface. Figure 5 compares a Galvalume coating that was etched using the electrochemically monitored process to one that was exposed for 2.5 years at an industrial site. In both cases the coatings appear similar. This indicates that the same phases will be reactive during atmospheric exposure and during the etching process. Thus, by monitoring potential one can estimate the extent to which active phases from the coating have been removed.

This method has also been applied to other coatings (Al/Zn/Mg/Si alloys) containing interdendritic microstructures and to Galvalume containing a chemical pretreatment. Etching curves for Al/Zn/Mg/Si alloys are similar to those for Galvalume except that they contain an initial region of Mg + Zn dissolution at a potential of $\sim -1.2 \rightarrow -1.3$ V vs SCE. Etching of samples containing a chemical pretreatment also cover the same potential region as those for NCT Galvalume, but the time required for etching is significantly extended. Metallographic analyses of samples containing a chemical pretreatment have confirmed that the same etching process occurs for these samples. We feel that this method is most appropriate for use on samples that do not contain a chemical pretreatment or on samples that have had the

pretreatment removed.

B.) Effects of Methods on Formed Samples

Since many applications of Galvalume and other Al/Zn alloy coatings use these materials in various formed configurations, it was important to determine the applicability of this method to the monitoring of formed samples. Forming-induced coating fracture may alter the behavior observed during etching. Figure 6 compares an etching curve for a flat Galvalume specimen to one for a Galvalume specimen containing a v-bend. Note that the relevant potentials at each stage of the etching process are analogous, but that the time required for the etching to be completed is shifted. This most likely is due to the coating fracture that has occurred during forming. Similar results were obtained on formed samples of the other alloy coatings. Based on these data we felt confident that similar phase dissolution would occur on unpainted formed and flat samples and that the method was appropriate for use on formed materials.

C.) Results of Field Exposures

The greatest potential of the electrochemically monitored etch process is its applicability for the screening of new coating compositions and/or process modifications. Samples pre-exposed using the etch method and subsequently exposed outdoors or in a laboratory test should be able to be used to make coating life predictions. In order to verify this hypothesis a field exposure of materials with known performance histories was initiated. This field exposure of pre-etched Galvalume and of the other aluminum/zinc alloy coatings began on July 30, 1991, at the Homer Research Laboratories (HRL) industrial site in Bethlehem, PA. Hot-dip galvanized (G90) materials were included in this exposure for site calibration. All samples received a v-bend prior to any etching and were prepared in duplicate.

Three pre-exposure conditions were common to all of the materials (except the G90 which did not receive any etching); no exposure, exposure for 4 minutes, and exposure for 8 minutes to the etching solution prior to field exposure. In addition, some materials were exposed for other periods of time based on previous characterizations of their etching curves. These pre-etch times varied from sample to sample, but were chosen to correspond to a fractional percent of the total time necessary to deplete the active phases from the coatings. Direct comparison of material performance should be possible within each type of pre-exposure condition and for averages over all pre-etch conditions.

Sample ratings were completed weekly or bi-weekly during the early phase of exposure, and monthly or bi-monthly after the changes from rating to rating began to decrease. The rating scheme used to evaluate extent of bend rusting was one developed and used in recent years in our laboratory (10 = no red rusting or staining; 4 = severe red rusting) (9).

In order to evaluate the electrochemically monitored etching method for coating life prediction it was necessary to estimate the field performance of each of the coatings investigated. Nominally identical samples of several of the materials included in our field exposure have been on exposure at the HRL site since March 24, 1988. Ratings of rusting on t-bends, and dimples of two different sizes were collected for these materials on November 5, 1991.

Comparing the rating values and the ranking of materials using the electrochemically monitored etching prior to exposure followed by several weeks of field exposure to field data

for nearly four years exposure, we see good agreement between the two methods. Figure 7 is a bar graph comparing the values of bend rust ratings after 4, 14, 26, and 67 weeks of field exposure (pre-etched samples) to the field ratings after 3 years, 8 months of field exposure of nominally identical materials that were not etched. Average v-bend ratings over all the pre-etched samples are compared to average field ratings (over all deformation types). Note that both the rankings and the relative magnitude of the ratings are in good agreement for these exposure types at exposure times as early as 14-26 weeks. Although the agreement in rating magnitude was perhaps a bit fortuitous, agreement in the rankings was the target for validation of the method. These data provide significant support that the electrochemically monitored pre-etching method is an appropriate method for rapid prediction of field performance of these coated sheet products. Further detail regarding the field exposure and the electrochemically monitored etching method is reported elsewhere (9).

IV. Detection of coating defects using EIS

It is also important to identify defects in coatings applied to metallic substrates. These defects are sometimes quite pronounced, visible to the eye, but may only be observable on a microscopic level. Electrochemical impedance spectroscopy (EIS) is well suited to qualitative and even semi-quantitative estimation of defects in coatings. This study reports the use of EIS for the estimation of phosphate porosity on coated steel substrates. In addition, EIS has been applied to evaluate organic coating degradation, after forming operations, on coated steel substrates. EIS data, in both cases, are consistent with chemical analyses and/or microscopy of these samples.

A.) Phosphate porosity

The phosphate/primer interface has been identified as the site of attack in several corrosion studies. It is expected that all aspects of the pretreatment process including oiling, cleaning, and phosphating affect corrosion performance. The extent of the effects is likely related to substrate type. Galvanneal is a zinc-iron alloy coating prepared by the hot-dip process. The coating is applied to the steel by immersion of a cleaned substrate in a molten zinc bath. Just after leaving the molten zinc bath the material passes through an annealing furnace, alloying of the zinc and steel occurs, and the final product is a Zn/Fe coating containing approximately 8-12% Fe. Galvanneal coatings are different from most other hot-dip coatings in that they consist of a range of compositions (and contain a range of surface phases or morphologies) rather than a single composition. This could make them particularly susceptible to variations in the pretreatment process. Previous reports examined the relationship of galvanneal surface morphology to phosphatability and resulting corrosion performance (10). These studies indicated that galvanneal surface morphology affects phosphate coating weight and crystal refinement. GM SCAB (GM 9511P, cyclic humidity, salt exposure test) testing identified galvanneal coating weight and Fe% in the galvanneal coating as the most important variables controlling painted corrosion performance. Phosphate coating weight/quality also affected galvanneal corrosion behavior.

One key variable in evaluation of phosphate quality is the stability of the phosphate coating in an alkaline environment. During the corrosion process, phosphate coatings will be exposed to a very alkaline environment. Evaluation of the stability of phosphate coatings in alkaline environments is important in understanding the site and mechanism of corrosion failure. EIS is ideally suited to evaluation of changes in the phosphate coating coverage/stability. The alkaline stability of phosphates on galvanneal has recently been evaluated in our laboratory

using EIS (10). Samples of known phosphate coating weights (phosphated with P+A Bonderite 952) were exposed for short periods of time to 0.1M NaOH and coating weight was determined after exposure. Figure 8 shows a plot of the % of the phosphate coating removed after immersion in a NaOH solution vs the original coating weight. An approximately linear relationship was observed. This indicates that samples containing higher phosphate coating weights initially are likely to retain their phosphate coatings longer when subjected to an alkaline environment.

Electrochemical impedance spectroscopy (EIS) data were collected (in 0.1M Na₂SO₄) before and after exposure to 0.1M NaOH. Figure 9 is a plot of $R_{ct} + R_{pore}$ values extracted from EIS data vs final PO₄ coating weights. A decrease in the ($R_{ct} + R_{pore}$) magnitude (after exposure to the alkaline environment) occurs which parallels the decreases in initial phosphate coating weight. This provides further support for the trend observed in Figure 8. Samples containing higher initial phosphate coating weights are predicted to have greater alkaline stability. Thus phosphate coating weight can be used as an indicator of alkaline stability. In addition, since an approximately linear relationship exists between $R_{ct} + R_{pore}$ values and phosphate coating weight, EIS data can be used as an alternate means of evaluating phosphate coating weight. This could be an important technique in such evaluations since EIS measurements can often be non-destructive and conventional gravimetric phosphate coating weight analyses are always destructive.

B.) Organic coating degradation

Defects/deterioration of phosphate coatings are typically not visible. Other paint defects can be visible. One such defect is termed "paint crazing". This phenomenon occurs typically when an as-painted surface undergoes a forming operation of sufficient severity to cause the paint and/or the underlying metallic coating to crack. The role of crazed paint surfaces in accelerating corrosion attack is not well defined. It is expected that crazed paint/substrates may lead to accelerated attack in some exposure environments. It is important to have a method to probe the extent of such crazing to make predictions regarding the impact on corrosion behavior. EIS is also an appropriate technique to complete this type of testing. Initial evaluation of EIS for the detection of paint crazing was reported elsewhere (9).

To evaluate the sensitivity of EIS to detection of minor differences in crazing behavior a series of samples were prepared with varying extents of crazing. A single Galvalume substrate was used for these studies and all samples were painted with the same paint system (an epoxy-SMP). EIS data were collected in 0.1 M Na₂SO₄ for specimens that received impact dimples covering a range of deformation severities. Each material was given a paint crazing rating prior to testing (10 = no crazing, 0 = severe crazing). Figure 10 is a plot of the EIS data over the range of deformations. Note the drop in near DC impedance as a function of deformation severity. Figure 11 is a plot of the crazing rating of each of these coatings vs the log of the near DC impedance value. Note the wide range of EIS values for these samples. EIS appears to be quite sensitive to distinctions in crazing severity.

The EIS method was also applied to samples that were commercially prepared, containing a range of crazing severities. The Galvalume used in this study was produced by three different steel suppliers. These materials were roll formed panels designed for use as metal building panels. All materials were painted with the same paint system. Crazing ratings were assigned to each material prior to test. Materials were tested in a specially designed cell that exposed only the bend area to the electrolyte. EIS data were collected in 0.1 M Na₂SO₄ prior

to and after exposure to an aggressive chemical environment. A plot of the initial EIS is shown in Figure 12. Note that the near DC impedance varies over several orders of magnitude for a fairly small difference in crazing rating. These data indicate that EIS is very sensitive to distinctions in paint crazing ratings.

Thus, EIS could provide valuable insight into paint crazing severity and is applicable as a tool in evaluation of this phenomenon. Use of EIS in combination with other techniques should significantly enhance our ability to understand and make coating life predictions.

V. Conclusions

This manuscript has highlighted three primary applications of electrochemical techniques for the monitoring of metallic and organic coating degradation. The first was the development of an electrochemical monitor that utilized EIS for the detection of organic coating degradation. The monitor was used to assess maintenance paint degradation in a sulfur dioxide/high humidity environment. The second was the development of an electrochemically monitored etching method that enables rapid prediction of corrosion behavior of zinc/aluminum alloy coatings. The third was EIS for the detection of defects in phosphate and organic coatings. In each case, in-situ monitoring, accelerated testing of coating compositions, and defect evaluation, the use of electrochemical methods provided a complement to other methods of analyses. It is expected that future studies could build on these application areas to use electrochemical methods as powerful tools in assessing coating properties and corrosion behavior.

VI. Acknowledgements

The author would like to acknowledge J. D. Hoffman for his valuable input throughout these studies and for his technical help in performing most of the analyses reported in this manuscript. In addition, I would like to acknowledge my co-workers at the Johns Hopkins University and Martin Marietta Laboratories for their efforts in the development of the ATMEIS; H. E. Townsend, W. C. Unangst, and H. E. G. Rommal for their technical input throughout several of these studies; T. A. Suchy and T. W. Wunderler for preparation of samples used in the atmospheric exposures; and L. L. Hahn, L. Salvage and R. C. Nester for SEM, electron-microprobe, and metallographic analyses required for these studies. Development of the ATMEIS was funded under the NAPAP program by the US EPA under cooperative agreements CR 814347-01-0 and CR 814347-01-1.

VII. References

- 1) T. C. Simpson, H. Hampel, G. D. Davis, C. O. Arah, T. L. Fritz, P. J. Moran, B. A. Shaw, and K. I. Zankel, "Evaluation of the Effects of Acidic Deposition on Coated Steel Substrates", Progress in Organic Coatings, 20, (1992): p. 199.
- 2) T. C. Simpson, P.J. Moran, H. Hampel, G.D. Davis, B.A. Shaw, C.O. Arah, T.L. Fritz, and K.L. Zankel, "Electrochemical Impedance Measurements for Evaluating and Predicting the Performance of Organic Coatings for Atmospheric Exposure", in ASTM STP 1000, Corrosion Testing and Evaluation: Silver Anniversary Volume, American Society for Testing and Materials, Philadelphia, 397 (1990).
- 3) T. Comeau Simpson, P.J. Moran, H. Hampel, G.D. Davis, B.A. Shaw, C.O. Arah, T.L. Fritz, and K.L. Zankel, "Electrochemical Monitoring of Organic Coating Degradation During Atmospheric of Vapor Phase Exposure", Corrosion, 46 (4), (1990): p. 331.
- 4) T. Comeau Simpson, P.J. Moran, W.C. Moshier, G.D. Davis, B.A. Shaw, C.O. Arah and K.L. Zankel, "An Electrochemical Monitor for the Detection of Coating Degradation in Atmosphere", J. Electrochem. Soc., 136, (9), (1989): p 2761.
- 5) J. C. Zoccola, H. E. Townsend, A. R. Borzillo, and J. B. Horton, Atmospheric Factors Affecting the Corrosion of Engineering Materials, ed. S. K. Coburn, STP 646, (Philadelphia, PA: ASTM, 1979), p 165.
- 6) H. E. Townsend and J. C. Zoccola, Materials Performance, 18, (10), (1979): p 54.
- 7) H. E. Townsend and A. R. Borzillo, Materials Performance, 26, (7), (1987): p 37.
- 8) H. E. Townsend, A. R. Borzillo, W. D. Barker, "Performance of Al-Zn alloy coated sheet after twenty-two years of atmospheric corrosion testing", in Proceedings of the 2nd International Conference on Zinc Coated Steel Sheet, Rome, June 9-10, (1988); H. E. Townsend, Metalloberflache, 43 (1989): p 7.
- 9) T. C. Simpson, "An Accelerated Corrosion Test Method For Galvalume and Other Aluminum/Zinc Alloy Coatings", CORROSION, IN PRESS.
- 10) T. C. Simpson, J. D. Hoffman, and W. C. Unangst, "Phosphatability and Painted Corrosion Performance of Galvanneal Coated Sheet" SAE Technical Paper Series from the 5th Automotive Corrosion and Prevention Conference and Exposition, October 21-23, 1991; SAE 1991 Transactions, Section 5, Vol 100, Journal of Materials and Manufacturing, 1318.

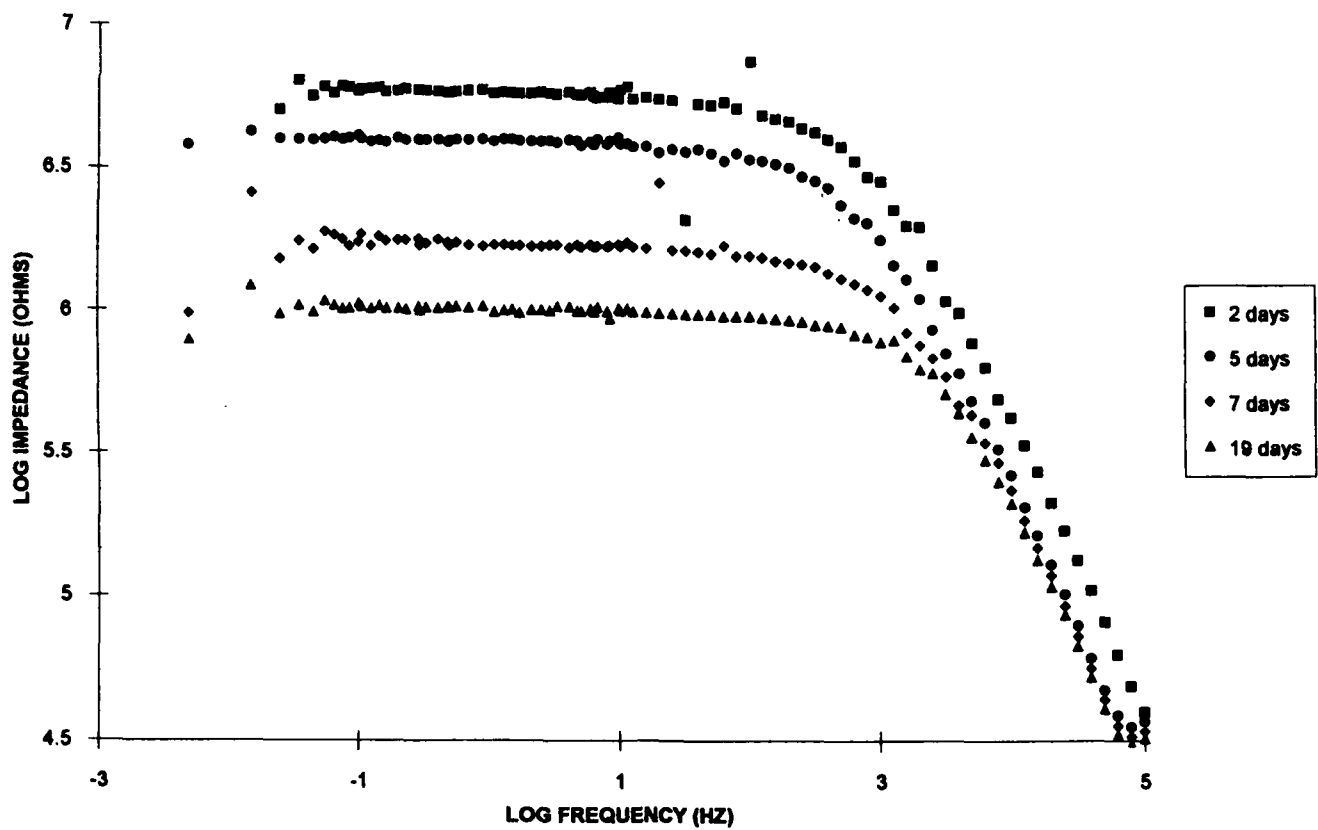


Figure 1: EIS data plotted in the Bode magnitude format, for an ATMEIS monitor after 2(■), 5 (●), 7(◆) and 19(▲) days exposure in an atmospheric exposure chamber to 1 ppm SO₂, 95% RH.

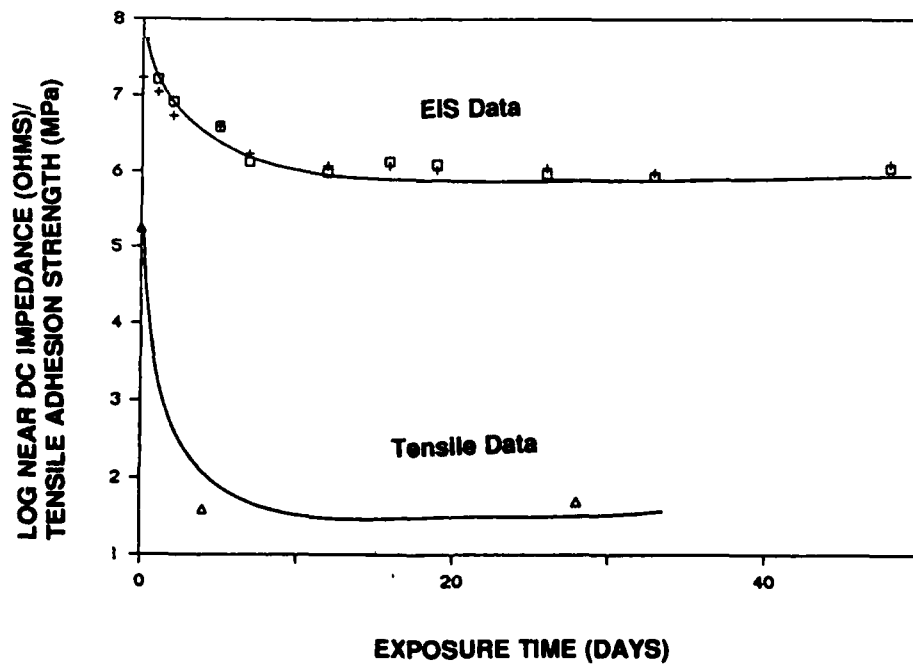


Figure 2: Comparison of near DC Impedance values (5-20 mHz) for two ATMEIS monitor specimens (□, +) to average tensile adhesion strength values (Δ) for conventional specimens as a function of exposure time in an atmospheric exposure chamber to 1 ppm SO₂ and 95% RH.

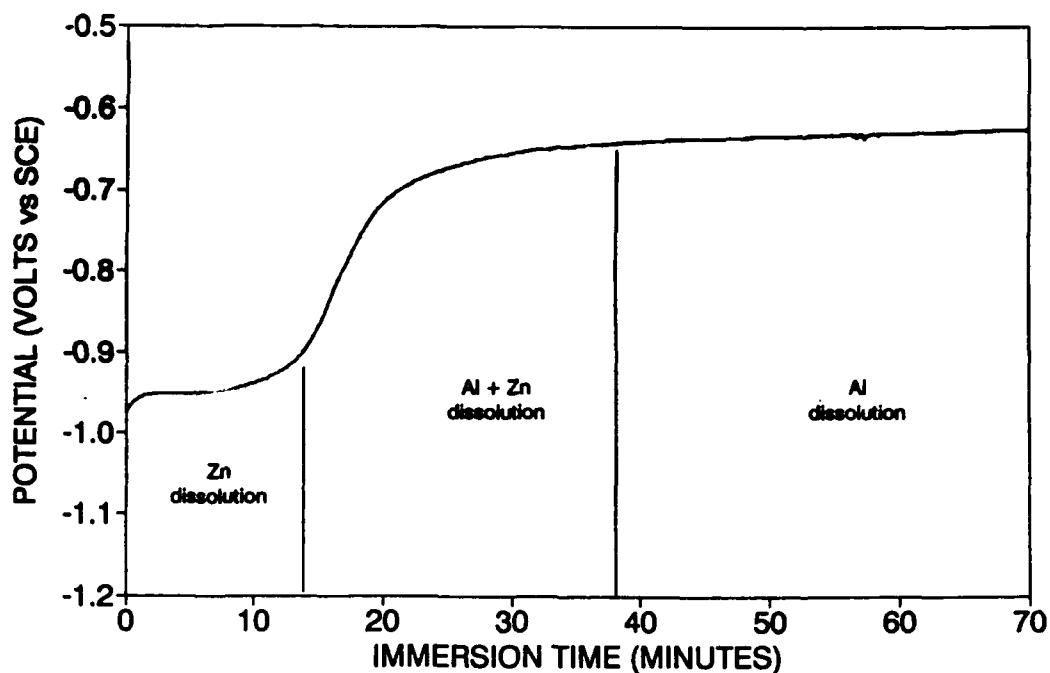


FIGURE 3: Typical electrochemically monitored etching curve in 0.5M H₂SO₄ for Galvalume. Potential regions are marked to indicate the dissolution expected to be occurring within each region.



15 minutes

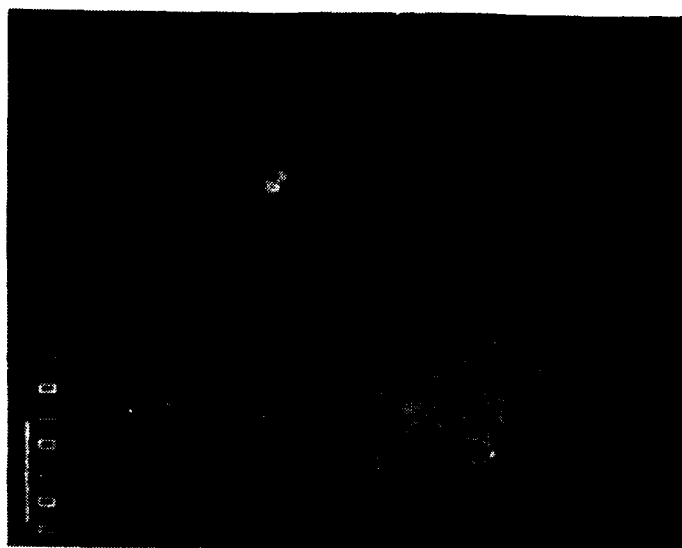


30 minutes

Figure 4: Cross sectional BEI (1500X) of Galvalume etched for 15 and 30 minutes in 0.5M H₂SO₄.



Sulfuric Acid Etch



HRL Industrial Site

Figure 5: Cross sectional BEI (1500X) comparing laboratory etched Galvalume to Galvalume exposed at the HRL industrial site for 2.5 years.

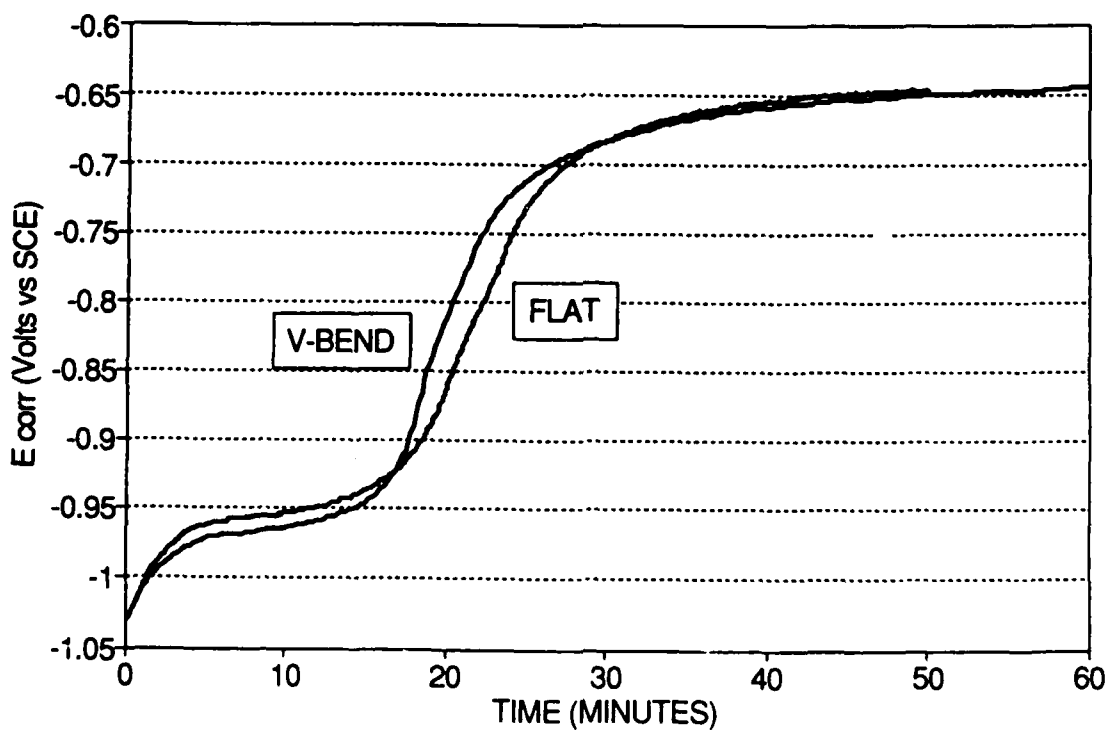


FIGURE 6: Comparison of typical Galvalume etching curves for flat and formed (v-bend) samples.

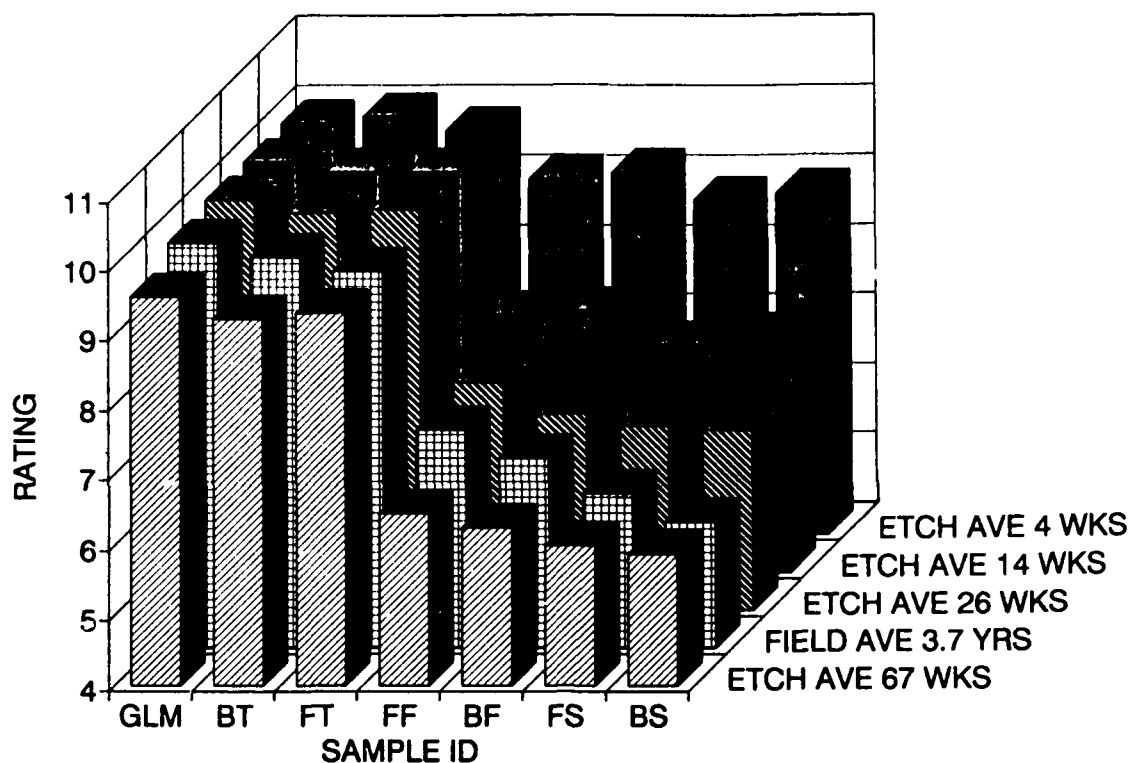


Figure 7: Comparison of field exposure data to data for electrochemical pre-etching followed by field exposure.

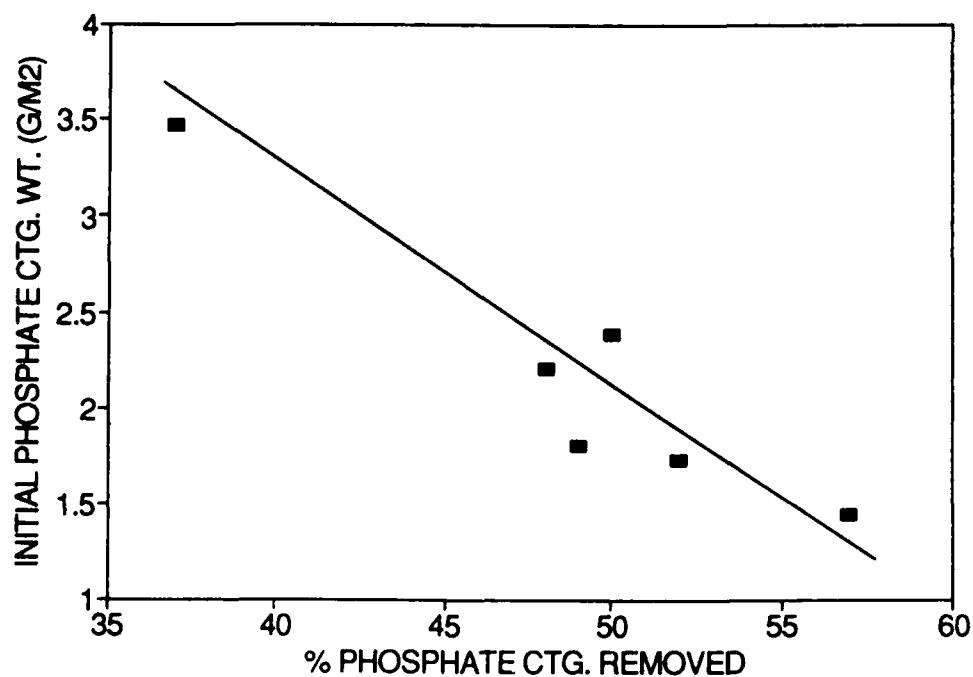


Figure 8: Plot of initial phosphate coating weight vs % of phosphate coating removed during exposure for 10 min. to 0.1M NaOH.

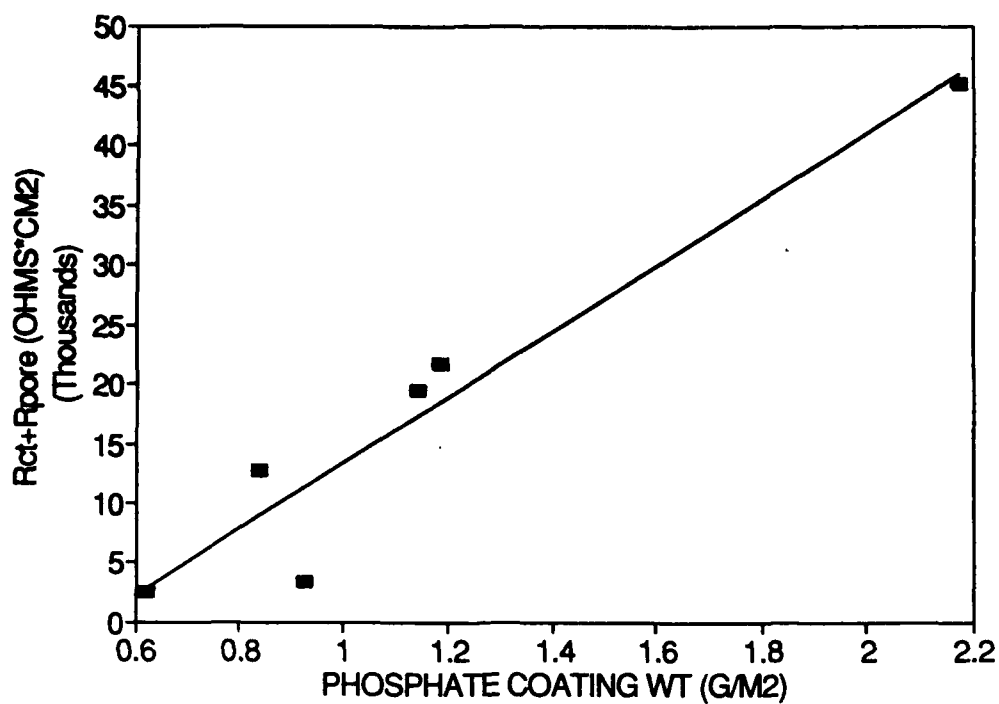


Figure 9: Final (Rct + Rpore) vs final phosphate coating weight of galvalume samples after 10 minutes exposure to 0.1M NaOH.

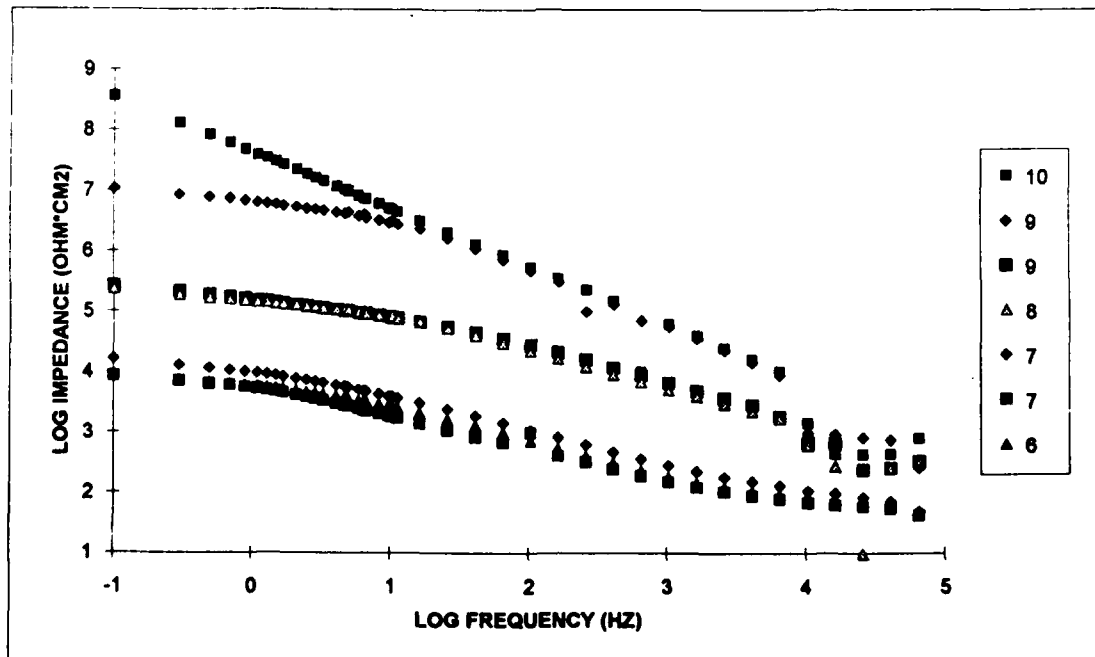


Figure 10: EIS data plotted in the Bode Magnitude format for samples of Galvalume containing impact dimples of varying severities. Crazing ratings of each sample are indicated in the figure legend.

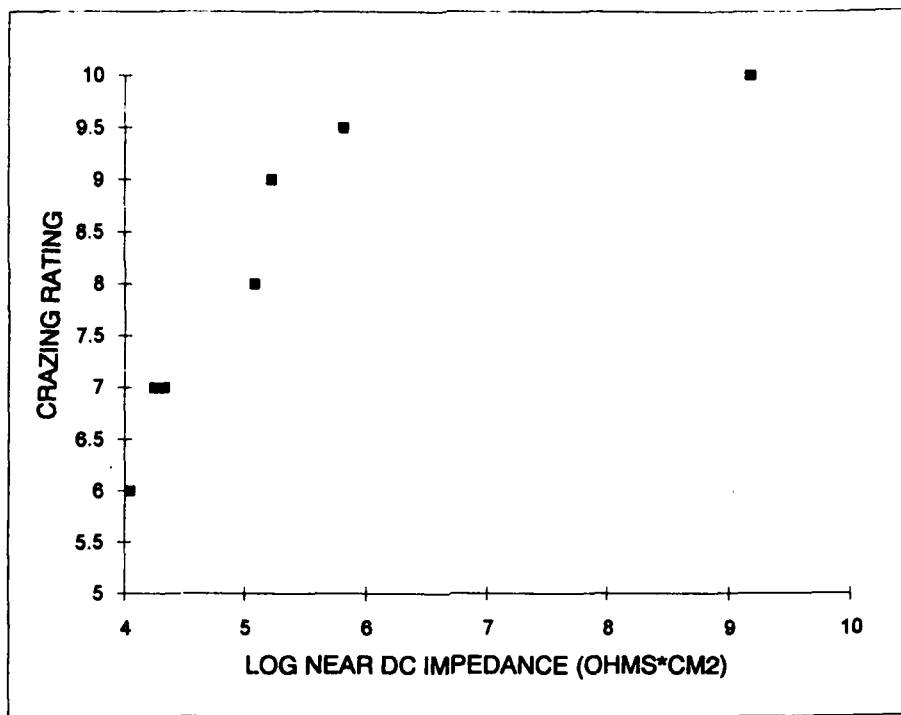


Figure 11: Plot of crazing rating vs the log of the near DC impedance value for a series of painted (epoxy-SMP system) Galvalume samples containing impact containing impact dimples of varying severity.

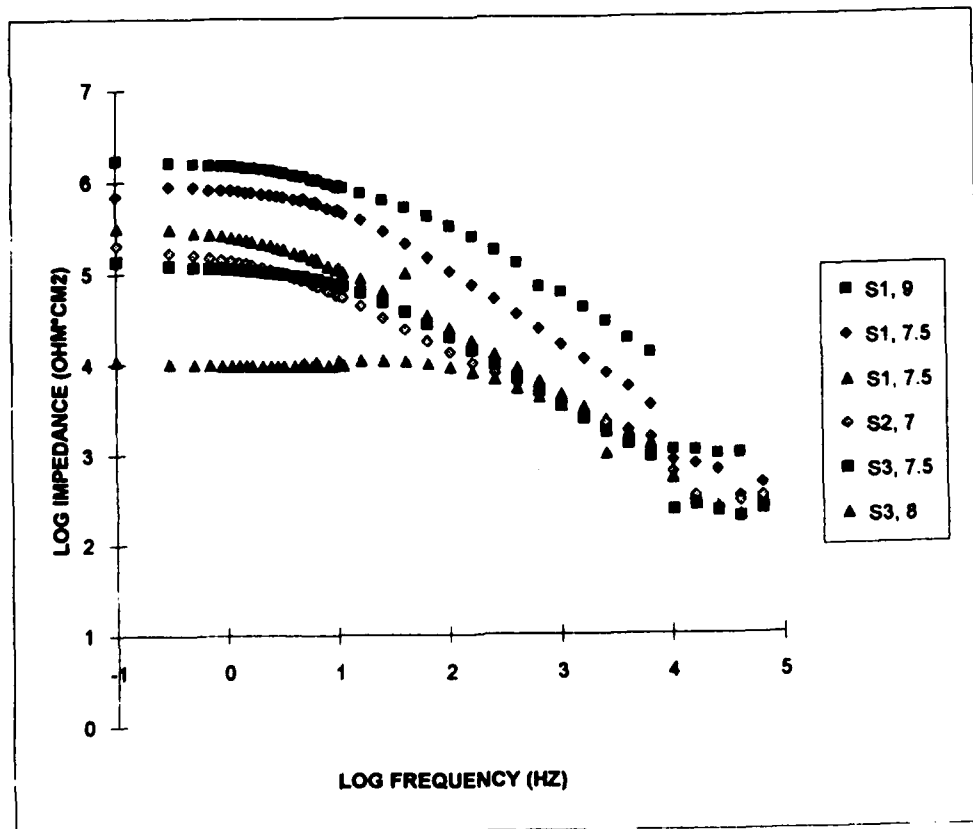


Figure 12: EIS data plotted in the Bode Magnitude format for a series of roll formed Galvalume samples. Galvalume samples were commercially produced by one of three suppliers. Galvalume supplier (S1, S2, or S3) and crazing rating for each sample are indicated in the figure legend.

Determination of Coating Delamination and Underfilm Corrosion during Atmospheric Exposure by means of Electrochemical Impedance Spectroscopy

Ahamed Amirudin
Swedish Corrosion Institute
Roslagsvägen 101, Hus 25
S-10405 Stockholm
Sweden

Per Jernberg
National Swedish Institute for Building Research
Materials and Structures Division
Gävle
Sweden

Dominique Thierry
Swedish Corrosion Institute
Roslagsvägen 101, Hus 25
S-10405 Stockholm
Sweden

Abstract

Electrochemical Impedance Spectroscopy (EIS) has been used to study the degradation of painted galvanised steel exposed to a Cyclic Corrosion Test with different concentrations of NaCl sprayed on the samples. For this purpose, a new electrochemical sensor that allows in-situ measurements to be made under atmospheric conditions has been developed. A comparison between the results obtained by EIS and the delaminated area obtained with a infrared thermography technique shows that the rate of delamination and corrosion beneath the coating may be monitored as a function of time by EIS and IR thermography. It is also shown that EIS gives advance knowledge of the mechanisms of underfilm corrosion.

Key terms: Electrochemical Impedance Spectroscopy, coated galvanised steel, cyclic corrosion test, atmospheric corrosion, IR thermography.

Introduction

A. General

Electrochemical Impedance Spectroscopy (EIS) has been widely used in the prediction of the life of organic coatings used for corrosion protection¹⁻³. It is generally agreed that the coated metal system may be described in term of the equivalent circuit presented in Figure 1, where C_c and R_c represent the capacitance and the resistance of the coating, R_u is the uncompensated resistance between the reference electrode and the working electrode and the term Z_m is related to the corrosion reactions in the defective areas of the coating. Z_m depends on the rate-controlling step of the electrochemical reactions, the presence of macroscopic defects in the organic coating and the pre-treatment of the metal surface before painting¹⁻⁴. However, it generally includes the double-layer capacitance, C_d , of the defective areas.

Almost all EIS investigations of the corrosion of polymer-coated metal have been carried

out in aqueous environments. The possibility of applying EIS to atmospheric corrosion of painted metals has been presented recently ^{6,7}. It has been demonstrated that the electrochemical sensor previously used lent itself to studies of the degradation of painted galvanised steel under various exposure conditions.

The purpose of this work was to further explore the possibility of monitoring the delamination rate of painted galvanised steel during an accelerated corrosion test using EIS measurements. The results are compared with an IR thermography method.

B. Determination of the delaminated area using EIS

The electrochemically active area under the coating has been often calculated by comparing the measured double-layer capacitance with the specific capacitance value, i.e. capacitance per unit area, according to the following equation:

$$\text{Area} = C_{\text{dmeasured}}/C_{\text{dspecific}} \quad (1)$$

Specific capacitance values have either been measured on the bare metal exposed to the same electrolyte or have been considered to be similar to that of mercury, i.e. 15-30 $\mu\text{F}/\text{cm}^2$.

However, this way of calculating the electrochemically active area requires the accurate determination of the equivalent circuit of the coated metal system, which can be rather difficult at an early stage of coating breakdown. Additional errors may occur, caused by corrosion products or passive layers on the metal surface, which may change the specific capacitance during exposure.

Recently, a new approach has been made by Haruyama ^{4,8}. He calculated the delaminated area from the high-frequency part of the impedance diagrams, relating it with the coating resistance according to the following formulae:

$$R_c = R_c^0/A_d \quad (2)$$

$$\text{where } R_c^0 = \rho \cdot d \quad (3)$$

$$C_c = (\epsilon \cdot \epsilon_0 \cdot A)/l \quad (4)$$

$$C_d = C_d^0 \cdot A_d \quad (5)$$

where C_d^0 and R_c^0 are the area-specific values, ϵ_0 is a constant, ϵ is the relative dielectric constant, l is the thickness of the paint coating, ρ is the specific resistivity of the coating, A is the total area of the specimen and A_d is the total delaminated area. This theory assumes that the EIS diagrams reflect only the metal surface on which the cathodic reaction occurs, which means that the electrochemically active area can be equated with the delaminated area.

It is also important to note that, according to Haruyama's method, it is assumed that the specific resistivity and the thickness of the coating remain more or less constant while delamination and corrosion proceed under the coating. These two parameters, however, are likely to change with the time of exposure.

It is also assumed that changes in the coating capacitance are only due to an increase of the dielectric constant of the organic coating which is caused by the penetration of water (see eq.4). This last assumption is probably not valid since changes in the coating

capacitance have been observed due to the initiation of the delamination process⁹.

In addition to the passive elements in the equivalent circuit, the frequency ("the breakpoint frequency") when the phase angle falls to 45 degrees in the high frequency range (the resistive and reactive impedances are equal) has been used as a direct measure of the delaminated area. The breakpoint frequency is derived from Haruyama's method (see equation 6) and, consequently, is subjected to the same limitations (i.e. the fact that coating capacitance, coating thickness and specific coating resistance remain constant during the delamination and corrosion processes).

$$f_b = 1/(2 \cdot R_c \cdot C_c) = A_d/(2 \cdot R_c^0 \cdot C_c^0 \cdot A) = f_b^0 \cdot A_d/A \quad (6)$$

$$\text{where } f_b^0 = 1/(2 \cdot \epsilon \cdot \epsilon_0 \cdot \pi \cdot \rho)$$

It should be noted that f_b^0 only depends on the coating parameters.

It must be stated that the exact physical meaning of the breakpoint frequency is not clear even if good correlations are generally obtained with the delaminated area¹⁰⁻¹¹.

C Determination of delaminated areas using the IR thermography method

Thermography and image analysis together can be used to measure defects, such as corrosion spots or delaminated areas, between a metallic surface and an organic coating¹²⁻¹³. The main advantage of this technique is that defective areas can be measured without removing the organic coating even in the early stages of the degradation process.

In some parts of the infra-red (IR) region, absorbance and reflectance are negligible for most types of coating used today. All organic binders have a "window" in the IR absorption spectrum in the wavelength interval 3.5-5.0 μm . Most pigments, fillers and additives also have little absorbance in this interval. A defect is detected as a contrast difference. This is made possible by the different IR-emissivity factors; an area covered by corrosion products has a factor of about 0.8, whereas a fresh glossy metal surface has a factor of about 0.2. A low emissivity factor implies high reflectance and vice versa. Thus, to stabilise the experimental conditions, there is a need to raise the sample temperature to about 20°C above the ambient temperature. Other defects, such as blisters, may introduce temperature differences giving rise to contrasts between intact and deteriorated areas.

Experimental

A. Samples and exposure conditions

Hot-dip galvanised steel panels (zinc coating thickness 8 μm) were phosphated and painted with either an electro-coated epoxy paint (ED-coated 20 μm) or a commercial top-coat system including an ED-coat, a sealer and a topcoat to give a total thickness of 110 μm . A gold grid was electron-beam deposited to a thickness of 4000 Å on the paints. The area of the gold electrode was 2 cm^2 corresponding to 10% of the total exposed area. A detailed description of the sensor and its validity has been given elsewhere⁵⁻⁷.

The Cyclic Corrosion Test (CCT) consisted of the following steps: the samples were sprayed with NaCl (0.5% or 5%), subjected to a wet period of 18 hours (98% relative humidity and 20°C), rinsed with deionised water and finally dried by an electric fan for a period of 6 hours. The cycle was repeated. All panels were scratched down to the steel substratum prior to exposure. The scratch was made manually which led to a certain scatter in the scratched areas among replicates. The exact scratched area was, however, measured for all samples using an image analyser prior to exposure.

B. EIS measurements

The experimental set-up used for EIS measurements has been described elsewhere ⁷. The EIS spectra were interpreted on the basis of a Non-Linear Least Squares (NLLS) fit giving the most probable equivalent circuit ¹⁴. The measurements were made at the end of the wet period of the CCT. All data presented are mean values of the results obtained on 7 specimens.

C. IR Thermography technique

The IR camera used was an AGEMA 880-SWB, spectral response 2.0-5.6 μm , equipped with a variable extension ring (15-25mm) for close-up imaging. The test panels were pressed on a sample holder consisting of a metallic/plastic frame and a soft rubber-like electrical plate. The sample holder and the camera were attached to a slide bench. The camera, with an adjustable height, could be moved along the bench and the sample holder perpendicularly to the bench in a horizontal direction. The sample area exposed at each shot was varied between $2 \times 2 \text{ cm}^2$ to $4 \times 4 \text{ cm}^2$. The image signal was transferred directly from the camera to the PC-based image analyser for area calibrations and measurement of defective areas. Figure 2 shows typical corrosion and delamination spots obtained with IR thermography technique.

Results and Discussion

A. EIS Measurements

1 EIS spectra. Figures 3 and 4 show Bode plots (i.e. modulus and phase angle versus frequency) obtained for electro-coated hot-dip galvanised steel exposed to the CCT for different lengths of time and for two different concentrations of NaCl sprayed on the samples. The impedance diagrams agree with what is generally obtained for coated metals in aqueous solutions. Two time constants are evident from the beginning of the exposure. The high-frequency region corresponds to the dielectric properties of the organic coating, while the low-frequency part corresponds to the corrosion reaction in the vicinity of the scratch. It may also be observed that for the samples sprayed with 5% NaCl, a third time constant appeared at the end of the exposure.

2 Equivalent circuit. Figure 5 shows the most probable equivalent circuit used to fit the data of Figures 3 and 4 together with the results obtained when applying this circuit to the experimental data of Figure 3 and the relative residuals for the data points. An excellent fit of the experimental data with very low relative residual errors for the data points is observed.

The physical meaning of the most probable equivalent circuit for the cyclic laboratory test has been discussed elsewhere ⁷. The constant phase element Q_c and the resistance R_c are due to the organic coating, C_d is the double-layer capacitance, and R_i and W are probably due to the charge transfer reaction. The physical meaning of R_i and W_i in series with the double-layer capacitance, C_d , is not totally understood. It should be noted that this time constant does not always appear, especially during the first few weeks of exposure. In this case the equivalent circuit reverts to the one presented in Figure 1. Impedance diagrams showing an extra impedance arrest at intermediate frequencies have recently been reported by Haruyama et al ⁴ and explained to be due to the presence of macroscopic defects.

Under the present experimental conditions, the samples are scratched prior to exposure. However, the total impedance of the system will depend on the climatic conditions used in the accelerated test such as the conductivity of the moisture film, the relative humidity and the temperature. Hence it is possible that the change in the shape of the impedance diagrams observed after few weeks of exposure could be related to an increase in the conductivity of the moisture film due to an accumulation of chloride ions in the scratched

area or to an increase in the concentration of chloride ions at the organic coating/metal interface in regions close to the scratch.

B. Determination of the delaminated area

1 IR Thermography technique. After the exposure period, the delaminated area was determined with the IR thermography technique before removing the organic coating and with an image analyser after mechanically removing the organic coating. The results are summarised in Table 1 and Table 2 for 5% NaCl and 0.5% NaCl respectively. It is obvious that classical visual observation leads to an underestimation of the delaminated area. Differences in the delaminated area measured with the two techniques were as high as 20% on some samples. It should also be noted that in the case of the CCT using 5% NaCl, delamination is observed even at distant points which are connected to the scribed area by still bonded coating.

The differences in the delaminated area between replicates are due to the fact that the samples had different scratch areas. This will be discussed in detail in the next section.

2 Breakpoint frequency. The breakpoint frequencies of all samples were determined from the Bode plot at the end of the exposure period. Figures 6 and 7 show the breakpoint frequency as a function of the delaminated area determined by the IR thermography technique for the CCT using 5% NaCl and 0.5% NaCl respectively. A good correlation (i.e. correlation factor 0.95) between the two techniques may be observed. This indicates -in agreement with other studies¹⁰⁻¹¹ - that the breakpoint frequency is a good estimation of the delaminated area. From Figure 6 it is also possible to calculate the constant f_b^0 corresponding to the totally delaminated coating. A value of 2×10^4 is obtained. This value is similar to that obtained by McCluney et al¹¹ for electro-deposited epoxy primer.

C. Corrosion mechanisms

1 Influence of the scratched area. As has been mentioned above, the results of Tables 1 and 2 were obtained using samples with different scratch areas. Figure 8 shows the variation of the delaminated area in connection to the scratch as a function of the scratch area (i.e. the surface of the exposed steel) for electro-coated hot-dip galvanised steel exposed to the CCT using 5% and 0.5% NaCl. A very good correlation is obtained. For the ED-coat the data of Tables 1 and 2 obtained by IR thermography technique were used.

Similar results are obtained for the top-coat system as shown in Figure 9. However, the delaminated area used in this comparison was that determined by the Image Analyser since the thickness of this system limits the use of IR thermography technique.

The results of Figure 8 and 9 indicate that the kinetics of the cathodic reaction on the steel surface determines the rate of delamination at the zinc/organic coating interface. However, higher delamination rates are observed for the ED-coat compared with the top-coat system for the CCT using 5% NaCl. This effect is not observed in the CCT using 0.5% NaCl where similar delamination rates are observed for the ED-coat and the top-coat system. This indicates that for the low delamination rates (i.e. CCT using 0.5% NaCl), the delamination is mainly controlled by the cathodic reaction at the scratch. The delamination rate will therefore be controlled by the access of oxygen and water to the scratch. This results in anodic dissolution of the zinc coating.

For the CCT using 5% NaCl, on the other hand, the delamination seems to be caused by several simultaneously acting mechanisms which will be discussed below.

2 Influence of chloride concentration. As shown in the preceding sections, the rate of delamination for both ED-coat and the topcoat systems, decreases by a factor of 3-4

when the chloride concentration in the spraying solution is decreased from 5% to 0.5% NaCl. Similar results have been obtained by Blekkenhorst et al¹⁷. This may be due to a combined effect of decreased ionic conductivity of the electrolyte, which may reduce the galvanic coupling between steel and zinc, and to decreased aggressivity of the electrolyte.

3 Proposed corrosion mechanisms. It has been observed by Shastry et al¹⁵ that for electro-coated electrogalvanised steel exposed to a salt-spray test, cathodic regions may be observed at the leading edge of the creep front. Similar results have been obtained by Van Ooij et al¹⁶ on electro-coated electrogalvanised steel exposed to atmospheric conditions in a coastal environment. However, in cyclic tests with high time of wetness and high chloride concentrations, this phenomenon is generally not observed and corrosion products are found throughout the delaminated area²¹. Hence, it is possible that the higher delamination rate observed for the ED-coat compared with the top-coat system in the CCT using 5% NaCl may be related either to a cathodic disbonding of the paint in front to the corrosion edge or to corrosion due to accumulation of chloride ions or both.

The two important variables in the present work which result in different deteriorations are the paint thickness and the concentration of chloride ions.

The diffusion coefficient of water for an epoxy paint is about $10^{-9} \text{ cm}^2/\text{s}$ ⁹. The time necessary for water to reach the interface zinc/organic coating will be therefore about 4 hours. In the case of top-coat system - due to the greater thickness - the time will be much longer (about 100 hours). Owing to the high chloride concentration in the electrolyte, the chloride ions may diffuse either laterally from the scratch or across the film. This will result in cathodic disbonding and formation of corrosion products ahead of the corrosion front advancing from the scratch. It is well known that in presence of large amounts of chloride and at pH's around 6.5, zinc hydroxychloride is formed¹⁸. In fact, SEM/EDAX analyses and Raman spectroscopy have shown that this corrosion product was found at the front of the degradation for thin paint layer on electrogalvanised steel in the same CCT with 5% NaCl as the one used in the present work at the front of the degradation¹⁹. The degradation mechanism, in the case of the ED-coat, therefore seems to be related to two simultaneously acting mechanisms: anodic zinc dissolution from the scratch and formation of corrosion products far from the scratch due to the combined action of high permeation rates and high chloride concentrations at the zinc/organic coating interface. This is in contrast to what is generally observed in outdoor exposures¹⁶ where small cathodic areas (i.e. "fingers") are found. The obvious conclusion is that the use of a 5% NaCl solution in accelerated tests may not be advisable.

In the case of 0,5% NaCl, where similar degradation rates were observed for the top-coat and the ED systems (i.e. no influence of the paint thickness), the rate of delamination is probably only controlled by the cathodic area of the exposed steel. This is consistent with practical experience using indoor and outdoor exposures on various zinc-coating materials²⁰ where the amount of zinc consumed from the scratch is inversely proportional to the zinc-coating thickness.

Conclusions

- * A good correlation between the breakpoint frequency and the delaminated area obtained by IR thermography has been observed. The former technique has the advantage of being used in-situ and for both ED-coat and top-coat systems.
- * For the CCT using 0,5% NaCl, the delamination rate is primarily controlled by the rate of the cathodic reaction on the exposed steel surface at the scratch.
- * For the CCT using 5% NaCl, two simultaneous mechanisms controlled the

delamination rate: the effect of the coupling to the exposed steel and the permeation of the corrosive species through the thickness of the film.

- * The IR thermography technique gives a good estimation of the delaminated area for the ED-coat electro-galvanised steel.

Acknowledgements

The authors thank The Swedish National Board for Industrial and Technical Development(NUTEK) for financial support. C. Barreau and D. Massinon (IRSID, France) are acknowledged for valuable discussions.

References

1. F. Mansfeld, M.W. Kendig and S. Tsai, Corrosion, **38**,(1982),p 478.
2. H. Leidheiser and M.W. Kendig, Corrosion, **32**,(1976),p 69.
3. G.W. Walter, Corrosion Science, **32**,(1991),p 1041.
4. R. Hiriyama and S. Haruyama, Corrosion, **47**,(1991),p 953.
5. T. Comeau Simpson, P.J. Moran, W.C. Moshier, G.D. David, C.D. Arah and K.L. Zankel, J. of Electrochem. Soc., **136**, (1989),p 2761.
6. C. Lecuyer, C. Barreau and D. Thierry, Revue de Met., **10**,(1991),p 691.
7. A. Amirudin , C. Barreau, D. Massinon and D. Thierry, Proc. 2nd Int. Conf. on Zinc and Zinc Alloys Coated Steel Sheet, Amsterdam (The Netherlands), (1992) p 549.
8. S. Haruyama, M. Asari and T. Tsuru, Proc. Symp. Corr. Prot. by Org. Coat., Manchester (England), (1987),p 197.
9. F. Geenen ,PhD Thesis, Delft University of Technology (The Netherlands),(1991).
10. H.P. Hack and J.R. Scully, J. of Electrochem. Soc., **138**,(1991),p 33.
11. S.A. McCluney, S.N. Popova, B.N. Popov, R.E. White and R.B. Griffin, J. of Electrochem. Soc., **139**, (1992),p 1556.
12. M.E. McKnight and J.W. Martin, ASTM STP 846, (1984),p 13.
13. P. Jernberg, Proc. Termosense XIII, (1991),p 295.
14. B. Boukamp, Ext. Abstr. 1st Int Symp. on EIS, Bombannes (France),(1989),p C1.11.
15. C.R. Shastri and H.E. Townsend, CORROSION/88, Saint Louis (USA), paper 50.
16. W.J. Van Ooij, H. Anderson and G. Ström, CORROSION/88, Saint Louis (USA), paper 51.
17. F. Blekkenhorst, E.N. Soepenbergh, M. Roelofsen and J.P. Schoen, CORROSION/88, Saint Louis (USA),paper 354.
18. D. Massinon and D. Thierry, CORROSION/91, Cincinnati (USA), paper 574.
19. A. Amirudin, C. Barreau, D. Massinon and D. Thierry, Material Science Forum, Vol **111-112**, (1992) p 291
20. M. Ström, G. Ström and W.J. Van Ooij, Proc. 2nd Int. Conf. on Zinc and Zinc Alloys Coat. Steel Sheet, Amsterdam (The Netherlands),(1992),p 521.
21. W.J. Van Ooij, A. Sabata and G. Ström, Proc. Corr. Rest. Aut. Steel Sheets, Chicago (USA)ASTM international, (1988),p 75.

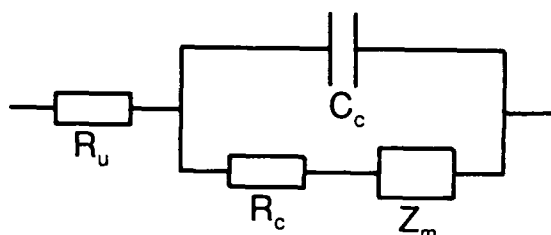


Figure 1. General equivalent circuit for a polymer-coated metal.



Figure 2. Typical delamination and corrosion spots seen by IR thermography.

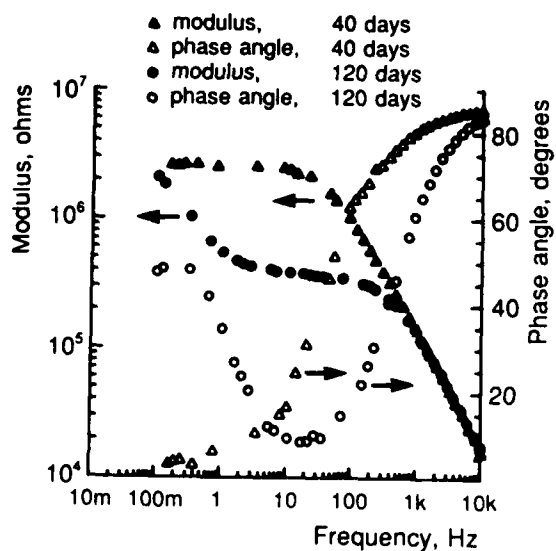


Figure 3. Bode plots for electro-coated hot-dip galvanised steel exposed to the CCT using 0.5% NaCl.

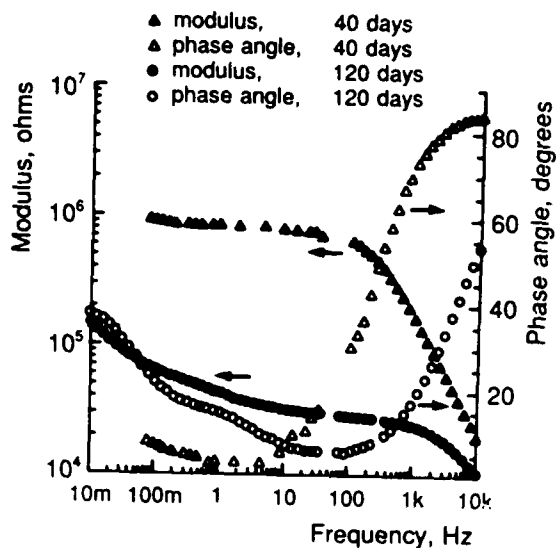


Figure 4. Bode plots for electro-coated hot-dip galvanised steel exposed to the CCT using 5% NaCl.

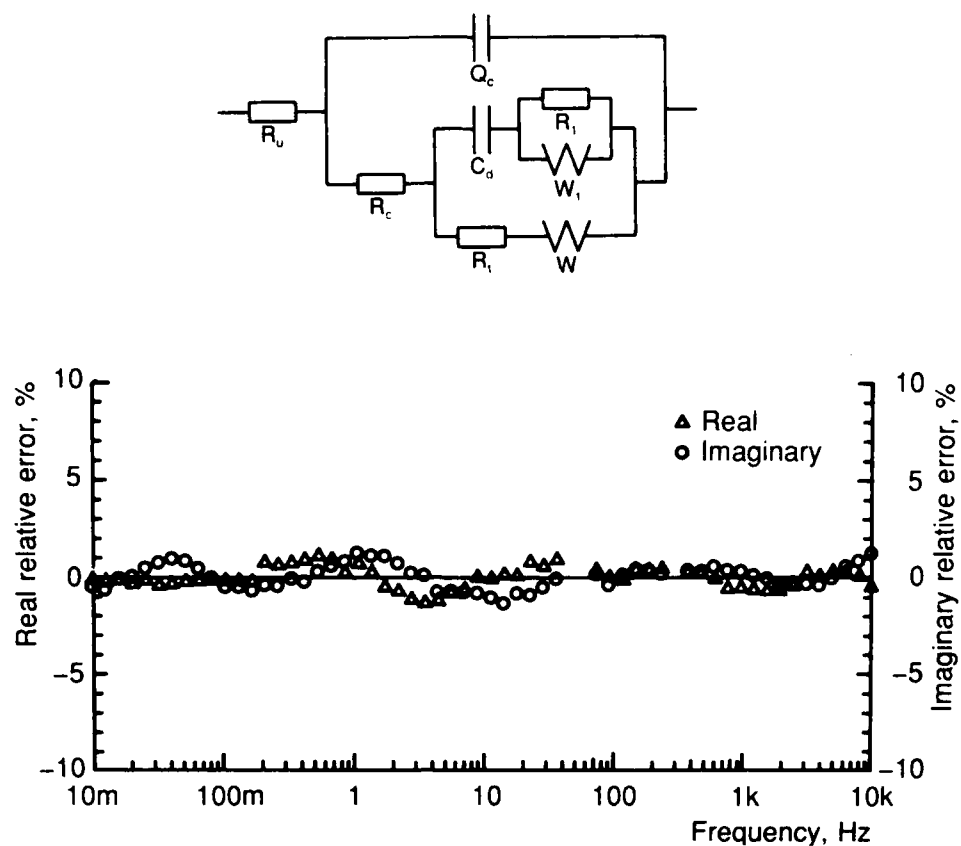


Figure 5. Most probable equivalent circuit and frequency error distribution for the data of Figure 3 (120 days).

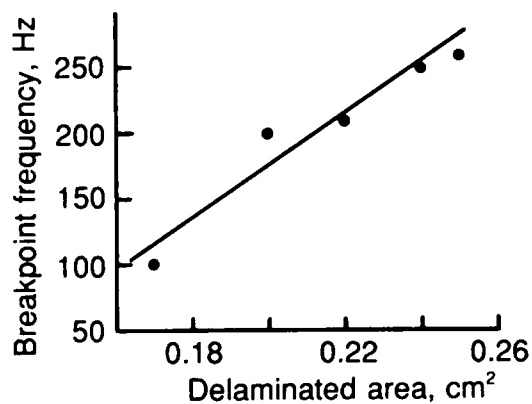


Figure 6. Breakpoint frequency as a function of the delaminated area in exposure to CCT using 0.5% NaCl

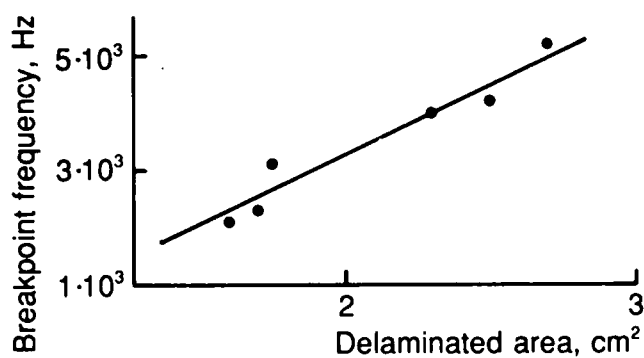


Figure 7. Breakpoint frequency as a function of the delaminated area in exposure to CCT using 5% NaCl

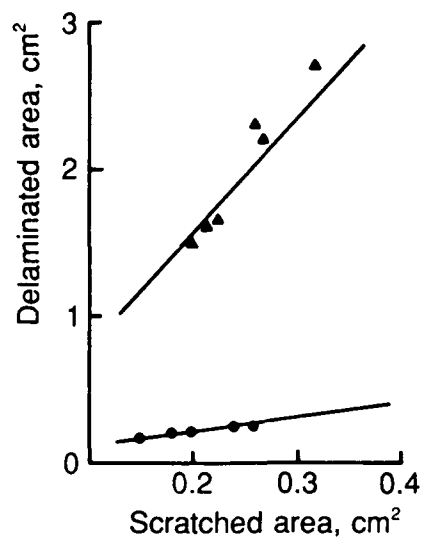


Figure 8. Delaminated area as a function of the scratched area for ED-coat.
 ▲ 5% NaCl, • 0.5% NaCl.

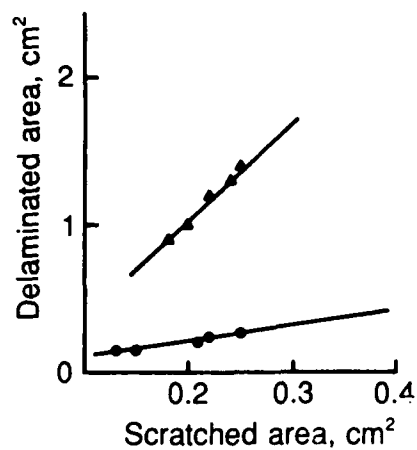


Figure 9. Delaminated area as a function of the scratched area for Top-coat.
 ▲ 5% NaCl, • 0.5% NaCl.

Table 1. Exposed scratched areas and delaminated areas for ED-coat hot-dip galvanized steel exposed to the CCT using 5% NaCl

Exposed scratched area, cm ²	Delaminated area, cm ²			
	Connected to scratch (after paint removal)	Not connected to scratch (after paint removal)	Total (after paint removal)	Total, by IR thermography
0.19	1.13	0.08	1.21	1.6
0.20	1.39	0.11	1.50	1.7
0.21	1.50	0.14	1.64	1.8
0.24	2.10	0.10	2.20	2.3
0.25	2.00	0.30	2.30	2.5
0.32	2.60	0.05	2.65	2.7

Table 2. Exposed scratched areas and delaminated areas for ED-coat hot-dip galvanized steel exposed to the CCT using 0.5% NaCl

Exposed scratched area, cm ²	Delaminated area, cm ²			
	Connected to scratch (after paint removal)	Not connected to scratch (after paint removal)	Total (after paint removal)	Total, by IR thermography
0.15	0.15	0	0.15	0.17
0.18	0.18	0	0.18	0.20
0.20	0.21	0	0.26	0.22
0.24	0.23	0	0.23	0.24
0.26	0.26	0	0.26	0.25

Characterization of Corrosion under Coatings by Electrochemical Noise Methods

D.J. Mills* G.B. Bierwagen* B. Skerry* D. Tallman*

* Dept of Polymers and Coatings
NDSU
Fargo
ND 58105

+ Sherwin Williams Company
Technical Center
Cleveland
OH 44113

Abstract

Electrochemical Noise (ECN) is the name given to the spontaneous fluctuations that continually occur in electrochemical systems. By simultaneously measuring both potential and current fluctuations (EVCN method), information can be extracted about corrosion processes. This technique was established with uncoated metal and has only recently been applied to painted metal. The long term aim of this work is to examine metal panels coated with Navy specification marine coatings using EVCN methods together with examination of identical systems by other corrosion test methods. This paper gives results for five alkyd primers on steel containing different inhibitive pigments. A novel type of experimental arrangement has been successfully employed. Specimens have been monitored using the EVCN method in dilute Harrison's solution and in 2 M NaCl. Blistering occurred in the latter environment and this seemed to relate to changes in the ECN parameters. Also sets of specimens were put through accelerated tests : Cycling Salt Spray and Hot (55 °C) Salt Bath. The latter also differentiated between the different pigments in the degree to which there was blistering. In the former test there was severe attack at the scratch which varied somewhat depending on the inhibitive pigment. Generally the work reported here has established the techniques for subsequent work with marine coating systems.

Key terms : anti-corrosive paints, electrochemical noise, accelerated tests

Introduction

Corrosion is an electrochemical process which occurs at the interface between the metal and the solution. Therefore electrochemical methods of analysis have been used extensively to generate quantitative performance information concerning corrosion and its inhibition. In essence, the method involves connecting the sample (usually immersed in solution) to an external source of voltage (either AC or DC). This causes a current to flow through the

external circuit. This is measured, as is the voltage with respect to some standard reference electrode. The exact way the measurement is made and how the subsequent data are treated varies with the technique. One common approach is to measure polarization resistance and considerable success has been achieved using this method to monitor uncoated metal.

Use of electrochemical techniques is generally more difficult with coated metal particularly when the coating is a paint with a high impedance ($> 1 \times 10^6 \text{ ohm-cm}^2$). Measurement of DC resistance *in situ* has frequently been used since the early work of Bacon Smith and Rugg showed it to be a successful way of monitoring and predicting coating performance¹. Measurement is made quickly, the technique is simple and the result is easy to understand. Recently much work has been done using AC Impedance. This produces very much more information but takes longer, requires complex equipment and the results are sometimes difficult to interpret. Generally then although both the methods above provide useful qualitative and occasionally e.g. with low resistance ($< 5 \times 10^5 \text{ ohms-cm}^2$) coatings, quantitative information, neither has as yet been able to produce the corrosion rate under a paint for the frequently encountered situation where the paint system has a resistance of say $> 5 \times 10^6 \text{ ohms-cm}^2$.

The monitoring and analysis of the spontaneous voltage and current fluctuations that occur during corrosion processes can give useful information. Voltage fluctuations are easily measured. This is the Voltage Noise method. It is a non-intrusive technique which can equally easily be made on coated as it can on uncoated metals. Early work applying this method to coatings on steel showed that the level of noise generated depended on the processes occurring on the specimen particularly blistering². A more recent article used the technique to indicate the onset of pitting corrosion under a thin phenol formaldehyde based coating³.

Eden *et al* extended the method when they reported that current noise fluctuations may be related to the amount of corrosion⁴. Current noise is generated by connecting together two nominally identical electrodes through a zero resistance ammeter. This is the Current Noise method. By simultaneously monitoring both voltage and current fluctuations corrosion rate information may be derived along with information about the mechanism of corrosion attack. The term EVCN will be used in this report to indicate this type of measurement.

Application of this to coatings has been conducted by one of the present authors. An advantage of the technique is that no externally applied signal is required in order to generate the signals to be measured. In early studies^{5,6} the voltage and current noise data obtained were analyzed in terms of simple statistics *i.e.* by computation of the mean and standard deviation of the noise signals. It was assumed that the amplitude of the Potential Noise (V_n) and the Current Noise (I_n) could be related by an Ohm's law analogy to produce a Noise Resistance (R_n). Useful results were obtained for painted electrodes. More recent work⁷ looked at four coatings with a range of anti-corrosive properties. The technique was able to differentiate paints in terms of both the extent and mechanisms of corrosion.

EVCN thus looks promising as a method for monitoring coated substrates but more results need to be gathered and on a greater range of paints. Particularly two and three coat systems need to be investigated. So one of the aims of the present Project is to study a range of marine coating systems. At the time of writing work on these coatings is incomplete. The results which are reported here use EVCN to monitor five alkyd primers. Because these coatings are thin (40-50 μm) and single coat it was expected that the test duration could be relatively short (around 200 hours). As some comparative data were available⁸ these primers were ideal for this preliminary study.

A second aspect to the project is in the development of suitable accelerated test method(s) for anti-corrosive paints particularly those for marine application. Recent work has indicated that a combination of a "Prohesion" cycle and a UV condensation cycle can effectively differentiate paints for industrial atmospheres⁹. For marine paints used above the water-line, it is expected that a cycling test similar to "Prohesion" but with a solution composition similar to sea water followed by UV/condensation cycle may be appropriate. For below water-line paints a Hot Salt Bath test *e.g.* exposure at 55°C in 0.5 M NaCl may be employed. This test has recently proved very successful in differentiating primers on both steel and zinc substrates¹⁰.

The work reported here is again preliminary work with alkyd primers. Data were generated in tests which lasted 350 hours ("Prohesion") or 170 hours (Hot Salt Bath). Longer test times are likely to be required to compare marine paint systems.

A summary of the on-going work with the marine paints is included. Many of the techniques used for that are the same as those described. However the results reported here were all obtained using the five alkyd primers.

Experimental

Materials

Coated Panels. These were received as 8" x 4" (220 x 100 mm) steel Q-Panel (R type *i.e.* slightly roughened) coated on one side with phenolic modified alkyd primer. Paints were applied using a #44 wirewound drawdown bar which gives 1.5 -2 mils (40-50 μm) dry film thickness. They were air dried at RT for three weeks before testing. The five paints had basically the same formulation. However the type of inhibitive pigment differed in four of them and the fifth contained no inhibitive pigment (blank). The total pigment loading was the same (48% PVC) for all five; the blank thus contained higher levels of the inert pigments (TiO_2 , Silica, Calcium Carbonate). The PVC of the inhibitive pigment varied between 7 and 14 %. Paints were designated 9102 (basic zinc molybdate), 9105 (zinc phosphate), 9106 (zinc chromate), 9107 (blank) and 9109 (barium metaborate). Four panels coated with each paint were supplied. They were cut into two to provide duplicate samples for the four exposure tests. The specimens for the EVCN work were from the bottom half

of the original panel and were used intact. Those for the accelerated tests were from the top half and, using a tempered steel blade, a 0.7 mm X-scratch was made through the paint on the top third of each specimen. The thickness of the paint was measured in 10 places on each specimen using an Elcometer 345 gauge. Paint thickness values on all specimens used for the EVCN experiments were highly reproducible, there was more scatter for the specimens used for the accelerated exposure tests. Because it is a critical factor in determining the level of protection afforded, all paint thicknesses are given in Table 1.

Solutions. These were made up in distilled deionized water using Reagent Grade chemicals (NaCl and $(\text{NH}_4)_2\text{SO}_4$). Dilute Harrison's solution (0.35 w/v $(\text{NH}_4)_2\text{SO}_4$ / 0.05 w/v NaCl) was used for one of the EVCN "runs" and was the solution in the Cycling Salt Spray Test. The other EVCN run used 2 M NaCl. The solution for the Hot Salt Bath test was 0.5 M NaCl.

Blanking Off Procedure. The backs and sides of the specimens were coated with a Colophony Rosin /Beeswax mixture (3/1). This is applied molten (m.p. 60°C) and is a highly effective, inert, high resistance ($> 1 \times 10^{12}$ ohms-cm²) protective coating. Fifty cm² of primer paint was left exposed.

Test Methods

EVCN. The EVCN equipment used was made by Capcis March Limited (CML). It is a computer controlled, automated digital electrochemical noise system. A block diagram showing the set-up is illustrated in Figure 1. Two nominally identical electrodes (joined together during measurement via a zero resistance ammeter) and a reference electrode comprise one probe. Up to 12 probes can be monitored. The machine interrogates each probe for say ten minutes and then moves on to the next. Monitoring is continuous and data can be gathered over a period of days weeks months or even years. The actual experimental cell arrangement was different to that used previously⁷. In order to be able easily to assess the effect of temperature and agitation, the three electrodes which comprise each probe were in the same container rather than in two different cells joined by a salt bridge. This set-up is illustrated in Figure 2. Data were acquired at 2 sec intervals to give a total of 256 data points in one set. The computer generates graphs of current and voltage against time and also a value of the mean Voltage (V_m), the mean Current (I_m) and the Resistance noise (R_n) over the ten minute period. R_n is calculated by dividing the mean of the standard deviation of the voltage by the mean of the standard deviation of the current. Probes 1-5 were the five paints in dilute Harrison's solution : molybdate, phosphate, chromate, blank, and metaborate respectively. This experiment was run for 250 hours. Probes 6-10 were the same five paints in 2 M NaCl and this ran for 185 hours. Tests were conducted at room temperature (around 22-23°C).

Cyclic Salt Spray Test. This was conducted in a Q-Fog Salt spray Cabinet made by Q-panel Company. This chamber is capable of running cycling or continuous tests. The temperature is variable between RT and 45°C and the cycle time (spray on or off) is also

variable. Conditions used were two hours RT with spray on, two hours at 40°C with spray off. The test was conducted using dilute Harrison's solution for 350 hours. This is essentially a "Prohesion" cycle.

Salt Bath Test. This is a simple test. The specimens were totally immersed in a 600 ml beaker (takes five specimens) containing 0.5 M NaCl. The beakers were contained in a water bath which keeps the temperature at 55°C. The test was run for 170 hours.

Panel Assessment Methods

Electrical. A Keithley Electrometer Model 617 was used to measure the DC resistance of the specimens. This effectively checks the success of the "blanking off". Also at the end of each test the DC Resistance of small areas was measured both on the face and at the scratch. This is a useful way of periodically monitoring panels in accelerated tests and the values obtained generally correlate with visual observation¹⁰. Results of these measurements are only briefly given here.

Visual. All panels were visually assessed at the end of each of the tests without removing the coating. The EVCN specimens were intact so only an assessment of the face was made. For blistering observed on the face, the visual observation data were converted to a number using Table 2. The ASTM Standard D614 covers blistering but because of the narrow range of the blistering observed in these tests, it was considered better to use a special scale. The behavior at the scratch for specimens put through the accelerated tests was assessed separately on a scale from 1 to 10 : 1 - lot of spread, lot of rusting to 10 - minimal spread, no rusting - see table 2.

Results

EVCN : 250 hour in dilute Harrison's Solution

The five probes were monitored continuously by EVCN. All gave similar results and illustrative plots of I_m and R_n for 9105 (phosphate) against time are shown in Figures 3 and 4. Values of I_m (avg.) and R_n (avg.) for all paints were obtained from the data plots and values are given in Table 3. The 9109 (metaborate) had a somewhat higher value of R_n (avg.) than the others. At the end of the test visually all the specimens rated 10 on the scale in Table 2 *i.e.* there was no visible rusting or blistering. DC resistance measurements made at the end were between 2×10^7 and 2×10^8 ohms-cm² with the metaborate paint having the highest resistance. Paint was stripped from two of the panels (molybdate and metaborate) and this confirmed that no attack had occurred.

EVCN : 185 hour in 2 M NaCl

There was a greater difference between paints both in their EVCN response and in their visual appearance. Most of the specimens blistered but the degree of blistering varied and

I_m and R_n values over the first 110 hours for a paint that showed minimal blistering *i.e.* 9102 (molybdate), are shown in Figures 5 and 6. On the same figures are plots of I_m and R_n for a paint that showed considerable blistering *i.e.* 9109 (metaborate). These plots show that the more highly blistered paint had higher I_m but lower R_n . Currents were generally higher than in dilute Harrison's solution. The average I_m and R_n values and visual assessment values for all five paints are given in Table 3. It was noted that the degree of blistering was often different on the two specimens which constituted one probe. Subsequent DC resistance measurements were in qualitative agreement with the R_n value at the end of the test. This DC resistance also differed between the two specimens with the one which showed the greater degree of blistering having a resistance between 2 and 10 times lower than the other. The paint was stripped from half of each of the ten panels. No immediately visible corrosion was observed. When further data are obtained it may be possible to correlate the sudden changes observed on the graphs with the onset of blistering.

Cyclic Salt Spray Test : 350 Hours

Results for visual observation of these specimens are given in Table 4. In general there was negligible attack on the face but heavy attack on the scratch. DC resistance measurements on small areas of the face at the end indicated a uniform high resistance ($> 1 \times 10^8$ ohms-cm²). The DC resistance of the scratch varied from 1.5×10^4 to 1.5×10^5 . The specimens with lower DC resistance showed more corrosion.

Hot Salt Bath Test : 170 hours

Results of visual observation of the face and at the scratch at the end of the test are also given in table 4. Here there was clear differentiation between the paints in terms of attack on the face and fairly good separation in terms of attack on the scratch. Subsequent DC resistance measurements (at RT) again correlated well with visual observation with values varying from $R > 1 \times 10^8$ ohms-cm² (chromate) to the $R < 1 \times 10^6$ ohms-cm² (metaborate).

Discussion

Electrochemical Noise Method

EVCN has been demonstrated to be a potentially useful technique for monitoring these alkyd primer paints on steel. Although none of the tests in dilute Harrison's solution at RT caused corrosion or blistering, the data obtained are useful as a record for this situation. In previous work⁷ (in 0.6 M NaCl) the currents were similar but the R_n values were higher when no corrosion occurred. The observed relatively low value of R_n might be a pre-cursor to later corrosion or it might be a consequence of having a not particularly impermeable (to ions) paint in a quite dilute (1/10 the ionic concentration of sea water) solution. The steady value of R_n militates in favor of the latter. It seems likely that all these paints would continue to protect steel for many months under these particular test conditions. The higher resistance of the metaborate paint may be due to its greater thickness (Table 1).

Results of EVCN in 2 M NaCl are more interesting. On several of the specimens the noise current is high and the R_n value low. This corresponds with those specimens which have noticeably blistered. Generally this paint appears to be sufficiently water permeable so that in high ionic strength solution, blistering can occur. This may well lead to subsequent corrosion. In this case the degree of protection is more dependant on the pigment. The relatively poor performance of chromate paint is worthy of comment. This pigment is somewhat soluble and may attract water to the interface. Apparently with this particular formulation and drying method the adhesion is not high enough to prevent what is probably osmotic and/or electro-osmotic blistering. The phosphate and molybdate gave better protection. These pigments are less soluble and therefore less likely to lead to osmotic blistering.

There is more information available in the data obtained during the EVCN experiments. This may be interpreted in terms of onset of blistering, changes in mechanism of protection etc. At the time of writing this data still await analysis.

The blanking-off method used here has proved very successful. Apart from being more convenient, experiments on the effect of flow can be conducted by stirring the solution. Also the solution temperature can be easily raised *e.g.* to 40°C or 50°C. This will greatly accelerate ionic permeability through the coating¹¹.

Accelerated Tests

The Cyclic Salt Spray Test was only run for a relatively short time with these specimens. Results confirm what had been observed in the EVCN immersion test that the intact paints, even at 40°C and cycling, all provide good protection in dilute Harrison's solution. This type of Cycling test however caused very severe attack at the scratch in even a short time. There was some difference in the behavior between specimens but none of them did well.

The Hot Salt Bath Test put the paints in the expected order viz chromate > molybdate > phosphate > metaborate > blank. The chromate pigment appears to prevent blistering under these conditions due perhaps to the higher temperature and lower ionic strength solution. Overall this test differentiated the primers well. Certainly if, in service a paint is likely to be exposed to a strong (1% or above) salt solution at temperatures of 30-40°C or higher then this test would appear to be an excellent choice. Paints exposed to direct sunlight can get quite hot (up to 65°C). For structures immersed in sea water where the actual temperature is unlikely to get above 30°C, the acceleration of ion transport produced by such a high temperature test justifies it.

Ongoing and Further Work

The above tests are being applied to a set of marine paints systems, both 2 and 3 coat systems. Immersion tests are in artificial sea water. Additionally some detached pieces of coating will have their ionic resistance behavior examined.

Conclusions

- 1) The feasibility of using the EVCN method with the CML equipment and with the new arrangement of cell design for continuously monitoring primer paints has been demonstrated.
- 2) In tests lasting 185 hr the EVCN method distinguished between paints which were blistering and those which were not. The value of R_p and I_m were particularly useful in this respect.
- 3) All five primers protected in dilute Harrison's solution which is about 1/10 the ionic strength of sea water. However blistering of some panels occurred within two weeks in 2 M NaCl.
- 4) Use of a Cycling Accelerated Test (2 hr RT spray on, 2 hr 40°C spray off) confirmed that these paints are not easily attacked or blistered on the face in dilute Harrison's solution. However they are all severely corroded at the scratch after a relatively short time (350 hr).
- 5) The Hot Salt Bath Test (170 hr at 55°C in N/2 NaCl) proved very effective at differentiating these paints.

Acknowledgements

Thanks are due to the Office of Naval Research for the Grant (ONR Contract No. N00014-93-1-0013) which made this work possible. Two undergraduates at NDSU Jeremy Jacobs and Peter Elliott have assisted on the experimental side. Rich Braun, an NDSU Graduate Student has been responsible for much of the accelerated test work. The assistance of Samy Abunaser on the computing side is also acknowledged. Finally, thanks are due to Charles Simpson (Sherwin Williams, Coffeyville) for providing the coated panels.

References

1. R.C.Bacon, J.J.Smith and F.M.Rugg, Ind. Eng. Chem., 40 (1948): p. 161.
2. J.P.Lomas, L.M.Callow, G.A.M. Sussex and J.D.Scantlebury, Mat. Sci Forum, 8 (1986): p. 327-350.
3. M.Metikis-Hukovic, E.Stupnisek-Lisac and M. Loncar, Bulletin of Electrochemistry 7 (March 1991): p 128-132.
4. D.A.Eden, K.Hladky, D.G.John and J.L.Dawson, NACE Corrosion Meeting March 1986, paper 274.
5. D.A.Eden, M.Hoffman and B.S.Skerry, ACS Symp. ser. 322 , Am. Chem. Soc. Washington D.C. (1986) : p. 36.
6. B.S.Skerry and D.A.Eden, Prog. Org. Coat., 15 (1987): p. 269-285.
7. B.S.Skerry and D.A. Eden, Prog. Org. Coat., 19 (1991): p. 379-396.
8. C.H.Simpson, Private Communication , March 1993.
9. C.H.Simpson, C.J.Ray and B.S.Skerry , J. Prot. Coat. Lin., 8 (May 1991): p 28-36.
10. D.J.Mills and P.J.Boden , Corrosion Science, 1993 : in press
11. D.J.Mills and J.E.O.Mayne, JOCCA, 65 (1982): p 138-142

Table 1: Thickness of Paints on all Test Panels (d.f.t.)

Exposure To/In	Panel	Paint Thickness in μm (avg. of ten readings)				
		Molybdate	Phosphate	Chromate	Blank	Metaborate
EVCN/ dilute Harrison's	ci	-	57 (+/- 2.3)	50 (+/- 1.8)	54 (+/- 1.3)	-
	di	50 (+/- 2.9)	51 (+/- 1.9)	50 (+/- 2.6)	54 (+/- 3.0)	60 (+/- 2.1)
EVCN/ 2 M NaCl	ai	40 (+/- 2.5)	43 (+/- 1.2)	53 (+/- 8.7)	40 (+/- 1.5)	57 (+/- 2.1)
	bi	65 (+/- 20)	43 (+/- 1.6)	40 (+/- 3.8)	54 (+/- 13.2)	42 (+/- 1.5)
Cycling Salt Spray	cii	50 (+/- 7)	46 (+/- 3.2)	44 (+/- 4.0)	39 (+/- 4.1)	46 (+/- 5.4)
	dii	43 (+/- 5.4)	43 (+/- 4.6)	45 (+/- 6.8)	45 (+/- 5.3)	42 (+/- 2.3)
Hot Salt Bath	aii	45.9	37.6	-	47.4	45.9
	bii	43.0	41.1	35.2	44.9	39.0

Table 2: Corrosion/Blistering Scale from Appearance

Value	Scratch
1	severe spread (several mm), heavy corrosion
2	severe spread in places, moderate corrosion
3	moderate spread (two mm), quite severe corrosion
4	some spread (up to 1.5 mm) in places, mod. corrosion
5	some spread (up to 1.5 mm) in places, some corrosion
6	only a little spread (1 mm or less), some corrosion
7	little spread, little corrosion
8	slight spread, (0.5 mm), slight corrosion
9	slight spread, virtually no corrosion
10	no spread, no corrosion
Value	Face
1	multiple blisters (60), rust, extensive loss of adhesion
2	lot of blisters (eg 40), some adhesion loss
3	lot of blisters but very little adhesion loss
4	several largish blisters plus some adhesion loss eg from edge
5	scattered but fairly numerous (eg 20) blisters
6	few blisters (10)
7	only a few blisters (< 5)
8	a very few isolated blisters
9	one or two isolated blisters
10	zero blisters and no corrosion or adhesion loss

Table 3: Electrochemical and Visual Results for EVCN Specimens

Paint	250 hours in dilute Harrison's			185 hours in 2 M NaCl		
	I_m^* (avg.)	R_p^+ (avg.)	Visual Assess. (2 panels)	I_m^* (avg.)	R_p^+ (avg.)	Visual Assess. (2 panels)
Molybdate	1×10^{-7}	8×10^5	10,10	3×10^{-7}	6×10^5	8,7
Phosphate	1.5×10^{-8}	1.3×10^6	10,10	1×10^{-7}	2×10^5	6,5
Chromate	2×10^{-8}	5×10^5	10,10	1.2×10^{-6}	3×10^5	5,3
Blank	2.5×10^{-7}	1×10^6	10,10	2.5×10^{-7}	3×10^5	5,4
Metaborate	1×10^{-9}	1×10^7	10,10	1.5×10^{-6}	4×10^{5x}	3,2

* units : amps

+ units : ohms-50 cm²

x ($1 \times 10^5 \rightarrow 1 \times 10^6 \rightarrow 1 \times 10^5$)

Table 4: Accelerated Test Results

Paint	Cycling Salt Spray (350 h) Protection Rating*		Hot Salt Bath (165 h) Protection Rating*	
	face	scratch	face	scratch
Molybdate	10	4	8	3
Phosphate	10	2,3	7	6
Chromate	10	4,5	9	8
Blank	10	2,3	5	5
Metaborate	10	2,3	6	4

* For scales used, see Table 2. Same for both panels unless indicated

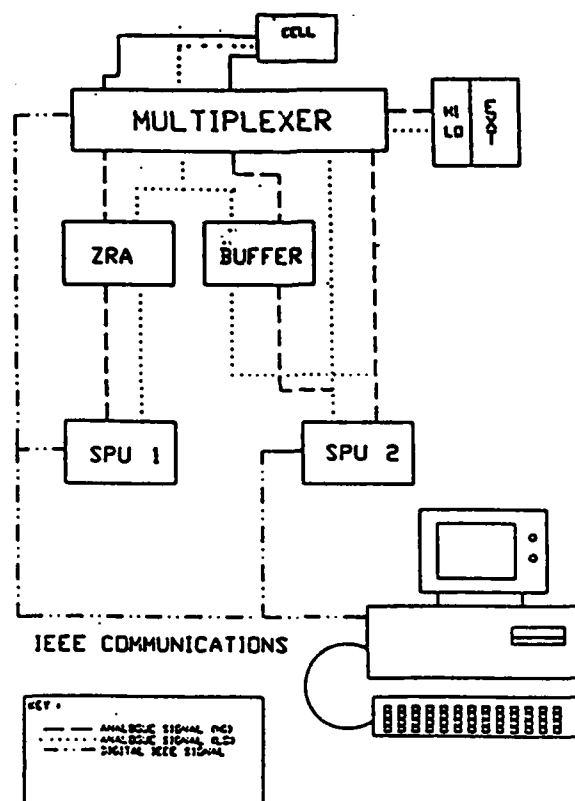


Figure 1: Block Diagram of the Electrochemical Noise Monitoring Instrumentation

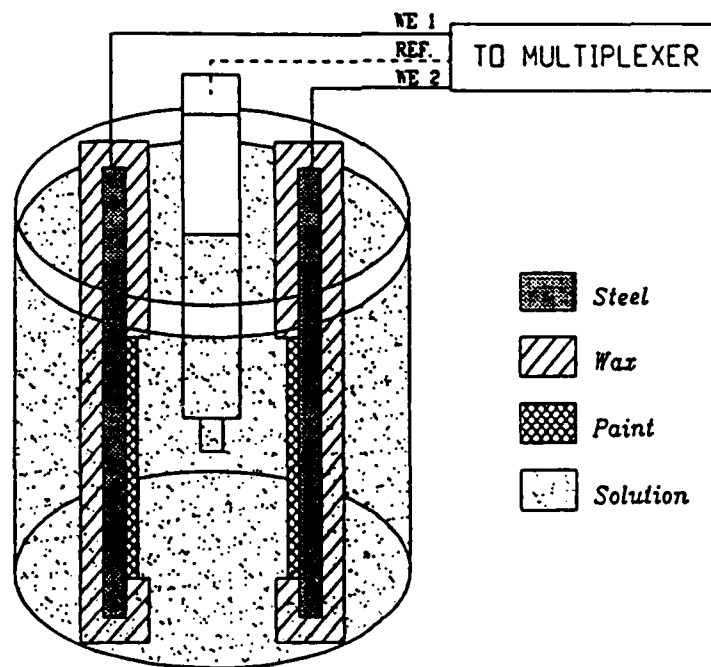


Figure 2: Cell Arrangement for Measuring Electrochemical Noise

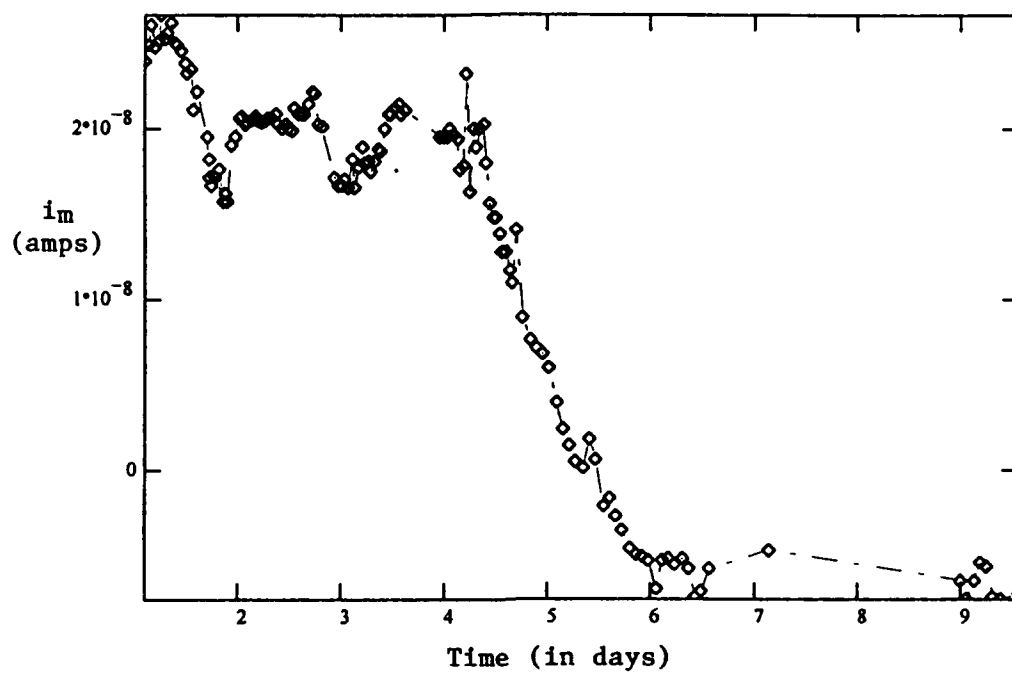


Figure 3: Mean Current vs time for Phosphate paint (probe 2) in dilute Harrison's solution

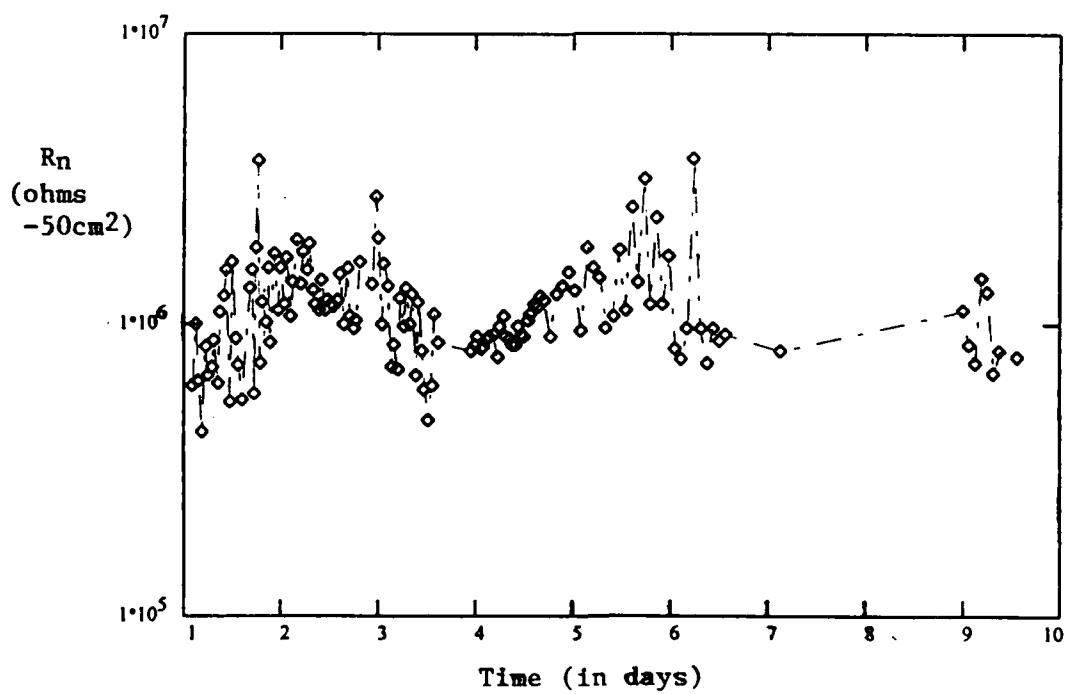


Figure 4: Resistance Noise vs time for Phosphate paint (probe 2) in dilute Harrison's solution

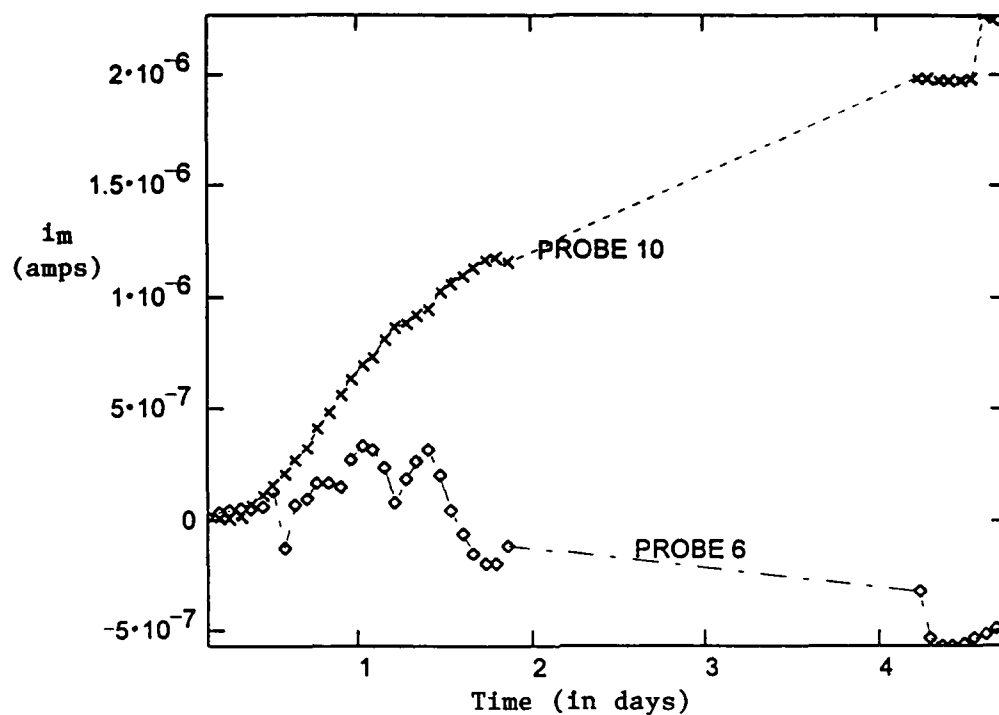


Figure 5: Mean Current vs time for Molybdate paint (probe 6) and Metaborate paint (probe 10) in 2M NaCl

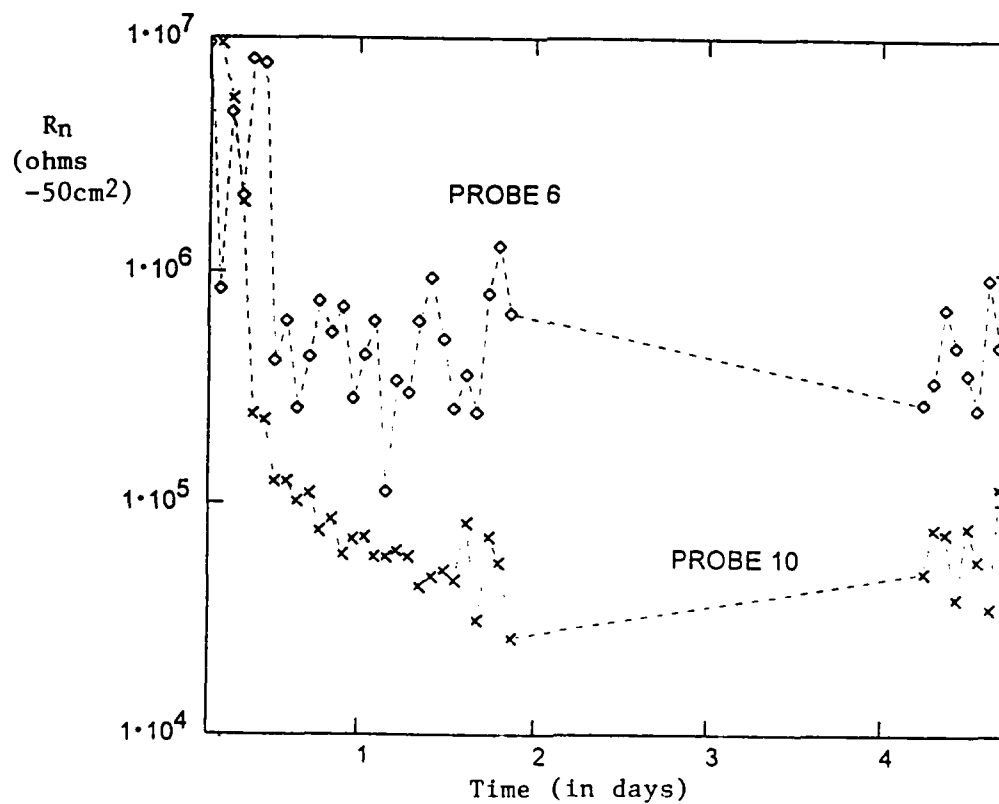


Figure 6: Resistance Noise vs time for Molybdate paint (probe 6) and Metaborate paint (probe 10) in 2M NaCl

NEW ACCELERATED TEST SIMULATING THE ATMOSPHERIC UNDERCOAT CORROSION

by Aldo Martello

abstract

The well known Salt Spray Test ISO - 7253 - 1984 and ASTM - B - 117 is not reliable for simulating the undercoat corrosion.

We have developed a new test feasible to reproduce the natural atmospheric undercoat corrosion with high fidelity, the same we find on the old painted facilities exposed outside in natural environment.

The new test simulates the natural environmental conditions as close as possible alternating spraying and drying phases.

The new test has been approved by Italian National Standard UNI - 9590 - 1985.

In addition using the same test cabinet with different environmental conditions we developed a new reliable test, simulating the undercoat filiform corrosion on steel and aluminum: test UNI - 9399 - 1984.

Both tests are accepted by ISO Standard TC - 35 as new designs.

Cabinet is named: **DRY CORROSION TEST CABINET** ®.

The same can be used for traditional salt spray tests.

Introduction

In this report I can make what I believe to be an important statement: "The old salt spray corrosion test, that everyone is familiar with, has been definitely sentenced to be no more considered such as a corrosion test"

This is not new because others, that have more authority than us, have stated the same.

ISO standard 7253 (1984) pronounced the same sentence 7 years ago and was approved by all the member states.

Before leaving this old test, another one had to be found to replace it, with advantages which would correct the defects of the old one.

Only with such advantages it can be said that the old test is really finished.

We are presenting this new test.

The automotive

The automobile, invented about 100 years ago, has become the most important and most commonly used means of transport in both industrialized and developing countries.

The expenses of a car are second only to the expenses for a house and it is likely to overtake it. But this product has a short life durability.

Efforts to make it last longer have met many obstacles. These efforts continue.

The life of the body, the only component which cannot be replaced, characterizes the life of the car. It is exposed to the destructive limits of atmospheric corrosion on the road.

Body corrosion is therefore important and it is a challenge to all automotive builders. Competition between builders is fought out on this ground, the life of the car being identified with its resistance to corrosion.

In marketing cars, the corrosion resistance has become the most important feature of guarantees.

Anticorrosion commitment

The fight against corrosion involves all the factors of automotive engineering from the birth of the project to the metallurgy, mechanics and components.

Materials other than iron are often used to prevent corrosion such as aluminum, zinc and plastic. Nevertheless, paint remains the principal element in this fight and it can be said that "corrosion begins where the paint ends".

Some of the structural parts of the body have tiny surfaces and gaps where the paint hasn't reached or isn't enough. It's difficult for the protective oils and waxes to reach these areas. When they reach them, sometimes they are not enough to be effective. Add to these problems the stone chips and scratches that damage the paint during use.

From these damaged or little protected points, the corrosion process starts and increases by road pollutants, weather factors and humidity. It is humidity, characterized by continuous wetting and drying, that is the main cause of corrosion. Iron oxide increases into voluminous microgranular forms that swell underneath the paint causing scabs and filiforms. This process continues until the substrate is destroyed.

The volume of iron oxide produced is about 10 times greater than the volume of oxidized iron. This is what makes the paint swell into small scabs. The scabs grow and split the overlying paint. Corrosion expands from these scabs and invades the substrate under the paint. Once this process starts it is practically impossible to stop it.

Attempts have been done to stop it by increasing the adhesion of the paint, the overall thickness of the paint, the metallurgical quality of the substrate or by using special surface treatments. All these attempts have been able to slow down this process but not eliminate it entirely.

To eliminate the wet and dry process completely, water repellents, waterproofer and corrosion inhibitors are necessary. But this is a field for future research on paint formulation surface treatment.

Simulated Tests

The electrochemical phenomenon of corrosion, its propagation under the paint film and the need to prevent it constituted the main subject of my previous work as a paint formulator for 30 years.

The environment in which a car operates is substantially different from that of a static laboratory test. However when the laboratory test meets certain requirements of reliability and is followed by a correct and careful evaluation, it becomes fundamental and irreplaceable as a key to predicting the life of a product which operates in a corrosive atmosphere. There are two points, mentioned further on, that are fundamental and essential for obtaining the results we have set.

Why the salt spray test is bound for extinction

The salt spray test is no longer reliable for two reasons:

1st it reproduces only one type of wet corrosion which seldom occurs in the different atmospheric environment;

2nd it simulates static temperature conditions, that in any case, are too low.

For these reasons the environmental conditions reproduced by the test are incapable of developing the microgranular, powdery corrosion consisting of insoluble iron oxides that we find on the product exposed to atmospheric corrosion.

The salt spray produces water-soluble iron hydroxides which cannot be transformed chemically into insoluble powdery oxides because the temperature is excessively low. Moisture is always present, ready to remove the water-soluble hydroxides as soon as they are formed.

So, once again, we repeat that the simulated environmental conditions of the salt spray test are absolutely different from the environmental conditions in which the automobile is used. For this reason, the test is no longer valid. The lab technicians have no choice but to remove their equipment from the laboratory or ship it off to an antique museum.

We have, however, taken two important characteristics from the salt spray test:

1st it is simple and repeatable;

2nd it is the most widely used and approved corrosion test found in laboratories everywhere in the world.

That is why we have decided, if possible, not to abandon these two advantages.

Therefore, we started from this type of equipment and developed another one which serves as a substitute to predict the behaviour of materials during use. Man has gone to the moon exploiting knowledge acquired through simulated tests on the ground and in laboratories.

This however was only possible under the following conditions:

1st the tests had to be reliable

2nd they were carefully and correctly evaluated

These are the 2 basic, absolutely essential, criteria for obtaining the results we have set; these are the criteria which have guided our research and given such excellent results.

We started from this type of equipment to develop a new test that would effectively replace it without losing the advantages of the old. There is nothing new in this.

Countless attempts have been made in the past to modify the salt spray test. Research laboratories throughout the world have studied it. But in my opinion the results have been very disappointing and not reliable.

The changes carried out have not been successful because they were conceived to maintain functioning as it was. They only concerned the salt concentration or alternate spraying and non spraying phases, or replaced with static moisture tests.

The reason why they haven't been successful is that they are too similar to the old tests. They haven't taken into

consideration, how important it is to reproduce the results in the field.

Our research has been oriented towards the results in the field. For this reason we started with a given objective: reproduce as closely as possible the results of corrosion found on the product.

In other words we started from the need to imitate, as faithfully as possible, the corrosion found on the product during actual use.

To do this, we had to use equipment which might also, but not necessarily, resemble a salt spray cabinet.

We succeeded in obtaining the result we had set for ourselves by making changes, which would preserve the form of the cabinet but substantially change others all other features.

We are satisfied with the results and happy to leave the old salt spray test without any regrets.

We are happy that the 78 years old test, created in 1914, can finally be retired with the approval and blessing of all those who used it.

It was useful in the past, but the time has come to move on.

The automotive industries and the Scab Corrosion tests

The automotive industries under the stimulus of commercial guarantees against corrosion: first the "passing through", and then the cosmetic, were forced to invent new simulations, because they could no longer trust the old salt spray test.

They soon realized, however, that while the new Scab Corrosion tests had improved there were still too many limitations and shortcomings. We asked the main automotive companies that use these tests (VW, Renault, General Motors, among others). All of them gave us the same opinion: "we are not happy with our test but we have to use it until we find a better one."

Now this better test, designed to satisfy the car industry engineers, actually exists and it is the one we are presenting to you. This is not our opinion, but it is supported by 250

zinc-coated steel which is widely used today in automotive manufacturing.

In the case of the zinc-coated steel, the method is important for evaluating adhesion of the painting system to the substrate. The adhesion of a painting system to the zinc-coated and phosphated steel is an important factor for the automotive industry.

In this case our test can give more useful and reliable data than those provided by the microscope. For this reason it can be used to advantage by all those who today are still using the salt spray test and observe the results under the microscope.

DRY CORROSION TEST CABINET®

figure 6

Dry Corrosion Test Cabinet is a trade mark registered by Angelantoni Climatic Systems S.p.A. who developed the equipment in its current form. DRY CORROSION is a contrast to the WET CORROSION of the salt spray test.

The equipment looks like a salt spray system. It functions by alternating the spraying of a low-concentrate salt solution with air drying. It is during the drying phase that it develops corrosive aggression. In this phase the soluble iron hydroxides are transformed into insoluble iron oxides, similar to powder, that gradually swell under the paint.

That's how the system got its name. However, we wish to emphasize that the old salt spray test and its derivatives can still be carried out with this equipment. This was done to satisfy all those who must still use the old tests because they are required in paint purchasing and by specifications.

Again, it is important to remember that the equipment, by setting up a different operating cycle, serves to perform a test for filiform corrosion separately from scab corrosion. The filiform corrosion test was approved by national Italian standards UNI 9399-1984.

Filiform corrosion test UNI 9399-1984

- ☐ duration of the test;
- ☐ repeatability of the test;
- ☐ amount of equipment used;
- ☐ manual operations during the test.

In determining the reliability of the test results, these points were considered:

- ☐ similarity of the corrosion with that observed "on" the product;
- ☐ similarity of the results with the test samples exposed outdoors in different locations on land and seaside;
- ☐ similarity with the results of the Volvo method.

The UNI 9590 method gives the number of hours it takes for the corrosion to pass through the steel.

This parameter is important in guaranteeing the automotive and in evaluating the quality of the steel used for stamping the body. The results reported in the table show how the UNI 9590 method is clearly better than others. It can also be used as a substitute for all the others to the satisfaction of technicians and everyone else concerned.

If we had to evaluate the old salt spray we would give it the following score:

- * 8 points for the method
- * 2 points for the results

We say that the salt spray test was used to measure the corrosion resistance of bare metals, while its use for painted substrates was an adaptation and therefore a compromise. This matter was discussed at the last meeting of the ISO (International Standard Organization) in Pretoria in May 1991 which I attended as member of this organization.

The UNI 9590 method can also replace the salt spray test for bare steel corrosion. This method is also very effective on

manufacturers using it, first among them the producers of automotive and industrial vehicles in Italy.

Some of these industries had been using the Scab Corrosion tests applied by the world's leading automotive industries, but they left and replaced them with ours because they got better results. Our new test equipment is named the DRY CORROSION TEST CABINET®. We'll explain this name further on.

Comparison of simulated Scab Corrosion tests (fig. 1)

The automotive manufacturers use different methods.

Each one of the five groups listed below uses its own method of testing Scab Corrosion:

1. Swedish group method Volvo
2. American group method APG-G.M:
3. German group method VDA-VW
4. French group method Renault-PSA
5. Italian group method Ferrari-PPG-FIAT-IVECO

I had to repeat all these tests many times during the 30 years I worked for a leading international paint producer that supplied automotive companies belonging to these groups or to their licensees.

We examined the methods to make a comparative evaluation. We were as objective as possible, considering the limitations and possibilities of error.

The results of our evaluations agree with the opinions I received in interviews with engineers from the above groups.

Parameters of evaluation

We evaluated the methods and the reliability of the laboratory results compared to field tests.

In evaluating the method, the following points were considered:

Compatibility of Organic Coatings with Flame Spraying Zn, Al and Zn-Al Alloy Coatings

Xin Zhaoqing
Wuhan Research Institute
of Material Protection
PO BOX 430030
Wuhan, China.

Abstract

They were studied Electrochemical Impedance Spectroscopies (EIS) of the specimens of organic coatings that are polyurethane, epoxy-polyurethane, epoxy-coaltar and copoly vinylacetal-vinyl chloride etc based on spraying Zn, Al and Zn - 15Al alloy coating in 3% NaCl solution. During 1200 hours galvanic current between the polyurethane coating defect specimens in 3% NaCl solution was measured. Salt fog 4000 hours, sea water immerse and splasa zone two years test were made. The results show: compatibility of the Organic coatings with spraying Zn and Zn-15Al coating is wide ranging. compatibility of the organic coatings with spraying Al depend on if containing a appropriate inhibitor in the coatings. In studing coating system, compatibility of wash primer+chromate primer+polyurethane or epoxy-polyurethane paint with spraying Zn, Al as Zn-15Al alloy coatings is best in the test conditions.

Key terms : sea water, compatibility, organic coating, spraying metal coating.

Introduction

From half of the century steel structures against corrosim by flame spraying Zn, Al and Zn-Al alloy coatings subsequently brushed with organic coatings has achiered good results. But it requeres a great deal of further research in the area of compatibility of organic coatings with spraying Zn, Al and Zn-Al alloy coatings.

The studing results of America Navy had shown organic paints on flame sprayed Zn were better than the same paints on steel and far superior to the same paints on flame-sprayed Al. When the paints blistered and be gan to fail the zinc provided protection from rusting and did not deteriorate the paint. Surprisingly, the sprayed Al coatings were degraded by the app-

-lication of paints. sprayed Al rapidly degraded the paint and in turn was degraded when the paint began to fail. Definitive and mechanistic studies are needed of the interaction between sprayed-Al coatings and organic top-coat paint in marine environments [1]. Koehler [2] had studied galvanic current between organic coating defect and bare aluminum in air saturated PH 3.5 0.5% NaCl at 100° F. In all cases, the bare aluminum became cathodic to the anodes developing under the organic coating from the point defects. Leidheiser [3] had studied rate controlling steps in cathodic delamination of 10 to 40 μ m thick polybutadiene and epoxypolyurethane coatings from metallic substrates of aluminum, steel and zinc (galvanized steel). Cathodic delamination was negligible, relative to steel and galvanized steel in all electrolytes when aluminum was used the substrate.

Above information suggests that compatibility of organic coatings with Al is different from Zn which are used the substrate. But the informations of iron and steel structures against corrosion by spraying Zn and Al coatings show that pay great attention to different compatibility is insufficient [4, 5, 6, 7].

This work deals with the following problems through electrochemical impedance spectroscopies, galvanic current tests, salt fog tests and sea water expose tests: We studied compatibility of the organic coatings that are polyurethane, epoxy-polyurethane, epoxy-coaltar and copoly vinylacetal-vinyl chloride etc. with the spraying Zn, Al and Zn-15Al alloy coating. The effect of the inhibitors containing in primer on compatibility is studied. It is obtained that the organic coatings which are compatible with the spraying Zn, Zn-15Al and Al coatings.

Experimental Method

A. Specimens

The size of specimens is $5 \times 10 \times 0.3$ (for EIS and salt fog test) or $10 \times 20 \times 0.3$ cm (for sea water test). The front and back sides and four edges of the steel (containing 0.2% c) specimens are sprayed with 150-200 μ m thick Zn, Al and Zn-15Al alloy coatings by means of flame spraying with pure Al (99.7%) wire, pure Zn (99.9%) wire or 85% Zn-15% Al alloy wire. The spraying technology is based on standard method. The paint is brushed on the front and back side of the spraying specimens. Two primers i.e. chromate primer and phosphate primer are selected to compare the inhibitive results of the different pigments in the primers. The coating with chromate primer is brushed with prephosphorized wash primer first, while the coating with phosphate primer is directly brushed with the phosphate primer without prephosphorized wash primer. The total thickness of painted film is controlled by the layer of painted film.

One layer of primer one add layer of paint its thickness is about $60\mu\text{m}$. Two layers of primer add two layers of paints its thickness is about $120\mu\text{m}$.

B. EIS

EIS was measured by Solartron 1250 transfer function analyser. The cell is a rectangle box. the auxiliary electods are two 316 stainless steel tubes. The test solution is 3% NaCl.

C. Galvanic Current Test

Just before the experement was intiated, the center of the specimen was damped by pressing a pointed instrument into the organic coating. The exposed sprayed metal diameter approximately 0.01cm. The defect specimen and corresponding bare sprayed metal coating specimen were immersed in 3% NaCl. The galvanic current was measured by PARC 350 A corrosion measure-ment system.

D. Artificial Sea Water Immersion and Salt Fog Alternate Test.

Artificial sea water was made by ASTM D1141-75. Salt fog test in SUGA ISO test box (Japan) made accord with ISO 3768. During 24 hours every day spraying fog is continuous. The experement was conducted alternally by immersion test 1000 hours and salt fog test 1000 hours.

E. Sea water immersion and splash zone test.

The lacate of the test situated in the San Yia city i.e. $18^{\circ} 23'$ north latitude and $109^{\circ} 35'$ east longitude. Sea water immersion test. the speci-mens are put 0.2-1.5m below sea water surface. Splash zone test the spe-cimensare put 0-0.5m above average high tide line.

Results and Discussions

A. Electrochemecal Impedance Spectrosopies (EIS):

They were studied EIS of the specimens of organic coatings that are polyurethane (PU), epoxy-polyurethane (EU), epoxy-coaltar (ET) and copoly vinylacatal-vinyl chloride (VN) ect based on spraying Zn, Al and Zn-15Al alloy coating in 3% Nacl solution. During immersing at 7, 60 and 100 day. the Nyquist and Bode plots measured can sum up 3 types. They are show re-spectively figure 1, 2, 3. The organic film resistance (R_p) and the undefilm corrosim electrochemical reaction resistance (R_t) was calculated respec-tively from Nyquist high and low frequence semicircle show the tabel.

Above rebults show: When above organic coatings (except VN) contain a phosphat-chromat inhibitor, ei. wash primer add chromate primer, they are compatible with the spraying Zn, Al and Zn-15Al alloy coatings. When the total thick of organic coatings is $60\mu\text{m}$, at 100 there is days, only the high frequency semicirde in Nyquist plots (figure 2), ei. one time constant, which represent the resistance of the organic film measured. the organic film resstance R_p is equated to or is more than $10^6\text{ohm} \cdot \text{cm}^2$. When the total thick of organic coatings are $120\mu\text{m}$. at 100 day. a complete Nyquist high

frequency semicircle can not be still measured (figure 1) estimating R_p is more than $10^9 \text{ohm} \cdot \text{cm}^2$. But when the organic coatings do not contain a appropriate inhibitor, i.e. there is only the phosphate primer, they are not compatible with the spraying Al coating. At the specimens are immersed 60 days, there are two time constances, i.e. the high and low frequency semicircle can be measured (figure 3), the organic film resistance calculated from the high frequency semicircle is equated to or is less than $10^6 \text{ohm} \cdot \text{cm}^2$, and blistering of organic film is observed. Low frequency semicircle shows underfilm corrosion of spraying Al coating. It is interested in that same organic coating specimens based on spraying Zn or Zn - 15Al alloy coating although occur the blisters at immersed 60 days, only the high frequency semicircle which represents the resistance of the organic film is measured, but it can not be measured the low frequency semicircle which represents underfilm corrosion of the Zn or Zn-15Al alloy coatings. The results show the electrochemical reaction had been led to the blisters of the organic film is stopped. Therefore above results can show different compatibility between the spraying Zn, Zn-15Al alloy and Al coatings with the organic coatings. It is taken note of adhesive strength of Vinyl film is very bad, therefore inhibitor in primer can not prevent underfilm corrosion of the spraying metal coatings.

B. Galvanic Current test

During 1200 hours galvanic current between the polyurethane coating defect specimens and corresponding bare spraying coating specimens in 3% NaCl solution was measured, the current-time curves shown figure 4, 5, 6. The results show: polyurethane coating defect specimens based on spraying Zn and Zn-15Al alloy coating are the galvanic cathode and a development of the damage does not observed at the defect of the polyurethane coating, no matter if the inhibitors are contained in the polyurethane coatings. But the polyurethane coating defect specimens which substrate is the spraying Al coating are the galvanic cathode or anode that depend on if containing a appropriate inhibitor in the polyurethane film. When the film contain appropriate inhibitor, i.e. wash primer add chromate primer, the specimens are the galvanic cathode, the development of the damage at the defect of the film is not observed. When the inhibitor in film is not appropriate, i.e. there is only phosphate primer, potential of the defect specimens transform from cathode to anode in galvanic cell, and it become stable anode, the polyurethane film blisters seriously and underfilm corrosion of the spraying Al coating is serious too. When there is not inhibitor in film, the defect specimen are anode, blister of polyurethane film and underfilm corrosion of the spraying Al coating are very serious. with the result that the underfilm corrosion rate of spraying Al coating is much greater than the free-corrosion rate of bare spraying Al coating. PH is 3-4 in the blister of the polyurethane film. It seems the underfilm corrosion

spraying Al coating is crevice corrosion. Direction of galvanic current reflect Al coating of under film is passivity or activity. There are only appropriate inhibitor in the organic film, the Al coating of under the organic film can keep stable passivity, the blister of organic film and underfilm corrosion of spraying Al coating do not occur, otherwise organic films not only can not protect the spraying Al coating, opposite they can accelerate the damage of the Al coating. Therefore the results of galvanic current tests prove furtherly different compatibility between the spraying Zn, Zn-15Al coating and Al coating with the organic coatings.

C. Artificial sea water immersion-salt fog alternate tests:

After artificial sea water immersion-salt fog alternate test for 4000 hours the test results of the specimens are shown table 1.

It is seen from Table 1 that the primer is one of the factors to decide the corrosion resistance of the entire painted film. It is seen from the comparison test that the specimens with prephosphorized wash primer and chromate primer coatings are much more resistant to corrosion than the specimens only with a phosphate primer coating, which is the same for the specimens either with Zn, Al coating as substrate or with Zn-15Al coating as substrate. When the total thickness is basically same, the former is generally 1-2 grades higher than the latter if grading according to the standard GB 1766-79. The points that best explains it are epoxypolyurethane system and polyurethane system. As for the specimens with 60 μ m thick painted film of prephosphorized wash primer+epoxy-polyurethane chromate primer+epoxy-polyurethane paint (or+polyurethane paint) after artificial sea water immersion-salt fog alternate test for 4000 hours, the majority exhibit no change on the surface except that the few exhibit several blisters on the surface. Thus being graded as excellent or good. When the film thickness is up to 120 μ m, there exhibits no change on the surface of specimen after tests, thus being graded as excellent. The specimens with 60 μ m thick painted film of epoxy-polyurethane phosphate primer and epoxy-polyurethane paint (or polyurethane paint) exhibit blisters in varying degrees on the painted film after tests, thus being graded as good or medium. When the total film thickness increases to 120 μ m, the majority of specimens reach to excellent grade, but part of the specimens exhibit blisters on the surface, thus being graded as good.

The vinyl film is sprayed with prephosphorized wash primer subsequently brushed with vinyl chromate primer and vinyl paint and is different from the aforesaid painted films for the breakdown. After the above-mentioned tests, the painted film peels off largely, but is still complete. When the peeled zone of the film is cut by blade, the inside of the film is full of liquids and the prephosphorized wash primer film on the surface of specimen is still visible. All this shows that vinyl film peels off the prephosphorized wash primer and the entire painted film may be torn off the

specimen. The above tests demonstrate that the binding force of prephosphorized wash primer film with vinyl primer film is very poor because of the lack of heteropolar bond in the vinyl resin, which results in the poor adhesion on the painted film and restricts the application of the painted film.

Above results of salt fog tests show identical law on compatibility organic coatings with the spraying Zn, Al and Zn-15Al alloy coatings. But the results of salt fog tests can not reflect accurately different compatibility such as EIS and galvanic current test, because underfilm corrosion can not be measured by means of the salt fog.

D. Sea water immersion tests:

The results of the sea water immersion and splash zone test are shown table 2. It is identical with the results of the salt fog tests. When the wash primer+the chromate primer+polyurethane or epoxypolyurethane painting, its total thick is $120\mu\text{m}$, the organic coatings are compatible with Zn, Al and Zn-15Al alloy. After two years, the organic coatings on the specimens are excellent. But when there is only phosphate primer, the blister of the specimens occur, but underfilm corrosion of the spraying Al coating is not enough to develop serious crevice corrosion during two years, it is possible that the inducing time of crevice corrosion of the spraying Al coating is more than two years.

Conclusion

The results of EIS and galvanic current tests show: compatibility the organic coatings with flame spraying Zn and Zn-15Al alloy is wide ranging in 3% NaCl solution, but for spraying Al coating, only when there are appropriate inhibitor (phosphate-chromate) in the primer, the compatibility is very good, otherwise spraying Al rapidly degrades the paint and in turn is degraded when the paint begins to fail. The corrosion of sprayed Al is crevice corrosion. Compatibility of wash primer +chromate primer+polyurethane or epoxy-polyurethane paint with spraying Al, Zn and Zn-15Al alloy coating is best. Salt fog 4000 hours test, water immerse and splash zone two years test show identical law.

Acknowledgements

I wish to acknowledge my debt to the fund commission of the machinery electron industry ministry provided the support for the study and permit to publish the paper. I wish to acknowledge my debt to Mr. Zhang Yue, Mr. Jia Jianxin, Mr. Xiang Nengquan, Mr. Hu Yongquan who participated in a part of work.

References

1. Metallized coatings for corrosion control of naval ship structures and components, NMAB-409, National Academy Press, Washington, D.C. 1983. pp. 35-36.
2. E. L. Koehler, Localized corrosion, NACE 1974, p. P. 117.
3. H. Leidheiser, jr and W. Wang, Corrosion Control by Organic Coating, NACE, 1981, P. 70.
4. F. W. Gartner, 8th International Thermal Spraying Conference.
5. J. C. Bailey. idem.
6. R. Bensimon, idem.
7. BS 5493:1977, code of practice for protective coating of iron and steel structures against corrosion.

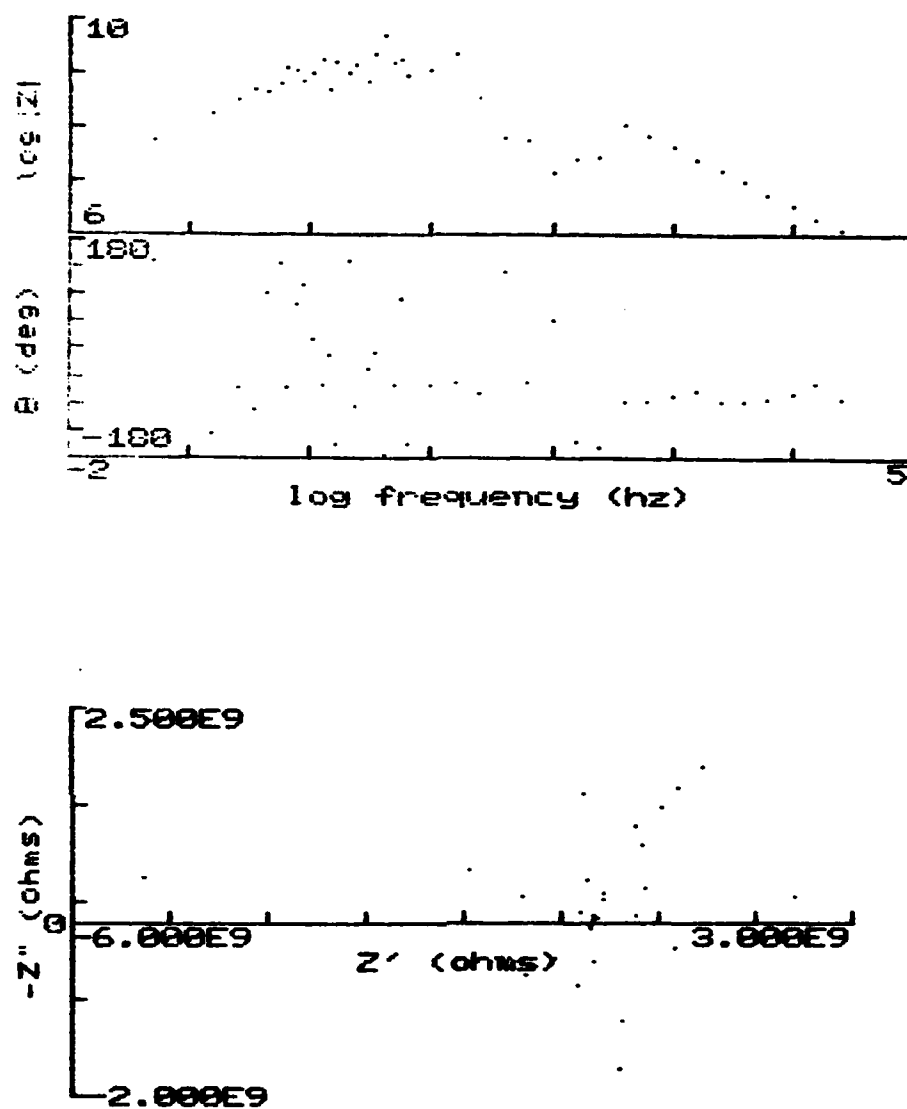


Figure 1. EIS, R_p is more than 10^9 ohm.

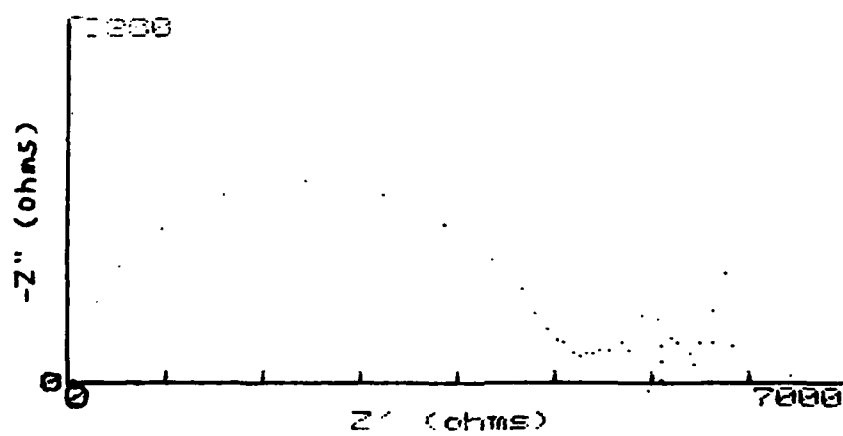
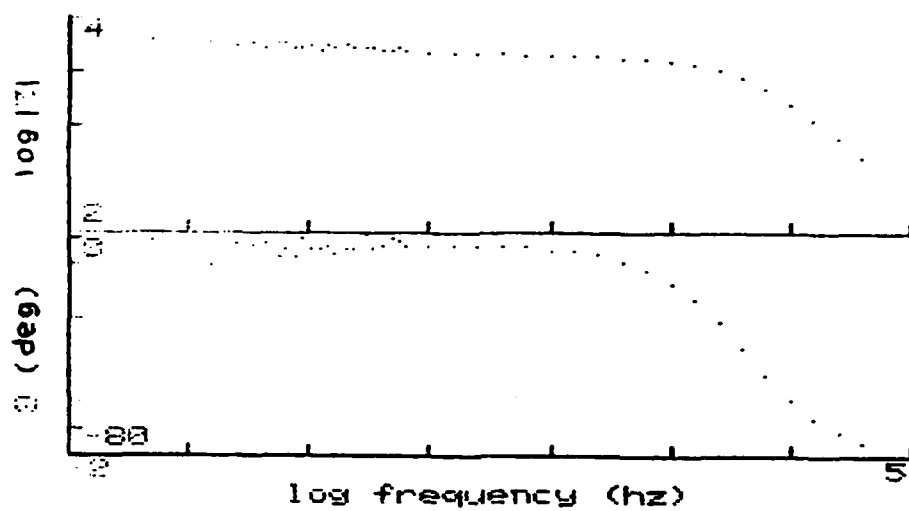


Figure 2. EIS, One time constant.

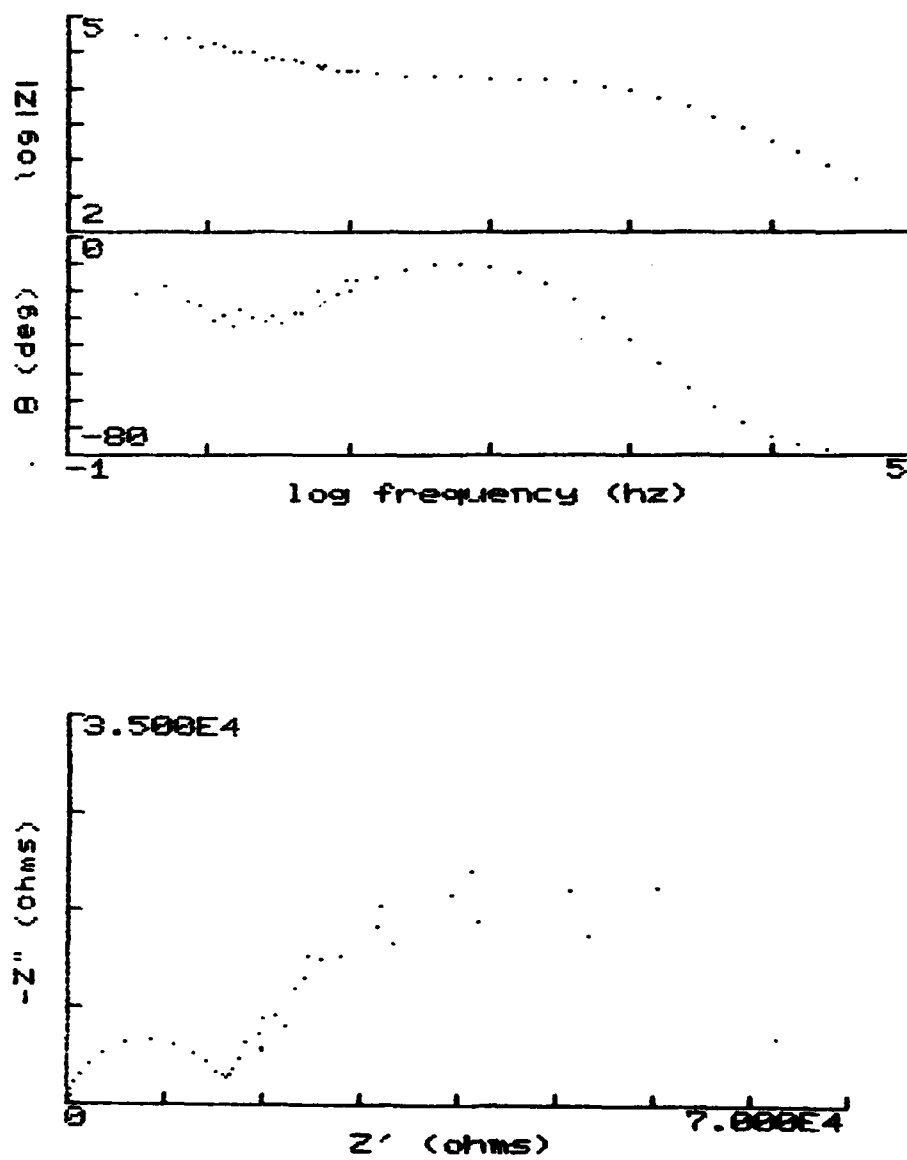


Figure 3. EIS, two time constant.

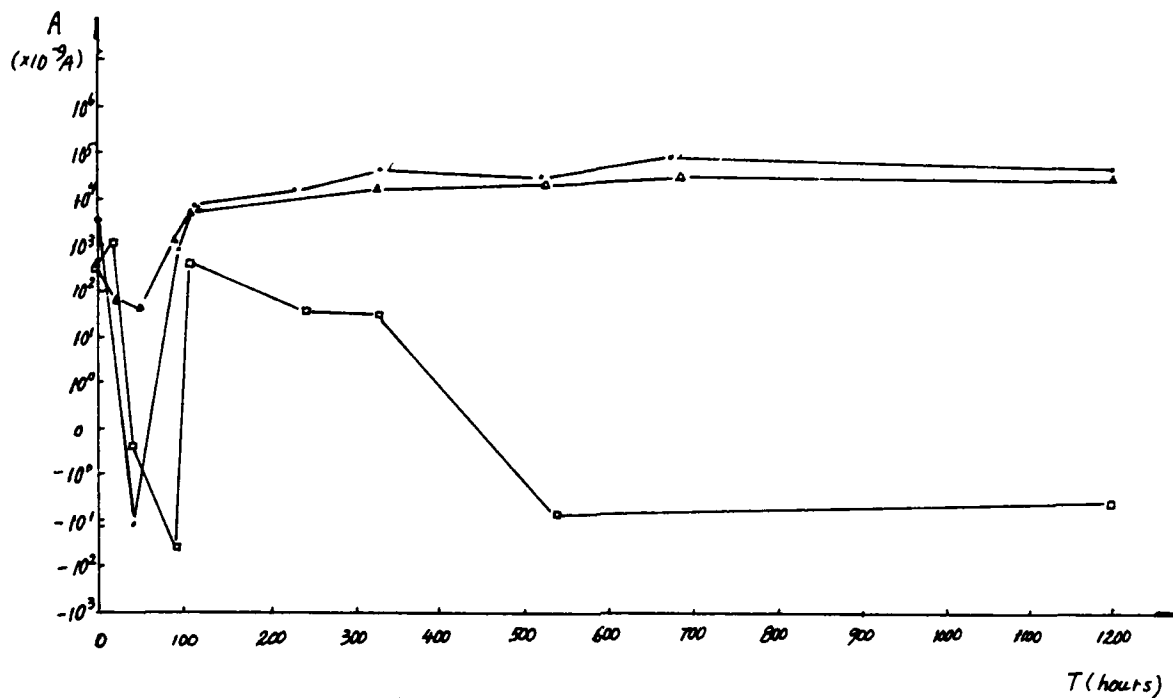


Figure 4. Galvanic current-time curve.

sign	organic coating electrode	bare spraying metal electrode
—□—	AISP+EP+EUZC × 1+PU × 1	AISP
—•—	AISP+EUZP × 1+PU × 1	AISP
—△—	AISP+PU × 2	AISP

Note. AISP: spraying Al coating

EP: wash primer

EU: epoxy-polyurethane

PU: polyurethane

ZC: chromate

ZP: phosphate

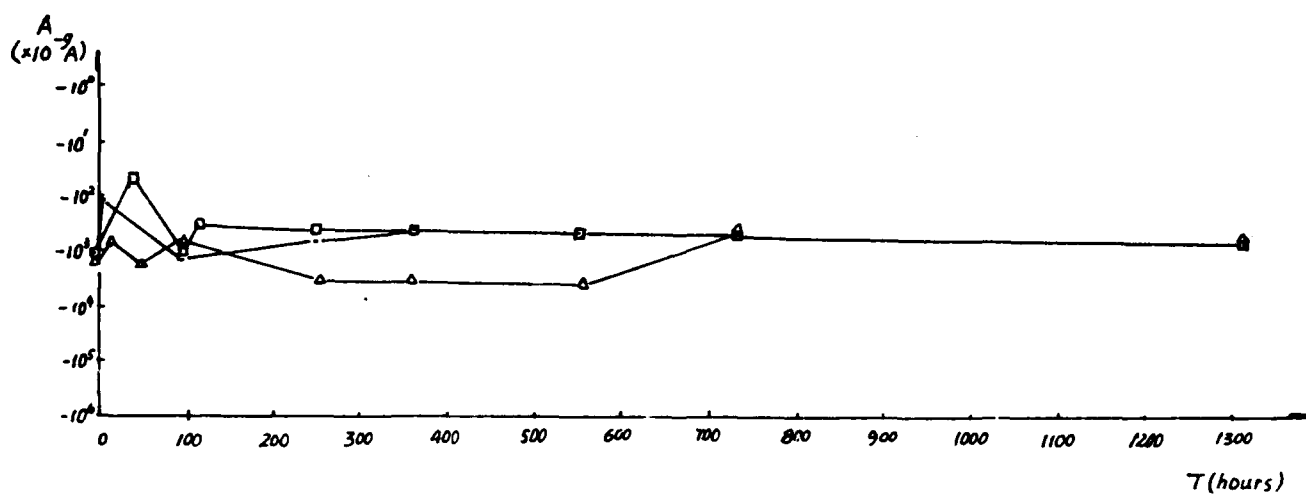


Figure 5. Galvanic current-time curve

sign	organic coating electrode	bare spraying metal electrode
—□—	Zn-AISP+EP+EUZC \times 1+PU \times 1	Zn-AISP
—•—	Zn-AISP+EUZP \times 1+PU \times 1	Zn-AISP
—△—	Zn-AISP+PU \times 2	Zn-AISP

Note. Zn-AISP: Zn-15Al alloy sprayed coating
other are same with note of figure 4.

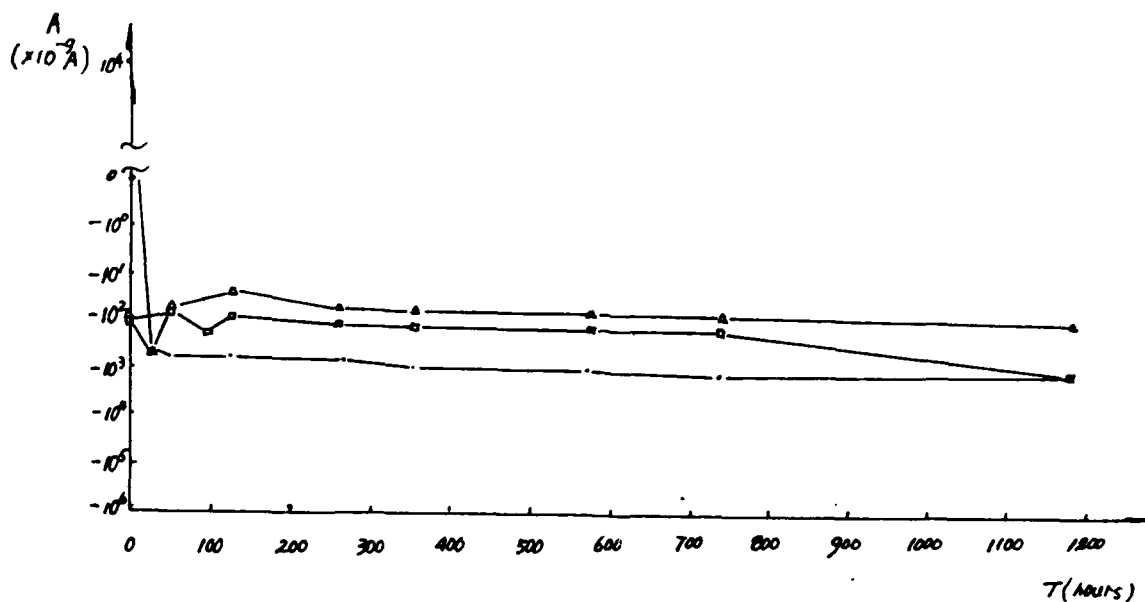


Figure 6. Galvanic current-time curve

sign	organic coating electrode	bare spraying metal electrode
—□—	ZnSP+EP+EUZC \times 1+PU \times 1	ZnSP
—•—	ZnSP+EUZP \times 1+PU \times 1	ZnSP
—△—	ZnSP+PU \times 2	ZnSP

Note. ZnSP: Zn sprayed coating
other are same with note of figure 4.

**Table 1. Simulative sea water immersion—
saltfog alternate test 4000hours results of
the typical painted film on the thermally
sprayed Zn, Al and Zn-15 Al alloy coatings**

number	coating systems	thickness of painted films (μm)	simulative sea water immersion—salt fog alternate test results (4000 hours)	
			appearance of specimen	grading
1	AlSP+EP+EUZC \times 1+EU \times 1	60	very few blisters	+
2	AlSP+EP+EUZC \times 2+EU \times 2	120	no change	0
3	AlSP+EUZP \times 1+EU \times 1	60	medium few blisters	++
4	AlSP+EUZP \times 2+EU \times 2	120	very few blisters	+
5	ZnSP+EP+EUZC \times 1+EU \times 1	60	no change	0
6	ZnSP+EP+EUZC \times 2+EU \times 2	120	no change	0
7	ZnSP+EUZP \times 1+EU \times 1	60	medium few blisters	++
8	ZnSP+EUZP \times 2+EU \times 2	120	very few blisters	+
9	ZnSP+EP+EUZC \times 1+EU \times 1	60	very few blisters	+
10	ZnSP+EP+EUZC \times 2+EU \times 2	120	no change	0
11	ZnSP+EUZP \times 1+EU \times 1	60	medium few blisters	++
12	ZnSP+EUZP \times 2+EU \times 2	120	very few blisters	+
13	AlSP+EP+EUZC \times 1+PU \times 1	60	very few blisters	+
14	AlSP+EP+EUZC \times 2+PU \times 2	120	no change	0
15	AlSP+EUZP \times 1+PU \times 1	60	medium bense blisters	+++
16	AlSP+EUZP \times 2+PU \times 2	120	medium few blisters	++
17	ZnSP+EP+EUZC \times 1+PU \times 1	60	no change	0
18	ZnSP+EP+EUZC \times 2+PU \times 2	120	no change	0
19	ZnSP+EUZP \times 1+PU \times 1	60	medium few blisters	++

Continue Table 1

number	coating systems	thickness of painted films (μm)	simulative sea water immersion—salt fog alternate test results (4000 hours)	
			appearance of specimen	grading
20	ZASP+EUZP × 2+PU × 2	120	no change	0
21	ZnSP+EP+EUZC × 1+PU × 1	60	very few blisters	+
22	ZnSP+EP+EuZC × 2+PU × 2	120	no change	0
23	ZnSP+EUZP × 1+PU × 1	60	medium few blisters	++
24	ZnSP+EUZP × 2+PU × 2	120	very few blisters	+
25	AlSP+EP+EUZC × 1+ET × 1	60	ET localized peel	+
26	AlSP+EP+EUZC × 2+ET × 2	120	ET localized peel	+
27	AlSP+EUZP × 1+ET × 1	60	medium dense blisters	+++
28	AlSP+EUZP × 2+ET × 2	120	very few blisters	+
29	ZASP+EP+EUZC × 1+ET × 1	60	no change	0
30	ZASP+EP+EUZC × 2+ET × 2	120	ET localized peel	+
31	ZASP+EUZP × 1+ET × 1	60	medium dense blisters	+++
32	ZASP+EUZP × 2+ET × 2	120	no change	0
33	AlSP+EP+VNZC × 1+VNX1	60	no change	0
34	AlSP+EP+VNZC × 2+VN × 2	120	large size blisters(1 inch)	+++
35	ZASP+EP+VNZC × 1+VN × 1	60	no change	0
36	ZASP+EP+VNZC × 2+VN × 2	120	no change	0

Note 1. AlSP, ZnSP, Zn-AlSP is respectively spraying Al, Zn and Zn-15Al alloy coatings, thick: 150–200μm.

EP: prephosphorized wash primer, ZC: chromate, ZP: phosphate, EU: epoxy-polyurethane, PU: polyurethane, ET: epoxy-coal tar paint, VN: copoly vinylacetal-vinyl chloride paint.

Note 2. grading: 0: excellent

+: good

++: medium

+++ : bad

Table 2. Sea water immersion and splash zone two years test results of the typical painted film on the spraying Zn, Al and Zn-15Al alloy coatings

number	coating systems	thick of painted films (μm)	corrosion grading	
			Immersion test	splas zone test
1	AlSP+EP+EUZC \times 2+EU \times 2	120	0	0
2	ZnSP+EP+EUZC \times 2+EU \times 2	120	0	0
3	Zn-AlSP+EP+EUZC \times 2+EU \times 2	120	0	0
4	AlSP+EUZP \times 2+EU \times 2	120	/	++
5	ZnSP+EUZP \times 2+EU \times 2	120	/	++
6	Zn-AlSP+EUZP \times 2+EU \times 2	120	++	0
7	AlSP+EP+PUZC \times 2+PU \times 2	120	0	0
8	ZnSP+EP+PUZC \times 2+PU \times 2	120	0	0
9	Zn-AlSP+EP+PUZC \times 2+PU \times 2	120	0	0
10	AlSP+EUZP \times 2+PU \times 2	120	++	+
11	ZnSP+EUZP \times 2+PU \times 2	120	++	0
12	Zn-AlSP+EUZP \times 2+PU \times 2	120	++	+
13	AlSP+EUZP \times 2+ET \times 2	120	+	0
14	AlSP+EP+VNZC \times 2+VN \times 2	120	++++	0
15	Zn-AlSP+EP+VNZC \times 2+VN \times 2	120	++++	0
16	AlSP+EUZP \times 2+VN \times 2	120	++++	0

Note1. AlSP, ZnSP, Zn-AlSP is respectively spraying Al, Zn and Zn-15Al alloy coatings, thick: 150-200 μm .

EP: prephosphorized wash primer, ZC: chromate, ZP: phosphate, EU: epoxy-polyurethane, PU: polyurethane, ET: epoxy-coal tar paint, VN: coply vinylacetal-vinyl chloride paint.

Note 2.grading: 0: excellent

+: good

++: medium

+++ : bad

++++: very bad

Surface Modification by Chemical and Electrochemical Processes

F. Mansfeld

Corrosion and Environmental Effects Laboratory (CEEL)
Department of Materials Science & Engineering
University of Southern California
Los Angeles, CA 90089-0241

Y. Wang

Corrosion and Environmental Effects Laboratory (CEEL)
Department of Materials Science & Engineering
University of Southern California
Los Angeles, CA 90089-0241

S. H. Lin

Corrosion and Environmental Effects Laboratory (CEEL)
Department of Materials Science & Engineering
University of Southern California
Los Angeles, CA 90089-0241

L. Kwiatkowski

Corrosion and Environmental Effects Laboratory (CEEL)
Department of Materials Science & Engineering
University of Southern California
Los Angeles, CA 90089-0241

Abstract

The concept of corrosion protection by surface modification focuses on the replacement of environmentally hazardous chemicals such as hexavalent chromium by processes which only involve environmentally acceptable chemicals. Examples will be given for surface modification of Al alloys by a combination of chemical and electrochemical processes leading to "stainless aluminum". The Ce-Mo process involves immersion in boiling solutions of $\text{Ce}(\text{NO}_3)_3$ and CeCl_3 followed by anodic polarization in Na_2MoO_4 . Significant improvements of the resistance to localized corrosion have been obtained. Remarkable improvements in the passive behavior of stainless steel have been achieved in the AV passivation process in which the stainless steel is polarized in the passive region with superposition of a potential square wave. A reduction of the critical current density for passivation of SS 304 in 0.2 N H_2SO_4 by a factor of 100 has been obtained.

Key terms: Al alloys, stainless steel, localized corrosion, passive film, impedance spectroscopy, polarization curves, passivation.

Introduction

The concept of corrosion protection by surface modification focuses on the replacement of environmentally hazardous chemicals such as hexavalent chromium by processes which only involve environmentally acceptable chemicals. Examples will be given for surface modification of Al alloys by a combination of chemical and electrochemical processes. The Ce-Mo process involves immersion in boiling solutions of $\text{Ce}(\text{NO}_3)_3$ and CeCl_3 followed by anodic polarization in Na_2MoO_4 . Significant improvements in the resistance to localized corrosion have been obtained. Al 6061-T6 treated in the Ce-Mo process did not show any indication of initiation of pits during immersion in 0.5 N NaCl open to air for 60 days during which time the impedance remained capacitive over the entire frequency range. Ce and Mo apparently produce a synergistic effect since boiling in hot water followed by polarization in the molybdate solution or boiling in the Ce-solutions followed by polarization in a borate buffer did not produce lasting corrosion resistance. Samples of Al 6013 treated in the Ce-Mo process have passed the salt spray test according to ASTM B 117, while the as-received samples were severely corroded. Initial results for Al 7075-T6 indicate that the Ce-Mo process needs to be modified for this alloy since immersion in boiling CeCl_3 causes pitting.

Remarkable improvements in the passive behavior of stainless steel in acid media have been achieved in the alternating voltage passivation process (AVPP), in which a potential square wave is applied for a certain length of time at a constant dc bias potential. The effects of the process parameters dc bias potential E_0 , pulse length P , pulse amplitude A and ratio R_0 of the duration of the anodic to the cathodic portion of the pulse on the passive properties of 304 SS have been evaluated using a factorial design experiment. The surface properties have been determined by recording the critical current density i_{crit} and the passive current density i_p as well as the time t_p for open-circuit potential decay in 0.1 M H_2SO_4 . The values of i_{crit} and i_p were recorded after the open-circuit potential decay. The significant decrease of i_{crit} and i_p and the increase of t_p after AVPP suggest that the passive film has become more resistant to attack in acid media. The objective of the research presented below is an evaluation of the process parameters on the protective properties of the passive film on stainless steel. The experimental approach used in AVPP and some typical result will be discussed below for type 304 stainless steel.

Experimental Approach

Al Alloys

The materials studied were Al 6061-T6 and Al 6013-T6. The standard procedure for surface modification consists of immersion in boiling 10 mM $\text{Ce}(\text{NO}_3)_3$ for 2 hours followed by immersion in boiling 5 mM CeCl_3 for 2 hours and polarization at + 500 mV (SCE) in 0.1 M Na_2MoO_4 for 2 hours at RT. This procedure is referred to as the Ce-Mo Process [1-3] in the following. A number of tests were performed in order to determine the effects of the various process parameters on corrosion resistance and to optimize the Ce-Mo Process. A 2^2 factorial design experiment was carried out for Al 6061 to determine the effects of molybdate concentration and polarization time on the resistance to localized corrosion. In

another set of experiments the immersion step in boiling Ce-solutions was replaced by immersion in boiling water or the polarization step in the molybdate solution was replaced by polarization in borate buffer. Corrosion tests were carried out in 0.5 N NaCl, open to air. EIS-data were collected as a function of exposure time at the corrosion potential E_{corr} . The analysis of the EIS-data was performed with the software package PITFIT [4]. dc measurements were carried out to characterize the electrochemical behavior of the modified surfaces.

Stainless Steel

Flat disks of 304 SS were abraded, rinsed in distilled water in an ultrasonic bath and cathodically polarized in 0.05 M H_2SO_4 at -750 mV vs. SCE for 5 minutes. After this cleaning step and rinsing in distilled water, the electrode was immediately immersed in 0.05 M H_2SO_4 and polarized at E_o with a superimposed potential square wave. A factorial design experiment was applied to determine the optimum values of A, P, E_o and R_o (see Fig. 1). All AV passivation experiments were performed with a PAR potentiostat model 173 combined with a PAR Universal Programmer model 175. Electrochemical methods were chosen to characterize the corrosion resistance of the modified passive layers. The decay of the open-circuit potential after AV passivation was recorded in 0.1 M H_2SO_4 in order to determine the layer stability. An anodic polarization curve was then recorded (10 mV/s) starting at the corrosion potential E_{corr} reached in the previous open-circuit decay experiment. The values of the time to activation t_p , the critical current density for passivation i_{crit} and the passive current density i_p were the criteria of the stability of the modified passive film. These experiments were carried out using a PAR model 173 potentiostat with a 276 GPIB interface card which was controlled by an IBM XT computer.

In order to compare the rate of oxygen reduction for as-received and modified surfaces cathodic polarization curves were recorded in an aerated borate - boric acid buffer at pH = 8.4. Cyclic polarization studies were performed in deaerated buffer at a potential sweep rate of 100 mV/s. Auger electron spectroscopy (AES) was used to determine concentration profiles of Fe, Cr, O and S in the modified surface layers.

Experimental Results and Discussion

Improvement of Pitting Resistance of Al Alloys by the Ce-Mo Process

Al 6061-T6 treated by the Ce-Mo process possesses enhanced resistance to pitting in chloride containing environment as indicated by impedance spectra (Fig. 1), which show capacitive behavior during exposure to NaCl for 30 days. No changes of the impedance spectra have been observed for time periods indicating that the modified surface is very stable. The experimental results from dc measurements suggest that the significant improvement of the pitting resistance can be attributed to the separation of the pitting potential E_{pit} and E_{corr} (Fig. 2) and the reduction of the rate of oxygen reduction on the modified surface as compared to the as-received surface (Fig. 3). The passive current density (c.d.) for the modified surface was extremely small ($< 1 \text{ nA/cm}^2$). Therefore it can be concluded that the surface treated in the Ce-Mo Process behaves like an insulator

allowing neither anodic or cathodic reactions to take place at appreciable rates.

In order to collect more information about how the properties of the modified surface may be affected by polarization in Na_2MoO_4 , a 2^2 factorial test was designed to evaluate the effects of molybdate concentration and length of polarization. The polarization times were 0.5 h and 2 h and the concentrations of Na_2MoO_4 were chosen to be 0.01 M and 0.1 M. The effects of the process parameters on the corrosion resistance are reflected in the impedance spectra (Fig. 4). For the shorter polarization time, the impedance decreases, the capacitance increases and the transmission line impedance, which is typical for the occurrence of pits on Al alloys [4-6], is clearly indicated at lower frequencies (curve 1 and 3). Similar changes are observed for a decrease in the concentration of molybdate at a fixed polarization time (curve 4 and 2). A small deviation of the impedance from capacitive behavior is observed for the sample treated with the Ce-Mo Process (curve 4). This difference to the results shown in Fig. 1, where a small sample (1 cm^2) with very few surface defects such as scratches, etc. was selected from a large sheet, is considered to be due to the use of a larger sample (20 cm^2) in the tests of Fig. 4 which contained surface defects which apparently contribute to the overall impedance behavior.

The results of the analysis of the factorial design experiment are shown in Fig. 5 for various parameters which describe the localized corrosion behavior of Al alloys [5,6] and are obtained from the analysis of impedance spectra such as those shown in Fig. 4 using PITFIT. The pitting time t_0 is the time at which the first pits were detected by visual observation. In Fig. 5, F is the pitted area fraction determined after 30 days, R_p° is the polarization resistance of the passive surface at time t_0 and $C_{i,1}$ and $C_{i,t}$ are the values of the total capacitance C_i obtained after 1 day and 30 days immersion in NaCl, respectively. The polarization resistance of the growing pits R_{pit}° and the transmission line parameter K° were calculated for the time t_0 and have been normalized to the pitted area $A_{pit} = 2FA$, where A is the total area of the test sample [5,6].

In general, the process parameter used in the Ce-Mo Process produce the best resistance to localized corrosion (Fig. 5). The results of the quantitative analysis of the effects of concentration c and polarization time t on the parameters, which characterize the resistance to localized corrosion, are also given in Fig. 5, which shows that significant interaction effects can affect the observed results. The pitted area fraction F , after 30 days, decreases with increasing t , but increases with increasing c . The interaction effect ct leads to a decrease in F . A similar result is obtained for the pitting time t_0 , for which increasing c reduces t_0 , while an increase of t and especially the interaction effect ct increase the time at which pits were first observed. The capacitance C_i contains contributions from the passive surface and from the growing pits. The ratio $C_{i,t}/C_{i,1}$ can therefore be used as an estimate of pit growth. Both an increase of c and t have a beneficial effect; however, the interaction effect ct reduces this beneficial effect to some extent.

In order to understand the roles of Ce and Mo in the Ce-Mo Process in more detail, three sets of Al 6061 samples were prepared with different procedures, which are the Ce-Mo standard procedure (Ce/Mo), immersion in 10 mM $\text{Ce}(\text{NO}_3)_3$ at 100°C for 2 hours, followed by immersion in 5 mM CeCl_3 at 100°C for 2 hours and polarization in borate buffer + 500

mV for 2 hours (Ce/Borate buffer), and boiling in distilled water at 100°C for 2 hours followed by polarization in 0.1 M Na_2MoO_4 at 500 mV for 2 hours (water/Mo). Corrosion tests were performed in 0.5 N NaCl by collecting EIS data continuously for at least 15 days. The EIS spectra (Fig. 6) show that the Ce/Mo treated sample is capacitive after immersion for 15 days (curve 1), the other two samples show impedance spectra which agree with the pitting model [4-6] from the first day of the corrosion test.

The water/Mo treated sample has the smallest capacitance C_i (Fig. 7). Apparently, boiling in distilled water increases the thickness of the aluminum oxide film, but does not improve the pitting resistance. For the Ce/Mo treated sample, the highest values of R_p and C_i were determined, which suggests that the modified oxide layer has the lowest dissolution rate despite the fact that it is thinner than the oxides formed by the other two treatments (Fig. 7). Anodic polarization in borate buffer, after treating in Ce-solutions, can improve the pitting resistance marginally. Pit growth rates as determined qualitatively by R_{pit}^0 are lower for samples treated in the Ce/borate buffer process than in the water/Mo process (Fig. 7). Significant improvements of the pitting resistance can only be achieved by the use of both the Ce and Mo steps in the Ce-Mo Process. The results presented here indicate that Ce and Mo produce a synergistic effect as was also concluded by Kendig and Thomas [7].

The Ce-Mo Process was also applied to Al 6013-T6. The impedance spectra obtained after 1 day and two weeks are presented in Fig. 8. Significant differences in the impedance spectra are observed for the two sets of samples. For the as-received sample, pits initiated over the entire surface in a short time and uniform corrosion was also observed. The impedance spectra showed an increase of C_i and the frequency dependence at low frequencies which is typical for the pitting process of Al alloys [4-6]. However, for the Ce-Mo modified sample, for which very few small pits were first observed after exposure to NaCl for 3 days, the impedance did not change significantly during the test period of 36 days. The estimated values of the pitted area fraction F (Fig. 9) show that the growth rate of pits on the treated sample was much lower than for the as-received surface. For the as-received surface about 12% of the exposed area was pitted after 15 days, while for the treated surface only 0.7 % was pitted after one month (Fig. 9). Exposure of samples of Al 6013-T6 to the salt spray test according to ASTM B117 for 15 days did not result in pitting for the sample treated with the Ce-Mo Process, but caused severe corrosion for the untreated sample.

Surface Modification of Stainless Steel by the Alternating Voltage Passivation Process (AVPP)

The principle of AVPP is illustrated in Fig. 10, which shows the polarization curve for type 304 stainless steel in 0.05 M H_2SO_4 and the potential square wave which is applied at the dc potential E_0 . The main process parameters are pulse amplitude A , pulse width P , E_0 and the ratio R_0 of the duration of the anodic to the cathodic portion of the pulse.

As described elsewhere [9], the direction of change of i_{crit} , i_p and t_p as a function of A and P were determined in a 3^2 factorial designed experiment using combinations of $\{A\} = 450, 900, 1350$ mV and $\{P\} = 50, 100, 150$ ms. The results obtained by the method of least

squares fitting are presented in Fig. 11. Optimum values of E_o and R_o have been established earlier from the analysis of 2^2 factorial design experiments, where it was found that E_o and R_o should be fixed at $E_o = 300$ mV and $R_o = 4:1$. For a fixed pulse width P an increase in amplitude A decreases i_{crit} and i_p (Fig. 11 a and b). This effect is especially significant for A changing from 450 mV to approximately 950 mV. In the range of A changing from 950 mV to 1350 mV i_{crit} is low and not very sensitive to the changes of A and P , while i_p increases. The time to reactivation t_p increases with increasing A up to 950 mV and decreases in the range 950 - 1350 mV (Fig. 11 c). For a fixed value of A an increase of P affects all three parameters, but its influence seems not to be so significant as the effect of A . From these results, one may conclude that the amplitude A of the alternating voltage (AV) exerts a larger effect on the protective properties of the surface layers than does the pulse width P . However, as has been discussed elsewhere [9], there is no simple relationship between improvement of the passive layer stability and AV amplitude alone, due to significant interaction effects between A and P . The results in Fig. 11 provide the A and P values necessary for achieving values t_p , i_{crit} and i_p which describe the most stable passive layers achieved by AVPP. Considering average effects, $\{A, P\} = \{1050 \text{ mV}, 90 \text{ ms}\}$ were chosen as optimum parameters.

The open-circuit potential decay curves obtained for an as-received sample, after DC passivation and after optimized AVPP (Fig. 12 a) as well as the anodic polarization curves (Fig. 12 b) show significant improvement of the oxide film stability after AVPP. The efficiency of AVPP can be judged by the efficiency ratios $R_{tp} = t_p/t_p^o$, $R_{ic} = i_{crit}/i_{crit}^o$ and $R_{ip} = i_p/i_p^o$ where $t_p^o = 33$ s, $i_{crit}^o = 3700$ mA/cm² and $i_p^o = 40$ mA/cm² are the results recorded for the as-received 304 SS. For the results shown in Fig. 12 $R_{tp} = 100$, $R_{ic} = 80$ and $R_{ip} = 4$. It is important to note that the values of i_{crit} and i_p were determined after open-circuit potential decay. The large decrease of i_{crit} seems to suggest that the passive film formed by AVPP dissolved only at a few weak spots during open-circuit potential decay and therefore less anodic charge was needed for repassivation.

In preliminary investigations, it has been observed that surface modification by AVPP affects the hydrogen evolution reaction [8]. Another important reaction especially in neutral or alkaline environments which exerts an influence on the corrosion behavior of the metal is cathodic reduction of oxygen. Cathodic polarization curves for the as-received sample as well as after the treatment are shown in Fig. 13. The polarization curves clearly show that the rate of oxygen reduction is considerably faster on the as-received SS 304 than after DC or AV passivation. In the latter case the lowest cathodic currents in the entire potential range were observed.

One reason for the beneficial effect of AVPP is the greater thickness of the film in comparison with DC or untreated samples [12]. An increase of the thickness of the passive film on modified surfaces can be deduced from Fe and O elemental profiles determined with AES (Fig. 14). An increase of the passive film thickness due to AVPP was found independently from cathodic reduction curves in deaerated borate buffer of pH = 8.4, in which the largest cathodic charge was consumed for the reduction of the passive film formed on 304 SS by AVPP [10]. Another important result shown in Fig. 14 is the much smaller amount of S in the passive film after AVPP as compared to dc passivation. AES

measurements indicate Cr enrichment in passive films after AVPP (Fig. 15). Qualitative conclusions about the changes in the chromium content or stoichiometry after AVPP may also be drawn from cyclic polarization curves carried out in deaerated borate buffer (pH = 8.4) (Fig. 16). It is seen that dc passivation and AVPP of 304 SS lead to the appearance of well-defined peaks in the transpassive region just before the onset of oxygen evolution. The peak height is the largest for the surface after AVPP. This irreversible process may be governed by the Cr phase in the surface film, i.e. its form and amount. An influence related to Ni should also be taken into account [11]. This effect will be studied in more detail in further investigations. In general, the results reported here are further evidence for the observations reported elsewhere [11] that AVPP shifts the stoichiometry of the Cr component in the modified passive film from that of $\text{Cr}(\text{OH})_3$ closer to a less hydrated compound such as CrOOH or Cr_2O_3 .

Summary and Conclusions

Surface modification of Al 6061 and 6013 by the Ce-Mo Process [1-3] produces "stainless aluminum", i.e. Al alloy surfaces which are extremely resistant to uniform and localized corrosion. It has been shown that both the Ce and the Mo step are needed in the Ce-Mo Process since Ce and Mo produce a synergistic effect. Immersion in boiling water followed by polarization in molybdate produces surfaces with poor corrosion resistance. Replacement of the molybdate solution by a borate buffer solution also produces surface with less resistance to localized corrosion than those formed in the Ce-Mo Process. Lowering of the molybdate concentration or the time of polarization in molybdate decreases the corrosion resistance. Further work is aimed at applying the Ce-Mo Process to Al 7075 and Al 2024. Preliminary results indicate that some modification of the process parameter might be necessary for these alloys with higher Cu content.

AVPP leads to significant improvements of the passive properties of 304 SS exposed to aerated 0.1 M H_2SO_4 in comparison to untreated or DC passivated samples. The resistance of the passive film to attack by an acidic medium is greatly increased as evidenced by the increase of t_p of about 100 - 130 and the decrease by a factor of 80 - 100 and 4 - 10 for i_{crit} and i_p , respectively. The exact values of these parameters depend on the choice of the AVPP process parameters. The results obtained with factorial design experiments indicate that significant improvements of the passive film properties are obtained for higher amplitudes and wider pulses of the potential square wave, but certain limits have been found. The optimum process parameters should create conditions in which the anodic potential is located near, but below the transpassive region. The cathodic pulse should contain a reductive component, since earlier results with $E_o = 50$ mV for square waves located within $E = -150$ and 275 mV were rather poor. The beneficial effects of AVPP are considered to be due to a greater thickness of the passive film in comparison with as-received or DC passivated samples and Cr enrichment along with the change in stoichiometry to less hydrated chromium oxide. The present investigations have been limited to studies in acid media. Further research is planned to evaluate the resistance of modified surface layers on stainless steels to localized corrosion in chloride containing media. The results of these studies will be applied in future research to improve the passive properties of low-Cr stainless steels.

Acknowledgement

The project on surface modification of Al alloys has been sponsored by the Office of Naval Research (Dr. J. Sedriks) under Contract No. N00014-91-J-1041. The work performed on surface modification of stainless steel has been sponsored by a grant from the National Science Foundation (DMR-9100174).

References

1. F. Mansfeld, Y. Wang and H. Shih, J. Electrochem. Soc. 138, L74 (1991)
2. F. Mansfeld, Y. Wang, and H. Shih, Electrochim. Acta 37, 2277 (1992)
3. U. S. Patent 5,194,138
4. H. Shih and F. Mansfeld, Corrosion 45, 610 (1989)
5. F. Mansfeld, Electrochim. Acta 35, 1533 (1990)
6. F. Mansfeld, Y. Wang, H. Xiao and H. Shih, Proc. Symp. "Critical Factors in Localized Corrosion", The Electrochem. Soc., Proc. Vol. 92-9, 469 (1992)
7. M. W. Kendig and C. Thomas, J. Electrochem. Soc. 139, L103 (1992).
8. L. Kwiatkowski and F. Mansfeld, J. Electrochem. Soc., 140, L39 (1993)
9. F. Mansfeld, S.H. Lin and L. Kwiatkowski, "The Effects of Process Parameters on Alternating Voltage Passivation of 304 Stainless Steel", Corrosion Science (in press).
10. L. Kwiatkowski and F. Mansfeld, unpublished data.
11. P. Schmuki, H. Boehni and F. Mansfeld, "A Photo-Electrochemical Investigation of Passive Films Formed By Alternating Voltage Passivation", submitted to J. Electrochem. Soc.

13. Cathodic polarization curves for 304 SS in aerated borate buffer, pH=8.4, after different treatments.
14. AES concentration profiles for Fe, Cr, S and O for the 304 SS surfaces for the as-received sample (a), after DC passivation (b) and after AV passivation (c).
15. Relative Cr contents in the passive films on 304 SS after different surface treatments obtained from AES profiles.
16. Cyclic voltammograms at 100 mV/s for 304 SS in deaerated borate buffer for different surface conditions: as-received (curve 1), DC passivation (curve 2) and AVPP (curve 3).

Figure Captions

1. Impedance spectra of Al 6061-T6 modified by the Ce-Mo Process and exposed to 0.5 N NaCl during 30 days.
2. Anodic polarization curves in 0.5 N NaCl (open to air) for Al 6061-T6, as-received (curve 1) and modified by the Ce-Mo Process (curve 2).
3. Cathodic polarization behavior in 0.5 N NaCl for Al 6061-T6, as-received (curve 1) and modified by the Ce-Mo Process (curve 2).
4. Impedance spectra as a function of the polarization time and Na_2MoO_4 concentration for Al 6061-T6 exposed to 0.5 N NaCl.
5. Estimated effects of polarization time t and Na_2MoO_4 concentration c on characteristic parameters for the pitting behavior for Al 6061-T6 in 0.5 N NaCl (data of Fig. 5).
6. Impedance spectra in 0.5 N NaCl for Al 6061-T6 treated by three different processes
7. Time dependence of C_p , R_p° and R_{pit}° for Al 6061-T6 treated by different processes and exposed to 0.5 N NaCl (data of Fig. 6).
8. Impedance spectra in 0.5 N NaCl for Al 6013-T6, as-received and modified by the Ce-Mo Process.
9. Pitted area fraction F as a function of exposure time for Al 6013-T6, as-received and modified by the Ce-Mo Process.
10. Schematic illustration of the measurement principle:
 - a) anodic polarization curve for 304 SS in 0.05 M H_2SO_4 ;
 - b) location of the square wave in comparison with the polarization curve, where A , P , $R_o = t_a : t_b$, and E_o denote pulse amplitude, pulse width, anodic to cathodic polarization time ratio and dc bias potential, respectively.
11. Results of 3^2 factorial design in terms of functional dependence of i_{crit} , i_p and t_p on A and P at $E_o = 300$ mV and $R_o = 4 : 1$. Time of treatment 20 min.
- 12a. Open-circuit potential decay for 304 SS exposed to 0.1 M H_2SO_4 ; curve 1: as-received; curve 2: after DC passivation at $E = 500$ mV for 20 min.; curve 3: after AVPP for 20 min. with $\{A, P\} = \{1050 \text{ mV}, 90 \text{ ms}\}$, $E_o = 300$ mV, $R_o = 4 : 1$.
- 12b. Anodic polarization curves in 0.1 M H_2SO_4 after potential decay (Fig. 12 a).

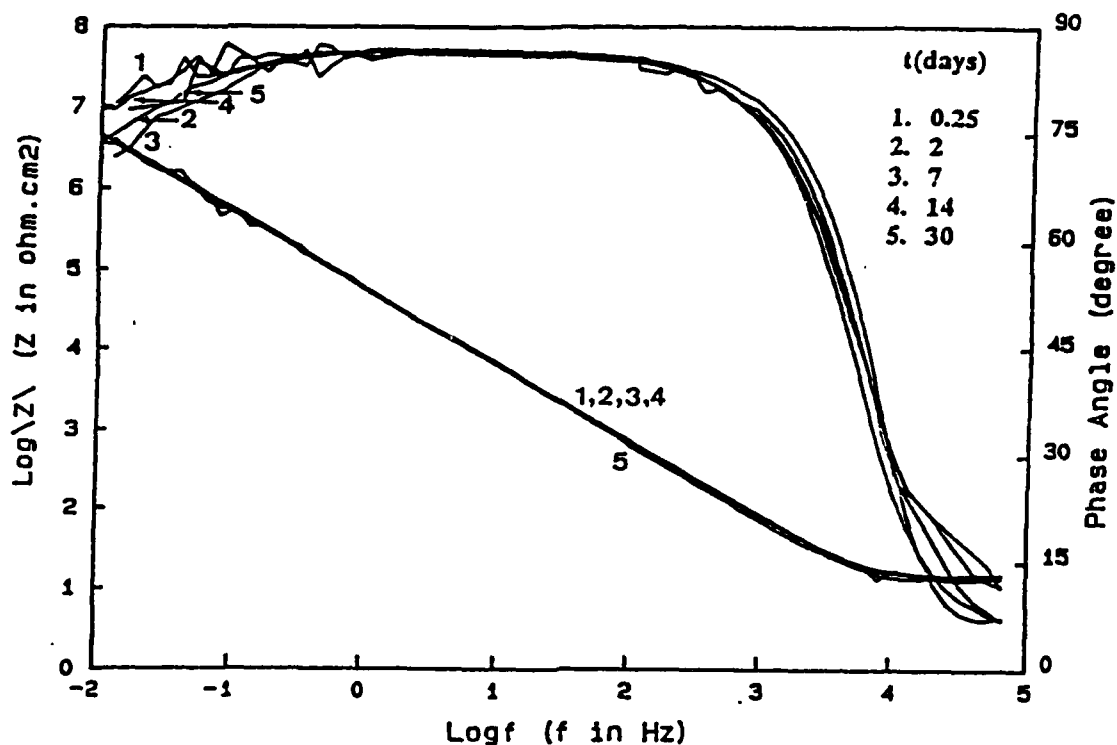


Fig. 1. Impedance spectra of Al6061-T6 modified by the Ce-Mo Process and exposed to 0.5 N NaCl during 30 days.

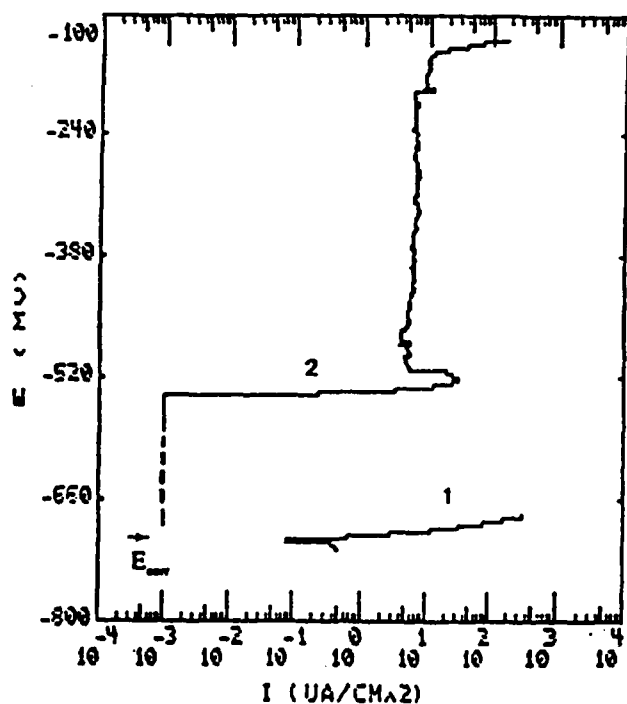


Fig. 2. Anodic polarization curves in 0.5 N NaCl (open to air) for Al 6061-T6, as-received (curve 1) and modified by the Ce-Mo Process (curve 2).

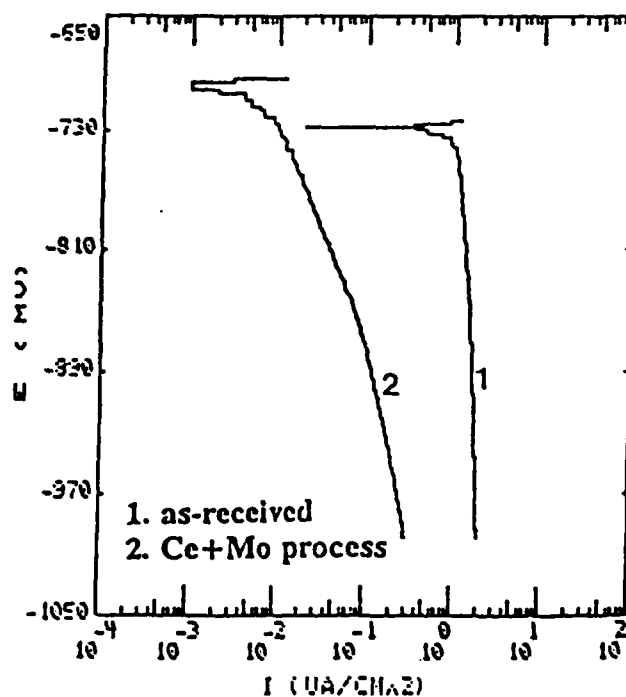


Fig. 3. Cathodic polarization behavior in 0.5 N NaCl for Al 6061-T6, as-received (curve 1) and modified by Ce-Mo Process (curve 2).

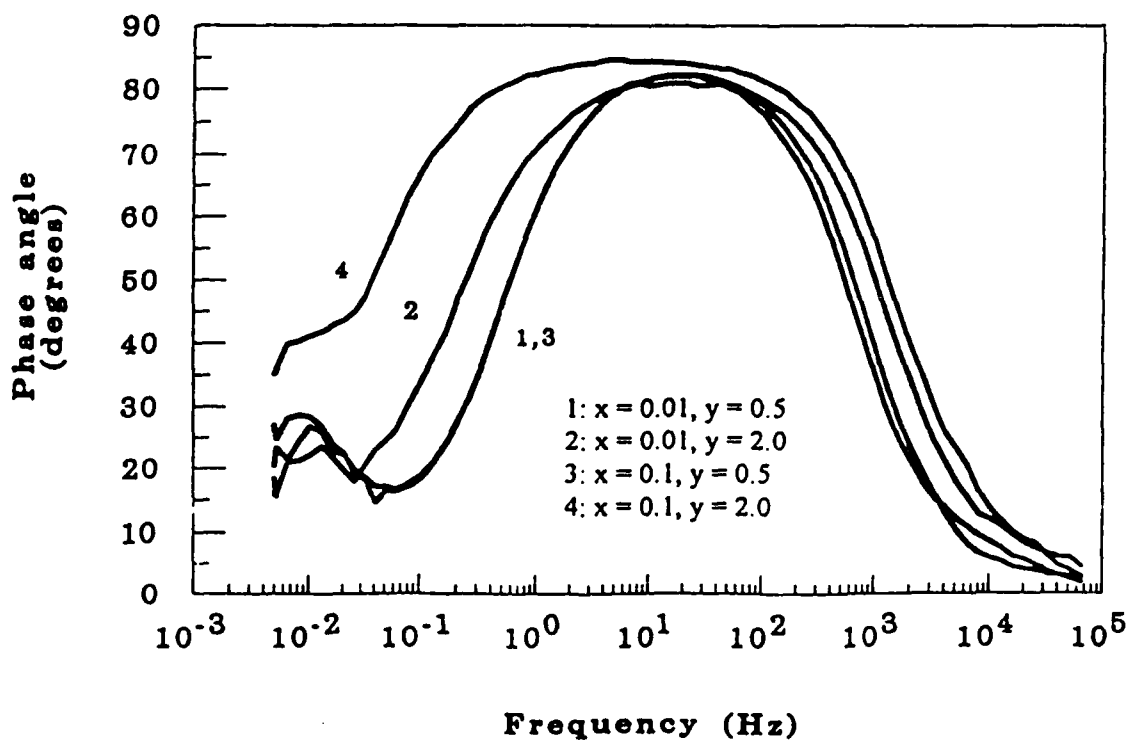
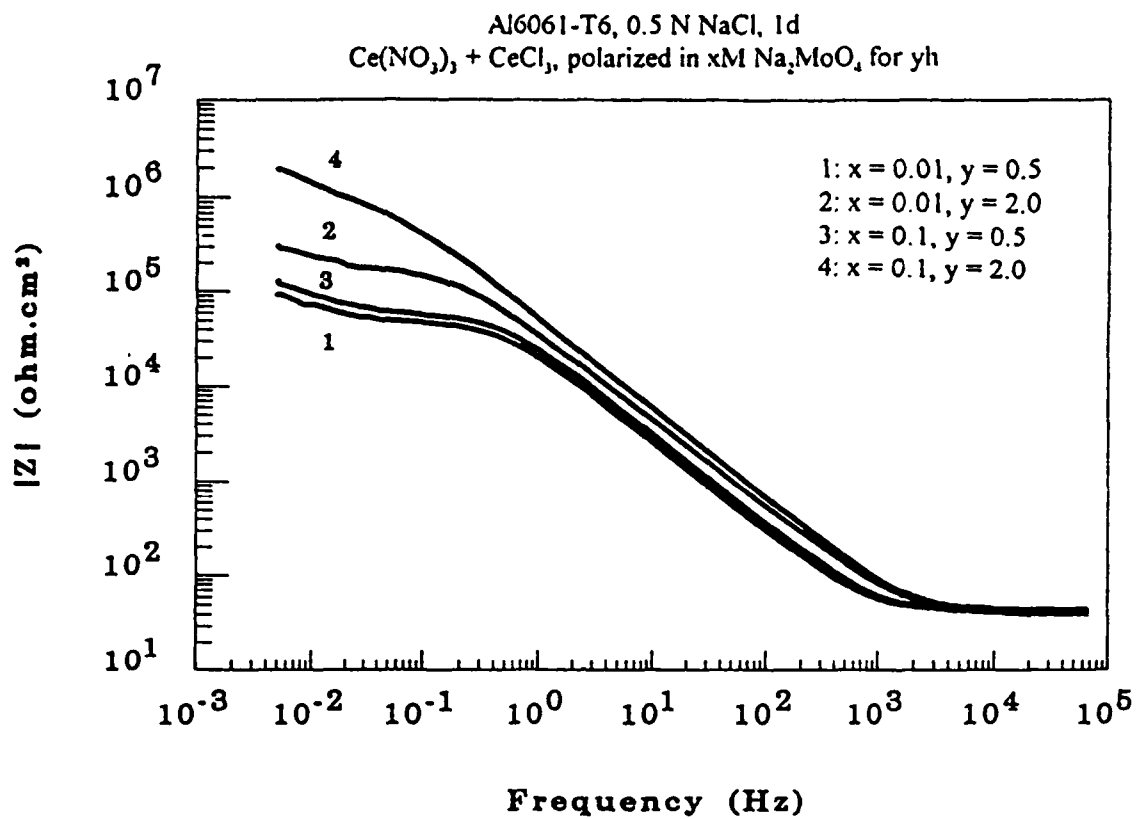
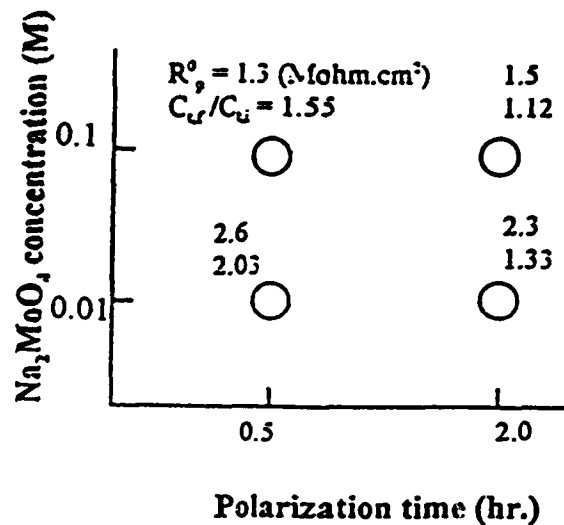
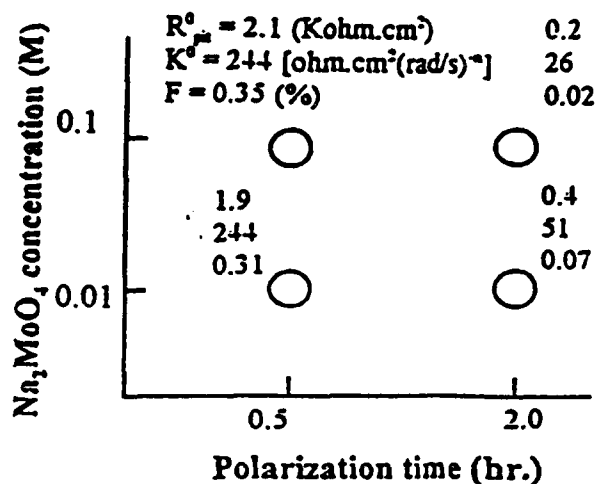


Fig. 4. Impedance spectra as a function of the polarization time and Na_2MoO_4 concentration for Al 6061-T6 exposed to 0.5 N NaCl.



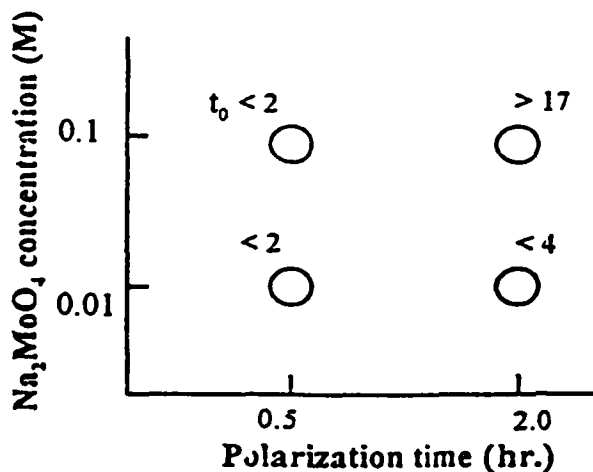
$$R_p^0 \text{ (10}^3 \text{ ohm.cm}^2\text{)} = 2.36 - 0.97t + 4.17c - 2.92ct$$

$$K^0 \text{ [ohm.cm}^2\text{(rad/s)}^{-1}\text{]} = 307 - 127t + 93c - 185ct$$

$$F \text{ (\%)} = 0.38 - 0.15t + 0.78c - 0.67ct$$

$$R_p^0 \text{ (10}^6 \text{ ohm.cm}^2\text{)} = 2.86 - 0.24t - 16.3c + 3.70ct$$

$$C_{ur}/C_u = 2.33 - 0.49t - 6.3c + 2.00ct$$



F: the pitted area fraction (30 days)
 t_0 : the time when pits were first observed
 C_u : total capacitance calculated from the first EIS measurement (1 day)
 C_{ur} : total capacitance calculated from the last EIS measurement (30 day)
 R_p^0 and K^0 were determined at the time t_0
 R_{pit}^0 was determined at $t - t_0 = 1$ (day)
 R_{pit}^0 and K^0 are normalized to the pit area

$$t_0 \text{ (d)} = 1.8 + 0.4t - 48.2 + 96.3ct$$

Fig. 5. Estimated effects of polarization time t and Na_2MoO_4 concentration c on characteristic parameters for the pitting behavior for Al 6061-T6 in 0.5 N NaCl.

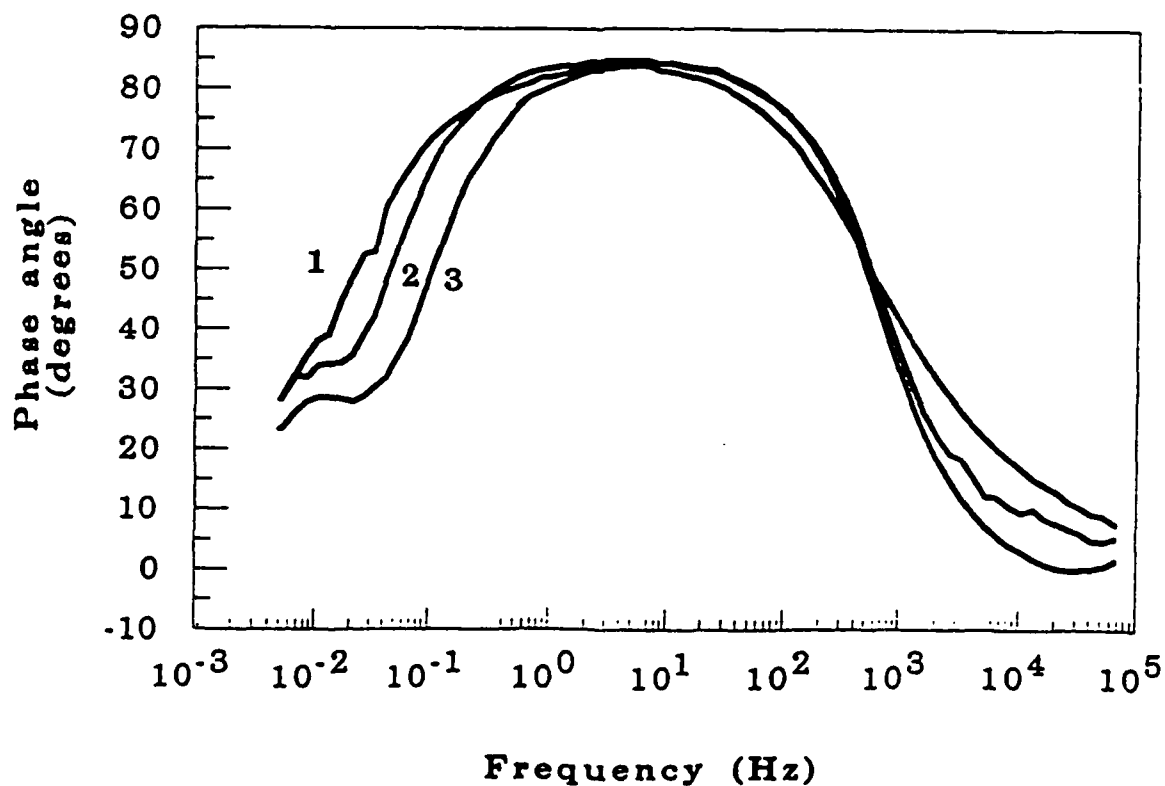
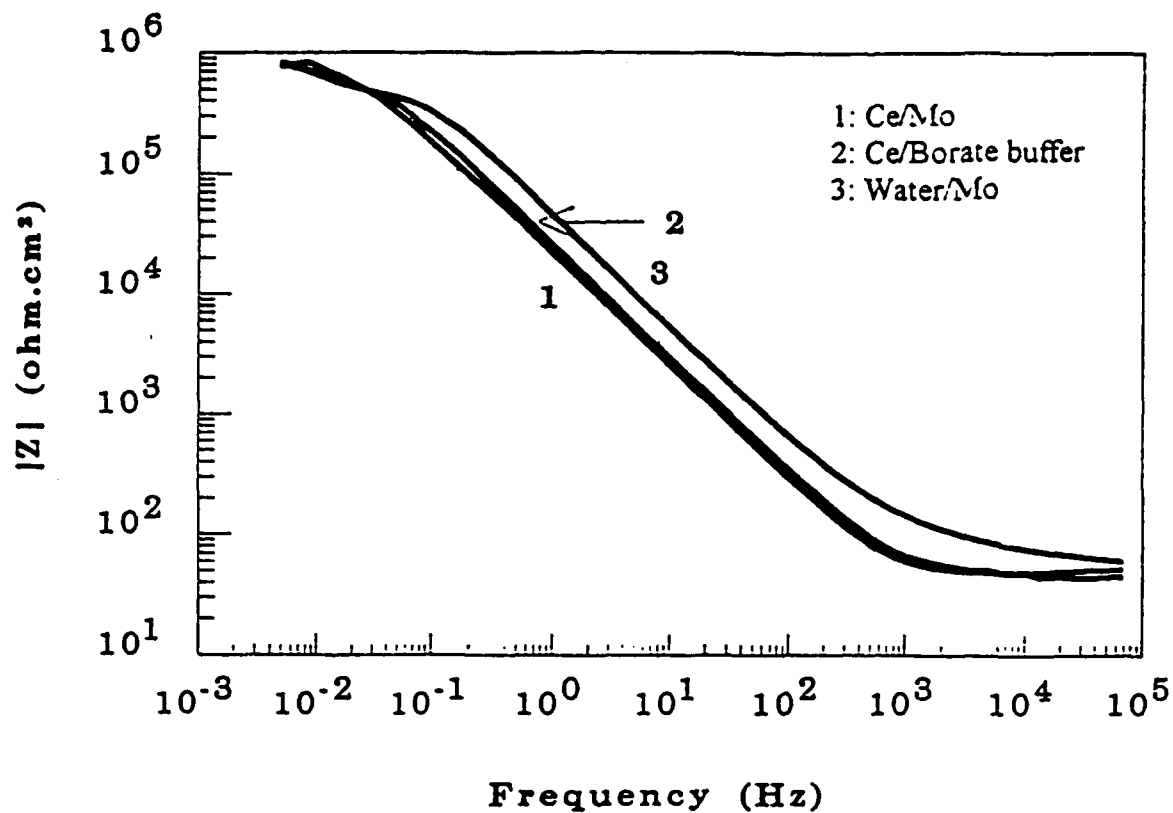


Fig. 6. Impedance spectra in 0.5 N NaCl for Al 6061-T6 treated by three different processes.

Al6061-T6/0.5 N NaCl

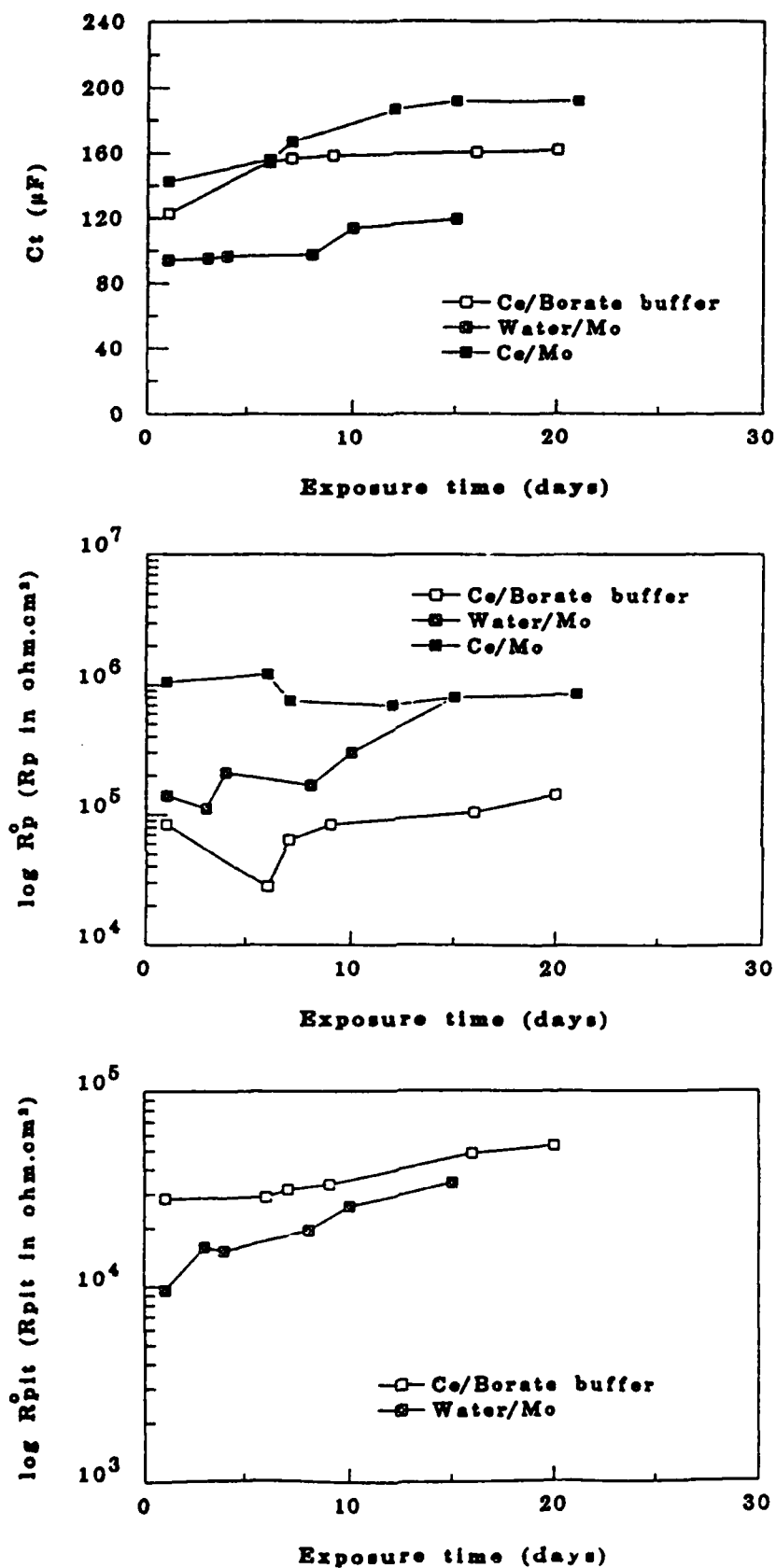


Fig. 7. Time dependence of C_t , R_p and $R_{p pit}$ for Al 6061-T6 treated by three different processes and exposed to 0.5 N NaCl (data of Fig. 6).

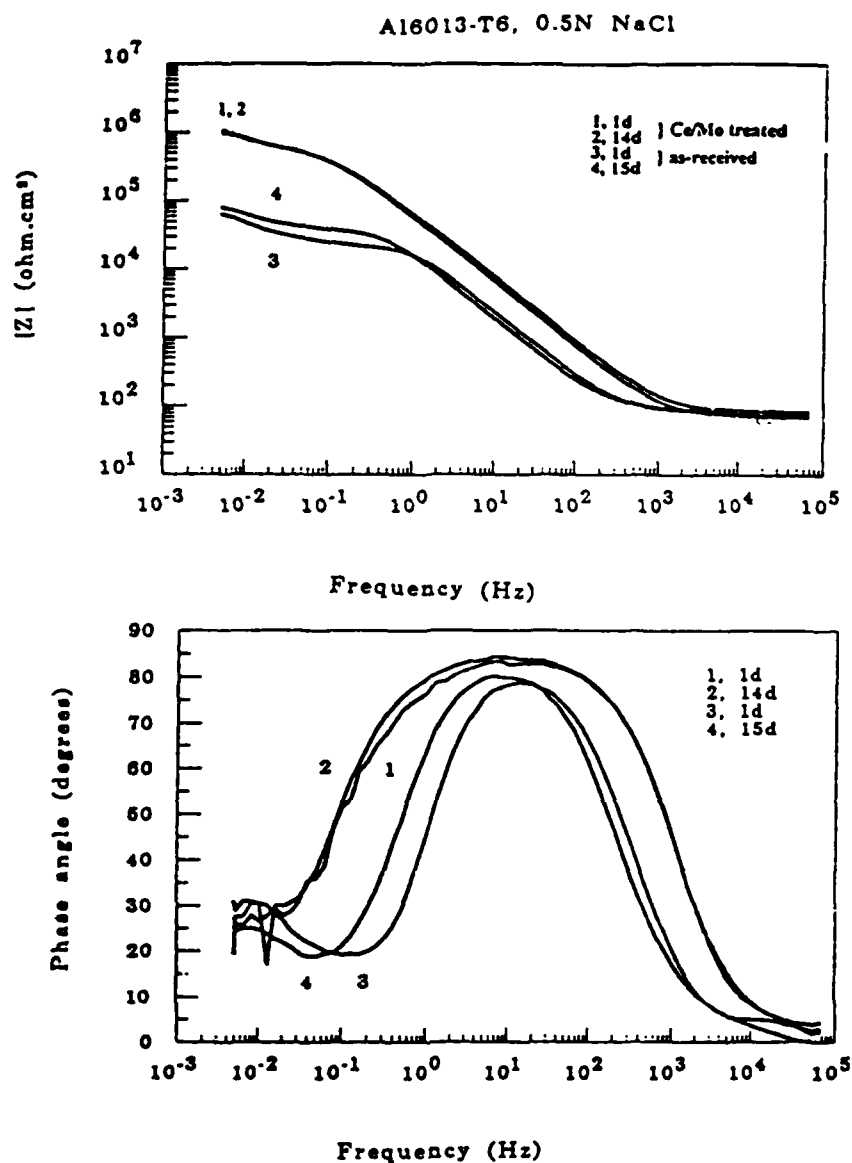


Fig. 8. Impedance spectra in 0.5 N NaCl for Al 6013-T6, as-received and modified by the Ce-Mo Process.

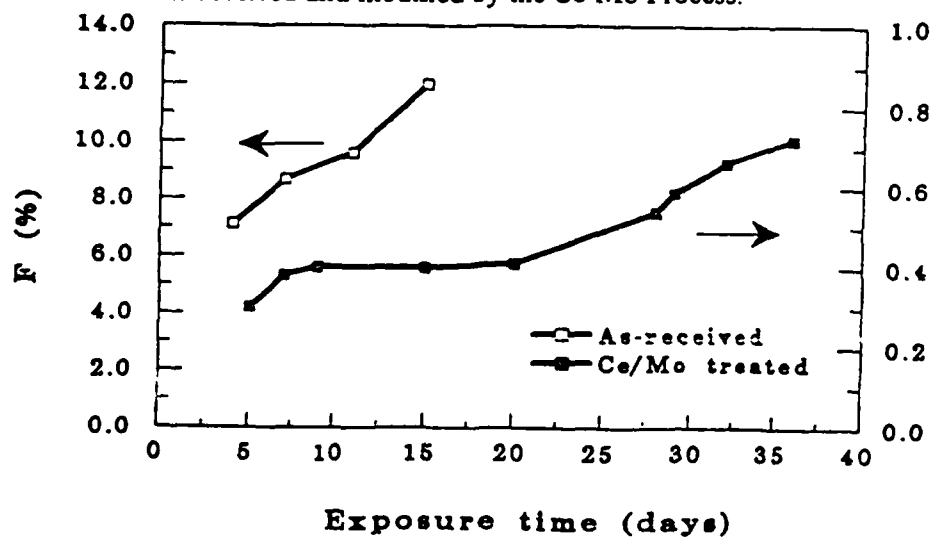


Fig. 9. Pitted area fraction F as a function of exposure time for Al 6013-T6, as-received and modified by the Ce-Mo Process.

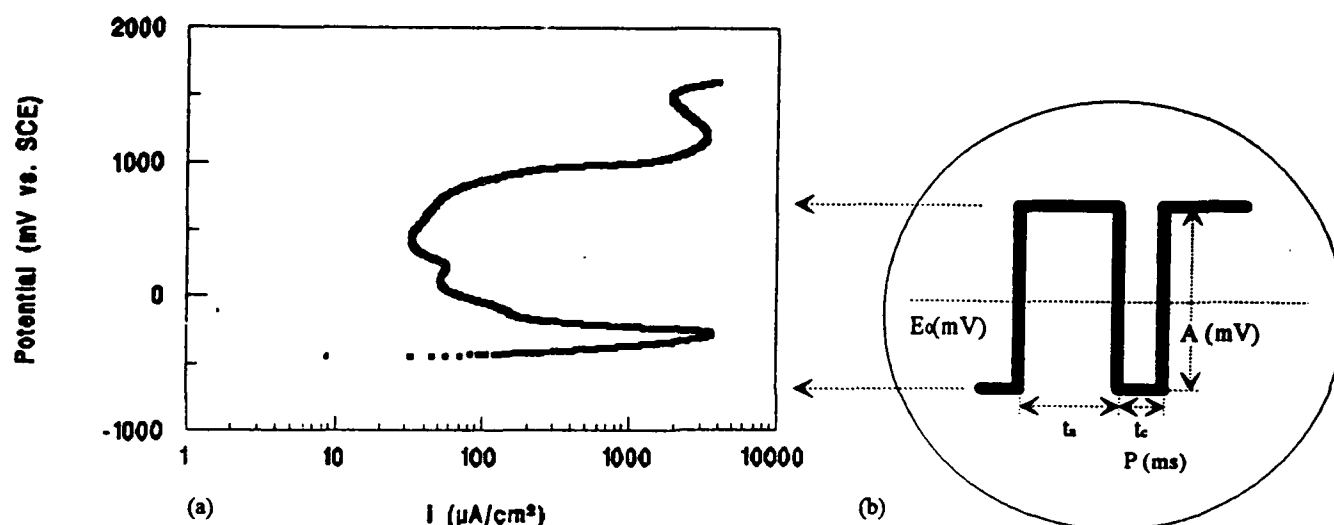


Fig. 10. Schematic illustration of the measurement principle: a) anodic polarisation curve for 304 SS in 0.05 M H_2SO_4 ; b) location of the square wave in comparison with polarisation curve, where A , P , $R_0 = t_a:t_c$, and E_0 denote pulse amplitude, pulse width, anodic to cathodic polarisation time ratio and dc bias potential, respectively.

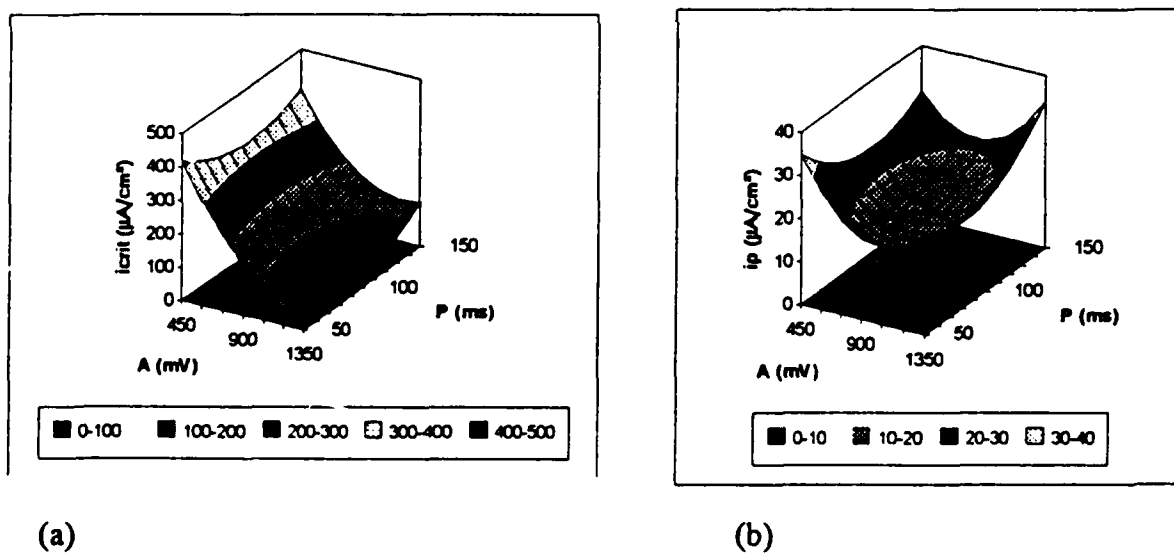


Fig. 11. Results of 3^2 factorial design in terms of functional dependence of i_{crit} (a), i_p (b) and t_p (c) on A and P at $E_0 = 300$ mV and $R_0 = 4 : 1$. Time of treatment 20 min.

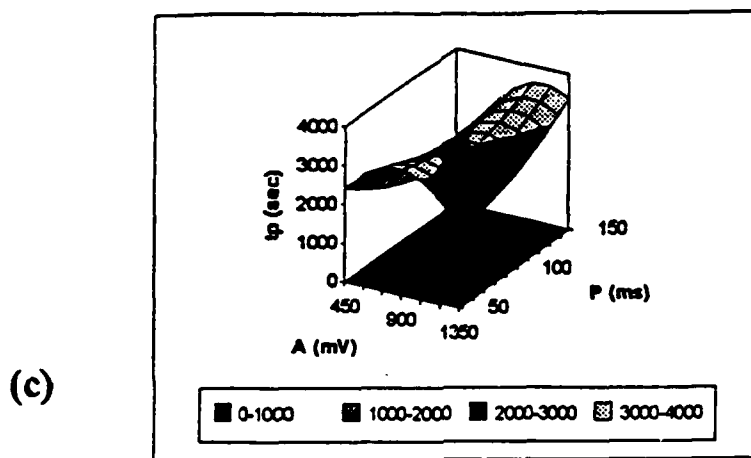


Fig.11. Results of 3^2 factorial design in terms of functional dependence of i_{crit} (a), i_p (b) and t_p (c) on A and P at $E_o = 300$ mV and $R_o = 4 : 1$. Time of treatment 20 min.

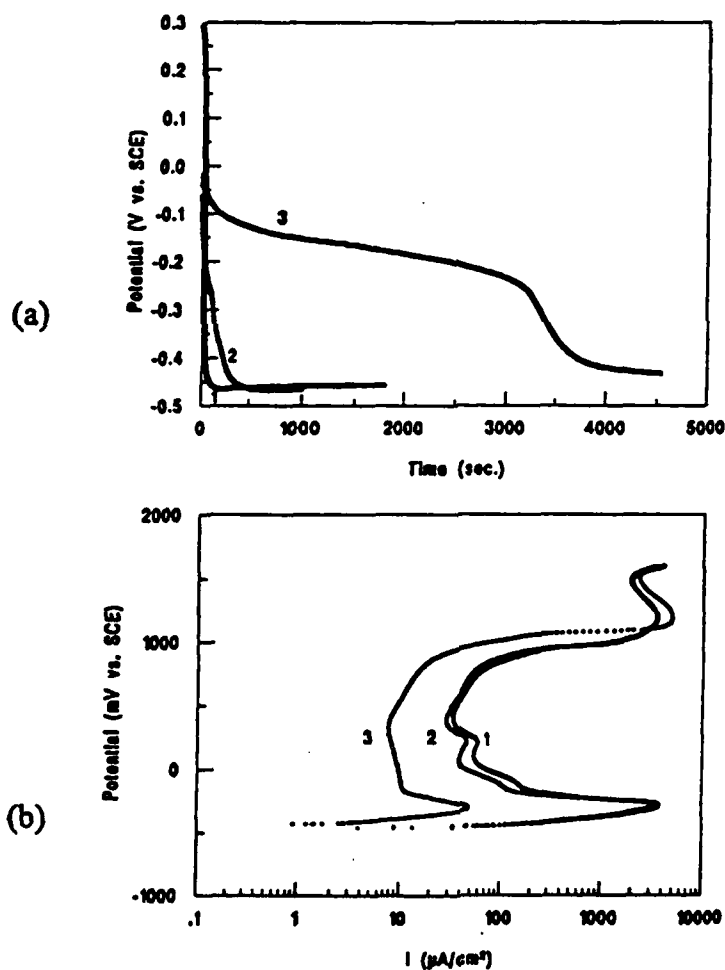


Fig.12a. Open-circuit potential decay for 304 SS exposed to 0.1 M H_2SO_4 : curve 1. as-received; curve 2. after DC passivation at $E = 500$ mV during 20 min; curve 3. after AVPP, with $\{A, P\} = \{1050$ mV, 90 ms $\}$, $E_o = 300$ mV, $R_o = 4 : 1$, time = 20 min.
Fig.12b. Anodic polarisation curves in 0.1 M H_2SO_4 after potential decay (Fig.3a).

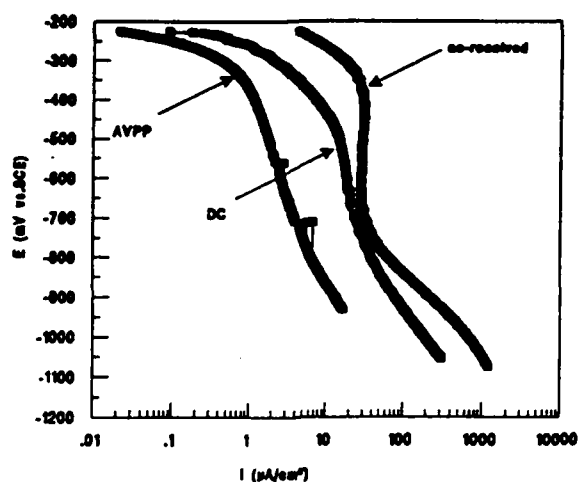


Fig.13. Cathodic polarization curves for 304 SS in aerated borate buffer, pH = 8.4, after different treatments.

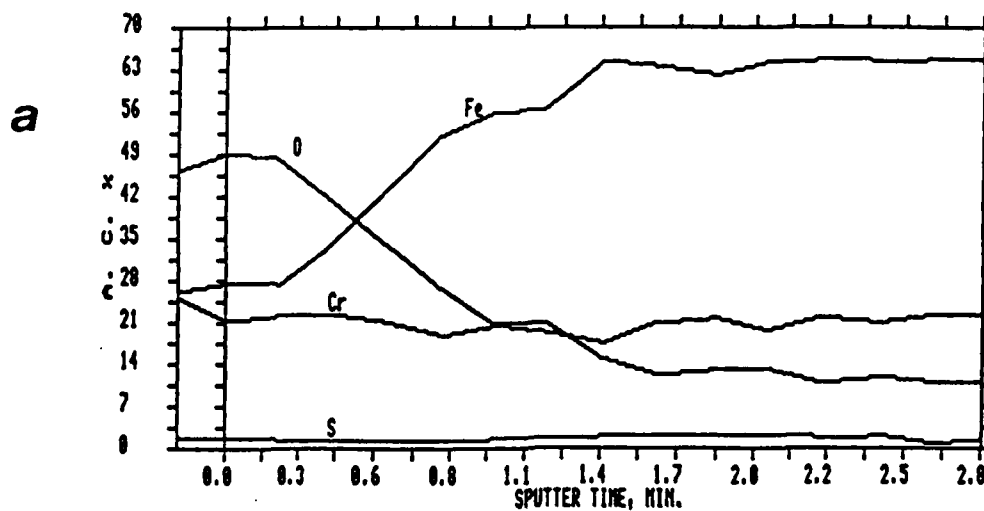


Fig.14. AES concentration profiles for Fe, Cr, S and O for the 304 SS surfaces for the as-received sample (a), after DC passivation (b) and after AV passivation (c).

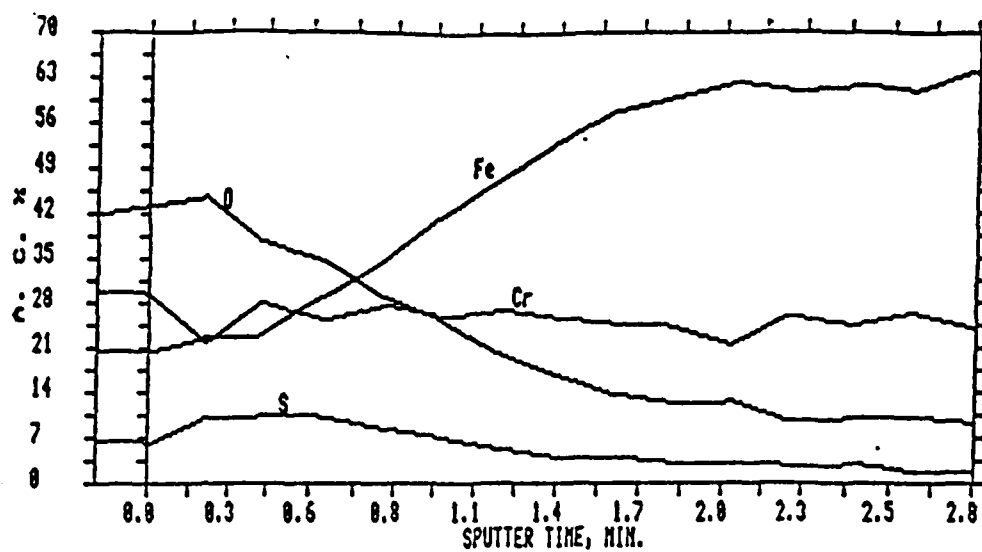
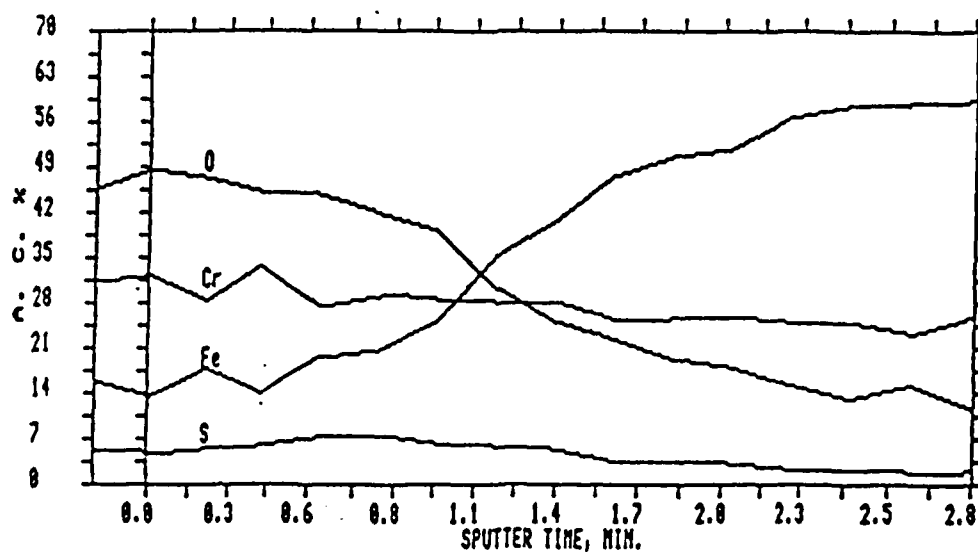
b**c**

Fig.14. AES concentration profiles for Fe, Cr, S and O for the 304 SS surfaces for the as-received sample (a), after DC passivation (b) and after AV passivation (c).

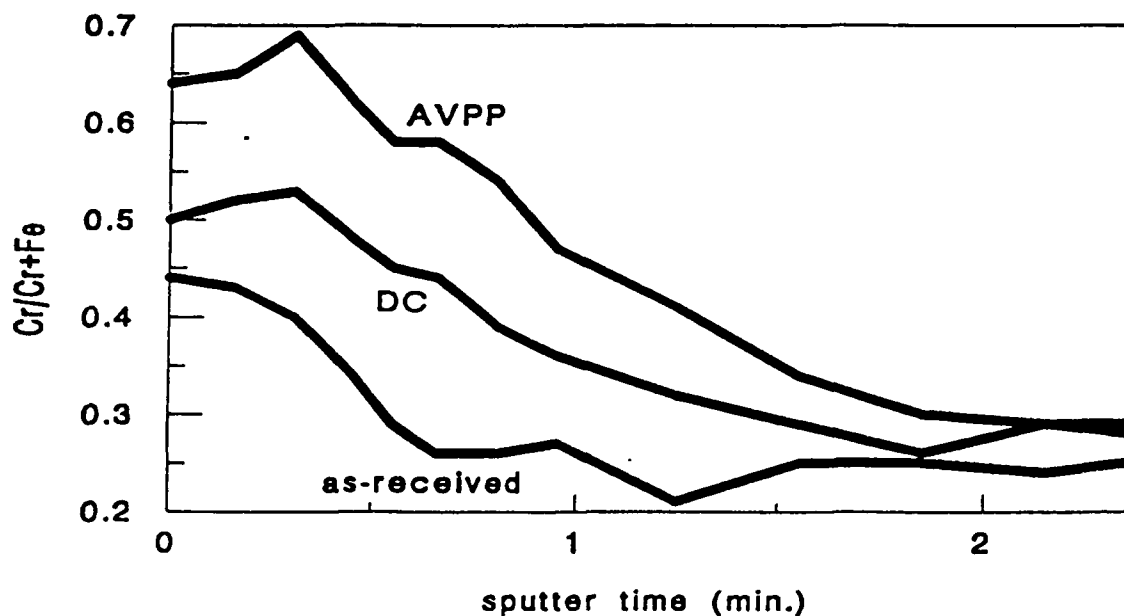


Fig.15. Relative Cr contents in the passive films on 304 SS after different surface treatments obtained from AES profiles.

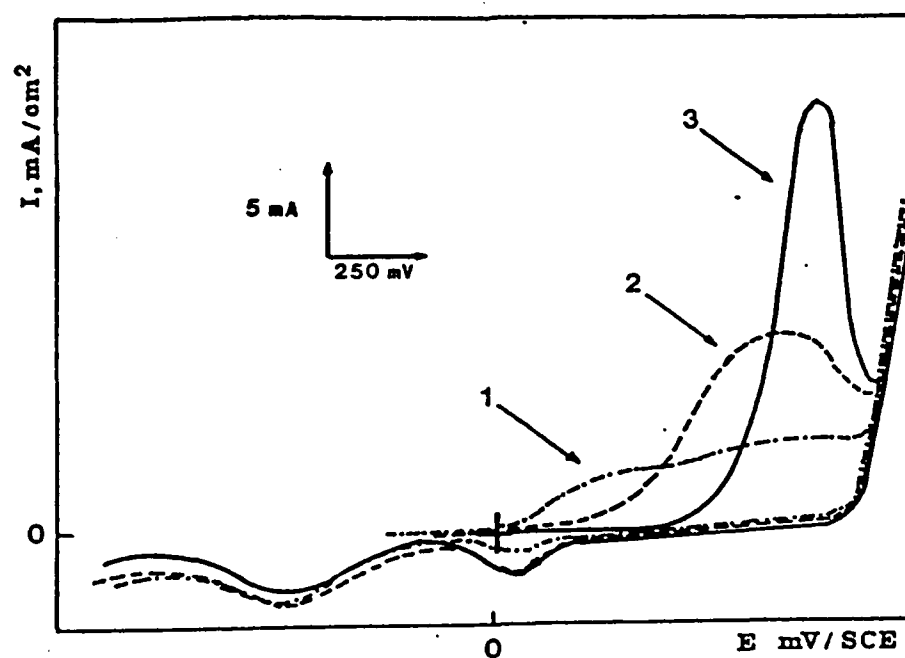


Fig.16. Cyclic voltammograms at 100 mV/s for 304 SS in deaerated borate buffer for different surface conditions: as-received (curve 1), DC passivation (curve 2) and AV passivation (curve 3).

LASER MELTING OF PLASMA-SPRAYED ALUMINA COATINGS

M.L. Escudero, V. López, A. Jiménez-Morales,
E. Vida and J.C. Galván.
Centro Nacional de Investigaciones Metalurgicas, C.S.I.C.
Av. Gregorio del Amo, 8
28040 Madrid. Spain.

Abstract

The effect of laser melting of a plasma-deposited pure alumina coating (γ -alumina) on a microalloyed steel was analyzed. The thicknesses of the alumina coatings were 100, 200 and 380 μm . These coatings were subjected to a multimode laser beam with an elliptical cross-section, with 4 and 6 mm axes and output power of 5, 2.5 and 1.5 kW. The scanning rate was varied between 4.5 and 172 m/min in order to achieve different surface states.

The main aim of this study is to change the alumina coating characteristics obtained by plasma projection. Although this coating is a good thermal barrier and resistant to wear, it is permeable and hence an unsuitable protection barrier against corrosion. We therefore attempted to achieve a coating melt to seal coating porosity and use it as a corrosion barrier.

Optical microscopy and scanning electron microscopy (SEM) were used to analyze how the melting process affected the alumina layer, the thickness which had melted, possible defects in the coating and transformations in the alumina. Corrosion behaviour was evaluated by the polarization resistance method and anodic polarization curves.

Complete melting of the coating leads to the formation of nonporous alumina layers which exhibit macroscopic cracks and a loss of adherence to the base material. Partial melting of the coating leads to a reduction of the porosity in the alumina layer, although microscopic cracks appear in a grid formation over the melted material. The melting of the alumina layer results in a transformation into α -alumina. Corrosion tests show that the laser-melted coating is less permeable than the plasma-deposited coating. In both cases, however, the corrosion behaviour of the metallic material covered by alumina is always controlled by that of the base material.

Key terms: alumina coatings, porosity seal, corrosion barrier

1. Introduction

In previous studies of plasma-sprayed alumina coatings on austenitic stainless steel, it has been shown that corrosion resistance is not altered by the presence of an external alumina layer but, in contrast, is influenced by intermediate coatings between the steel and the ceramic layer, which ensure good adherence^{1,2}.

This work is aimed to seal the inherent porosity of plasma-deposited alumina coatings for use as thermal barriers and against the wear, and also as a protection barrier against corrosive media. Laser melting of plasma sprayed ceramic coatings can be an effective technique to meet this objective.

2. Experimental

In the present study, a series of alumina coatings were used with thicknesses of 100, 200 and 300 μm obtained by plasma spraying over 140x70x10mm³ microalloyed steel sheets. The base steel had the following chemical composition (in mass %): 0.10%C, 0.34%Si, 1.37%Mn, 0.009%P, 0.002%S, 0.032%Nb, 0.014%Ca, 0.032%Al, 0.06%Cr and 0.15%Cu.

Each coated sheet was cut mechanically into four 70x35x10mm³ parts for laser treatment. The melting treatments were carried out at the Navarra Laser Centre using a Spectra Physics 975 model continuous carbon dioxide laser with a power of 5 kW. A multimode beam with an elliptical cross-section with 6 and 4 mm major and minor axes was used in the experiments.

Series of tests were done on the three thicknesses of the plasma-sprayed ceramic coatings. Beam powers and scanning rates are summarized in Table 1.

Optical microscopy and scanning electron microscopy (SEM) were used to analyze how the melting process affected the alumina layer, the thickness which had melted, possible defects in the coating and transformations in the alumina. X-ray diffraction was used to assess the structural state of the alumina before and after laser treatment.

Corrosion resistance was determined by means of two characteristic parameters: the evolution over time of the corrosion potential, E_{corr} , and the corrosion current density, I_{corr} . The latter parameter was calculated using the polarization resistance technique³. Susceptibility to pitting corrosion was assessed by plotting anodic polarization curves. The polarization scan rate was 1 mV.s⁻¹. The electrochemical tests were conducted in tap water at room temperature.

3. Results

Figure 1 shows an SEM surface image of a 100 μm -thick plasma-sprayed alumina coating in its initial state without laser treatment. The last alumina particles deposited during spraying can be seen. The images of the samples with thicker coatings (200 and 380 μm) are also similar to that shown in Figure. 1. At a higher magnification (Figure 2), one can observe microcracking of surface droplets or particles of alumina which have not undergone any laser treatment. This microcracking is present also in the thicker alumina layers. Using X-ray diffraction, it was observed that the coating structure was metastable face-centred cubic γ - alumina.

Surfaces of samples treated by isolated beam scans are shown in Figure 3. The tracks were obtained with a 5kW beam output applied over the samples with different alumina coating thicknesses. The scanning rates were 4, 5, 6.5, 8.5, 10, 17 and 34 $\text{m}.\text{min}^{-1}$. The whole alumina layer melted on samples with 100 μm when the scanning rate was $\leq 17 \text{ m}.\text{min}^{-1}$. However, in samples coated with 380 μm , the laser treatment led to accumulation of molten material in local zones of the track. Molten alumina solidified in the form of droplets or on the edges of craters. The relief of the alumina accumulations is high in the 380 μm thickness layer and diminishes with an increase of the scanning rate. The thickness of molten alumina can be estimated on the basis of the beam power/scan rate ratio (P/R in $\text{kW}.\text{m}^{-1}.\text{min}$), which is proportional to the amount of energy supplied by the laser.

Figure 4 illustrates how the thickness of the molten layer varies according to the P/R quotient in the 100 μm coating. When operating the beam with 1.5kW and 137 $\text{m}.\text{min}^{-1}$, no melting in the alumina layer was observed. Operating with more energetic beams and/or slower scan rates resulted in total or partial melting. The energy supplied by the melting process changes as the melt zone progresses. If melting affects a large part of the coating, there will be a significant heat transfer to the base material. However, if the alumina layer is not melted it will act as a heat shield.

Complete melting of the coating leads to the formation of alumina layers free of internal microdefects (Figure 5). Although microcracks initially seen in the sprayed alumina (Figure 2) disappear, other cracks develop during laser melting and fully penetrate the coating in a direction normal to the surface. The molten alumina layer also shows a clear discontinuity in the zone near the base steel. In a particular case of these treatments (5 kW and 17 $\text{m}.\text{min}^{-1}$) the steel near the coating is quenched to martensite in the zones where perlitic formations were located in the original state (Figure 5).

Connect to previous paragraph X-ray diffraction indicates that there was a recrystallization including the formation of hexagonal, rhombohedral, stable α -alumina (Figure 6).

Given the nature of the substrate, tap water was used to test the corrosion behaviour of the alumina-coated microalloyed steel sheets. Values of E_{corr} , R_p and I_{corr} obtained from samples coated with 200 μm plasma-sprayed untreated coatings and treated specimens with a melted alumina layer thickness of 25 μm were compared. The results of an immersion test for eight days, are shown in Table 2.

Following the test, oxide appeared on the surface of the alumina coating. Although the corrosion behaviour in both cases is a reflection of the behaviour of the base steel.

Anodic polarization curves for the same specimens subjected to the same medium (Figure 7) indicate no passivation in the test range of polarization between -700 and 100 mV. These curves indicate that a laser-treated coating offers a better impediment to corrosion than the plasma-coating sprayed although it is not a protective barrier.

4. Discussion

The results show that laser melting of alumina coatings may lead to diverse forms. One may opt for complete melting of the ceramic material or a partial melting that is restricted to the coating surface.

Partial melting of the outermost alumina layer commences at extremely high scan rates of the laser beam. Although the time of interaction with the beam at a scan rate of 172 m.min⁻¹ is only two thousandths of a second, the dimension and power of the beam are extremely high, supplying large densities of power to the coating, and since, the thermal conductivity of the outermost layer of alumina is low, heat will be localized.

A small unmelted fraction of the alumina layer must remain in order to allow a significant heat transfer to the base steel (Figure 4). Otherwise, the ceramic material acts as a heat barrier.

Complete melting of the alumina layer is not a viable alternative for practical purposes. In addition to thermally affecting the support material, a discontinuity will occur between the coating and the base material. This tends to favour spallation of the whole layer. The possible advantage of obtaining a compact alumina layer that is free of the initial microcracks (Figure. 2), is counteracted by the appearance of other types of cracks that are less numerous but more open and pass through the whole coating (Figure 5).

Partial melting of the plasma-sprayed ceramic layer offers more possibilities. The more restricted the coating thickness subjected to melting, the greater the surface finish of the final product. In spite of cracks that appear on the molten surface, the corrosion test indicates that the permeability of the layer diminishes (Figure 7). This reduction is not enough, however, to consider the coating to be protective.

5. Conclusions

1. Complete melting of the ceramic layer thermally affects the base material and results in a discontinuity between the coating and the base material. In the porosity-free molten ceramic layer, cracks appear that fully traverse the coating.
2. If there is partial melting of the alumina layer, grid shaped cracks and microporosity appear even when the treatment affects a small depth of around $10\mu\text{m}$. Although the water permeability through the coating diminishes, an effective seal is not achieved.
3. The melting of the γ -alumina leads to its transformation into α -alumina.

Acknowledgments

This research was funded by CICYT under Grant No. PPA 86-0443-CO₂-O₂: "Caracterización y evaluación metalúrgica de los materiales tratados superficialmente con láser".

References

1. M.L. Escudero, J.A. González and J. Ruiz, British Corrosion Journal, 22 3(1987): p.182.
2. M.L. Escudero, J.A. González and J. Ruiz, Werkstoffe und Korrosion, 39 (1988): p.364.
3. M. Stern and A.L. Geary, Journal Electrochemical Society. 104 (1957): p.56.

Table 1. Beam powers and scanning rates used on the three coating thicknesses of the plasma-sprayed ceramic coatings.

Power, kW	Scanning rate, m.min⁻¹
5	4, 5, 6.5, 8.5, 10, 17, 34, 51, 85, 125, 137, 172
2.5	68, 125, 137, 172
1.5	51, 85, 137

Table 2. Values of E_{corr} (vs. a Saturated Calomel Electrode), and R_p and I_{corr} in tap water solution for plasma-sprayed in the as-received condition and laser-melted alumina samples.

Parameters	Plasma sprayed	Laser melted
E_{corr} (mV/SCE)	- 654	- 582
R_p ($\Omega \cdot \text{cm}^2$)	5448	6000
I_{corr} ($\mu\text{A} \cdot \text{cm}^2$)	4.7	4.3

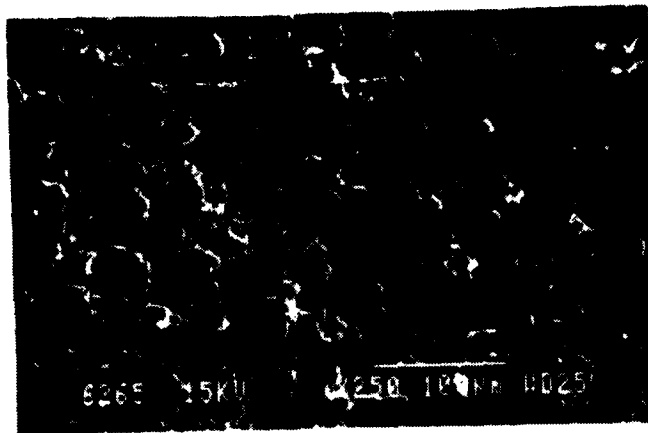


Figure. 1.- Surface morphology of a plasma-sprayed 100 μ m thick alumina coating before laser treatment.

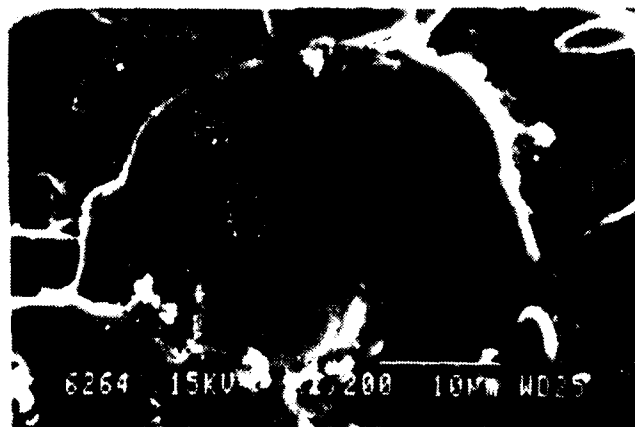


Figure. 2.- Microcracks observed on the coating in Figure 1.

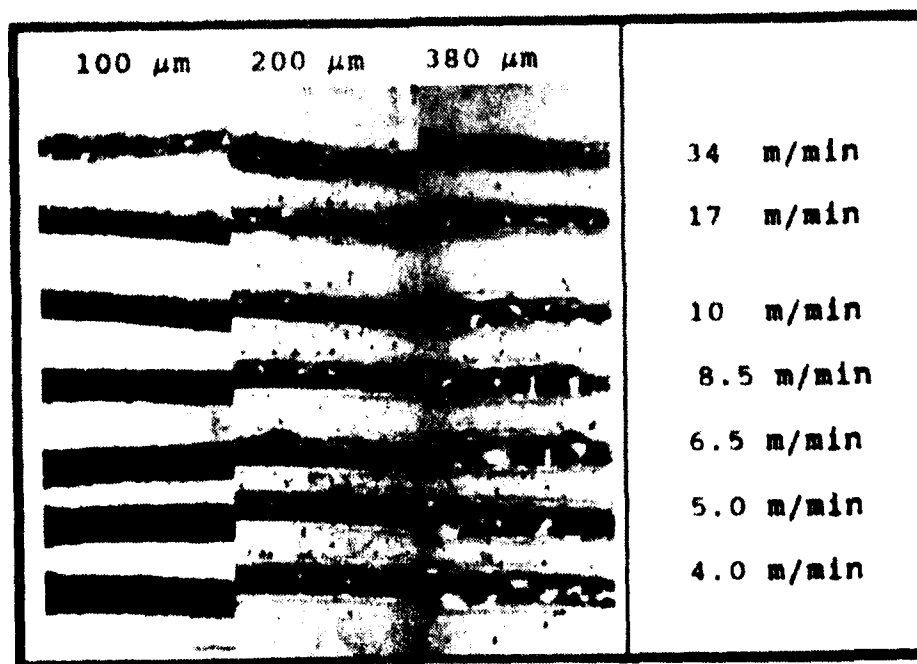


Figure. 3.- Tracks created by a 5 kW beam at different scan rates over specimens with alumina coatings of different thicknesses (x 1).

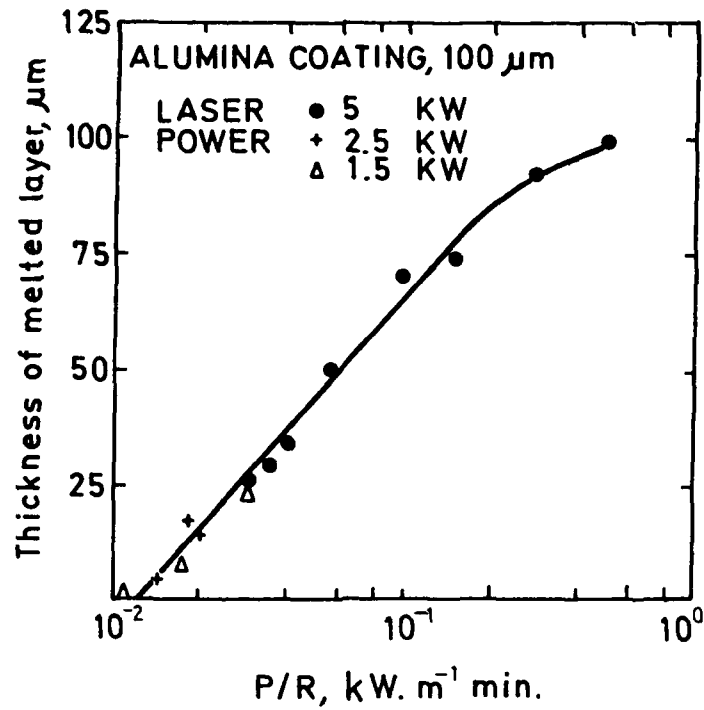


Figure. 4.- Variation of molten alumina layer thickness with beam operating conditions.

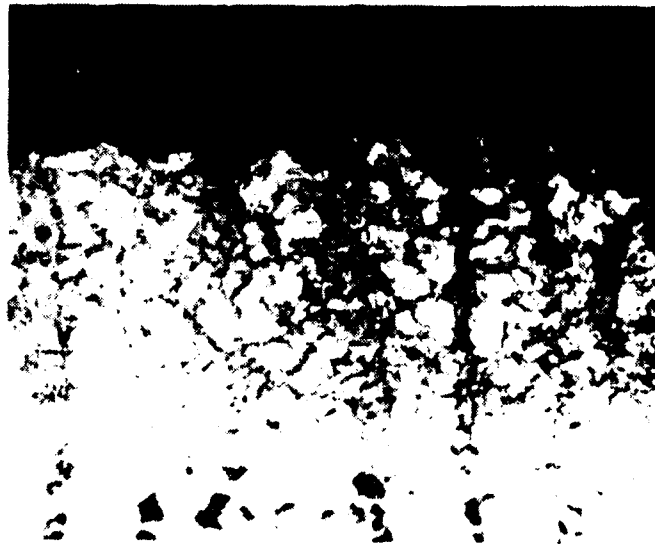
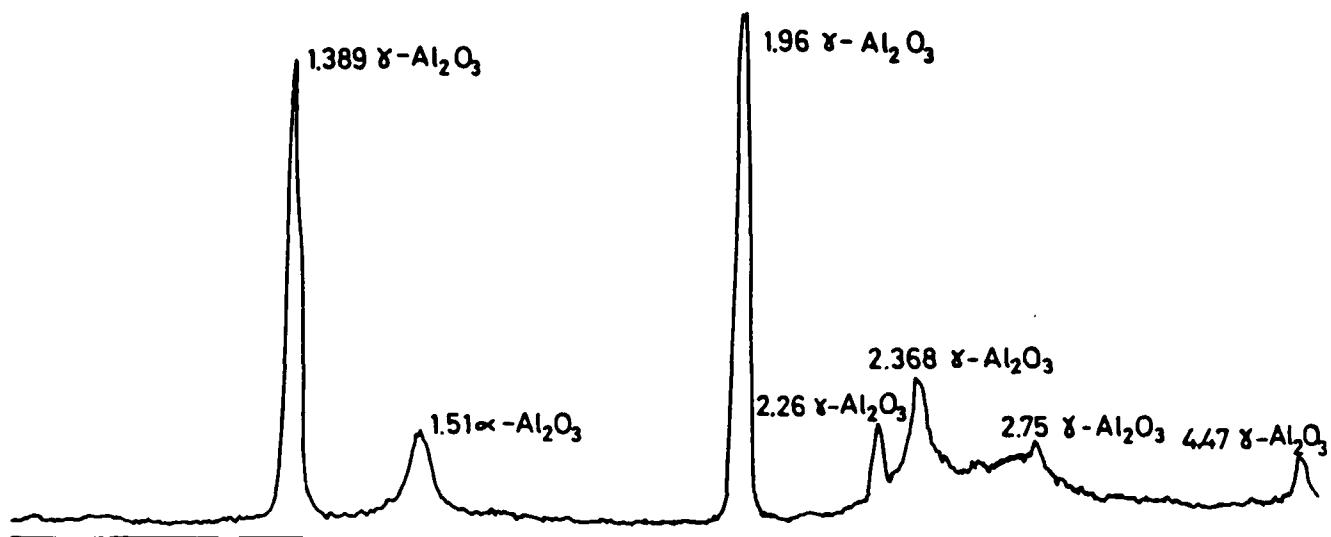
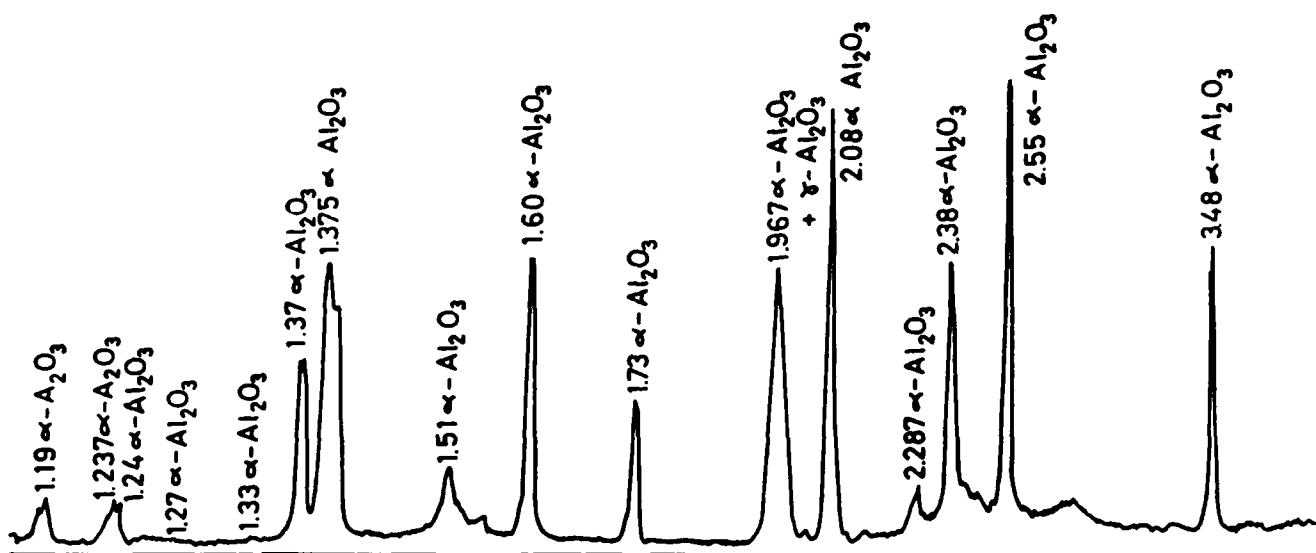


Figure. 5.- 100 μm -thick alumina coating melted with a 5kW beam scanning at rate of 10 m.min⁻¹.



(a)



(b)

Figure. 6.- X-ray diffractograms of the alumina coating:
(a) before melting, and (b) after complete melting of the coating.

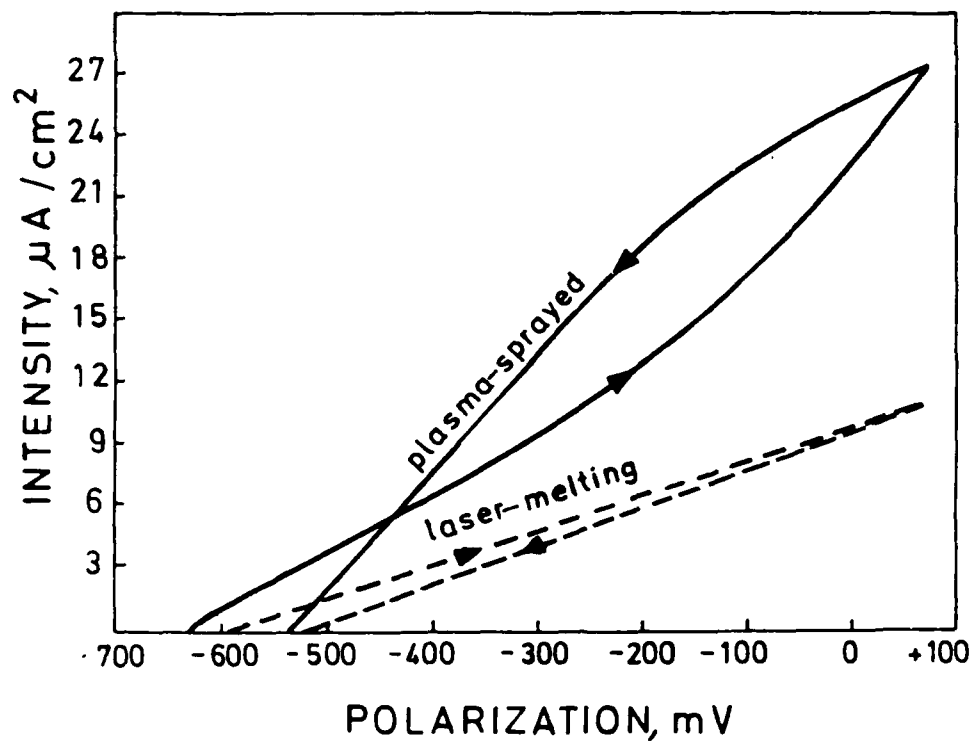


Figure. 7.- Anodic polarization curves of untreated and treated plasma-sprayed alumina coatings.

CORROSION AND OXIDATION BEHAVIOR OF TI-AL SURFACE ALLOYS FORMED USING LASER IRRADIATION

A.S. Khanna
Corrosion Science and Engineering
Indian Institute of Technology, Bombay, India.

V.H. Desai
Materials Science and Engineering Program
Mechanical and Aerospace Engineering
Univ. of Central Florida, Orlando, USA.

G.L. Goswami
Bhabha Atomic Research Center
Bombay, India.

ABSTRACT

This paper presents the results on the investigations made on the formation of surface coatings of titanium aluminide by irradiating the aluminum coated titanium substrates with laser. The characterization of the coatings and their effect on the high temperature oxidation behavior has been described.

Key terms: high temperature oxidation, laser surface alloying, titanium aluminide, intermetallics

INTRODUCTION

Titanium, a potential base for refractory alloys, is particularly suitable for aerospace applications, mainly due to its low density and high strength. It forms a protective oxide film which readily heals in water thereby making it an important metal for oil, chemical and marine industries. Quite recently, the metal is being recommended for condenser tubes especially where sea water or brackish water is used for cooling. There is however, a limitation on the use of this metal. Above 350°C the metal dissolves excessive oxygen, which makes it very brittle. Alloying improves the strength as well as increases the utility temperature limit to about 550°C, beyond which again the oxygen dissolution dominates^[1]. It seems unlikely that bulk alloying could impact a further improvement in the use of this metal beyond this temperature. The alternate way to achieve this is by applying some coatings which prevent oxygen permeation^[2].

Intermetallics of Ti with Al have very good high temperature properties. They have been found to be suitable for high temperature applications beyond 600°C^[1]. The aim of this research is to develop surface films for titanium and titanium alloys which push their utility temperature beyond 500°C. A combination of spray coatings followed by laser irradiation was chosen as the route to form such coatings.

Laser irradiation is now becoming a suitable method to form thin protective layers or surface alloys by irradiating the coated surface with a laser beam^[3-5] or incorporating the alloying constituent by simultaneously adding the alloying element^[6]. Such coatings have been found to be more dense, uniform and relatively strongly bonded to the substrate^[7]. Further, an intense heat source such as a laser beam, melts a very specific area very fast followed by rapid cooling, giving rise to a novel microstructure which could improve the corrosion and oxidation properties^[8].

EXPERIMENTAL

Pure titanium metal (having trace amounts of Fe, Cr and Al) was coated with aluminum (99.95%) using spray coating techniques. Flame spraying using oxy-acetylene gas and arc spraying were used to coat titanium with aluminum powder. For convenience, specimens were designated as FT1, FT2, FT3, AT2, LT1, LT2 and LT3, where "F" refers to flame sprayed specimens and "A" arc spray specimens. Numbers 1, 2 and 3 refers to original thickness of aluminum deposited on the specimens, viz. 100, 200, and 300 μm respectively. The final coating thickness obtained was slightly higher than that planned.

Nd:YAG pulsed laser with 300 watts and pulse time of 1-20 ms was used for carrying out laser treatment. Several trial runs were carried out at different values of the total pulse energy (5 - 18 Joules) on the coated specimens. The pulse width of 15 ms, beam diameter of 2 mm and sweep speed was kept constant throughout the experiments. Laser treatment were carried out in a specially designed chamber where a constant flow of Argon provided a protective atmosphere.

Pure titanium, aluminum coated titanium and the laser treated specimens were subjected to high temperature oxidation by exposing the specimens in air at 600°C and 700°C for about 250 hours. Before oxidation, laser treated specimens were characterized for surface structure, composition and diffusion of Al into the matrix using scanning electron microscopy/energy dispersive X-ray spectroscopy (SEM/EDS). Oxygen dissolution was estimated using microhardness indentation technique. Specimens after oxidation were analyzed using SEM/EDS.

RESULTS AND DISCUSSION

Characterization of Laser Treated Specimens

Figure 1 shows the optical micrograph of the flame sprayed specimen. The aluminum coating thickness appears to be more than 400 μm and it is highly porous and uneven.

Laser treatment can make the aluminum coating very dense. However, the laser parameters used, were not always adequate to melt the substrate or improve the bonding of the coating with the substrate (Figure 2). For a specimen with a lower coating thickness (100 μm), a laser melted zone is formed which is highly bonded to the substrate (Figure 3).

The composition of the surface alloy formed and the depth of the alloyed zone are related to the material properties in a complex manner. Since, the physical properties such as low melting and boiling points and high vapor pressure of Al are not favorable for laser irradiation, it was difficult to get the desired composition of the alloy by using a pure Al coating. Many trial runs were carried out at various coating thickness and total energy of laser per pulse. Figure 4 shows the distribution of aluminum in the titanium matrix from the free surface at various levels of total pulse energy for 100 μm thick coated specimens. Figure 5 shows the same for the specimens with 200 μm aluminum coating. Results from both of these analysis can be summarized as follows:

- i) Low pulse energy is able to give higher concentration of aluminum at the top of laser melted zone.
- ii) At high energy, more of the substrate melted and some Al got vaporized. The Al distribution is a bit more uniform when compared to low pulse energy.
- iii) At high pulse energy, the laser melt zone extends much deeper into the substrate matrix which is not desirable. Desired depth may be obtained by increasing the scanning speed, coating thickness or beam diameter.

The location of microhardness measurements in the laser melt zone and the substrate are shown in Figure 6. The results indicate that the laser melt zone is much harder (H_V 303) compared to the titanium substrate (V_H 144).

Arc Coated Specimens

Specimens that were arc spray coated had Al thickness of either 200 or 450 μm . The coating was relatively uniform and dense. Trial runs were carried out by choosing various laser parameters. Pulse energy (10 to 18 J/pulse) and pulse duration (8 to 12 ms) were the main parameters varied. Figure 7 and Figure 8 show respectively distribution of Al within the laser melted zone for Ti coated with 200 and 450 μm thick Al coating. The laser energy used for alloying were similar at 15 J per pulse and 16 J per pulse respectively. Among the two specimens, one coated with 200 μm of Al shown more uniform Al distribution in the melt zone.

Oxidation Tests

Weight gain vs time data for the oxidation of bare titanium substrate, Al coated Ti and laser treated Al/Ti specimens are shown in Figures 9 and 10. The oxidation tests were run in air at 600°C and 700°C for about 250 hours.

- i) Oxidation rate of Ti metal decreases as a result of aluminum coating alone and the rate of oxidation does not vary significantly with the coating thickness. A slight increase in oxidation rate at coating thickness in excess of 100 μm could be due to higher porosity.

- ii) As expected, arc coated specimens show better oxidation resistance, likely, because the coating was more dense and uniform.
- iii) Laser treatment further reduces the oxidation rate which assures better corrosion resistance probably due to densification of coating, better substrate-coating bonding, fine microstructure of the alloyed zone and the formation of TiAl or Ti₃Al intermetallics.

Samples on which high temperature oxidation tests were run formed mainly alumina at 600°C and TiO₂ at 700°C respectively. A comparison of the products formed on the oxidized and non-oxidized samples after laser treatment is given in Table 1 as identified by X-ray diffraction.

Dissolution of oxygen in the titanium matrix during oxidation was observed. The initial increase in oxidation rate is due to oxygen dissolution which makes the matrix brittle^[9]. An increase in hardness from V_H 144 for Ti to V_H 182 after oxygen dissolution confirms this view. The dissolution increased further at 700°C increasing the hardness value to V_H of 260. Coating on the surface, especially after laser treatment, reduced the extent of oxygen dissolution in the matrix, thus confirming the advantage of such coatings in improving the mechanical behavior at high temperatures.

CONCLUSIONS

The present work is a preliminary study on the formation of titanium aluminide intermetallic coatings by an insitu laser irradiation method. The work has shown that oxygen dissolution which is the main culprit in deteriorating the high temperature utility of titanium is drastically reduced by forming surface coatings especially of titanium aluminide. Formation of proper coating and selection of suitable laser parameters is the main requirement for a suitable impervious coating. Addition of certain alloying elements which improve the room temperature ductility of the coatings should be an important parameter for future consideration.

REFERENCES

1. J. Stringer, Acta Met., 8 (1960), p758.
2. N.W. Kearns et. al., Proc. 6th World Conf. on Titanium, Vol.4, (1988) p1753, France.
3. A.S. Khanna, W.J. Quadackers, M. Schuster, E.W. Kreutz, K.Wissenbach and A. Gasser, Structure and Reactivity of Surfaces, C. Morterra, A. Zecchina and G. Costa (edts), Elsevier Publication, (1989) p535, Amsterdam.
4. A.S. Khanna, R.K. Singh Raman, E.W. Kreutz and A.L.E. Terrance, Corrosion Science, 33 (1992) p949.

5. J.G. Smeggil, A.W. Funkenbusch and N.S. Bornstein, High Temperature Science, 20 (1985) p163.
6. L.J. Li and J. Majumdar, 'Laser processing of Materials', AIME, K. Mukharjee and J. Majumdar, (eds.), 1989, p35.
7. R. Streiff, M. Pons and P. Mazars, Surface and Coating Technology, 32 (1987) p85.
8. F.H. Stott, P.K.N. Barret and G.C. Wood, Mater. Sci. & Eng. 88 (1987) p163.
9. Mathew J. Donachie, 'Titanium' A technical guide, ASM International, Metal Park, 1990, p223.

Table1 Types of phases detected on the surface of the various samples (a). unoxidised (b). oxidised at 600°C (c). Oxidised at 700°C.

a

Samples	Types of phases observed.
LT1	Ti, TiAl
LT3	Al

b

Samples	Types of phases observed.
T1	TiO ₂
FT1	TiAl ₃ , α-Al ₂ O ₃
FT3	TiAl, α-Al ₂ O ₃
LT1	TiAl, TiAl ₃ , α-Al ₂ O ₃
LT3	Al, α-Al ₂ O ₃

c

Samples	Types of phases observed.
T1	TiO ₂
FT4	TiAl, α-Al ₂ O ₃
FT4 ^a	TiAl ₃ , α-Al ₂ O ₃
AT1	TiAl, α-Al ₂ O ₃
LT1	TiO ₂ , α-Al ₂ O ₃
LT3	TiAl, α-Al ₂ O ₃

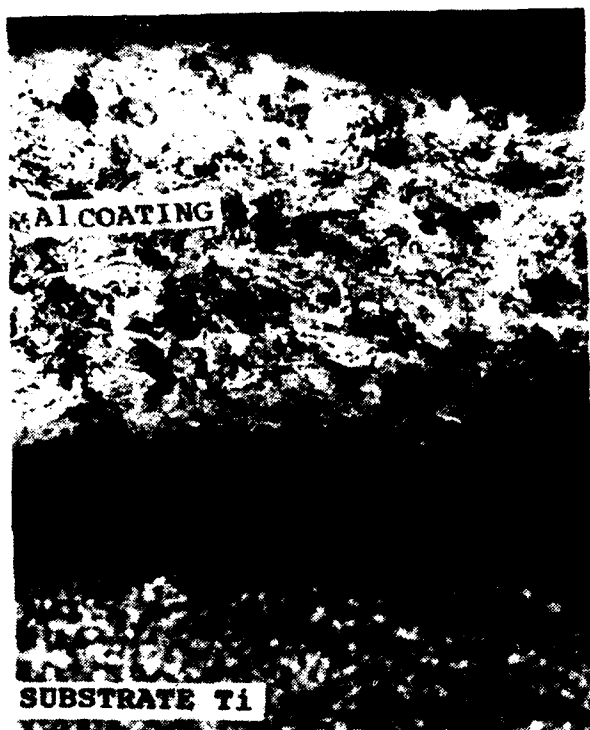


Fig. 1 Optical Micrograph of Flame Sprayed Sample (FT3)

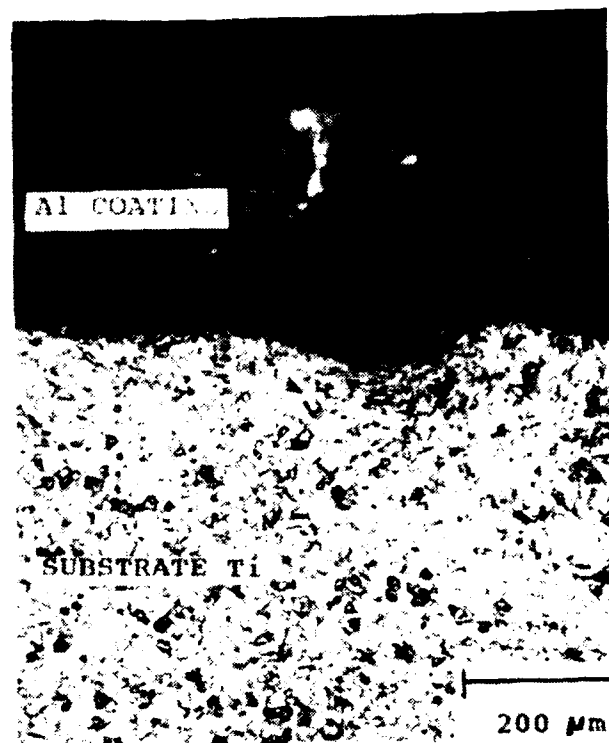


Fig. 2 Optical Micrograph of Laser Treated Sample (LT2)

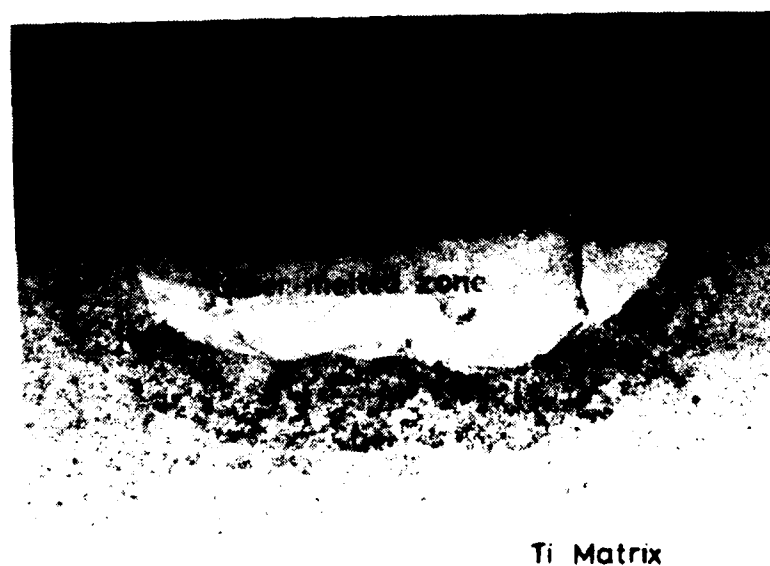


Fig. 3 Optical Micrograph of Laser Treated Specimen (LT1)

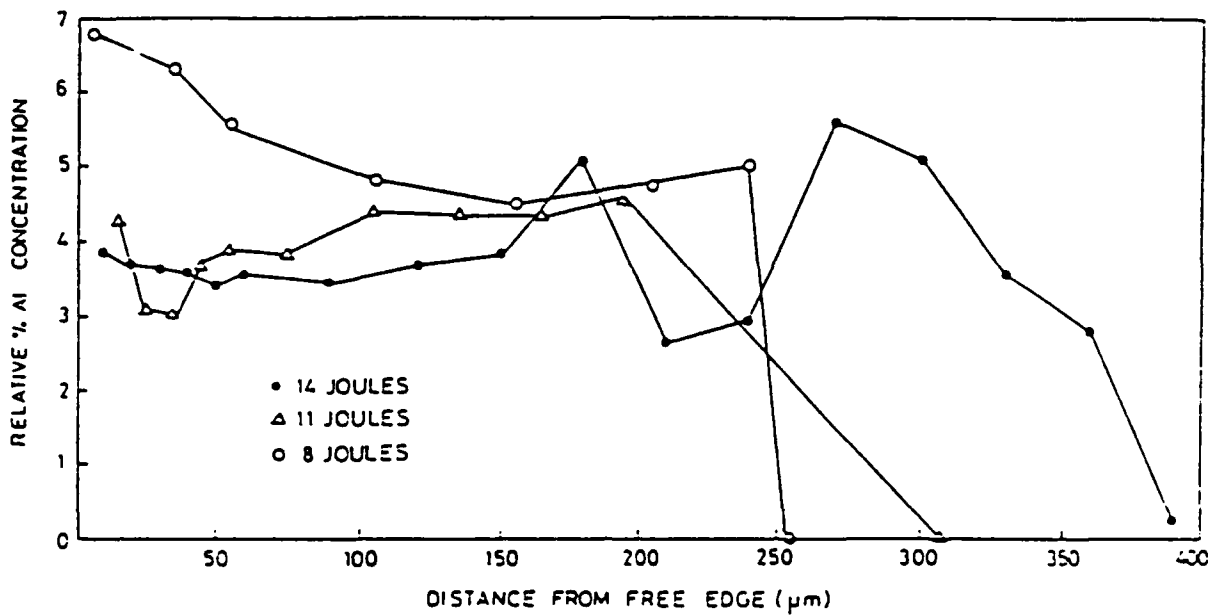


Fig. 4 EDS Analysis of LSA for the Irradiated Sample (FT2)

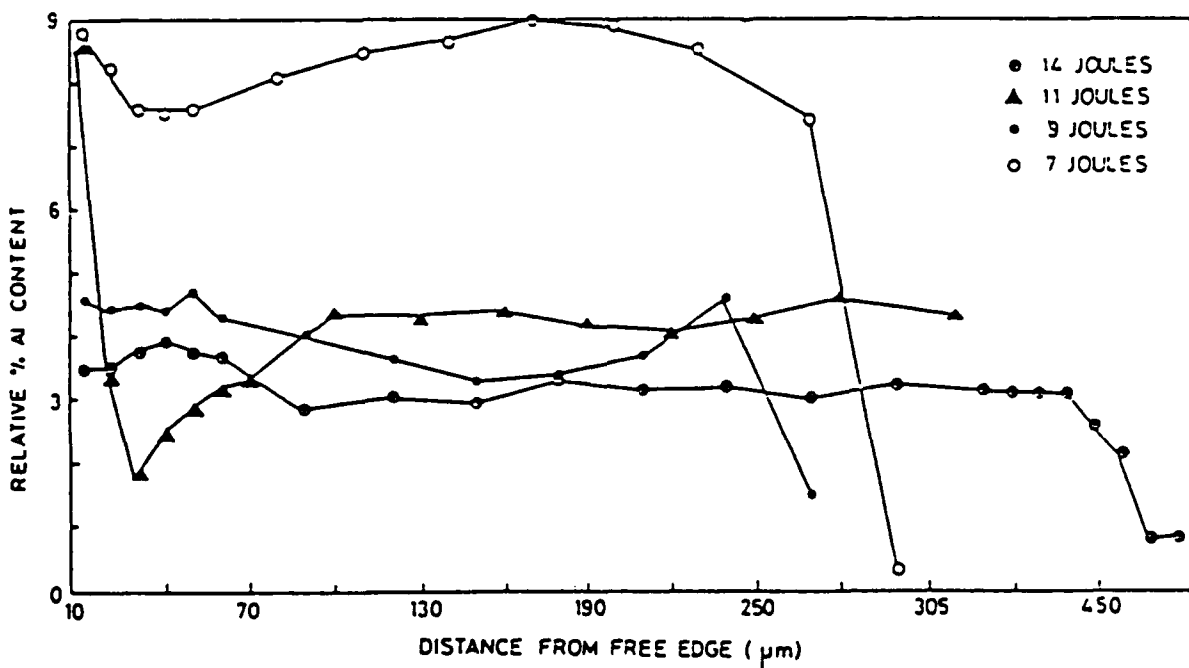


Fig. 5 EDS Analysis of LSA for the Irradiated Sample (FT3)

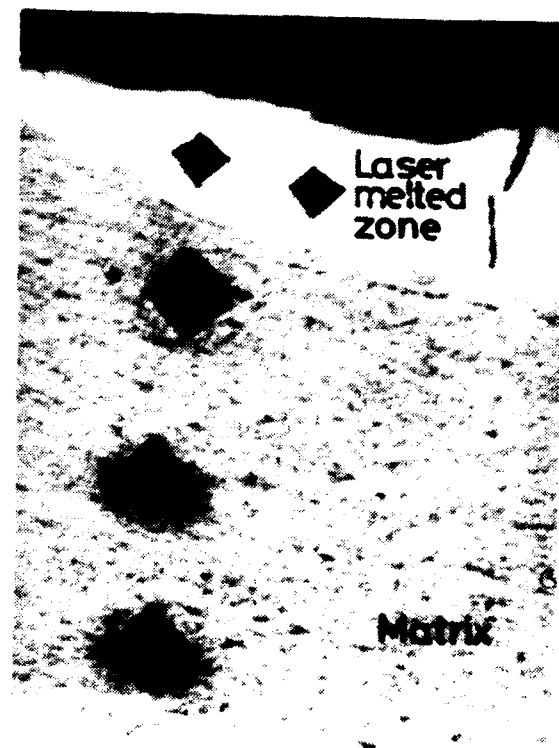


Fig. 6 Results of Microhardness on Laser Treated Sample (LT1)

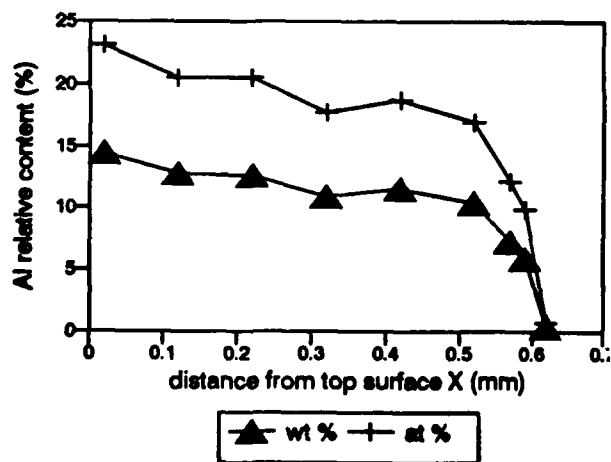


Fig. 7

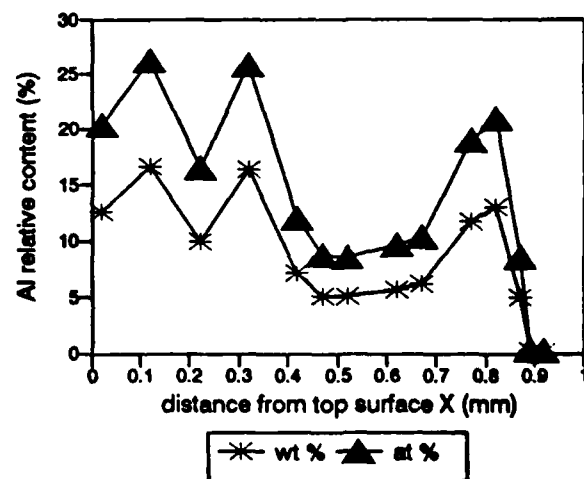


Fig. 8

EDS Analysis of (Fig. 7) 200 μ m Thick and (Fig. 8) 400 μ m Thick Arc Coated Aluminum Followed by Laser Treatment.

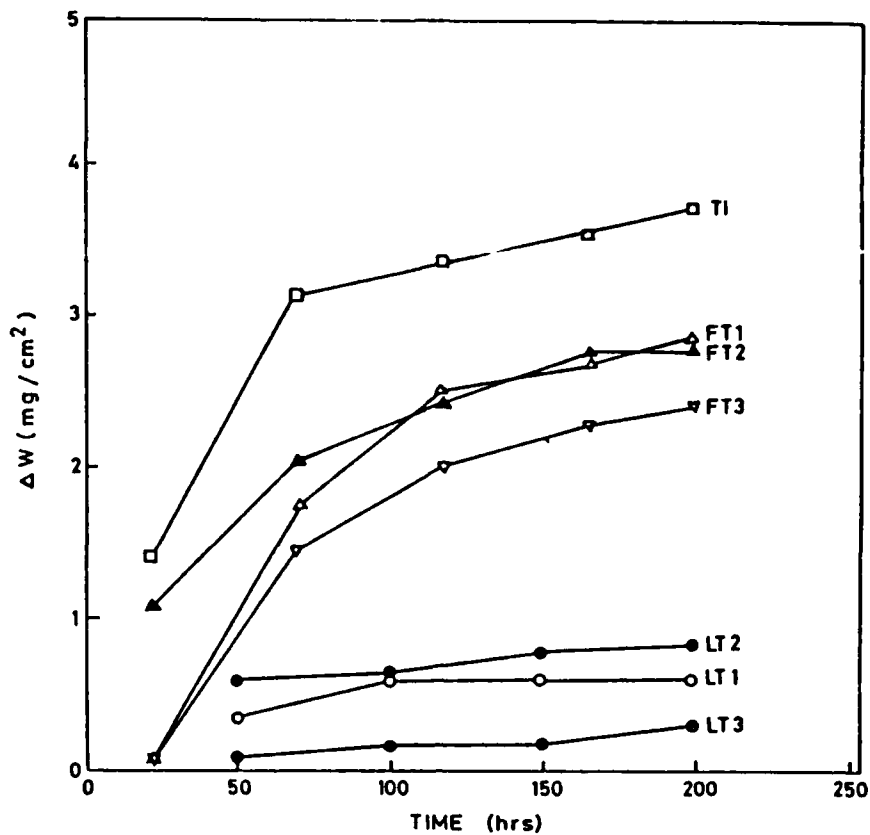


FIG.9. WEIGHT GAIN VS. TIME PLOT FOR THE OXIDATION OF PURE Ti AND ALUMINIUM COATED Ti AT 600 °C

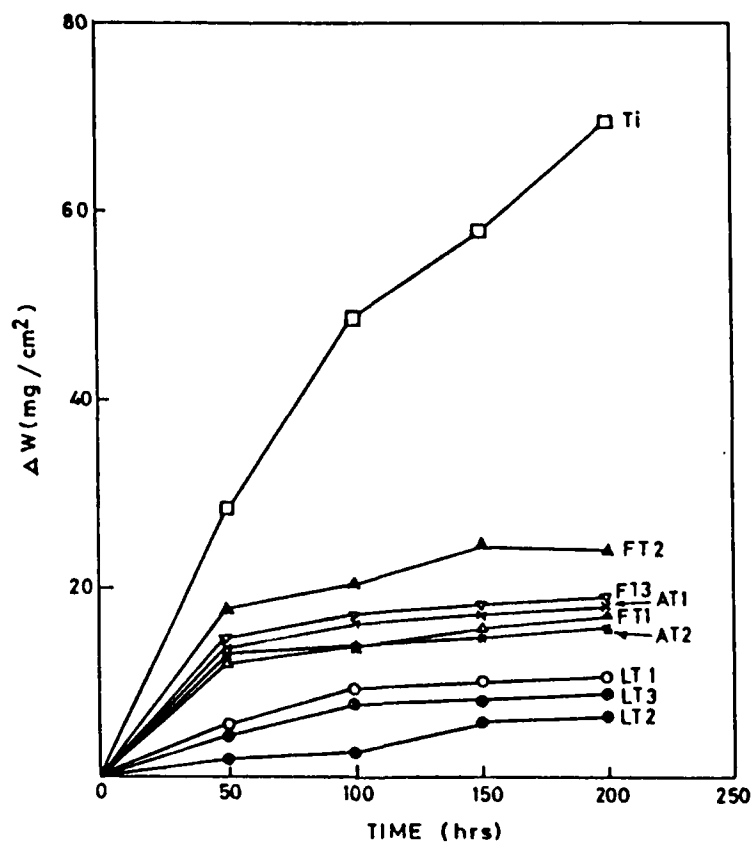


FIG.10. WEIGHT GAIN VS TIME PLOT FOR THE OXIDATION OF PURE Ti AND ALUMINIUM COATED Ti AT 700 °C

CORROSION AND HEAT RESISTANCE OF ALUMINA COATED IRON TO ALKALI CARBONATE AT 700°C

Masaru OKUYAMA

Oyama National College of Technology
771 Nakaguki, Oyama, 323, Japan

Takuji Noshiro

Oyama National College of Technology
771 Nakaguki, Oyama, 323, Japan

Satoshi Kambe

Faculty of Science and Technology, Teikyo University
1189-4 Nishi-kitayama, Nagaoka, Utsunomiya, 320, Japan

Abstract

In order to develop heat and corrosion resistant materials for molten alkali carbonates which are used as electrolytes for Molten Carbonate Fuel Cells, alumina was coated on a metallized iron substrate by the plasma-spraying method. From previous investigations, it was found that chromium was a superior metallizing material to give good heat and corrosion resistance. Moreover, compared with electrolytic chromium powder, ductile chromium one (99.9% purity) has been found to be a superior material. In this study, corrosion and heat resistivity of the alumina-coated samples and alumina-chromium concentration-graded coating samples using ductile chromium powder were examined through polarization experiment in 53mol%Li₂CO₃-47%Na₂CO₃ at 700°C and microscopic observation and SEM analysis after rapid cooling.

The ductile chromium-metallized double layer coatings gave a half time smaller corrosion current densities than those of the electrolytic-chromium metallized ones and were not generally cracked by rapid cooling from 700°C. It could be recognized that ductile chromium gave both better heat and corrosion resistance as a metallizing material. Furthermore, the three-stepwisely chromium/ alumina concentration-graded coatings were superior than the chromium-alumina double layer coatings in both corrosion and heat resistance. It was also found that the concentration of chromium in the Cr/Al₂O₃ mixed middle layer and the film thickness of the alumina top-coat gave strong effect on the corrosion current density. Minimum corrosion current was observed for the sample containing 30 to 40 atm% Cr in the middle layer and the thicker alumina layers gave the smaller corrosion current density.

1. Introduction

Recently, advanced technologies for application of molten salts have been developed. One of the current attractive subjects is molten salt fuel cell (MCFC). Molten alkali carbonates used in MCFC are so aggressive that metallic materials easily pass an allowance of corrosion¹⁾⁻⁵⁾. The authors have investigated development of ceramic-coated materials available for this environment by using a plasma spray technique⁶⁾. Ceramic-coated materials are required to satisfy both corrosion and heat resistance. From our recent results, the followings were found out. Alumina coating films were the most corrosion-resistant to molten alkali carbonates among several ceramic coatings tested. When iron is employed as a substrate material for economic reasons, chromium metal is necessary as a metallizing material for protection and contact of iron substrates⁷⁾.

Since plasma-sprayed alumina films were porous and thus molten salt penetrated through pores, metal substrates reacted with the molten salt. Chromium gave comparably low corrosion current and, moreover, had a similar thermal expansion coefficient to that of alumina. For fabrication of the coatings, electrolytic chromium powder was mainly employed. In this experiment, the alumina-chromium coatings of double layer structure were not satisfied because

Key terms: molten alkali carbonate, plasma-sprayed alumina coatings, hot corrosion

they frequently cracked during rapid cooling, but alumina/chromium concentration-graded coatings especially improved heat resistivity. These results have been published⁸⁾. However, it was also found that use of a ductile chromium substrate instead of iron much improved both corrosion and heat properties of the alumina-coated samples. In this paper, for more development, characteristics of alumina coating samples using ductile chromium powder as a metallizing material are investigated through polarization experiments in molten alkali carbonates and chemical analysis of the layers. Results are compared with electrolytic chromium powder.

2. Experimental

A pure iron rod of 3 mm was cut into 50 mm length. One end of the rod was sharpened to obtain homogeneous coatings and avoid direct exposure of the substrate iron to molten salt. After roughening the surface with a sand blast, ductile chromium powder (99.9% purity) was sprayed for metallizing and then alumina powder was sprayed as an outermost layer. During application the iron sample was rotated. In some cases, an alumina/chromium mixed layer was sandwiched between them. Models of chromium distribution in the concentration-graded alumina/chromium coating layers are exhibited in Fig. 1 (A) with a schematic diagram of the experimental apparatus (B). The alumina powder provided by Showa Denko Inc. was a commercial product of 5 to 20 μm in diameter for spraying. Electrolytic chromium was prepared by grinding metal pieces up to a size smaller than 40 μm . The ductile chromium powder used had an average diameter of 29 μm and was provided by Toso Inc. The fabricated alumina-coated samples were characterized using SEM and EPMA analysers. Thickness of the coating layers were measured with a reading microscope. Corrosion resistance of the samples in molten alkali carbonates was measured by their stepwise potentiostatic polarization experiments in 53mol% Li_2CO_3 -47% Na_2CO_3 at 700°C under 1 atm CO_2 . Polarization was carried out from 0 V vs the Ag/10mol%AgCl reference electrode in the less noble direction to -2.0 V every 0.05 V for 1 minute, which is called the first scan. Reversing polarity, polarization was performed up to 1.0 V, which is called the second scan. Heat resistance of the samples was measured by applying them rapid cooling, which was provided by removing the sample from the operating furnace at 700°C.

3. Results

3.1. Comparison between polarization curves of alumina-chromium double layer coatings on iron using electrolytic and ductile chromium powder

Alumina-chromium double layers were coated on iron by plasma spraying. The corrosion and heat resistance of the metallizing materials were compared between electrolytic and ductile chromium powder. Figure 2 shows the first and second polarization curves of both samples in 53% Li_2CO_3 -47% Na_2CO_3 at 700°C under closed atmosphere of 1 atm CO_2 . For the sake of comparison, the polarization curve of iron directly covered with an alumina layer without any metallizing is also given in Fig. 2. In the case of the directly alumina-coated iron sample, the substrate iron reacts through the alumina porous layer and thus, indicates the corrosion potential of iron in this media. On one hand, the sample metallized with electrolytic chromium has much less noble potential than iron, which corresponds to that of a metallic chromium electrode, and reduces corrosion current density to about a half. The sample using ductile chromium powder for metallizing shows about 0.2 V more noble potential than that of the sample metallized with electrolytic chromium and gives about half corrosion current density, which seems to be in passive state. Heat resistance of these coating samples were measured by microscopic observation after polarization experiment followed with rapid cooling in air by taking them out of the furnace. Figure 3 exhibits their surface stereo-microscopic photographs. The alumina layer coated on the non-metallized iron substrate was completely broken. That of the sample metallized with electrolytic chromium was not significantly broken but slightly cracked. While, the sample metallized with ductile chromium can be observed to have no crack. Therefore, it was found that ductile chromium powder was superior as a metallizing material to give both high corrosion and heat resistance.

3.2. Polarization experiment of chromium/alumina concentration-graded coating samples

In most cases when ductile chromium was employed as a metallizing material, the alumina coating layers were not cracked after rapid cooling from 700°C. However, it was found that they were cracked in rare cases if their thickness was less than 100 μm . For more improvement, three stepwisely concentration-graded coatings were fabricated layer by layer, which were composed of chromium layer (undercoat) / a mixing layer of alumina-chromium / alumina layer (topcoat). Changing in the mixing weight ratio of chromium powder to alumina one from 1:2 to 1:49, a middle layer was sprayed. Figure 4 exhibits the 1st scanning polarization curves of the samples with a middle layer sprayed with a mixed powder of 1:2, 1:9 and 1:19 in weight ratio. Since the sprayed chromium in the coating films react with the salt, similar profiles of polarization curves can be seen. It is also found that both anodic and cathodic current decreases with decreasing mixing ratio and accordingly, corrosion current density decreases. After taking the samples out of the furnace and then cooling, none of them were cracked.

3.3. Characterization of the coating samples after their polarization experiment followed with rapid cooling

The cross sections of the coating samples after their polarization experiment at 700 °C followed with rapid cooling in air was examined by SEM observation and EPMA line analysis. Figures 5 shows the SEM photograph and chemical line analysis on Al and Cr components by EPMA for a chromium-alumina double layer coating after the polarization experiment. The SEM photograph indicates no cracks in any part of the coating and it was possible to estimate rough values of the layer thickness. The chemical line analysis of aluminum and chromium components in the coating shows clear discrimination of a metallized chromium layer and an alumina layer with a narrow overlapping range (< 35 μm). Variation of the intensity in the chromium layer (330 μm) is rather smooth in spite of powder spraying, which means low porosity of the layer. While, variation of aluminum intensity in the alumina layer (290 μm) was fairly rough. This means that the sprayed alumina powder does not display sufficient cohesion and thus, the layer has some large pores.

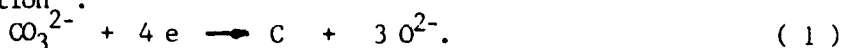
Figure 6 shows the SEM photograph and the Al and Cr distribution in a Cr- Al_2O_3 concentration-graded coating (a triple layer) after the polarization experiment, which has the middle layer sprayed with a mixture of Cr and Al_2O_3 powder in equi-molar ratio after the polarization experiment. Maintenance of a compact coating with no cracks can be seen even after a polarization experiment followed by rapid cooling. The mixed layer is comparably so thin (150 μm) that distribution of Cr and Al is not clear, but atomic chromium fraction can be roughly estimated to be 83 % in average. This means that chromium powder is more easily sprayed than alumina powder. Therefore, mixing ratio of chromium powder to alumina for spraying should be reduced for reduction of corrosion current. Figure 7 shows the photographs of the sample with a middle layer sprayed in mixing powder weight ratio of 1:9 after a polarization experiment followed by rapid cooling. The thickness of the three layers was measured to be 370, 100 and 360 μm outerwards. The chemical line analysis reveals that chromium atomic fraction in the middle layer is estimated to be 65 % in average. The SEM and EPMA line analysis of the sample using powder weight ratio of 1:19 for spraying the middle layer is exhibited in Fig. 8. The thickness of the three layers was measured to be 260, 105 and 290 μm outerwards. The analyzed chromium atomic fraction in the middle layer is estimated to reduce to 30 %. Taking into consideration the result from the polarization experiments, which indicate that the reduction of the mixing ratio of powder, Cr to Al_2O_3 diminished corrosion current, quantity of chromium in the middle layer seems to play an important role in determining corrosion rate.

4. Discussion

4.1 Corrosion reaction and advantage of ductile chromium powder

It was found that the profiles of the polarization of the chromium-alumina double layer coatings on the substrate iron were different between the first scan (0 to -2.0 V) and the

second one (-2.0 to 1.0 V). Especially, a big discrepancy of about 0.5 V was observed between the corrosion potential ($I = 0$) in the first scan and that in the second one. It was reported that the cathodic reduction was the deposition of carbon according to the following reaction⁹⁾:



Carbon deposited in the cathodic process on the first scan reversibly dissolved in the anodic process on the next second scan. Therefore, the corrosion potential of the first scan shift to the carbon/carbonate reversible potential. Since the anodic polarization curve on the first scan is attributable to anodic reaction of the substrate metals, the polarization curves in the first scan can give corrosion current by extrapolation of their expected Tafel lines. From the first scanning polarization curves of chromium-metallized alumina (double layer) coatings, the measured corrosion potential of the sample using electrolytic chromium powder was located at around -1.2 V, but that of the sample using ductile chromium powder is at around -1.0 V (Fig.2). This difference means that electrolytic chromium was more active than the ductile chromium because the former existed nearer to the active state. However, the cathodic current can be observed to give almost the same value on both samples. This seems to be because the cathodic reaction rate is controlled by diffusion process in the porous alumina coating layer or becomes independent of the samples as the reaction takes place on the deposited carbon in the layer. The estimated corrosion current density is listed in Table 1 with the thickness of layers in the coatings. It is found that the corrosion current density of the sample using ductile chromium powder was less than a half of the corresponding one using electrolytic chromium powder and that cooling shock caused no significant cracking or destroying on the former (Fig.5), but often did on the latter. Therefore, use of ductile instead of electrolytic chromium powder much improved both corrosion and heat resistance. This is because ductile chromium has more similar heat expansion coefficient, $7.5 \times 10^{-6} \text{K}^{-1}$ ¹⁰⁾ to that of alumina and smaller corrosion current due to high purity (99.9%).

4.2 Corrosion and heat resistance of Cr/alumina graded coatings

Ductile chromium/alumina stepwisely concentration-graded coatings were fabricated, which consisted of three layers; metallized chromium layer, chromium-alumina mixed middle layer and alumina top layer. Their corrosion current densities were estimated from the first scanning polarization curves and listed on Table 1. The corrosion currents of the concentration-graded coatings are generally smaller than those of the double layer coating. Whether their heat resistance was improved or not is not clear from the rapid cooling test, but no crack were generated on any samples.

It can be understood from Table 1 that the corrosion current density of the stepwisely Cr/Al₂O₃ concentration-graded coating samples diminishes when the mixing ratio of chromium to alumina powder for spraying of the middle layer is reduced. However, the chromium and aluminium line analyses revealed that their practical ratio in the middle layer is remarkably shifted. This is because the two powders are very different in their gravity, powder size, particle figure and spraying efficiency even if the two powders were completely mixed in the preliminary process. The effect of sprayed ratio of Cr to Al₂O₃ in the middle layer on the corrosion current density was examined. To avoid disturbance of the coating film thickness, data on the samples with an alumina topcoat of similar thickness (140 - 200 μm) are used. The result is shown in Fig. 9. It can be seen that the corrosion current density strongly depends on the concentration of chromium in the middle layer. It decreases with decreasing chromium content but a minimum is observed at around 30 to 40 % below which it increases again. Decrease in the corrosion current density can probably be understood as follows. Anodic reaction is attributable to dissolution or oxidation of chromium in the middle layer. Decrease in the chromium concentration reduces reaction surface area and probably does electric contact. Less concentration than 30 % becomes more advantageous, but simultaneously loses role of a binder between alumina powders and thus, the middle layer seems to become more porous. Finally, the corrosion current density corresponds to that of a Cr-Al₂O₃ double layer coating if the curve extends to zero chromium concentration. Therefore, the Cr/Al₂O₃ concentration-graded coatings with the middle layer which was sprayed by powder weight ratio of Cr/Al₂O₃ = 1:19 (real concentration in the layer = 30 to 40 atomic%) gives the best corrosion

resistance.

On heat resistance, Cr-Al₂O₃ double film coatings rarely cracked after polarization experiment followed by rapid cooling, but no crack was observed on the surface of any type of Cr/Al₂O₃ concentration-graded coating samples as long as ductile chromium powder was used.

4.3 Effect of thickness of layers composing Cr/Al₂O₃ concentration-graded coatings on corrosion resistance

Plasma-sprayed alumina coatings were reported to have about 8 % porosity¹¹⁾. Therefore, corrosion reactions take place on the substrate metals through a porous alumina top coating layer. Therefore, it can be expected that the thickness of coatings or individual layers composing them gives a strong effect on corrosion current density. Figure 10 shows the effect of thickness of Al₂O₃ top layer (A), the middle Cr-Al₂O₃ mixing layer (B) and metallized chromium layer (C) on corrosion current density using all of the data given in Table 1. Although the thickness dependence of the metallized chromium layers and the mixed middle layers is difficult to recognize, that of the Al₂O₃ top layer seems to be distinguishable. This is because the porous Al₂O₃ layer becomes a barrier to reaction of chromium in the middle layer and/or of the metallized chromium layer.

As discussed in the previous section, the corrosion current density strongly depends on the chromium concentration in the middle layer of the three-stepwisely concentration-graded coatings. Therefore, the corrosion current density depends not only on thickness of the Al₂O₃ top-coat film but also on the concentration of chromium in the middle layer. If the data of the samples with the same chromium concentration in the middle layer are connected by a line, the dependence of the film thickness of the Al₂O₃ top layer become more clear as shown in Fig. 11. The simplest interpretation of these relations may suggest diffusion control. However, the anodic polarization curves obeyed Tafel relations. Therefore, it seems to be because increase in Al₂O₃ thickness causes reduction of the number of channelings to reaction sites.

5. Conclusion

In order to develop heat and corrosion resistant materials for the molten alkali carbonates which are used as electrolytes for Molten Carbonate Fuel Cells, alumina was coated on a metallized iron substrate by the plasma-spraying method. Through this investigation, it was found that chromium was a superior metallizing material giving good heat and corrosion resistance. Up to now, electrolytic chromium powder was mainly used, but ductile chromium (99.9% purity) powder has been found to be superior. In this investigation, heat and corrosion resistivity of the alumina-coated samples and alumina/chromium concentration-graded coating samples using ductile chromium powder as a metallizing material were examined through polarization experiment in 53%Li₂CO₃-47%Na₂CO₃ at 700°C and microscopic observation and SEM analysis after rapid cooling. The results are as follows.

(1) The corrosion current density of Al₂O₃-chromium double layer coatings using ductile chromium was one half that of the samples using electrolytic chromium. The electrolytic-chromium metallized double layer coatings were destroyed very often after applied thermal shock but no crack was observed for most of those using ductile chromium. It could be recognized that ductile chromium was superior to give both heat and corrosion resistance as a metallizing material.

(2) The stepwisely Cr/Al₂O₃ concentration-graded coating (a triple layer) was sprayed on the iron substrates and tested. Their corrosion and heat resistance were better than the chromium-alumina double layer coatings.

(3) It was found that the concentration of chromium in the Cr/Al₂O₃ mixed middle layer of the three-stepwisely concentration graded coatings was much higher than the mixing ratios of their powders for spraying and that it gave strong effect on the corrosion current density. Minimum corrosion current density was observed at the sample with 30 to 40 atm% Cr in the middle layer.

(4) The effect of film thickness of each layer composing coatings on corrosion current density was examined. Relationship between corrosion current density and thickness of the Al_2O_3 top-coat layer could be recognized. The corrosion current density linearly decreased with increasing film thickness. This seems to be because the Al_2O_3 top coat films are a barrier to anodic reaction of chromium in the coatings.

Reference

- 1) H.Numata, A. Nishikata and S.Haruyama, Boshoku Gijutsu, 33, 103 (1984)
- 2) R.A.Rapp, Proc. 11th Intern. Corros. Congress (1990.4, Florence), Vol. 4, 11
- 3) R.A.Donado, L.G.Marianowski and J.R.Selman, J. Electrochem. Soc, 131, 2535 (1984)
- 4) D.A.Shores and P.Singh, Proc. Sympo. on Molten Carbonate Fuel Cell, Electrochem. Soc, 271 (1984)
- 5) H.S.Hsu, J.H.Devan and M.Howell, J. Electrochem. Soc, 134, 3038 (1987)
- 6) M.Okuyama, A.Tsurumi, Y.Itoi and S.Kambe, Proc. 11th Intern. Corros. Congress (1990.4,Florence), Vol.4, 29
- 7) M.Okuyama, M.Ushioda and Y.Itoi, Proc. Corros. Protec.'91 (1991.5, Tokyo), 69
- 8) M.Okuyama, M.Ushioda and Y.Itoi, Denki Kagaku, 60, 508 (1992)
- 9) M.D.Ingram and G.Janz, Electrochim. Acta, 10, 783 (1965)
- 10) Private report from Toso Inc.
- 11) Y.Sekimoto, Study on Industrial Safety (Oyama National College of Technology), No.8, 109 (1987)

Table 1 List of film thickness of each layer composing sprayed coating films, chromium concentration in middle layer analysed by EPMA and measured corrosion current densities

Chromium layer (μm)	Middle layer (μm)	Alumina layer (μm)	Powder mixing weight ratio for spraying middle layer	Cr at % in middle layer by EPMA	Corrosion current density (A/m^2)
*290	0	0	-		8.0
300	0	0	-		7.0
310	0	140	-		5.8
250	0	240	-		5.0
310	0	270	-		5.0
330	0	290	-		4.0
260	200	140	Cr:Al ₂ O ₃ =3:2	96	4.7
340	240	320	3:2		3.0
270	150	280	1:2	85	3.5
300	120	410	1:2		2.2
420	100	170	1:9	69	3.5
330	160	370	1:9		2.8
320	110	170	1:19		2.2
160	170	190	1:19	35	2.0
270	80	150	1:49	13	4.6
120	110	170	1:49		3.2
210	90	200	1:49		4.5

* Electrolytic chromium powder was used, the others were ductile chromium

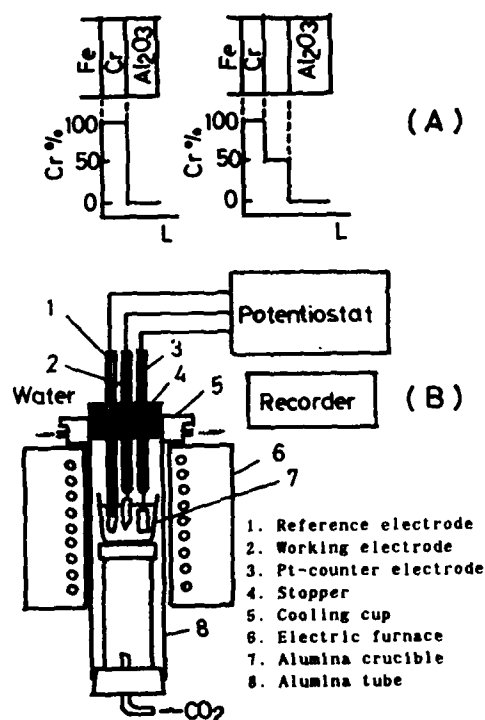


Fig.1 Models of coating layers and chromium distribution for plasma-sprayed Cr/Al₂O₃ stepwisely concentration-graded coatings (A) and schmatic figure of apparatus for polarization experiment in molten 53%Li₂CO₃-47%Na₂CO₃ at 700°C

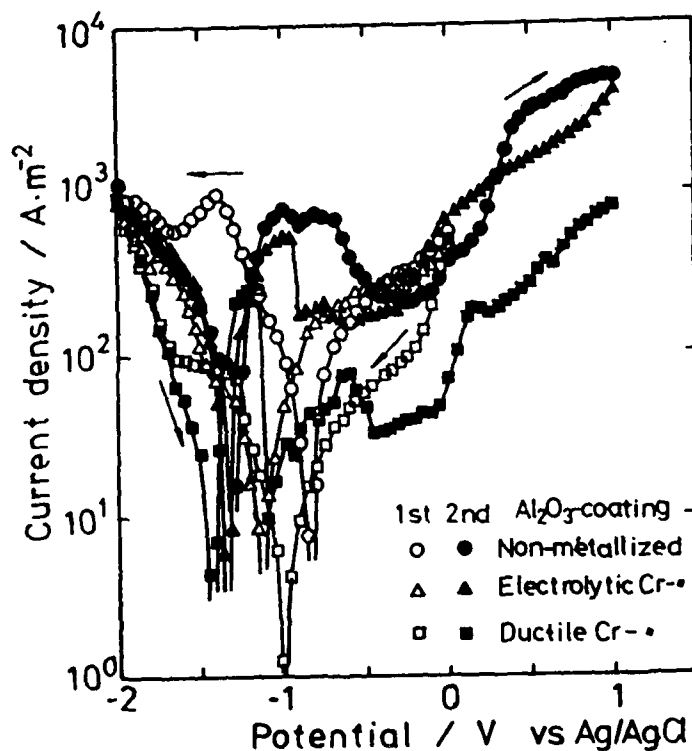


Fig.2 1st and 2nd scanning polarization curves of electrolytic Cr-, ductile Cr- and non-metallized Fe coated with Al₂O₃ in molten 53%Li₂CO₃-47%Na₂CO₃ at 700°C

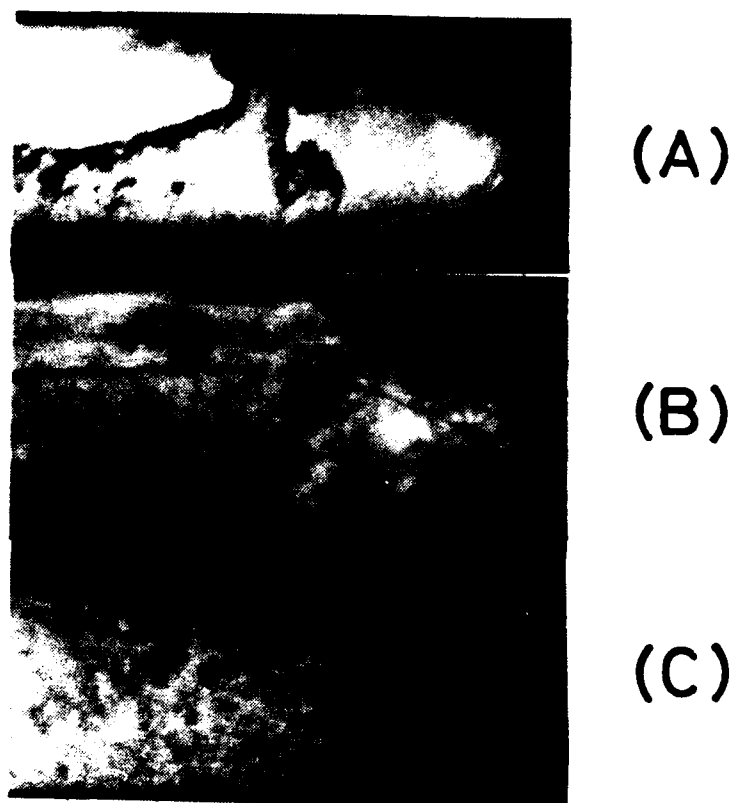


Fig.3 Stereo-microscopic surface photographs of non- (A), electrolytic Cr- (B), and ductile Cr- (C) Fe coated with Al_2O_3 after polarization experiment followed with rapid cooling

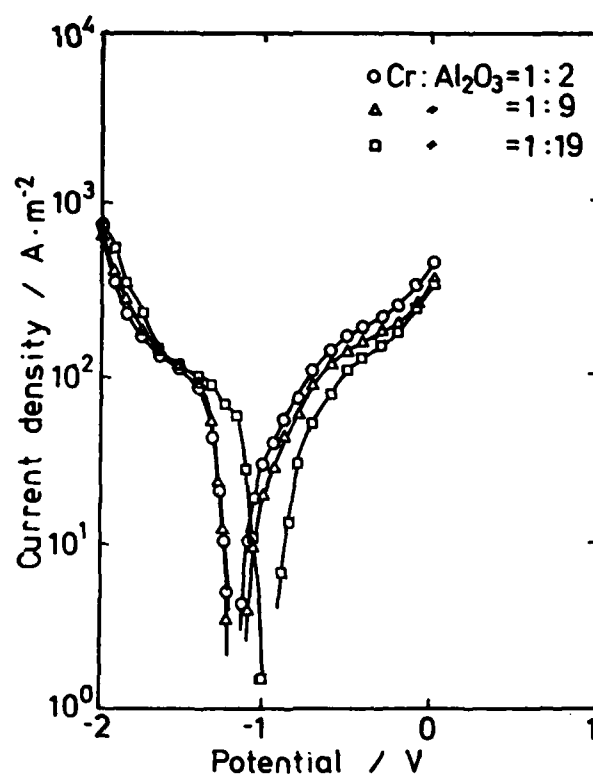
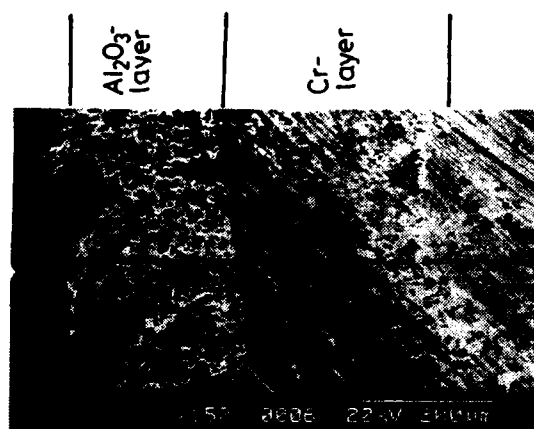
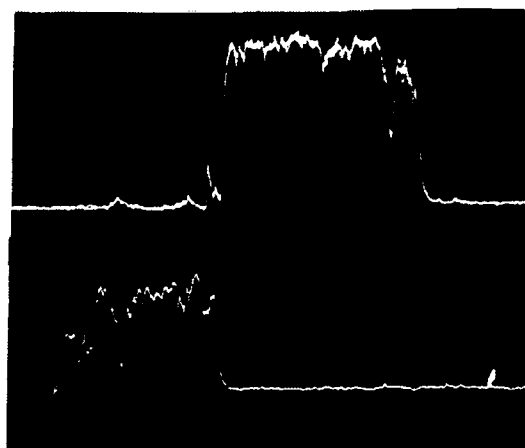


Fig.4 1st scanning polarization curves of three-stepwisely concentration-graded coatings with a middle layer sprayed with a mixed Cr and Al_2O_3 powder in various ratios



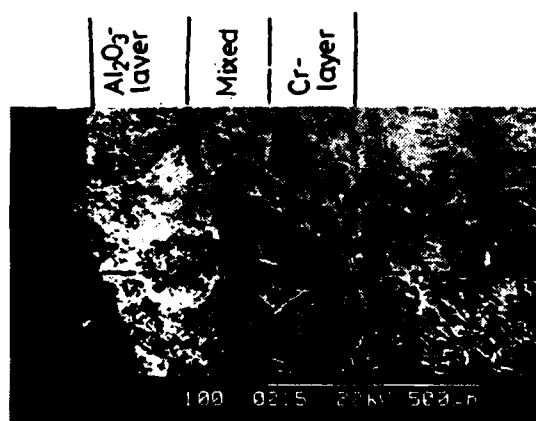
SEM photograph

Intensity profile
of chromium



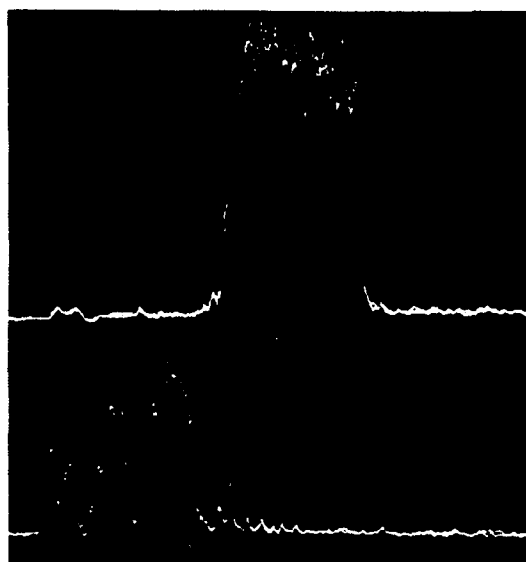
of aluminum

Fig.5 SEM photographs and Cr and Al line analysis of cross section of ductile chromium-metalized Fe coated with Al_2O_3 after polarization experiment followed with rapid cooling



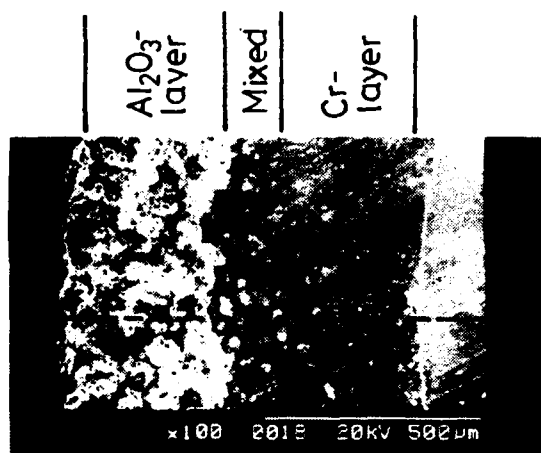
SEM photograph

Intensity profile
of chromium



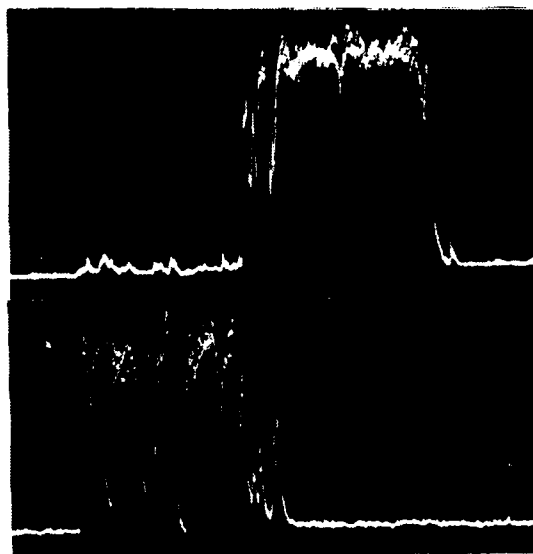
of aluminum

Fig.6 SEM photograph and Cr and Al line analysis of cross section of a 3-stepwisely concentration-graded coating of Cr and Al_2O_3 powder in ration of 1:2 after polarization experiment followed with rapid cooling



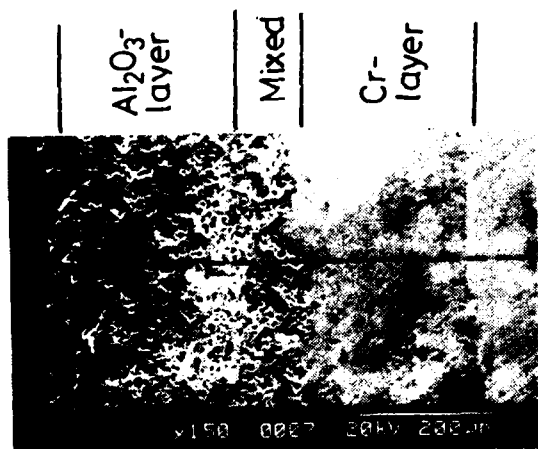
SEM photograph

Intensity profile
of chromium



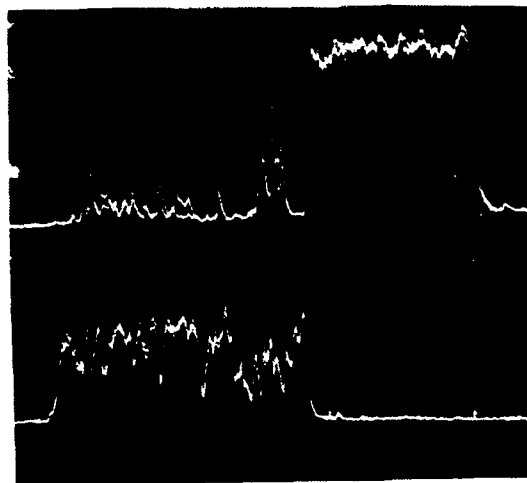
of aluminum

Fig.7 SEM photograph and Cr and Al line analysis of cross section of a 3-stepwisely concentration-graded coating of Cr and Al_2O_3 powder in ration of 1:9 after polarization experiment followed with rapid cooling



SEM photograph

Intensity profile
of chromium



of aluminum

Fig.8 SEM photograph and Cr and Al line analysis of cross section of a 3-stepwisely concentration-graded coating of Cr and Al_2O_3 powder in ration of 1:19 after polarization experiment followed with rapid cooling

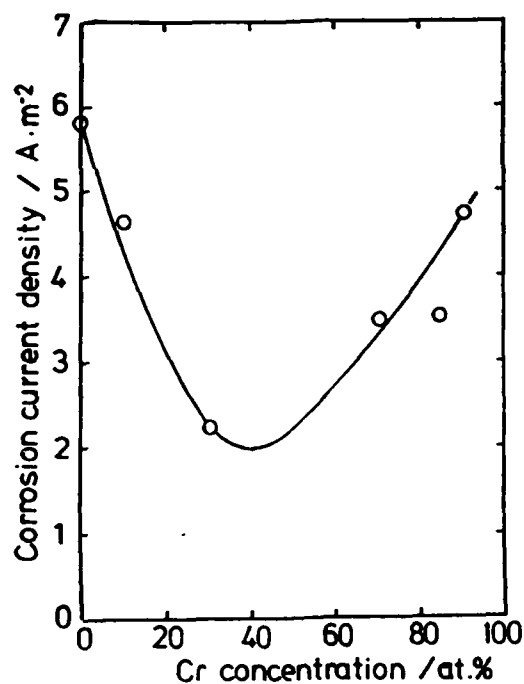


Fig.9 Effect of practical Cr concentration in the middle layer of 3-stepwisely concentration-graded coatings on corrosion current density

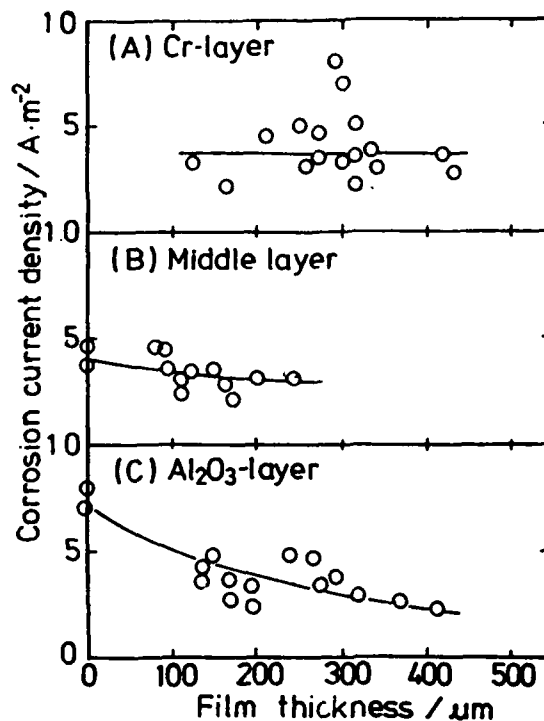


Fig.10 Effect of film thickness of each layer composing 3-stepwisely concentration-graded coatings on corrosion current density. (A) Cr-layer, (B) middle mixed layer, (C) Al₂O₃ layer

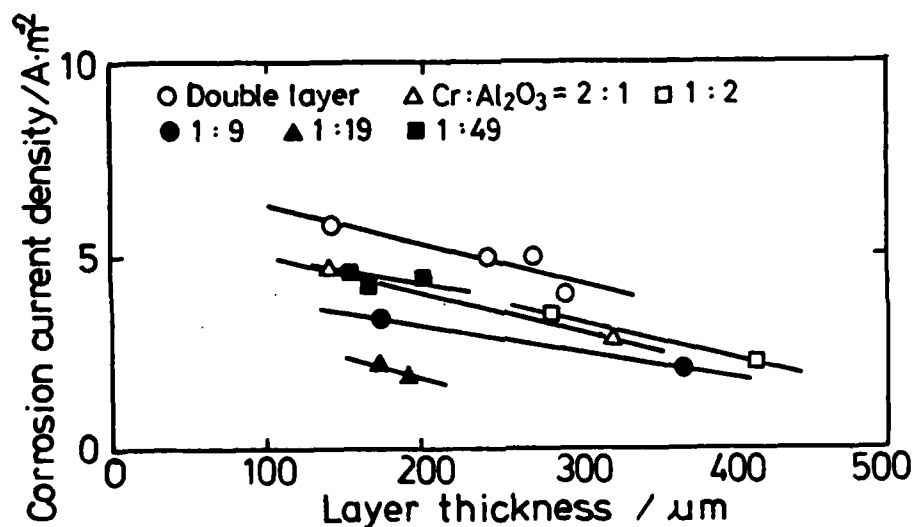


Fig.11 Effect of film thickness of Al₂O₃ layer of 3-stepwisely concentration-graded coatings on corrosion current density

Corrosion Resistance of Amorphous Plasma Sprayed Coatings

Nacer Bacha
Universit de Blida
Institut de Mcanique
Route de Soumaa - B.P 270
Blida (Algeria)

Clermont Roy
Universit de Sherbrooke
Sherbrooke (Qubec)
J1K 2R1 Canada

Abstract

A study for corrosion behaviour of two amorphous coatings produced by thermal plasma spraying was carried on iron based and nickel based alloys. The corrosion resistance of both coatings was evaluated by mass-loss measurements and electrochemical methods in hot acids.

The results show that FeCrPC amorphous coating has exhibited spontaneous passivation and has demonstrated corrosion resistance superior to the stainless steel. The NiCrBSi amorphous coating has exhibited a good corrosion resistance but was slightly poorer than type 316L SS. The heat treatment of amorphous coatings led to the formation of second phase precipitation which significantly deteriorates their corrosion resistance.

Although the plasma sprayed coatings possess attractive overall properties, the generation of an amorphous state suffers from local material degradation at the particle boundaries.

Key words: amorphous coatings, plasma spraying, iron based alloys nickel based alloys, corrosion resistance.

Introduction

Metallic glasses are single-phase alloys without long-range order characteristic of the crystalline state. These features of the structure are responsible for a number of a unique mechanical, physical and chemical properties, including high corrosion resistance. First results ^[1-3] on the corrosion behaviour of metallic glasses reported that several metallic glasses, in ribbon form, possess corrosion-resistance properties superior to those of crystalline alloys of stainless steel.

Plasma spraying is a well established technology that allows selective modification of the surface properties of materials without adversely affecting the bulk properties of the materials. However, despite its wide use for coatings deposition to combat wear and corrosion, very little has been reported on the behaviour of corrosion resistant amorphous metallic coatings. The lack of attention on this problem can in part be attributed to the availability of amorphous metals in the form of ribbons or thin sheets which has little practical value. Therefore the development of techniques by which uniform protective metallic glass coatings can be applied to production equipment could be cost effective and further could allow designs in which expensive materials can be replaced by cheaper coated materials.

The present work is aimed at obtaining fundamental information on the corrosion resistance of two amorphous coatings deposited by plasma spraying.

I. Experimental Procedures

A. Coatings Preparation

The powders supplied by Alloys Metals Inc., were standard feedstock, having specifications given in table 1. Two types of supports were formed for the corrosion study :

For mass loss tests, supports in form of a disc of 2.54 cm in diameter and 0.4 cm thick, were grit blasted with Al_2O_3 60 grit and then inserted in a closed autoclave 48 hours before plasma spraying operation. This precaution was necessary to diminishing drastically adhesion of coatings and then pull out them easily from their supports after spraying deposition.

For electrochemical tests, supports were in the form of a cylinder of a 1 cm in diameter and 1 cm in height. Eight specimens could then be coated at the same time in one deposition experiment.

All coatings were sprayed onto mild steel substrates with plasma torch D.C in a controlled atmosphere vessel. During plasma spraying a high-velocity inert gas (He) was directed onto the freshly deposited layer to quenching the coating.

X-ray diffraction together with scanning electron microscope (SEM) studies were used to identify the microstructure and the phases generated after plasma spraying.

B. Mass-loss tests

The corrosion rates of the coatings were determined by mass-loss measurements. Prior to immersion, the coupons were ultrasonically cleaned with alcohol, air-dried and weighed to a precision of 0.1 mg.

Solutions employed in the testing were 1 N H_2SO_4 and 1 N HCl . These corrodents were made using distilled water and reagent grade chemicals. The duration of tests was 24 hours for both solutions. The test temperatures were $34 \pm 1^\circ\text{C}$ and $55 \pm 1^\circ\text{C}$.

The corrosion rate was calculated using mass loss, total surface area, sample density and exposure time.

C. Electrochemical tests

Anodic and cathodic potentiodynamic polarization scans were made in 1 N H_2SO_4 and 0.2 N HCl at both temperatures of $34 \pm 1^\circ\text{C}$ and $55 \pm 1^\circ\text{C}$. Potentiodynamic scans were performed with the model 342 C SoftCorr corrosion measurement system, which consist of an EG&G PAR 273 potentiostat driven by software from an compatible IBM AT computer and a corrosion cell of three electrode compartment. After each experiment, the scans were analyzed according to standard procedures using corrosion software programs and graphical interpretation of the data. The polarization curves were initiated at -800 mV (SCE) with a potential sweep rates of 2mV/min. The test solution was deaerated using nitrogen for 30min prior to beginning the run. Continuous deaeration was maintained during experiments. All of the potentials were measured vs Saturated Calomel Electrode (S.C.E.) that was isolated from the cell using a Luggin probe. The working electrode was designed as shown in figure 1. Coated support was encapsulated in Pyrex tubing and sealed with epoxy resin to ensure that only the surface of as sprayed coating was exposed to the test solution.

In the case of the 316L SS specimens, working electrode was as the same design as shown in figure 1. The specimens, in form of a disk of 1 cm in diameter and 0.2 cm thick, cut into cold rolled sheet, were attached to the cylinder support with conductive Ag contact paint. In both cases, the surface area of the electrode was 0.78cm^2 .

II Results and Discussions

A. Mass-loss tests

Mass-loss data for the amorphous coatings and SS 316 L are summarized in table 2. The iron-base amorphous coatings with phosphorous as a major metalloid exhibited fully satisfactory resistance in the hot acids. The NiCrBSi amorphous coatings did not exhibit nearly as good a corrosion resistance particularly in 1 N H₂SO₄ and 1 N HCl at 55 °C. The corrosion of 316 SS coupons exposed to the 1 N HCl at both temperatures was characterized by pitting corrosion. The severity of attack was greatest for coupons exposed at 55 °C.

The heat treatment at high temperature (500 °C) of rapidly solidified coatings was associated with a large mass-loss. The severity of attack on the amorphous aged coatings particularly those of NiCrBSi base was exemplified by the presence of a voluminous deposit of corrosion products. On the contrary, coatings in amorphous state exposed to both acids showed no significant build up of corrosion products.

These observations confirm that the absence, in the amorphous metals, of grain boundaries, second phase or major chemical potential differences, enhances the formation of a uniform and homogeneous passive film on the coatings.

Figure 2 show SEM micrograph of an amorphous NiCrBSi coating immersed in 1 N H₂SO₄ during 24 hours. Much of the apparent corrosion damage is concentrated at the rim of the particles flattened upon impact.

During plasma spraying, a molten particle impinging on the substrate spreads out radially in form of a thin disc. Because of the internal compressive stresses introduced during solidification, the weaker adherence to the substrate is observed at the periphery of the disc compared to the centre^[4]. This results in a relatively porous and/or heterogenous zone of material at the periphery of flattened particles and then offers potential sites for crevice corrosion.

It seems probable that the flattened particle boundaries in amorphous coatings, similarly to grain boundaries in crystalline alloys, prevent the formation of a fully uniform passive film over the entire glass surface.

B. Electrochemical tests

The potentiodynamic polarization curves were performed for preliminary and rapid assessment of the corrosion behaviour of the amorphous sprayed coatings in hot acids. The polarization characteristics of 316L SS were inserted for comparison. Typical results are shown in figure 3. The FeCrPC amorphous coatings are characterized by smaller critical current densities and primary passivation near or equal to the steady-state corrosion potentials which are indicative of a spontaneous passivation in both solutions. Passive range extends to + 1 volt (SCE). The nature of passive film was not determined but as the composition of FeCrPC contain more than 10 % at Cr and 9 % at P, it was probably the same nature as was found by Naka et al.^[1] on amorphous ribbon FeCr₁₀P₁₃C₇, which consists mainly of hydrated chromium oxy-hydroxide.

The NiCrBSi amorphous coatings exhibit a good corrosion resistance in 1 N H₂SO₄ at both temperatures. In spite of their relatively higher critical current densities than those of 316L SS, their passive range extends up to + 1 volt (SCE). However, their passivation occurs by anodic polarization. In aqueous solution containing Cl⁻ ions, the NiCrBSi amorphous coatings are less corrosion resistant because their capability to passivate decreases significantly.

Conclusion

-High corrosion resistance in hot acids of amorphous coatings deposited by thermal plasma spraying underline the tremendous potential of this technology to produce coatings with unique tribological^[5] and chemical properties on any shape substrate.

-A better control of plasma spraying parameters is required to improve coating quality and then increase corrosion resistance of amorphous coatings.

Acknowledgment

The authors acknowledge the financial support from the Ministry of Energy, Mines and Ressources Canada. The authors express their gratitude to Prof. A.Lasia for corrosion tests facilities. Thanks are also due to A.Rami for assistance in experimentation.

References

1. N.Naka, K.Hashimoto, T.Masumoto, Journal of Japan Institute of Metal, 38 (1974): p. 835.
2. K.Hashimoto, T.Masumoto, S.Shimodaira, Proceedings USA-Japan Seminar, (Houston, TX: National Association of Corrosion Engineers, 1975), p. 34.
3. K.Hashimoto, T.Masumoto, Treatise on Materials Science and Technology, 20 (1981): p. 291.
4. D.Apelian, M.Paliwal, R.W.Smith, W.F.Schilling, International Metals Reviews, 28 5 (1983): p. 271.
5. N.Bacha, C.Roy, J.Masounave, (Eleventh International Thermal Spraying Conference, Montreal, Canada, 1986) p. 435.

Table 1: Chemical composition (at %)

Alloy	Element								
	B	Co	Se	Si	C	Cr	P	Fe	Ni
Ni base coating	2.5 to 3.2	1.0 max	0.003 max	4.0 to 5.0	0.03 max	12.0 to 14.0		3.0 to 5.0	bal.
Fe base coating					1.42	11.45	9.19	bal.	

Table 2: Corrosion rates of amorphous coatings and crystalline stainless steel in hot acids.

Alloy		Corosion rates (mmpy)			
		1 N H ₂ SO ₄ solution		1 N HCl solution	
state		at 34 °C	at 55 °C	at 34 °C	at 55 °C
316L SS	crystalline	0.040	---	3.730	11.048
FeCrPC coating	amorphous	0.010	0.366	1.837	2.634
NiCrBSi coatings	amorphous aged	1.230 5.262	2.258 45.156	1.936 11.345	4.958 70.309

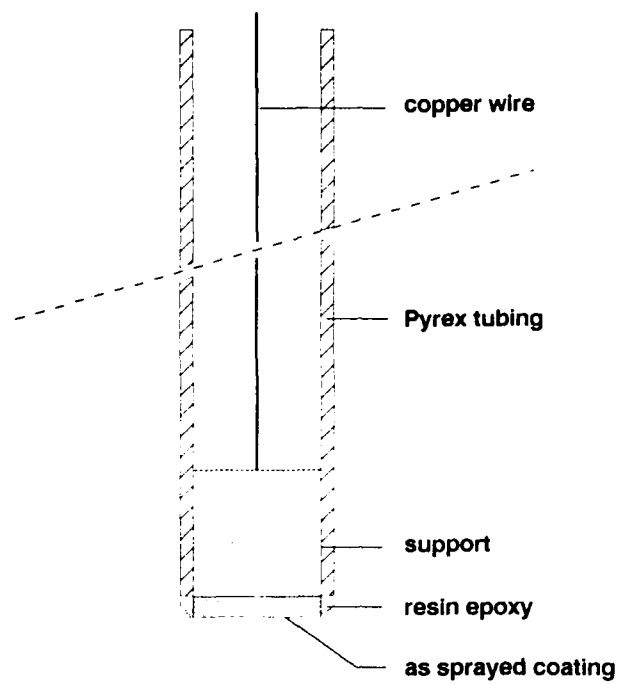


Figure 1: Schematic representation of working electrode

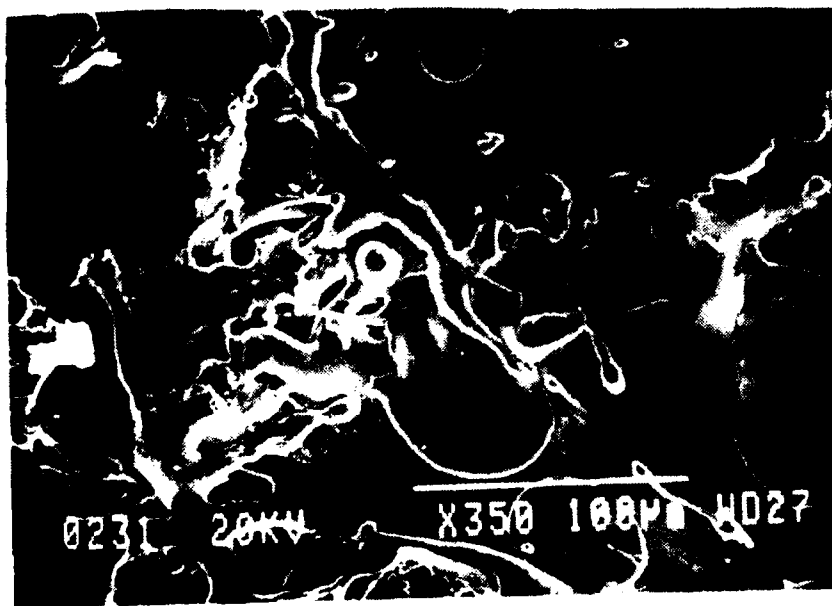


Figure 2: Corrosion features on NiCrBSi amorphous coating in 1 N H₂SO₄ at 55 °C during 24 hours.

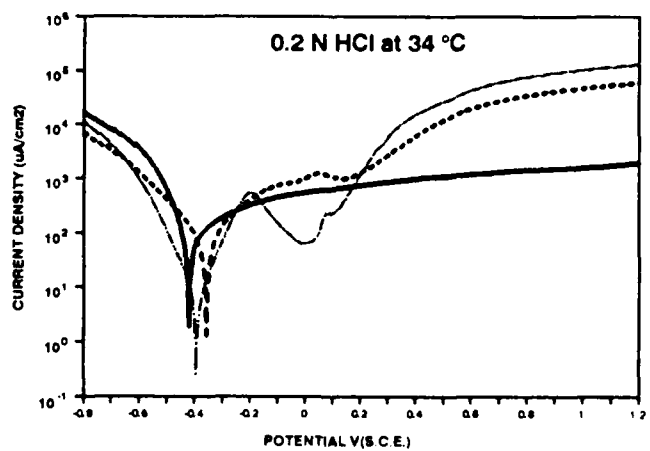
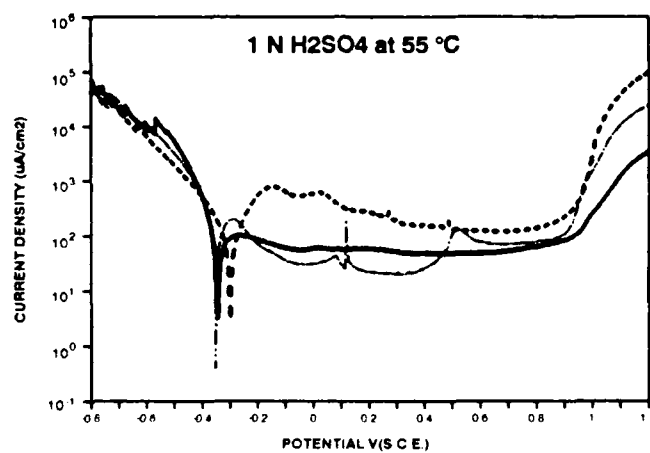
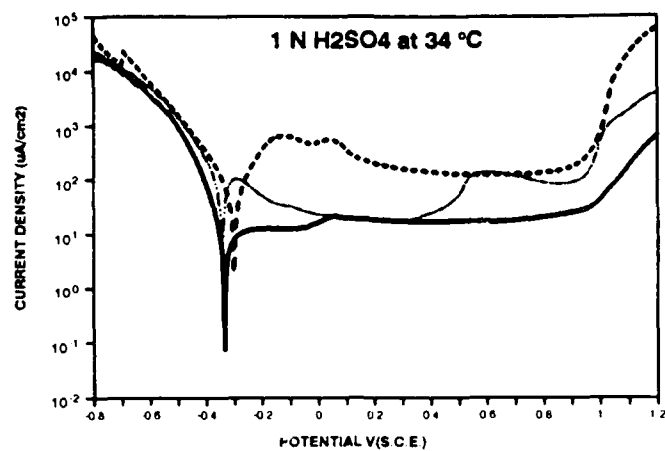


Figure 3: Potentiodynamic polarization curves of:

- FeCrPC amorphous coatings
- NiCrBSi amorphous coatings
- · - · - 316L SS

Formation of Protective Wearresistent Oxide Coatings on Aluminium Alloys by the Microplasma Methods from Aqueous Electrolyte Solutions.

Alexander V. Timoshenko
Moscow Institute of Steel and Alloys
Leninsky Prospekt, 4, Moscow, Russia

Boris K. Opara
Moscow Institute of Steel and Alloys
Leninsky Prospekt, 4, Moscow, Russia

Yulija V. Magurova
Moscow Institute of Steel and Alloys
Leninsky Prospekt, 4, Moscow, Russia

Abstract

While aluminum alloys are oxidized in aqueous alkaline solutions at AC and forming voltage achieves 250 V, microplasma discharges appear on the metallic surface. This phenomenon allows to form uniform oxide coatings with high protective properties, wearresistance and electrical resistance.

Taking into account the influence of electrolyte composition and its aggregate state on coating properties, following classification of oxide application processes has been suggested: as to the polarization type, as to the polarization nature, as to the nature of discharges, as to the nature of processes, as to the type of electrolytes, as to the aggregate state. It is pointed out, that oxidation process overchanges from sparkless process through spark oxidation, through microarc oxidation to arc process consecutively.

After the initial oxide layer has been formed first sparks appear on the anode oxide surface because of the voltage drooping on the oxide layer achieves break-down values. Propagation of the break-down executes by overchanging from corona discharge near the pores bottoms to the spark discharge in the coating pores.

When microarc oxidizing following processes exist: space charge forming in the oxide body; gaseous discharge in the oxide pores; melting of the coating material because of heating up by sparks; diffusion processes, promoted by heating up in oxide body; deposition of the colloid particles at the oxide surface from electrolyte; migration of the negative colloid particles into discharge channels; plasmochemical and thermochemical conversions.

Coating formation is realized by alloy components oxidation, as well as by electrolyte components penetration into growing oxide. Taking into account the colloid state of the electrolyte components, it is pointed out that the oxide properties depend upon chemical composition and sizes of solution articles.

Now there are some fields of practical employment of microplasma oxide coatings to protect from corrosion, to increase wearresistant and electrical strength of the material surface.

Introduction

When oxidizing metals in electrolytic solutions, bear in mind that there exists a limit value of the voltage at the bath. If this value is higher, spark discharges appear on the surface being oxidized. This phenomenon was described in detail by Gunterschulze and Betz [1, 2]. The authors pointed out that this phenomenon deteriorates the properties of the oxide layer. At the same time the later works have shown it is possible to form oxide coatings with high operational properties with the voltage being higher than the sparking voltage. At the present time there are review works pertaining to the processes of application of the coatings in different electrolytes [3 to 5]. The review [5] shows advantages of deposition of the coatings by the anodic spark method - considerable economy in energy as compared with other methods, uniformity of coatings and their quick application, possibility in regulation of the microstructure and properties, as well

as obtaining new microstructures of coatings. It is pointed out that the anodic-spark processes may be used for a wide range of materials.

The process of coating formation from the electrolytic aqueous solutions greatly depends upon the electrolytic composition, chemical composition of the material being oxidized, as well as upon polarization mode and conditions. The processes are carried out at the DC, AC or pulse current polarization. Depending upon the composition of electrolyte the coatings may be formed both due to oxidation of the base and due to deposition of the electrolyte components.

1. Classification and Main Stages of Coating Application Processes

The works of Markov and others [6] give the most systematized classification of the processes of application of inorganic nonmetal coatings. The given classification is based mainly on the type of polarization and does not cover considerable group of the processes which take place during microplasma treatment of the metal surface.

To our mind it is necessary to perform the classification as to the wider class of signs characterizing the process essence. It is known from the literature that the formation of coatings takes place effectively in the sparking mode [7], when heated in the electrolytic plasma [8] and during plasma-electrolytic anodizing [9]. The composition and aggregate state of electrolytes play an important role. Therefore, we suggest the following classification of the coating application processes:

1. Anodic, cathodic and heteropolar as to the polarization type.
2. Pulse and continuous as to the polarization nature.
3. Spark, microarc and arc as to the nature of discharges.
4. Oxidation, electrophoresis, thermal transformation as to the nature of processes.
5. Alkaline, acid, salt, combined as to the type of electrolytes.
6. From solutions, colloid systems and from finely divided systems as to the aggregate state.

Using such an approach to the classification it is possible to divide the processes to a great extent as to distinctive features. For example, oxidation of the aluminium alloys in the sulfuric acid solution at AC voltage of 400 to 460 V [10] may be classified as the anode continuous microarc oxidation from the solution. Formation of coatings on steels from electrolytes containing 12-molybdatephosphoric acid [8] may be related to the anode continuous salt arc process of thermal transformations on steel from solution. The coating application described in [11] may be related respectively to the heteropolar pulse microarc electrophoresis and thermal transformation from the finely divided system in the combined electrolyte, etc.

It is possible to select the distinctive features typical for any microplasma process.

Firstly, for appearance of the microplasma discharge there should be high electric field strength in the volumes directly adjoining the metal surface. Therefore, the first stage required for appearance of the microplasma discharges should be the formation of the dielectric or semiconductor layer on the metal surface. If such a layer fails to be formed due to any reason, the microplasma treatment does not also occur. The dielectric layer may be preliminarily applied to the metal surface by natural method, which provides for the progress of the subsequent treatment.

Secondly, the appearing microplasma discharge should ensure formation of the coating. This may be achieved, first of all, by changing the electrolyte composition, as well as due to change of the polarization conditions. If the metal was not subjected to the microplasma oxidation the formation of coatings may be ensured by introduction (into the electrolyte) of the components capable of undergoing the thermal transformations in the plasma discharge and whose transformed products are capable of interacting with the metal surface. In some cases the similar transformations may be ensured by preliminarily applying to the metal surface the layer of chemical compounds which are capable of forming the chemical compounds with the metal under the action of microplasma discharges.

Thirdly, to obtain the coatings having the required complex of properties, it is necessary to create definite conditions for heat removal from the burning zone of the microplasma discharges, as well as diffusions and migrations of the components of the plasmocchemical reactions. The temperature in the discharge channel

is, first of all, determined by the plasma composition and heat removal conditions. In its turn, the thermal characteristics of the process may be changed both by changing the electrolyte composition and by changing the polarization conditions, particularly the shape of polarizing pulses and the pulse repetition frequency.

Possible stages of the microplasma processes when forming the coatings are presented in Table 1.

It should be pointed out that many important processes taking part in formation of the coatings, such as adsorption of ions on the coating surface, gas liberation due to the electrolysis of the electrolytic solution, formation of the space charge zone in the coating structure, redistribution of phases in the process of the coating growth, processes of crystallization, melting and evaporation of the system components, electrophoresis and dielectrophoresis phenomena, etc. were not covered by the present diagram.

II. Formation of Coatings on Aluminium Alloys

The coatings were applied from the aqueous solution of the electrolyte containing (g/l): 2.5 of sodium hydroxide, 3 of sodium aluminate and 3 of sodium hexametaphosphate.

The polarization was performed on the AC with a frequency of 50 Hz from the capacity source. The initial level of the polarizing current was set up and further on the current value was not regulated. When determining the chemical stability a drop of solution containing hydrochloric acid and copper chloride was applied to the coating surface and then a probe was placed which was connected to the device used to determine the time till the coating failure. The anodic polarizing curves were taken in the solution of the sodium chloride in the potentiodynamic mode at the potential sweeping rate of 1 mV/s to determine the electrochemical behavior of alloys with coatings.

Subjected to examination were aluminium alloys, type 1099, 2024 and alloys with different content of copper up to 5 per cent by mass.

In the process of oxidation when rising both cathodic (U_c) and anodic (U_a) voltage amplitude, relative fraction of cathodic component increases and ratio U_a/U_c decreases accordingly [12].

The static treatment of the obtained results with the use of multiple correlation method made it possible to obtain the empirical dependence of U_a/U_c upon the oxidation time (t , min) and current initial density (i_0 , A/dm²) in the form of:

$$U_a/U_c = 7.3 - 0.024 t - 0.123 i_0 \quad (1)$$

Examinations of the coating properties and observance over the nature of spreading of spark discharges over the surface have shown that there is a certain value of U_a/U_c below which the process nature sharply changes. Instead of microarc discharges uniformly moving over the surface there appear discharges concentrated and burning more longer at the same sections of the surface. After changing over to such a mode the coatings are partially damaged at the places of burning of discharges. On alloy 2024 the U_a/U_c ratio approximately equal to three corresponds to the changeover to the arc mode. Considering this ratio as a critical one, after substituting into the equation (1) we obtained the dependence of the critical oxidation time (t_{cr}) on the initial density of the polarizing current:

$$t_{cr} = 191 - 5.5 i_0 \quad (2)$$

Taking into account the fact that the time can not take negative values, we obtain from the equation (2) the current critical density $i_{cr} = 35$ A/dm². During polarization with the initial density of the current exceeding i_{cr} the process immediately gets changed over into the arc mode. Nonuniform coatings are formed and in some cases there are local failures of the coatings up to through failures of thin-walled parts.

Investigations of the coating microstructure have shown that failure of the film formed in the sparkless mode is observed in the mode of the spark oxidation at the initial stages. Through damage to coatings are also observed in this case. The fraction of the melted surface is not great.

The chemical stability of coatings becomes lower than that of the coatings formed in the sparkless mode (Table 2). Further buildup of the coating results in changeover to the mode of microarc oxidation. The voltage at the bath rises to values exceeding 300 to 350 V. Protective properties of the coatings get also better (Table 2). The coating material gets melted over the entire surface. The number of open pores as compared with the coatings made in the spark mode is considerably reduced. The coating properties also depend upon the chemical composition of the alloy being oxidized. For example, when treating alloys 1099 and 2024 at the same conditions, considerable difference in properties of the coatings (Table 3) is observed. Such an increase in the coating properties is likely to be specified first of all by change of their chemical composition.

The X-ray phase analysis of coatings on alloys with different content of copper has shown that coating contains α -Al₂O₃, γ -Al₂O₃ and mixed oxide CuAl₂O₄. As a duration of the oxidizing rises, there exists accumulation of α -Al₂O₃ and CuAl₂O₄ in place near the metal-oxide boundary, and of γ -Al₂O₃ in external part of the coating.

Increase of the concentration of copper in alloy aids in growth of the thickness, microhardness and of protective properties of the coatings (Fig. 1).

Fixing the change of momentary values of voltage, current density and light impulses, when forming the coating at AC, it may be to bring out the main mechanisms of growth of the coating.

For all of oxidized alloys curves of momentary values of voltage (U), current density (I) and light impulses (L) have characteristic form in the anodic half-period (Fig. 2). So three areas may be resolved.

In the first area voltage grows monotonously. For all that during some time when increasing the voltage the current through the system is not observed. Time up the anodic half-period starts to the moment of the current appears is denoted by t_{br} (break-down). At the voltage U_{br} current rising begins. Then current fast reaches up to ultimate value.

After fast increasing current, anodic voltage is stabilized at maximum (second area).

At last when decreasing voltage (third area) the current drops smoothly to zero. So period ends at the nothing current. Voltage at which absence of the current appears again is denoted by U_{qu} (quench voltage).

In the cathodic half-period current exists during all time. The voltage U_c is well below U_a .

At oxidizing not only U_a/U_c but also shape of current curve change. After 30 minutes oxidizing second maximum on the current curve appears. And both maximums I_1 and I_2 (Fig. 2b) are observed in the second area.

From this data minimum resistance in anodic (Fig. 3) and in cathodic half-periods and the maximum value of light (Fig. 4) impulse were calculated.

As the content of copper in alloy increases the break-down voltage (U_{br}), corresponding to 5 minutes oxidizing, increases too. U_{br} (30 minutes) not depends upon copper content in alloy (Fig. 5) break-down time (t_{br}) behaves similar. Amplitude of light impulse (30 min. oxidizing) not depends upon copper content in alloy, but drops with increasing content of copper (5 min. oxidizing).

Calculation of the volt-ampere characteristics shows that in first and in third areas linear ranges may be described by the equations:

$$I = K_1 U (U - U_{br}) \quad (3)$$

$$I = K_2 U (U - U_{qu}) \quad (4)$$

K_1 and K_2 - constant.

In the second area of the curve range near the maximum of the current density may be linearized and described by:

$$I = A \exp(B \cdot U) \quad (5)$$

A and B - constant.

After calculations (date of 5 minutes oxidizing) it has been established, that K_1 (3) linearly rises with increasing content of copper in alloy. K_2 (4) not depends upon copper content and equals $1.4 \cdot 10^{-6} \text{ sm}/(\text{V s})$ (Fig. 6). After 30 minutes oxidizing K_1 values corresponding all of AL-Cu alloys equal $10^{-5} \text{ sm}/\text{V s}$, but it is below one corresponding 1099-alloy by 20 %. K_2 has not dependence upon copper content and upon oxidation time (Fig. 7).

According to gaseous discharge theory [13, 14] equations (3) and (4) correspond volt-ampere-characteristic (VAC) of the corona discharge.

Constant K in the equation is determined by mobility of charge carriers and by geometrical factors initiating distortion of the electrical field near the electrode.

Corona discharge is known to appear in the area where field strength in gaseous range reaches maximum value [13, 14]. So when evolving discharge at micro-arc oxidation distortion maximum should exist near the pore bottom in anode oxide, near the external side of the barrier layer.

Barrier layer formed in sparkless mode shows high dielectric properties and during some time (up to t_{br}) holds the voltage increasing under anodic polarization. At U_{br} near pore bottom exists ionization of gaseous particles produced by electrochemical reactions and by thermal actions. So corona discharge appears. Current in corona discharge is due to mobility of the charge carriers.

Negative particles move in the direction to the anode, and cations - in the opposite direction. In such case as negative particles may be ionized oxygen and electrolyte anions. Besides that high field strength may break loose electrons from gaseous and electrolyte molecules. Mobility of the negative particles is defined by their charge, mass and by collisions with opposing stream of the positive particles.

Further voltage rising creates conditions for corona discharge changes over to the spark discharge. So resistance of this system drops down because of short circuit electrodes in some places in the coating. Sparking results in stabilization of the voltage. Light emission increases and depends upon current intensity through the spark discharge channel.

Generalizing this date it may be to present following mechanism of the coating formation on aluminium alloys.

When conducting electrical current through electrolyte anode oxide film deposits at oxidized surface. At the internal boundary metal-oxide-system waterless barrier layer appears. This layer maintains high value of the voltage drop due to it's high dielectric properties. At external boundary porous layer being polymer oxide structure with electrolyte components inclusions (anions and water molecules) is formed. Due to pores existing new portions of electrolyte may be transported to barrier layer surface. With anodic polarizing electrical field causes the moving of oxidized metal ions from metal into electrolyte. Metal cations including into the alkaline electrolyte form hydrate aluminates in the colloid state. Colloid particles assume negative charge and are driven from cathode to anode by electrical field. Particularly colloid particles are deposited at the coating surface; particularly colloid particles hit again the pores, where lose their water by the joule heat sustaining growth of the barrier layer from external side.

Oxygen, extracted at the pores bottom, fills them and makes added range of the voltage drop in anodic oxide. So if the voltage drop in gaseous interval exceeds the voltage of gaseous ionization, corona discharge appears in area with maximum field strength.

If the voltage of this system keeps increasing, corona area may occupy all gaseous volume; so steamer spark discharge arises between metal and electrolyte electrodes [13, 14].

When anodic polarizing spark discharge travels from external interface (gas - solution) to internal interface (barrier layer - gas).

When closing discharge distance with barrier layer surface, it is failed by the instantly extracting large energy. Energy extracting results evaporating or melting pore bottom material (oxides, hydroxides, metals). Because of the discharge exists in a brief space of time, processes exhibit explosion character. Gases and melted particles are dumped from the discharge channel to electrolyte making lower pressure space. After ending discharge electrolyte particles stream into lower pressure space, and there is processes recurrence.

Failing initial barrier layer when existing spark discharge is corroborated by some decreasing protective properties of oxide in comparison with anodic oxide (Table 3).

Direct contact of the metal with the gaseous space sustains high concentration of metal particles (vapors, cations, metal containing anions) in discharge plasma. So both particles containing aluminium and particles containing alloying elements fall within discharge space. Because of direct contact of the metal with gaseous space exists, alloying elements are observed to influence oxide properties and discharge conditions.

After ending discharge sweating of liquid and gaseous spark processes products at pores walls and pores bottoms results in oxide coating growths.

Spark discharge throws one's components into solution, where they form colloid particles and gain negative charge.

During future spark discharges negative colloid particles are pulled by the electrical field in spark channel and are dehydrated, ionized, melted, evaporated by the high temperature. This phenomenon favours oxide coating growth.

Zone where oxide growths is area with the electrical field maximum. In anodizing it is external boundary of the barrier layer; in spark oxidizing it is area near metal surface in places of the barrier layer destroys.

However in time thickness of the plasmochemical and thermochemical reactions products increases. So during spark discharge through breakdown is not observed.

In crystallizing from melted state there is forming oxide layers with the high electron conductivity. So future spark discharges end not on the metal surface, but on the surface of the oxide layer formed earlier. This layer is known by X-ray analyses to consist of high temperature modification α - Al_2O_3 and of the phase CuAl_2O_4 .

Due to the heating up to the high temperature diffusing in coating is facilitated and layers adjoining interface metal - oxide are enriched with the metal. On the other side of the layer quantity of the metal decreases. So areas of negative and positive space charge are appear. Their contact exhibits valve properties.

When oxidizing at DC under constant voltage conditions, with space charge zone growths, current density should drop up to zero values, that is observed in experiments [15].

When forming sufficiently thick layer, containing space charge on metal-oxide boundary conditions of the oxide growth change.

Because of discharge not runs into the metal surface, ions of the alloying elements take place in plasmochemical reactions to a less extent. So constant K (3) not depends upon the content of copper in alloy.

Detaching area of the space charge from the metal-oxide boundary is accompanied by arising second maximum on the current curve I_2^{max} (Fig. 2b).

In contrast to the spark mode in this case the voltage drops not only on gaseous interval, but also on the area of space charge. As is the case with spark mode corona discharge appears in the gaseous face. However results in increasing resistance of energy barrier and in dropping current density after I_1^{\max} (Fig. 2b). In this case spark discharge arises in consequence of the breakdown of both space charge and gaseous interval.

It should be give attention to characteristic properties of AC oxidizing. Experiments have showed, that there exist rectifying at all stages of oxidizing.

At the anodize stage this effect is not great and is explained by existing space charge on external surface of barrier layer, by particular reducing oxide in cathodic polarizing, or by the current by defects in cathodic half-period [16].

At the spark oxidizing stage when existing through breakdown of oxide, rectify effect is a result of different mobility of particles in gaseous interval.

In cathodic polarizing electrical current is due to moving cations through oxide layer and due to moving electrons to oxide - electrolyte interface. At the same time oxide is cooled and it's resistance increases. This makes added difficulties for gaseous discharge in the next anodic halfperiod.

When overchanging into anodic half-period pores in oxide coating are filled by hydrogen. However there exists electrochemical extracting oxygen. In poreless places of coating energy barriers form by the concentrating not leading charge carriers near the interface between space charge areas. Due to these processes, up to the moment of the corona discharge arising, electrical current through the system is absent, but voltage is increasing (Fig. 2). Arcing oxygen-hydrogen plasma in spark discharge results in strong heating oxide layer. So one's electrical resistance decreases again and anodic current fast increases. In the second half of the anodic half-period when reducing anodic current there exist condensing products of the plasmochemical and thermochemical reactions at pores walls and pores bottom. This results in some increasing electrical resistance. Some reduce of current density in the second half of anodic half-period also may be connected with decreasing amount of charge carriers in plasma after proceeding plasmochemical reactions.

III. Practical Employment of Microplasma Coatings

Reasoning from the data given in the literature on the properties of the oxide coatings and taking into account the requirements of the industry to new materials, one can assume the basic fields of the industrial employment of the microplasma processes of the coating formation (Table 4) even at the present time.

References

1. A. Gunterschulze, H. Betz, Z. Physik, 78 (1932): s. 196.
2. A. Gunterschulze, H. Betz, Z. Physik, 91 (1934): s. 70.
3. V.I. Chernenko, L.A. Snezhko, I.I. Papanova, Production of Coatings by Anodic-Spark Electrolysis, (Leningrad: Chemistry, 1991).
4. A.B. Liptchansky, V.A. Zvetkov and others, Microarc Oxidation - New Method of Formation of Metal-Ceramic Materials and Coatings, (Moscow: CNII "Elektronika", Review on electrons equipment, Series 7, 1991).
5. G.P. Wirtz, S.D. Brown, W.M. Kriven, Mater. and Manuf. Proc., 6, 1 (1991): p. 7.
6. G.A. Markov, O.P. Terleeva, E.K. Shulepko, Collective Works of Moscow Institute of Petrochemical and Gas Industry, 185 (1985): p. 54.
7. P. Kurze, W. Krysmann, G. Marx, Wiss. Z. d. Tech. Hochsch. Karl Marx Stadt, 24, 6 (1982): s. 665.
8. N.A. Polotebnova, V. N. Duradzi. Physica i Chimija Obrabotki Materialov, 5 (1985): p. 90
9. E.E. Averyanov, Reference Book on Anodization, (Moscow: Mashinostroenie, 1988)

10. G.A.Markov, V.V.Tatarchuk, I.K.Mironova, Izvestiya SO AN SSSR, ser. Chim. Nauk, 3, 7 (1983): p. 34.
11. G.A. Markov, E.K. Shulepko and others, A.S. SSSR, No 926O84 (1982)
12. A.V. Timoshenko, B.K. Opara, A.F. Kovalev, Zashita Metallov, 27, 3 (1991): p. 417.
13. Y.P. Rayser, Physics of gaseous discharge, (Moscow, Nauka, 1987)
14. Gaseous Electronics. v1. Electrical Discharges, (NY, Academic Press, 1978)
15. A.V.Nikolaev, G.A.Markov, B.I.Peshevitskiy, Izvestiya SO AN SSSR, Ser.Chim.Nauk, 5, 12 (1977):p.32.
16. L. Young, Anodic Oxide Films, (London and New York, Academic press, 1961)

Main Stages of Process of Microplasma Application of Coatings

Stage	Examples
1. Formation of the dielectric of semiconductor layer on the metal surface.	1. Formation of anode coating at the first stages of oxidation. 2. Formation of the gas discharge gap at high current density (steam-gas mixture). 3. Creation of artificial dielectric or semiconductor layers on the metal surface.
2. Appearance of discharge.	1. Electric break-down of the gas discharge gap. 2. Electric break-down of dielectric layer or zone of the space charge. 3. Thermal break-down of the space charge zone on the surface or in the volume of the dielectric or semiconductor.
3. Flow of plasmachemical and thermochemical reactions.	1. Ionization of atoms and molecules $\text{Me} - \text{ne} \rightarrow \text{Me}^{n+}$ $\text{X} + \text{me} \rightarrow \text{X}^{m-}$ where X - oxidizer. 2. Formation of chemical compounds in the discharge plasma $a\text{Me}^{n+} + (an/m)\text{X}^{m-} \rightarrow$ $\rightarrow \text{Me}_a\text{X}_{(an/m)}$ where X - oxidizer. 3. Water thermolysis $2\text{H}_2\text{O} \rightarrow 2\text{H}_2 + \text{O}_2$ 4. Thermal decomposition of compounds $\text{Al}(\text{OH})_3 \rightarrow \text{Al}_2\text{O}_3 + 3\text{H}_2\text{O}$ 5. Formation of chemical compounds from atoms and molecules $\text{Al}_2\text{O}_3 + \text{CuO} \rightarrow \text{CuAl}_2\text{O}_4$ $\text{TiO}_2 + \text{BaO} \rightarrow \text{BaTiO}_3$
4. Heat and mass transfer to and out of the discharge zone.	1. Heat removal to electrolyte, metal and coating. 2. Diffusion of ions from metal through the oxide layer to the discharge zone and in the reverse direction. 3. Transfer of electrons and ions from metal through the coating layer under the action of the field. 4. Transfer of ions from the electrolyte to the discharge zone.

Table 2

Protective Properties of Coatings Formed on Alloy 2024

Oxidation mode	Thickness, μm	Chemical stability, min
1. Sparkless mode $U_a = 90 \text{ V}$, time = 2 min	3 ± 1	6 ± 2
2. Spark mode, $U_a = 200 \text{ to } 250 \text{ V}$, time = 15 min	13 ± 2	7 ± 2
3. Microarc mode, $U_a = 400 \text{ to } 500 \text{ V}$	46 ± 4	29 ± 3
	58 ± 5	39 ± 5
	83 ± 6	42 ± 6
4. Arc mode, $U_a 570 \text{ V}$	106 ± 10	14 ± 4
	139 ± 12	16 ± 3
5. Thick-layer anodization in sulphuric acid (20 %) at -5°C	15 ± 2	11 ± 2
	43 ± 4	16 ± 2

Table 3

**Properties of Microplasma Coatings on Aluminium and Alloy 2024
Formed at Current Initial Density of 10 A/dm^2**

Alloy	Treatment time, min	Thickness, μm	Microhardness, GPa	Electric strength, $\text{V}/\mu\text{m}$	Chemical stability, min
Al	30	34 ± 4	6 ± 2	18 ± 3	18 ± 3
	60	45 ± 4	8 ± 2	20 ± 3	21 ± 3
2024	30	38 ± 4	12 ± 3	26 ± 4	27 ± 4
	60	58 ± 5	17 ± 3	39 ± 5	34 ± 5

Practical Employment of Microplasma Coatings

Corrosion protection	Chemical equipment Construction Pump elements Vessels Medical equipment Tubes, sheet
Wear-resistant coats	Plain bearings Constructions Engine elements Erosion protection Mechanisms, mashines Tubes, sheet
Electroprotective coats	Electronic Chemical equipment Power industry
Catalyst carriers	Chemical equipment
Decorative coats	Apparatus Civil engineering Household engineering
Chemical composition and pressure transducers	Chemical equipment Medical equipment Constructions

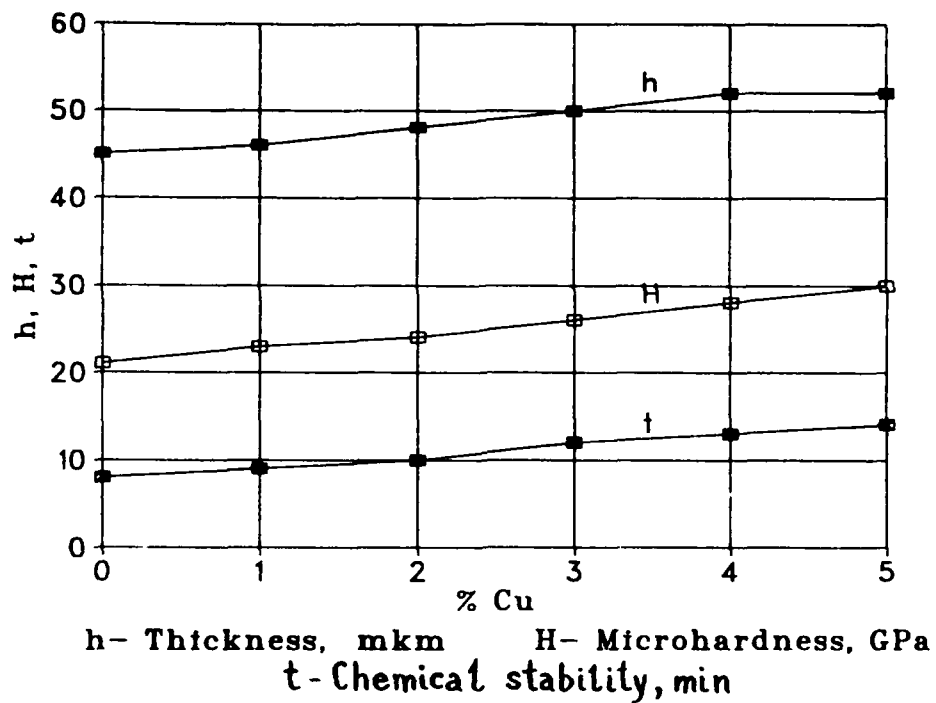


Fig. 1. Dependence of thickness, microhardness and chemical stability upon copper content in alloy

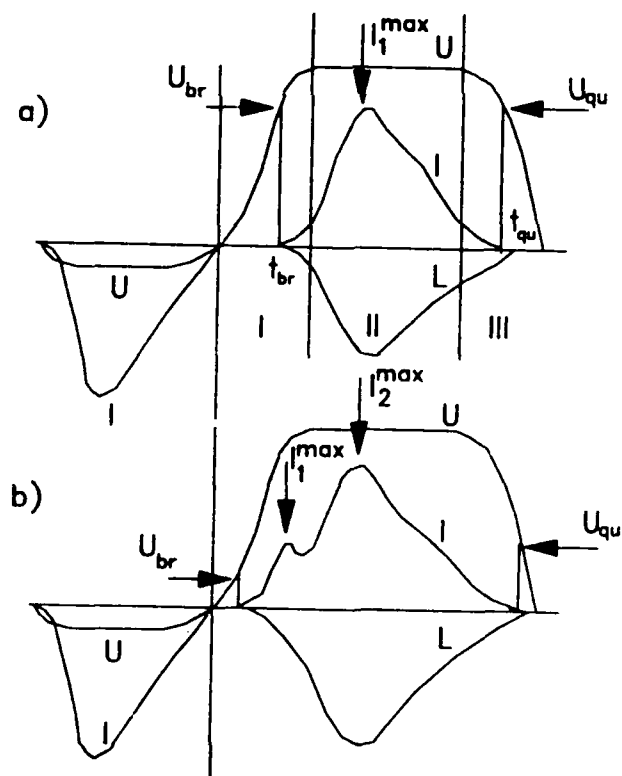


Fig. 2. Typical changes of voltage, current density and light impulse during one period of AC
a) 5 min oxidizing; b) 30 min oxidizing

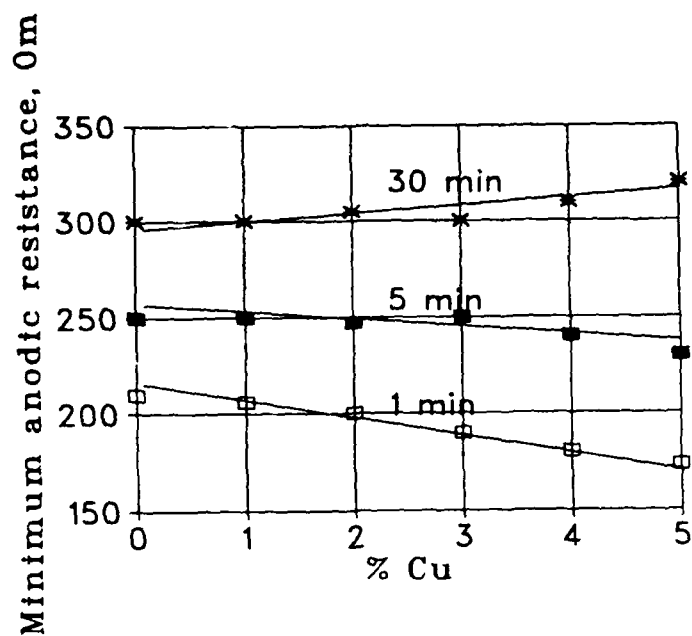


Fig. 3. Dependence of minimum anodic resistance upon copper content in alloy

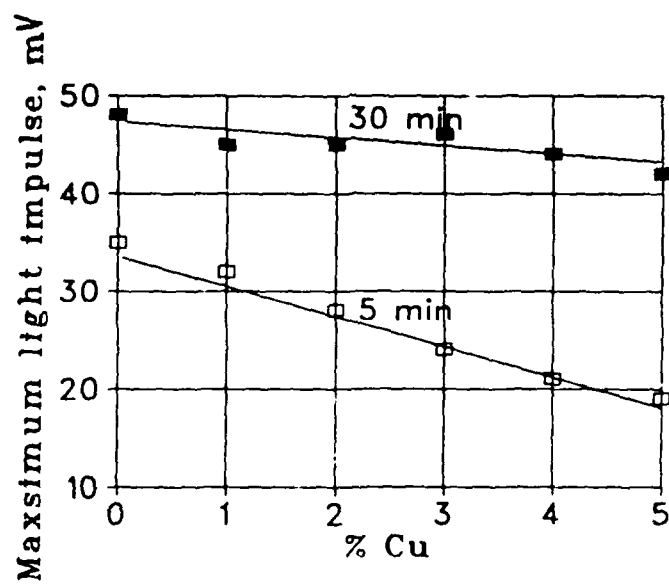


Fig. 4. Dependence of maximum light impulse upon copper content in alloy

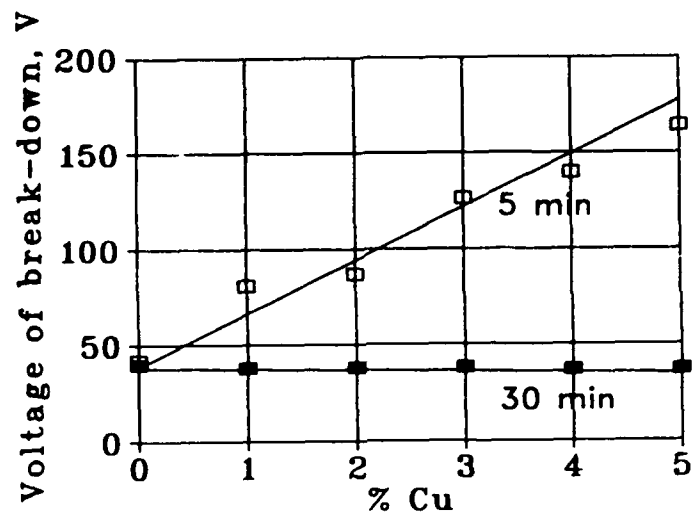


Fig. 5. Dependence of voltage of break-down upon copper content in alloy

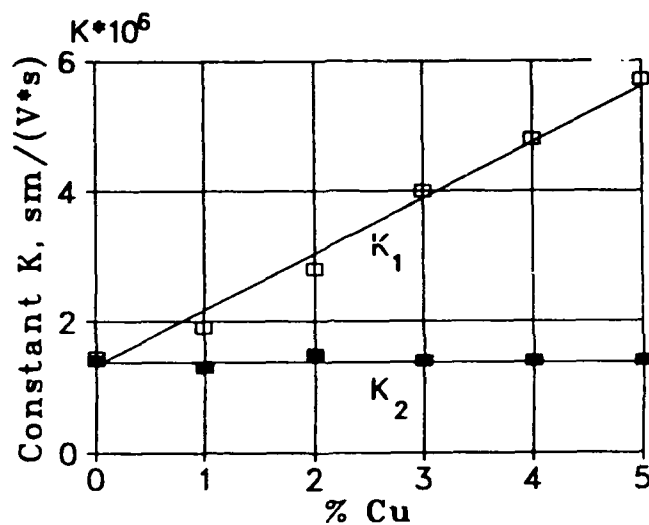


Fig. 6. Dependence of constant K from (3), (4) equations upon copper content in alloy, 5 min oxidizing

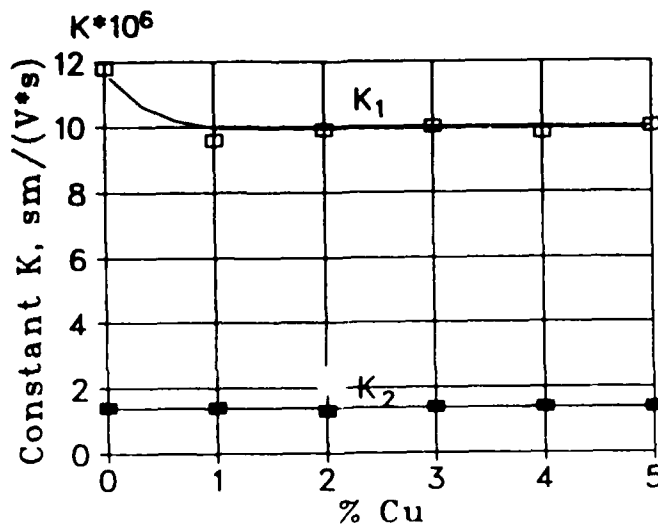


Fig. 7. Dependence of constant K from (3), (4) equations upon copper content in alloy, 30 min oxidizing

Superior Corrosion Resistance by Niobium Coating

Yläsaari S., Turkia M., Forsén O.
Laboratory of Corrosion and Material Chemistry
Helsinki University of Technology
SF-02150 Espoo, Finland
Tel. 358-0-451 2745
Fax. 358-0-451 2660

Polyakov E., Maslov V.
Institute of Chemistry
Kola Science Centre of the Russian Academy of Sciences
14 Fersman Street, 184200 Apatity Murmansk region, Russia

Abstract

Niobium is a reactive metal which passivates spontaneously in many aggressive environments. Niobium metal also has favourable thermal and mechanical properties for use in the chemical process industries as process equipment or ancillary components which require high reliability and extensive service life. Niobium coatings can be used in applications where superior resistance against aqueous corrosion or erosion in hot-gases is needed.

In this study the corrosion resistance of electrodeposited niobium on AISI 316 stainless steels in acid media has been studied. The coatings were manufactured by Kola Science Centre of the Russian Academy of Sciences. Niobium coating deposition from molten halide electrolytes is also described in this paper. The structure and composition of niobium coatings are reviewed. The morphology, microstructure and defects were studied using a scanning electron microscope. In short term experiments the electrolyte was 30 % H_2SO_4 at a temperature of 298 K and during long term measurements the electrolyte was 1 M H_2SO_4 . Both Alternating Current (AC) and Direct Current (DC) electrochemical methods were used to characterize the corrosion behaviour of base material and coating-base material -system. Short term measurement procedure for coated samples consisted of four different measurements: Electrochemical Impedance Spectroscopy, Linear Polarization, Potentiostatic Exertion and Long Cyclic Anodic Polarization. In long term immersion tests, corrosion currents and rest potentials versus saturated calomel electrode (SCE) were measured.

Polarisation resistance values measured by electrochemical impedance spectroscopy showed that the corrosion resistance of niobium coatings was related to the development of a passive layer on the niobium surface. The Long Cyclic Anodic Polarization curves showed that electrodeposited niobium coatings are capable of isolating the substrate material completely from the electrolyte. The Potentiostatic Exertion measurements showed that the corrosion resistance of electrodeposited niobium coatings was five orders of magnitude better than of the base material AISI 316 in 30 % H_2SO_4 electrolyte. The long term measurements showed the excellent corrosion resistance of niobium and the fact that electrodeposited niobium coating is dense.

Key terms: Niobium, coatings, electrodeposition, electrochemical methods

Introduction

With the progress of process technology physical and chemical requirements for structural materials are becoming more severe. Under such circumstances, attention has been paid to surface treatment technologies to ensure entirely different material properties for the surface of a structural part. Relatively thin layers of coating material can act as a barrier between the base metal and its environment and so prevent its corrosion.

At present a clear-cut tendency to the expanded use of tantalum, titanium¹, zirconium and niobium² applications in chemical industry has become a reality. Various pipelines with valves, pumps, syphons and compressors; heat exchange gear, stirrers, autoclaves, columns, centrifuges etc. are fabricated of these materials.

Niobium is an intrinsically reactive metal which spontaneously passivates very effectively under many very aggressive chemical conditions. It is known that niobium is resistant to most aqueous solutions below 100 °C except hydrofluoric acid and concentrated alkaline solutions because it readily forms a protective oxide film of Nb_2O_5 .³ Niobium metal has also favourable thermal and mechanical properties for use in the chemical process industry as both direct containment equipment and as ancillary components which require high reliability and extensive service life.

In this study the electrodeposition of niobium coatings on stainless steel, the structure and composition of the coatings and the corrosion resistance of electrodeposited niobium on stainless steels in acid media has been studied. Both Alternating Current and Direct Current electrochemical methods were used to characterize corrosion behaviour of base material and coating-base material system. Niobium coated carbon steels were used as a reference material. The morphology and tribology of niobium coatings are considered as well.

I. Niobium Deposition from Molten Chloride-Fluoride Electrolytes

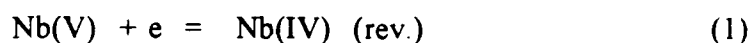
Tantalum and, to a lesser degree, niobium are rather expensive and rare metals which hinders their use in industry. Since for the applications considered here only surface properties of the equipment are significant, it is cost-effective to use composite materials where a less expensive base material having high strength and heat conduction performs the mechanical function, while a thin transition metal surface layer protects the structure from corrosion. Some of the most accessible plating methods for protection of rather large surfaces by non-porous rare metal layers deserve emphasis. These methods include cladding by explosion and molten salt electrolysis, the latter being markedly advantageous in protecting complex shaped equipment. The method of niobium coatings electrodeposition has been developed in Kola Science Centre of the Russian Academy of Sciences since the sixties and by now an appreciable number of papers covering this area have been published including overviews⁴⁻⁶.

In niobium coatings electrodeposition chloride-fluoride electrolytes based on NaCl-KCl-CsCl ternary eutectic ($m.p. = 480^\circ\text{C}$) doped with K_2NbF_7 are preferable⁷. The electrochemical deposition cell consisted of a steel chamber containing a glassy carbon crucible. The electrode leads and other tubes are made of nickel and entered through a rubber closure protected by a Teflon protector. A graphite rod of spectral purity serves as the counter electrode. The indicating electrode is a 1 mm platinum wire welded to a nickel lead in turn fixed to a threaded sleeve enabling the depth of immersion of the electrode to be determined.

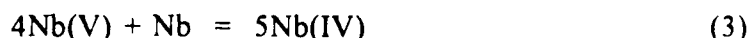
A silver electrode protected by the graphite capsule is used as a reference electrode. Metallic niobium is used as anode material. The electrolyte used consisted of a eutectic mixture of cesium, potassium and sodium chlorides (68.1:16.3:15.6 w/o) with the addition of K_2NbF_7 (10 w/o).

The temperature of the cell is controlled by potentiometer to within $\pm 3^\circ$. The chamber is first evacuated at a room temperature and then heated under vacuum in steps of $200^\circ C$ up to a residual pressure of $2 - 3 \times 10^{-2}$ mmHg. The cell is then filled with dry argon, the temperature adjusted to its final value and the electrodes inserted into the melt. The process temperature is $700^\circ C$ and cathodic current density up to $200 A/dm^2$. Niobium coated steel samples, were obtained in hermetically sealed electrolyzer in the atmosphere of carefully purified and dried argon. The electrolyzer is fitted with a valve and the hermetical chamber permit the rapid replace of the coated parts. Prior to coating deposition the specimens are degreased and dried. On completion of deposition process and specimen removal from the molten electrolyte, the salt residue is washed with water.

Investigations of the electrode process mechanism has revealed that the reduction of the Nb(V) complexes in these melts proceeds in two sequential stages:



On contact with metallic niobium employed as soluble anode, vigorous interaction between Nb and the melt containing complex Nb(V) ions occurs:



and this reaction equilibrium is essentially shifted to the right. Average oxidation states of anodically dissolved niobium in these electrolytes in a wide range of current density are also close to (IV) which allows to represent electrochemical processes taking place in chloride-fluoride melts at niobium coatings deposition as a sum of two electrode reactions, an anodic reaction:



and a cathodic reaction:



The above described electrolyte is quite stable in the interval of working temperatures of 680 - 750°C, dissolves in water and is readily removed from coated part surface; it is virtually unhygroscopic and gives the possibility to raise the rate of the process by increasing the cathodic current density. The rate of the niobium coating deposition reaches 150-200 $\mu\text{m/h}$.

II. Structure and Composition of Niobium Coatings

The morphology, microstructure and defects were studied using a scanning electron microscope (SEM). Both coating surfaces and cross-sections were studied. Cross-sectional scanning electron microscopy showed that all niobium coatings had a fine and dense structure without any porosity or cracking at the substrate-coating interface. The adhesion of the niobium coatings appeared to be of high quality as judged on the basis of SEM (Fig. 1). The adhesion of niobium coating to substrate was determined with the aid of a tearing machine. The specimen was glued to counter plate made of carbon steel preliminary treated with a jet of silicium carbide power (particle size 500-1000 μm) at the pressure of 5-15 MPa for 3 hours at 175°C. Niobium coating to substrate adhesion attained the value 8 kg/mm² notwithstanding the absence of components active interdiffusion on steel. Fe and Nb distribution on the Nb-stainless steel interface after electrolysis was studied by microprobe analyzer (Fig 2). Scanning electron micrograph observations of the upper surface of the specimens showed no structural defects but mountain-like surface consisted of Nb (Fig. 3). Breaking surfaces were made by first freezing the coated specimens by liquid hydrogen and then breaking them immediately. Niobium coatings on stainless steel were hard to break (Fig. 4a), but niobium coated carbon steel breaks quite easily because of the temperature of -196 °C (Fig. 4b). The transition temperature of pure niobium T_c is < -126°C, so niobium is a very ductile metal⁸. According to ASTM standards B 708 and B 393 the tensile strength should be 125 MPa, the yield strength 85 MPa and the elongation 25 % to niobium sheets (R 04210 quality).

Both metals, niobium and tantalum, are susceptible to hydrogen embrittlement. To prevent hydrogen embrittlement the "platinum spotting" technique has been applied to test samples manufactured by Kola Science Centre of the Russian Academy of Sciences. The "platinum spotting" technique, whereby platinum is applied to the surface in isolated spots as thin as 10 μm with the area ratio 10000:1, enables to convert hydrogen into a molecular form which is not adsorbed by the metal at temperatures lower than 200°C, and thus produces no detrimental effect on mechanical properties of the base. If the possible cathodic reaction is hydrogen evolution, then the reaction is catalysed by platinum the end product being H₂O. Optical study of the cross section of niobium coated stainless steel sample is in figure 5. The columnar structure of the coating and the absence of detectable continuing porosity are distinctly seen. A comparatively weak texture with the axis direction <110> increases in the course of the coating thickness growth. The microhardness of niobium layer was determined with 50 g loading. Owing to the low level of impurities the microhardness of niobium coating on specimens cross-section was 90-100 kg/mm² and the elongation ranges up to 5.0 mm in Erichsen test. The chemical composition of the niobium coating in table 1. indicates its high purity. The chemical composition of the niobium coating (mass-%) was determined by spark mass spectrometer, the depth of spark treatment being 5 μm . Electron-beam melted 99.9 w/o niobium was used as a standard.

III. Experimental

The base materials were AISI 316 stainless steel (SS) and carbon steel (CS). The coatings used in this study were electrodeposited niobium described in previous sections. They were manufactured by Kola Science Centre of the Russian Academy of Sciences. The thickness of the coatings was 50 μm .

In short time experiments the electrolyte was 30 % H_2SO_4 (5.6 M H_2SO_4) at 298 K temperature and in long term measurements 1 M H_2SO_4 . Potentials were measured versus saturated calomel electrode, SCE, and platinum plate was used as a counter electrode. The surface areas of the test specimens were 0.79 cm^2 . Short term electrochemical measurements were made with a computer-controlled measurement system developed at the Helsinki University of Technology^{9,10}. The system uses a NF2000 potentiostat and NF5050 frequency response analyzer.

Measurement software is written in Basic and data processing is carried out with commercial software packages.

Short term measurement procedure for coated samples consisted of four different measurements: Electrochemical Impedance Spectroscopy EIS, Linear Polarisation LP, Potentiostatic Exertion PE and Long Cyclic Anodic Polarization LCAP.

Electrochemical Impedance Spectroscopy EIS.

Impedance spectrum was measured using logarithmic sweep with 5 frequencies per decade at frequency range 1 mHz to 100 kHz. Amplitude of the excitation voltage signal was 10 mV. Elimination of the phase shift at high frequencies was done by installing a capacitive coupling with platinum wire and 1 μF capacitor parallel to the reference electrode. Ohmic drops were insignificant between the test electrode and the SCE reference electrode on grounds of EIS measurements.

Determination of linear polarization resistance, R_p .

R_p was determined in the potential domain $E_{\text{corr}} \pm 10$ mV using alternating anodic and cathodic polarization. The overpotential sequence was +1, -1, +2, -2 +10, -10 mV and the time between measurements was 2 seconds.

Potentiostatic Exertion PE.

Determination of i vs. t curves was made with potentiostatic exertion method using polarization of 1200 mV vs. SCE for 7200 seconds. The potential used in PE was selected on the basis of anodic polarization measurements. It was in the transpassive region for the stainless steel substrate.

Long Cyclic Anodic Polarization LCAP.

Anodic polarization curves were made with potentiostatic polarization method using 10 mV steps at 6 second intervals. Polarization scan started at -800 mV vs. SCE and at 2000 mV vs. SCE the polarization changes direction towards starting point unless the current density first reaches the threshold current density 5 mA/cm^2 , where the polarization scan direction is automatically reversed.

Long term immersion tests were carried out by a measurement system consisting of two potentiostats, Hewlett Packard 34703A multimeter and Grants Instruments 1200 series Squirrel meter/logger. For a 40 day period four samples, niobium coated AISI 316 and two niobium coated carbon steels and pure Nb were immersed in 1 M H_2SO_4 electrolyte at room temperature. One of the Nb/CS samples was held at a potential which was 200 mV higher than the corrosion potential of the base material, CS ($E_{\text{corr}} = -450$ mV vs. SCE) and the other

Nb/CS sample was held at a the potential of 300 mV over E_{corr} of base material. Corrosion current of Nb/CS samples and rest potentials vs. SCE of Nb/AISI 316 specimen and pure niobium were measured.

IV. Results and Discussion

Linear polarization resistance measurements turned out to be nearly impossible because of low current densities at E_{corr} . When a niobium coating is covered by a dense and uniform oxide layer, the current densities are of the order of $1 \mu\text{A}/\text{cm}^2$. The polarization resistance of the base material AISI 316 steel in 30 % H_2SO_4 electrolyte was approximately $40 \Omega\cdot\text{cm}^2$ ($E_{\text{corr}} = -290 \text{ mV} \pm 10 \text{ mV}$ vs. SCE) when R_p of niobium coated specimen was approximately $516 \text{ k}\Omega\cdot\text{cm}^2$ ($E_{\text{corr}} = 270\text{-}440 \text{ mV}$ vs. SCE). The polarization resistance of the reference material, pure Nb, was approximately $142 \text{ k}\Omega\cdot\text{cm}^2$ ($E_{\text{corr}} = 140 \text{ mV} \pm 10 \text{ mV}$ vs. SCE).

The polarization resistance values measured by EIS showed that the corrosion resistance of niobium coatings was related to the development of a passive layer on the niobium surface. The XPS studies of Grunder and Halbritter show that the anodic film over the niobium surface is composed of a thin NbO film, with an average thickness of 1 nm, and an approximately 6 nm thick external layer of Nb_2O_5 ¹¹. The NbO layer is insoluble and inhibits the ionic transport of Nb^{5+} ions.

When the niobium coatings over the AISI 316 specimens were destroyed purposely by a diamond drill, the polarisation resistance values decreased as can be seen from Bode diagrams in figure 6. EIS spectra were measured at the potential $E = -311 \text{ mV}$ vs. SCE, which is in the activity range of the base material.

The R_p values of all specimens (coated or not) measured by EIS were higher when the potentials of specimens were in the passivity range of the base material AISI 316 as can be seen in figure 7. Even the carbon steel specimen coated with niobium was as good as the Nb/AISI 316-system according to EIS measurements in 30 % H_2SO_4 electrolyte. Impedance spectra, measured in the active range of the AISI 316 stainless steel (Fig. 8.) showed the vital importance of the niobium oxide layer. A strong relation between the potentials and the polarisation resistances of Nb coated specimens, (Fig. 9.) exist. R_p values measured by EIS can be related to the formation of the oxide film or the existing film is becoming dense. The oxide film thickness increases at the same time as the potential is becoming increasingly more anodic until some saturation point in passive range.

LCAP curves for niobium coated specimens measured in 30 % H_2SO_4 solution are shown in figure 10. The uncoated base material (AISI 316) and niobium on carbon steel were used as reference samples for the corrosion measurements. All niobium coated samples had better corrosion resistance than the stainless steel substrate. The shape of the curves shows the fact that these electrodeposited niobium coatings can isolate the substrate material almost completely from the electrolyte. The base material shows rapid dissolution at low anodic overpotentials. The dissolution rate decreases owing to the formation of a protective film. The passive nature of the AISI 316 substrate is seen at potentials from 10 mV (SCE) to 1000 mV (SCE). Above 1000 mV (SCE) in transpassive region, decomposition of water is initiated and oxygen evolution begins on the base material. Niobium coated samples remained passive from 1 mV (SCE) to 1500 mV (SCE). After that either the oxygen evolution gives some effect to the polarization curve or the activation could depend on the modification of the oxide passive layers by hydration or dissolution with subsequent repair^{12,13}. However, in none

of the tests did a breakdown of the surface layer take place, even up to potentials of 4 V vs. SCE. The current densities in the passive range for coated specimens were one order of magnitude lower than the stainless steel current densities in the passive range. All current densities of coated samples were so low that ohmic drops were insignificant between the test electrode and the saturated calomel electrode. On a valve metal the passive film is an extremely adherent dielectric oxide film and it will protect the metal from anodic dissolution until a critical breakdown potential is reached, and above this potential metal will show pitting corrosion. In chloride solutions this breakdown potential is for titanium about 10-14 V vs. NHE, but niobium and tantalum can remain passive up to 100 V. The breakdown potentials of niobium and tantalum are so high that in practice neither chloride concentration nor temperature changes will affect them^{14,15}.

The potential exertion measurement confirms the fact that the electrodeposited niobium coating can isolate the substrate from electrolyte almost perfectly. This potential exertion method reveals whether or not there are any pores or cracks in the coating. Measured current densities increased immediately if a direct path existed between the base material and the electrolyte. However, if the failed coatings had time to passivate, those direct paths were probably blocked by reformed Nb_2O_5 -layer. This reformed layer is not as dense and uniform as it is in good coatings, which can be seen as overall higher current densities in current vs. time -curves. The current densities of uncoated substrate materials were almost five orders of magnitude higher than the current densities of coated specimens, which were approximately $0.005 \mu\text{A}/\text{cm}^2$ (Fig. 11.).

The long term measurements showed again the excellent corrosion resistance of niobium and the fact that the electrodeposited niobium coating is dense and able to passivate even at the lower potentials. The corrosion currents of two Nb/CS samples under the potentiostatic exertion (-250 and -150 mV vs. SCE) were so negligible that no corrosion current could be measured during a 40 day period. The corrosion currents of Nb/CS samples and the rest potentials of pure niobium and niobium coated AISI 316 samples were monitored for every hour and the only signals to observe were the rest potentials. The corrosion potentials measured for the pure niobium were at first 10 days about 80 mV (SCE) lower than the corrosion potentials for the niobium coated sample. After 30 days the potential difference between niobium coated sample and pure niobium was diminished. The coated system was also much more stable than the pure niobium in 1 M H_2SO_4 electrolyte during the 40 days test period, which is probably due to the different surface morphology and activity of the test samples (see Fig. 3).

7. Conclusions

EIS measurements indicated the fact that the corrosion resistance of the coatings was strongly related to the dense oxide layer of niobium. The Long Cyclic Anodic Polarization curves showed that electrodeposited niobium coatings are capable of isolating the substrate material almost completely from the electrolyte. The potentiostatic exertion measurements showed that the corrosion resistances of the electrodeposited niobium coatings were five orders of magnitude better than the corrosion resistance of the base material AISI 316 in 30 % H_2SO_4 electrolyte.

VI. References

1. Ya.M. Kolotyркиn, N. Agafonova, Ts. Zalkind, Moscow, NIITEKHIM, (1985), 42p
2. P.E. Sullivan, In Proc. Int. Sym. Tantalum and Niobium. Orlando (USA), (1988), pp. 595-618.
3. R.T. Webster, Niobium in Industrial Applications. In: Refractory Metals and Their Industrial Applications. ASTM 849, R.E. Smallwood, ed. American Society for Testing and Materials. Philadelphia.(1984) pp. 18-27.
4. A. Baraboshkin, Electrocrystallization of metals in molten salts, Moscow, Nauka, (1976), 280 p.
5. D. Inman, In "Molten Salt Chemistry", Proc. NATO Adv. Inst., Camerino, (1987), pp. 417-424.
6. Molten Salt Technology - Edit. D. Lovering, N.Y., Plenum Press, (1982), 460p.
7. Pat. USSR N1448774, 06.04.87, C25D 3/66, S. Kuznetsov, V. Maslov, E. Polyakov.
8. R.W. Balliett, M. Coscia, F.J. Hunkeler, Niobium and Tantalum in materials selection, Journal of Metals, 38, (1986), pp. 25-27.
9. J. Aromaa, K. Knuutila, O. Forsén, S. Yläsaari, A Compact Micro Computer System for Electrochemical Experiments, Proceedings of the 5th Asian-Pacific Corrosion Conference, 23.-27. November 1987, Melbourne, Australia.
10. M. Tavi, O. Forsén, J. Aromaa, Corrosion Testing of ZrN and TiN films, Electrochemical Methods in Corrosion Research, Proceedings of Symposium, 12.-15. July 1988, Zürich, Switzerland. Edited by Elsener, B., Trans Tech Publications, (1989), pp. 15-27.
11. M. Grunder, J. Halbritter, Journal of Applied Physics, 51, (1980), p. 397.
12. E. Lugscheider, H. Eschnauer, B. Häuser, D. Jäger, Vacuum Plasma Spraying of Tantalum and Niobium, J. Vac. Sci. Technol. A3 (6), Nov/Dec (1985), pp. 2469-2474.
13. C.V. D'Alkaine, L.M.M. De Souza, F.C. Nart, The Anodic Behaviour of Niobium I, II, III, Corrosion Science, Vol. 34, No. 1. (1993), pp. 109-149.
14. W.R. Jacob, Corrosion Prevention & Control, August (1975), pp. 6-20.
15. A. Nidola, Technological Impact of Metallic Oxides as Anodes, In Electrodes of Conductive Metallic Oxides, part 11B, Edited by S. Trasatti, Elsevier Scientific Publishing Company, (1981), pp. 627-659.

[Table 1 to page 4.] The chemical composition of the niobium coating (mass-%).

Zn, V, Co, Ni, Mn, Al, Mg, Cu	Sn, Si, Mo	W	Ti, Ca	Cr	O, N, C
$< 2 \times 10^{-4}$	$< 5 \times 10^{-4}$	$< 8 \times 10^{-4}$	$< 1 \times 10^{-3}$	$< 6 \times 10^{-3}$	< 0.01

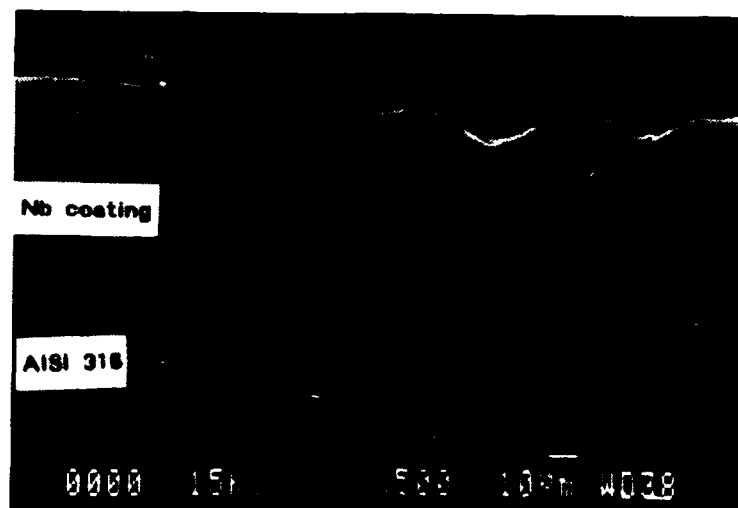


Figure 1. Cross-sectional scanning electron micrograph of the niobium coating stainless steel interface.

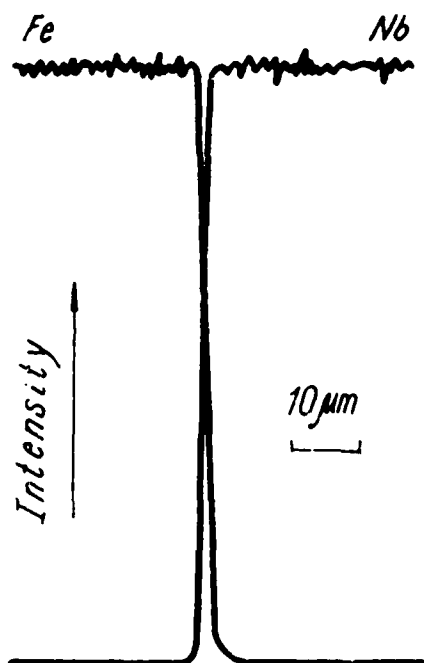


Figure 2. Distribution of components on niobium stainless steel interface after electrolysis.



Figure 3. Mountain-like upper surface of niobium coated stainless steel.

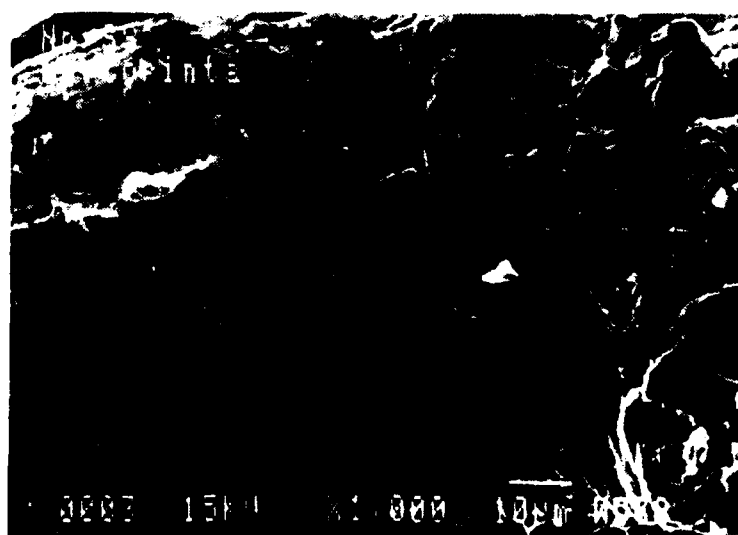


Figure 4 a. Breaking surface of niobium coated stainless steel.

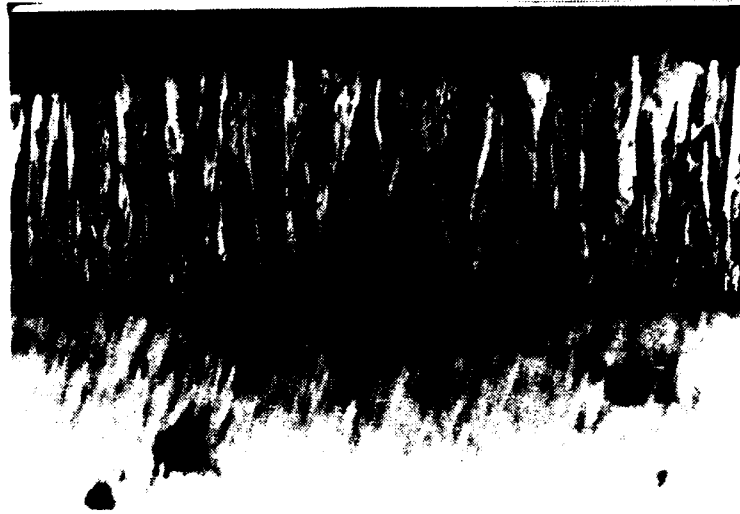


Figure 4 b. Breaking surface of niobium coated carbon steel.

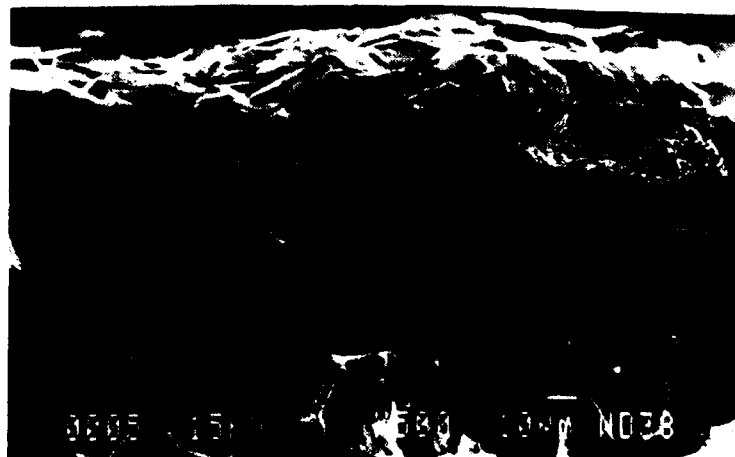


Figure 5. Cross-section of niobium coated stainless steel ($\times 500$).

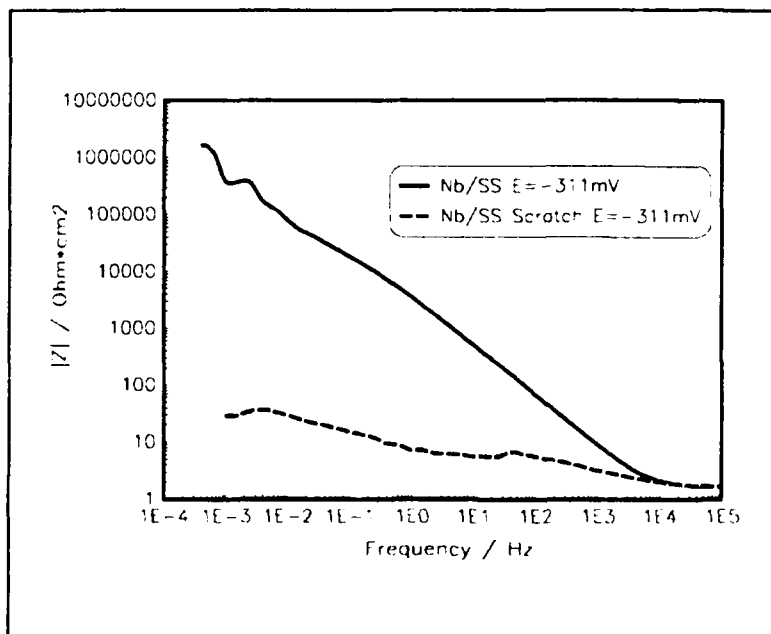


Figure 6. Nb/AISI 316 with and without a scratch in 30% H_2SO_4 .

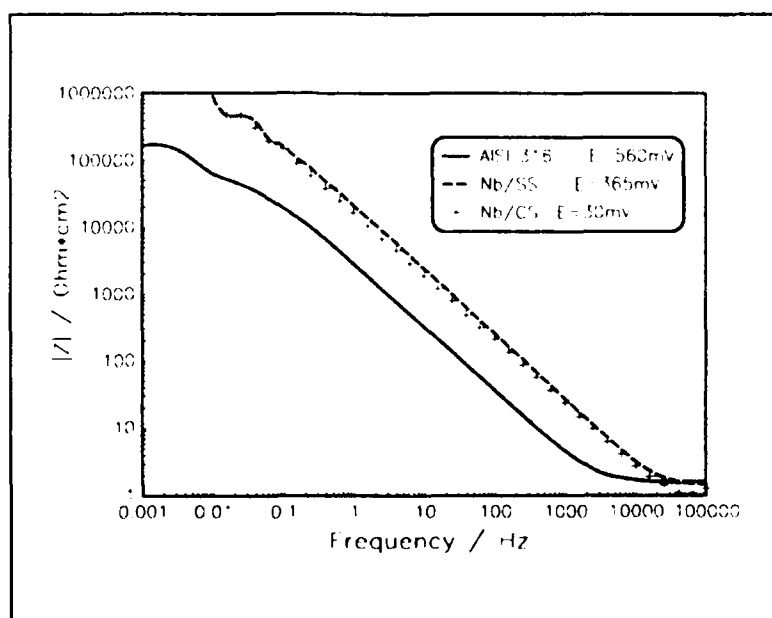


Figure 7. Bode diagrams measured at the passive range of AISI in 30% H_2SO_4 .

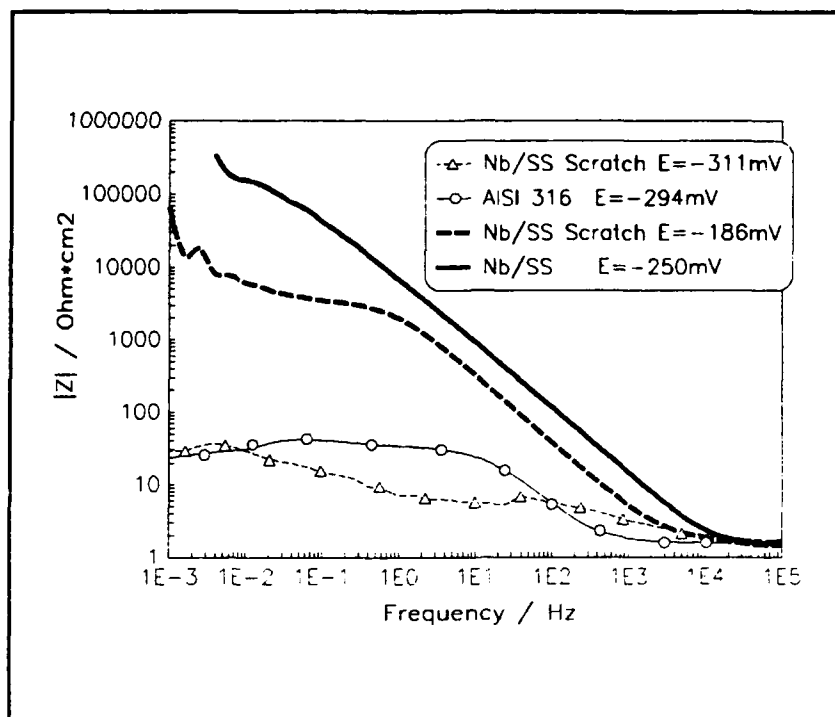


Figure 8. EIS measurements at the active range of AISI 316 in 30% H_2SO_4 .

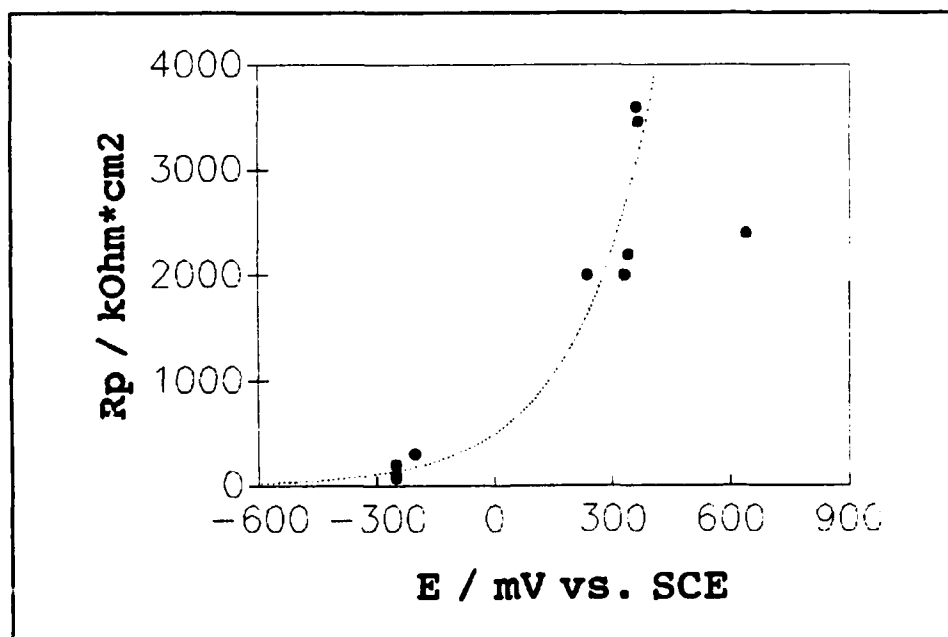


Figure 9. R_p values measured for the Nb/AISI 316 system at different potentials (see LCAP curves) can be related to the formation of the oxide film.

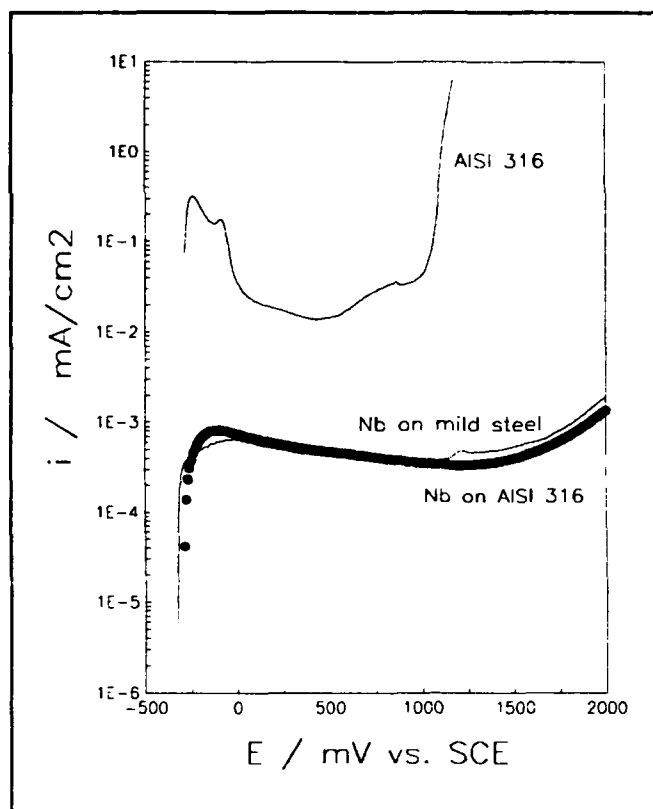


Figure 10. LCAP curves for AISI 316, Nb/mild steel and Nb/AISI 316 in 30% H_2SO_4 .

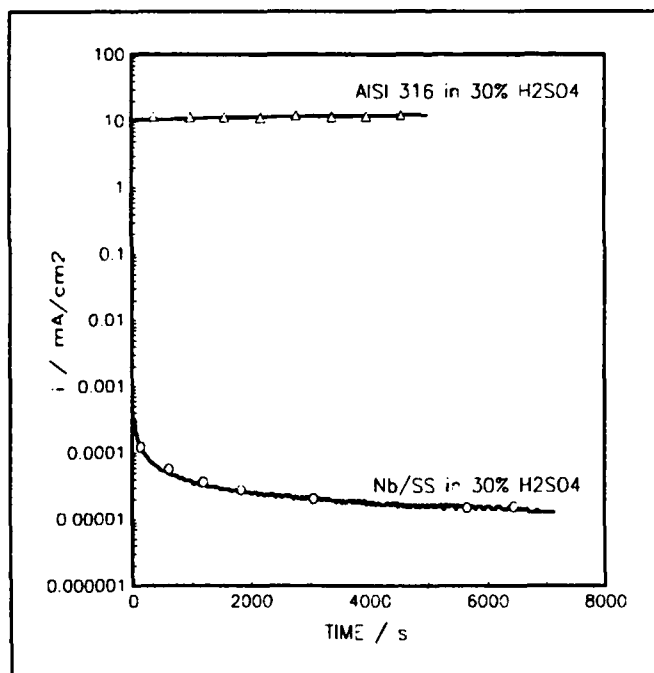


Figure 11. PE measurements at 1200 mV vs. SCE for 2 h.

The Effect of Laser Transformation Hardening on the Corrosion Resistance of AISI 01 Tool Steel

L.J. Yang,
S. Jana,
S.C. Tam,
L.E.N. Lim,
M.W.S. Lau.

School of Mechanical & Production Engineering,
Nanyang Technological University,
Nanyang Avenue,
Singapore 2263.
Republic of Singapore.

Abstract

ASSAB DF2 tool steel has been used widely for a number of applications including tools, moulds and dies. However, due to high humidity and the corrosive nature of some raw materials, they corrode easily if inadequate precaution is taken. Therefore, a study on the corrosion resistance of ASSAB DF2 tool steel specimens with both conventional and laser transformation hardening was done, using a salt spray chamber to simulate accelerated corrosive environment. Three types of specimens were used. These included plain as-received specimens, specimens hardened to hardnesses of 40 and 60 HRC by the conventional hardening process; and specimens which were pre-hardened to a hardness of 60 HRC after which they were hardened by a laser. The coatings used were zinc phosphate coating, manganese phosphate coating and black oxide coating.

Both zinc and manganese phosphate coatings were found to be effective in enhancing the corrosion resistance of the Assab DF-2 tool steel specimens. However, black oxide coating was found to be ineffective in corrosion protection under such testing conditions. Conventional heat treatment was found to reduce the corrosion resistance of ASSAB DF2 tool steel specimens; the higher the hardness, the lower is the corrosion resistance. For laser hardened specimens, the pre-hardened specimens and the specimens hardened with a lower heat input power were found to be more corrosion resistant.

Key terms: AISI 01 tool steel, Laser transformation hardening, Protective coatings, Corrosion rates.

Introduction

AISI-01 is a cold work alloy tool steel which has been used widely for a number of applications including tools, moulds and dies. However, due to the high humidity of the environment and the corrosive nature of some plastic raw materials, e.g. PVC and acetate, they corrode easily. Due precautions must, therefore, be taken to ensure that the tools made of the steel be adequately protected in industrial applications.

In recent years, laser has been used for welding, cutting, trimming, marking and scribing. Furthermore, high intensity laser has been used for laser heat treatment and laser cladding to improve the wear and corrosion resistance of the substrates [1-3]. A study was therefore carried out to investigate the effect of laser transformation hardening on the corrosion resistance of ASSAB DF2 cold work tool steel specimens heat-treated by both the conventional and laser transformation hardening [4]. The effect of protective coatings in enhancing the corrosion resistance of the tool steel was also studied. These coatings include zinc phosphate, manganese phosphate and black oxide coatings.

Equipment Used

Salt Spray Chamber

The Atlas Electric Devices Salt-Fog cabinet, measuring 1300 x 760 x 1730 mm, was used in this investigation. It is capable of producing uniform, free falling spray mists with uniform collection rates. The cabinet is manufactured with an inert continuous vinyl lined steel. It has a transparent acrylic cover to allow operator to control the even distribution of fog inside the test cabinet.

The salt spray chamber has two reservoirs: the top bubble tower liquid level reservoir and the external salt solution reservoir. The external reservoir supplies salt solution to the dispersion tower inside the cabinet. The float in the dispersion tower maintains the salt solution level. The distilled water level inside the bubble tower is maintained at two third full through the use of an auto level water valve. Air enters the bottom of the tower through the micro bubble aerator. It leaves the top of the tower heated and saturated with water vapour. The dispersion tower is installed in the cabinet chamber to provide the salt fog. The saturated air from the bubble tower goes to the atomizer on top of the tower reservoir. The salt solution is then siphoned into the saturated air stream to provide a properly maintained and uniform salt fog out of the top of the dispersion tower.

Laser Unit

The Maho Laservav YAG laser system was used for laser transformation hardening of the specimens. The continuous CW output of the laser unit is 0-400 W while the maximum pulsed output is 20 kW. The wavelength is 1.06 microns. The maximum pulse energy is 0-55 Joules with a pulse duration of 0.3-20 milliseconds and pulse repetition rate of 0.2-500 Hz. The beam diameter is 10 mm. The process parameters chosen for the laser transformation hardening of the specimens are listed in Table 1.

Experimental Procedure

The ASSAB DF2 tool steel selected for this investigation has a typical analysis of C=0.90%, Mn=1.20%, Cr=0.50%, W=0.50% and V=0.10%. The material came in the form of precision ground plates of size 6 x 40 x 500 mm and were cut into specimen sizes of 6 x 40 x 60 mm. These specimens were either used in the as-received soft annealed condition, or heat treated to 40 and 60 HRC conditions using conventional method or with laser transformation hardening after the conventional heat treatment process mentioned earlier. All the specimens were either treated with a zinc phosphate, or a manganese phosphate or a black oxide coating after heat treatment and prior to salt mist testing. Two types of coating thicknesses were used; 0.007 and 0.015 mm thick for both zinc and manganese phosphate coatings and 0.004 and 0.010 mm thick for black oxide coatings. The thicknesses of the coatings were determined by using a scanning electron

microscope after typical selected specimens were sectioned, moulded onto a plastic holder, ground and polished.

The laser transformation hardening technique is used to increase the surface hardness of ferrous alloys by heating a thin layer of the substrate rapidly into austenitising temperature and subsequently cooling it at a very fast rate due to self-quenching by conduction of heat into the bulk body, to produce a martensitic structure. However, the efficiency of laser heat treatment depends on the absorption of light energy by the workpiece. Since the absorptivity of light energy by a bare steel specimen is very low, some absorbent coatings are almost always used during laser transformation heat treatment. Hence, for the specimens to be used for laser transformation hardening, a manganese phosphate coating of 0.015 mm thick was applied before they were laser transformation hardened. The laser transformation hardened specimens were then subjected to corrosion test as the rest of the specimens. Although laser hardening had vaporized the original manganese phosphate coating, however no further coating was applied to these specimens since the purpose of the study was to evaluate the corrosion resistance of these hardened specimens.

The specimens were loaded into the salt spray machine and exposed to the salt spray mist (5% NaCl) for a time period of about 144 to 168 hours. Recommendations from ASTM B117-85 salt spray (fog) test were followed as closely as possible. At an interval of about 24 hours, the samples were taken out to evaluate their corrosion rates by measuring their weight losses. The test rack that was used to support the specimens had slots with an angle of 20 degrees. The salt solution was prepared by dissolving 200 grams (5 parts) by weight of sodium chloride into 3.8 litres (3,800 grams or 95 parts) of distilled water. The air supply was set at a pressure of 15 psi or 103 kPa.

Experimental Results and Discussion

Figure 1 shows the corrosion rate against exposure time for the 'as-received' ASSAB DF2 specimens without any coating and with different types of coatings. It can be seen from the figure that the uncoated specimen has extremely high corrosion rates as compared with those which have zinc and manganese phosphate coatings on them. The use of a black oxide coating does reduce the corrosion rate slightly. However, it is still ineffective when it is compared with zinc and manganese phosphate coatings. It is further observed that there is a tendency for the corrosion rate to reduce as the exposure time is increased. This is due to the formation of a more inert oxidised surface on top of the specimen which prevents it from active corrosive attack by the salt mist. Figure 1 also shows the effect of coating thickness on the corrosion rate. A thicker coating in all cases reduces the corrosion rate especially at the early stage. However the effect is no longer there after an exposure time of about 100 hours.

Figure 2 shows the effects of heat treatment conditions on the corrosion rates of the specimens. The specimens were in the as-received, hardened to 40 and 60 HRC hardness conditions and were coated with zinc phosphate coatings of two thicknesses. Lower corrosion rates are observed on the as-received specimens as compared with those heat treated to 40 and 60 HRC hardness and for both coating thicknesses. It seems, therefore, that the slightly higher corrosion rates of the specimens hardened to a higher hardness value is probably related to the higher residual stress and lattice distortion set up in the specimen during the hardening process.

Figure 3 shows the effect of laser transformation hardening on the corrosion rates of the specimens. The specimens were hardened with different heat input powers as mentioned in Table 1. It is noted that, in case of the as-received specimens, the specimens which received a lower heat input power during laser transformation hardening have lower corrosion rates as compared

with those specimens which received higher input powers during laser transformation hardening.

For the pre-hardened to 60 HRC and subsequently laser hardened specimens, the corrosion rates for the specimen hardened with a 200 W heat input power is higher than those obtainable with the specimen hardened with a 360 W heat input. The corrosion rates of both these two specimens are, however, higher than those of the specimen hardened with a 100 W heat input power during laser transformation hardening.

It has been observed that, for the pre-hardened to 60 HRC specimens, the average hardnesses of the specimens after laser transformation hardening were 959.0, 963.4, 949.8 VHN for specimens hardened with an heat input power of 100, 200 and 360 W respectively. The specimen which received the heat input power of 200 W has the highest average hardness value and also the corrosion rate. For the as-received specimens, the corresponding hardnesses of the specimens were 886.5, 886.2, 874.0 VHN for specimens hardened with an heat input of 100, 200 and 360 W respectively. In this case, the specimen which has the lowest average hardness value of 874.0 VHN has slightly higher corrosion rates. However, this might have been due to experimental scatters. It seems, therefore, that the corrosion rate is affected by the residual stress set up during laser transformation hardening. The higher heat input would have caused higher residual stress and lattice distortion which in turn probably affects the corrosion rate of the specimens.

It should be noted from Fig. 3 that the corrosion rate of laser transformation hardened specimens also depends on the prior heat treatment condition of the parent material, i.e. whether it is in the as-received soft annealed or pre-hardened condition. Previous study has also indicated that hardness and heat affected zones of a laser transformation hardened specimen is affected by its pre-heat treatment condition of the parent material [5]. However, the exact mechanism on why the corrosion resistance of the pre-hardened specimens is higher is not clear. It is possible that prehardening by conditioning the specimens to produce a more homogeneous matrix (as opposed to the discrete carbide particles in ferrite of the as-received samples) produces a less stressed, less distorted and more homogeneous hardened specimen upon subsequent laser heat treatment. This could translate into better corrosion resistance.

Conclusion

The investigation has shown that both zinc and manganese phosphate coatings can enhance the corrosion resistance of ASSAB DF2 tool steel. However, black oxide coating was found ineffective under salt mist testing conditions. It is found that conventional hardening has an effect of reducing the corrosion resistance; the higher the hardness, generally the higher is the corrosion rate. For the laser transformation hardened specimens, it is found that the heat input power can affect the corrosion rate. A higher heat input power used during laser transformation hardening of the specimen may increase its corrosion rate. Furthermore, it is found that the pre-hardened specimens have lower corrosion rates as compared with those of the as-received soft annealed specimens.

Acknowledgement

The authors gratefully acknowledge the financial support provided by Applied Research Grant #30/88 and Ministry of Finance R&D Grant #04/89 . They would also like to thank Mr Koay

Choon Meng, past undergraduate student, technicians from CNC laboratory, School of Mechanical & Production Engineering, Nanyang Technological University, for the technical support provided.

References

- [1] P. Pizzi: "Lasers in Automobile Production", in "Laser Welding, Cutting and Surface Treatment", The Welding Institute, 1984.**
- [2] J. F. Ready (Editor), "Lasers in Modern Industry", Society of Manufacturing Engineers, 1979.**
- [3] J. Mazumder: "Laser Heat Treatment: The State of the Art", Journal of Metals, vol.35, No.5, May 1983. pp. 18-26.**
- [4] C. M. Koay: "The Corrosion Resistance of Steel Specimens", FYP Report #B136, School of Mechanical & Production Engineering, Nanyang Technological University, 1992.**
- [5] Yang L. J., Jana S. and Tam S. C.: "The Effects of Prehardening on Laser Transformation Hardening of Tool Steel Specimens", Jnl of Materials Processing Technology, Vol. 25, No 3, April 1991, pp. 321- 332, Elsevier Science Publication B. V., Amsterdam, The Netherlands.**

Table 1- Parameters used in laser transformation hardening of specimens.

S/N	SPOT DIAMETE R (mm)	LASER POWER (W)	PULSE ENERGY (J)	PULSE FREQUENCY (Hz)	PULSE HEIGHT (%)	PULSE WIDTH (ms)
1	3.6	100	12.5	8	58.9	1
2	3.6	200	25.0	8	88.3	1
3	3.6	360	45.0	8	100	1.6

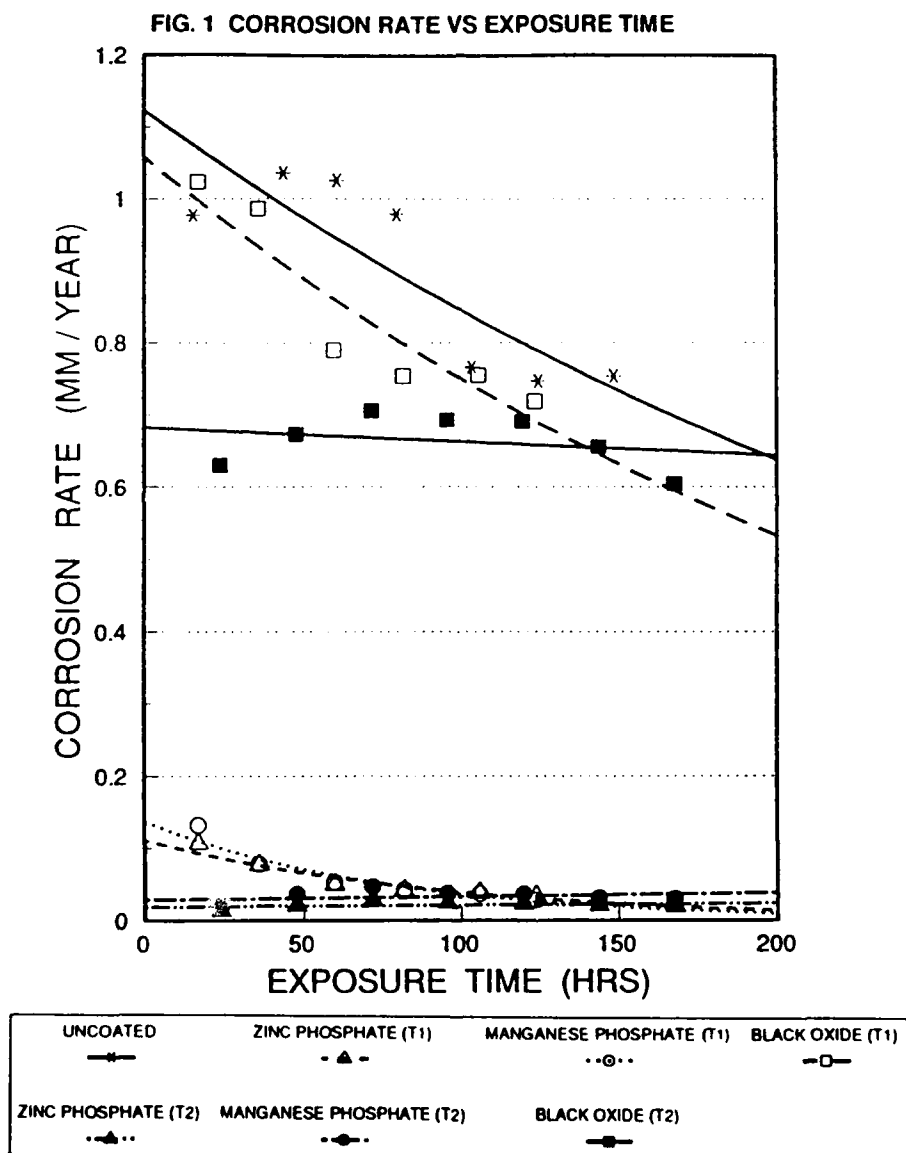


Fig. 1 Corrosion rate vs exposure time for 'as-received' ASSAB DF2 specimens, both uncoated and coated with zinc phosphate, manganese phosphate and black oxide coatings with two different thicknesses (T1=0.007mm and T2=0.015mm for zinc and manganese phosphate coatings; T1=0.004 mm and T2=0.007 mm for black oxide coatings).

FIG. 2 CORROSION RATE VS EXPOSURE TIME

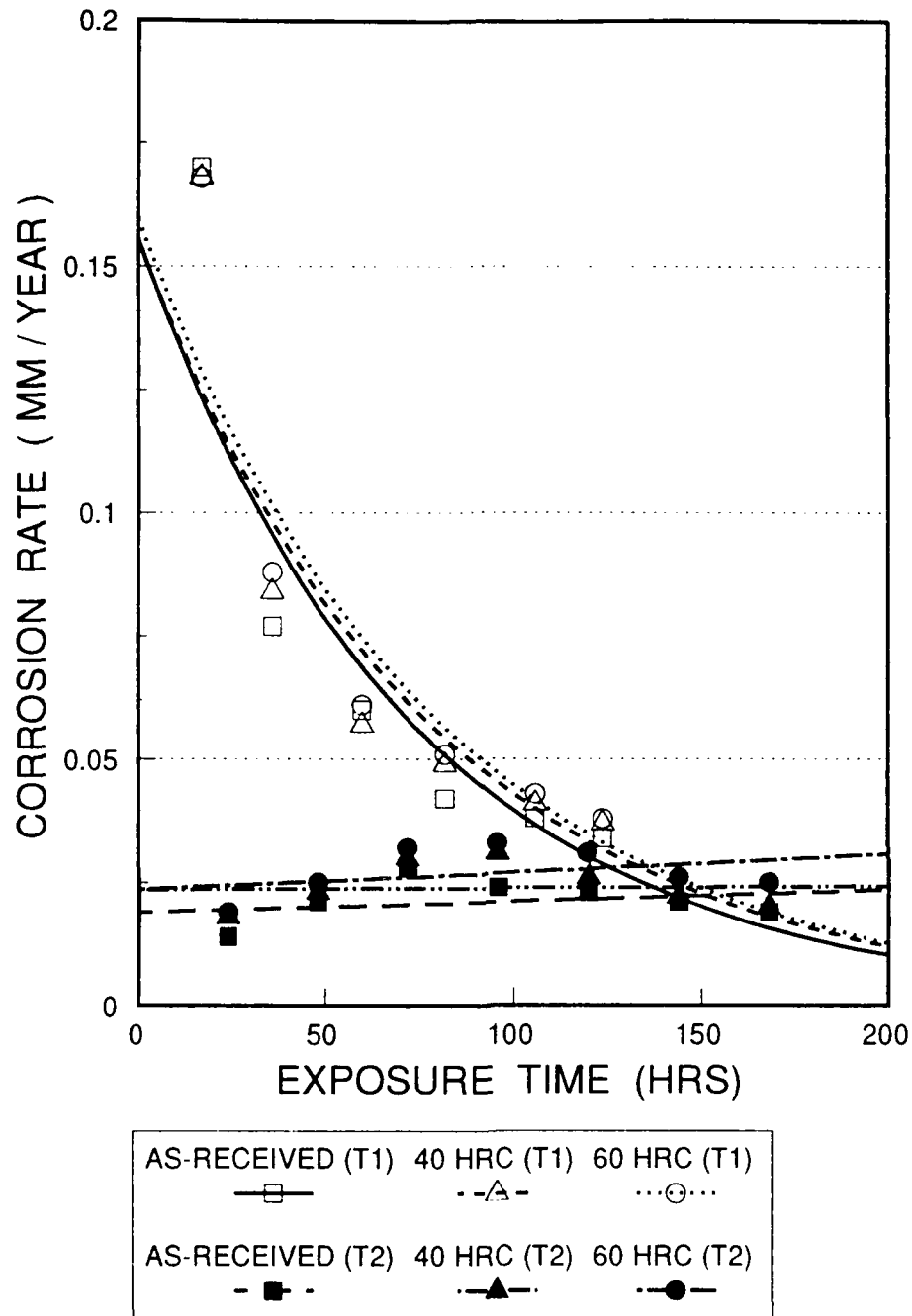


Fig. 2 Corrosion rate vs exposure time for 'as-received' and hardened to 40 and 60 HRC hardness ASSAB DF2 specimens coated with zinc phosphate coatings with two different thicknesses (T1=0.007mm and T2=0.015mm).

FIG. 3 CORROSION RATE VS EXPOSURE TIME

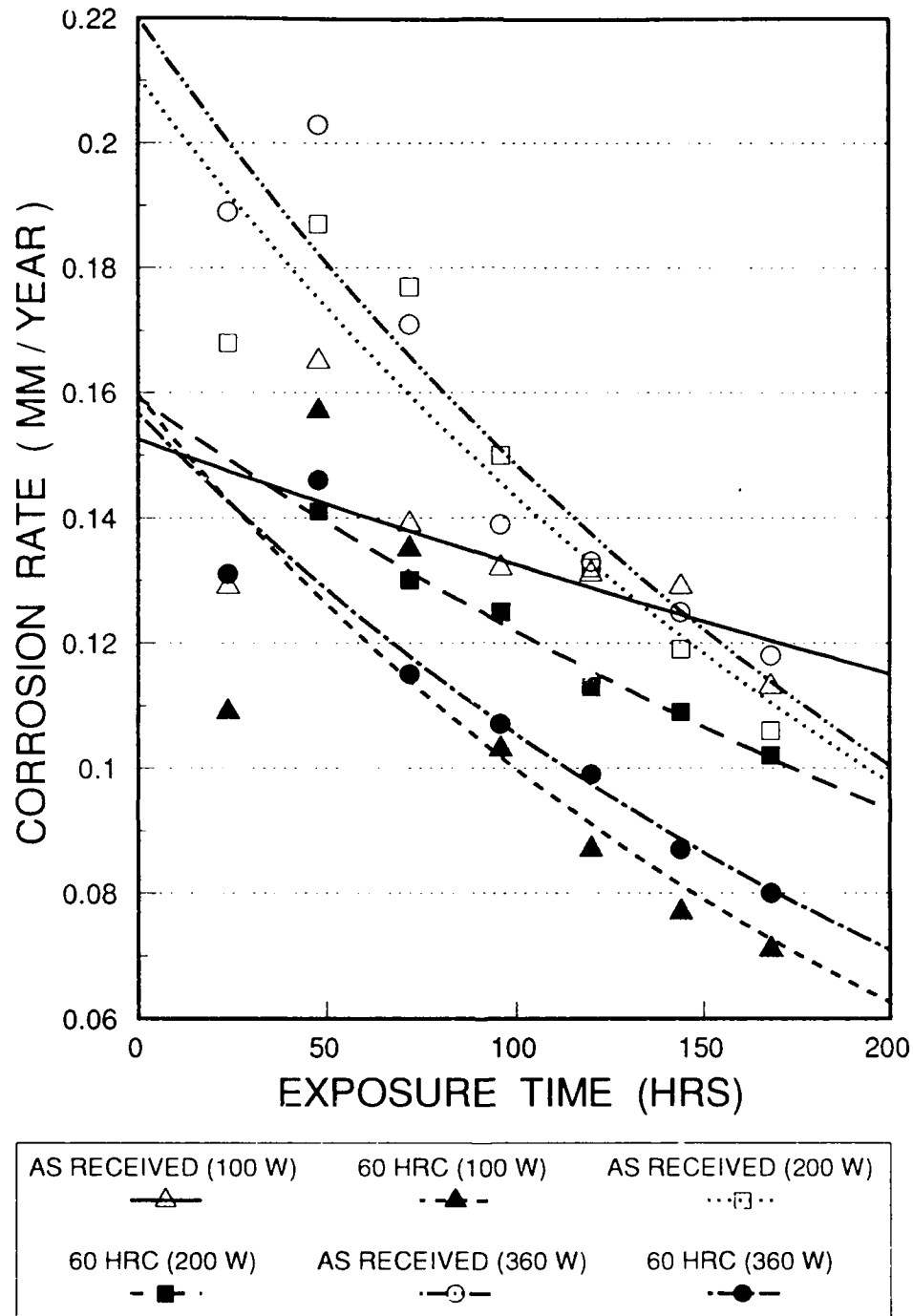


Fig. 3 Corrosion rate vs exposure time for 'as-received' and pre-hardened to 60 HRC hardness ASSAB DF2 specimens, laser transformation hardened with 100W, 200W and 360W heat input powers.

A Comparison of the Corrosion Properties of Thick Layers of Chromium and Its Alloys with Nickel Deposited from Chromium (III) Electrolytes

A. Watson
Department of Chemistry
Paisley University
Paisley
UK

M. R. El-Sharif
School of Engineering
Glasgow Caledonian University
70 Cowcaddens Road
Glasgow G4 0BA
UK

X. Wang
School of Engineering
Glasgow Caledonian University
70 Cowcaddens Road
Glasgow G4 0BA
UK

C. U. Chisholm
School of Engineering
Glasgow Caledonian University
70 Cowcaddens Road
Glasgow G4 0BA
UK

Abstract

In recent years the electrodeposition of thick layers of chromium and its alloys has become possible from environmentally more acceptable chromium (III) electrolytes, allowing their corrosion and wear resistant properties to be exploited. In contrast to the conventional chromium (VI) the chromium (III) electrolytes allow codeposition of a range of alloys. These alloys offer a choice of metallurgical properties. Single metal chromium is very hard but brittle. Such brittleness can be a problem in corrosion protection. The hardness can be sacrificed for greater ductility by alloy formation. The codeposition of nickel can offer the possibility of adjusting the balance of wear resistant and corrosion properties to a given problem. The present paper will describe a comparison of the corrosion properties of a chromium-nickel alloy coating to a single metal chromium deposited from a similar electrolyte and with a single metal chromium deposited from a commercial electrolyte modified for thick deposits. The techniques used include salt spray and Tafel plots. The corrosion properties were related to deposition parameters and to the age of the electroplating electrolytes, since chromium (III) electrolytes are often unstable towards aging. In general the corrosion protection offered by the chromium-nickel alloy was found to be better than the single metal chromium. With the chromium-nickel alloy corrosion currents fell with increasing deposit thickness to an optimum thickness of about 40 μm beyond which no improvement occurred. In contrast the single metal chromium deposit had corrosion currents which fell only to 1-3 μm beyond which they rose again markedly. Microscopy showed that the latter was associated with major microcracking in the more brittle deposit. On the other hand the corrosion currents produced by the single metal chromium, prior to this cracking, were less sensitive to variations in the age of the electroplating electrolyte. The single metal chromium examined appeared to offer a poorer corrosion performance than a conventional chromium (VI) process.

Key terms: **Electrodeposition, Chromium Alloys, Chromium (III) Electrolytes, Corrosion Resistance**

Introduction

In recent years the sustained deposition of thick coatings of chromium and its alloys has become possible¹⁻⁴ from the environmentally more acceptable chromium(III) electrolytes. A major advantage of chromium (III) electrolytes, in addition to their environmental acceptability, is that they offer the possibility of electro-codeposition of chromium alloys. This is not practicable from chromium (VI) electrolytes. Thick coatings of chromium are used both for wear resistance and corrosion protection, taking advantage of the hardness of electrodeposited chromium and its resistance to corrosion. However hard chromium deposits are also brittle. The important attribute of alloy codeposited coatings is that they offer the ability to adjust and tailor a range of properties for a specific application. For example, sacrificing some of the hardness for a higher fracture toughness may enhance wear and corrosion performance in some applications. A comparative study of the corrosion properties of single metal chromium with its alloys with nickel and iron was appropriate.

Experimental Details

Deposition of the Coatings

Electrolytes

The common electrolyte used was as follows. For single metal chromium and chromium-nickel deposition the appropriate metal salts were eliminated:-

0.8 mol $[\text{Cr}(\text{H}_2\text{O})_4\text{Cl}_2]\text{Cl} \cdot 2\text{H}_2\text{O}$ (green modification)
0.2 mol $\text{NiCl}_2 \cdot 6\text{H}_2\text{O}$
0.03 mol $\text{FeCl}_2 \cdot 6\text{H}_2\text{O}$
0.5 mol NH_4Cl
0.5 mol NaCl
0.15 mol $\text{B}(\text{OH})_3$

Several baths were prepared from this electrolyte using :-

A. dimethylformamide electrolytes

for chromium and chromium-nickel:-

750 g N,N-dimethylformamide

250 g deionised water

for chromium-nickel-iron

500 g N,N-dimethylformamide

500 g deionised water

B. urea electrolytes

8.0 mol urea

make up to 1 litre with deionised water

A commercial decorative chromium(III) electrolyte modified for sustained deposition of thick coatings was also used for comparison.

All solvents and reagents were of AnalaR grade. Due to the slow ligand exchange reactions of chromium(III) a standard procedure of electrolyte preparation is essential. For the dimethylformamide electrolytes the chromium salts were dissolved in the amide without heating while the other reagents were dissolved in the water. The two solvents were then mixed without heating. For the other electrolytes the main complexant/solvent was dissolved first in most of the water, followed by the other reagents, the chromium salt being last. During dissolution of the chromium salt no heating was applied. Finally the solution was made up to the mark with deionised water. These electrolytes were employed at make up pH without further adjustment of pH.

Electrodes

High conductivity AnalaR copper, high density graphite and mild steel were used as cathodes, the size of the cathode area exposed for deposition being $2.5 \times 2.5 \text{ cm}^2$. The non-working area was insulated with a non-conducting lacquer. After preparation all cathodes were immediately transferred wet to the plating cell.

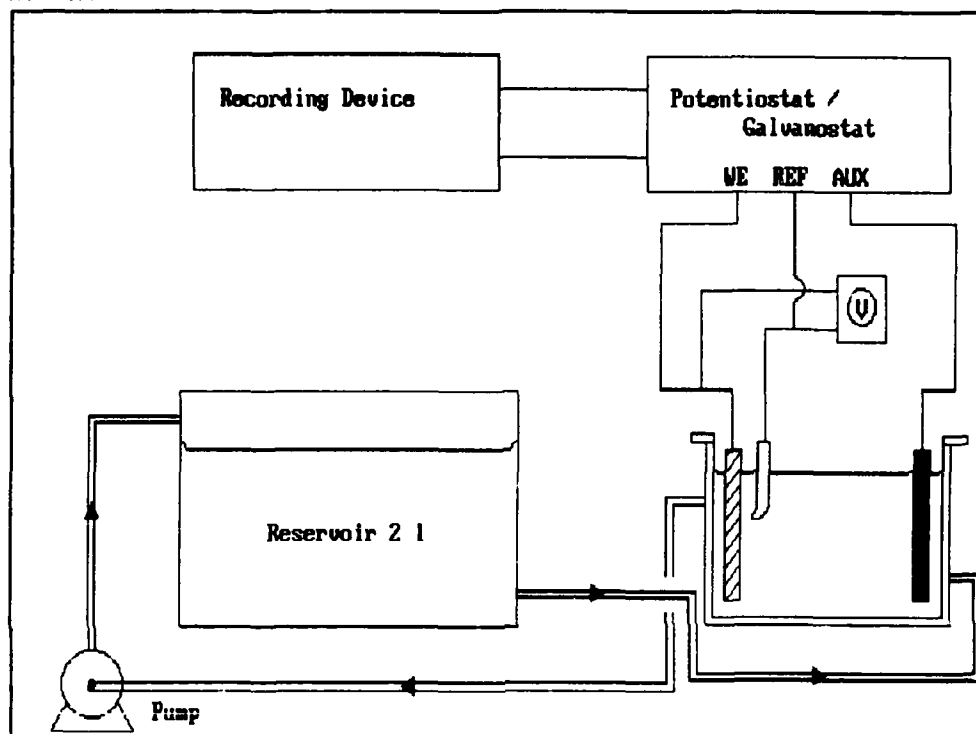
Copper cathodes were prepared, by degreasing in acetone, electropolishing at 900 mV in 80% v/v phosphoric acid, 10% v/v water and 10% v/v methanol, and finally rinsing with flowing deionised water.

Mild steel cathodes were degreased with carbon tetrachloride, followed by an anodic etch in 50% sodium hydroxide for 5 minutes at 5 A/dm^2 at 90°C . After rinsing the cathodes were etched for 15 seconds in 50% hydrochloric acid and then rinsed in deionised water.

Insoluble high density graphite anodes were employed. The reference electrode was a standard 'sticktype' calomel electrode.

Cells

The electrodeposition apparatus consisted of a rectangular thin walled plastic cell (10 cm length, 4 cm wide, 8 cm depth). To circulate the electrolyte the cell was fitted with outlets leading via a peristaltic pump (Watson and Marlowe) to a 2 litre reservoir, with return by gravity feed to the cell. The flow was from anode to cathode with the outlet so placed as to arrange a gentle agitation at the cathode. A flow rate of 80 ml/min was maintained.



All the electrolytes were maintained at 25°C

Electrochemical Investigation of the Deposits

In the studies of electrochemical properties a three electrode cell system (Versastat model 352) was used in which the sample was used as the working electrode, platinum and saturated calomel electrode as the auxiliary and reference electrodes respectively. Each sample was degreased with acetone and coated with lacquer to give an exposed area of 4cm² before the immersion into a non-deaerated 0.05M H₂SO₄ solution at 20°C. Tafel plots were characterized with a potentiodynamic scan rate at 5mV/min and the corrosion current for each coating was estimated by Tafel line extrapolation. The corrosion currents were obtained by the polarization resistance method, using the Stern-Geary equation⁵.

In the laboratory accelerated salt spray corrosion tests, 5% neutral salt spray was used according to ASTM Specification B117, with a Weiss Technik SSC450 salt spray testing chamber.

Discussion

Preliminary investigations by salt spray test followed by microscopy confirmed that the corrosion of the work piece is generally by corrosion of the substrate from under the coating rather than of the chromium alloy coating itself. This indicates the importance of coating thickness.

The corrosion current was investigated as a function of the thickness of the deposit, from a number of different deposits. Chromium/nickel and chromium/nickel/iron deposits from dimethylformamide electrolytes show a steady decrease in corrosion current with increased thickness, as can be seen in Fig.2. This would be expected as less microcracks penetrate from the coating surface to the substrate surface. A maximum protection is offered, for chromium/nickel, at about 20 μm , beyond which there is little improvement, up to a thickness of 50 μm . The equivalent optimum value for chromium/nickel/iron is about 5-10 μm , beyond which a small loss of protection occurs to 30 μm .

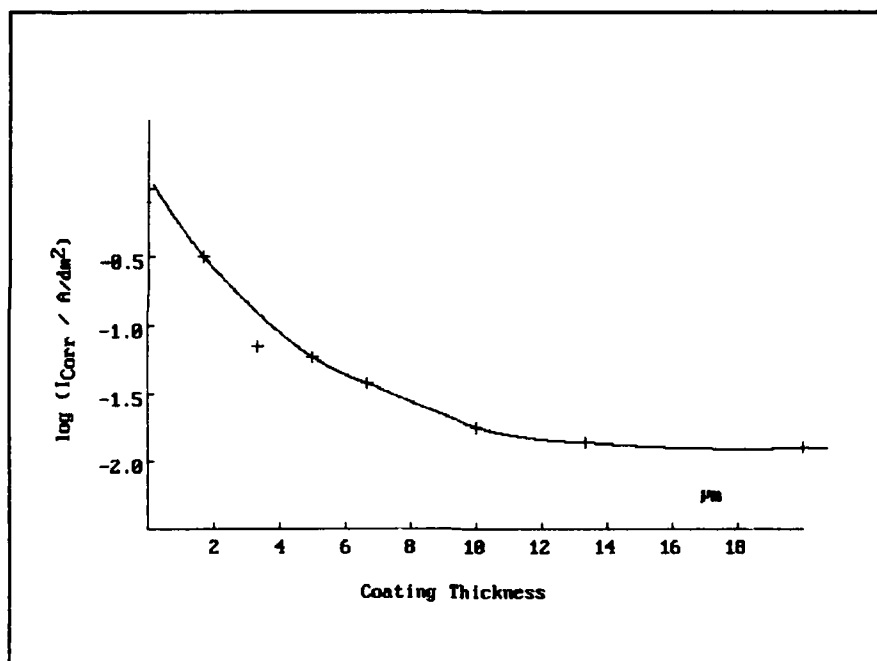


Figure 2 The corrosion current for a chromium/nickel alloy deposited from DMF as a function of coating thickness.

A considerably different behaviour was shown by single metal chromium deposits. Fig.3 shows the corrosion current versus coating thickness for a single metal chromium deposit from a commercial decorative chromium(III) process based on a carboxylate electrolyte and modified for sustained deposition of thick layers. This shows a short initial decrease in corrosion current with increased thickness. However this is followed by a sudden major increase in corrosion current. With further increase in thickness the current again decreases somewhat but the corrosion currents become of poor reproducibility with periodic jumps in current.

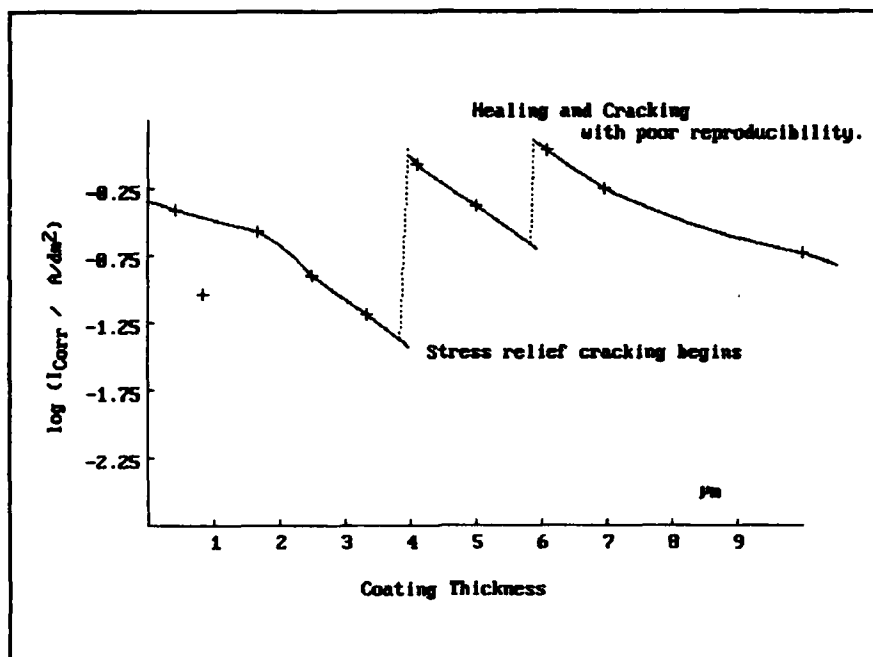


Figure 3 The corrosion current for single metal chromium from a commercial carboxylate electrolyte as a function of coating thickness.

Microscopy shows that the sudden jumps or increases in corrosion current are associated with a sudden increase in the degree of microcracking due to stress relief. These new microcracks might be better thought of as narrow macrocracks. Microscopy also shows healing of the cracks with continuing deposition and a temporary improvement in protection. However once significant cracking has occurred the cycle of cracking and healing is not reproducible in nature. The optimum thickness for corrosion protection for this coating is only about 3 μm. which is insufficient for wear protection etc.. Single chromium metal coatings from dimethylformamide and urea electrolytes showed a similar although less extreme pattern, allowing a greater thickness, 15-20 μm, before loss of protection occurs.

The chromium/nickel and chromium/nickel/iron deposits did not display the sudden increase in penetrative crack count on increased coating thickness associated with the single metal chromium coatings investigated. This no doubt reflects the greater ductility of the alloys. The commercial carboxylate process produced a single metal chromium with a microhardness of 1200 HV, a particularly high value most likely to be associated with its lack of ductility and its failure through internal stress.

Microscopy indicated that corrosion for 10 minutes at 100-200 mV anodic of the corrosion potential, produced corrosion pits. These pits were clearly associated with extensive corrosion of the substrate. Broken layers of chromium or its alloy could be seen undercut by corrosion of the substrate. The pits were found to contain loosely adherent quantities of chromium alloy. No direct evidence was found of corrosion of the coating itself. Its loss appears to be associated with loss of substrate support. No pits were found confined within the coating thickness. The coating

surface either appears unaffected or extensive corrosion of the substrate is associated with loss of the coating. For example Fig.4 shows a photomicrograph of a chromium coating on mild steel after corrosion. Electron probe analysis shows the staining around the cracks to be iron compounds presumably from the steel substrate, while the chromium alloy surface appears intact. In general the pits appeared to have some limited association with the microcracking pattern.



Figure 4 A photomicrograph of a chromium deposit on mild steel at magnification X 400, after corrosion for 4 minutes at 100 mV anodic of E_{Corr} .

Corrosion is therefore generally to be associated with the effective porosity of the coating rather than its own inherent corrosion properties.

Polarisation Curves

Potentiodynamic polarisation curves, in sulphuric acid pH 0.5-2, for single metal chromium and chromium/nickel coatings on copper substrates did not show any clearly defined passive region while those obtained on mild steel did show a narrow passive region with a high passive current. This is probably consistent with corrosion of the substrate through the coating, rather than the properties of the coating itself, as copper does not display passive behaviour at this pH.

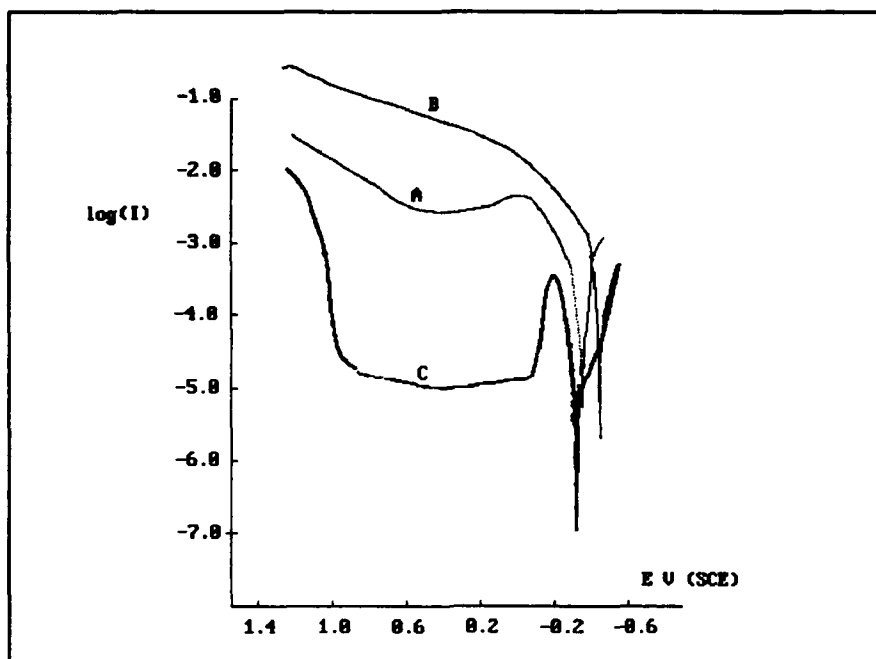


Figure 5. The potentiodynamic curves in 0.05 M H_2SO_4 for A a 80% Cr chromium nickel deposit from DMF on mild steel, B a mild steel and C a 302 stainless steel.

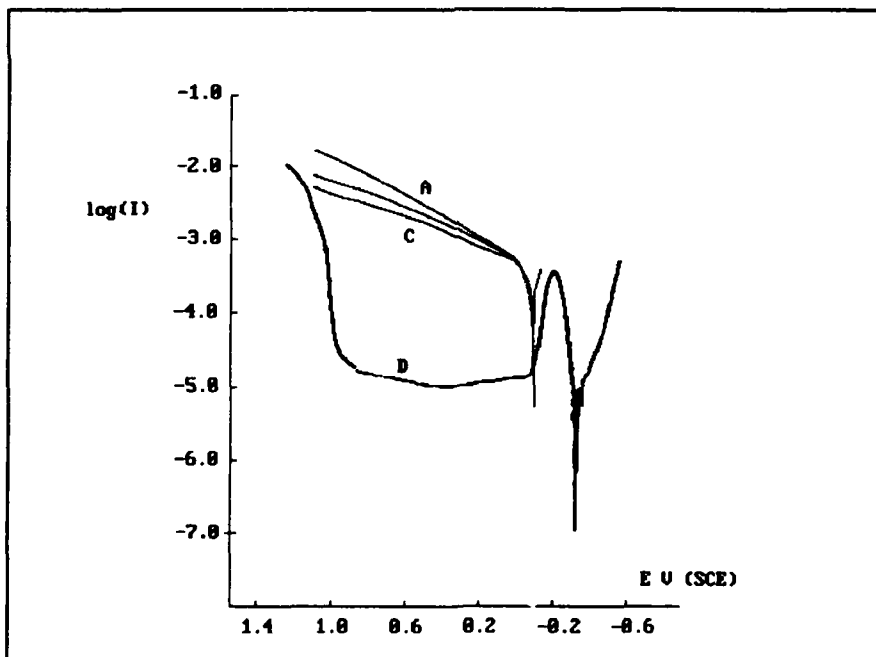


Figure 6. The potentiodynamic curves in 0.05 M H_2SO_4 for A, B, C a 80% Cr chromium nickel deposit from DMF of 5, 10 and 20 μm respectively on copper, and D a 302 stainless steel.

Currents in both the corrosion and possible passive region decrease with the thickness of the single metal chromium and chromium/nickel deposit on both copper and mild steel, until a maximum is reached or until a marked increase in stress relief cracking occurs. The chromium/nickel/iron deposits are the most ductile and most crack free of the deposits examined. A distinct passive region was found for the latter deposits both on mild steel and on copper substrates. This would suggest that the curve is responsive to both coating and substrate.

The currents for the ternary alloy deposited on both mild steel and copper are significantly lower than for single metal chromium and chromium/nickel. It can therefore be suggested that the corrosion properties of single metal chromium and chromium/nickel deposits are dominated by their porosity through the extent of microcracks penetrating from surface to substrate, while in the less porous chromium/nickel/iron deposits the lower corrosion currents also in part reflect the coating itself.

Fig.7 shows a comparison of chromium/nickel/iron deposits on mild steel from dimethylformamide and urea electrolytes with stainless steel and a mild steel. A narrower passive region with higher passive current could reflect a more active coating surface and corrosion of the substrate. The curves will reflect the corrosion of a composite rather than just the coating itself.

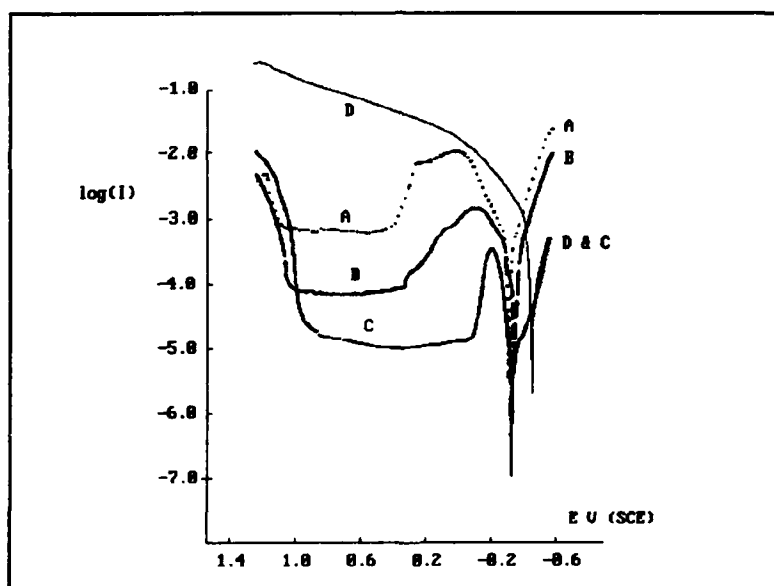


Figure 7, The potentiodynamic curves in 0.05 M H_2SO_4 for A 10%Cr,23%Ni,67%Fe deposit from dimethylformamide
B 11%Cr,40%Ni,50%Fe deposit from urea,
C a 302 stainless and D a mild steel.

More prolonged corrosion of the chromium/nickel/iron deposits leads to eventual partial exposure of the substrate, which in turn results in the undercutting of the coating by corrosion of the substrate observed with single metal chromium and chromium/nickel. Corrosion appears to increase the population of microcracks penetrating to the substrate.

At transpassive potentials massive corrosion of all the coatings occurs.

The Influence of Metallic Composition

An increase in the chromium content of the chromium/nickel alloys (>80% Cr) studied had the effect of increasing the corrosion current. This effect is likely to be due to a loss of ductility with increasing chromium, resulting in a greater concentration of penetrating microcracks.

Increasing the chromium content of the chromium/nickel/iron alloys had the effect of decreasing the corrosion currents, up to about 40-50% Cr. Above this a increase in corrosion currents occurs associated with increased cracking.

Table I The Corrosion Potentials and Currents, in 0.05 M H₂SO₄, of 5µm Cr/Ni/Fe coatings deposited from the DMF electrolyte.

Potential V (SCE)	Cr%	Ni%	Fe%	E _{Corr} V (SCE)	I _{Corr} mA/dm ²
-1.4	6.1	38.9	55.0	-0.355	20.2
-1.6	18.0	29.4	52.7	-0.311	8.76
-1.8	37.2	20.3	42.5	-0.292	2.95
302 steel	18	8	74	-0.291	0.83

The increase in corrosion protection offered by these chromium/nickel/iron deposits with increased chromium content suggests that the corrosion currents are indeed those of the coating, since increased chromium is unlikely to decrease the extent of microcracking. The optimum minimum corrosion currents found for deposits with about 40% Cr and 20% Ni do in fact approach the performance of 18/8 stainless steel with a similar corrosion potential and corrosion currents only about three to five times greater. This however depends on a minimum of microcracking. Should such effective microcracking increase markedly corrosion current also rise markedly, overwhelming the effect of chromium content on the nobility of the coating.

The influence of complexant

The urea and dimethylformamide electrolytes examined offered better corrosion protection with single chromium deposits than a commercial chromium(III) carboxylate electrolyte for single metal chromium. For chromium/nickel/iron deposits, the urea electrolyte appears in general to give coatings offering a superior performance to those obtained from dimethylformamide at lower chromium contents, while at higher chromium contents the dimethylformamide offered the better performance.

Table II Corrosion parameters in 0.05 M H₂SO₄, of 5µm Cr/Ni/Fe coatings deposited from the DMF and Urea electrolytes.

Electrolyte	E _{Corr} V (SCE)	I _{Corr} mA/dm ²	I _c mA/dm ²	I _p mA/dm ²	Passive range V (SCE)
DMF 10%Cr 22%Ni	-0.357	49.14	641	57.5	-0.377 - 1.043
Urea 10%Cr 40%Ni	-0.391	27.2	127	9.85	-0.297 - 1.015
302 steel	-0.379	1.06	33	1.54	-0.108 - 0.929

The Effect of the Age of the Chromium(III) Electrolyte

A general observation can be made that the corrosion protection offered by these coatings becomes poorer with ageing of the electrolyte, with an increased instance of penetrative microcracking.

Table III The increase in corrosion current for a 5µm chromium/nickel deposit with the age of the chromium(III) dimethylformamide electrolyte used for the deposition.

Age	fresh	60 min	120 min	24 hr	30 days	1 year
i _{Corr} mA/dm ²	59.5	78.4	127	132	110	89.9

In Table III the shorter times refer to time of electrolysis, while the longer times include both electrolysis and storage.

Ageing in these electrolytes is believed^{2,4} to be due to formation of µ-hydroxo bridged oligomeric and polymeric chromium(III) species in the higher pH (pH ≈ 4) of the cathode diffusion layer catalysed by transient chromium(II) formed as an intermediate in the electrodeposition. Once formed these species will survive in the lower pH of the bulk electrolyte due to the slow ligand exchange reactions of chromium(III). Inclusion of these polymeric species in the deposit would be likely to increase internal stress and hence the concentration of effective cracking leading to some loss of corrosion protection. Longer times of storage between electrolysis may lead to some very slow reversal of the polymerisation reaction as perhaps indicated in Table III.

The chromium/nickel/iron coatings from dimethylformamide electrolytes in fact showed some initial improvement in corrosion protection during the first ten hours of deposition, followed by a period of stability. The results in Tables I, II and IV and Fig. 3 are all from pre-aged solutions with at least 10 hours of previous electrolysis. This probably represents the initial completion of complexation through chromium(II) catalysis. This effect was less marked for urea electrolytes which are believed to reach completion of complexation more rapidly^{2,4}. However much longer term ageing of these two chromium/nickel/iron electrolytes does indeed result in loss of protection as with the chromium/nickel deposits, due to increased penetrative microcracking with corrosion of the substrate taking over from corrosion of the coating material. Again µ-hydroxo bridged chromium(III) polymer formation is to be indicated. The period

of relatively crack free chromium/nickel/iron coatings, with corrosion parameters as shown in Table I, varies from 50-150 hours depending greatly on exact conditions.

The Effect of Heat Treatment

There have some claims^{6,7} that the corrosion performance of chromium/nickel/iron deposits can be improved by heat treatment. The deposits, from dimethylformamide, investigated in the current study were also subjected to heat treatment.

Table IV The effect of heat treatment on a Cr/Ni/Fe deposit from DMF, on its corrosion potential and current in 0.05 M H₂SO₄.

Temperature °C	Time min	E _{corr} V (SCE)	I _{corr} ² mA/dm ²
as deposited	-	-0.311	8.76
600	30	-0.188	22.99
1000	30	-0.142	10.2

The effect of heat treatment is to produce a more positive, that is more noble, corrosion potential. This would suggest a less reactive coating. However the corrosion currents in fact increase. Heat treatment leads to a loss of corrosion protection.

The deposits contain considerable organic inclusions with ≈1% carbon. On heat treatment the total carbon content of the deposit falls somewhat as part of the organic material is lost by vaporisation. The rest becomes elemental carbon which can interact with the metal components of the coating. Chromium carbide precipitation has been confirmed by X-ray diffraction. As a result the homogeneity of the coating is altered by heat treatment. The heat treatment will also have its effect on the all important cracking and microcracking. Both increased cracking has been observed, as well as some limited healing of the cracks. These effects will vary with the heat treatment parameters, however increased cracking is more common and no heat treatment conditions were found to reduce the corrosion currents.

Comparison with Chromate(VI) Processes

It is difficult to make a meaningful comparison between the corrosion performance of chromium from trivalent and hexavalent processes, since the latter have had decades of research development, while the trivalent processes are of more recent origin. However in general single metal chromium generated from chromium(III) electrolytes often has a great microhardness and may be more brittle than chromium from conventional chromium(VI) processes. Deposits obtained from the conventional chromium(VI) processes are microcracked. A difference in the nature of the microcracks from trivalent processes may be indicated. There is evidence that the microcracks in conventional hard chromium contain oxides. They may also be less interconnecting than in deposits from trivalent processes. The further development of trivalent chromium deposits for corrosion protection will thus require considerable attention to the problem of microcracking.

Comparison with Stainless Steel

Most of the coatings examined offered very much poorer corrosion resistance than thermally prepared stainless steel, as might be expected. The best protection was offered by chromium/nickel/iron deposits with an optimum composition of ~ 40% Cr, 20% Ni, 40% Fe with corrosion currents about only 3-4 times those of 18/8 stainless steel. Many previous workers appear to have sought electrodeposited coatings with the 18% Cr, 8% Ni composition. This composition has no particular significance for electrodeposited coatings since the nature of these alloys does not resemble thermally prepared alloys of the same metal content, as the former has much a higher oxygen content and the higher total carbon content is present as organic inclusions etc.

Conclusions

The relative corrosion protection offered by chromium and chromium alloys coatings, electrodeposited from the chromium(III) electrolytes investigated, is dominated by the extent and character of the microcracking. The best corrosion protection, for the work piece, is offered by the most ductile of the deposits, chromium/nickel/iron although it is inherently less resistant in itself than the single metal chromium or chromium/nickel. The worst protection was offered by single metal chromium deposits which suffered significant stress relief cracking beyond thicknesses of only a few μm . Chromium/nickel deposits showed a corrosion protection controlled predominately by the porosity of the coating. Only chromium/nickel/iron deposits could be obtained whose corrosion characteristics were inherently those of the coating material itself - rather than those of the composite, with corrosion of the substrate dominating as for chromium/nickel. Optimum corrosion protection was obtained at relatively low thicknesses. 5-10 μm for chromium/nickel/iron. Greater thicknesses offer no advantages and excessive thicknesses can lead to cracking even with chromium/nickel/iron. The best quality chromium/nickel/iron electrodeposited coatings did approach the corrosion resistance of stainless steel with corrosion currents about 3 to 4 times those of stainless steel.

References

- [1] A. Watson, M R el Sharif and C U Chisholm, Transactions of the Institute of Metal Finishing, 64, 149-153, 1986.
- [2] A. Watson, A.M.H. Anderson, M.R. El-Sharif, and C.U. Chisholm, Proceedings of Eurocorr., Vol. 1, (1991), 228
- [3] A Watson, M R el Sharif and C U Chisholm, Transactions of the Institute of Metal Finishing, 66, 34-40 1988.
- [4] A.M.H. Anderson, A Watson, M.R. el-Sharif, and C.U. Chisholm, Trans. Inst. Metal Finishing. 69 26-32 (1991)
- [5] M. Stern, Corrosion J., 13, (Sept. 1958), 440
- [6] C. Domnikov, Metal Finishing 68 (2), 57, 1970.
- [7] T. Takahashi, K. Sugiyama and K. Hayakaw, J Electrochem Soc. 34, 153, 1966.

Studies of Chemical Conversion Treatments of Electrodeposited Zinc-Chromium and Zinc-Nickel-Chromium Alloys

M. R. El-Sharif
School of Engineering
Glasgow Caledonian University
70 Cowcaddens Road
Glasgow G4 0BA
UK

Y. J. Su
School of Engineering
Glasgow Caledonian University
70 Cowcaddens Road
Glasgow G4 0BA
UK

A. Watson
Department of Chemistry
Paisley University
Paisley
UK

C. U. Chisholm
School of Engineering
Glasgow Caledonian University
70 Cowcaddens Road
Glasgow G4 0BA
UK

Abstract

Chromate treatments for zinc and many other metals suffer from highly toxic process solution containing Cr(VI) and hence require costly treatments before disposal of spent liquors. Thus economic consideration, coupled with an increase in environmental awareness, have accelerated efforts to find non-toxic alternatives to chromates. A novel process to generate chromium based conversion coatings has been proposed as to introduce chromium into zinc or zinc alloy coatings and then oxidise their surfaces in powerful oxidising media. In this paper, conversion coating treatments of electrodeposited Zn-Cr and Zn-Ni-Cr alloy coatings in aqueous solutions of permanganate and persulfate have been examined.

The results indicate that in both permanganate and persulfate solutions conversion coatings with similar characteristics can be obtained on Zn-Cr and Zn-Ni-Cr alloy coatings. The formation of conversion coatings in these non-chromates solutions can be described by a dissolution-oxidation-precipitation process. The electrode potential - time profile and the activation-passivation behaviour during the formation of conversion coatings were studied. The studies show that the optimum immersion time can be determined from the activation-passivation behaviour of the coating surface under given operating conditions. The surface appearance of the conversion coatings was characterised by optical microscopy and it is suggested that the conversion coatings such formed contain both Cr(III) and Cr(VI) species, which are widely regarded as more effective on corrosion resistance. The effects of concentration of oxidising agents, immersion time, pH value, temperature and film aging were investigated. The electrochemical properties of the coatings were examined in sodium chloride solution.

Key terms: Electrodeposition, Zinc alloy, Conversion treatment, Chromating, Corrosion resistance

Introduction

Zinc is commonly used as a sacrificial coating to protect steel substrate against corrosive attacks and its protective value can be greatly enhanced by chromate conversion treatments, which effectively delays the formation of the initial corrosion product known as the white rust [1,2]. Recently notable achievements have been made in the development of zinc alloys such as zinc-nickel and zinc-cobalt, which possess superior corrosion resistance to single metal zinc. Yet the difference in corrosion resistance when comparing unchromated zinc alloys and chromated zinc alloys is large [3,4,5]. This means that chromate conversion coating could be a primary choice to zinc alloys once better corrosion resistance is desired. Chromate treatments suffer from environmentally undesirable chromium (VI) [6,7,8] and much recent efforts to replace this process have indicated the beginning of the end of using chromate treatments in metal finishing industry [9, 10]. Many types of non-chromates based conversion coatings such as molybdates or tungstates have been proposed [11,12]. The analogy of molybdates and tungstates to chromates exists in the sense of being corrosion inhibitors but comparison have shown that better corrosion resistance was given by the chromates based conversion coatings [13,14]. Although these alternatives to chromate treatments have not been fully established it could mean that chromates is in fact a better corrosion inhibitor.

In previous papers the present authors [15,16] have reported that a novel process for generating chromates based conversion coatings on zinc and its alloys. The method which is aimed at retaining the effectiveness in corrosion inhibition of chromates while eliminating the chromate solutions in conversion treatments. This was achieved by the electrodeposition of zinc-chromium and zinc-nickel-chromium alloy coatings on steel and the oxidation of these alloys in solutions which contain no chromates but powerful oxidant such as potassium permanganate. The object of the present work is to investigate and compare different types of oxidant capable of generating chromates based conversion coatings with an anti-corrosion property and to study the effects of different types of electrodeposited alloy on the formation of the conversion coatings.

Experimental method

The electrolytes composition and the operating conditions employed to obtain Zn-Cr and Zn-Ni-Cr alloy deposits are shown in Table 1. Analytical grade chemicals were used in the electrodeposition of alloys, formation of conversion coatings, and electrochemical measurements. In the investigation of electrodeposition behaviour and formation of conversion coatings, copper and mild steel cathodes were used. The working area of each cathode was $2.5 \times 2.5 \text{ cm}^2$. The copper cathodes were degreased in acetone and electropolished at 900 mV in a solution containing 80% (v/v) phosphoric acid, 10% (v/v) deionised water and 10% (v/v) methanol, and then rinsed in deionised water. The mild steel cathodes were polished with silicon carbide paper grade 500, treated cathodically in a solution containing 50-70 g/l alkaline cleaning agent with a current of 5 A/dm^2 for one minute at 80°C , followed by a rinse in deionised water. High density graphite was employed as an anode. Electrodeposition was conducted under potentiostatic mode, with circulated electrolyte to ensure sustained deposition [17,18]. Cathode vertical movement was used to minimise the negative influence of gas bubbles and improve quality of the deposits. In the formation of conversion coating electrodeposited alloys were pre-treated in a 3% nitric acid solution for 10 seconds and then rinsed in deionised water. This was followed by the immersion of the coatings into a solution containing permanganate, persulfate, or peroxide at various pH and temperature. The coatings were rinsed again in deionised water, and dried in hot air or idled for a certain period of time. The composition of the alloys was determined by X-ray fluorescence in a JXA-50A Electromicroscope attached with a Link electro microprobe analysis unit. Coating thickness were determined both with simple weighing technique and a Buechler Omnimet-1 Image analysis system. Surface appearance of alloys and conversion layers were examined under optical microscope. Electrochemical measurements were carried out with a EG&G-352 corrosion measurement system, and in a non-deaerated 1.0 M NaCl solution of pH 6.0 and at 30°C . The anodic and cathodic polarisation curves in the Tafel or linear

region were obtained with a typical potentiodynamic scan rate of 10 mV/min. The corrosion currents, I_{corr} , can be calculated from Tafel Constants (β_a and β_c) which were obtained from Tafel plots, and from the Polarisation Resistance, R_p , which was determined from the slope at the origin of polarisation curve, using the Stern-Geary equation [19]

$$I_{\text{corr}} = (\beta_a \times \beta_c) / [2.303 \times R_p \times (\beta_a + \beta_c)] \quad (1)$$

In the present case where dissolved oxygen exists in the solution it was assumed that the cathodic reaction was diffusion controlled and $\beta_c \gg \beta_a$. Thus the corrosion currents can be calculated from a simple form of equation (1) as

$$I_{\text{corr}} = \beta_a / (2.303 \times R_p) \quad (2)$$

Table 1. Bath composition and operating conditions for Zn-Cr and Zn-Ni-Cr alloy deposits

Constituents (g/l)	Zn-Cr bath	Zn-Ni-Cr bath
ZnSO ₄ ·7H ₂ O	57	57
CrCl ₃ ·6H ₂ O	215	215
NiCl ₂ ·6H ₂ O	-	48
Urea	240	240
Secondary complexant	38	38
H ₃ BO ₃	9	9
NH ₄ Cl	27	27
NaCl	29	29
Cathode potential, (-V, SCE)	1.6 - 1.85	1.4 - 2.2
Bulk pH	2.0 - 3.0	2.5 - 3.0
Temperature, (°C)	20 - 25	20 - 25
Agitation	Cathode movement vertical	Cathode movement vertical

Results and discussion

Electrodeposition of alloys

Zinc and chromium contents in electrolytes are both critical to influence the quality and chromium content of Zn-Cr deposits [15]. Thin deposits containing up to 35% Cr were obtained from low zinc bath (< 0.1 mol/l), but thick deposits were obtained only when zinc level was maintained around 0.2 mol/l and chromium level above 0.8 mol/l. Current efficiency was up to 45% in optimum range of cathode potential. The use of cathode movement vertically was found to be effective to minimise the negative influence of the hydrogen gas bubbles.

In Zn-Ni-Cr alloy deposition, an optimum chromium level in the electrolytes was found similar to that used in Zn-Cr deposition, and zinc level should be maintained between 0.2 to 0.3 mol/l [20]. The range of cathode potential which produced bright deposits was found much wider than that in the Zn-Cr deposition, that was from - 1.4 to - 2.2 V(SCE). The results show that chromium in deposits was sensitive to the change in cathode potential while nickel in deposits remained about the same, between 11% and 13%, which is the reported optimum content for corrosion resistance of zinc-nickel alloys [21,22]. The increase of pH in bulk solution or increase of temperature increased nickel content but reduced chromium content of deposits.

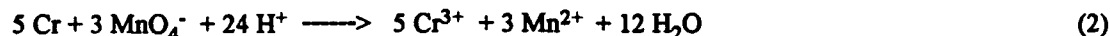
Studies of formation of conversion coatings

Mechanism of formation of conversion film on zinc alloys

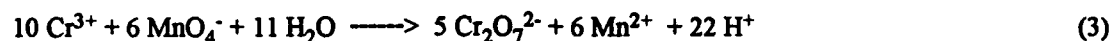
The solutions used for the formation of chromium based conversion film on zinc alloys were highly acidic (pH = 1.5 - 1.8) containing powerful oxidant such as permanganate, film-forming activators, and organic acids. In the case of zinc-chromium, as the alloy is immersed into such a solution zinc from the alloy is preferentially dissolved and reacts with hydrogen ions in the metal-solution interface.



Chromium content near alloy surface is enriched and activated and its dissolution takes place after being oxidised by a oxidant such as permanganate, represented simplistically by



A portion of chromium(III) is expected to be further oxidised into chromium(VI)



As reactions (1) and (2) can be regarded as predominating reactions the hydrogen ions within the metal-solution interface are consumed very quickly and this results in a rapid increase of pH in the interface. When pH reaches a critical value a complex chrom gel containing chromium (III) and chromium (VI) oxo/hydroxo species as well as zinc hydroxide and zinc chromate species is formed and precipitated on the surface of the alloy.

Effect of oxidising agent and concentration

Fig. 1 (a) shows the potential - time curves obtained in the formation of conversion coating for Zn-Cr alloys of 4%Cr in solutions at 20°C with different oxidising agents, which is also compared with that obtained from chromate treatment of zinc. The solutions used in the formation of conversion films are listed in Table 2. Details of each curve in Fig. 1(a) can be seen when plotted in their own corresponding potential range in Fig. 1 (b) - (d) respectively. It is noted that all curves show an initial decrease (more electronegative) in potential, indicating the metal surfaces were effectively activated. The activators in chromate solution to zinc are well known as chloride and sulphate^[23], which prevent an initial passivation from occurring by facilitating the dissolution of zinc. Some of the present solutions contained sulphate ions which obviously revealed activation in the absence of chromate. Iridescent conversion films were obtained from these solutions. It is also noted that each curve has a major peak at about 10 sec. and the reason is under investigation. The potential started to increase at different points of time depending on the solution involved (70 sec in chromate, 50 sec in permanganate, and 30 sec in persulfate). A certain period of immersion time such as 30 sec produced thinner film from persulfate than other solutions, and this may be associated with the shorter period when the surface of an alloy was in activated state in the persulfate. Also from Fig. 1(a) the variations of potential in chromate and permanganate solutions within 100 sec were similar, 55 mV (SCE) and 65 mV (SCE) respectively, while the potential variation in persulfate was 13 mV (SCE).

Table. 2. Solutions used in the conversion treatments (pH = 1.5 - 1.8)

Composition	I	II	III	IV	V
$\text{Na}_2\text{Cr}_2\text{O}_7 \cdot 2\text{H}_2\text{O}$ (g/l)	200				
KMnO_4 (g/l)	2	5	10		
$\text{Na}_2\text{S}_2\text{O}_8$ (g/l)				5	10
HNO_3 (ml/l)	5	10	10	10	10
H_2SO_4 (ml/l)	10	20	20	20	20

The effect of permanganate concentration on the potential - time of Zn-Cr (4%Cr) can be seen in Fig.2. Unlike the 5 g/l KMnO_4 solution, the potential in 10 g/l KMnO_4 decreased more rapidly at the beginning and increased very slowly thereafter and its overall potential was shifted towards more negative values. Thicker conversion films were obtained from this more concentrated permanganate solution. The effect of oxidising agents and their concentration on weight gain of conversion film was studied, on Zn-Cr alloys of 4%Cr in permanganate and persulfate solutions (Fig.3). A general rise of film weight gain with concentration of oxidising agent was found, markedly in 10 g/l KMnO_4 in the initial 40 sec. The increase of persulfate concentration had less effect on the weight gain of the films than that of permanganate concentration.

Effects of chromium content of alloy and immersion time

The chromium content of the alloy is significantly important to the chromium content and state in the conversion coating as it is the only source providing chromium species needed in the conversion coating. A number of Zn-Cr and Zn-Ni-Cr alloys containing chromium between 0% and 10% (12%-14%Ni in Zn-Ni-Cr alloys) were used to form permanganate conversion coating and the visual surface appearance is described in Table 3. When immersion times were less than 30 seconds light yellow conversion films were obtained on the alloys of 2%Cr while iridescent films were obtained from the alloys of 6% and 10% Cr. Although film thickness was one of the factors influencing the film colour there was a correlation between the chromium percentage of alloy and the distribution ratio of green-blue to orange-red area of the film surface under optical microscope. The higher the chromium content of the alloys the higher the ratio of the orange-red colour was found, provided the solutions and operating conditions were identical, indicating a larger portion of chromium from the alloy was transformed into hexavalent chromium. Immersion times beyond 60 seconds produced thicker films with increase in increasing micro cracking. The surface appearance of films on Zn-Ni-Cr were generally darker than those on Zn-Cr and a bright blue colour was commonly seen. This bright blue colour was likely to be associated with oxidised nickel products in the conversion films.

Table 3. Surface appearance of conversion films on Zn-Cr and Zn-Ni-Cr alloys (obtained from 5 g/l KMnO_4 solution, pH = 1.5 -1.8, 25°C)

Alloy	Immersion time (seconds)	chromium content of alloy		
		2%	6%	10%
Zn-Cr	10	very light yellow	light iridescent	iridescent
	20	light yellow	iridescent	iridescent
	40	light yellow	iridescent	dark iridescent
	60	dark yellow	dark iridescent	brown-iridescent
	90	yellow-brown	brown-iridescent	brown-iridescent
Zn-Ni -Cr	10	yellow	iridescent	dark iridescent
	20	yellow	iridescent	iridescent-blue
	40	dark yellow	iridescent-blue	blue
	60	yellow-brown	iridescent-blue	blue
	90	yellow-brown	dark-blue	dark blue

The potential of Zn-Cr with 8%Cr was found to be less dependent on time of immersion despite the initial sharp decrease observed both in 5 g/l and 10 g/l KMnO_4 solutions at 20°C (Fig. 2). In comparison with 4%Cr alloys, 8%Cr resulted in more positive potentials in the solutions. Fig. 4 is the potential-time profile of Zn-Ni-Cr (12% - 14%Ni) in 5 g/l and 10 g/l KMnO_4 solutions at 20°C. In 5 g/l solution a sharp increase of potential at about 50 sec was found both for alloys containing 2% and 4%Cr. For 6% and 8%Cr, similar sharp increases in potential were also found but they took place at much early stage of the immersion. These were consistent with those observed in Zn-Cr alloys, indicating that 8%Cr resulted in a rapid passivation of the surfaces. An immersion time of 40 sec of 8%Cr alloy produced thicker but much rougher films than those obtained on 2% - 6%Cr alloys. The outer layers of the film on 8%Cr Zn-Cr alloys were thus not expected to be formed by the

dissolution-oxidation-precipitation procedure because if a thin layer of passive film was formed too soon after the immersion it could suppress the zinc dissolution, as well as the dissolution and oxidation of chromium. This was similar to the zinc chromating where an initially formed CrO_3 film can stop zinc dissolution [22]. It was also found in Fig. 4 that the increase in chromium content of the Zn-Ni-Cr alloys or the decrease in oxidant concentration of the solutions increased the overall potential during the film formation, the same as for Zn-Cr alloys.

Effects of temperature and pH

The effect of temperature on potential-time profile was also investigated (Fig. 5). The increase of temperature shifted the surface potential of Zn-Cr alloys (4%Cr) towards more negative value. At 20°C potential reached a maximum negative value before becoming more positive, but at 40°C and 50°C the potentials decreased throughout the 100 sec of immersion except for the first 10 sec, and the range of variation were found not too large. This longer period of surface activation is associated with the diffusion rate of active species within the metal-solution being increased with temperature. The effect of temperature on weight gain of above alloys was shown in Fig. 6, where the rise in temperature caused increase in weight although the difference was not significant. However, the conversion films formed at higher temperatures generally had rougher surfaces and micro-cracks being developed. The pH below 1.0 resulted in a rapid dissolution of initially formed conversion film, even the alloy coating itself. The increase of pH from 2.0 generally produced dark films and increasingly less iridescent colour.

Aging of the conversion coating

The as-formed conversion coatings were normally weak and susceptible to scrape damages. The aging of the coatings were conducted in two ways, drying in hot air flow at 60°C and drying in air at room temperature for 24 hr. Stronger coatings were obtained from the former technique. The surface appearance of the coatings was also found somewhat different by using these two different drying technique, with more iridescent colour from the higher temperature drying. The structure of the coatings and the chromium state are expected to be influenced by higher temperature drying, as the molecular weight of the polymeric species can be changed and the conversion of hydroxo bridging to oxo bridging can be speeded up by the increase of temperature.

Electrochemical investigation of conversion coatings

The results presented in Fig. 7 (a) - (b) show the effect of immersion time and the concentration of KMnO_4 in the conversion treatments. The corrosion potential of the coatings obtained from 10 g/l KMnO_4 were generally more positive than those obtained from 5 g/l KMnO_4 and their corrosion current were found to be much higher (Table 4). The activation-passivation behaviors of Zn-Cr(4%Cr) in conversion treatment can be seen in Fig. 2, where, in contrast to 5 g/l KMnO_4 , the activation of the surface in 10 g/l KMnO_4 was carried out at much more negative potentials and the passivation was not clearly seen as the potential remained much the same after the initial 20 sec. This indicates a severe dissolution and a possibility of losing chromium content and other species needed in the conversion films into the bulk solution even when the immersion time was properly controlled, resulting in poor quality of the coatings. The immersion time of 40 sec was found to be optimum in 5g/l KMnO_4 for producing conversion coatings that have lower corrosion rate. This suggested that to obtain the best conversion coatings the immersion should be completed at the time after the activation step was completed plus a short period when the surface was in the activated state and the dissolution-oxidation-precipitation process still continued (Fig. 1c). The passivation can be then completed during the taking out and the rinsing of the samples. However, this did not suit the case in 10 g/l KMnO_4 , in which immersion time of 40 sec or beyond resulted in much higher corrosion rate.

Tafel curves (Fig. 8) and corrosion parameters (Table 4) show the effects of chromium content of alloys and the operating temperature in conversion treatments. It is found that as the chromium content of the alloys increased, the corrosion potentials shifted towards more positive direction and the corrosion currents decreased, indicating more chromium species were contained in the conversion coatings. Those coatings obtained at higher temperature conversion treatment revealed poorer corrosion resistance but no significant change in corrosion potential was found as a result of change in

temperature. Fig. 9 shows the effect of different solutions used in the conversion treatments. There was no significant difference in corrosion potential and corrosion current between using 5g/l KMnO_4 and 5g/l $\text{Na}_2\text{S}_2\text{O}_8$ (Table 6). The influence of nickel in Zn-Cr alloy is also presented in the linear polarisation curve (Fig. 10) and Table 6. It is found that the alloying of nickel in Zn-Cr alloy greatly changed the corrosion potential towards more positive direction and reduced the corrosion current.

Table 4. The corrosion parameters influenced by operating conditions in conversion treatment at 20°C, with Zn-Cr (4%Cr)

Immersion time (second)	Concentration of KMnO_4 (g/l)	E_{corr} (V,SEC)	I_{corr} ($\mu\text{A}/\text{cm}^2$)
20	5	- 0.950	5.52
40	5	- 0.926	3.14
60	5	- 0.970	6.82
20	10	- 0.922	8.01
40	10	- 0.944	17.73
60	10	- 0.963	17.59

Table 5. The corrosion parameters influenced by chromium content of alloy and temperature in conversion treatment (Immersion time 40 sec, in 5g/l KMnO_4)

Zn-Cr Cr (%)	Temperature in conversion treatments (°C)	E_{corr} (V,SCE)	I_{corr} ($\mu\text{A}/\text{cm}^2$)
4	20	- 0.926	3.14
4	40	- 0.966	8.27
6	20	- 0.915	2.79
6	40	- 0.920	6.27
6	50	- 0.925	12.36

Table 6. The corrosion parameters influenced by type of alloy and solution used in the conversion treatment (Immersion time 40 sec, 20°C)

Type of alloy	Solution used in conversion treatment	E_{corr} (V,SCE)	I_{corr} ($\mu\text{A}/\text{cm}^2$)
Zn-Cr(4%Cr)	5g/l KMnO_4	- 0.926	3.14
Zn-Cr(4%Cr)	5g/l $\text{Na}_2\text{S}_2\text{O}_8$	- 0.986	4.23
ZnCr(4%Cr,13%Ni)	5g/l KMnO_4	- 0.845	0.71

Conclusion

The quality of the conversion coatings is influenced particularly by treatment time, chromium content of alloys, and concentration of oxidising agent in the treatment solutions. Conversion coatings obtained from persulfate are generally thinner and lighter than those obtained from permanganate. However, the electrochemical measurements show little difference on corrosion properties between them. The best conversion coatings can be obtained at 5 - 10 sec after the activation process is completed in specific solution, but this time controlling method is not applied to the case when server dissolution takes place during the conversion treatment. A combination of operating conditions which results in long or virtually no activation period is not favourable to good quality conversion coatings. The addition of nickel to Zn-Cr alloy coatings greatly improved the corrosion properties of the conversion coatings.

References

- [1] E. J. Wilhelm, *U. S. Patent*, 2,035,380 (1936)
- [2] L. F. G. Williams, *Plating*, Oct. (1972) 931
- [3] J. W. Dini and H. R. Johnson, *Met. Fin.*, Sept., (1979) 53
- [4] R. R. Sizelove, *Plating and Surf. Fin.*, March (1991) 26
- [5] A. P. Shears, *Trans. Inst. Metal Finish.*, 67 (1989) 67
- [6] P. Kodak, *Plating and Surf. Fin.*, 76, 11 (1989) 30
- [7] A. Bittner, *Surface Coatings Australia*, 27, 5 (1990) 6
- [8] R. J. Heller and C. H. Roy, *Plating and Surf. Fin.*, 73, 11(1986) 22
- [9] J. Holmes, *Met. Fin.*, 87, 11 (1989) 65
- [10] J. A. Albanese, *Plating and Surf. Fin.*, 77, 5 (1990) 120
- [11] W. Paatsch, *Met. Fin.*, (1985) 79
- [12] G. D. Wilcox, D. R. Gabe and M. E. Warwick, *Corrosion Reviews*, 6, 4 (1988) 577
- [13] G. D. Wilcox and D. R. Gabe, *Bri. Corro. J.*, 22, 4 (1987) 254
- [14] G. D. Wilcox and D. R. Gabe, *Met. Fin.*, Sept. (1988) 71
- [15] M. R. El-Sharif, Y. J. Su, C. U. Chisholm, and A. Watson, *Proc. of the International Conference on Advances in Corrosion and Protection, UMIST, Manchester, UK, 1992*
- [16] A. Watson, Y. J. Su, M. R. El-Sharif, and C. U. Chisholm, *Trans. Inst. Metal Finish.*, 71, 1 (1993) 15
- [17] A. Waston, M. R. El-Sharif and C. U. Chisholm, *Trans. Inst. Metal Finishing*, 64 (1986) 149
- [18] M. R. El-Sharif and C. U. Chisolm, *Trans. Inst. Metal Finishing*, 66 (1988) 34
- [19] M. Stern, *Corrosion J.*, 13, Sept. (1958) 440
- [20] M. R. El-Sharif, Y. J. Su, A. Watson, and C. U. Chisholm, *Proc. of the International Conference of Corrosion Asia'92, Singapore, 1992*
- [21] A. Abivsi, N. R. Short and J. K. Dennis, *Trans. Inst. Metal Finishing*, 69 (1991) 45
- [22] N. R. Short, A. Abibsi and J. K. Dennis, *Trans. Inst. Metal Finishing*, 67 (1989) 73
- [23] L. F. G. Williams, *Surface Technology*, 4 (1976) 355

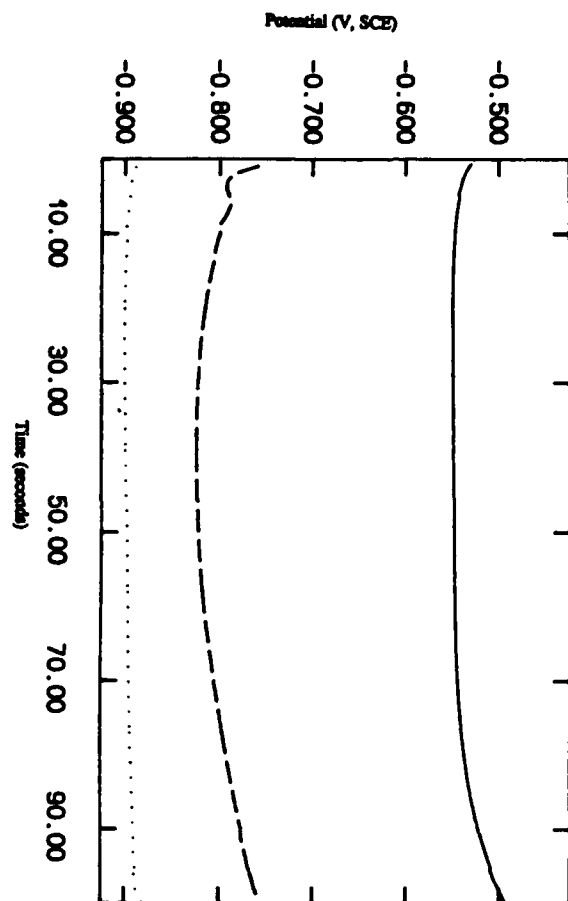


Fig. 1 (a). Potential - time curves for zinc in chromate (—), Zn-Cr (---), and Zn-Cr (4%Cr) in 5 g/l $\text{Na}_2\text{S}_2\text{O}_8$ (.....), and at 20°C

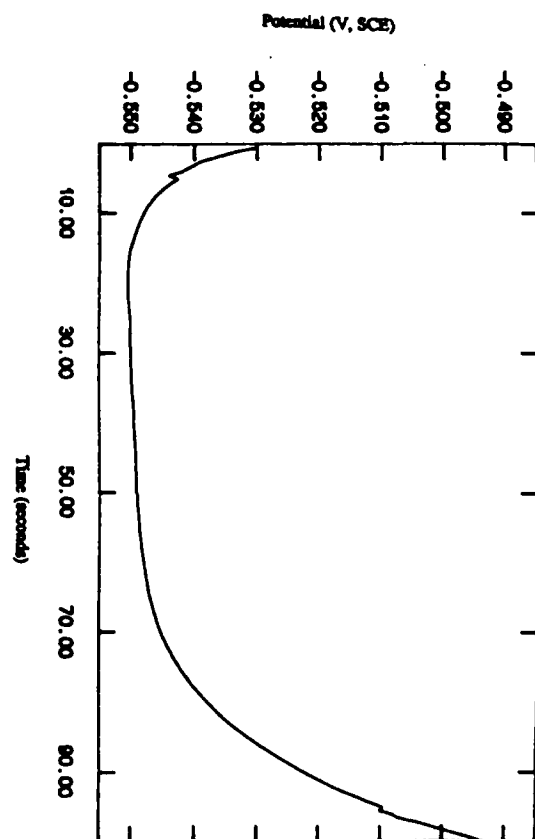


Fig. 1 (b). Potential - time curve for zinc in chromate, and at 20°C

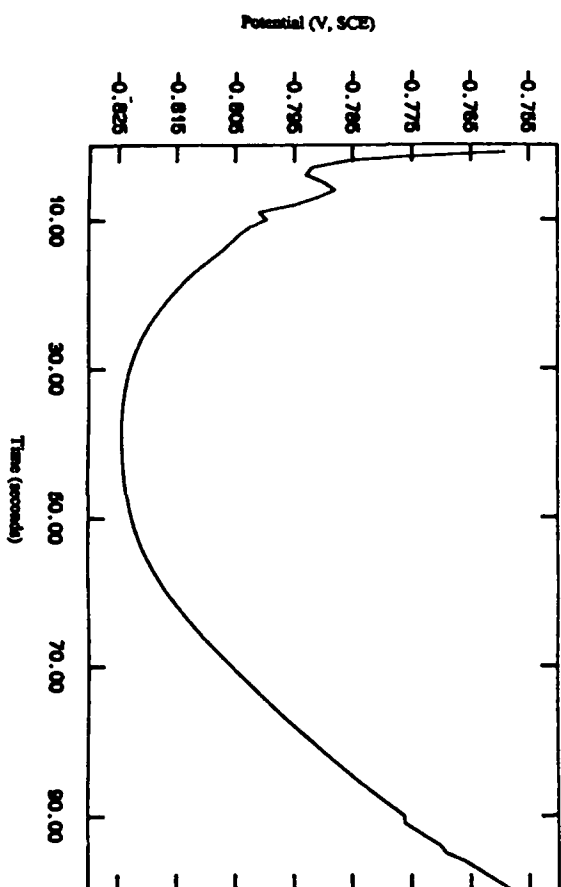


Fig. 1 (c). Potential - time curve for Zn-Cr (4%Cr) in 5 g/l KClO_4 , and at 20°C

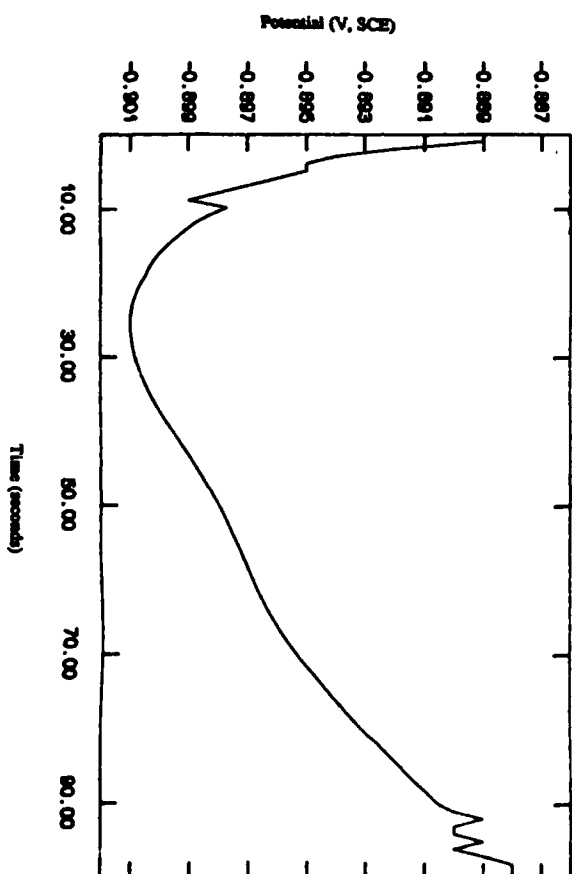


Fig. 1 (d). Potential - time curve for Zn-Cr (4%Cr) in 5 g/l $\text{Na}_2\text{S}_2\text{O}_8$, and at 20°C

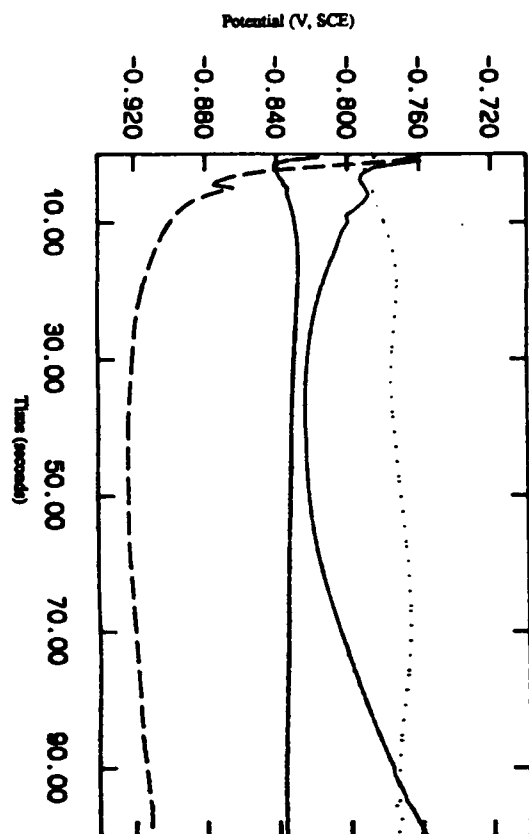


Fig. 2. Potential-time curves for Zn-Cr (4%Cr) in 5 g/l K_2MnO_4 (—), Zn-Cr (4%Cr) in 10 g/l K_2MnO_4 (---), Zn-Cr (8%Cr) in 5 g/l K_2MnO_4 (....), Zn-Cr (8%Cr) in 10 g/l K_2MnO_4 (---), and at 20°C

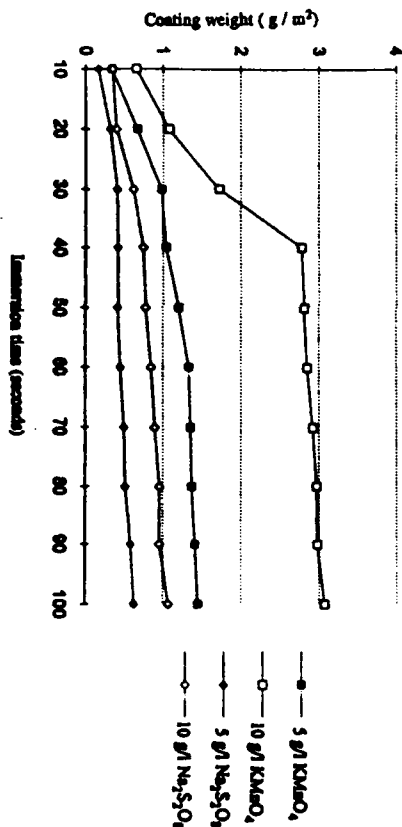


Fig. 3. Effect of oxidizing agent and its concentration in conversion treatment on weight gain of conversion coating, with Zn-Cr (4%Cr), and at 20°C

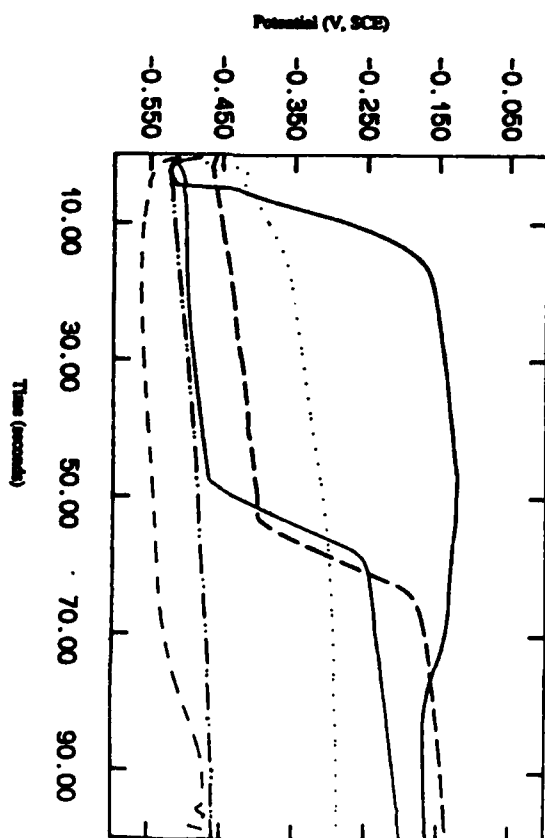


Fig. 4. Potential-time curves for Zn-Ni-Cr (7%Cr) in 5 g/l K_2MnO_4 (—), Zn-Ni-Cr (4%Cr) in 5 g/l K_2MnO_4 (---), Zn-Ni-Cr (6%Cr) in 5 g/l K_2MnO_4 (....), Zn-Ni-Cr (7%Cr) in 5 g/l K_2MnO_4 (---), Zn-Ni-Cr (4%Cr) in 10 g/l K_2MnO_4 (---), and at 20°C (all alloys contain Ni% = 12-14)

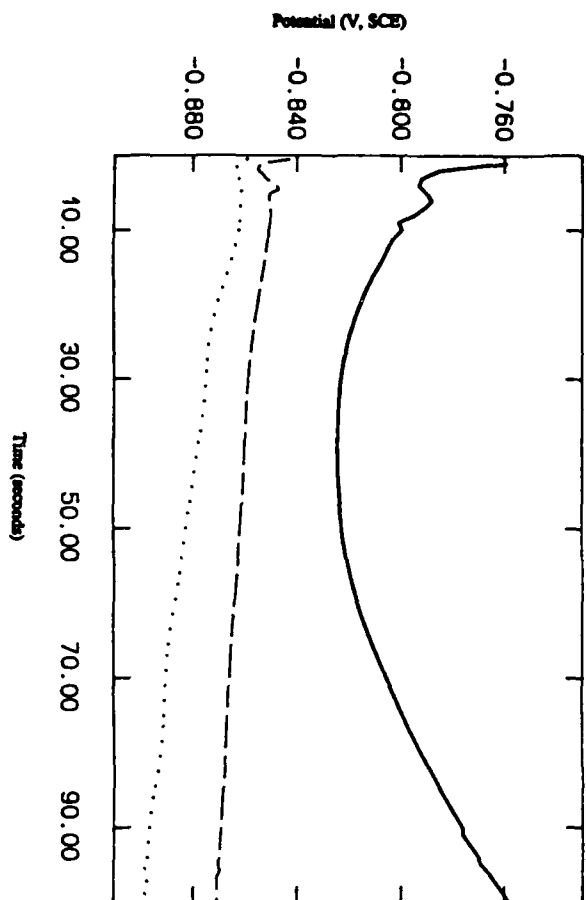


Fig. 5. Potential-time curves for Zn-Cr (4%Cr) in 5 g/l KMnO_4 at various temperatures: 20°C (—), 40°C (---), and 50°C (....).

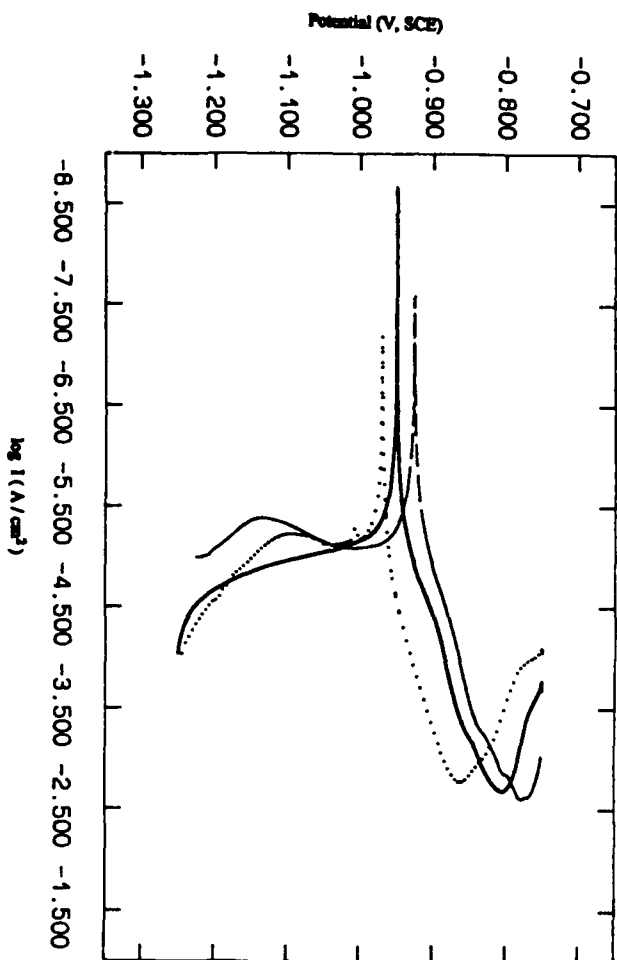


Fig. 7 (a). Polarization curves showing the effect of immersion time in conversion treatment, with Zn-Cr (4%Cr) in 5 g/l KMnO_4 , for 20 sec (—), 40 sec (---), and 60 sec (....).

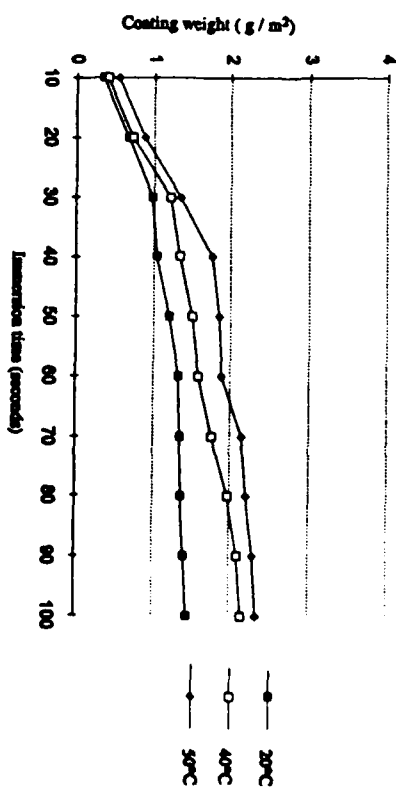


Fig. 6. Effect of temperature in conversion treatment on weight gain of conversion coating, with Zn-Cr (4%Cr) in 5 g/l KMnO_4 .

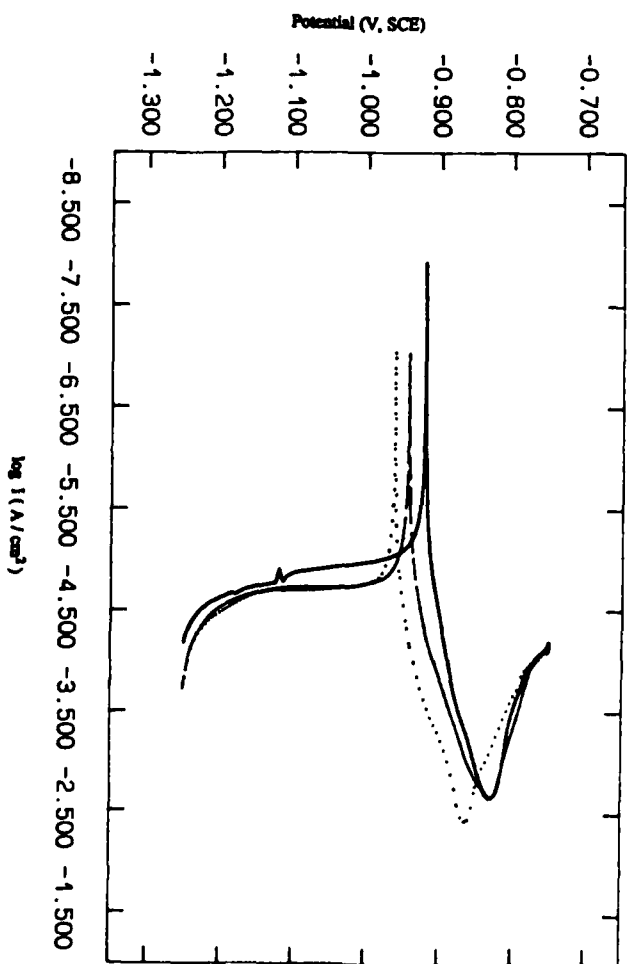


Fig. 7 (b). Polarization curves showing the effect of immersion time in conversion treatment, with Zn-Cr (4%Cr) in 10 g/l KMnO_4 , for 20 sec (—), 40 sec (---), and 60 sec (....).

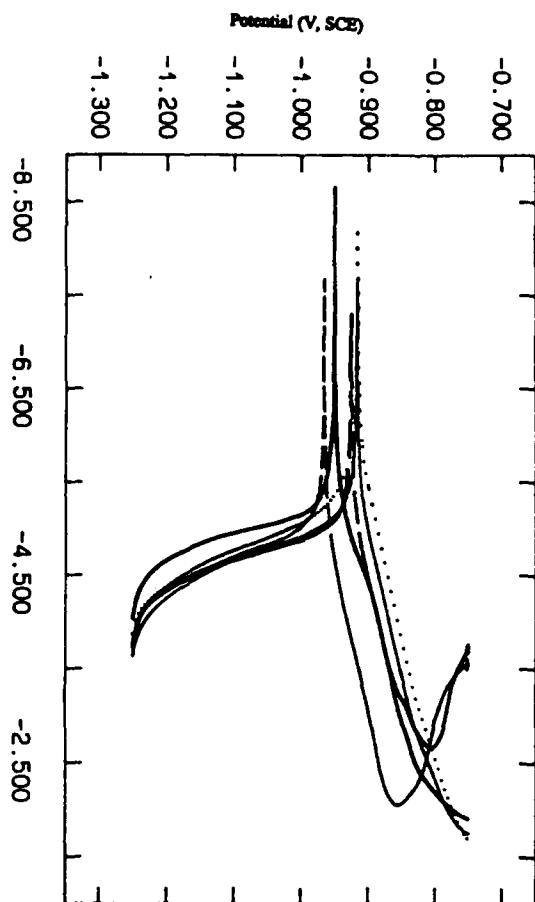


Fig. 8. Polarization curves showing the effect of Cr% in Zn-Cr alloys and temperature in conversion treatment, for Zn-Cr (6%Cr) at 20°C (—), Zn-Cr (6%Cr) at 40°C (---), Zn-Cr (6%Cr) at 50°C (···), and Zn-Cr (6%Cr) at 40°C for 40 sec (-·-·-), in 5 g/l KMnO_4 .

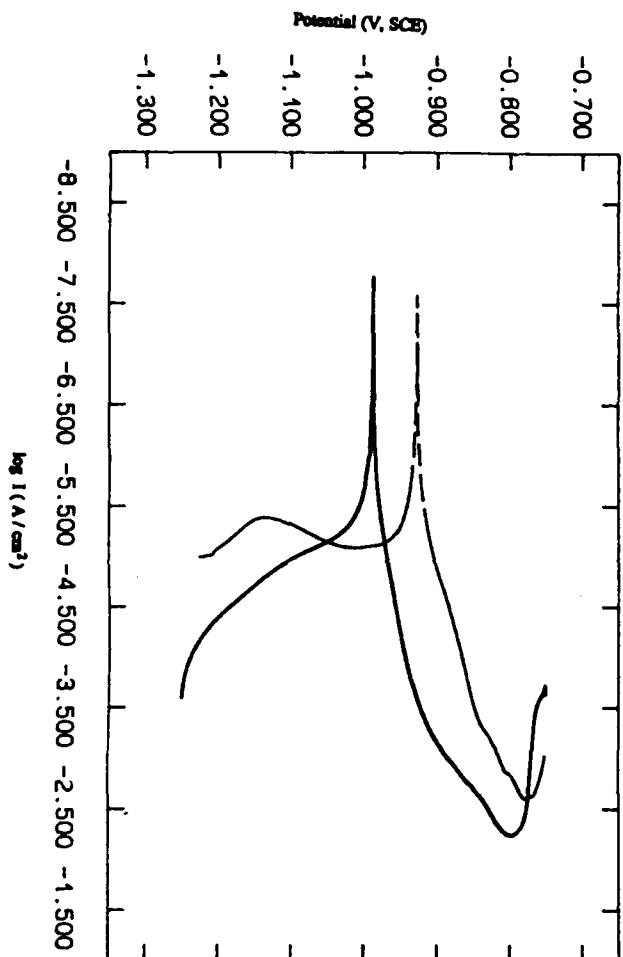


Fig. 9. Polarization curves showing the effect of solutions used in conversion treatment, with Zn-Cr (6%Cr) in 5 g/l Hg_2SO_4 (—), and 5 g/l KMnO_4 (---), at 20°C for 40 sec (-·-·-).

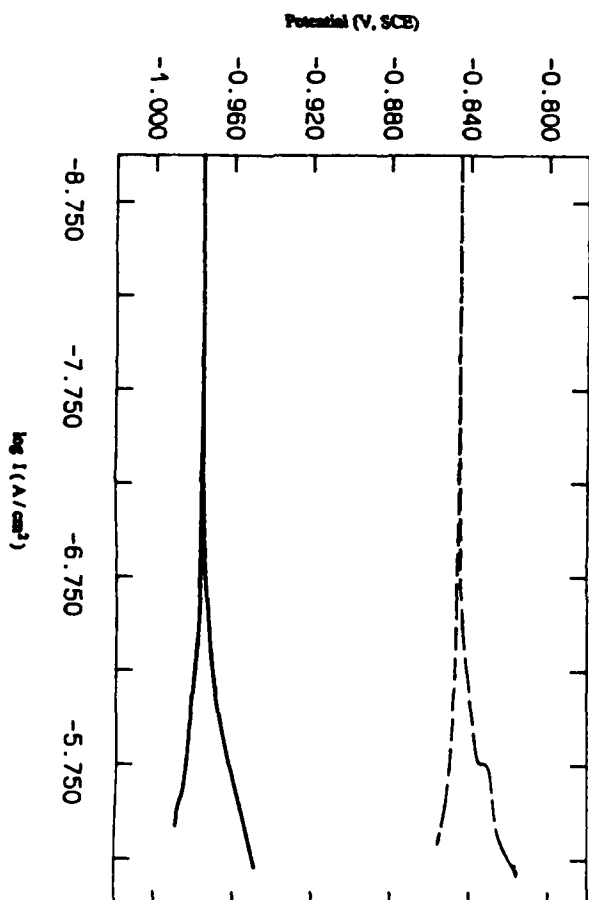


Fig. 10. Polarization curves showing the effect of alloy type used in conversion treatment, with Zn-Cr (6%Cr) (—) and Zn-Ni-Cr (6%Cr, 13%Ni) (---), in 5 g/l KMnO_4 at 20°C for 40 sec.

Study of Corrosion Resistance of Electroless Ni-P Platings

Li Yi

South China University of Technology

Guangzhou 510641

People's Republic of China

Yao Xin Dong

South China University of Technology

Guangzhou 510641

People's Republic of China

Xuan Hao Wen

South China University of Technology

Guangzhou 510641

People's Republic of China

Abstract

The Corrosion rates were measured by neutral salt spray test and by polarization curve. The effects of concentration of hypophosphite, operating temperature, pH, complexing agent, heat treatment and pretreatment process on corrosion resistance were studied systematically. It can be concluded that elements which affect corrosion resistance of the coatings can be divided into two aspects: macroscopic element and microscopic element. Macroscopic element is pretreatment process. Microscopic element includes concentration of hypophosphite, operating temperature, pH, complexing agent and heat treatment. This paper has also used some advanced techniques including scanning electron microscope, X-ray diffraction, etc.

Key terms: corrosion resistance, electroless Ni-P plating

Introduction

As a surface treatment technique, electroless Ni-P plating has been widely used in various industry departments since it was discovered by Brenner and Riddell in the 1940's, for it offers unique deposit properties including wear and abrasion resistance, ductility, lubricity and especially excellent corrosion resistance. But it still leaves some problems in theory and process which need to be discussed. For example, how to improve the corrosion resistance, how to determine the process conditions, etc. So it is advisable to study the relationship between the corrosion resistance and the process conditions. Therefore, this paper will show the rules of the relationship.

Experimental

The test material was A₃ steel. All the steel samples were machined into cylindrical plate specimens. The electroless solutions were prepared from chemically pure grade reagents and deionized water. The corrosion rate was measured by neutral salt spray test and by polarization curve tested with HCl electrolyte. The heat treatment period was two hours. The solution for neutral salt spray was 3.5% NaCl and the temperature was maintained between 30°C and 35°C. Twenty-four hours was a cycle, including eight hours(spraying) and sixteen hours(not spraying). Some advanced test techniques were also used including scanning electron microscope, X-ray diffraction to test the electroless Ni-P platings. And the P content of the Ni-P platings were determined by using a scanning electron microscope(SEM).

Discussions

1. The Effect of Concentration of Hypophosphite on the P Content during Ni-P Plating

Process conditions: Nickel sulfate: 20g / l
Sodium citrate: 15g / l
Addition I : 2g / l
Addition II : 10ml / l
pH: 4.5
Temperature: 85°C

Sodium hypophosphite g / l	20	25	30
P content wt%	8.809	11.930	13.753

Table 1. Relationship between P content and sodium hypophosphite.

Table 1. shows that when the concentration of sodium hypophosphite increased, the P content of the Ni-P plating increased.

2. The Effect of pH on P content of the Ni-P Plating

Process Conditions: Nickel sulfate: 20g / l
Sodium hypophosphite: 25g / l
Sodium citrate: 15g / l
Addition I : 2g / l
Addition II : 10ml / l
Temperature: 85°C

pH	3.5	4.5	5.5
P content wt%	12.889	11.930	10.747

Table 2. Relationship between pH and P content.

Table 2. shows that when pH increased, the P content of the Ni-P plating decreased. That is to say, we can increase the P content of the Ni-P plating by abating the pH.

3. The Effect of Temperature of P Content of the Ni-P Plating

Process Conditions: Nickel sulfate: 20g / l
Sodium hypophosphite: 25g / l
Addition I : 2g / l
Addition II : 10ml / l
Sodium citrate: 15g / l
pH: 4.5

T °C	70	80	90
P content wt%	8.741	11.020	12.743

Table 3. Relationship between P content and the solution temperature.

Table 3. reveals that temperature increased the P content of the plating.

4. The Effect of the Concentration of the Complexing Agents on P Content of Ni-P Plating.

Process Conditions: Nickel sulfate: 20g / l
Sodium hypophosphite: 25g / l
Addition I : 2g / l
Addition II : 10ml / l
pH: 4.5
Temperature: 85°C

Sodium citrate g / l	15	20	25
P content wt%	11.930	12.816	13.661

Table 4. Relationship between P content and concentration of the complexing agents:

Table 4. reveals that when the concentration of the complexing agents increased, the P content of the plating increased. It is clear that the process conditions which affect the P content of the Ni-P plating are concentration of sodium hypophosphite, pH, temperature and concentration of the complexing agents, etc.

5. The Relationship Between P Content of the Ni-P Plating and Its Corrosion Resistance

In order to identify the trends, three systems were tested. These three systems were, P% = 8.809, P% = 11.930, P% = 13.753.

5.1. The Results of Neutral Salt Spray Tests.

After 720 hours neutral salt spray test:

P content wt%	Corrosion
13.753	No rust
11.930	Some rust
8.809	More rust

Table 5. Results of neutral salt spray tests.

Table 5. Reveals that the higher the P content, the better the corrosion resistance.

5.2. Measuring the Corrosion Rate by Polarization Curve

From the Figure 1, 2 and 3, it is clear that cathodic polarization exhibits a Tafel behavior over a wide range of current densities. EN plating becomes passive under anodic polarization. So we can't extrapolate the anodic Tafel line to obtain the corrosion current, but we have employed the cathodic Tafel region for each extrapolation. This can lead to a reliable estimate of I_{corr} only if the cathodic polarization exhibits a well defined Tafel line:

P content wt%	8.809	11.930	13.753
Corrosion Rate $\mu A / cm^2$	56.2	31.6	19.9

Table 6. Relationship between P content and corrosion rate.

Now we can find the conclusions made by the above two measuring method are equal. Thus, when the P content of the EN plating is increased the corrosion resistance is increased. Therefore, we can improve the corrosion resistance of the EN plating by increasing the P content of the plating.

Fig.4, 5 and 6 are X-ray diffraction figures of three different P content platings. These three figures indicate that when P content increased, the X-ray diffraction peak broadened, i.e., the plating became

more noncrystalline. This is because P can affect the crystal lattice of Nickel and when P content increased, this kind of effect increased too. Therefore, the crystalline grains became smaller, and finally lost the feature of the crystal changing into noncrystal. So we can say noncrystallinity is an uniform system. There are no crystal boundaries in it. So it is more stable in corrosion media.

Thus, when P content increases, the noncrystallinity increases and then corrosion resistance of the EN plating improves.

6. The Relationship Between Corrosion Resistance and Heat Treatment Temperature

Neutral Salt Spray Test:

Heat Treatment Temperature 600℃	Rust appeared after 240 hours
400℃	Rust appeared after 288 hours
200℃	Rust appeared after 720 hours
No Heat Treatment	Rust appeared after 720 hours (more bright)

Table 7. Relationship between corrosion resistance and heat treatment temperature.

In order to study the relationship between corrosion resistance and the heat treatment temperature, the X-ray diffraction figures under the above four conditions were investigated.

Figure 7 to Figure 10 indicate that when the heat treatment temperature was 200℃, the noncrystalline alloy changed into one exhibiting crystallinity. The diffraction increased, the diffraction peak sharpened. At that time crystalline boundaries appeared. They significantly decreased the corrosion resistance of the EN plating. Photo 1, 2 are two photos taken with a scanning electron microscope.

7. The Relationship Between the Corrosion Resistance and Pretreatment

From the experiment, we discovered that different pretreatment lead to different corrosion resistance of the plating. Table 8 are two samples were tested in neutral salt spray. One had been polished and another had not. Photo 3, 4 show their scanning electron micrographs(200X).

After polishing	Rust appeared after 720hrs
No polishing	Rust appeared after 336hrs

Table 8. Relationship between the corrosion resistance and pretreatment.

Why were these two samples' corrosion resistance so different? We think this is because the sample which had no polishing deposited not so uniform and this was easy to cause local corrosion.

Conclusions

Now, we have studied three parameters which affect the EN plating's corrosion, they are:

- (1) The elements which affect the P content of the EN platings: concentration of hypophosphite, operating temperature, pH and complexing agent.
- (2) Heat treatment temperature.
- (3) Pretreatment process.

References

1. A. Brenner and G.E. Riddell, U.S. patent, 2532, 283-4(1950).
2. E.A. Grasharf, et al., Metal Finishing, 81 11(1983).
3. Donaldw, Badrand, CEF, Plating and Surface Finishing, 70 12 24(1983):p.24.

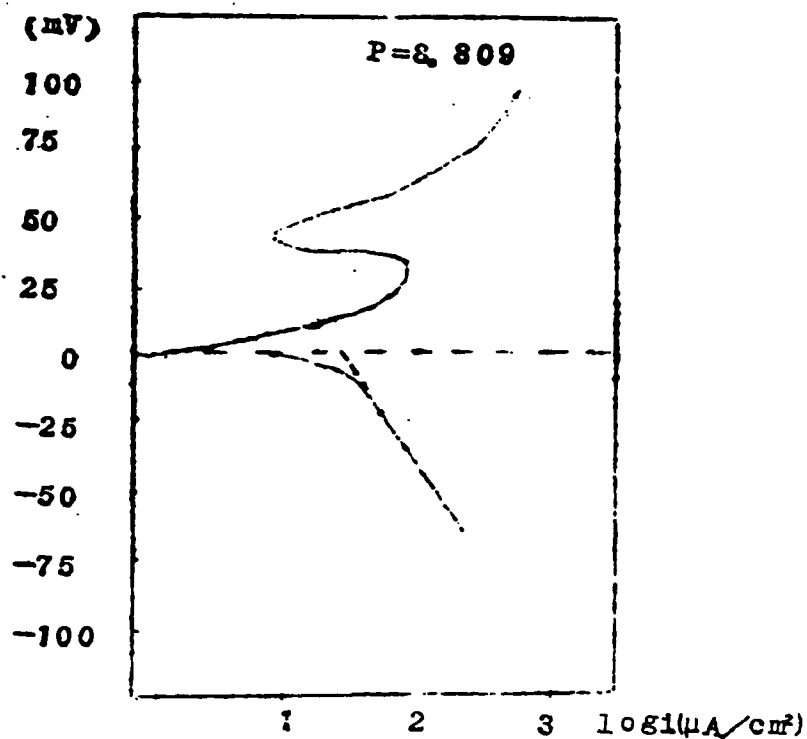


Figure 1. The plating's polarization curve($P\% = 8.809$)

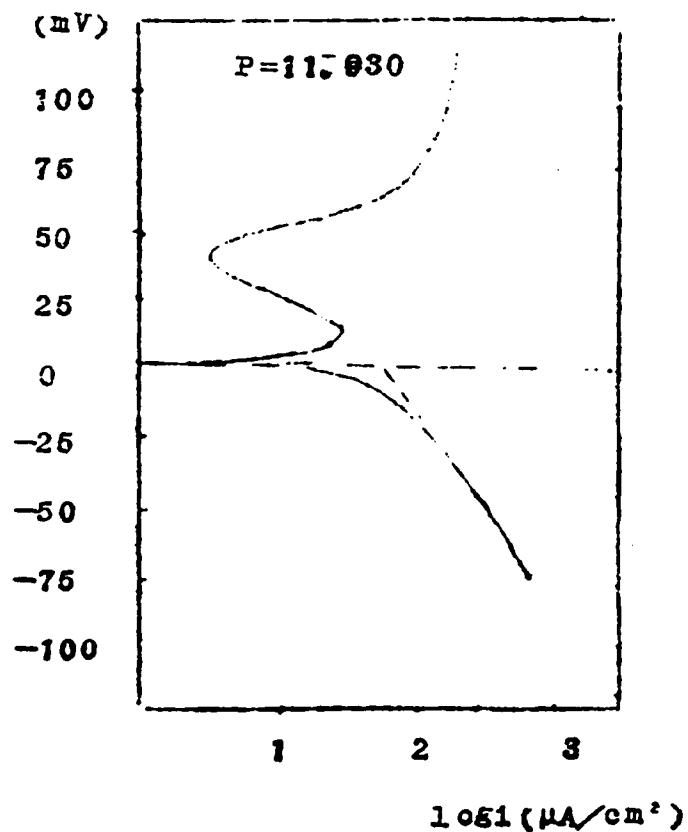


Figure 2. The plating's polarization curve($P\% = 11.930$)

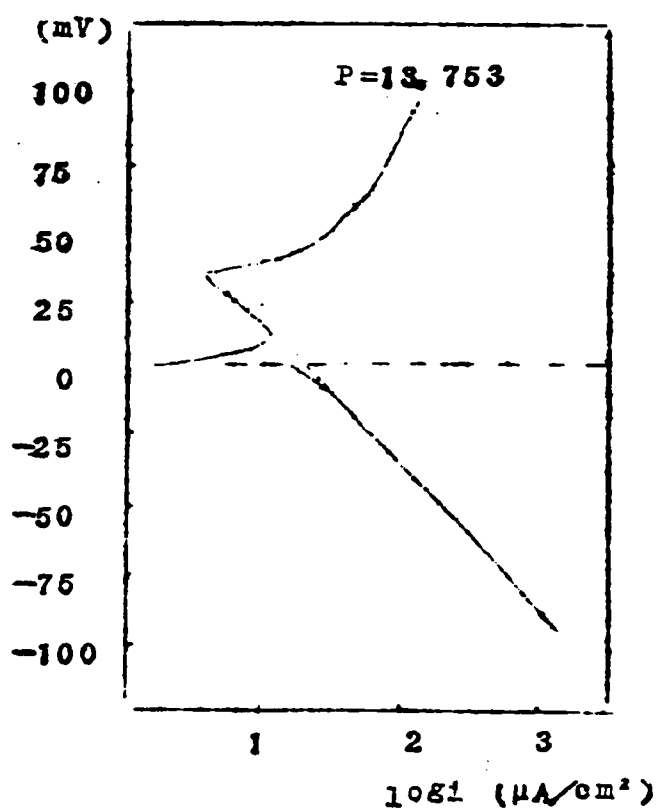


Figure 3. The plating's polarization curve($P\% = 13.753$)

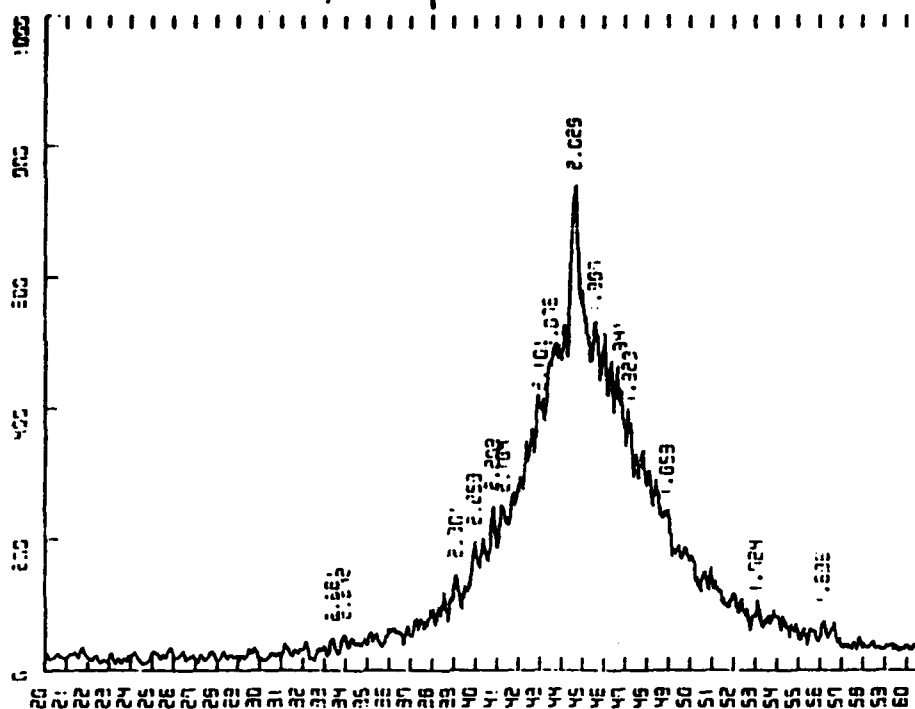
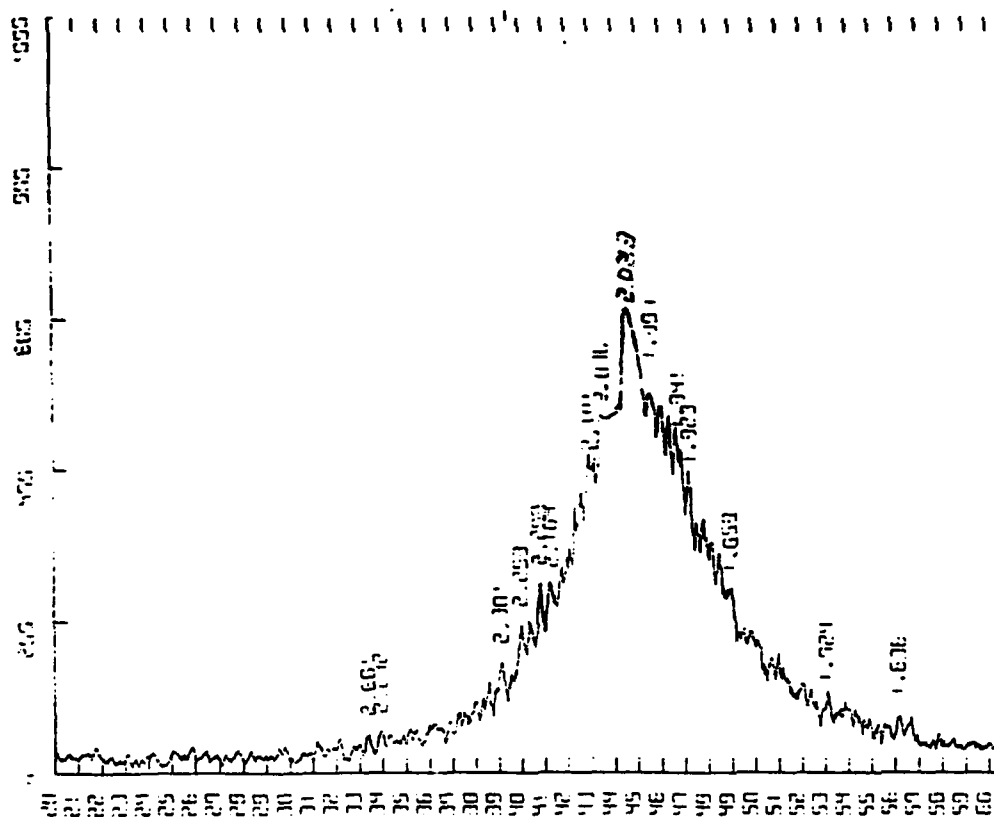


Figure 4. EN plating's X-ray diffraction figure(P content = 8.809%)



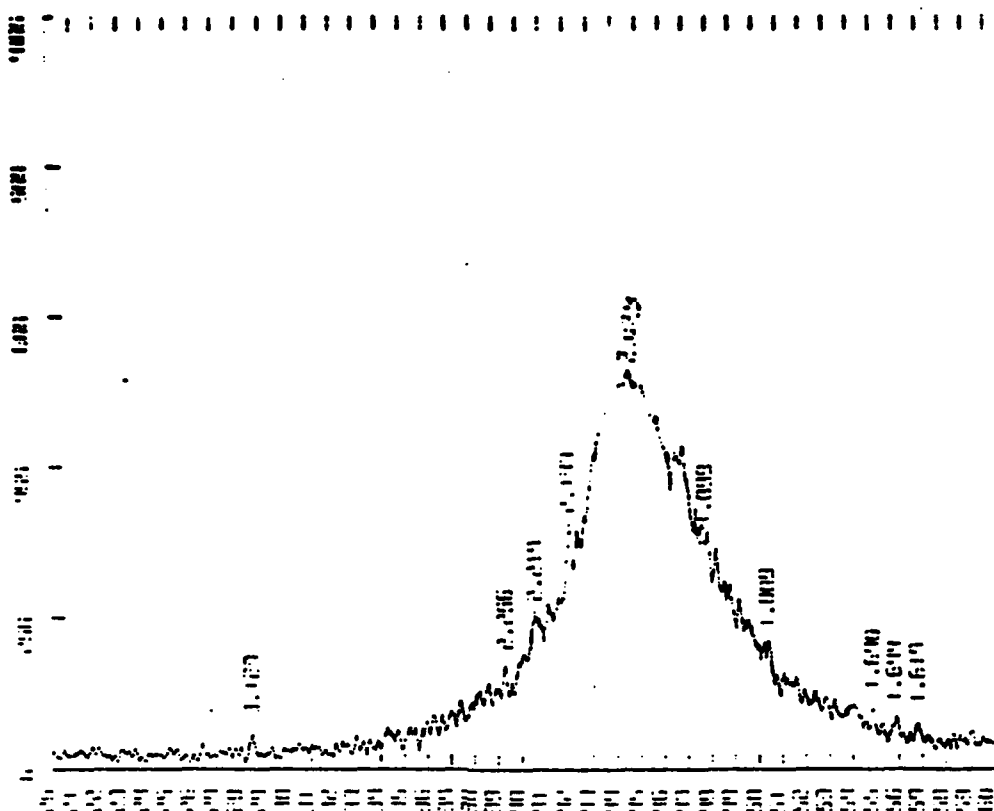


Figure 6. EN plating's X-ray diffraction figure(P content = 13.753%)

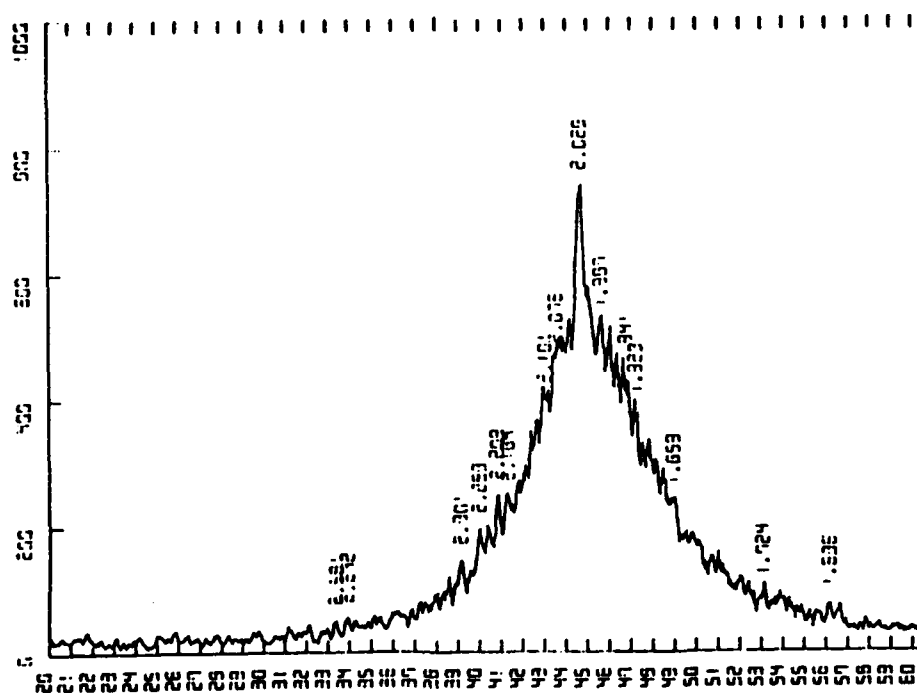


Figure 7. EN plating's X-ray diffraction figure(no heat treatment)

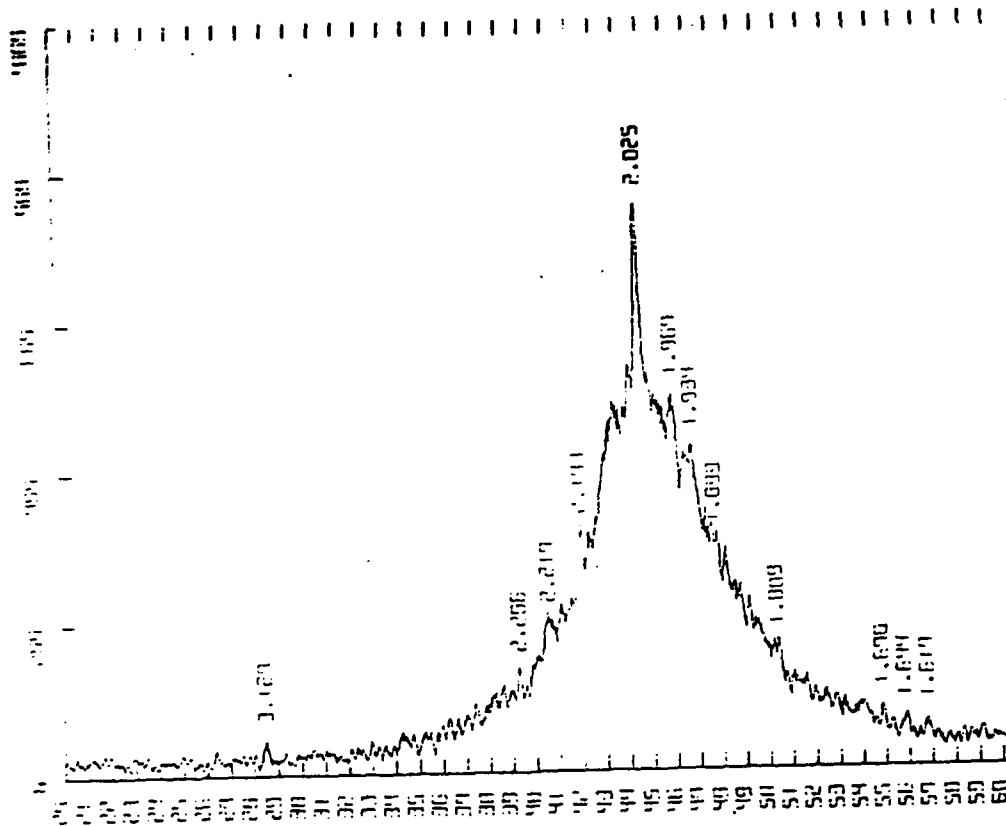


Figure 8. EN plating's X-ray diffraction figure(heat treatment temperature is 200℃)

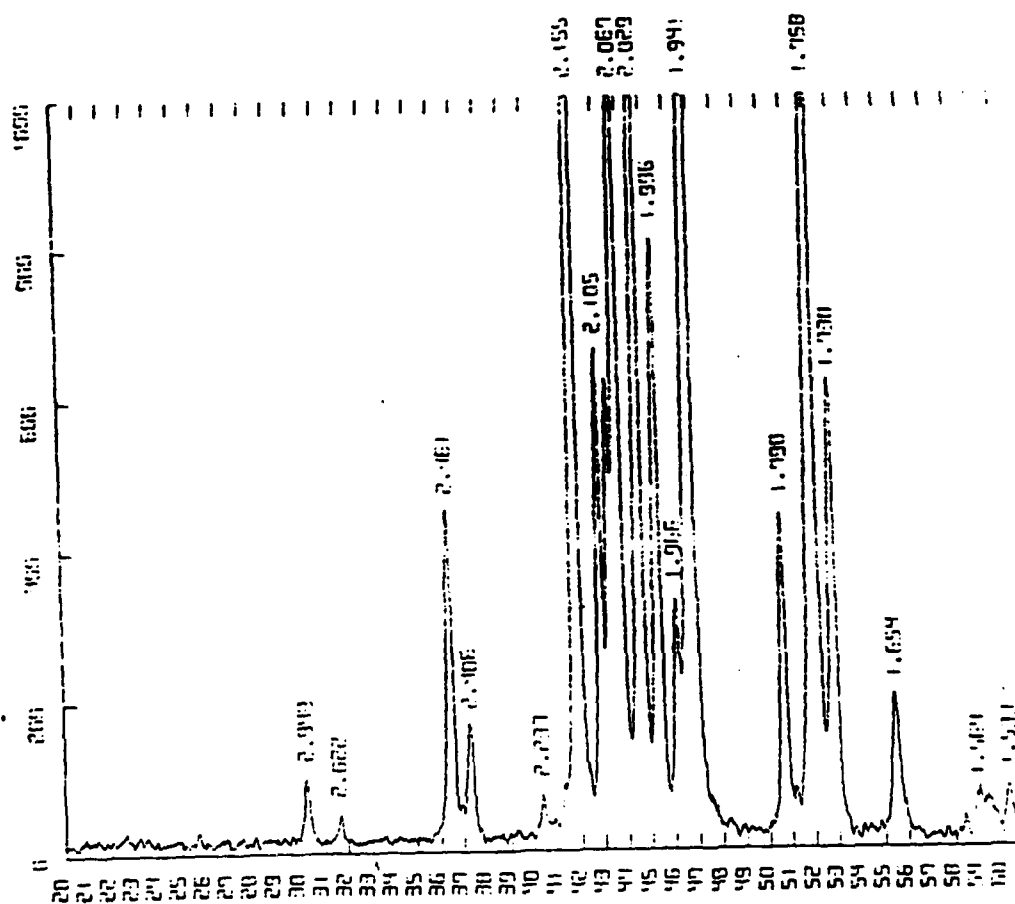


Figure 9. EN plating's X-ray diffraction figure(heat treatment temperature is 400℃)

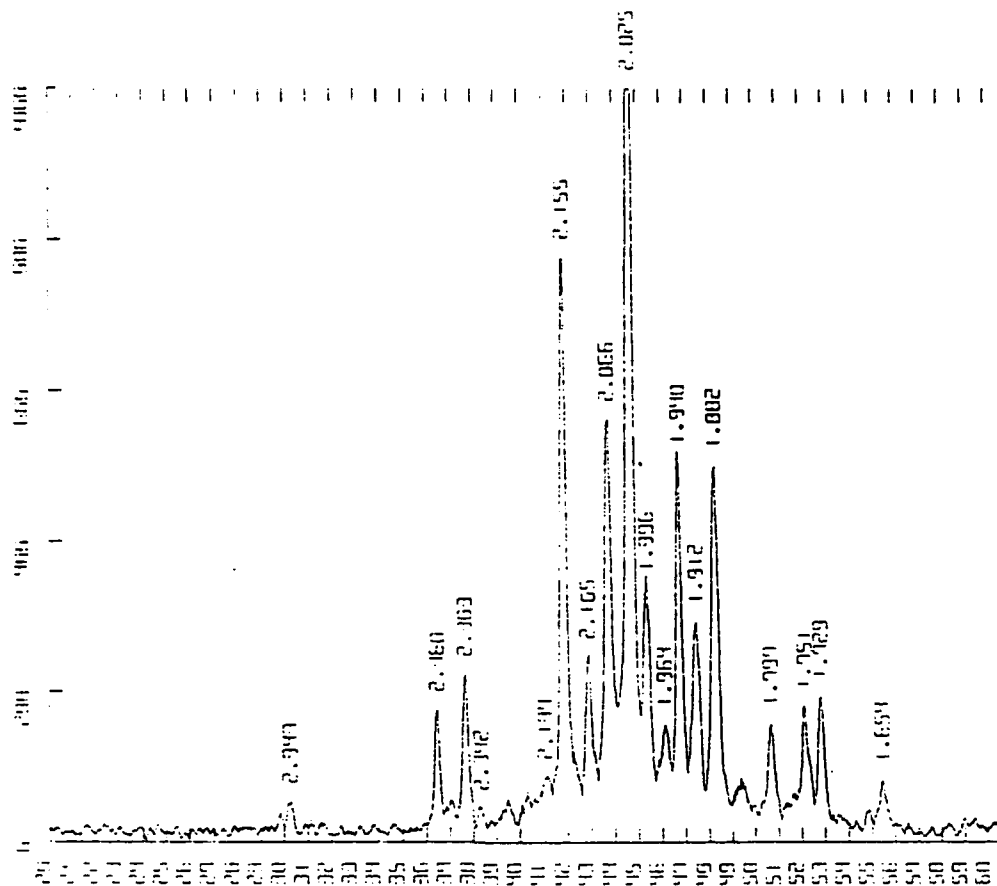


Figure 10. EN plating's X-ray diffraction figures(heat treatment temperature is 600°C)



Photo 1. Scanning electron micrograph of the surface which had no heat temperature

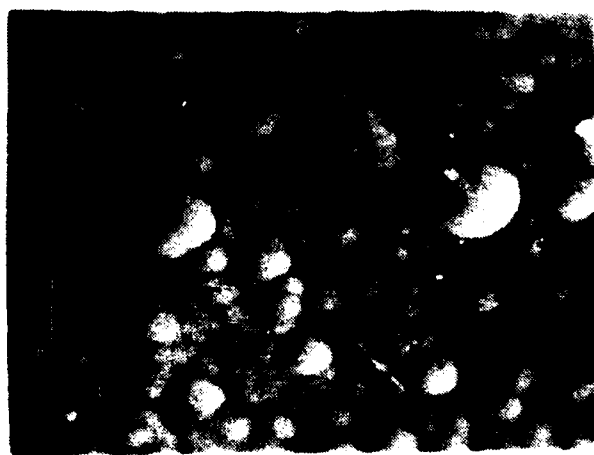


Photo 2. Scanning electron micrograph of the surface which had 400°C heat temperature



**Photo 3. Scanning electron micrograph
of the sample which
had polishing**



**Photo 4. Scanning electron micrograph
of the sample which
had no polishing**

Resistance to Aqueous Corrosion of Steels Protected by a Cr-Si Diffusion Coating

Xiaoru Wan[†], Ge Wang and Robert A. Rapp

Department of Materials Science and Engineering
The Ohio State University
Columbus, OH 43210

Abstract

The simultaneous deposition of Cr and Si to form a diffusion coating on two steels (AISI 1045 and 4140) was studied. In halide-activated cementation packs, the use of either a "ternary activator" (e.g., NaF+NaCl+AlF₃) combined with the elemental metal powders, or else a "dual activator" (e.g., NaF + NaCl) combined with a Cr-Si masteralloy powder, allows for the formation of a surface composition approximating 30Cr-3 to 4Si. Coated coupons were corrosion tested in either 1N H₂SO₄ or 3.5wt% NaCl solution at room temperature. Coupons coated using the Cr-Si masteralloy had superior corrosion resistance in 1N H₂SO₄, while steels coated in packs containing elemental metal powders suffered pitting corrosion. The coated coupons were not adequately resistant to pitting corrosion in 3.5wt% NaCl solution.

Introduction

Plain carbon steels and high-strength low alloy (HSLA) steels suffer from severe corrosion in environments containing sulfuric acid or in a marine environment, primarily owing to their low contents of the beneficial alloy elements (e.g. Cr, Mo, etc.). High-strength stainless steels are not only expensive relative to low alloy steels, but may also suffer from stress corrosion cracking (SCC) in these environments. The formation of a coating with high alloy content on low-alloy steels could offer a means to combat corrosion in aqueous environments.

In sulfuric acid or seawater, resistant alloy compositions require a high Cr content combined with either Mo, Si, V, Ni or Re[1]. Coatings produced by electroplating or physical vapor deposition are susceptible to spallation or delamination, both because of growth stresses in the coating and the lack of strong bonding between the coating and the substrate. The halide-activated pack cementation coating technique has been extensively used to produce protective coatings to combat high-temperature, "dry" corrosion. Owing to the superb coating/substrate bond produced by the diffusion process and the capability of inexpensively coating large or complex objects with multiple alloy components, the coatings success in hot dry gas may also prove to be cost-effective in aqueous environments.

Because of the difficulty involved in depositing Mo and other refractory metals by pack cementation, a recently developed ternary alloy coating of Fe-Cr-Si composition was chosen for this study[2-4]. The beneficial effect of Si in both pitting resistance and sulfuric acid corrosion resistance has been noted by many authors[1, 5-7]. The presence of Si in an 18Cr-14Ni stainless steel greatly improves its resistance to 0.5N FeCl₃ solution[5], a widely accepted test for pitting resistance. An addition of 3.3wt% Si to this steel resulted in a reduction in corrosion rate comparable to an addition of 2.75wt% Mo in the test[5]. An addition of 4.45wt% Si to 18Cr-8Ni stainless steel produced a duplex microstructure which resulted in a ten-fold decrease in the general corrosion rate in 1N H₂SO₄ [5].

The growth of a ferritic Cr-Si diffusion coating by pack cementation on a medium-carbon steel encounters two major problems. First, the codeposition of Cr and Si to achieve the desired composition (i.e., 25-30wt.%Cr and 3-4wt.%Si) requires an exact control of the fluxes of Cr and Si from the pack to the steel during the coating process. Second, to avoid the formation of chromium carbide at the surface, the carbon activity and flux in the metal at the surface must be minimized. To solve the first problem, the "dual activator" concept introduced by Harper and Rapp[2,3] is adopted here. After selection of a Cr-Si masteralloy with the desired component activities, the use of a proper ratio of salts as a dual activator can serve to adjust the partial pressures of chromium chloride and silicon fluoride almost independently, thus setting the fluxes of the Cr and Si into the steel in the right proportion. To solve the second challenge (forming a blocking Cr carbide at the surface), a third activator (AlF₃) and a two-stage heatup scheme were introduced in this study. Because of its high vapor pressure at elevated temperatures, AlF₃ evaporates preferentially during an initial lower temperature

step, thus preliminarily depositing silicon and initiating a ferrite layer with low carbon solubility. The strong thermodynamic repulsion between silicon and carbon hence serves to drive carbon inwards, thereby preventing chromium carbide formation at the surface during the later high temperature step when Cr is deposited. Also because silicon and aluminum are ferrite stabilizers, the initial phase transformation from austenite to ferrite at the surface greatly reduces the surface carbon content to eliminate carbide formation.

This paper reports the deposition of a Cr-Si diffusion coating on a medium-carbon steel (1045) and an HSLA steel (4140), and the results of the corrosion testing of the coated coupons in either 1N H₂SO₄ or 3.5wt% NaCl solution at room temperature.

Experimental Procedures

AISI 1045 and 4140 steels were cut into coupons of approximately 2x1x0.2 cm by a low-speed diamond saw. The coupons were ground through 320 grit SiC abrasive paper, and cleaned ultrasonically in water then in acetone. The exact dimensions and weight of each coupon were then measured.

Diffusion coatings from two different kinds of cementation packs were evaluated. As demonstrated previously[2,3], 20wt% of 90Cr-10Si masteralloy as the alloy source, and 2wt% of a dual activator of approximately 95NaF-5NaCl along with SiO₂ as the filler in the pack was chosen for one type of pack. The second kind of pack involved a 20 wt% mixture of elemental Cr and Si powders of 90Cr-10Si composition, and 2.5wt% ternary activator mixture of approximate composition 30AlF₃-67NaF-3NaCl, along with the SiO₂ filler.

In each case, a set of 2 to 4 cleaned coupons was uniformly embedded in a pack mixture inside an alumina crucible. The charged crucible was dried in an oven at 100°C for about an hour. The crucible was then covered by an alumina lid and sealed by a high-temperature ceramic cement. The sealed crucible was cured at 100°C for another hour, and then positioned inside a horizontal alumina tube which was heated by an electrical resistance furnace. A type K thermocouple was placed in direct contact with the sealed crucible for monitoring and controlling the coating temperature. During the heating, high-purity argon was purged through the entire system to prevent oxidation. After heating at the the desired temperatures (850°C-1050°C) for various times, the crucible was furnace-cooled to room temperature.

The coated coupons were cleaned ultrasonically, and their dimensions and weights were recorded. Some of the coupons were X-rayed and then mounted, sectioned, ground and polished for metallographic examination. The polished mounts were etched with 10% nital solution, and examined by an optical microscope. The compositions of the coatings were determined using Energy Dispersive Spectroscopy (EDS) on a JEOL-JXA-35 scanning electron microscope (SEM). The spectroscope was calibrated weekly and the quantitative analysis was made by comparing against a standard alloy specimen whose composition was established by NIST. Sometimes, microhardness profiles were also measured across the coatings.

For sulfuric acid solution testing, some coated coupons were submerged into 1N H₂SO₄ at room temperature (23°C), and weight changes were measured periodically. To simulate seawater testing, other coupons were submerged into 3.5wt% NaCl solution at room temperature (23°C) for either 12 days or 40 days, and the pit formation was recorded.

Results and Discussion

Coating Development

Codeposition of Cr and Si into low-carbon steels by using a Cr-Si masteralloy has been reported by Harper and Rapp[2,3]. The main focus of this research, however, was to extend the method to develop similar coatings for medium-carbon steels and HSLA steels by using elemental Cr and Si powders, which would prove to be less expensive and more readily recycled than the Cr-Si masteralloy. Table 1 illustrates the results of preliminary experiments to establish the sensitivity of the coating composition and structure to the pack composition. Table 2 describes successful coatings produced using a Cr-Si masteralloy with a "dual activator", and Table 3 presents the coating characteristics for packs with a mixture of elemental Cr and Si powders using a ternary activator. All these coatings were bright and shining, and the surface compositions were consistently around 25-30wt% Cr and 3.5wt% Si. The cementation packs using higher silicon contents often resulted in a slightly higher silicon content in the coatings.

Figures 1 and 2 present representative coating morphologies and composition profiles for a 1045 and a 4140 steel, respectively. For these coatings, the Cr-Si

masteralloy and dual activator were used. Figures 3 and 4 show the coating morphologies and the composition profiles for a 1045 and a 4140 steel, respectively. In this case, the coating pack consisted of a mixture of Cr and Si elemental powders, and the ternary salt activator. For all four of the coatings shown, the introduction of both Cr and Si at the high temperature stabilized a ferrite surface layer on the austenite interior. Upon rather slow cooling, the interior converted to ferrite plus carbide, and indeed, the ferrite grains of the coating grew inward to eliminate the coating/core interface which existed at the high temperature. Thus, in most cases, the ferrite grains of the coating extend readily into the substrate, providing an excellent bond of the coating to the substrate. The fine lines in the micrographs which seem to separate the coating from the substrate result from preferential etching during metallographic preparation, but they do not constitute interfaces. Also shown in Figures 1 to 4 are many irregular "pegs" along the original α - γ boundaries at the coating temperature. These pegs are actually ghosts of the triple points where the original grain boundaries met at the high temperature (about 1050°C). The adherence of such coatings without interfaces should be excellent. Figure 5 presents a hardness profile for the coating; the coating is not alarmingly hard and must exhibit significant ductility.

An important deleterious phenomenon occurred during the coating process; a carbon depletion zone developed in the core underneath the coating. The extent of this depletion zone was a function of the pack chemistry as well as the coating temperature and time. In future studies, the decarburization suffered during the coating process will need to be minimized by limiting the process temperature and time.

Numerous preliminary runs were performed to identify and rationalize the optimal pack chemistry. The results of some of these runs, as listed in Table 1, led to the following interpretations:

1. *Effect of elemental silicon in the pack.* The greatest difficulty in chromizing medium-carbon steels at high temperature is the formation of a blocking chromium carbide at the surface. This chromium carbide layer reduces greatly the diffusion of chromium into the substrate, except after extended heating at a relatively high temperature (1150°C). The preliminary introduction of a carbon-repulsive and ferrite-stabilizing third element (e.g. Si) into the coating greatly reduces the carbon activity in the coating and therefore retards the formation of chromium carbide at the surface. The surface compositions for run C8 in Table 1 indicate that the silicon activity generated by

the silica filler alone is not sufficient to prevent the formation of a chromium carbide layer at the surface. On the other hand, 5wt% elemental silicon in the pack eliminates the availability of chromium to the steel (run C11 in Table 1). The composition from run CK1 suggests that a significant amount of silicon can be established at the surface either during the heating-up or by a three hour isothermal treatment at 850°C.

2. *Effect of fluorine activity in the pack.* The fluorine activity also has a significant effect on Si gaseous species in the pack. A calculation performed by Harper and Rapp[2,3] suggests that in a "dual activator" Cr-Si cementation pack, chlorine primarily increases the vapor pressures of chromium gaseous species, whereas fluorine primarily increases the vapor pressures of silicon gaseous species. Therefore, by adjusting the ratio between chloride and fluoride in the "dual activator", different proportions of chromium and silicon content in the coating can be achieved. Run C12 in Table 1 shows that the absence of fluoride in the pack caused the formation of chromium carbide at the surface, even though the silicon content in the pack seems about adequate when compared to run 163 in Table 1.

3. *Effect of the filler.* The use of different fillers in the cementation pack also has a significant effect on the resultant coatings. The silica filler usually resulted in a smooth and shining surface finish of the coated coupons, while the alumina filler gave a metallic gray surface. Quite often, using an alumina filler also resulted in a net weight loss of the coated coupon as opposed to a net weight gain expected for an inward-grown diffusion coating. Harper and Rapp[2,3] have pointed out that the silica filler in a Cr-Si cementation pack using sodium halides is not inert. In fact, sodium would react with silica to form sodium silicate, and release silicon into the gas phase. As such, the silica filler plays a significant role in controlling the overall activity of silicon gaseous species in the cementation pack. However, the silicon released by the silica filler alone does not suffice to generate an adequate coating, as mentioned earlier (run C8 in Table 1).

4. *Surface finish.* Chromium-silicon coatings showing good corrosion resistance generally had a shining, smooth surface finish. Inadequate coatings often had a dull, rough surface. A comparison of these two different surface morphologies reveals that the rough surface always results from a significant outward-grown layer which entraps pack powders, as shown in Figure 4.

Corrosion Testing

1. *Corrosion in 1N H₂SO₄*. The rates of uniform corrosion were determined by periodically weighing the coated coupons immersed in the acid. Corrosion test results for coated coupons in sulfuric acid are plotted in Figure 6. An initial fast weight loss followed by a slow weight loss was noted for all the coated coupons, while the uncoated coupon exhibited a constant weight loss rate, which after 13 days was about triple that for the coated coupons.

2. *Corrosion in 3.5wt% NaCl solution*. Corrosion test results in 3.5wt% NaCl solution are listed in Table 4. All the coated coupons exhibited pitting corrosion, and this preferential attack probably occurred along residual continuous Cr carbides in the grain boundaries of the coatings.

Conclusions

1. The simultaneous deposition of Cr and Si diffusion coatings with surface composition of approximately 25-30wt% Cr and 3-5wt% Si on 1045 and 4140 steels has been achieved using either a "ternary activator" with elemental Cr and Si powders, or a "dual activator" with a Cr-Si masteralloy.

2. The optimum cementation-pack compositions are

- a) metal source: 15wt% Cr + 2wt%Si
activator: 2wt% (95NaF+5NaCl) + 1wt%AlF₃
filler: SiO₂
- b) metal source: 20wt% (90Cr-10Si) masteralloy
activator: 2wt%(96NaF+4NaCl)
filler: SiO₂

3. A two-stage of coating process, i.e. 850°C for 3hr followed by 1050°C for 16hr, was most effective in producing the desired coating compositions for a pack involving elemental Cr and Si powders.

4. All coated coupons with the desired coating composition had much lower corrosion rates in 1N H₂SO₄ than uncoated coupons. But the coated coupon did not exhibit adequate pitting resistance in 3.5wt% NaCl solution.

Acknowledgement

This work was sponsored by Oak Ridge National Laboratory (R.R. Judkins, contract FWP-FEAA028).

References

1. J. F. Mason, Jr., in "*Source Book on Stainless Steels*", (ASM, Metals Park, OH, 1976), pp. 107-120.
2. M. A. Harper and R. A. Rapp, in *Heat Resistant Materials*, K. Natesan and D. J. Tillack, eds., (ASM Int., Materials Park, OH, 1991), pp. 379-286.
3. M. A. Harper and R. A. Rapp, in "*Surface Modification Technologies IV*", T. S. Sudarshan, D. G. Bhat, and M. Jeandin eds. (TMS Publications, Warrendale, PA, 1991) p. 415.
4. R. Bianco, M. A. Harper, and R. A. Rapp, *Journal of Metals*, **43**, (1991) 20.
5. N. D. Tomashov, G. P. Chernova, and O. N. Marcova, *Corrosion*, **20** (1964) 166t.
6. B. E. Wilde, *Corrosion*, **44** (1988) 711.
7. M. G. Fontana, *Corrosion Engineering*, 2nd Ed. (McGraw Hill Book Co. New York, 1978).

List of Tables

Table 1	Results of preliminary experiments to establish the effects of cementation-pack composition on coating composition and thickness.
Table 2	Successful coatings produced using the optimized cementation pack chemistry and the treatment procedures.
Table 3	Successful coatings produced using the optimized cementation pack chemistry and the treatment procedures.
Table 4	Corrosion test results of the coated coupons in 3.5wt.% NaCl solution at room temperature.

Figure captions

Figure 1	Concentration profiles and microstructure for coating on 1045 steel using 90Cr-10Si masteralloy with 2 wt% (95NaF-5NaCl) activator diffused at 850°C for 3 hours + 1050°C for 16 hours (SiO ₂ filler).
Figure 2	Concentration profiles and microstructure for coating on 4140 steel using 90Cr-10Si masteralloy with 2 wt% (95NaF-5NaCl) activator diffused at 850°C for 3 hours + 1050°C for 16 hours (SiO ₂ filler).
Figure 3	Concentration profiles and microstructure for coating on 1045 steel using 15 wt% Cr + 1 wt.% Si, 2 wt% (95 NaF-5 NaCl) + 1wt% AlF ₃ activator diffused at 850°C for 3 hours + 1050°C for 16 hours (SiO ₂ filler).
Figure 4	Concentration profiles and microstructure for coating on 4140 steel using 15 wt% Cr + 1 wt% Si, 2 wt% (95 NaF-5 NaCl) + 1 wt% AlF ₃ activator diffused at 850°C for 3 hours + 1050°C for 16 hours (SiO ₂ filler).
Figure 5	Microhardness profile of coupon from coating on 1045 steel using 15 wt%Cr + 1 wt%Si, 2 wt% (95 NaF-5 NaCl) + 1 wt% AlF ₃ activator diffused at 850°C for 3 hours + 1050°C for 16 hours (SiO ₂ filler).
Figure 6	Weight losses of coated coupons C2123, C2324 and a coupon without coating in 1N H ₂ SO ₄ solution at room temperature.

Table 1 Results of preliminary experiments to establish the effects of cementation pack composition on coating composition and thickness.
(Treatment: 850°C for 3 hours followed by 1050°C for 16 hours)

Run No. internal code	Cementation Pack Composition (wt. %)					Coating (wt. %) Surface Comp	Thickness (μm)	Comments
	Activator		Metal Powder					
	dual activator		AlF ₃	Cr	Si			
	NaF	NaCl						
C163	1.9	0.1	1	15	1	25.3	180	ferrite
C8	1.9	0.1	1	20	0	90.0	20	carbide
C11	1.9	0.1	1	10	5	0.4	310-280	ferrite
C12	0	2	1	20	1	94.8	30-35	carbide
CK1*	1.9	0.1	1	15	2	0.9	20	ferrite

* CK1 was treated only at 850°C for 3 hours

Table 2 Successful coatings produced using the optimized cementation pack chemistry on 1045 steel
(Treatment: 850°C for 3 hours followed by 1050°C for 16 hours)

Run No. internal code	Cementation Pack Composition (wt. %)					Coating (wt. %) Surface Comp	Thickness (μm)	Comments
	Activator		Metal Powder					
	dual activator		AlF ₃	Cr	Si			
	NaF	NaCl						
C1733	1.9	0.1	1	15	1	28.3	150	bright
C1832	1.9	0.1	1	15	1	37.1	260	bright
C1931	1.9	0.1	1	15	1	30.9	220	bright
C2031	1.9	0.1	1	15	2	25.7	320	bright
C2131	1.9	0.1	1	15	2	34.4	300	bright

Table 3 Successful coatings produced using the optimized cementation pack chemistry on 4140 steel
(Treatment: 850°C for 3 hours followed by 1050°C for 16 hours)

Run No. internal code	Cementation Pack Composition (wt. %)				Coating (wt.%) Surface Comp		Thickness (μm)	Comments	
	Activator		Metal Powder		Cr	Si			
	dual activator		AlF ₃	Cr					Si
	NaF	NaCl							
C1723	1.9	0.1	1	15	30.5	3.3	150	bright	
C1822	1.9	0.1	1	15	40.7	3.2	250	bright	
C1921	1.9	0.1	1	15	33.0	3.6	200	bright	
C2021	1.9	0.1	1	15	27.1	4.4	290	bright	
C2124	1.9	0.1	1	15	34.9	3.6	300	bright	

Table 4 Corrosion test results of the coated coupons in 3.5wt% NaCl solution at room temperature

Run No. internal code	Cementation Pack Composition (wt. %)					substrate	Corro. Time (days)	Corro. observed
	Activator		Metal Powder					
	dual activator		AlF ₃	Cr	Si			
	NaF	NaCl						
C1724	1.9	0.1	1	15	1	4140	12	pitting
C1734	1.9	0.1	1	15	1	1045	12	pitting
C1824	1.9	0.1	1	15	1	4140	12	pitting
C1834	1.9	0.1	1	15	1	1045	12	pitting
C2121	1.9	0.1	1	15	2	4140	40	pitting
C2325	1.9	0.1	0	20 (90Cr-10Si)MA		1045	40	pitting

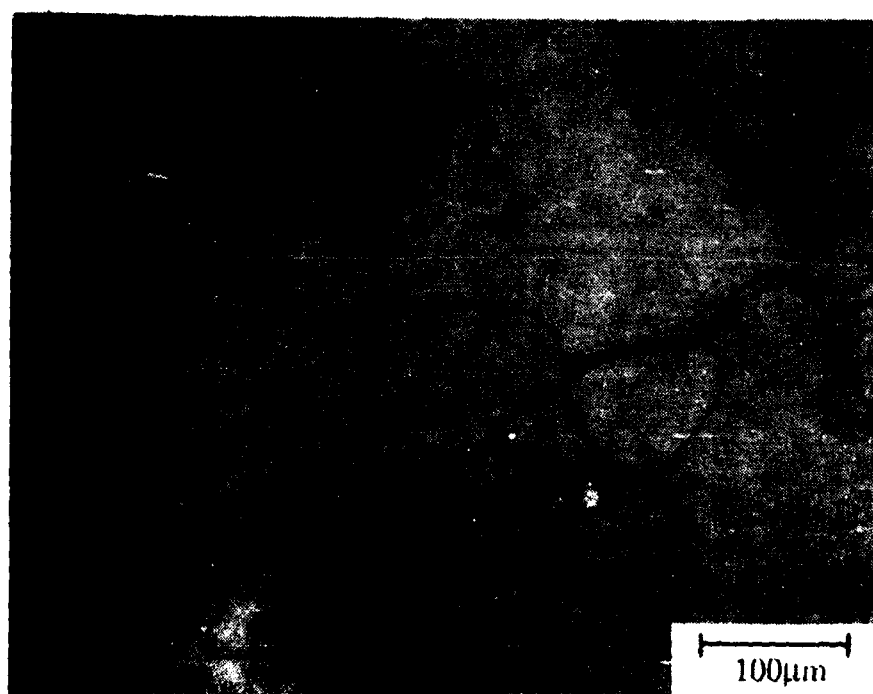
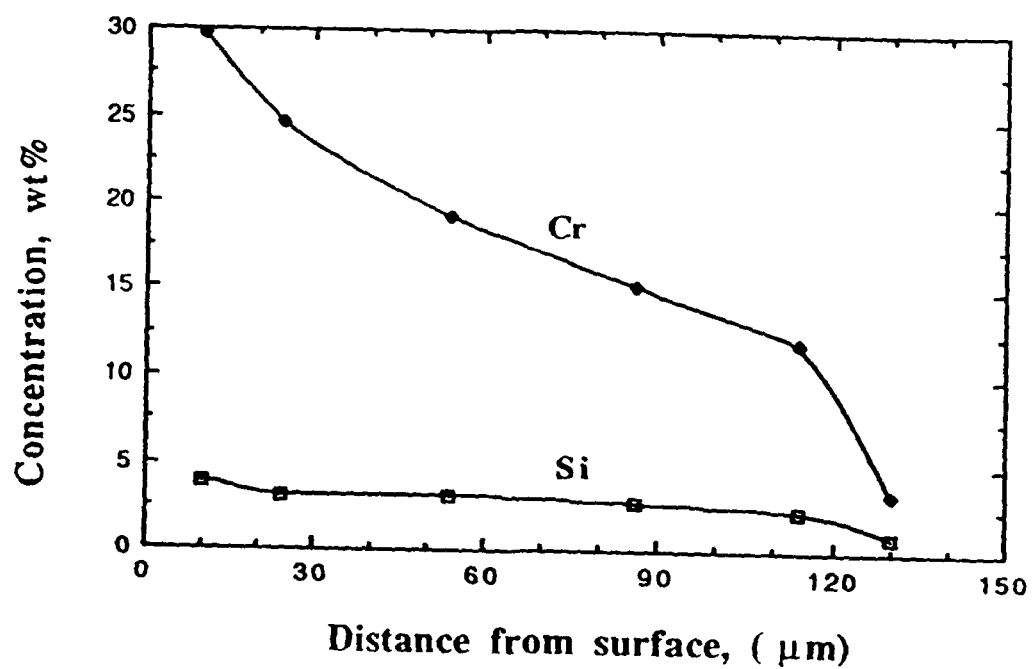


Figure 1 Concentration profiles and microstructure for coating on 1045 steel using 90Cr-10Si masteralloy with 2 wt% (95NaF-5NaCl) activator diffused at 850°C for 3 hours + 1050°C for 16 hours (SiO₂ filler).

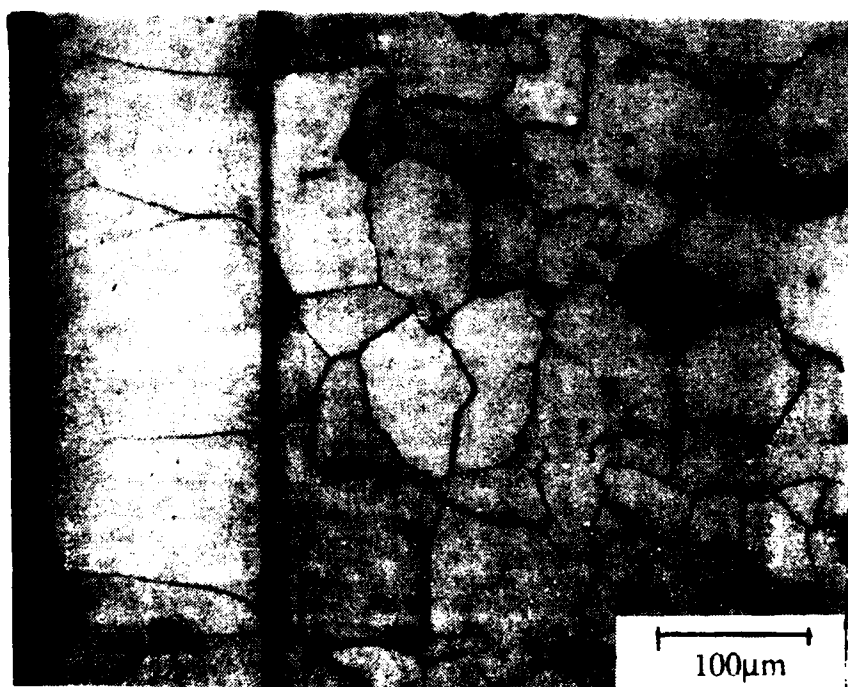
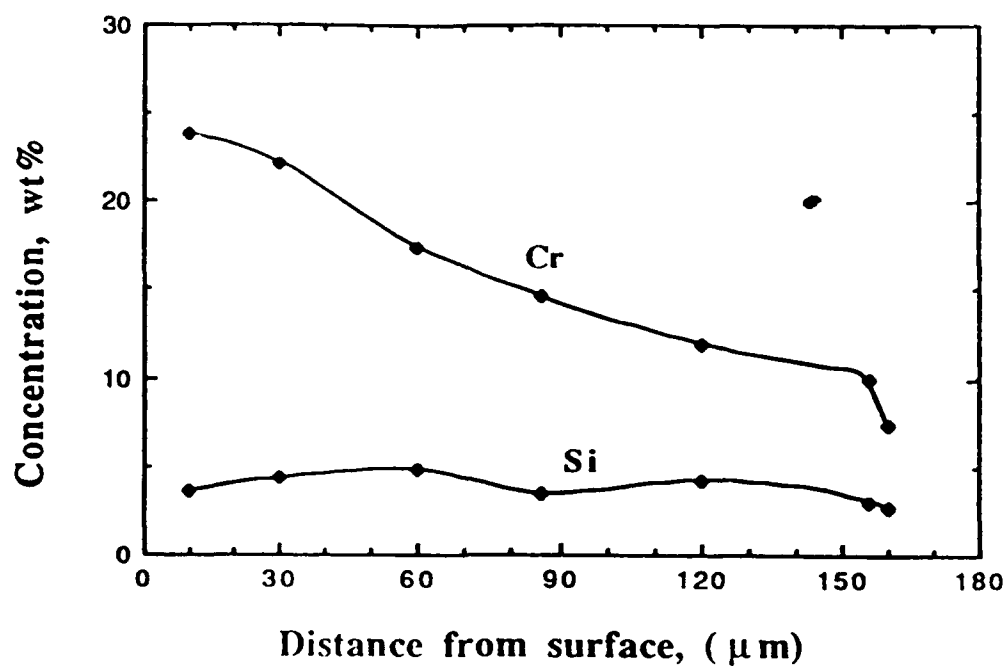


Figure 2 Concentration profiles and microstructure for coating on 4140 steel using 90Cr-10Si masteralloy with 2 wt% (95NaF-5NaCl) activator diffused at 850°C for 3 hours · 1050°C for 16 hours (SiO₂ filler).

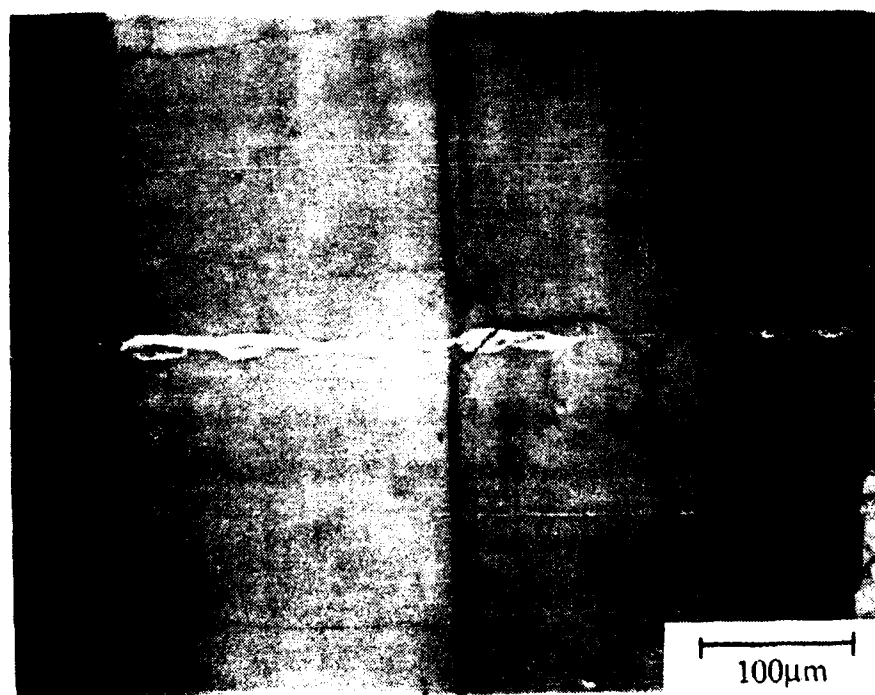
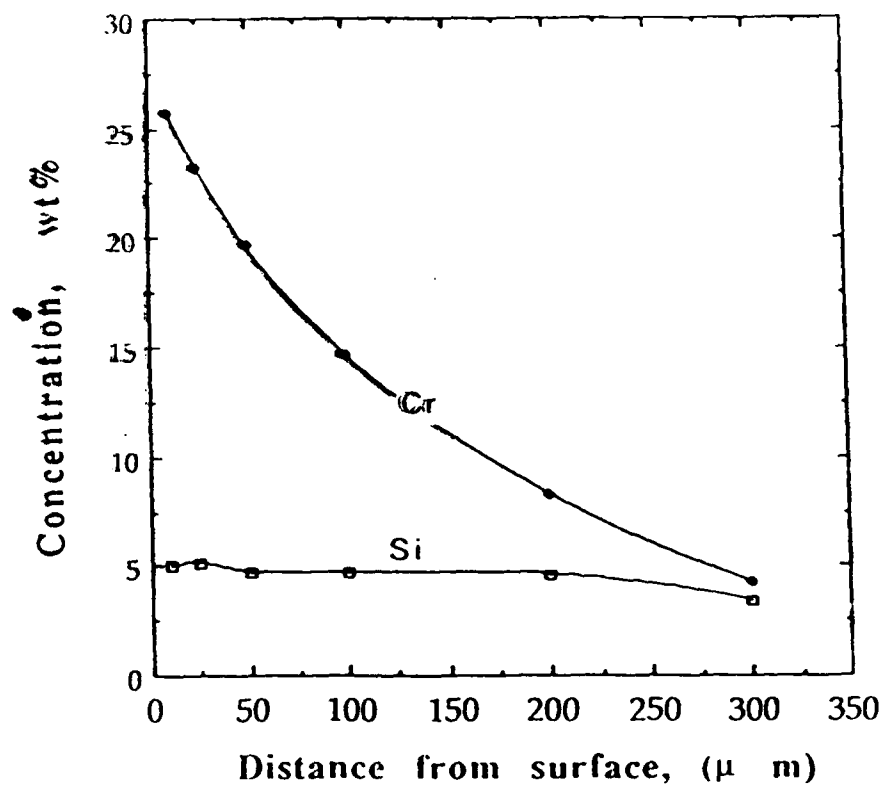


Figure 3 Concentration profiles and microstructure for coating on 1045 steel using 15 wt% Cr + 1 wt.% Si, 2 wt% (95 NaF-5 NaCl) + 1wt% AlF_3 activator diffused at 850°C for 3 hours + 1050°C for 16 hours (SiO_2 filler).

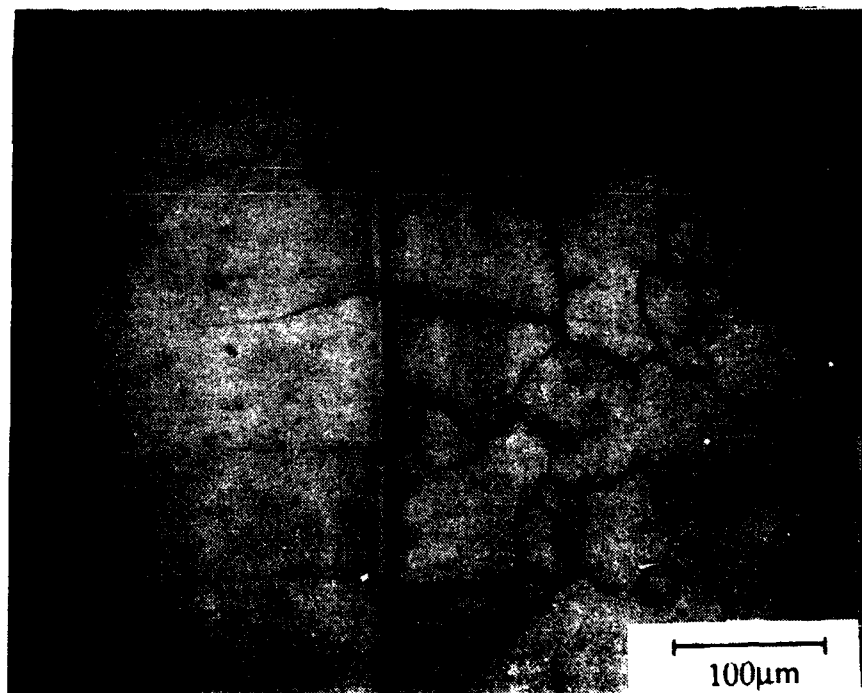
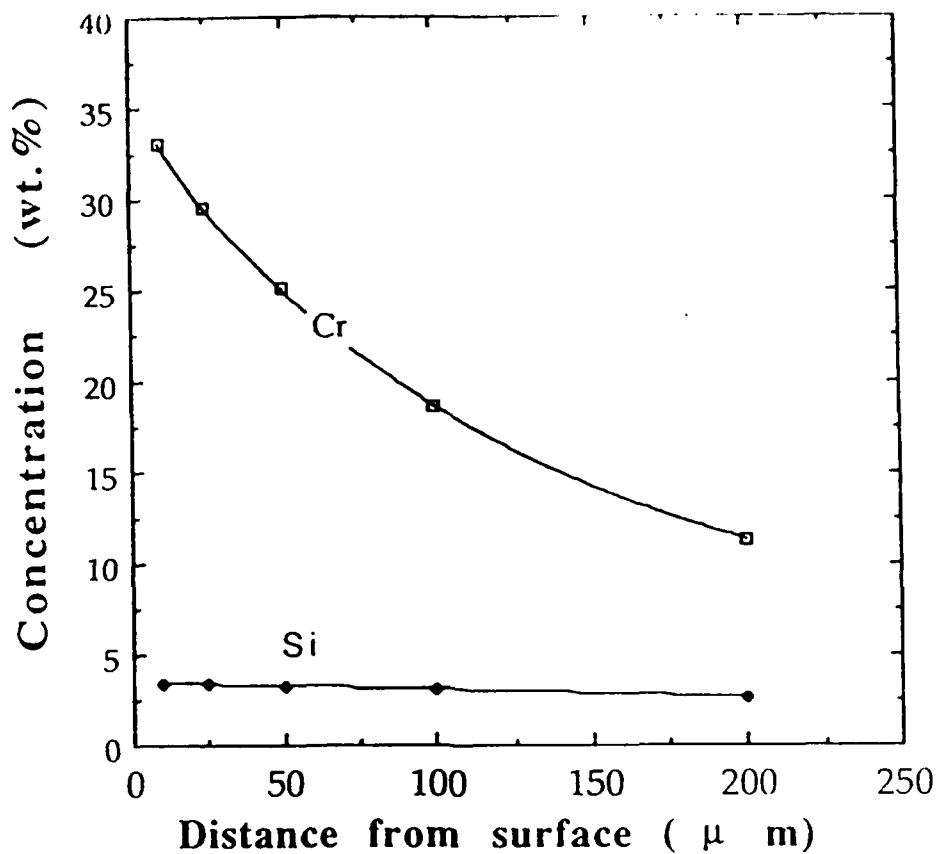


Figure 4

Concentration profiles and microstructure for coating on 4140 steel using 15 wt% Cr + 1 wt% Si, 2 wt% (95 NaF-5 NaCl) + 1 wt% AlF_3 activator diffused at 850°C for 3 hours + 1050°C for 16 hours (SiO_2 filler).

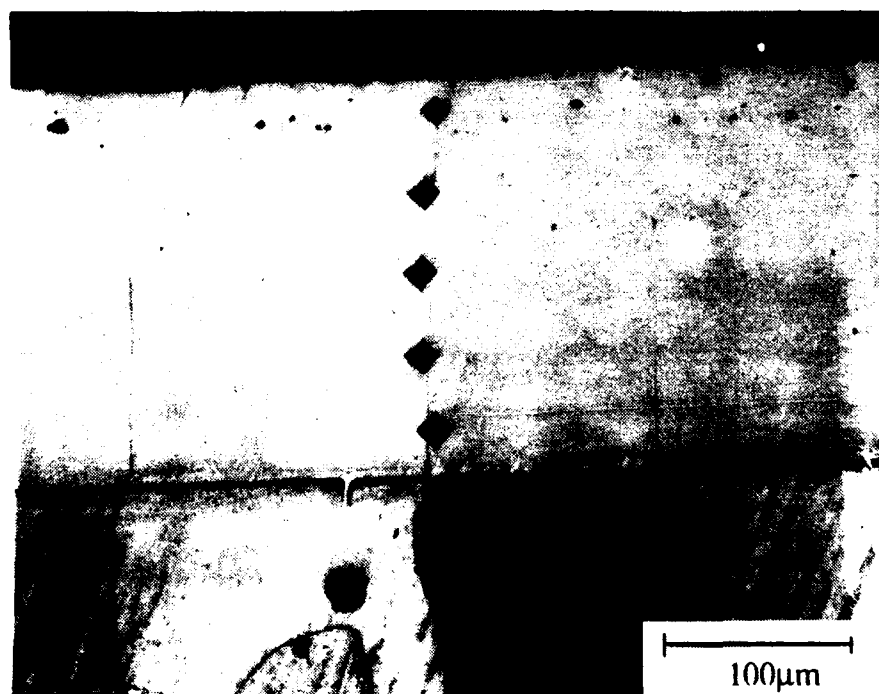
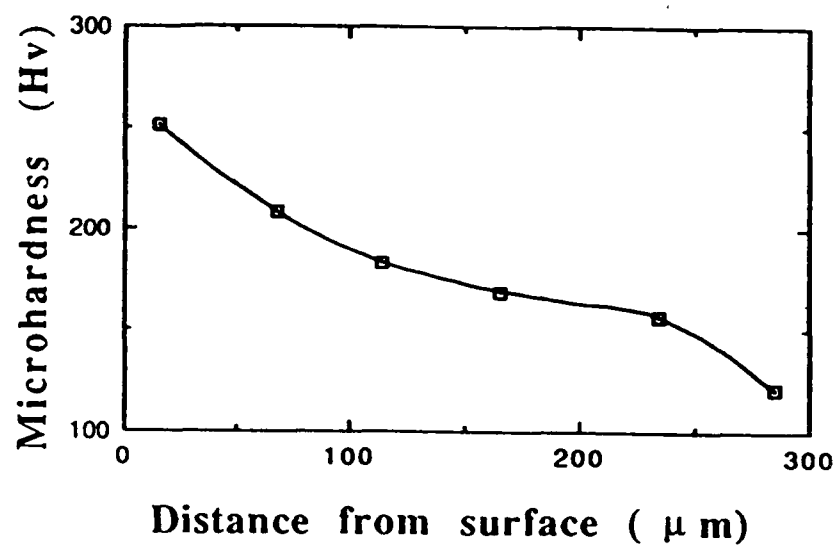


Figure 5 Microhardness profile of coupon from coating on 1045 steel using 15 wt%Cr + 1 wt%Si, 2 wt% (95 NaF-5 NaCl) + 1 wt% AlF₃ activator diffused at 850°C for 3 hours + 1050°C for 16 hours (SiO₂ filler).

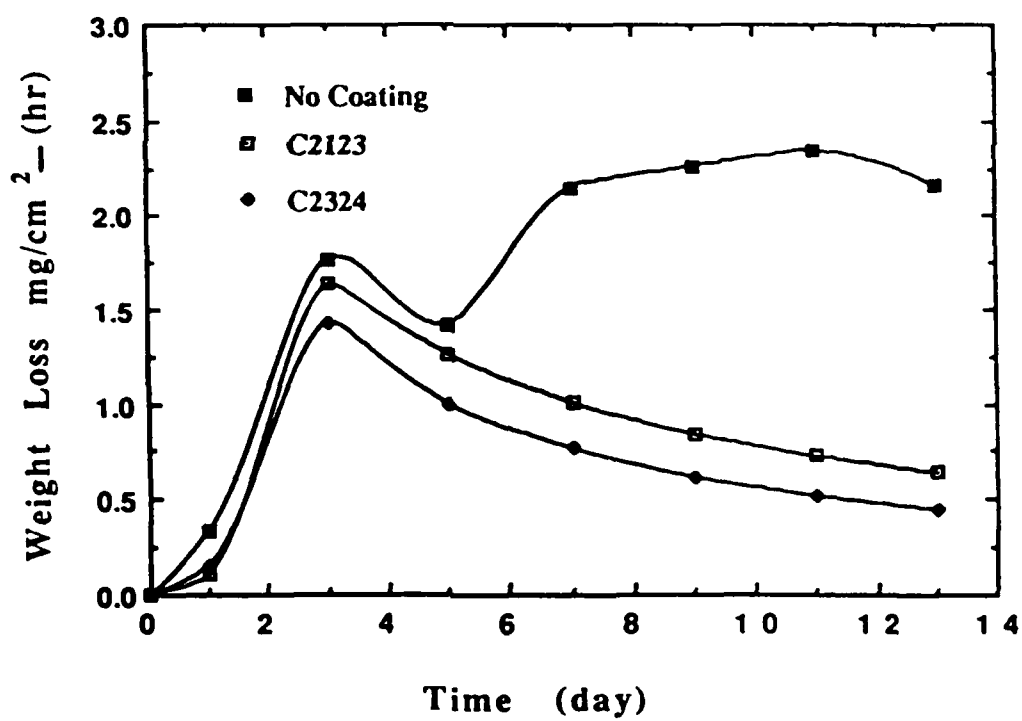


Figure 6 Weight losses of coated coupons C2123, C2324 and a coupon without coating in 1N H_2SO_4 solution at room temperature.

FLUORESCENT MATERIALS AS CORROSION SENSORS FOR COATINGS

Richard E. Johnson
Department of Chemistry
LeTourneau University
Longview, Texas, U.S.A.

Vinod S. Agarwala
Naval Air Warfare Center
Aircraft Division
Warminster, Pennsylvania, U.S.A.

Abstract

The objective of this study was to investigate the possibility of using fluorescent materials as early warning indicators of coating degradation during corrosion of metals. A number of compounds were screened for fluorescence activity by themselves and as complexes with metal ions. Five compounds were found to exhibit distinct oxidation-reduction (redox) behavior and showed promise as indicators for corrosion (oxidation) when it occurs. Three of these compounds showed high fluorescent activity, and thus were investigated further by UV and IR spectroscopy as well as cyclic voltammetry to determine their redox behavior. All five materials were tested by themselves and in standard paint coatings on aluminum alloy panels and were found to show fluorescence under 365 nm UV light when the paint surface was scratched and moistened, as in coating failures. Other fluorescent materials may also offer similar applications, and thus, would be part of the future study as well as the work on actual mechanisms and kinetics of these redox reactions. These fluorescent materials would make possible inspection of aircraft or painted surfaces in a darkened area utilizing UV light and photographic or video recording of the fluorescent spots for forthcoming corrective measures.

Key terms: Fluorescent materials, corrosion of steels and Al alloys, coating degradation, early warning sensors

Introduction

Corrosion of metal alloys in aircraft and ships is a very expensive problem in the least and may even prove dangerous to human lives if critical parts fail because of undetected corrosion. Previous work by V. Agarwala has shown that certain redox indicators could be mixed with primer paint and used to detect scratches in the paint by the color change produced [1]. The objective of this work was to investigate fluorescent materials that could be used in a similar way and be detected by using UV light that would show up fluorescent areas in paint coatings where corrosion could begin.

A variety of fluorescent materials are now utilized for analytical techniques such as acid-base titrations, precipitations or metal complexing reactions. It was in screening some of these materials that the behavior of fluorescence with redox reactions was also investigated.

Several substances showed promise as redox indicators by the change in fluorescence activity with their oxidized and reduced forms. The work described in this paper deals mainly with two of these compounds, fluorescein and columbia blue dye-D298¹.

Experimental

The fluorescent dyes and other chemicals were used as purchased without further purification. Fluorescence spectra were obtained with a Shimadzu Model 5000U Spectrofluorometer, however, some screening of compounds was done using a hand held 365 nm UV light from Spectronics Corporation. Cyclic voltammetry work was done using the Gamry Instruments CMS100 Corrosion Measurement System.

The fluorescent dyes were mixed with standard primer and applied to aluminum alloy plates and this was followed by a polyurethane white top coat of paint. Fluorescence was seen in scratched areas of the plates after exposure to moisture using the 365 nm lamp for illumination. About twenty-five compounds were screened for fluorescent activity with and without metal ions. Some of the compounds were specific for aluminum or iron ions, however, the fluorescence was weak and in some cases the compound itself had some fluorescence. Possible dyes that could be used included eriochrome blue black-R, morin, 8-quinolinol and rhodamine-B.

Results and Discussion

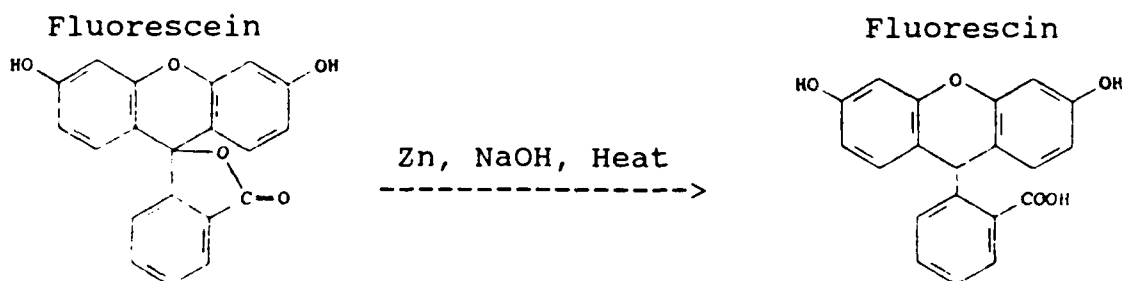
Most of the work was concentrated around the two dyes, fluorescein and columbia blue-D298. Fluorescein has a good emission band centered at 520nm and columbia blue has an emission

¹Trademark of Dayglo Corp., Cleveland, OH.

band centered at 466nm. The excitation spectra for fluorescein and columbia blue for these emission bands are shown in Figures 1 and 2. Fluorescein has strong excitation at 504 nm, medium at 245 nm and weaker at 336 nm. Columbia blue has a strong, broad excitation band at 382 nm and another weaker band at 256 nm. When using the hand-held lamp of 365 nm for excitation, this probably overlaps with the 336 nm band for fluorescein and the 382 nm band for columbia blue for excitation.

Both fluorescein and columbia blue were reduced in alkaline medium with zinc metal and heat. The dramatic decrease in fluorescence emission are shown in Figures 3 and 4 for the 520 and 466 nm bands respectively. These dyes are then redox indicators, having no fluorescence in the reduced states and fluorescing strongly in the oxidized states. The change in fluorescein from oxidized form to reduced form is shown below.

The elimination of the oxygen bridge by reduction also eliminates the fluorescence. Generally, the more rigid the ring structure by bridging with metal ions or other atoms, the more likely the compound will have fluorescent activity.



FTIR was utilized to determine if there are differences in solid fluorescein and fluorescin. Fluorescin is prepared by making a fluorescein solution in alkaline medium and then concentrating it by heating followed by acidification of the solution. When reduced fluorescin acid precipitated out, it was filtered and stored in a vial under a nitrogen atmosphere. If this fluorescin could be distinguished from fluorescein on a surface, further studies of this system could be done adsorbed on a solid surface or possibly bonded to a solid surface. This could have applications to the actual use of this material as a corrosion indicator. The FTIR spectra are shown in Figure 5. The spectra are of the dyes in KBr pellets. In the range of 1450 to 1500 wavenumbers, fluorescin has a ratio greater than one for the 1502 peak to the 1446 peak intensities. For similar peaks the ratio is much less than one in fluorescein. This same effect is true in the 740 to 760 wavenumber range although not as large as the previous one. These are not due to any sodium salt formation as

the spectrum for the sodium salt of fluorescein was also used for comparison. These differences indicate the potential to look at the oxidized and reduced forms of fluorescein with IR techniques.

The redox behavior of these fluorescent dyes were further investigated using cyclic voltammetry (CV). The instrumentation used was a Gamry Instruments CMS100 Corrosion Measuring System interfaced to an AT compatible 386 computer. The data were obtained using the cyclic polarization program that was built into this system. Two platinum electrodes were used for the working and counter electrodes and the reference electrode was a standard saturated calomel electrode. For all solutions a 1.0 M potassium sulfate supporting electrolyte was used and nitrogen was bubbled through the solutions except when actual data were being taken. The voltage scan range was 1.0 V to -0.6 V. Figures 6 and 7 illustrate the CV data for the dyes of fluorescein and columbia blue. All potentials are relative to the standard saturated calomel electrode. Fluorescein had a reduction peak at about -0.2 V, but may oxidize back in two steps indicated by small waves at 0.0 V and 0.7 V. Columbia blue dye showed a reduction peak at 0.2 V and a slight reversible oxidation at 0.3 V, but appeared to have an irreversible oxidation at -0.3 V. More work needs to be done to verify oxidation and reduction steps. Many organic compounds have some oxidation or reduction steps that appear irreversible, but may be limited by the potential range in a water system. Other electrode systems could possibly be used to verify these redox reactions.

Fluorescein and columbia blue were added to epoxy primer paint for tests on aluminum alloy panels. The dyes were added straight at about 1% concentration, adsorbed on powdered alumina and adsorbed on vesicular titanium dioxide. The primer was sprayed onto the test panels, dried for one day and then covered with a white polyurethane topcoat. Only the panels with 1% pure dyes added to primer showed fluorescence upon scratching and applying moisture to panels.

Conclusions

From this initial study it is concluded that the use of fluorescent materials as "smart coatings" or corrosion indicators is possible. After screening many compounds, five appear to be promising at this time. More extensive work has been done on fluorescein and columbia blue dye-D298 and that was reported in this paper. Further work would be needed on the actual oxidation-reduction mechanisms of these dyes and also on the kinetics of re-oxidation with variables such as temperature and humidity. Also catalytic or inhibiting effects of paint resins and alloy surfaces would be important to future applications.

Further work could be done to try and put the reduced form of the dye (non-fluorescent) into the primer and see if it fluoresces upon exposure to air and moisture through scratches in the painted surface. Whole airplanes or metal parts could be inspected in a darkened area by using UV light and either photographing or video recording of the fluorescent spots on the

surface. Again, the potential for cost savings with this early method of corrosion detection is great and merits further work.

Acknowledgment

The authors gratefully acknowledge the technical assistance of Mrs. Chris Dickey and Ms. Sarah Kwang with the fluorescence and FTIR spectra. The first author also acknowledges the support of the American Society For Engineering Education and the Naval Air Warfare Center (NAWC) for the summer research grant. The supports from ILIR program of the NAWC and U.S. Air Force Wright Laboratory are highly appreciated.

References

1. V.S. Agarwala, "Chemical Sensors for Integrity of Coatings", Proc. of Tri-Service Conference on Corrosion, Plymouth, MA, Ed. M. Levy, U.S. Army Materials Technology Laboratory, Watertown, MA, pp. 341-349, 1992.

Figure 1. Excitation Spectrum for Fluorescein Emission at 519 nm.

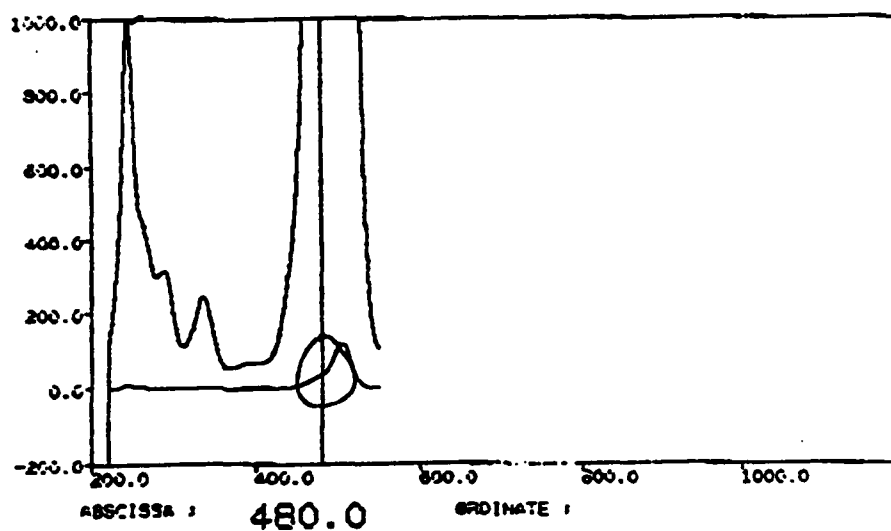


Figure 2. Excitation Spectrum for Columbia Blue Emission at 466 nm.

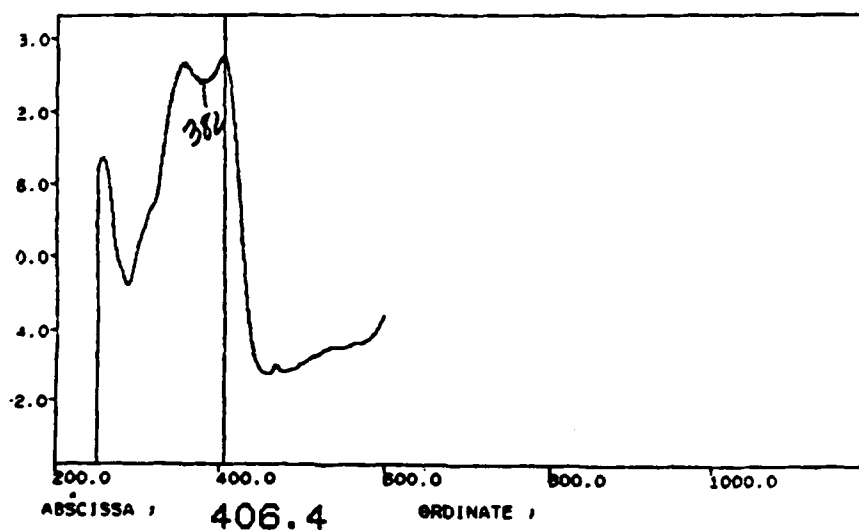


Figure 3. Emission at 520 nm for Oxidized and Reduced Fluorescein.

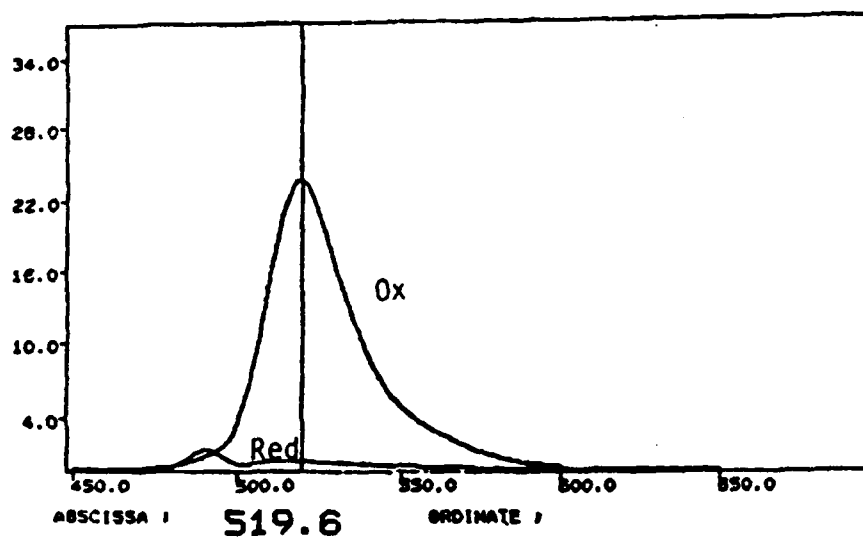


Figure 4. Emission at 466 nm for Oxidized and Reduced Columbia Blue.

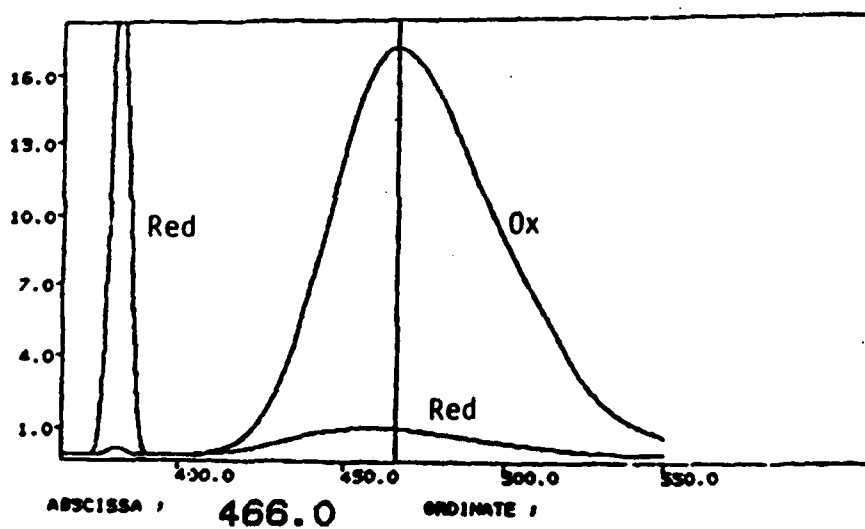
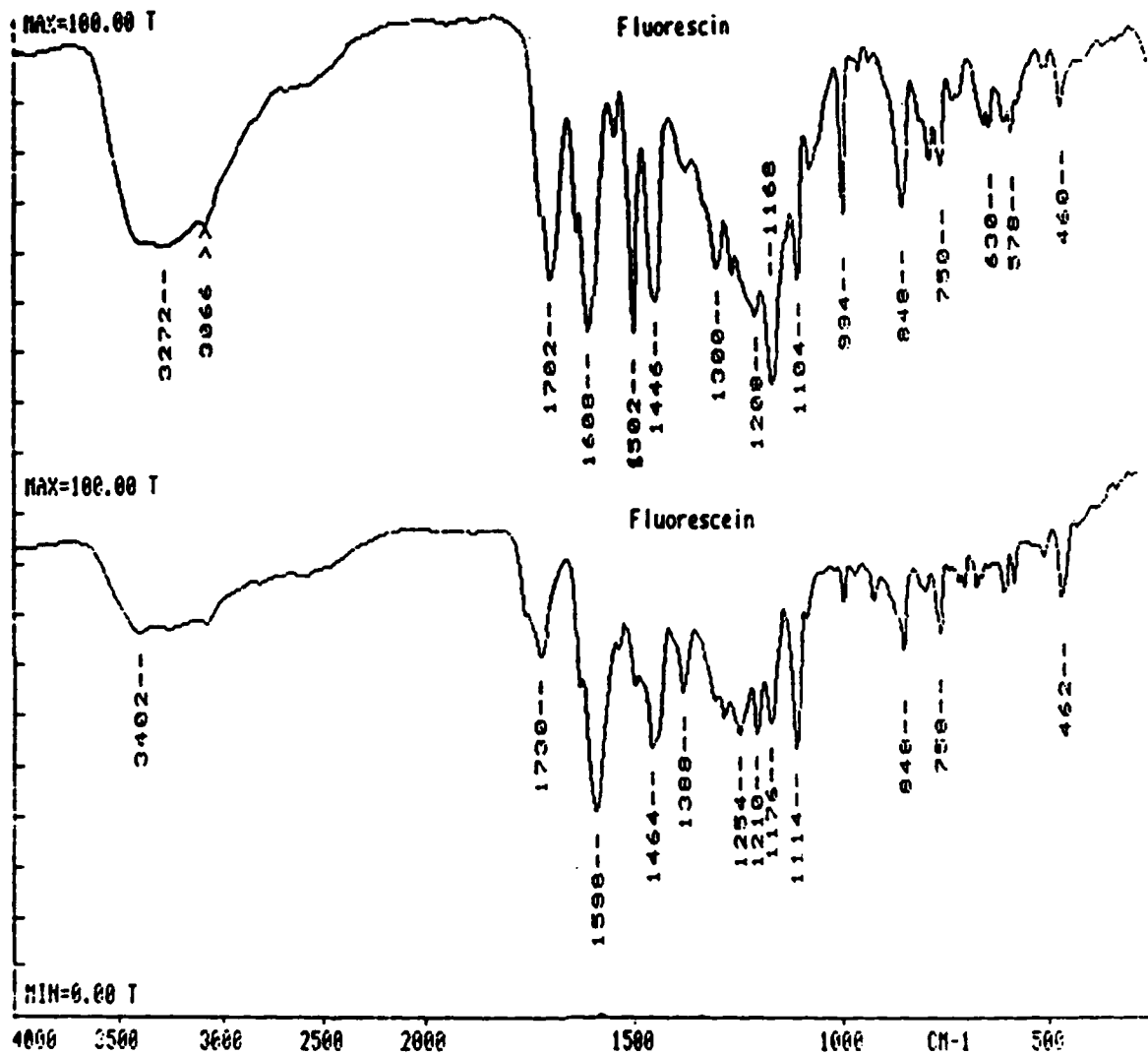


Figure 5. FTIR Spectra for Oxidized and Reduced Forms of Fluorescein.



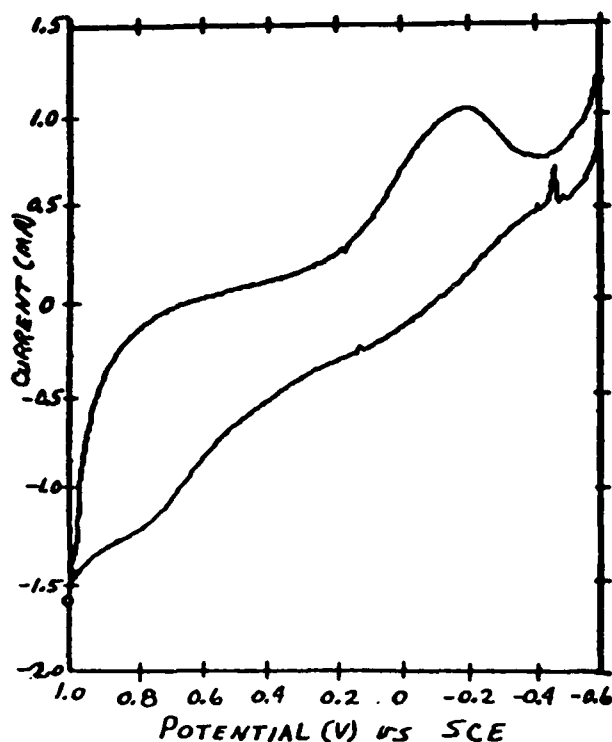


Figure 6. Cyclic Voltammogram of 0.6% (w/v) Fluorescein in 1 M Potassium Sulfate. Water solution purged with Nitrogen.

Potat #1
 Fwd Scan: 1 V to -0.6 V, 50 mV/s, 0.1 s/pt
 Rev Scan: -0.6 V to 1 V, 50 mV/s, 0.1 s/pt
 EOC: 0.178367 V
 Conditioning: OFF
 Delay: ON, 60 s
 IR Comp.: OFF

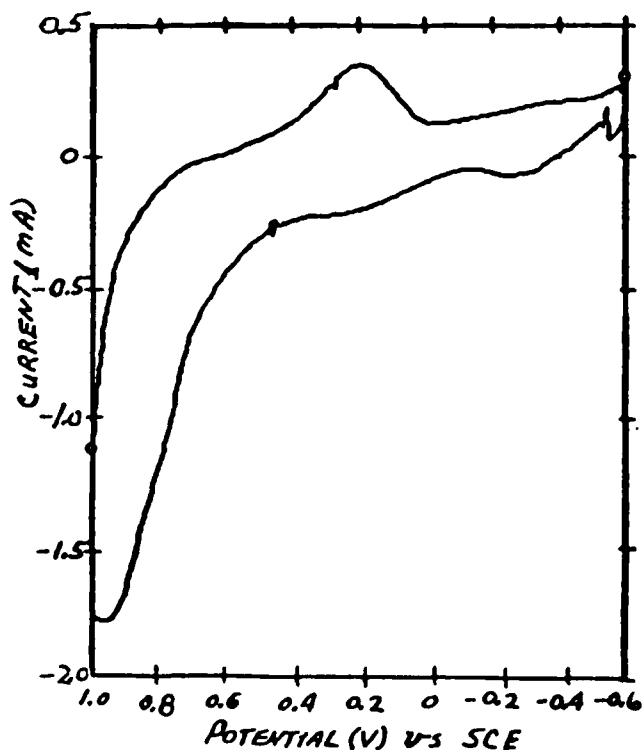


Figure 7. Cyclic Voltammogram of 0.02% Columbia Blue Dye-D298 in 1 M Potassium Sulfate. Water (90%) - Isopropanol (10%) solution purged with Nitrogen.

Potat #1
 Fwd Scan: 1 V to -0.6 V, 50 mV/s, 0.1 s/pt
 Rev Scan: -0.6 V to 1 V, 50 mV/s, 0.1 s/pt
 EOC: 0.268168 V
 Conditioning: OFF
 Delay: ON, 60 s
 IR Comp.: OFF

The Investigation of a New Autodeposition Coating System

Zhaoji Pan, Dajian Qiu, Zhongliu You and Yuan Zhao
Wuhan Research Institute of Material Protection (WRIMP)
Baofung Erlu 182, 430030 Wuhan
PR China

Abstract

A new autodeposition coating system of acrylic copolymers has been attained. The coating subjected to neutral salt spray test(NSS) for 600 hours without chromate rinse.

Hydrophilic monomer MAA improves the stability of the latexes and SEM photos show that the particles are smaller and rounder when more MAA is used so that the stability of the latex is better. A function of calculation the MFT of acrylic emulsion has been attained and the deviations between the measurement and the calculation is satisfied. The facts of the latexes effecting on salt spray resistance have been discussed. The autodeposition parameters and the bath stability have been also discussed.

Key terms: autodeposition, acrylate, monomer, copolymer, latex, the minimum film-forming temperature (MFT)

Introduction

Autodeposition is a process for depositing an organic coating on metal surface. The process involves the controlled releases of multivalent metal ions from the metal surface which destabilizes dispersed polymer particles in the bath so that a coating builds up on the metal surface[1].

Autodeposition saves the procedure time and equipment space comparing with conventional pretreatment / electrodeposition system. It reduces the air and water pollution because organic solvent usage is avoided. It also significantly reduces the energy and sharply decreased fire risk by avoiding the use of electric current in the coating bath[2].

The surfactants of the latexes for autodeposition coatings must be lower than the critical micell concentration (CMC) due that a good thickness of the coating can be attained. And the stability of the latex becomes a problem. Hydrophilic functional groups would be concentrated on the particle surface facilitating the unfolding of macromolecules[3]. The studies have shown that the adsorption of sodium alkylsulfonate onto such copolymer latexes was 40–50% less than that onto others[4].

Coalescing agents can not be used in autodeposition bath, and H_2O in the autodeposited wet film is less than 20%, and the minimum film-forming temperature (MFT) of emulsion should be in proper range in order to attain uniform and continuous film. Yamazaki[5] studied

the effects of methyl methacrylate and ethyl acrylate on MFT. Protzman[6] studied the effects of the polarity of polymers on MFT. And Z. Pan[7] studied the effects of the structure of particles on MFT.

Corrosion protection by organic coatings is considered to electrochemical resistance of the coating and to cathodic or anodic polarization or delay of the supply of water and oxygen[8]. Mayne[9] considered that the electrolytic resistance of coating was the most important factor. For autodeposition coatings, the system without chromate rinse have not been found, and the acrylic autodeposition coating with chromate solution treatment subjected to neutral salt spray test(ASTM B-117) only for 336 hours[2]. It is necessary to improve corrosion resistance of the acrylic autodeposition coating system.

Experiment

Materials

BA butyl acrylate	STY styrene
AA acrylic acid	MAA methacrylic acid
AN acrylonitrile	HPA 3-hydroxypropyl acrylate
CL crosslinker	

Experiments

The latex is prepared by the seed emulsion polymerization. The MFT is attained according to GB9267-88. The neutral salt spray(NSS) test is according to ASTM B-117. The autodeposition process consists of following stages: Sample surface cleaning — Water rinse — Deionized water rinse — Autodeposition coating — Immersion rinse — Curing in oven.

Result and Discussion

The improvement of the stability of the latexes

MAA monomer of the latex increases from A1 to A4 (table 1), and STY of the latex decreasing correspondingly. The total amounts of MAA and STY is unvaried. The results show that the sludges of the latex sharply decrease and the performance of the latex becomes more transparent with MAA monomer increasing. It is to say, MAA monomer improves the stability of the latexes significantly.

The SEM photos of this series show in Fig.1. The results indicate that the percent of single particles of A3 and A4 are much more than that of A2 and A1. The particles of A2 are smaller and rounder while that of A1 are bigger and longer. This means that for stable latexes there are higher percentage of single particles and coalescing particles are smaller and more regular than that of the unstable latexes.

MFT of emulsion

The main factors effecting on MFT of the emulsion are Tg of copolymers, the polarity of copolymers and the structure of the particles. The results have been discussed by Z. Pan[7]. And

here we only discuss the function of calculating MFT. When the difference of the latexes are content of BA, HPA, MAA, and STY in latex, the MFT of the latexes can be expressed as the following function:

$$T_i = T_m - k(BA_i - BA_m) + 0.8(MAA_i - MAA_m) + 0.55(HPA_i - HPA_m) \quad (1)$$

Where:

$k = 1.5$ when $AN = 0$

$k = 3.7$ when $AN > 10\%$

T_i is the calculated MFT of the latex i

T_m is the measured MFT of the latex m

BA_i , MAA_i , HPA_i correspond its percentage in latex i

BA_m , MAA_m , HPA_m correspond its percentage in latex m

A series of designed latexes according to quadrature $L9(3^4)$ is shown in table 2. And the MFT of the calculation is attained by the function (1): CL amount of the latexes of M2, M4, M9 is the same, and the difference between these latexes is BA, MAA, HPA and STY percentage. In this case, T_2 , T_4 can be calculated by T_9 , the measured MFT of M9. By the same way we can calculate others. The results show that the deviations between the calculation and the measurement of the latexes are from -1.2 to $+0.9$ °C.

The factors effecting on corrosion resistance of the coating

CL composition of the latexes in table 3 increases from CL₁ to CL₄ and STY decreases correspondingly. The results show that the average molecule weight of acrylic copolymers increases with CL increasing. And salt spray test shows that corrosion resistance of the coating is satisfied when the average molecule weight of copolymer resin is about 8×10^6 .

AN composition of the latexes from AN₁ to AN₄ in table 4 increases and STY decreases correspondingly. The results show that corrosion resistance of AN₁ which the latex is without AN monomer is the best and satisfied. However, that of AN₂, AN₃ and AN₄ which AN composition is more than 10% is worse. In another way, AN effects on NSS of coating significantly.

MAA composition of the latexes increases from MA₁ to MA₆ and AA composition of the latexes decreases from MA₁ to MA₃ while STY of the latexes decreases correspondingly and maintaining the total contents of MAA, AA and STY constant (table 5). The results show that corrosion resistance of the coating greatly improved when MAA composition increases. But corrosion resistance of the coating becomes worse when percent of AA composition increases.

Showing in table 6, MAA total composition of the latexes are the same, just MAA distribute differently in particle core / shell. The results show that corrosion resistance is better when the shell contain 5.0–7.5% MAA.

Process parameters control

The autodeposition process parameters investigation is conducted through neutral salt

spray testing . The autodeposition bath consists of a latex emulsion resin, hydrofluoric acid, hydrogen peroxide(oxidizing agent), ferric fluoride and deionized water. The resin solid in operating bath, dipping time of the steel panels, surface tension of the bath, ferric ion concentration, pH, ferrous ion concentration and temperature of the bath are the effective parameters on autodeposition rate, bath activity, thickness and corrosion resistance of the coating.

The surface tension of the bath is a very important factor, the activity of autodeposition bath increases with the enhancing surface tension of the bath. The film thickness is unacceptable if the surface tension of the bath is less than 45 dyn / cm. (see in table 7). Higher surface tension can result in bath unstable, the suitable surface tension of the bath is 50–60 dyn / cm.

Concentration of ferric ion in bath has influence on autodeposition rate(see in figure 2) , the thickness of the coating increases with increasing of ferric ion concentration, the ferric ion acts as a destabilizing agent for the colloidal latex particles in the bath, causing their deposition onto the metal surface. The latex may coalesce if ferric ion concentration is more than 3.5 g / l, so the proper concentration of the ferric ion in the bath is 1 –1.5 g / l. Ferrous ion affects the anodic etch so the ferrous ion in the bath must be transferred to ferric ion by adding oxidizing agent, the redox potential is controlled within 300–400 mV. The pH of the bath affects anodic etch also, it is controlled within 2.5–3.5. The proper dipping time of the metal panels in the bath is 90–150 seconds at 20–30 °C. When the bath parameters are adjusted in these ranges, the bath has suitable activity and a proper coating thickness can be achieved.

The coating thickness affects on salt spray resistance of the coating, the thicker coating has better corrosion resistance and when the thickness of the coating is more than 15 µm, the corrosion resistance of the coating is acceptable.

It is reported in early literatures[2,10] that the autodeposited coating of acrylic system must be treated with chromate rinse after deposition. It is well known that the chromate rinse can bring about environmental problem though it can greatly increase adhesion and corrosion resistance of the coatings. Table 5,6 shows the corrosion resistance of the autodeposited coating without chromate rinse in our experiments. The results indicate that the coating autodeposited from acrylic emulsion latex which omitting chromate rinse has an acceptable salt spray resistance and is comparable with the result in other reports[2,10] which have chromate rinse in autodeposition process. The particles structure of the latex is an important factor on corrosion resistance of the coating. This is principle of coating having acceptable corrosion resistance which omitting chromate rinse.

Bath stability

The bath parameters can be controlled by manual or automatic with equipments. The additives such as fluoric acid and hydrogen peroxide can be added continuously or timely. With the autodeposition processes, the impurities can be carried in by the panels and dissolve from the panel surface, the buildup of the impurities in the bath can conduct the appearance and corrosion resistance of the coating bad, and may interfere the stabilization of the bath. It must be maintained within a proper range.

In autodeposition processes, ferric ion dissolved from metal surface by etching of the acid can diffuse into the bath through the porous wet coating. Some of the ferric ions may be carried out by panels, the others remain in the bath, the concentration of ferric ion will build up. With the consuming of the resin solid in the bath, the addition of replenishing resin and deionized water is needed, this reduces the concentration of the ferric ion in the bath. The amounts of ferric ion dissolve from the metal surface are influenced by the activity of the bath, dipping time of the panels, the concentration of ferric ion in the bath, pH of the bath and temperature. When the bath parameters such as pH, dipping time and temperature are maintained within a suitable range, the activity of the bath is a main factor on the buildup of ferric ion in the bath. When a latex has higher autodeposition activity, the buildup of ferric ion is less than 20% in one turnover (When the amounts of the replenishing resin adding to the bath is equal to the total amounts of resin solid in the bath, we say, this is one turnover). The experiment results indicate that, with a latex describe as above which has higher autodeposition activity and maintaining suitable bath parameters, the ferric ion dissolved into the bath is maintained in balancing with the amounts of ferric ion carried out by panels, the concentration of ferric ion is controlled within a range of 1–1.6 g/l, this is in a tolerable range. Thus the bath maintains in stable for more than 10 turnovers.

Conclusion

The coating prepared by autodeposition with the new developed acrylic emulsion latex has a satisfactory corrosion resistance (pass 600 hours neutral salt spray test) without chromate reactive rinse. The autodeposition bath can maintain in stable for a long time (more than 10 turnovers) in processing when using a higher activity latex and adjusting the bath parameters in proper ranges.

Reference

1. USP 4,313,861
2. EP 0,186,113
3. V.I. Elisceva, *Acta Chim. Acad. Sci. Hung.* 71(1972): p.465
4. T. Matsumoto, M. Okubo, *Kobunshi Ronbunshu*, 34(1977): p.557
5. Yamazaki, *Kobunshi Ronbunshu*, 33(1976): p.663
6. T.F. Protzman and G.L. Brown, *J. Appl. Polym. Sci.*, 4(1960): p.108
7. Z. Pan etc. '92 International Conference on Colour Materials, (1992 Osaka, Japan): p.32
8. *Progress in Organic Coatings*, 9(1981): p.85
9. S.E. Mayne, *Off. Dig.*, 24(1952): p.127 or *Research*, 6(1952): p.278
10. M.J. Johnson, *Plating and Surface Finishing*, 71 7(1984): p.58

Table 1 Effect of MAA on the stability of the latex

the latex	MAA (%)	the sludge (%)	performance of the latex
A ₁	2	6.8	opaque
A ₂	4	2.5	translucent
A ₃	6	1.2	transparent
A ₄	8	none	transparent

Table 2 the MFT of calculation and the measurement

the latex	BA	MAA	HPA (%)	CL	STY	T _m	T _i (°C)	T _i -T _m
M ₁	36	4	8	2	50	46	46.7	+0.7
M ₂	40	4	4	1	51	36	36.6	+0.6
M ₃	44	4	6	3	43	31	31	0
M ₄	36	6	6	1	51	46	45.3	-0.7
M ₅	40	6	8	3	43	41	39.8	-1.2
M ₆	44	6	4	2	44	34	34	0
M ₇	36	8	4	3	49	44	44.9	+0.9
M ₈	40	8	6	2	44	44	42.8	-1.2
M ₉	44	8	8	1	39	36	36	0

Table 3 Effect of CL on corrosion resistance

the latex	CL (%)	\bar{M}_n (10 ⁴)	thickness (μm)	NSS (hour)
CL ₁	0	0.08	33	121
CL ₂	1	8.12	35	336
CL ₃	2	14.48	36	168
CL ₄	3	18.46	33	91
CL ₅	4	17.05	34	42

Table 4 Effect of AN on corrosion resistance

the latex	AN (%)	thickness (μm)	NSS (hour)
AN ₁	0	35-33	360
AN ₂	10	34-31	96-121
AN ₃	17	33-31	96-121
AN ₄	22	31-30	121

Table 5 Effect of MAA on corrosion resistance

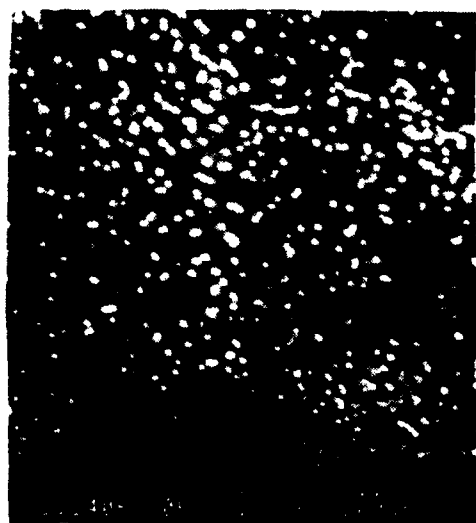
the latex	AA (%)	MAA (%)	thickness (μ m)	NSS (hour)
MA ₁	4	0	39	96
MA ₂	2	0	33	168
MA ₃	0	2	31	336
MA ₄	0	4	34	480
MA ₅	0	6	32	600
MA ₆	0	8	35	600



A₁



A₂



A₃



A₄

Fig.1 MAA effects on the latex coalescing

The Influence of Adsorbed Layers of Silane Coupling
Agents on Protective Properties of Polymer Coatings.

M.A. Petrunin,
Physical Chemistry Institute,
Russian Academy of Sciences
31, Leninsky pr., Moscow,
117915, Russia.

A.P. Nazarov,
Physical Chemistry Institute,
Russian Academy of Sciences
31, Leninsky pr., Moscow,
117915, Russia.

Yu.N. Mikhailovski
Physical Chemistry Institute,
Russian Academy of Sciences
31, Leninsky pr., Moscow,
117915, Russia.

Abstract

The adsorption of different ethoxysilanes on aluminum and iron was studied. The influence of the surface coverage of the metal by silane on the adhesion and water resistance aluminum-epoxy adhesive joint was revealed. The improve of adhesion, hydrothermal and cathodic delamination stability of polymer coatings to the steel by adsorbed silanes was shown. An adsorption of silane monolayer is capable to inhibit the hydration of the surface oxide and Al corrosion in water. The formation of the surface siloxane polymer by modification of metals inhibits the corrosion under coatings. It is caused by the siloxane oligomers chemisorption and negative charging of the metal surface. The presence of negatively-charged layers cause difficulties of an electrostatic character for the migration of Cl^- ions to the metal surface.

Key terms: silane, adsorption, adhesion, inhibition, polymers, coatings.

Introduction

Polymer coatings are widely used for protection of metal constructions from corrosion. The protective properties are largely determined by the strength of the adhesion bond between metal and polymer, and by its stability to the action of aqueous media. Organic silanes have found wide use as promoters of adhesion and water resistance of polymer coatings on mineral

substrata [1]. The specific feature of these compounds is the universal promoting effect with regard to substrata and polymers of various types [2-4]. However, despite the intensive studies of the effect of silane adhesion promoters the mechanism of the effect of modifiers on strength and stability of the adhesion compounds metal-polymer is still not clear. The structure and properties of the surface compounds forming during modification and the interphase bonds nature, responsible for increased adhesion and water resistance at the interface metal-silane polymer are also needed to investigate.

The study of the mechanism of the promoting effect of silanes may help to determine the perspective ways of improving and making new anti corrosion polymer coatings with increased adhesion and water resistance. The subject of the present work was a study of the mechanism of the ethoxysilane adsorption layers formation on the aluminum surface and their effect on the strength and stability of adhesion joints in the systems metal-silane-polymer.

Experimental procedure

The adsorption of silanes on the Al surface was studied by the methods of piezoquartz micro weighing [5] and ellipsometry. A vacuum cell for this experiments was used for piezoquartz investigations. Quartz of the AT-cross-section with the basic oscillation frequency of 8000 kHz was used in the work. After a preliminary evacuation of air (a pressure of 10^{-6} mm Hg) a 100 nm thick aluminum film was deposited by thermal sputtering on the surface of the piezoquartz transducer from two sides. The thermal sputtering was carried out from a tungsten boat. The accuracy of the mass measurements was $6.9 \cdot 10^{-9}$ g/cm². The oscillation frequency of the resonator was measured using a frequency meter.

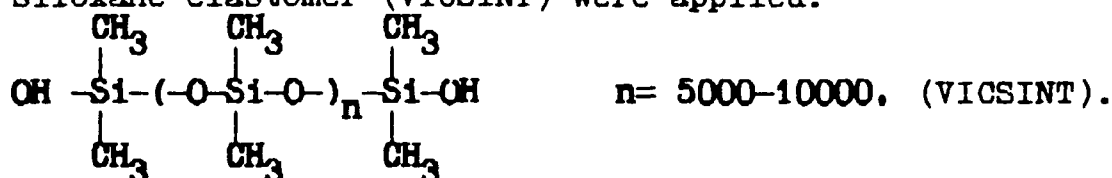
"The true surface area" of the metal was measured by the use of the BET method [6]. n-Octane with a vapor pressure of 10 mm Hg at 293 K (a landing site of its molecule is equal to 0.61 nm² [7]) was used as adsorbate.

To evaluate the adhesion strength we used the method of separation of the metal foil at the angle of 180°. To obtain each experimental point 5-7 samples were tested. The stability polymeric coatings to the cathodic delamination was studied by technique [8] in 0.3 M Na₂SO₄ at -0.8 V and -1.3 V. Peeling time and cathodic current were monitored. The working surface area was 7 cm².

Electrochemical experiments were made by the potentiodynamic method with the potential sweep speed equal to 1 mV/sec. The potential values are given relatively normal hydrogen electrode.

The structure and composition of the silanes used are given in Table 1.

The epoxy resin ED-20, copolymer of ethylene with vinylacetate SEVILEN and siloxane rubber LETSAR with primer on the basis of siloxane elastomer (VICSINT) were applied.



Results and discussion

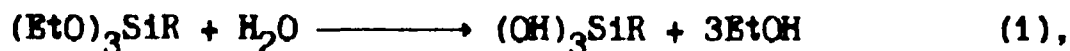
The piezoquartz weighing study of adsorption of silanes from a vapor phase was shown both reversible and irreversible adsorption for mono- (MS) and triethoxysilane (VS, PS, APS). The amount of the irreversible adsorbed silane is about one monolayer. The values of the "landing sites" (S) of silane molecules have been calculated (Table 2). There is the vertical location for APS and MS. The relatively high values S for VS and PS may point to their plane orientation with regard to the metal due to an additional interaction of the organic radicals with the surface. According to the BET equation [6] the energy of interaction of the adsorbate with the surface was calculated (Table 2). The low values indicate the presence of weak van der Waals interactions (H-bonds), arising during adsorption of silanes on the metal from the vapor phase.

To study the effect of water on the silane adsorption Al sputtered on piezoquartz was kept in H_2O vapour. Then the physically sorbed H_2O was removed, and the adsorption of silanes was measured. It was established that the presence of small quantities of water ($p/p_{\text{H}_2\text{O}} = 0.1$) decreases adsorption of

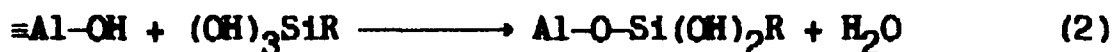
MS and VS [4]. Increasing the water content on the surface in the range of $p/p_{\text{H}_2\text{O}} = 0.2-0.5$ led to a proportional increase in

the amount of silane. The study of the adsorption of silanes on Al, kept in water vapour at high relative pressures ($p/p_{\text{H}_2\text{O}} \approx 1$)

showed that APS and VS during adsorption displace $\text{H}_2\text{O}_{\text{ads}}$ to the vapour phase. The experiments show, that a necessary condition of the formation of the covalent bonding of silane molecules with metal oxide of the surface is the presence of adsorbed water on the surface. The mechanism of silane chemisorption includes hydrolysis to form silanol:



and the condensation with hydroxyl groups of the surface:



The increase in the amount of adsorbed water leads to an increase in the surface concentration of silanol molecules and consequently, in the amount of the chemisorbate.

The investigations of silane adsorption on the metal surface from solution were made by the ellipsometry (from toluene, Fig. 1) and piezoquartz micro balance (from water, Fig. 2). It was established that triethoxysilanes adsorbed on the surface of aluminum and Fe as a polymolecular layer both from toluene and water solution. The thickness of vinylsilane adsorbed layer is 20 nm (Fig. 1, curve 2,3). A quartz microweighing study of the adsorption of silanes in aqueous solution showed (Fig. 2) that the amount of the irreversibly adsorbed silane in this case was 5-30 statistic mono layers : VS -30; PS - 10 ; APS - 5 mono layers. Vinyltriethoxysilane has the highest adsorption ability, 2-3 layers of vinylsiloxane oligomers are formed on the aluminum surface already at the concentration of 10^{-5} M. Monoethoxysilane (MS), incapable of the reaction of polycondensation, is adsorbed on metal as a monolayer, with the participation of only surface hydroxide groups (Fig.2, curve 3) and thickness of layer is 1 nm (Fig. 1, curve 1).

A quantitative evolution of the adsorption of silanes on Al may be applicable to the study of the promotion by silanes of the polymer adhesion on metals. We studied the effect of the degree of the filling by silanes of the metal surface on adhesion properties of the Al-epoxy adhesive joints. APS was used as a coupling agent. Silane was deposited on the Al foil surface from the vapor phase, its quantity was controlled by microweighing. According to the adsorption isotherm (Fig. 3, curve 1) silane was adsorbed on Al at several $p/p_{0\text{APS}}$. Then, epoxy resin was deposited on the Al, and the adhesion was measured. The samples with the APS adsorption at $p/p_0=0.05$ and with the coverage $\theta=0.3$ monolayer have the highest adhesion $F \approx 250$ g/cm. The adhesion strength increased by a factor of 2.5 as compared to the non-modified Al (80 g/cm). Increasing the degree of filling by silane (up to 1 monolayer) decreases the adhesion strength (Fig.3, curve 2). The preliminary keeping the foil with deposited silane in saturated water vapour led to an increase in dry adhesion (180 g/cm) with increasing the coverage of Al by silane (Fig. 3, curve 3). It was shown above, that the chemisorption of silane is determined by the concentration of $\text{H}_2\text{O}_{\text{ads}}$. The adsorbed water, which is not removed by evacuation [5] is found on the Al foil surface. The amount of this H_2O is necessary for chemical bonding of only a part of silane ($\theta \leq 0.3$). The adhesion is provided by molecules of APS bonded covalently with the surface and by the interaction of the functional groups (epoxy-, amino-) of the polymer with active centers of the metal surface. The increase in the coverage by the adsorbate molecules ($\theta > 0.3$) that do not have chemical bonds with the surface (due to lack of H_2O on the

Al surface) prevent the formation of adhesion bonds between functional groups of the epoxy coating and of the metal and the adhesion is decreased. Keeping the silane-coated Al surface in H₂O vapour leads to the formation of covalent bonds for all the adsorbed silane molecules. Therefore the adhesion strength remains constant (Fig. 3, curve 3) with increasing silane quantity. This indicates that the promotion of adhesion is only due to formation of the aluminosiloxane bonds Al-O-Si.

One of the most significant characteristics of polymer coatings is water stability. The study of the water resistance of epoxy resin on aluminum modified by APS shows that the presence on the surface of a chemisorbed silane monolayer is not suffice for providing high resistance of the coating in water (a full delamination is after 2 days, without modification - 1 day) (Fig. 3, curve 1,2). The modification of the surface from an aqueous solution ($10^{-4} < [\text{APS}] < 0.017 \text{ M}$) leads to an increase in the time of separation of the coating (6 days). At the concentration of the modifying solution 0.017 M and higher, aluminum-epoxy joint preserved high adhesion strength (>200 g/cm) after a 20 day's test (Fig. 3, curve 3). In this case a polymolecular siloxane layer is adsorbed on the surface. At the interface the diffusion of epoxy resin and amino siloxane occurs to form "interpenetrating network" and the covalent bonding of the modifier and polymer components. As a result transition zone bonded with the metal is formed. This is necessary for providing high water resistance of coatings.

The results obtained for epoxy resin may be used for other polymer coatings. The adhesion and hydrothermal stability of siloxane rubber with polymethylsiloxane primer VICSINT was studied. It was noted that the chemical nature of the organic radical of the silane has a marked effect on the adhesive strength of the coating to the metal. Thus with the use of APS which has a polar group in the organic radical - we find that there is some reduction in the adhesion of the coating ($F = 0.3 \text{ kg/cm}$). In the cases of GPS, DES, VS, we saw an increase in adhesive strength (1.0, 1.2, 1.4 kg/cm, respectively) compared to the unmodified specimens (0.5 kg/cm). The character of the separation from the modified surface was for most part cohesive, while it was always adhesive failure in the case of the unmodified surfaces (100% of the primer remain on the strip). In order to create the transition zone bonded with the steel we grafted amino groups onto the primer by introducing APS. A GPS having an epoxy group in the organic radical was applied to the steel surface. The amino groups will be react with surface epoxy groups (eq. 3). In adhesive strength tests of such a coating, we observed 100% cohesive separation ($F = 1.0 \text{ kg/cm}$).



The hydrothermal stability of this joint was investigated. The

complete peeling for the non-modified steel surface was 24 h. In the presence of the silanes, cohesive separation of the coating from the metal was seen when the specimens were held in boiling water for 1000 h. Thus, no significant hydrolysis of the Me-O-Si chemical bonds of the coating occurred during the tests.

Adhesion promoters of silanes at metal-polymer interface may be expected to prevent overcoats from cathodic peeling. The steel samples were primed with the silanes and overcoated with a siloxane rubber or copolymer of ethylene and vinylacetate (SEVILEN). The coating integrity was determined by the time required for complete peeling and by the change in cathodic current at -0.8 V in $0.3 \text{ M Na}_2\text{SO}_4$. As seen in Table 3 an increasing number of silane adhesion centers can lengthen peeling time of a coating by a factor of 50 to 1000 and thereby raise its service life on cathodically protected structures.

In our recent work [9] is shown adsorption silane and silanol to results in formation of surface siloxane complexes with Fe-O-Si bonds. This considerably raised the adhesion and water resistance of siloxane polymer to the mechanical action of evolving hydrogen. We believe the adsorption of silanol can decrease the hydrolysis of surface iron oxide (Fe_2O_3) and convert it to hydroxide with less cohesion. In addition, the presence of silane adsorbed layer at the metal-polymer interface leads to the inhibition of interfacial bonds hydrolysis.

Besides the adhesion and water stability it is important to control the corrosion processes at the interface metal-polymer. The occurrence of the corrosion under the polymer coatings is determined by the presence at the interface of a phase water film [10]. Corrosion tests of the modified samples were carried out to study the behavior of Al in water. For this one silane monolayer was sorbed on aluminum sputtered on a piezoquartz resonator. After that it was kept in water, dried in vacuum and the hydration rate of Al_2O_3 was measured (Fig.4). The obtained data indicate that the monolayer chemisorption of silane can decrease by 1.5-2 times the interaction rate of the metal with H_2O . According to the degree of the hydration inhibition of the oxide film the silanes may be arranged in the following series: $\text{VS} > \text{PS} > \text{APS} > \text{MS}$. The strongest effect was observed in triethoxysilanes, which are able to form surface linear siloxane chains: $=\text{Al-O-Si(R)-O-Si(R)-O-Al}=$ or to bond the neighboring Al atoms: $=\text{Al-O-(OH)Si(R)-O-Al}=$ of the surface.

In our recent work [11] was shown the inhibition the local corrosion of metals by formation at the interface metal-electrolyte negative charged surface layers (10-20 nm). In 0.001 M NaCl unmodified Al undergo a pitting corrosion with marked weight loss (Fig.5 curve 1). This data was obtained by the piezoquartz microweighing. The negative charged silane layer decreases of Cl^- adsorption at the interface. The

The ion-exchange and charging properties of silane surface layer are maintained in the presence of coating. The electrochemical investigations of coated metal electrodes are carried out. The systems Al-epoxy and steel-siloxane were used. For electrochemical experiment, we chose specimens have coatings of the same thickness and similar ohmic resistance. The anodic polarization curves are shown in Fig. 6,7. It was shown that the presence of positive charged APS ($-\text{CH}_2\text{NH}_3^+$) at the interface Al-epoxy lead to increase of anodic current of metal dissolution under coating (Fig.6, curve 2) in comparison with unmodified Al (curve 1). The modification of Al by GPS, forming the negative charged layer ($=\text{Si}-\text{O}^-$ groups) on the surface, reduce anodic current (curve 3). The siloxane elastomer (VICSINT) is modified by the introduction of silanes into a polymer matrix. It is shown that APS increase and the ethoxysilanes, which have negative charges in molecules, inhibit the anodic dissolution of steel under siloxane coating (Fig.7). The polymer layer in close proximity to the surface has properties of a ion-exchanger. In the case of positive charged modifier (APS) the epoxy resin and siloxane have properties of anion-exchanger and there is the promotion of aggressive ions (Cl^- , SO_4^{2-}) penetration through coating to the interface metal-polymer. That give rise to the increase of the rate of Al corrosion and anodic dissolution of steel. In the case of negative charged silanes (GPS, DES) the polymer matrix is the same as a cationexchanger and prevent the Cl^- adsorption and corrosion of metals. Hence, the addition of charged silanes at the interface metal-polymer is the perspective way of improving of anticorrosive properties of polymer coating.

References

1. E.P. Pluddemann, Silane coupling agents, (Plenum Press, N.Y., 1982), 263 p.
2. P.E. Cassidy, B.J. Yager, J.Macromol.Sci.-Revs.Polymer Technol, 1 (1971): p.1.
3. H. Leidheiser, M. De Costa, R.D. Granata, Corrosion, 43 6 (1987): p. 382.
4. Nazarov A.P., Petrunin M.A., Mikhailovsky Yu.N., "The role of the adsorption of silane coupling agents in the interfacial interactions metal-polymer coatings", 11th INT. COR. CON., (Florence, Italy, 1990) V.1, p.225.

5. P.V.Strekalov, A.A.Mikhailov, Yu. N. Mikhailovsky, Zashita metallov, 19 (1983): p.179 (rus).
6. S. Brunauer et.al., The solid-gas interface, E.A. FLOOD Ed., (Marcel Dekker Inc., N.Y., 1967), p.347.
7. A.L. McCellan, H.F. Harnsberger, J.Colloid and Interface Sci., 23 (1967): p. 577.
8. M.A.Petrinin, A.P. Nazarov, Yu. N. Mikhailovsky, Zashita metallov, 26 4 (1990): p.759 (rus).
9. M.A.Petrinin, R.M. Zaitzev, A.P. Nazarov, Yu. N. Mikhailovsky, Zashita metallov, 26 5 (1990): p.587 (rus).
10. W. Funke, JOCCA, 68 (1985): p. 229.
11. A.P. Nazarov, M.A.Petrinin, Yu. N. Mikhailovsky, Zashita metallov, 28 (1992): p.564 (rus).

Table 1. The structure formulae of the used silanes.

Name	Chemical formula
MS	$(\text{CH}_3)_3\text{Si}(\text{OC}_2\text{H}_5)$
VS	$\text{CH}_2=\text{CH}-\text{Si}(\text{OC}_2\text{H}_5)_3$
PS	$\text{C}_6\text{H}_5-\text{Si}(\text{OC}_2\text{H}_5)_3$
GPS	$\text{CH}_2-\text{CH}(\text{O})-\text{CH}_2-\text{O}-(\text{CH}_2)_3\text{Si}(\text{OC}_2\text{H}_5)_3$
APS	$\text{NH}_2-(\text{CH}_2)_3-\text{Si}(\text{OC}_2\text{H}_5)_3$
DES	$(\text{CH}_3)_3\text{Si}-\text{O}-\text{C}(\text{O})-(\text{CH}_2)_{10}\text{Si}(\text{OEt})_3$
IDC	$\text{Na}^{2+}[(\text{CH}_2\text{COO})_2\text{NCH}_2-\text{CH}(\text{OH})-\text{CH}_2-\text{O}-(\text{CH}_2)_3\text{Si}(\text{OC}_2\text{H}_5)_3]^{2-}$
TA	$\text{J}[(\text{C}_2\text{H}_5)_3\text{N}^+\text{CH}_2-\text{CH}(\text{OH})-\text{CH}_2-\text{O}-(\text{CH}_2)_3\text{Si}(\text{OC}_2\text{H}_5)_3]$

Table 2. Values of the "landing sites" and the adsorption heats of the ethoxysilane molecules.

Adsorbate	S, nm/mol		Adsorption heat kcal/mol
	BET equation	Langmuire eqn.	
VS	0.77	0.65	1.75
APS	0.40	0.35	2.31
PS	0.94	0.52	1.86
MS	0.33	0.31	1.66

Table 3. Time of total delamination (t) of siloxane polymer (VICSINT) and copolymer ethylene with vinylacetate (SEVILEN) during cathodic polarization in 0.3 M Na₂SO₄. Metal (carbon steel) electrodes are modifiede by silanes.

Coating on steel (Pol)	t, min	Coating on steel (Pol)	t, min
VICSINT, E=-0.8 V (nhe)		SEVILEN, E=-1.3 V (nhe)	
Pol	0.6	Pol	30
APS + Pol	395	APS + Pol	1720
VS + Pol	310	Methacril + Pol silane	360
VS + (Pol + APS)	1160	(GPS + APS) + Pol	1160
Pol + APS	54	GPS + Pol	180

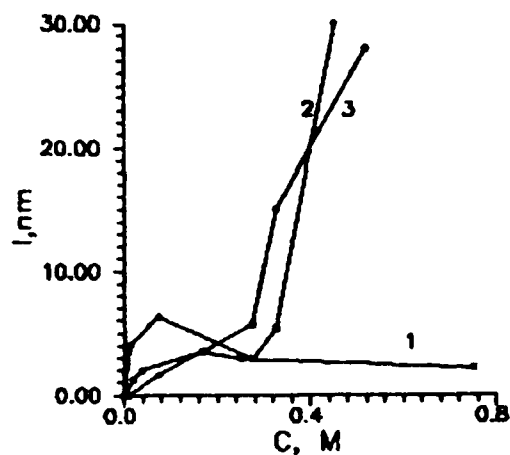


Fig. 1

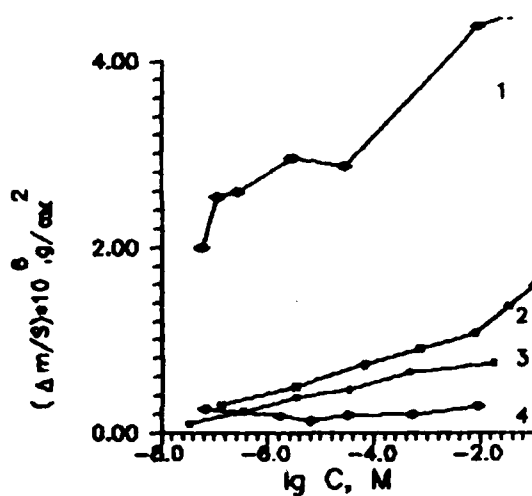


Fig. 2

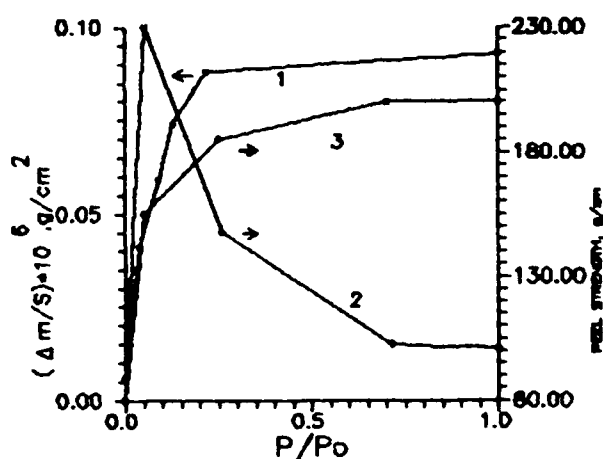


Fig. 3

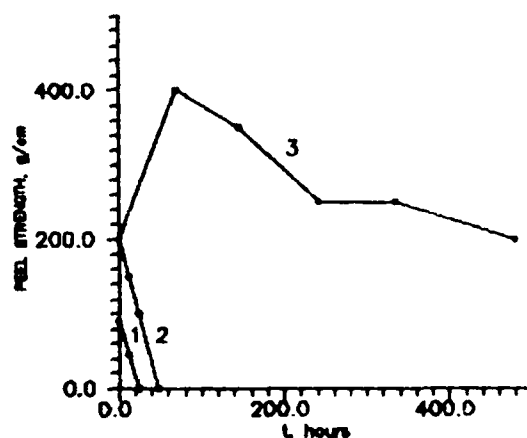


Fig. 4

Fig. 1. Isotherms of adsorption of silanes on Al from toluene solution on aluminum (1,2) and iron (3), 1-TS, 2,3- VS. Results was obtained by ellipsometry.

Fig. 2. Isotherms of adsorption of silanes on Al from water solution 1-VS, 2-APS, 3-TMS, 4-PS. Results was obtained by quartz microbalance.

Fig.3. Isotherm (1) of irreversible adsorption APS on Al and adhesion strength (2,3) of joints epoxy-APS-Al foil (2) and epoxy-APS- Al foil preliminary keep in H_2O vapour (3).

Fig. 4. Hydrothermal stability of adhesive joints Al-epoxy (1). Al is modified by APS : 2.- 1 monolayer from vapour phase; 3.- from aqueous solution $[APS] = 0.017 M$.

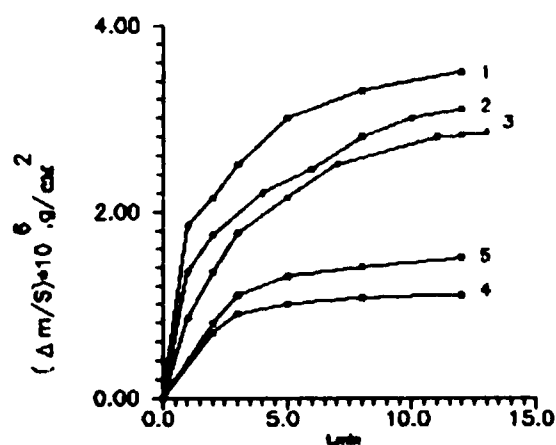


Fig. 5

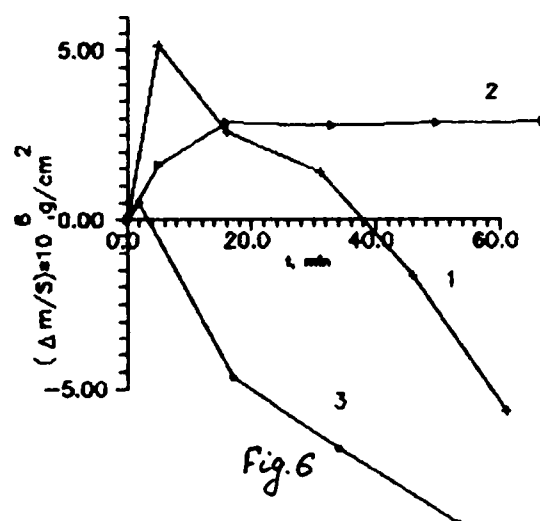


Fig. 6

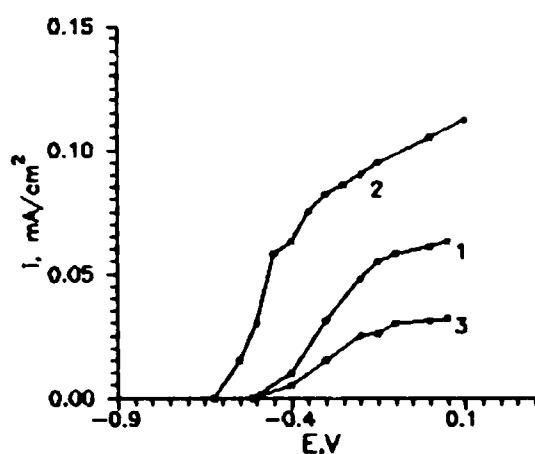


Fig. 7

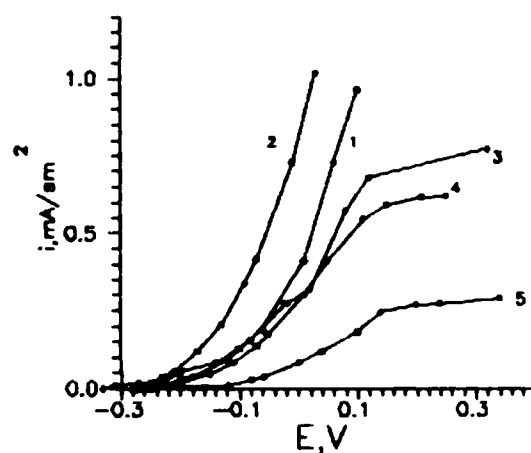


Fig. 8

Fig. 5. Kinetic of hydration of oxide film on Al modified by silanes (1 monolayer deposition from vapour phase) in distilled water. 1.- Al; 2.- TMS; 3.- APS; 4.- VS; 5.-PS.

Fig. 6. Corrosion of Al (1) modified by silanes (1 monolayer) 1.- Al; 2.- IDC; 3.- TA, 0.001 NaCl, pH 6.

Fig. 7. Anodic polarization curves of Al(1) with epoxy resin ED-20 in 0.1 M NaCl pH 6.5. The electrodes are modified by silanes 2 - APS; 3 - GPS.

Fig. 8. Anodic polarization curves of carbon steel (1) with siloxane coating VICSINT in 0.1 M Na₂SO₄ pH 6.5. The silanes APS (2), GPS (3), DES (4), VS (5) are introduced into polymer matrix.

Research of Weather Resistant Bridge Paint and Wear Resistant Primer and Finish Paints for Bridge Cover Plates

Yu Shaoyu
China Academy of Railway Sciences
Wei Gong Cun, Haodian District
Beijing, China, 100081

Abstract

Large quantity of steel, therefore, large quantity of paints and coatings are used on Chinese Railways. For the purpose of improving the service life of steel bridges, power transmission towers, and wagons, reducing maintenance work high above the ground, and extending re-coating period, lamellar micaceous iron oxide (abbreviated as MIO) pigment, weather resisting MIO bridge paint, wear resisting primer and finish paints for bridge cover plates have been developed.

After years of research and trial, grey and red MIO pigments have been produced successfully. Physic-chemical tests including scanning electronic micrographic and X-ray diffraction methods have verified that the main content of the pigment is $\alpha\text{-Fe}_2\text{O}_3$. It has features of lamellar structure, inert, non-toxic and weather resistant.

A series of MIO finish paints, under coat paints and primer paints with different special characteristics have been developed using MIO pigment and different sorts of resins. Sample plates painted with these mated coatings were subjected to accelerated ageing, humidity, salt spray tests and outdoor exposure tests. Test results has shown that mated coatings have excellent performances. MIO mated coating on the Nanjing Yangtze River Bridge, the Wuhan Yangtze River Bridge, the Yellow River Bridge and other railway bridges has shown 3-4 times longer service life than the coating used in the past. Up to June 1991, the MIO mated coating on the Nanjing and Wuhan Yangtze River Bridge claimed 15 years of service and will continue to be in service. The economical benefits due to extended repainting cycle are significant. This kind of armour paint is also applied to the Jiujiang Yangtze River Bridge and a Burmese Bridge to which China rendered assistance in its construction. They are also expected to find application on high-speed and heavy haul railway bridges.

To meet the needs of the Nanjing and Wuhan Yangtze River Bridge, the SO6-1 cover plate prime and SO4-2 cover plate finish have been developed. For these, corrosion inhibiting pigment and the wear resistant pigment were used together with polyurethane vehicle (two packages). Laboratory test showed the abrasion resistance of the paints was 9 times that of the paint products used in past. Up to the moment, 16 years have passed since they were coated on the Nanjing Yangtze River Bridge.

Introduction-MIO Bridge Paint Enjoys a High Reputation

Chinese railways own more than 3,800 steel bridges amounting to over 240 km in length, and a great quantity of paints is required for their protection. In the past, 316 grey finish, formulated by granular zinc white, TiO and long oil alkyd resin (316 finish in short) was used. It has only a service life of 2-4 years. Afterwards, 66 finish paint, formulated by aluminum-zinc powder and long oil alkyd resin, was used having a service life of 10 years in Beijing area [1,2]. Finally, CO4-9 grey MIO modified alkyd enamel finish paint (CO4-9 finish) was developed by a research group led by CARS. The CO4-9 finish paint has a service life of more than 15 years.

The research group has set a MIO pigment production base in China. The crude MIO ore is put into a process of selection, milling, dressing and etc.. The final products are grey color and red color MIO pigments. A lot of work has been done on studying the technological process and the effect of MIO particles on the performance of the paint. Red and grey MIO pigments are used in producing red MIO primer paint and grey MIO finish paint respectively. Both of them have anti-ageing performance better than 66 grey finish paint. The grey MIO finish Paint saves TiO and zinc powder, while red MIO primer paint can replace iron red primer when added with some corrosion resistant pigment.

Laboratory test data show that the CO4-9 finish presents a service life 3-4 times longer than the former paints. Its service life estimated under the climatic conditions in Beijing area may last over 15 years. It is the first such kind of paint produced in China, and makes Chinese bridge coatings join the ranks of the technical advanced world. It also won a Prize from the International Surface Technique and Anti-Corrosion Products Exhibition in 1991. It has been approved by an official appraisal organized by the Science and Technology Department of the Ministry of Railways.

We have also developed SO6-1 polyurethane primer and SO4-2 polyurethane finish formulated with anti-wearing pigment for bridge cover plates which laid under sleepers on the bridge sustaining successive vibration and abrasion, and corroded by water or liquid drops.

Properties of Lamellar MIO

Micaceous iron oxide is by definition an iron oxide with mica appearance. It is a natural mineral ore formed 280 million years ago in the carbonic period. It is a kind of hematite also named as iron glance with shinny black-grey color. The fine ground MIO particle is black shinny tiny tablets. But the tablets turn into red-brown color and transparent while the tablets become very small and thin.

MIO has a constituent of α -Fe₂O₃ and some protoxides, SiO₂, Al₂O₃, Ca, Mg Salt, etc.. Its main constituent α -Fe₂O₃ is non-toxic. It is chemically inert to acid, alkali, salt, etc., and capable of reflecting ultra-violet light, thus protecting the coat from degradation and chalking. MIO has an inherent ability of insulation. Therefore, MIO paint film can prevent the surface from dewing. It is not poisonous nor sensitive to light. It can very

well stand the damaging effect of high temperature, sunlight, rain, dew and snow. MIO lamellae, when used as a pigment in paint, lap and overlap each other parallel to the paint surface. This formation makes the paint inherently resistant to moisture permeation, raises the durability of the coating 10-20 years. Therefore, the MIO coating has a reputation of "armour coating". In the recent several decades the MIO paint has been popularly applied abroad [3,4,5,6,7]. Special paints prepared with MIO pigment can be applied to bridges, cars, steel towers, gas tanks, petroleum storage tanks and pipe lines, ship building, chemical plants and exposed to industrial exhaust gases and chemical atmosphere.

Study, Test and Their Results

I. MIO pigment study, test and their results [1,2,8]:

The crude MIO ore is put into a process of selection, milling, dressing for study purpose and a grey MIO is successfully developed for preparation of finish and undercoat, and a red MIO pigment for Primer paint. Technical index for MIO pigment has been mapped out. In order to get MIO pigment with thin lamellar structure, we have explored several mineral sources, studied different processing technologies on the effect of the formation of the lamellar. The test results are as follows:

A. China Tieyanfan (MIO 1-4) grey MIO pigment, contains more than 93% Fe_2O_3 has a lamellar structure as shown in Fig.1.

B. x-ray diffraction indicates that the MIO has a high content of very stable $\alpha\text{-Fe}_2\text{O}_3$, as shown in Fig.2.

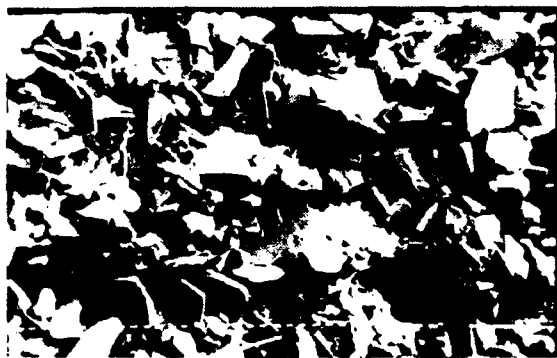


Fig.1 SEM of China Tieyanfan (MIO 1-4)

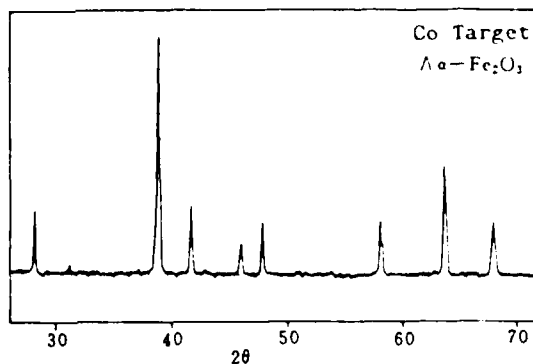


Fig.2 X-ray diffraction pattern of China Tieyanfan MIO pigment

C. The physical and chemical properties of the MIO pigment are given in Table 1 and 2.(see Appendix).

II. Study of long-life weather resistance bridge paint (CO4-9 grey MIO modified alkyd enamel paint) [1,2,8,9,]:

The CO4-9 finish and the epoxy polyamide finish (H51-19) with good resistance to chemicals have been developed through a series of formulation experiments based on the MIO pigment as the chief component added with long oil alkyd and others of good weatherability, anti-settling agent, solvent, drier, etc., all being mixed at high speed.

The results are as follows:

A. The physical and chemical properties are given in Table 3. (see Appendix)

B. The test results for artificial ageing and film thickness decrease due to chalking are given in Fig.3.

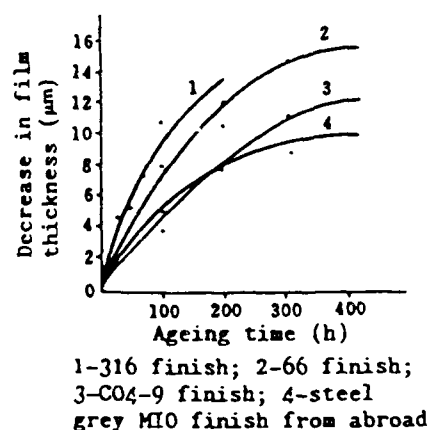


Fig.3 Film thickness decrease rate due to ageing and chalking

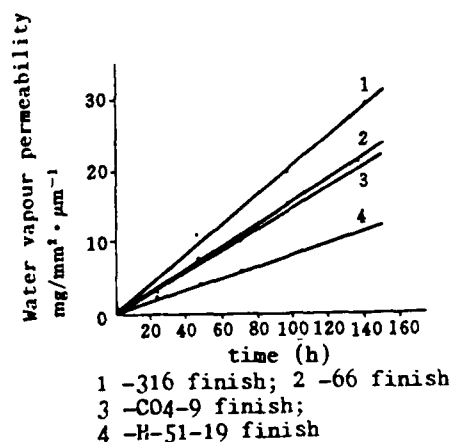


Fig.4 Water vapour permeability

Through weight loss by chalking method we have learned: when the weight loss by chalking curve of alkyd finish paints exposed in the outdoor atmosphere coincides with weight loss by chalking curve obtained by modified artificial ageing testing machine in our laboratory, then the 24-hour artificial ageing corresponds to 1-year exposure in Beijing area [9]. Therefore, we can learn from our artificial ageing tests that, the CO4-9 finish has its chalking resistance and weatherability 1-3 times better than the 66 finish. 66 finish has a service life of about 10 years, and starts chalking in 120 hours, corresponding to 5-year exposure in Beijing area, while tested in an improved ageing testing machine. On the other hand, CO4-9 finish paint shows no chalking after 200 hours, shows slow decoloration, and keeps basically the same after 400 hours ageing. 400 hour-ageing corresponds to a service life of 15 years in Beijing area according to the comparison between ageing samples and samples exposed outdoor. From the surface appearance, it can be deduced that CO4-9 finish paint has a service life of 15 years if used in Beijing area. From the determination of weight loss due to chalking, the CO4-9 finish has a lower thickness decrease rate than both the 316 and the 66 finishes.

C. Exposure tests conducted in Guangzhou with different mated coatings have revealed that: 66 finish usually took 4 months before chalking slightly and 10.5 months before chalking significantly, while 7.5-21 months were necessary for CO4-9 grey MIO alkyd finishes to become slightly chalky and 21-36 months to become significantly chalky. That is to say, MIO paints got chalky in 1-3 times as much time as 66 finish. 66 finish has a service life of over 10 years in the Beijing area, so MIO alkyd finishes are expected to be in effective service for at least 15 years.

D. The results from film moisture permeation test are given in Fig 4.

E. The results from film ultraviolet reflection test are given in Fig 5.

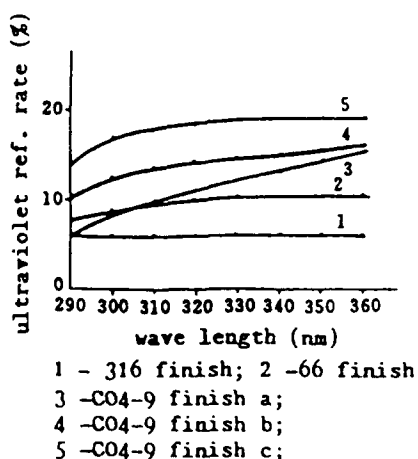
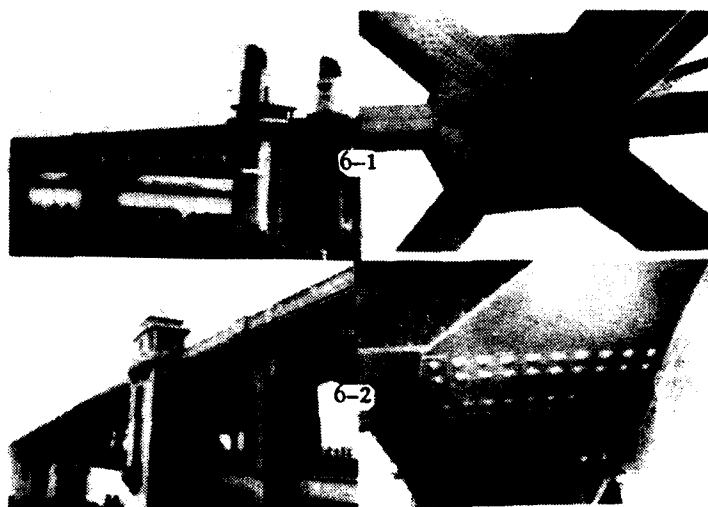


Fig.5 Film ultraviolet reflection rate



Figs. 6-1 & 6-2 Nanjing Wuhan Yangtze River Bridges applied CO4-9 finish film in good condition after 15 years

III. Test results of wear resisting primer and finish paints for bridge cover plates [8] The successfully developed SO6-1 yellow-brown polyurethane corrosion resistant primer finish has properties of strong adhesion, high anti-corrosion, tough film, water resistant, humidity and heat resistant and non-active to chemicals. It combines very well with the fusion spraying zinc layer, and is proper to be the primer finish for cover plates. SO4-2 grey polyurethane finish paint for bridge cover plates possess an excellent wear resistance. The paint film is hard but not brittle, anti-impact, quick in drying, and can be very thick.

SO6-1 and SO4-2 mated coating passed through physical and mechanical properties tests, and met all the technical requirements. While tested on Taber Abraser, tests results revealed that, SO6-1 and SO4-2 mated coating has a wear resistance 9 times of that of the mated coating previously used. The mated coating has been coated on fusion spraying and non-spraying layers of the cover plates on the Nanjing and Wuhan Yangtze River Bridge. The coating has been proved to be high wear resistant, and a service life of 16 years is expected.

Field Coating Investigation

During the months from May to June in 1976, the CO4-9 finish was applied to the Yangtze River Bridges at Nanjing and Wuhan (on the existing coat). The steel bridges had been shot blasted to Sa 2 1/2 class and then immediately sprayed with red lead primer or MIO/polyurethane primer. The total dry film thickness of finish and primer was over 200 micrometers. In June 1991, after a weathering and corrosion resistance test of 15 years on these two bridges, a field investigation was taken to find that the film was in good condition, without any corrosion (see Fig 6-1, 6-2), still glossy at the shaded part, with good adhesion, without obvious chalking, cracking or spalling (except places with accumulated water or liable to impacts) [10,11]. It has been applied to the Yellow River Bridge and many bridges in various railway administrations for many years with satisfactory results. The H51-19 finish together with zinc rich epoxy primer and MIO undercoating have been applied to locomotive frame with good results. A Railway Ministerial Standard TB 1572-84 "Railway Steel Bridge Protective Coating" was issued in 1984. National Standard GB 8755-86 for the MIO pigment was brought into effect in 1986.

SO6-1 and SO4-2 mated coating for bridge cover plates has been applied on large numbers of bridges.

Conclusions

MIO pigment and Weather Resistance Bridge Paint CO4-9 and Wear Resistant cover plate paint have the following good properties:

1. MIO pigment has a lamellar structure, small water-vapor permeability, good water and humidity resistance.
2. Good chemical stability, weak sensitivity to light and durable against sunlight, rain, dew, frost, snow etc.
3. Good shielding effect for the primer and interfacial bonding between the finish and primer paints.
4. Excellent resistance to weathering with a service life over 15 years in Beijing area under the condition of specified coating requirements.
5. The estimated service life based on laboratory test data agrees with the figure of 15 years obtained from the observed data on field bridge coatings. CO4-9 finish is a weather resistant bridge paint and can also be applied to outdoor steel structures.
6. The over plate mated coating has excellent properties especially good in wear resistance. It lasts 9-times longer than the coating used in the past.

Besides, in cooperation with related units, the author has also developed MIO coating series for use in different areas. Such as, B825 acrylate polyurethane mated coating, organic zinc rich primer and MIO under coating, MIO chloride rubber mated coating and MIO chlorosulfonated polyurethane mated coating. All of them have been put into service.

Appendix:

Table 1 Physical & Chemical Properties of MIO Pigment

Item	Indices	Product conformity to indices	Test method
Iron content expressed as Fe_2O_3 , Min. (%)	93.0	93.0	GB6755-86 2.1
SiO_2 content, Max. (%)	3.0	3.0	GB6755-86 2.2
Volatile matter at 105°C , Max. (%)	0.5	0.14	GB5211.3-85
Matter soluble in water Max. (%)	0.1	0.09	GB5211.2-85
Residue on sieve of mesh 63 μm , Max. (%)	1.0	0.8	GB1715-79 method A
pH of aqueous extract	6.0-8.0	7.2	GB1717-86
Oil absorption value (%)	9.0-12.0	11.3	GB1712-79
Appearance	steel grey lamellar powder	same as left	

Table 2 MIO Pigment Resistance to Chemicals

Item	Grey MIO 1-1 Weight loss*
HCl(1;3)	1.93%
HNO_3 (1;3)	0.85%
H_2SO_4 (1;3)	1.54%
10% NaOH	0.29%
3% NaCl	0.31%
Loss on ignition (900°C)	0.31%

* Weight loss in 10 days at normal temperature.

Note: Thickness and lamellar size of MIO pigment must be as specified.

Table 3 Physical & Mechanical Properties

	66 finish	C04-9 finish	H-51-19 finish (packed separate)	Remark
Colour & appearance	neat & smooth film	grey to silver grey, neat & smooth	neat & smooth	GB1729-79
Viscosity, min. (s) Tu-4 Visc. cup at $25^\circ\text{C} \pm 1^\circ\text{C}$	45	145	145	GB1723-79
Fineness (μm)	75	80	80	GB1724-79
Drying time(h): at $25^\circ\text{C} \pm 1^\circ\text{C}$				
surface dry	12	10	2	GB1728-79
dry hard	24	24	24	
Toughness (mm)	1	1	1	GB1731-79
Impact strength (kg · cm)	50	50	50	GB1732-79
Adhesion grade, max.	2	2	2	GB1720-79
Humidity cabinet test, at $47 \pm 1^\circ\text{C}$ for 420h, RH over 95%	local small blisters	no change except turning yellowish	no change	GB1740-79 GB1765-79
Salt spray test 3.5% NaCl for 400 h, at $40 \pm 1^\circ\text{C}$	small blisters	no change	no change	GB1771-79

REFERENCES

1. 铁科院金化所防腐室等三单位: 新型云母氧化铁桥梁面漆研究试验报告 1978. 4
2. 余少玉、吴秀霞、穆瑞君: 采用云母氧化铁颜料延长钢梁面漆使用寿命的研究 1978. 8
3. 山本洋一: 涂料の研究 NO72. 1969 5-9
4. FANCUTT, F: Paint Munufacture V. 35, 12 1965
5. Nassberg, B: American Paint J. V. 54. 1970 68
6. Bishop, D.M. JOCCA, V. 64. 1981. 57-74
7. Claxton, A. E., Official Digest, 36, (470), 1964, 268
8. 余少玉: 我国桥梁涂料的发展<<涂料工业>> (2) 1985. 36-39
9. 铁科院金化所防腐室: 油漆大气暴晒与人工老化相关系数试验小结(粉化失重法) 1976. 12
10. 武汉长江大桥桥工处: 灰色云母氧化铁桥梁面漆检查报告 1991. 6. 23.
11. 南京长江大桥管理处: 灰色云母氧化铁桥梁面漆在南京长江大桥上使用情况介绍 1991. 6. 29.

Determination of Water Transport Properties of Organic Coatings with EIS

L. Nicodemo, T. Monetta and F. Bellucci

Department of Materials and Production Engineering
University of Naples Federico II
Piazzale Tecchio 80125, Naples, Italy

Abstract

The Electrochemical Impedance Spectroscopy (EIS) technique was used to evaluate the water transport properties of free standing polyimide (Kapton® and PMDA-ODA) and polyethyleneterephthalate (PET) membranes at 25 and 40 °C, respectively, and in supported PMDA-ODA-coated metals. Transport properties of free standing films were also obtained by using the MacBain quartz spring balance in order to assess the reliability of the EIS method when compared to the classical technique.

Results from this work show that transport properties obtained with EIS are in reasonable agreement with those obtained with the classical gravimetric method. In addition, the theoretical analysis presented in this paper indicates that transport properties of water through free standing and applied films (paints) can be obtained from EIS only when specific requirements are met.

Key terms: EIS, organic coatings, transport properties

Introduction

Changes in electrical properties during the exposure of organic coating systems to aqueous environments have been the subject of many investigations starting principally with the work of Wormwell and Brasher¹ in the early '50s, followed by the papers of Brasher and Kingsbury² and of Gentles³. In these papers an electrical capacitance method was first introduced to evaluate the water uptake of paint films on metal immersed in sea water. The method of calculating the water uptake of a paint film from observed capacitance values used by the authors cited above is based on a modification of an original formula given by Hartshorn, Megson and Rushton⁴. The application of this formula to a paint containing water at any time t and at zero time requires the assumption that the distribution of water into the paint film is random and uniform, and leads to:

$$\phi = \frac{\text{Log}(C_t/C_0)}{\text{Log}\epsilon_{\text{H}_2\text{O}}} \quad (1)$$

where, C_t is the capacitance at time t , C_0 the capacitance at time $t=0$, and the dielectric constant of pure water. The value of C_0 is obtained by a linear extrapolation of $C_t(t)$ for $t \rightarrow 0$ ^{1-3,5}. The capacitance at $t=\infty$, C_∞ , is taken as the value of the capacitance after the appearance of a plateau, indicating that equilibrium has been reached and the film is fully saturated with water. The equilibrium water uptake is obtained using equation 1 with $C_t=C_\infty$. Less attention has been paid in

the literature to: (i) the determination of the water diffusion coefficient via capacitance data, (ii) the method of obtaining C_0 , and (iii) the testing of the capacitance method on free standing polymeric films.

The aim of this work is to compare the capacitance or EIS method with the more usual gravimetric method of measuring water uptake on free standing polymeric films. Then, the EIS method will be applied to supported films (on metallic substrate) in order to ascertain the influence of the electrochemical reaction at the metal-polymer interface on the capacitance change with immersion time. As will be shown in the following, a correct use of the EIS method will allow to evaluate the water diffusion coefficient through coatings in both the free standing and the coated configuration.

Theory

The model proposed in this paper to evaluate water transport properties of polymeric films using the EIS is based on the assumptions that: (i) the change in capacitance is due entirely to the permeation of water into the film, (ii) the permittivity of the absorbed water is constant (equal to 78.54 and 73.35 at 25 and 40 °C, respectively), and (iii) the swelling of the polymer film can be ignored. As far as point (i) is concerned, two different models will be presented and discussed. In the first model (Discrete Model, DM), the electrical analog of the free standing film is represented by a capacitance in parallel with a resistance; in the second model (Continuous Model, CM) the film is represented by an infinite series of capacitance and resistance in parallel. A schematic of the equivalent circuits of these models as related to the water concentration profile in a film of thickness L at time t , is shown in Fig. 1a and b, respectively. In the following sections these two models will be described in detail.

DM Model: According to this model it is assumed that the water concentration profile into the homogeneous polymer is flat at any time t between zero and infinity (equilibrium). Water profiles variations occur, in this case, by step and the water concentration is a function of time t not of the abscissa x . The equivalent analog can be assumed as composed by a parallel RC circuit. Equation 1 is used as basic relationship between mass uptake, expressed as volume fraction, ϕ , and capacitance change, expressed as C_t/C_0 . To use this equation, however, the dry film capacitance C_0 , should be a known value. Since this value is not known "a priori" it must be extrapolated from the the time behavior of the capacitance itself as will be shown below. Assuming that equation 1 holds true, one has:

$$\frac{C_t}{C_0} = e^{\alpha\phi} \quad (2)$$

where α is a constant given by: $\alpha = 2.3 \text{Log} \epsilon_{\text{H}_2\text{O}}$. For small values of the equilibrium water uptake ($\phi_{\infty} \ll 1$) equation 2 can be expanded in series yielding:

$$\frac{C_t - C_0}{C_{\infty} - C_0} = \frac{\phi}{\phi_{\infty}} \quad (3)$$

where $(C_t - C_0)/(C_\infty - C_0)$ is defined as the dimensionless film capacitance (DFC). Since the volume fraction $\phi = \phi_\infty M_t / M_\infty$ (where M_t denotes the total amount of diffusing substance which has entered the film at time t , and M_∞ the corresponding quantity after infinite time), it can be concluded that all kinetic expressions M_t / M_∞ reported in the literature and describing the uptake of water in polymers, can be easily translated into DFC equations by using the relationship 3. In the case of a free film of thickness L , exposed to a uniform and constant concentration of diffusant with a zero initial concentration of the diffusant into the film, taking the expression of M_t / M_∞ from the literature (Fickian diffusion)^{6,7}, one has:

$$\frac{C_t - C_0}{C_\infty - C_0} = 4 \left(\frac{Dt}{L^2} \right)^{1/2} \left(\frac{1}{\pi^{1/2}} + 2 \sum_{n=0}^{\infty} (-1)^n \operatorname{ierfc} \frac{nL}{2(Dt)^{1/2}} \right) \quad (4)$$

Equation 4 gives a unique curve when plotted as DFC versus $\tau^{1/2}$, where $\tau = Dt/L^2$, is a dimensionless time. For relatively small values of τ , corresponding to $\text{DFC} < 0.6$, equation 4 reduces to:

$$\frac{C_t - C_0}{C_\infty - C_0} = \frac{4 t^{1/2}}{\pi^{1/2} L} D^{1/2} \quad (5)$$

Equations 4 and 5 describe the application of the EIS to the uptake of solute into polymers when Fick's law is obeyed. There are cases, however, in which the transport of diffusants in polymers is not described by the simple Fick's law. The relationship between the amount of substance absorbed, M_t , and the time t is, in this case, more complex and requires the application of cumbersome methods to extract the diffusion coefficient from the mass uptake⁸⁻¹⁰. Equation 5 shows that in order to extract the diffusivity from the capacitance time decay plot, a plateau (C_∞) must be observed in this plot. Furthermore, equation 5 shows and the dry film capacitance, C_0 , can be obtained as the extrapolated value of C_t for $\sqrt{t} \rightarrow 0$. Once the values of C_0 and C_∞ have been determined, then the capacitance data can be arranged according to equation 5 to extract the diffusivity D .

CM Model: According to this model, the film is divided in layers of thickness Δx . Due to the the water concentration profile across the film (see Figure 1b), each layer contributes to the overall film capacitance C_t with its own value. Applying equation 2 to this layer one has:

$$C_t(\Delta x) = C_0(\Delta x) e^{[\alpha \phi(\Delta x)]} \quad (6)$$

where $\phi(\Delta x)$ is the volume fraction of water in a layer of thickness Δx , and C_0 is the dry film capacitance given by:

$$C_0(\Delta x) = \frac{C_0 L}{\Delta x} \quad (7)$$

Since all layers are in parallel, the film capacitance, C_t , can be calculated by the following equation:

$$\frac{1}{C_t} = \lim_{\Delta x \rightarrow 0} \sum_{x=0}^{x=L} \frac{1}{C_t(\Delta x)} = \frac{1}{C_0 L} \lim_{\Delta x \rightarrow 0} \sum_{x=0}^{x=L} \Delta x e^{-\alpha \phi} \quad (8)$$

Taking the limit of the right hand part of equation 8, one has:

$$\frac{1}{C_t} = \frac{1}{C_0 L} \int_0^L e^{-\alpha \phi} dx \quad (9)$$

When no water is absorbed into the film, ($\phi=0$), equation 9 reduces to the trivial case $C_t=C_0$. Integration of equation 9 for small values of the equilibrium water uptake ($\phi_\infty < 1$), yields:

$$\frac{1}{C_t} = \frac{1}{C_0 L} \left[L - \frac{\alpha}{\rho S} M_t \right] \quad (10)$$

where ρ is the density of water and S the surface. Equation 10 is the relationship between the total mass uptake, M_t , and film capacitance, C_t , valid for $\phi_\infty < 1$. Following the same procedure as that used for the DM model, the analytical expression of M_t can be substituted into equation (10) leading to:

$$\frac{C_t - C_0}{C_\infty - C_0} \left(\frac{C_\infty}{C_t} \right) = 4 \left(\frac{Dt}{L^2} \right)^{1/2} \left(\frac{1}{\pi^{1/2}} + 2 \sum_{n=0}^{n=\infty} (-1)^n \operatorname{ierfc} \frac{nL}{2(Dt)^{1/2}} \right) \quad (11)$$

where the inverse of the dry film capacitance, $1/C_0$, is obtained as the extrapolated value of $1/C_t$ for $\sqrt{t} \rightarrow 0$. Finally, from equation 11, the following relationship is derived for short times:

$$\frac{C_t - C_0}{C_\infty - C_0} \left(\frac{C_\infty}{C_t} \right) = \frac{4 t^{1/2}}{\pi^{1/2} L} D^{1/2} \quad (12)$$

The left hand term in equations 11 and 12, represents the DFC derived according to the CM model. Equation 12 shows that to calculate the diffusion coefficient D from the capacitance data, these data must exhibit a plateau (C_∞ is known) and must be arranged as DFC versus \sqrt{t} . In addition, according to equation 11, all capacitance data when plotted as DFC versus $\tau^{1/2}$, will lie on a unique curve also in this case. When the equilibrium water uptake ϕ_∞ is not small compared to 1, then equation 12 is not valid anymore and the diffusion coefficient D cannot be evaluated.

Experimental Procedure

Materials. Freestanding Kapton® films were cut from sheets of thicknesses varying between 7.5 and 125 μm which were provided by E.I. du Pont de Nemours, Electronic Department, Wilmington, DE. PMDA-ODA is the synthetic analogue of

Kapton[®] polyimide and was also supplied by E.I. du Pont de Nemours, as the amic acid solution of poly[N,N'-(p,p'-oxy-diphenylene) pyromellitimide]. The procedure to obtain free standing PMDA-ODA polyimide is reported elsewhere¹¹. PET films of 22, 75 and 205 μm thickness were furnished by Texas Instruments, Attleboro, MA.

Methods. The gravimetric and the capacitance data reported in this paper, were obtained as described in the literature^{6,12,13} and the experimental procedure is, therefore, omitted for the sake of simplicity.

Results and Discussion

The impedance response of polyimide and PET films was determined by means of a Solartron 1255 transfer function analyser in the frequency range 100+1 KHz to evaluate the behavior of the film when fully saturated with water. Some results obtained with polyimide (in the free standing and applied configuration) are shown in Figure 2 in the form of Bode plot. Similar results were obtained with thick polyimide and with PET films. As can be seen from this figure, the polyimide film exhibits a pure capacitive behavior (slope of -1) in the frequency range investigated even when it is fully saturated with water suggesting that during the absorption experiments at constant frequency the film response is dominated by the film capacitance. Data presented in this paper were obtained at the excitation frequency f of 6.5 KHz and the capacitance of the film was evaluated as $C=1/(2\pi f I_m S)$, where I_m is the imaginary part of the impedance⁶.

Freestanding Films. Figure 3 shows the capacitance values C_t as a function of \sqrt{t} for the 75 μm thick PET film at 40 °C. The dry film capacitance, C_0 , and the film capacitance at equilibrium, C_∞ , are reported, with an arrow, on the left and right hand scale, respectively. Experimental findings obtained with the EIS method (Figure 3) can be arranged as dimensionless film capacitance, DFC, as a function of the square root of the dimensionless immersion time, τ . Since the diffusion phenomenon is Fickian, then all experimental data plotted as DFC (DM and CM models) must lie on a unique curve as described by equations 4, and 11. These results are shown in Figures 4 and 5 for the Kapton[®] and PET films, respectively. As can be seen from these figures, the diffusivity curves of Kapton[®] and PET compare satisfactorily with the theoretical curve, demonstrating that the experimental findings are well described by equation 4.

According to the theoretical analysis presented above, the diffusion coefficient D can be obtained from EIS data at constant frequency using equations 5 (DM model) and 12 (CM model) provided that the capacitance at equilibrium, C_∞ , is known. The diffusion coefficient values obtained in this way are reported in Table 1. It must be pointed out, however, that if C_∞ cannot be evaluated from the C_t time decay plot, then the diffusion coefficient D cannot be extracted from the capacitance data.

Transport properties values reported in Table 1 show that water diffusivity evaluated according to the DM and the CM model are in good agreement for low values of the film thickness. The higher is the film thickness, the largest is the discrepancy between the diffusion coefficient evaluated with the two models. This result suggests that a free standing film can be described by a simple parallel RC

circuit only for small values of the film thickness. Thick films can be properly described only by a series of parallel RC circuits. Since a free film of thickness L is equivalent, as far as the kinetics of water uptake is concerned, to a coated film of thickness $L/2$, it follows that only very thin coatings can be described by an electrical analog composed of a parallel RC circuit. This aspect will be further discussed in a subsequent section.

Gravimetric data for both free standing Kapton® and PET films are also reported in Table 1. It was not possible to carry out gravimetric measurements with thin Kapton® (7.5, 12.5 and 19 μm) and PET (22 μm) films, due to both the high value of D and the small film thickness. Results reported in Table 1 show good agreement between the EIS and the gravimetric method. The EIS method, however, also allows the evaluation of the diffusion coefficient of thinner films as indicated by the data obtained for the 7.5, 12.5, and 19 μm thick films. In addition, data for the 2.4 μm thick PMDA-ODA free standing film obtained with the EIS technique, are also reported in Table 1.

Supported Films. The presence of a metallic interface at one boundary, affects the geometry of the mathematical problem, hence a modified form of equation 5 must be used to obtain the diffusion coefficient from the EIS data. This equation is⁷:

$$\frac{C_t - C_0}{C_\infty - C_0} = \frac{4t^{1/2}}{\pi^{1/2}(2L)} D^{1/2} \quad (13)$$

where C_t is the film capacitance in the applied configuration. To extract the film capacitance from the capacitance of the coating/metallic system (that is what the EIS determines), a description of the typical $C_t = C_t(t)$ curve for painted metal exposed to salt solution (schematically shown in Figure 6) is necessary. There is a rapid increase in the film capacitance for short immersion times, associated with water uptake in the coating, followed by a steady state value before a further increase is observed. The final rise in the film capacitance has been associated in the literature to several factors as further water absorption¹⁵, homogeneous absorption into the homogeneous part of the coating contrary to the initial rise attributed to capillary absorption¹⁶, accumulation of interfacial water^{17,18}, or to corrosion initiation^{1,13}. Depending on the type of paints and on the film thickness, some authors observed a clear plateau in the film capacitance time decay plot, while others researchers observed a continuous rise of C_t with time.

As reported in the theoretical section, to extract the water diffusivity and the water uptake from the time behavior of the capacitance of coated metallic substrate, some requirements must be met. First of all, a clear plateau in the capacitance time decay plot must be observed as discussed above for the free standing films. When a plateau is not observed because of either the interfacial reaction (corrosion of the metallic substrate) or coating's delamination, then the experimental data cannot be arranged to extract the required film's parameter. The initial film capacitance, C_0 , however, can be always determined by a non-linear regression analysis of the capacitance data for short immersion times. Finally, the theoretical analysis reported above, suggests that the capacitance data of thin films can be analyzed using the DM

model, while the capacitance data of thick films should be analyzed using the CM model.

Figures 7 and 8 show the capacitance C_t as a function of \sqrt{t} for a 2.4 μm thick PMDA-ODA film supported on pure Cr and Al. These figures are representative of the type of results obtained with coated PMDA-ODA/metallic substrates investigated in this paper. Water diffusion in 2.4 μm thick free standing PMDA-ODA film was observed to be Fickian in nature as reported above. It is expected, therefore, a similar behavior when PMDA-ODA is applied to a metallic substrate.

Results shown in Figures 7 and 8, indicate that even for this simple system whose diffusion mechanism is known "*a priori*", different capacitance time decay plots were observed. In Figure 7 (PMDA-ODA/Cr), a clear plateau (equilibrium) is observed, while in Figure 8 (PMDA-ODA/Al) a continuous increase of the film capacitance with time is observed. The initial film capacitance C_0 can be calculated from the $C_t(t)$ values in both cases (these values are shown, with an arrow, on the left hand side scale), while the diffusivity of water can be obtained only for the case shown in Figure 7. Due to the small film thickness, the diffusion coefficient D was evaluated using equation 5 (DM model), while the equilibrium water uptake was obtained via equation 2 with $C_t=C_\infty$. The diffusivity of water ($1.67 \times 10^{-9} \text{ cm}^2 \text{ s}^{-1}$), and the water uptake (2.6 % by weight), are comparable with those of the freestanding film (see Table 1). The value of C_0 , ($107.98 \text{ pF cm}^{-2}$, $\epsilon=2.93$), is slightly lower than that of the free standing film. Since the capacitance data shown in Figure 8 do not exhibit any plateau, the water diffusivity in the coated PMDA-ODA/Al system cannot be determined in this case. The value of C_0 ($154.35 \text{ pF cm}^{-2}$, $\epsilon=4.2$) is, in this case, somewhat higher compared to that of free standing film and of that of PMDA-ODA/Cr. Since C_0 is associated with the unpenetrated coating/metallic interface, it can be concluded that pinholes or heterogeneities, and/or interfacial oxides must be present in the PMDA-ODA/Al systems of Figure 8. These results clearly indicate that even for a simple coated/metal system of which the transport mechanism of water is known "*a priori*", water diffusivity and water uptake cannot be deduced from impedance measurements unless some requirements are met. In addition, C_0 does not represent the dry film capacitance as in the case of free standing films. For coated films, C_0 represents the capacitance of the homogeneous part of the coating and of the oxides present at the metallic interface.

Conclusions

Results presented in this paper showed that the EIS and the gravimetric methods of evaluating transport properties of water across free standing Kapton® and PET films are in good agreement. When applicable, the capacitance method can be preferred to the gravimetric method because the transport properties can be evaluated without perturbing the system under study. In addition, with the capacitance method polymeric films as thin as few μm can be tested even for relatively high water diffusion coefficients (on the order of $10^{-9} \text{ cm}^2 \text{ s}^{-1}$). In order to use the EIS method the following items should be fulfilled:

- (i) a model for the effect of water on the capacitance change of the polymeric material should be available; the dry film capacitance, C_0 , is obtained by linear extrapolation of C_t for $\sqrt{t} \rightarrow 0$. From the values of C_0 and C_∞ , the equilibrium

water uptake can be easily evaluated. The diffusion coefficient, D , however, can be determined by simple equations only for "Fickian diffusion".

- (ii) as far as the kinetics of water uptake as determined with the EIS method is concerned, two models were presented and discussed. The DM model (a parallel RC circuit) can be successfully applied to thin films, while thick films are more conveniently described by the CM model (a series of parallel RC circuits). Water transport properties can be deduced from EIS measurements of coated metallic systems only if specific requirements are met;
- (iii) the initial film capacitance, C_0 , is the dry film capacitance when the coating is in the free standing configuration. For applied films, C_0 represents the combination of both the dry film capacitance and the capacitance of the oxides present at the metallic interface.

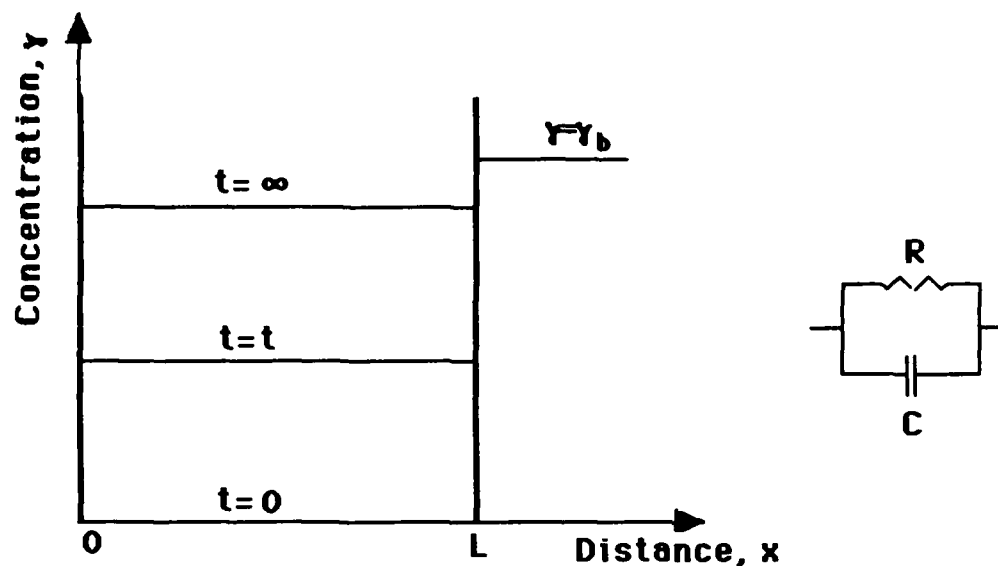
Acknowledgement: The authors wish to acknowledge S.D. Senturia of the Microsystems Technology Laboratory of Massachusetts Institute of Technology for providing the coated PMDA-ODA sample. The financial support of MPI (60% Funds) is also gratefully acknowledged.

References

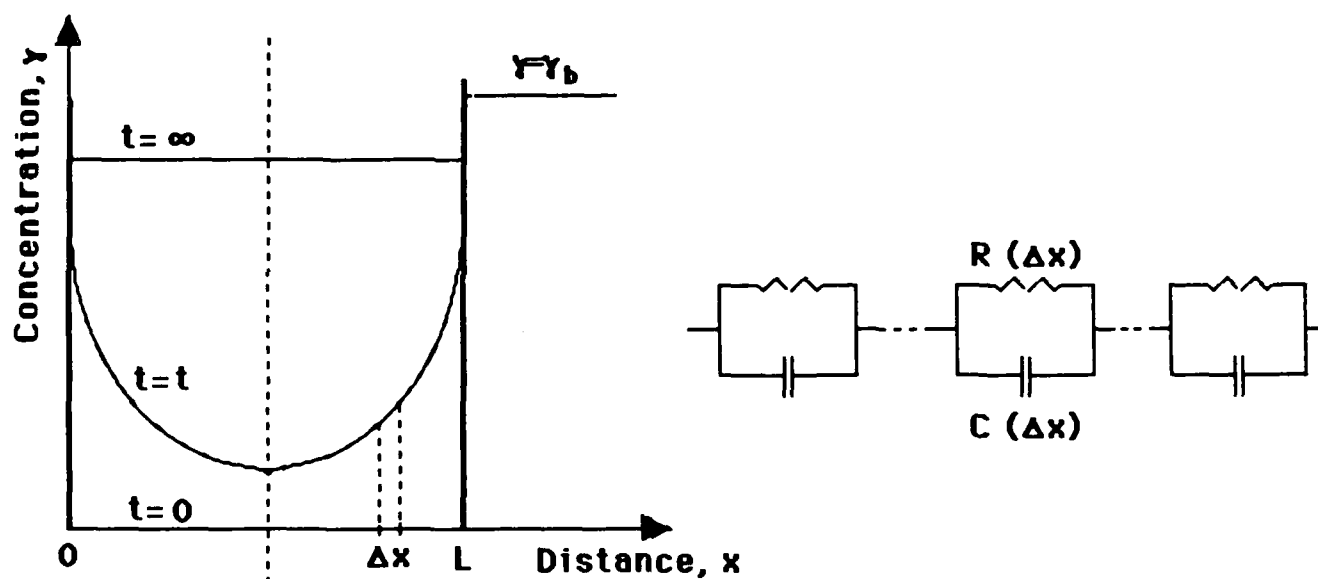
1. F. Wormwell, D.M. Brasher, J. Iron St. Inst., 164 (1950) p. 141.
2. D.M. Brasher, A.H. Kingsbury, J. Appl. Chem., 4 (1954) p. 62.
3. J.K. Gentles, J. Oil Colour Chemists Ass., 46 (1963) p. 850.
4. L. Hartshorn, N.J.L. Megson, E. Rushton, J. Soc. Chem. Ind. London, 56 (1937) p. 266T.
5. K.A. Holtzman, J. Paint Tech., 43 (1971) p. 47.
6. J. Crank, G.S. Park, Diffusion in Polymers, Academic Press, New York 1954.
7. J. Crank, The Mathematics of Diffusion, University Press, Oxford 1968.
8. Permeability of Plastic Films and Coatings to Gases, Vapors, and Liquids. Ed. H.B. Hopfenberg, Plenum Press, New York 1974.
9. D.J. Escore, H.B. Hopfenberg, V.T. Stannett, Polymer Eng. Sci., 20 (1980) p. 102.
10. A.H. Windle, in "Polymer Permeability", Chp 3, 75, Edr. J. Comyn, Elsevier Applied Science Publishers, London & New York, 1986.
11. A. Schussler, F. Bellucci, S.D. Senturia, R.M. Latanision, J. Appl. Polym. Sci. 42, (1991) p. 1567.
12. S.J. Downey and O.F. Devereux, Corrosion, 45 (1989) p. 675.
13. F. Bellucci, M.J. Kloppers, R.M. Latanision, J. Electr. Soc., 138 (1991) p. 40.
14. G.H. Walter, Corr. Sci., 26 (1986) p. 39.
15. S.A. Lindqvist, Corrosion, 41 (1985) p. 69.
16. R.E. Touhsaent, H. Leidheiser Jr, Corrosion, 28 (1972) p. 435.
17. F.M. Geenen, E.P.M. van Westing, J.H.W. de Wit, Proc. 9th Eur. Congr. Corr., Utrecht, The Netherlands 1989 CO-88.
18. F.M. Geenen, PhD thesis, University of Delft, (1991).

TABLE 1. Water diffusion coefficient, D , in $\text{cm}^2 \text{s}^{-1}$, water uptake, W , in % by weight, as a function of film thickness for free standing polyimide (PMDA-ODA, Kapton®) and PET films at the temperature of 25 (polyimide) and 40 °C (PET), respectively. Subscripts "g" and "c" indicate gravimetric and capacitance method, respectively

Material	L, μm	W_g	W_c		$D_g \times 10^9$	$D_c \times 10^9$	
			DM	CM		DM	CM
PMDA-ODA	2.4		2.39	2.31		1.42	1.49
KAPTON®	7.5		4.3	4.15		1.58	1.92
KAPTON®	12.5		4.63	4.31		1.85	2.14
KAPTON®	19		2.27	2.24		2.06	2.36
KAPTON®	25	1.8	3.59	3.55	2.08	2.37	3.10
KAPTON®	50	2.5	3.95	3.89	1.72	2.67	3.35
KAPTON®	75	2.5	3.57	3.53	2.01	2.77	3.53
KAPTON®	125	2.8	3.59	3.50	2.12	2.84	3.45
PET	22		0.95	0.94		2.11	2.18
PET	75	0.50	0.83	0.80	7.76	5.91	6.15
PET	205	0.46	0.54	0.50	13.10	9.97	12.61



(a)



(b)

Figure 1. Schematic of water concentration profile in a free film of thickness L and electrical equivalent circuit according to a Discrete (a) and Continuous (b) Model.

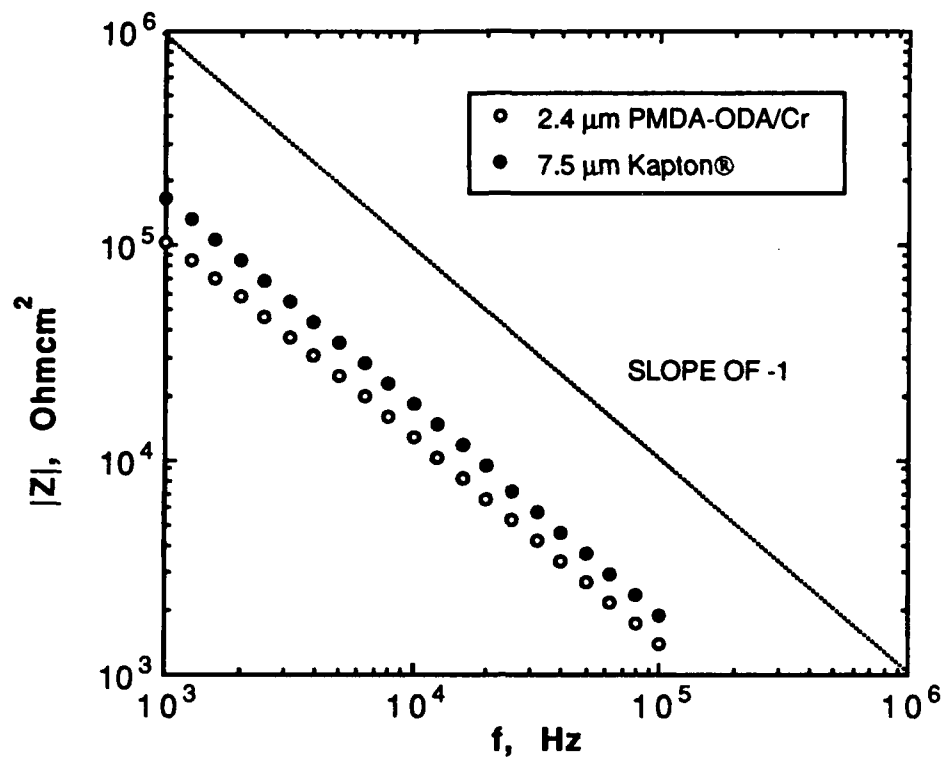


Figure 2. Bode plot for a 7.5 μm free standing polyimide film and for a 2.4 μm PMDA-ODA/Cr systems fully saturated with water at 25 $^{\circ}\text{C}$. Similar spectra were observed for thick polyimide and for PET films at 40 $^{\circ}\text{C}$.

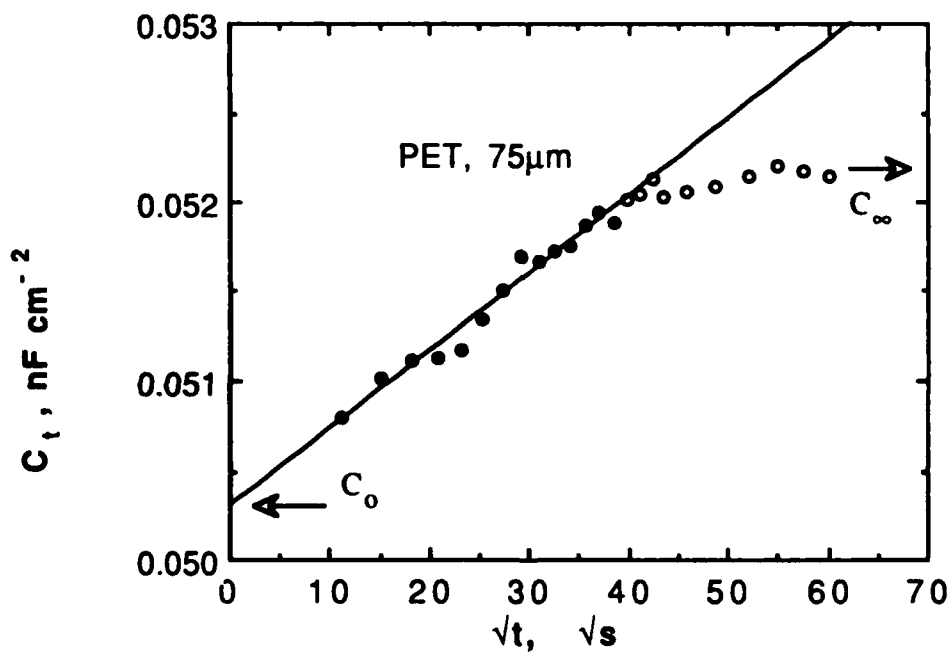


Figure 3. Film capacitance C_t , in nF cm^{-2} versus \sqrt{t} , in $\sqrt{\text{s}}$, for the 75 μm PET film at 40 $^{\circ}\text{C}$.

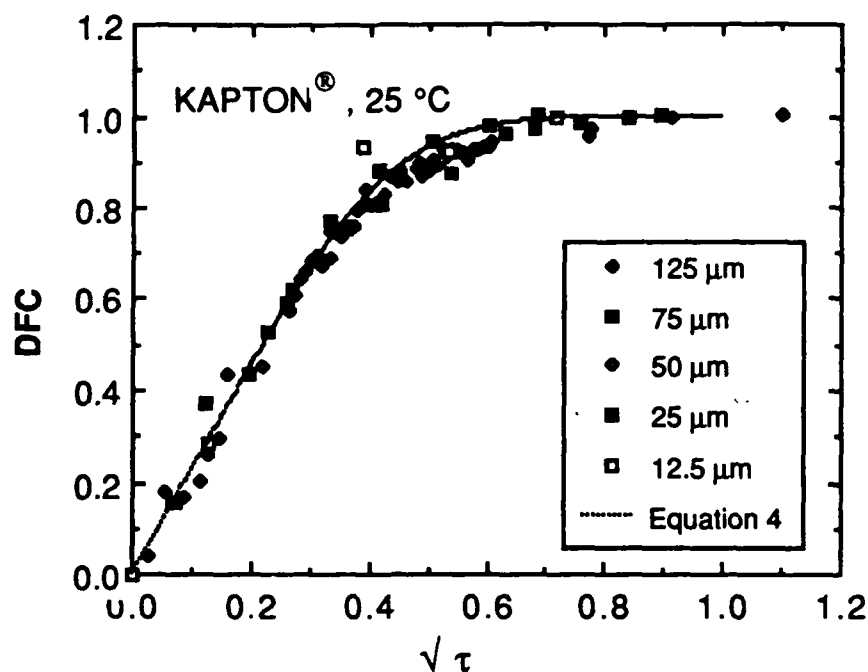


Figure 4. Dimensionless film capacitance, DFC, versus the square root of the dimensionless time, t , for the Kapton[®] films investigated in this paper. The dotted line was determined using equation 4.

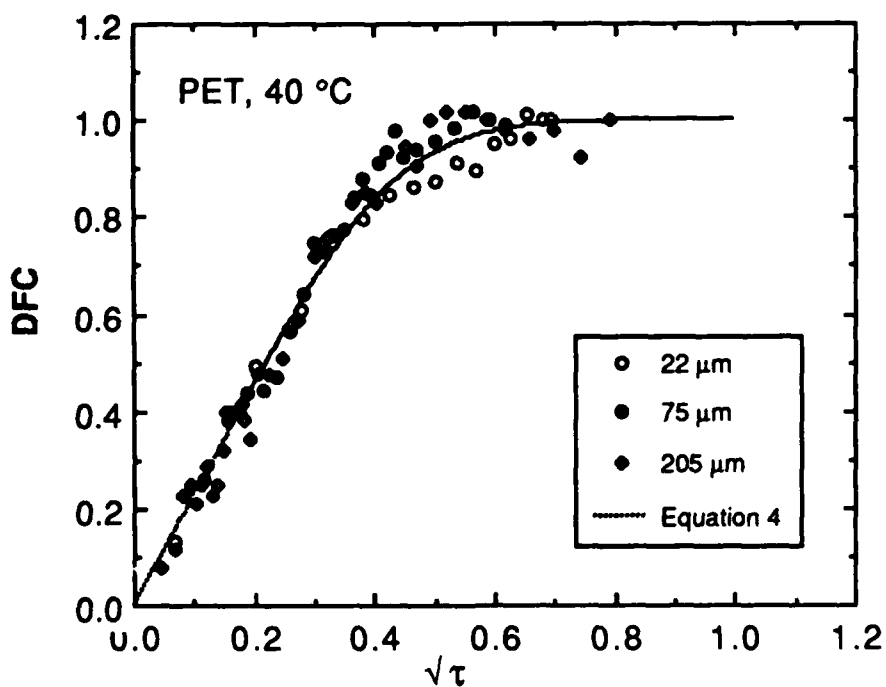


Figure 5. Dimensionless film capacitance, DFC, versus the square root of the dimensionless time, t , for the PET films investigated in this paper. The dotted line was determined using equation 4.

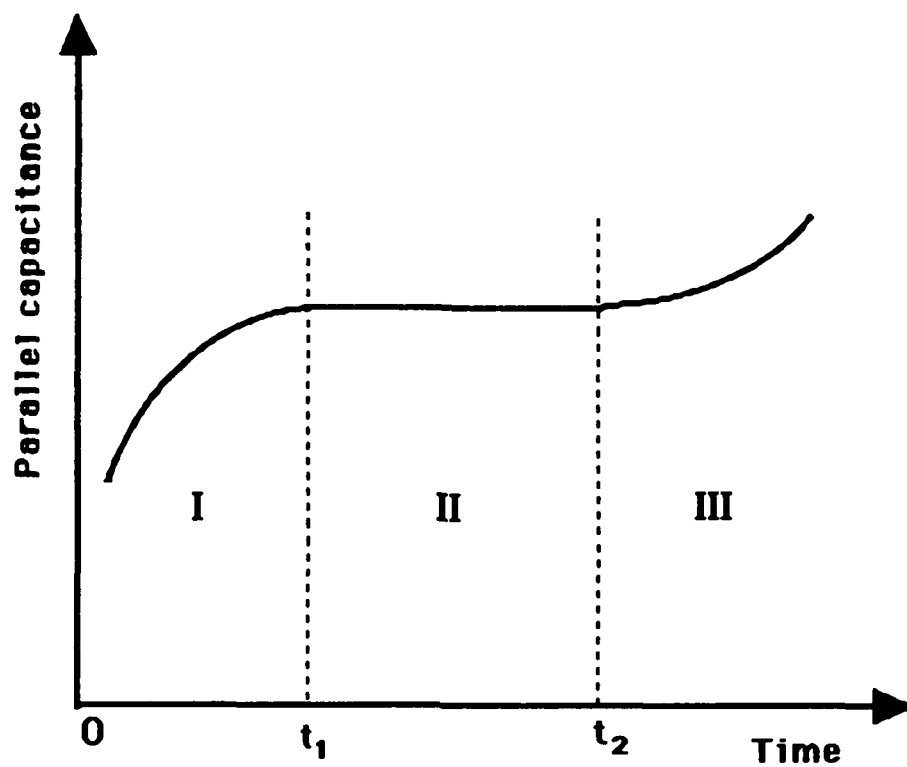


Figure 6. Schematic of capacitance time decay plot showing an initial film capacitance, followed by the appearance of a plateau and of a subsequent rise with time.

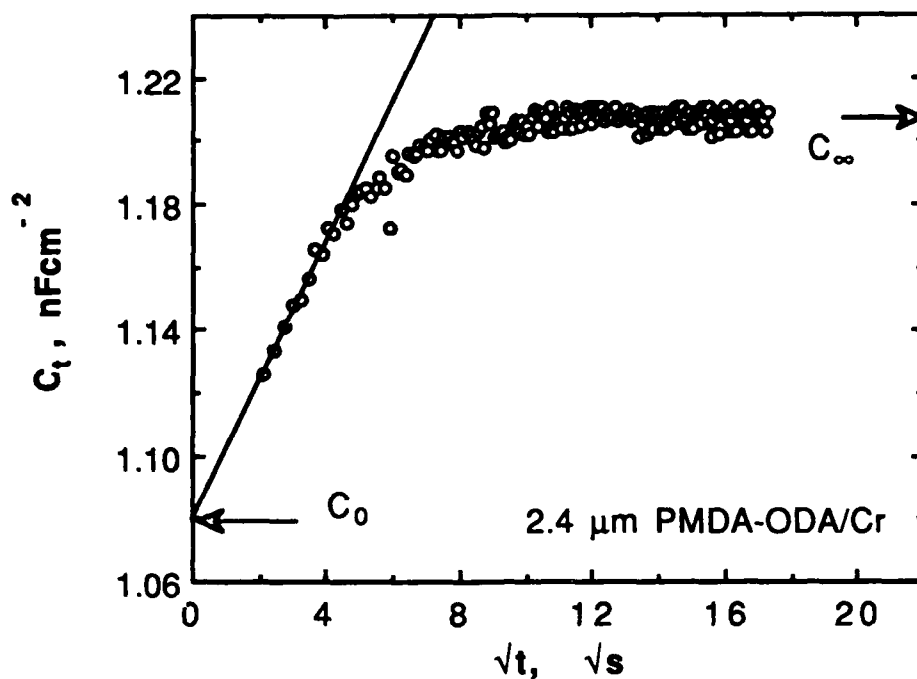


Figure 7. Film capacitance C_t , in nF cm^{-2} , versus \sqrt{t} in \sqrt{s} , at 25°C for a $2.4\text{ }\mu\text{m}$ PMDA-ODA polyimide applied on Cr as metallic substrate.

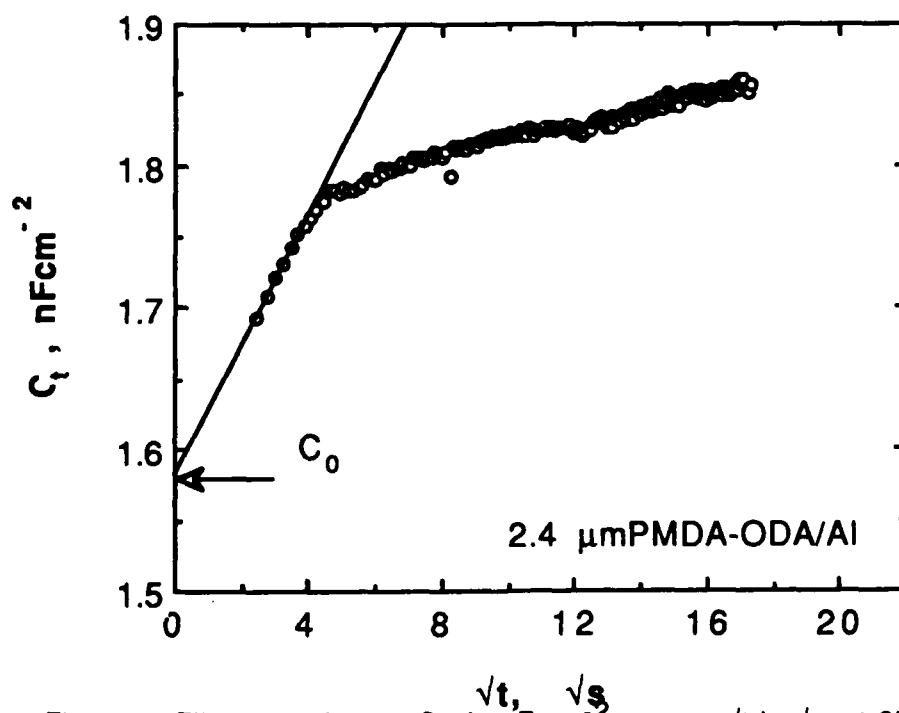


Figure 8. Film capacitance C_t , in nF cm^{-2} , versus \sqrt{t} in \sqrt{s} , at 25°C for a $2.4\text{ }\mu\text{m}$ PMDA-ODA polyimide applied on Al as metallic substrate.

Characterisation of Organic Coatings with Impedance Spectroscopy

J.H.W. de Wit

Materials Institute Delft
Division of Corrosion Technology, Electrochemistry and Spectroscopy
Rotterdamseweg 137
2628 AL Delft
The Netherlands

Abstract

The protective properties of organic coatings depend on the permeability of the coating and the adhesion of the coating to the metal. The water solubility and the penetration rate of water into the coating can be studied very well with impedance spectroscopy.

Also the corrosion reaction at the metal-coating interface can be detected in the very early stages of the process. Detailed analyses of equivalent circuits representing the different physical phenomena in the coating and at the metal coating interface in combination with other techniques as DSC and DMTA, give information on the performance of the coatings. By determining the Most Probable Impedance equivalent circuit (MPI), and comparing with data on natural ageing as well as with results from fast cyclic corrosion tests the life time expectancy can be judged. In situ determination of loss of adhesion of barrier epoxy coatings has become possible, using new EIS data and including new data from an dielectric sensor. The paper will give an overview of the evolution of the possibilities with impedance measurements for organic coatings evaluation, based on many recent publications* and newly obtained experimental data.

Key words:

Electrochemical Impedance Measurements, Organic Coatings, Water Permeation, Adhesion, Corrosion under Coating, Blisters, MPI Analysis, dielectric sensor

Introduction

The possibilities of EIM to characterise the quality and the protective behaviour of organic coatings have been known for some 15 years¹. Only since ten years highly sophisticated commercial equipment has come on the market. Because of the fast increase in the quality of both hardware and software the equipment has also become very much more user-friendly. As a result of the increased availability of this measuring technique, many industrial researchers obtained Impedance Spectroscopy units but became soon disappointed. The equipment offered too many possibilities for the average user.

Most problems during measuring do not result from the equipment itself, but from lacking stability of the system measured upon, lack of reproducibility of coatings, and poor experimental conditions like disturbance of the measurements due to the pick up of various signals by the normally very high impedant systems. An extra handicap was formed by the overwhelming amount of publications describing EIM on organic coatings, with simple interpretations suggesting that the technique could be used as a quickly learned stand-alone technique with which coatings could be easily characterised (see e.g. 2-4).

As a matter of fact, it is very difficult to interpret EIM measurements in a sensible way. Laboratory measurements on coated model panels are easily made, however, highly sophisticated software makes it seducingly easy to fit equivalent circuits to the measured data. The use of many time constants will always result in a good fit. Even the hierarchy of the so-called nested equivalent circuits can often be changed without changing the quality of the fit⁵. An alternative to fitting equivalent circuits would be to derive a complete transfer function starting from fundamental knowledge on all possible phenomena at the metal coating interface and in the coating dealing with transport of charge and deriving an impedance plot from this to be compared with measured data⁶. However, this is quite impossible for the very complicated system metal/organic coating due to overlapping time constants. Most of the parameters describing the various processes are interdependent invalidating this kind of analysis. So we have to rely on the use of equivalent circuits. It is the purpose of this paper to show how the interpretation of impedance data with equivalent circuits can be optimised using data from

various techniques, and by using time dependent electrochemical data which make it possible to find the Most Probable Impedance equivalent circuit (MPI) in accordance with a reliable physical model. In order to reach that goal most measurements were done on model transparent epoxy coatings. In this way it has been possible to follow and explain the water uptake, the curing, the adhesion, and the formation of corrosion products at the interface very precisely⁵⁻⁷. Based on the MPI-concept and making use of EIM-sensors and laboratory coated panels in relation with accelerated weathering tests, EIM becomes very relevant for industrial applications and provides a means for life time prediction of coatings.

Impedance analysis

Before analysing EIM performed on organic coatings, it is necessary to define the area of interest. Interpretation procedures do depend on the character of the phenomena studied. With EIM the following phenomena can be studied: water permeation, water condensation at the interface, swelling of the coating, curing of the coating, loss of adhesion including the delamination area, corrosion at the interface, and the formation of various defects including blisters.

Ideally interpretation should start with a physical model, which through the development of a transfer function would be transformed into an expression for the Impedance and eventually result in simulated impedance plots, including both the Faradaic and the non-Faradaic part of the Impedance. The simulated Nyquist and Bode plots can first be compared qualitatively with measured data. By changing the values for various parameters a quantitative fit can eventually result, giving realistic values for the physical parameters of the model. An alternative method is based on the development of a suitable equivalent circuit. The measured data are evaluated with optimised soft-ware like e.g. the software package *equivrt* by Boukamp in order to determine the number of time constants. An equivalent circuit taking into account the number of time constants found, is constructed, based on a basic physically relevant model, resulting from information determined with various also non-electrochemical techniques (DMTA, DSC, FTIR etc.). The equivalent circuit is fitted to the data. The fitting is optimised, so that the components of the equivalent circuit have physically realistic values. Both procedures should lead to the same result, which in some cases was shown to be possible⁶.

However, for the complicated coated systems discussed in this paper the transfer function analysis is not possible due to the fact that many parameters can not be treated as truly independent.

For the evaluation of the quality of coatings this often is not necessary either. Sometimes much simpler models can be used. This has resulted in the introduction of the so-called "breakpoint-frequency" method^{3,4} for delamination studies. For defect free coatings a standard simple equivalent circuit is used to determine the relevant breakpoint frequency in the Bode plot which gives information on the delaminated area. However, for defect containing coatings this model suffers from oversimplification of the physical model, by separating the defect area and the delamination area in the circuit, resulting in erroneous conclusions. Delamination under a coating without local defects would thus not be detected at all⁸. Using more complicated, physically relevant equivalent circuits, the method may in principle be useful as long as the breakpoint frequencies are well separated which is, however, difficult to foresee.

A more general procedure, which can be used to study not only delamination but also all other phenomena mentioned above, is the optimised equivalent circuit analysis method which leads to the Most Probable Impedance equivalent circuit the so-called MPI method.

The principles of the MPI method

A Nyquist plot of an impedance measurement on a non-barrier epoxy-coating is given in Figure 1. Graphical evaluation of the plot would result in two time constants. However, using the *immittance analysis program equivrt* 5 time constants could be found. For a physically relevant interpretation of the impedance behaviour of this coating it is necessary that the values of the parameters show a systematical variation with exposure time, which can be attributed to real physical changes of the system. Furthermore, the results must be insensitive to small variations of the system. This was tested by analysis of impedance measurements as a function of time of exposure using the same equivalent circuit. Only small variations of the values of the components of the eq.c. were indeed obtained. The impedance results were also compared with

results from potential measurements and visual inspection, as discussed in the paragraph on delamination and corrosion.

The MPI procedure proceeds along the following lines. Only so many fitting parameters, or elements in the equivalent circuit, should be used as to obtain an optimal fitting result, still allowing for a systematical variation of the results with exposure time in accordance with all other relevant physical data. Also the derivation of the hierarchy of the elements in the eq.c. is based on the condition of a stable fitting result with a minimal systematical deviation between measured and fitted result. When searching for the optimal hierarchy again a general theoretical model with physical relevance is taken into account. In Figure 2 A, B and C residual error plots are given for fits using respectively two, three and four time constants. From the error plots it became clear that it is necessary to use four (but not five!) time constants to eliminate the systematical error from the fit results. The Nyquist plot shows that these time constants are not well resolved. The resulting eq.c. as given in Figure 3 is quite complicated. The Q-factors in this circuit are CPE's which represent the deviation from true capacitive behaviour. The two parallel (RQ) circuits have an equal level in the eq.c. and interchanging the parameter values does not affect the impedance of the circuit. This uncertainty can only be resolved using non-EIM data. The Nyquist plot is further interpreted in the paragraph on adhesion and corrosion.

In some cases the eq.c. containing Q elements (CPE's) can be considered as the MPI. This is only acceptable if a good physical model exists to explain the deviation from ideal capacitive behaviour. The value of the CPE factor n must have physical relevance. One example will be treated in the paragraph on water-uptake. If no acceptable physical model exists to explain the CPE's, the last step in the determination of the MPI is the exchange of the Q-factors in the eq.c. for C's and W's (Warburg diffusion impedance) at the cost of some fitting accuracy⁵.

The example used to explain the MPI method described a non-barrier epoxy-coating. For ideal barrier coatings true dielectric behaviour will be observed, which requires a different analysis (9). However for life time prediction of practical coatings this is less relevant.

Two Examples Of EIM Interpretation With MPI Analysis

1. Water Uptake: The First Stage Of Coating Deterioration

Because the permeation of water in a coating can be considered to be the first stage of deterioration of the total coating system, it is important to obtain information on S and D , the solubility and the diffusion coefficient of water in the coating. Especially all deviations from ideal Fickian behaviour and from normal saturation are interesting, because these give information on the quality of the coating.

The uptake of water in a paint film introduces a change in the dielectric properties (the capacitance) of the material. The mixing relation given by Brasher and Kinsbury¹⁰ describes the relation between the volume fraction of water in the coating and the capacitance, under the assumption that the water is randomly distributed through the coating at interstitial sites. This assumption is reasonable for most coating systems:

$$\Phi = \frac{\log(C_t/C_0)}{\log 80} \quad (1)$$

where Φ	denotes :	the volume fraction of water in the coating
C_t	denotes:	the capacitance of the paint film at time t
C_0	denotes:	the capacitance of the paint film at time $t = 0$
and 80	is:	the relative permittivity of water at $T = 20^\circ\text{C}$.

The rate of penetration of water can in many cases be described by Ficks second law of diffusion. This equation can be solved, using the following boundary conditions: water is initially homogeneously dispersed in the coating, and the water concentration at the outside of the coating is constant. This yields the diffusion coefficient D for water in the coating.

A typical example of a change in C_{pf} as a function of time of exposure as a result of water permeation is shown in Figure 4. This Figure shows the four regimes that may be distinguished in the water permeation behaviour of supported coatings:

- i. Unbounded normal diffusion of water ($C_{pf} \approx \sqrt{t}$), also called Case I diffusion.
- ii. Anomalous diffusion: the water mobility and the polymer segment relaxation times are comparable.
- iii. Full saturation of the coating (C_{pf} is constant).
- iv. Deviation from normal saturation.
 - A: Clustering of water molecules at the coating/substrata or coating/pigment particle interface.
 - B: Case II diffusion, where the permeant mobility is much higher than the polymer segment relaxation rate. This behaviour is often observed when the coating suffers from swelling.

In Figure 4 Regime iv A has been given.

Before any mixing relation may be used, two characteristic quantities need to be determined from the $C_{pf}(t)$ diagram: The capacitance of the dry coating C_0 and the capacitance of the saturated coating C_s which may roughly be done graphically as visualised in Figure 4. However, an accurate determination of these parameters is vital in order to calculate an accurate value for D . Various methods do exist to determine these parameters as was discussed extensively before ^{5,7,11,12}. Here I will only mention a NLLS fit to the data of a modified Crank and Park equation: after solution of Ficks second law and incorporation of Equation 1 the following expression results:

$$\frac{\log(C_t/C_0)}{\log(C_\infty/C_0)} = 1 - \left[\frac{8}{\pi^2} \right] \sum_{i=0}^{\infty} \frac{1}{(2i+1)^2} \exp \left[-\frac{(2i+1)^2 \pi^2 D t}{4l^2} \right] \quad (2)$$

This equation can be used for a NLLS fit to the experimental data. In this way accurate values for both D and S can be obtained for those cases where ideal Fickian behaviour exists, and where saturation of the coating is easily obtained. However, the situation is often more complicated.

No constant value for the capacitance is obtained despite full saturation, due to swelling of the coating. A typical example of this behaviour is given in Figure 5. It is clear that when the water uptake of a coating is calculated using the NLLS method for this type of curve, the results will be strongly dependent on the length of the time interval chosen. The time intervals used here are 4, 10 and 16 hours. It is obvious that the coating is not behaving as an ideal dielectric. In that case the MPI is better given by $R(RQ)$, where the impedance for the CPE is given by: $Z = 1/Y_0(j\omega)^{-n}$.

In Figure 6 $n(Q)$ is given as a function of exposure time and as a function of Φ the amount of water in the coating. Clearly only for short exposure times n is independent of the water content of the coating. The water molecules hardly interact with the polarisable groups of the polymer. The diffusion is still Fickian and the water molecules fill up the interstitial space in the coating.

After about four hours a linear relation between n and Φ can be observed ⁷. This is typical for Case II diffusion, where due to swelling a nearly linear increase of the Capacitance (or Y_0) can be observed (see also Figure 5). A correction for this swelling effect must be applied. A linear term SC_t , where SC_c is the swelling coefficient obtained from Capacitance measurements ($[l/s]$) is added. Rewriting Equation 2 and adding the swelling term we arrive at:

$$\log(C_t/C_0) = \log(C_\infty/C_0) \left\{ 1 - \left[\frac{8}{\pi^2} \right] \right.$$

$$\sum_{i=0}^{\infty} \frac{1}{(2i+1)^2} \exp \left[-\frac{(2i+1)^2 \pi^2 D t}{4l^2} \right] \} + SC_{ct} \quad (3)$$

This new equation can be fitted to the experimental data, which for the measurement of Figure 5 results in the very good fit given in Figure 7. The fit result should be compared with the fit over 16 hours in Figure 5. The assumption that swelling was responsible for this linear increase of the capacitance, was verified by immersion of tri-angular pieces of paint film in Milli-Q water and measuring the dimensions using a microscope. The swelling reaches values of 2-3% after 50 hours in accordance with the correction used for the fit of Equation 3.

In this way using the MPI including a CPE more detailed information on the water-uptake process could be obtained than by using the most simple eq.c. Using this method it was also established that the deviation from ideal behaviour for the water uptake depends very much on the curing of the coating^{5,7}.

2. Loss of Adhesion/Corrosion

The long term anti-corrosion performance of a barrier type epoxy coating can also be evaluated by following the CPE parameters Y_0 and n as a function of time¹³⁻¹⁷. Figure 8b shows that after a steep increase of Y_0 (and a decrease of n) a nearly constant value is obtained around 100 hours, while a further increase is observed at 400 hours. An investigation of the interface substrata/coating with a stereo-microscope, possible due to the transparency of the model coating, showed the formation of some very small spots of corrosion products at the interface after 400 hours of exposure, thus showing that the CPE parameters are very sensitive to changes at the interface. The capacitance is less sensitive as can be seen in Figure 8a. The coating system was still very high impedant, while corrosion had started at the interface. Also for pigmented barrier type coatings it was possible to observe this behaviour, while the coating was still very high impedant and showed no visible deterioration.

Returning to the Nyquist plot of Figure 1 and the eq.c. of Figure 3 it will now be shown how the MPI procedure gives detailed information on the protective action of a practical coating system. The system discussed is a 75 μm epoxy coating containing red iron oxide and zinc phosphate⁶.

In evaluating this coating various components in the eq.c. were followed in time during exposure to a 3% NaCl solution. Changes in the values of E_{corr} , R_{pore} , R_{diff} and R_{ct} could be correlated with the development of corrosion spots at the interface. Most sensitive to the various changes in the coating/substrata system were the CPE parameters. The following model could be obtained from the measurements, also using data for transparent pigment free coatings, SEM micrographs and visual information on corrosion spots and blisters (see also Figure 9).

Certain areas of the coating swell excessively, followed by breaking of the adhesive bonding to the substrata. Intermolecular bonds will also be affected by this swelling. This is reflected in the changing values for Q_{pf} . Before rupture the values of Y_0 and $n(Q_{pf})$ increase and decrease resp., while after the rupture the values step back to values that represent the coating impedance without spots that exhibit swelling or corrosion under the coating. After breakthrough of the coating the substrata can corrode freely. The corroding area is not covered by the coating and the impedance can be separated from the coating impedance. Only after breakthrough of the coating the corrosion spot can become visible. The various stages of the formation of the corrosion spots are represented in Figure 9. In Figure 10 these stages are also visible in a schematical representation of the measured curves of Y_0 for Q_{pore} , Q_{dl} and Q_{diff} during the different stages of blister/corrosion spot formation. It is clear that a simpler eq.c. would not have resulted in this detailed interpretation. This was only possible by optimising the eq.c. to obtain the MPI, using all relevant data on the system.

Despite the fact that the discussed analysis gives relatively early information on the delamination of and corrosion under the coating it may be useful to increase the rate of deterioration of the coating in a well reproducible way, either to simulate practical situations where the coating has been externally damaged, or to investigate reaction mechanisms into

detail. Normally scribes are applied to the coated substrata. However, these are not easily reproduced. Therefore a new method was developed, using an excimer laser ablation technique 5, 18-20, not to be discussed in this paper.

The Wet-Dry Cycle Studied With a Dielectric Sensor.

In order to evaluate the interface behaviour as a function of the time during wet-dry cycles into more detail a transparent epoxy coating was applied to a dielectric sensor. When measuring the impedance at the interface direct evidence for the loss of adhesion due to water uptake can be obtained. The sensor consisted of a glass panel with a golden grid as given in figure 11. The results of dry-wet cycle are visible in figure 12, a,b, and c. A more schematised picture has been given in figure 13.

The time dependence during this cycle of the CPE parameters can be explained when considering the most probable concentration profiles for water in the coating for the various stages ⁷. These profiles have been given in figure 13b.

Five stages can be distinguished:

1. In stage 1 the coating is penetrated by water. The capacitance and Y_0 increase, while n decreases, indicating increased inhomogeneity of the coating system.
2. In stage 2 the water reaches the interface of the and causes loss of adhesion. The capacitance and Y_0 increase, while n decreases (indicating that the water at the interface causes further inhomogeneity). This can be explained by closer examination of the geometry of the sensor, as given in figure 14.
In figure 14a the field lines only enter the coating and the air above the coating, consequently the measured dielectric response is mainly caused by the coating. When the coated sensor is immersed the water at the coating surface immediately contributes to the impedance, yielding a stepwise increase of the capacitance and a stepwise decrease of n . In stage 2 the coating loses adhesion and a water phase is formed at the interface.
3. In stage 3 the coating is drying again and water diffuses to the coating surface. The amount of water in the coating decreases indicated by a decrease of the capacitance and Y_0 . The homogeneity increases indicated by an increasing value of N . Taking into account that water is still present at the interface, this water layer can be considered as a source for water to reach the surface for evaporating. The concentration gradient will resemble the curve figure 13b stage 3.
4. Stage 4 can only be observed in the plots of the CPE parameters. The capacitance is hardly changing. During this stage the total amount of water in the coating remains constant. The increasing inhomogeneity of the coating results from the local depletion of water at the interface, which eventually will lead to a lower water flow to the outer parts of the coating. This results in the ultimately lower capacitance in stage 5. The water will not totally disappear from the interface as the capillary forces will prevent this. Thus a thin water film will remain, as was found at the interface after peeling off the film.
5. During the last stage of the cycle a stationary situation is developing. The water in the coating is evaporating very slowly and finally the coating will be dry, except the very thin film at the interface. The concentration profile will resemble figure 14b-5.

The values of the CPE parameters after exposure are slightly different from the initial values before the cycle. This can be attributed to the thin water film at the interface, which is causing a little inhomogeneity and only a very small contribution to the capacitance.

The dielectric behaviour of the coating on the sensor was qualitatively the same as was found for the coatings on the steel panel when dehesion took place. The effect for the coatings on the dielectric sensor is more pronounced due to the size of the dehesion area. On the steel panels only minor spots, where due water penetration and condensation at the interface corrosion/blistering starts at local impurities, are responsible for the deviation from normal dielectric behaviour. Dielectric sensors are therefore very sensitive tools to study mechanisms for dehesion and interfacial corrosion beneath coatings.

Conclusions

It has been shown that EIM can be used very well to characterise the behaviour of organic layers. Using the concept of the MPI and by combining results from different techniques the water uptake, interaction between the water and the polymer, blistering and corrosion under the coating can be followed. Using model coatings in combination with laser defects and CPE analysis again leading to the MPI, detailed models for the various electrochemical events in and

under the coating can be obtained. Combination of these data with sensor techniques and modified accelerated weathering techniques will lead to early warning systems and improved life time prediction in near future.

References

1. L.M. Callow and J.D. Scantlebury: J. Oil. Col. Chem. Ass, 64,(1981)83.
2. F. Mansfeld, S.L. Jeanlaquet, M.W. Kendig: Corr.Sci., 26, (1986)734.
3. S. Haruyama, M.Asari and T. Tsuru: Proc. Symp. on Corr. Prot. by Org. Coat., M.W. Kendig, H. Leidheiser Jr. Eds., Pennington, N.J. Electro-chem.Soc., (1987)197.
4. R. Hirayama and S. Haruyama: Corrosion, (1991)952.
5. F. Geenen: Thesis T.U. Delft, (1991).
6. J.A.L. Dobbelaar and J.H.W. de Wit: J. Electrochem.Soc.,139(1992)716.
7. E.P.M. van Westing: Thesis T.U. Delft, (1992).
8. D.H. van der Weijde, E.P.M. van Westing, H.J.W. Lenderink and J.H.W. de Wit: submitted for publication.
9. P. Steeman: Thesis T.U. Delft (1992).
10. D.M. Brasher and A.H. Kinsbury: J. Appl. Chem., 4 (1954)62.
11. E.P.M. van Westing, F.M. Geenen, G.M. Ferrari and J.H.W. de Wit: Proceedings 16th Int. Conf. in Org. Coat. Sci. and Techn., Athens, July 1990, 9 pp.
12. F.M. Geenen, H.J.W. Lenderink and J.H.W. de Wit: Proceedings 5th Int. Conference on Electrochemical Methods for Corrosion Research, July 1991, Helsinki. C4/1-4.
13. F.M. Geenen, J.H.W. de Wit and E.P.M. van Westing: Progress in Organic Coatings, 18 (1990) 299.
14. F.M. Geenen, H.J.W. Lenderink, E.P.M. van Westing and J.H.W. de Wit: Proc. XXth FATIPEC Congress Nice (F) 1990, 13 pp.
15. F.M. Geenen en J.H.W. de Wit: Farbe und Lack, 98, 9 (1992).
16. E.P.M. van Westing, G.M. Ferrari and J.H.W. de Wit: Proc. 2nd Int Symp. Electrochem Imp. Spectr., July 12-17, Santa Barbara (1992).
17. E.P.M. van Westing, G.M. Ferrari, F.M. Geenen and J.H.W. de Wit: accepted for Progress in Organic Coatings, (1993).
18. M.M.M. Dings, R. de Jonge, S.M. Peters, E.J.H. Koot, F.M. Geenen, E.P.M. van Westing and J.H.W. de Wit: Proc. XXth FATIPEC Congress Nice (F) (1990).
19. F.M. Geenen and J.H.W. de Wit: Proc. CASS '90, New Zealand, November (1990).
20. F.M. Geenen, M.M.M. Dings, E.J.H. Koot, R. de Jonge, S. Peters and J.H.W. de Wit: Proceedings 5th Int. Conference on Electrochemical Methods for Corrosion Research, July 1991, Helsinki. C2/1-3.

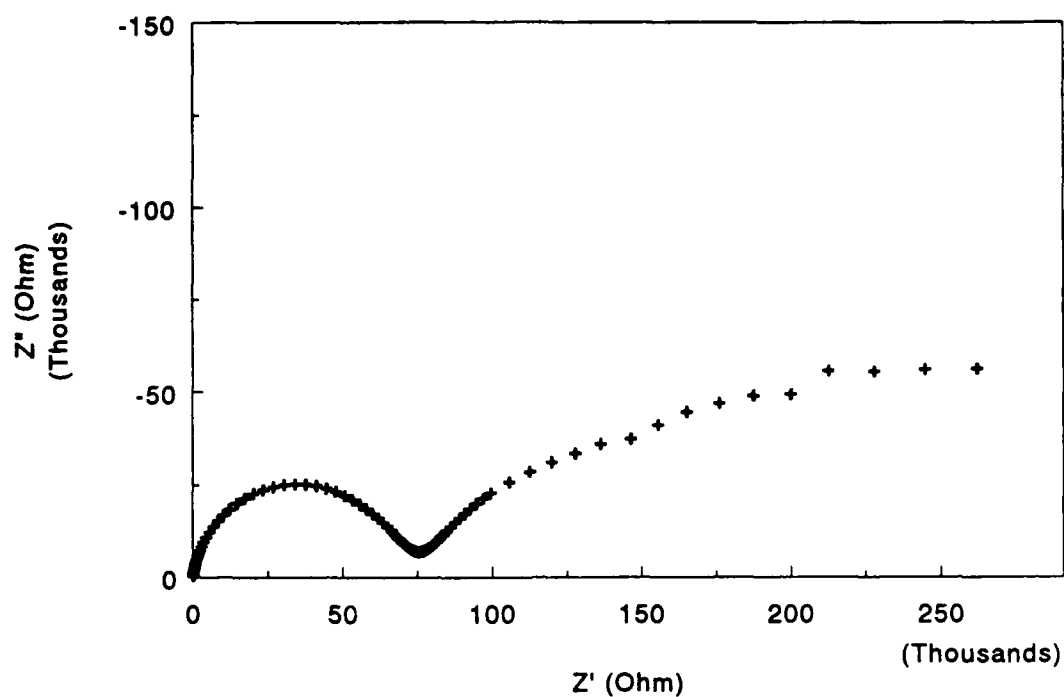


Fig. 1: Typical example of Nyquist plot of the impedance of a metal substrate coated with a non-barrier coating.

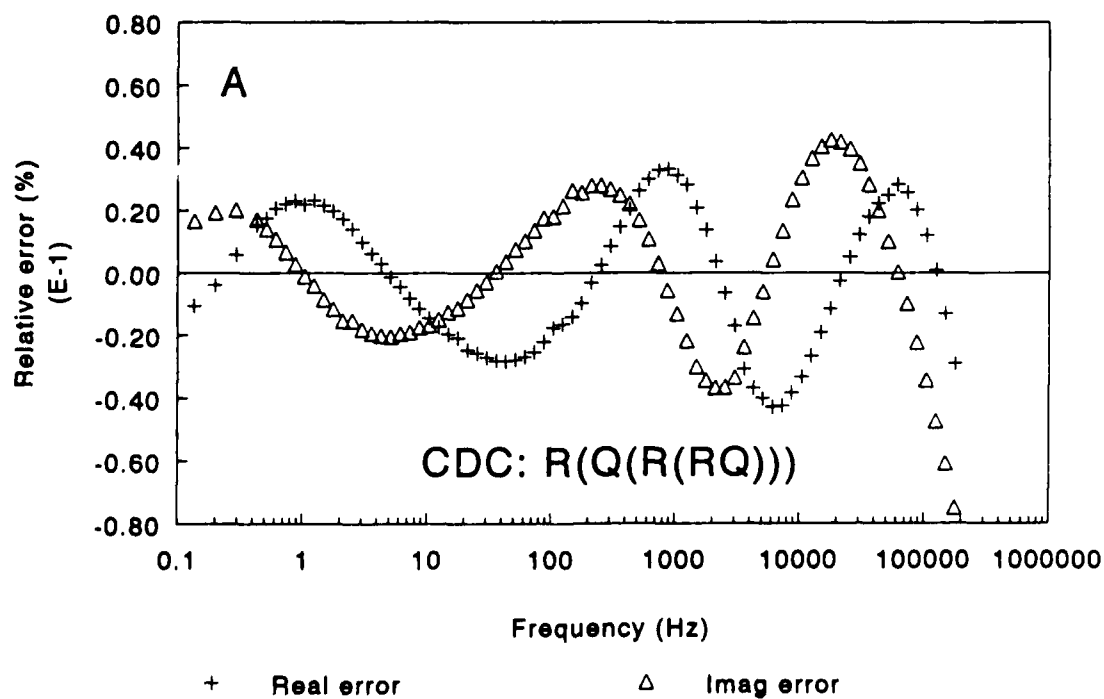


Fig. 2: Residual error plot of fit on impedance measurement of Fig. 1 using a) two time constants

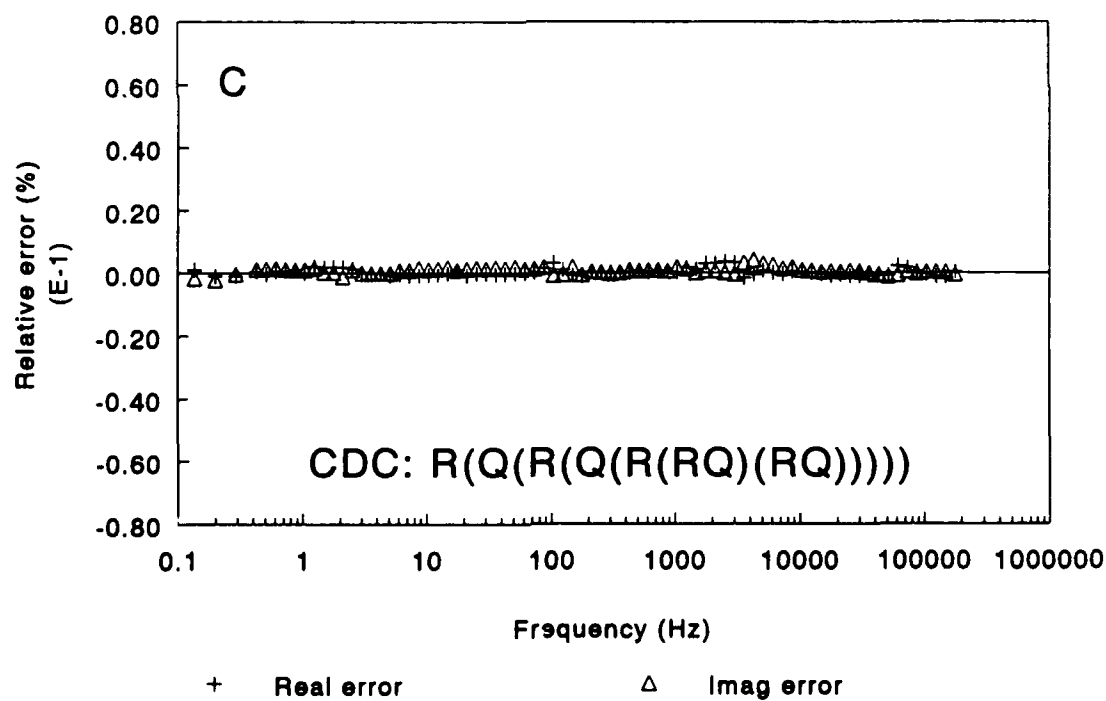
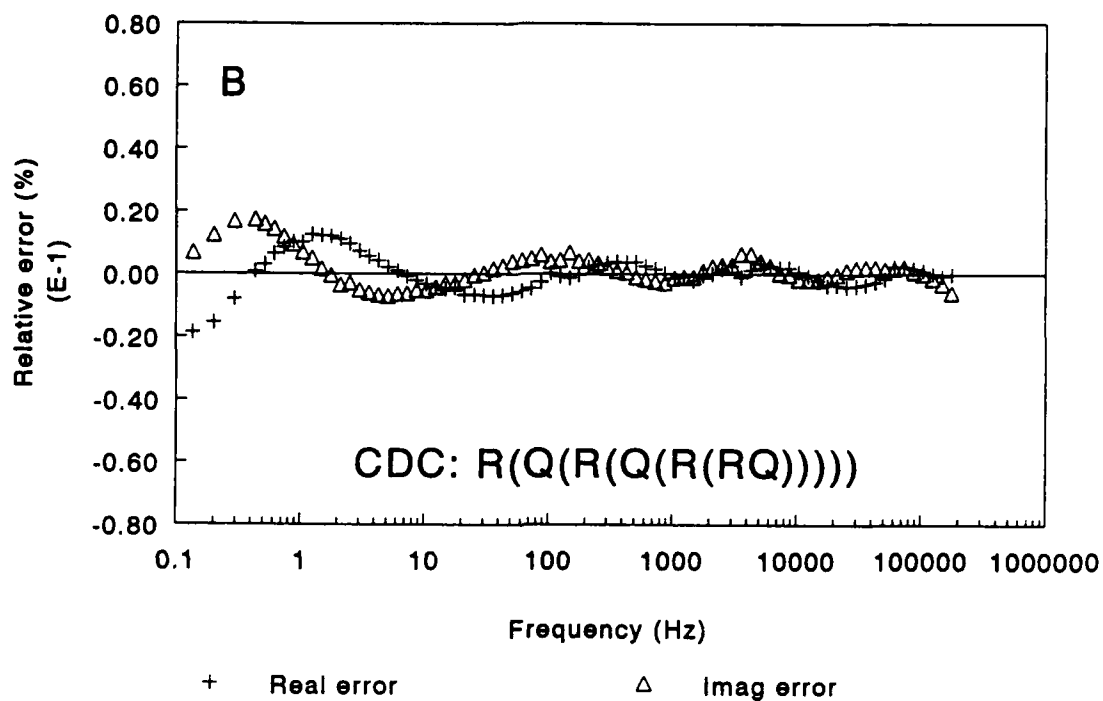


Fig. 2: Residual error plot of fit on impedance measurement of Fig. 1 using
b) three time constants and c) four time constants

Equivalent Circuit

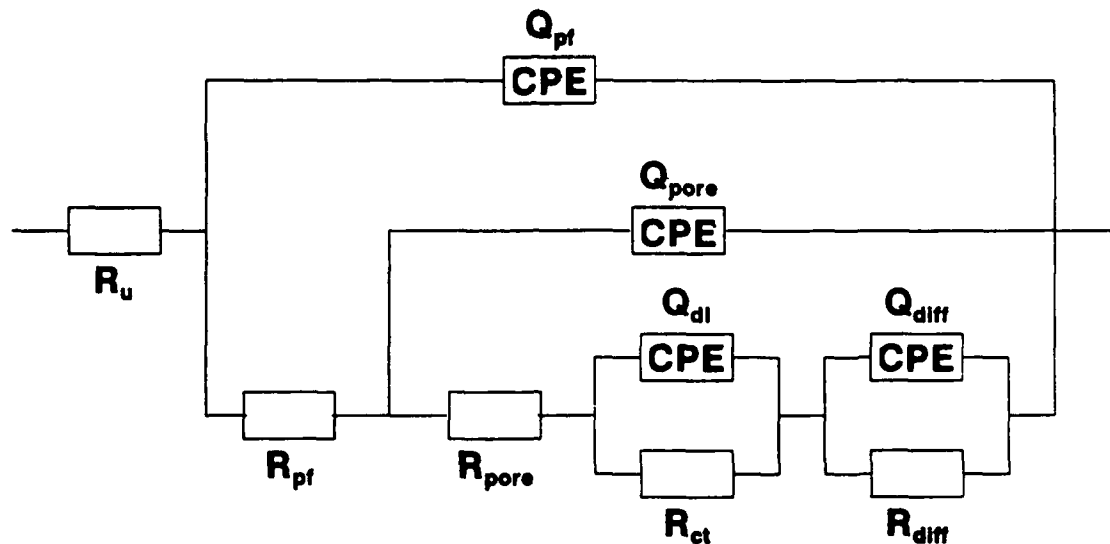


Fig. 3: The equivalent circuit of the impedance of barrier coating.
 CDC: $R_u(Q_{pf}Q_{pore}(R_{pore}(R_{ct}Q_{dl})(R_{diff}Q_{diff})))$.

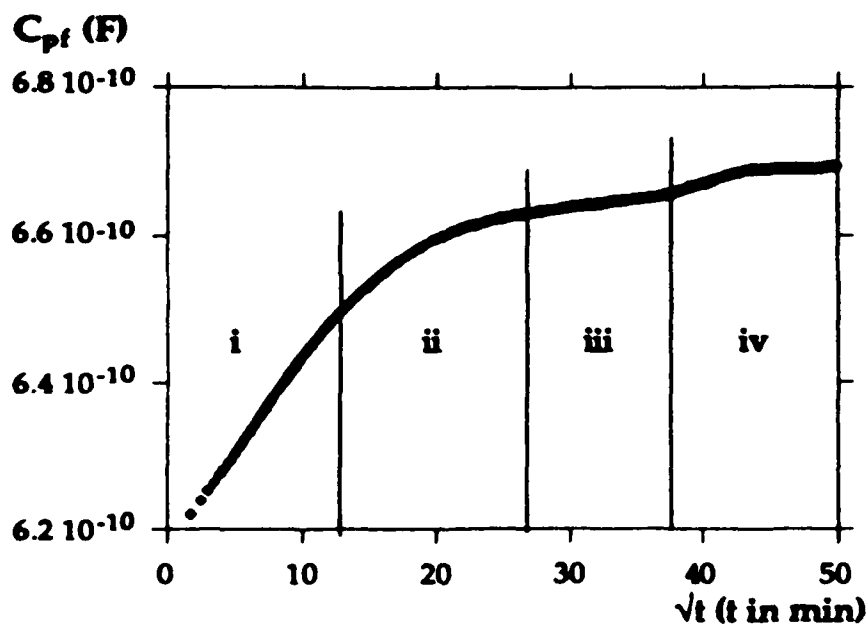


Fig. 4: Determination of the capacitance of the "dry" and water saturated coating C_0 and C_s .

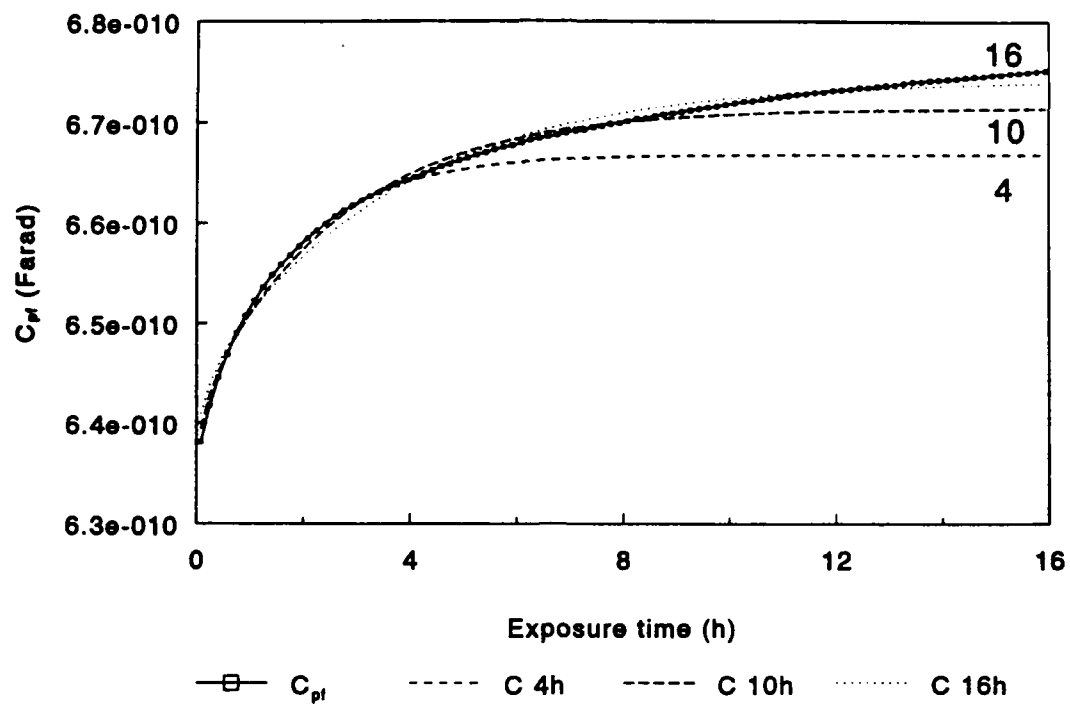


Fig. 5: Fit results on the curve of the capacitance increase as function of time during water uptake for different time intervals.

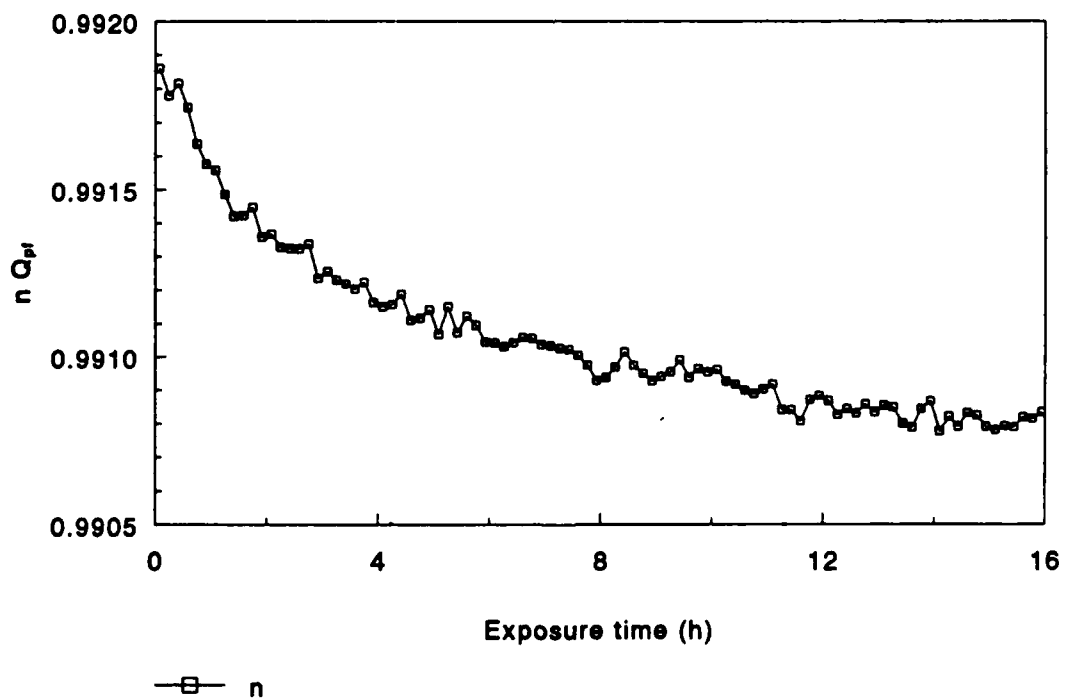


Fig. 6: a: The $n Q_{pf}$ of a coating as function of time during water uptake.

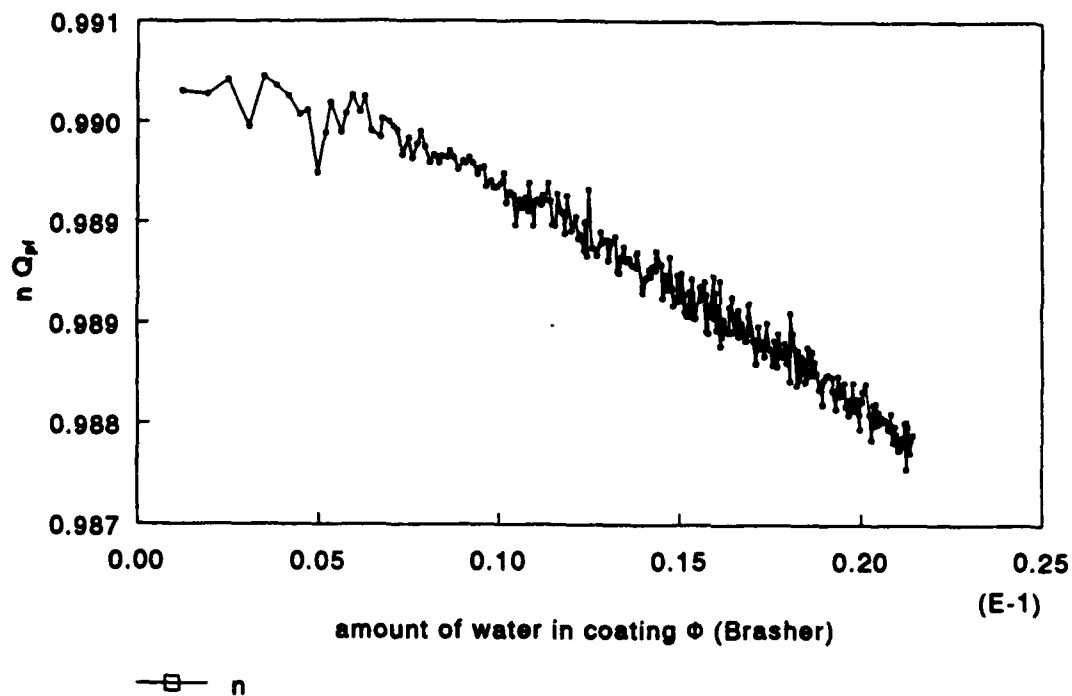


Fig. 6: $b:n_{Qpf}$ as function of Φ during the water uptake of a model epoxy coating with the exposure time as parameter.

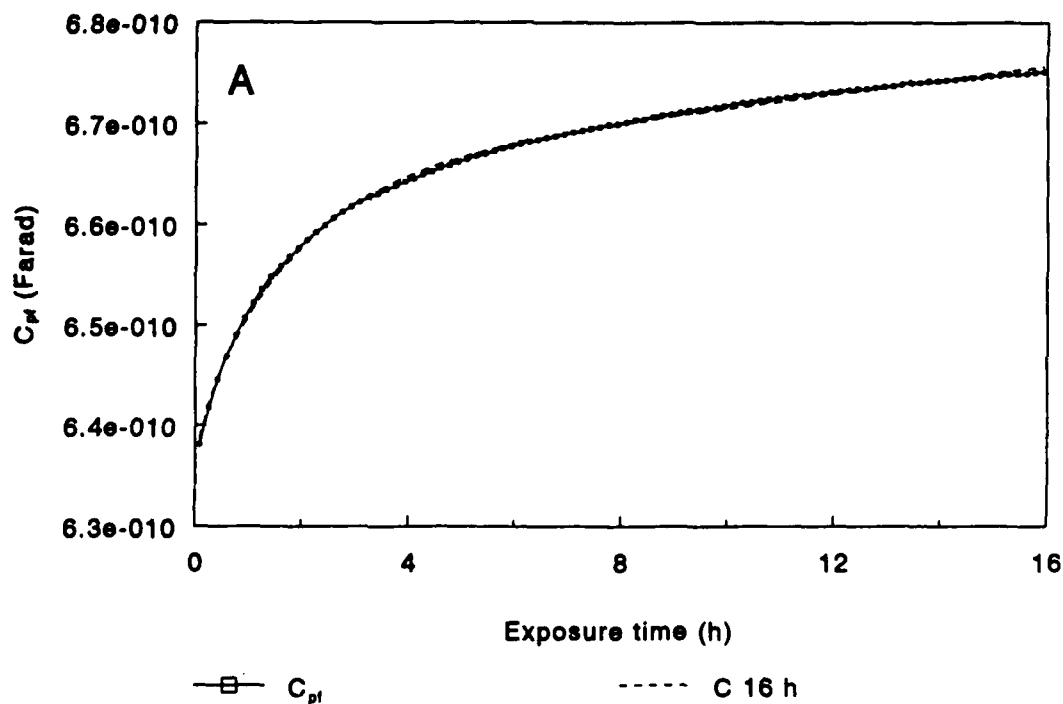


Fig. 7: Fit result on the curve of the coating capacitance C_{pf} as function of time of a coated dielectric sensor during water uptake. a) coating capacitance curve,

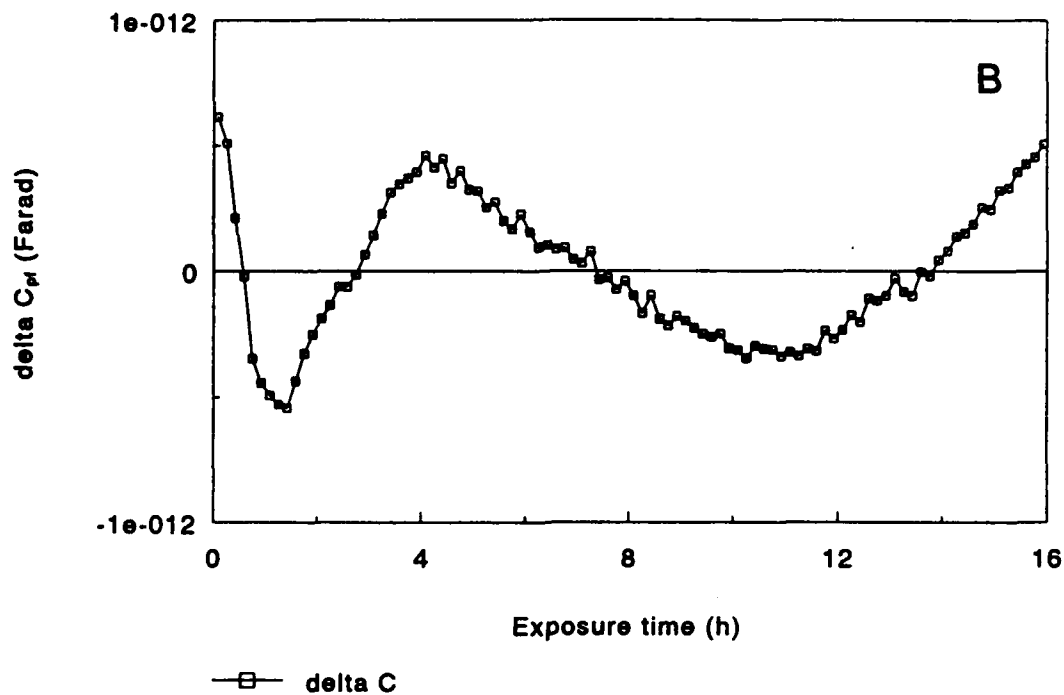


Fig. 7: Fit result on the curve of the coating capacitance C_{pf} as function of time of a coated dielectric sensor during water uptake.
b) error plot $C(\text{fit}) - C_{pf}$.

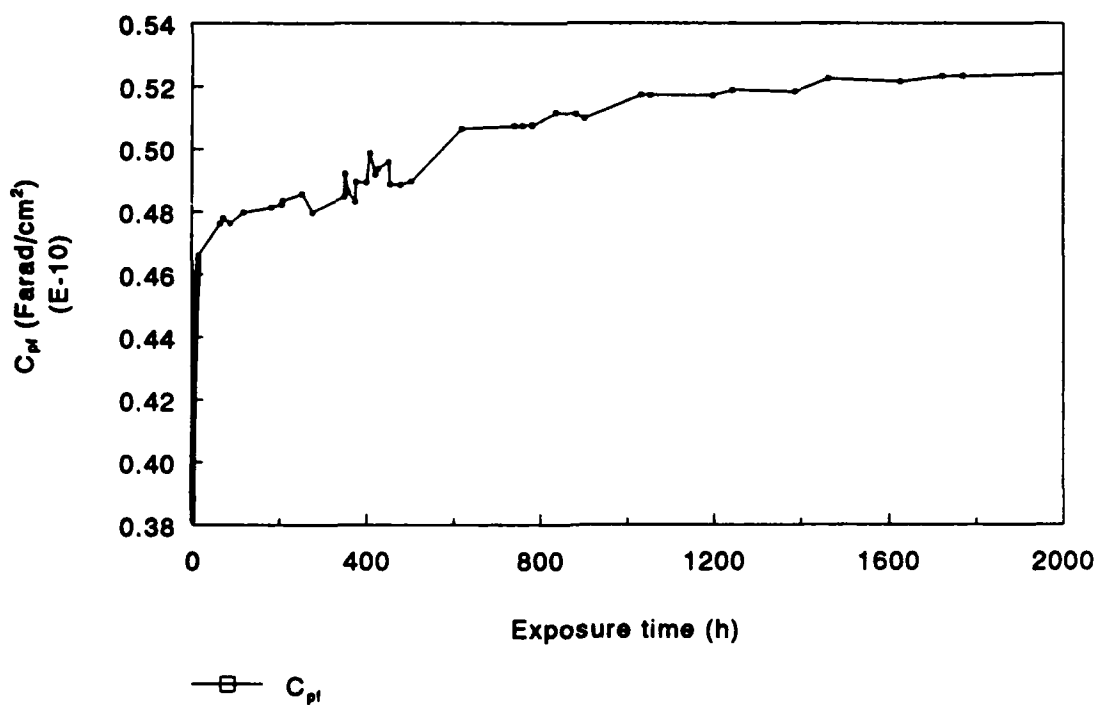


Fig. 8: a :The coating capacitance C_{pf} versus time during a long term exposure in a 3% NaCl- solution.

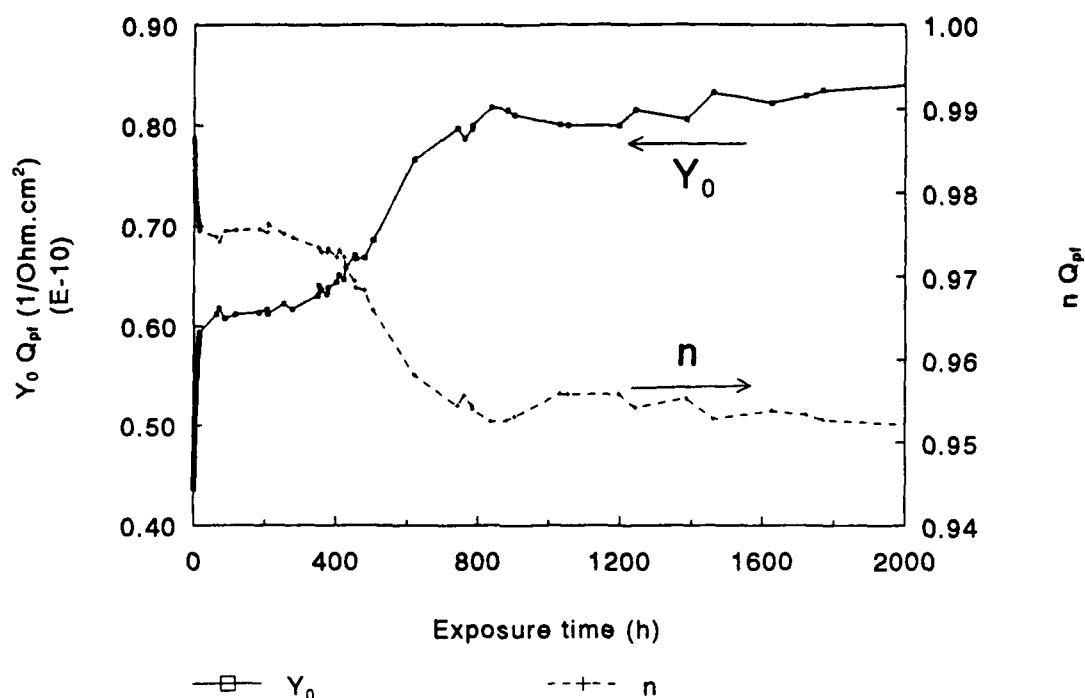


Fig. 8: b: The CPE-parameters Y_0 (left axis) and n (right axis) versus time during a long term exposure in a 3% NaCl-solution.

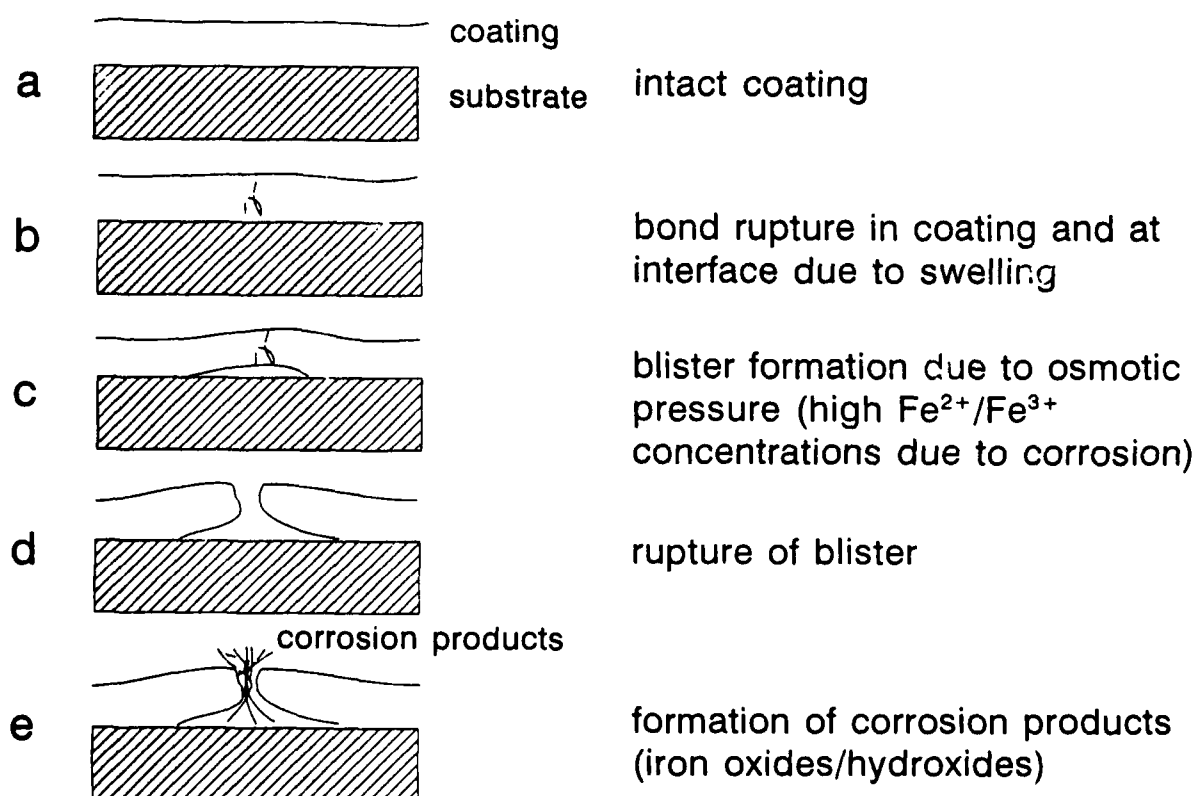


Fig. 9: Schematic view of the formation of corrosion spots under a coating.

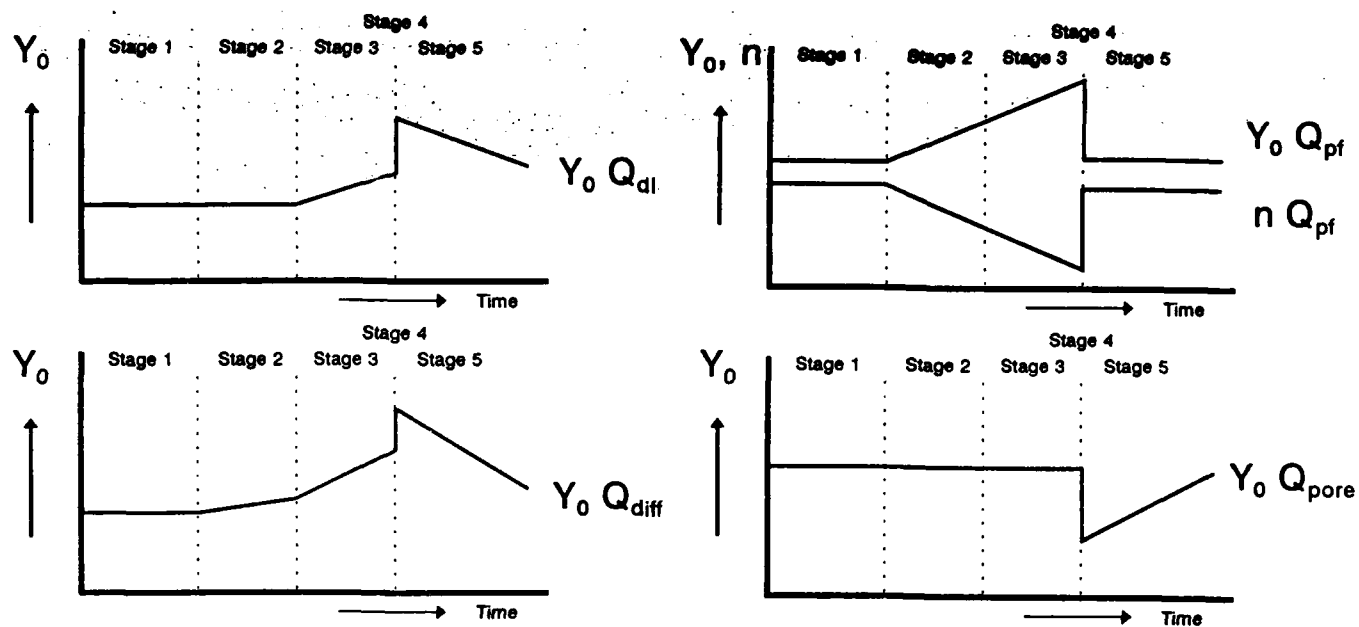


Fig. 10: A schematic representation of the curves of Y_0 (Q_{pore} , Q_{dl} and Q_{diff}) during the different stages of blister formation.

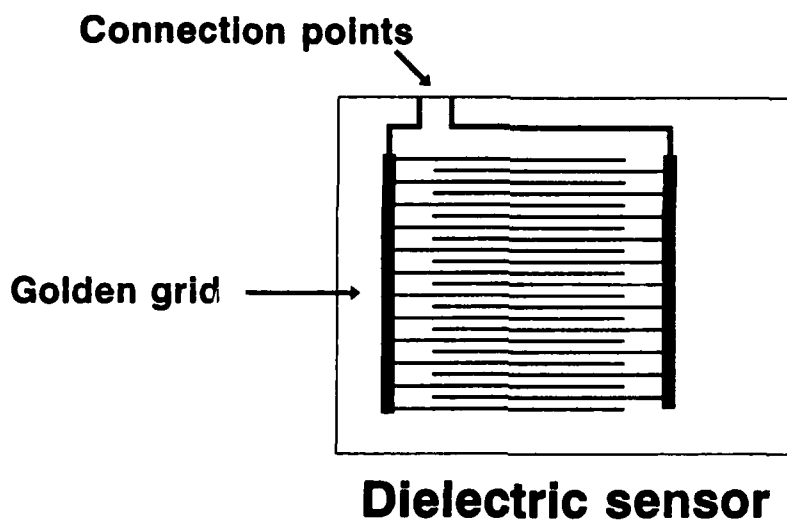


Fig. 11. Schematic view of the dielectric sensor

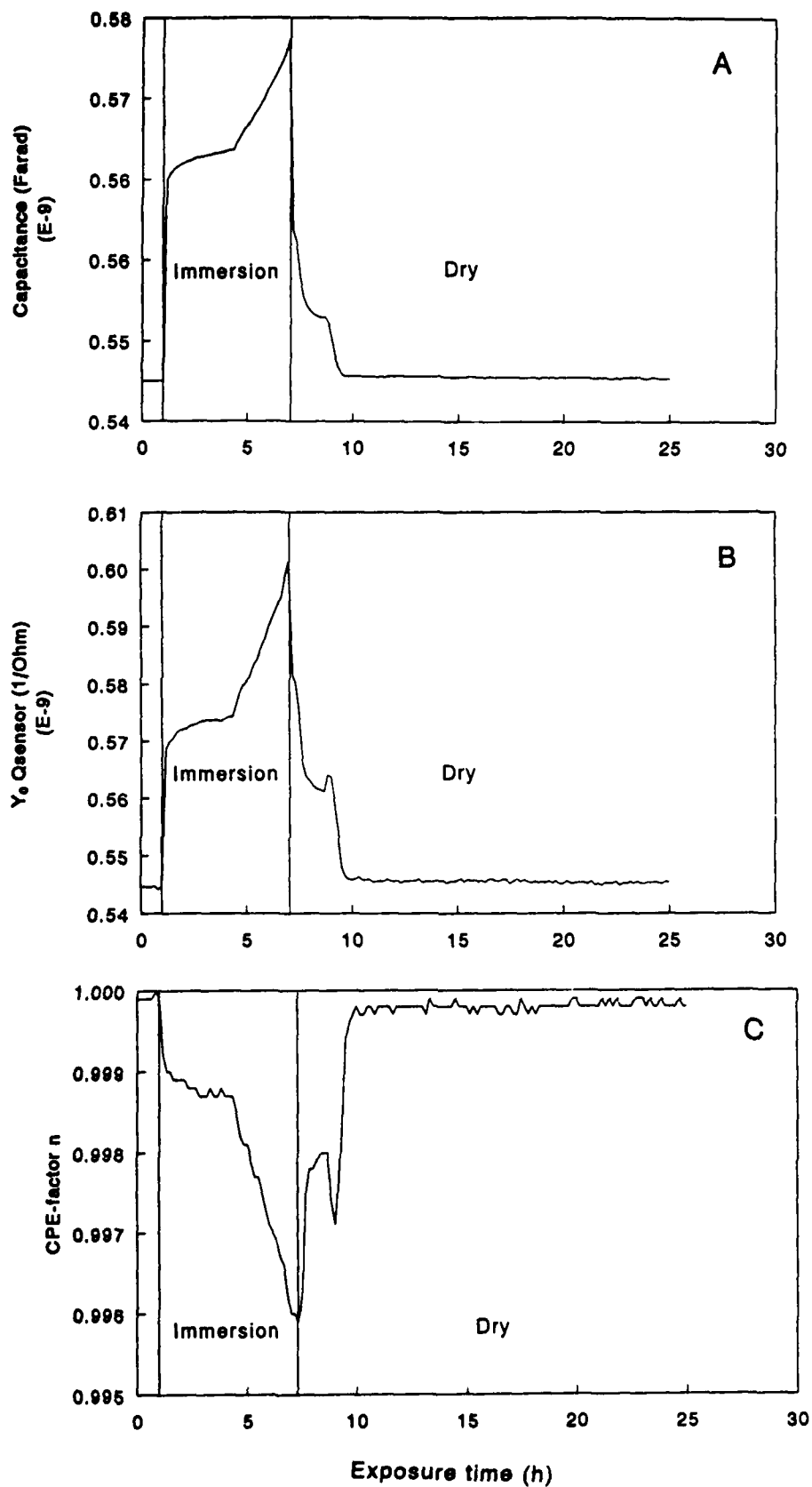


Fig. 12. The capacitance (12A) and the CPE parameters Y_0 (12B) and n (12C) of a dielectric sensor during a wet-dry cycle.

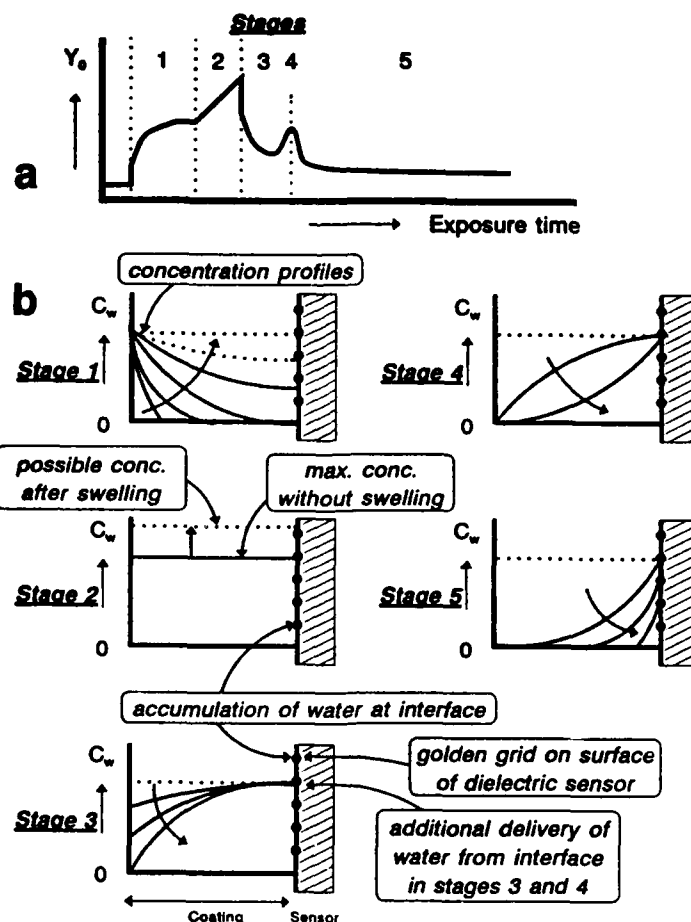


Fig. 13. a: Schematic view of Y_0 of the CPE of the dielectric sensor as a function of time during the dry-wet cycle.
b: The concentration profiles of water during the five stages of figure a.

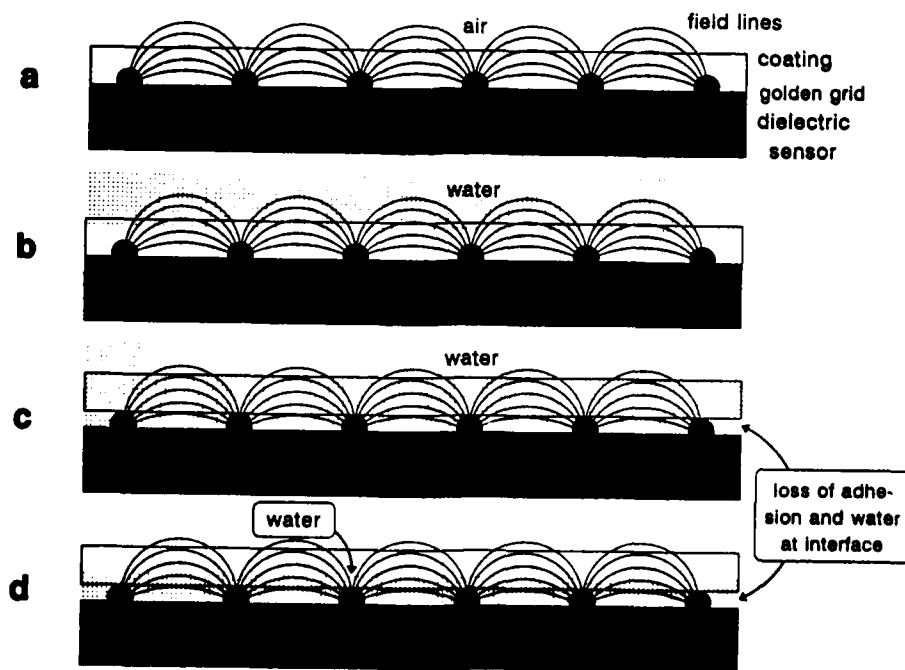


Fig.14. Schematic view of the field lines with the coated dielectric sensor:
a: dry unimmersed coating
b: Shortly after immersion
c: Coating adhesion is partly lost. a separate water phase is formed at the interface
d: Coating is drying with water at the interface.

Substrate effects on the corrosion performance of coated steels under immersed conditions

I. Costa
IPEN-CNEN/SP
Caixa Postal 11049
CEP 05422-970
São Paulo-SP-Brazil

S. E. Faidi
UMIST-Corrosion and Protection Centre
PO Box 88
Manchester

J.D. Scantlebury
UMIST-Corrosion and Protection Centre
PO Box 88
Manchester

Abstract

Little work has been reported in the literature concerning the influence of the substrate on the corrosion performance of coated metals under immersed conditions. In this study, effects of the substrate with minor compositional differences are specifically investigated.

Two mild steels and two low alloy steels, coated with a clear alkyd film, were studied under immersed conditions in a solution containing 3.5 % NaCl. The long term corrosion behaviour of these coated substrates was monitored by visual observation, potential-time measurements and electrochemical impedance spectroscopy. It was found that the observed trends in the corrosion performance were related to the inclusion content of the substrate and not to the small additions of alloying elements. Coated substrates which had the lowest inclusion content showed relatively longer times to failure.

The localised areas of corrosion attack, seen as black or brown spots, were associated with the distribution of the inclusions on the surface. A mechanism is proposed to account for the role of these inclusions on the overall performance of the paint.

Key terms: coated steels, substrate, inclusion content

Introduction

The work reported in the literature¹⁻⁶ concerning the influence of the substrate on the corrosion behaviour of coated systems compares metals of very different electrochemical properties. The general conclusion reached by the previous authors was that the corrosion performance of painted metals was dependent on the electrochemical nature of the substrate. Metal substrates with lower corrosion resistance produced faster rates of film deterioration^{1,3,5}.

When substrates of similar compositions were considered, some coating systems were observed to perform better on low-alloy steels as compared to carbon steels⁷. This would suggest that minor changes in the composition of the steel surface could have an important effect on the protective properties of organic coated systems when exposed to aggressive environments. This observation seems to be particularly true for atmospheric exposure of coated steels, since adherent and protective corrosion products which hinder further corrosion are formed on the defective areas of the coating. Nevertheless, for coated steels under immersed conditions very little work has been reported about the effect of the small addition of alloying elements on the corrosion behaviour of the steels.

Previous work carried out at UMIST⁸ suggested that differences are found between two types of steels, mild steel and low-alloy steel type, when coated and fully immersed in chloride solution. However only visual observations were carried out with no attempt to explain the reasons for the differences. In order to investigate the relationship between the steel substrate characteristics and the corrosion behaviour of the steel when coated and immersed in sodium chloride solution this work was carried out.

Experimental

Two mild steels (MS 1 and MS 2) and two low alloy steels (LAS 1 and LAS 2), whose chemical composition is shown in Table 1, were tested electrochemically in a solution containing 3.5% wt NaCl and at ambient conditions. The surface of the steels was prepared by grinding with silicon carbide grit paper (up to grade 1200). The specimens were then degreased with trichloroethylene in an ultrasonic bath, hot air dried, and immediately stored in a desiccator over silica gel for at least three days before the coating was applied. A long oil alkyd was applied by flood spinning. The coated specimens were left overnight in a desiccator, before finally being cured in an oven at 40°C for four hours. The dry thickness of the coating was found to be in the range of 20 to 30 μm . The resulting coating was transparent making the observation of corrosion, blistering or delamination processes easier. The edges of the specimen were blanked off leaving an area of 10 cm^2 to be exposed to the test environment.

The alkyd coated specimens were subsequently fully immersed in aerated 3.5% wt sodium chloride solution and, in most cases, allowed to remain until the complete breakdown of the paint. During the immersion period the corrosion behaviour of the tested specimens was monitored by measuring the electrochemical corrosion potential, the electrochemical impedance characteristics and visual observations of the steels surfaces.

The electrochemical impedance measurements were performed in the frequency range of 65 kHz to 20 mHz, with 7 readings per decade over extended time periods of around 500 days. The measurements were carried out under potentiostatic control at the open circuit potential as a function of the exposure time. The amplitude of the exciting voltage applied varied according to

the resistance of the coating film. For coatings with resistances $> 1 \times 10^7 \Omega \cdot \text{cm}^2$, the amplitude applied was 50 mV, and for lower resistance coatings it corresponded to 20 mV. The experimental cell consisted mainly of a working electrode, a saturated calomel reference electrode, and a large graphite auxiliary electrode. The reproducibility of the data was established by using 4 specimens of each substrate. The maximum test duration was 500 days.

In order to check if the impedance data reflected the corrosion behaviour of coated steels, the extent of corrosion was assessed visually. The corrosion potential, E_{corr} , was also monitored during these prolonged tests in relation to a saturated calomel reference electrode (SCE). Some of the specimens tested were removed from the solution after a certain period of immersion since no corrosion could be detected from the impedance spectra even though corrosion could be seen on the surface. For this reason only three specimens corresponding to most substrates were compared.

Results and Discussion

The values of coating resistance, R_{pf} , were estimated from the Nyquist impedance diagrams as the chord AC of the arc that best fitted the impedance data, as illustrated in Figure 1. The development of the impedance response with immersion time is exemplified in Figure 2 for one of the specimens tested corresponding to the substrate LAS 2. Figures 3 to 6 show the variation in R_{pf} values with immersion time for the following substrates MS 1, LAS 1, MS 2, and LAS 2, respectively. Table 2 presents a summary of the development of the coating resistance, R_{pf} , with immersion time of the various specimens tested. A curve fitting procedure was used to find the semicircle that best fitted the experimental data in the Nyquist plot. At the beginning of the immersion period an arc running almost parallel to the Z'' axis was produced for most coated specimens indicating an initial highly protective coating. This also indicated that the coating on the specimens used was not grossly defective, and there was no significant ionic transport through the coating.

From figures 1 to 4 and table 2 it can be deduced that the steel substrate seems to have an effect on the behaviour of the coated system. While the coating on the LAS 2 steel substrate remained very protective most of the time, relatively rapid deterioration of the protective properties of the coating occurred for most of the specimens corresponding to the substrate MS 1. The coating on one of the specimens of this latter substrate, (MS 1(4) table 2), however presented an exceptional resistance and it still showed a capacitive behaviour at the end of the test.

The performance of the coating-substrate system seemed to be ranked in the following order, LAS 2 $>$ MS 2 \approx LAS 1 $>$ MS 1. The criteria used for comparing the performance of the coated substrates was the time for failure and the time for a decrease in R_{pf} to values $\leq 10^6 \Omega \cdot \text{cm}^2$. It can also be noted that two of the LAS 2 coated specimens did not fail during the period of the test, even though the R_{pf} corresponding to these specimens had dropped to values of the order of $10^6 \Omega \cdot \text{cm}^2$, after 200 and 300 days immersion, indicating that some deterioration of the system occurred. This supports the idea that even for cases when the coating is losing its protective characteristics, the lower corrosion of the LAS 2 substrate retarded the complete failure of the system.

For the coatings which maintained their protective characteristics during all the test, the substrate did not seem to have affected the performance of the system. This is expected since the coating in these cases works as an almost "perfect barrier" to the corrosive environment.

Despite the low coating thickness used, proper coating application after adequate surface preparation might have been the cause for the resulting outstanding coating characteristics obtained. The highly resistant coatings were evidenced by a capacitive behaviour at the end of the test period (500 days). Another possible reason for the excellent properties of some coatings, even after long periods of exposure, might have been their high cross-linking density resulting from a complete cure of the coating.

Unfortunately, "perfect coatings" do not occur in practice and defective coatings are usually found. Defects can also develop during the service lifetime of coatings. In these common cases, "non-perfect" coated systems, the substrate electrochemical properties is believed to affect the corrosion characteristics of the system. In the cases where R_{pf} decreased with time, it is considered that the corrosion process at the interface might have enhanced conduction through defects in the coating. Thus, substrates more susceptible to corrosion would result in lower times for failure of the coated system.

Differences in the general trend to resist corrosion failure however could not be related to the chemical composition. An attempt was then made to explain the reasons for the different behaviour exhibited by the various coated substrates based upon their microstructural characteristics. The inclusions present in the various steels used were analysed by Optical Microscopy and Energy Dispersive Microscopy. These were found to consist mainly of MnS in the case of the mild steel types and oxide or mixed (oxide-sulphide) in the case of the low alloy steels used. The average number of inclusions per cm^2 , table 3, was also different for the various steels tested. For the steel MS 1 the average number of inclusions was 2 to 4 times larger than that of the other steels studied. The steel with the lowest number of inclusions was the LAS 2 and that was also the steel to resist the longest the corrosion failure of the coated system among the steels used.

The reasoning behind investigating the microstructure characteristics as a possible cause for the differences observed was that some of these features, which were later found to be related to the inclusions present in the steel, were easily revealed in the case of the steel substrate MS 1 after few days immersion. They were usually associated with small brown and black corroding spots, as illustrated in Figure 7 (a). In the case of the steel MS 1 the inclusions were aligned in the rolling direction as result of the production process being easily distinguished to the naked eye. Since sulphide inclusions are good electronic conductors and as such can take part in the electrochemical reactions they might contribute to the phenomenon of underfilm corrosion. They can also initiate pitting corrosion since they act as local cathodes for hydrogen evolution. Oxide particles on the other hand are poor electronic conductor and as such are not expected to be as effective as the sulphide types.

For most specimens tested localized corrosion was noted which was associated with small brown changing to black corrosion spots, Figure 7 (b) to (d). The localized corroding spots were most likely associated with "weak" areas of the coating which allowed localized attack of the substrate and production of alkali at the surrounding areas. These were either present initially or developed during exposure to the corrosive environment. Generally the corrosion of coated metals has its first step as the result of a galvanic effect with the anodic reaction being located at the bare metal exposed at a paint defect or "weak" area, and the cathodic reaction underneath the intact coating. The way the corrosion product acts subsequently is treated differently by three mechanisms. In one of the proposed mechanisms the corrosion product is considered to behave as inactive areas⁹. A second explanation assumes that the voluminous corrosion products affect mechanically the coating/metal bond, lifting the paint

and eventually causing the breakage of the interfacial bond¹⁰. A third hypothesis proposes that the corrosion products actively participate in the electrochemical reactions responsible for metal substrate corrosion and subsequent delamination¹¹.

It is believed that all the three proposed mechanisms might be operative depending on the characteristics of the coating and corrosion products formed. When the coating was highly protective during the whole test period, compact and not voluminous corrosion products consisting mainly of FeOOH (brown rust) were formed which might have blocked the access of corrosive species to the underlying metal without disturbing the bond metal oxide-coating. Since this type of rust is not a good electronic conductor it is unlikely to have taken part in the electrochemical reactions and the first mechanism is bound to have prevailed. This mechanism might have been operative in the case of the specimen MS 1(4) which showed small brown corrosion spots after few days immersion and was still unchanged when the test ended.

In some cases the corrosion black spot was surrounded by a delaminated area, Figure 7 (b), which was found to be related to the presence of sodium and hydroxide species detected by Auger and XPS analysis. Magnetite (Fe_3O_4), the black corrosion product, is an electronic conductor and thus might have participated actively in the electrochemical reaction eventually leading to delamination. The formation of voluminous corrosion products were only noticed in the late stages of corrosion of some of the specimens used and as such it is not believed to have played an important role in the cases studied.

The inclusions in the steels studied are believed to have an important effect on the initial stages of corrosion. The sulphide inclusions are cathodic to the ferrite matrix causing the creation of microgalvanic cells when an electrolyte is present. They work as nucleation sites for corrosion which might develop or not depending on the characteristics of the coating. Oxide inclusions although not metallic conductors might also affect the properties of coated steels by decreasing the adhesion of protective coatings¹². Thus the areas associated to the oxide inclusions are areas where water could be easily accumulated leading to corrosion initiation.

What happens after corrosion has started however depends on the characteristics of the coating. For highly protective coatings the corrosion product is deposited on the initial local sites restricting the access of the corrosion species to the underlying metal. The corrosion of the substrate is stimulated as a result of the bare metal exposed locally at the coating defect but if the interfacial bond of the coating-metal oxide does not deteriorate at areas distant from the corroding spot, corrosion is restricted to the "weak" area leading to localized corrosion. The deposition of insoluble corrosion products around the void or localized corroding area follows. Corrosion products develop and rise over the corroding area and its surroundings forming a layer or incrustation which isolates the environment within the cavity from the bulk electrolyte. This subsequently retards the diffusion of corrosive species, and once the defective area has been blocked by insoluble corrosion product, corrosion can stop. This situation can be maintained for long times in the case of highly resistant coatings, until corrosion is allowed to start on other areas of the specimen.

For less resistant coatings with the presence of defects, pores, or "weak" areas corresponding to free volume regions however corrosive species will have easy access to the underlying metal. If due to the low coating resistance the bond at the coating-substrate interface is disturbed this can result in the loss of adhesion between the coating and the substrate. Since water can be replenished at these areas of the interface it forms a layer which can sustain corrosion. Once water has accumulated on large areas of the surface the corrosion characteristics of the substrate are supposed to have a significant effect on the anti-corrosion

properties of the system. The boundary regions between inclusions and metallic matrix are the likely regions for corrosion initiation due to a microgalvanic effect.

Inclusions can also affect the movement of water through a capillary or pore which is easier under the influence of a potential gradient, by electroendosmosis¹². Consequently, galvanic couples at the interface may lead to a blister. In the blistered area, coating has lost its adherence and water may accumulate allowing generalized corrosion to start. Thus inclusions at the interface can act as additional corrosion promoters. Galvanic cells are set-up between the heterogeneity and the steel base. These cells are sufficient to activate the corrosion process as soon as the corrosive species reach the interface. MnS type inclusions which are cathodic relatively to bare metal can provide ideal nucleation sites for rusting. These when attacked by an acidic environment, produce HS^- and S^{2-} which in turn promote a faster dissolution rate of iron by decreasing its activation polarization¹³. Increasing acidity caused by hydrolysis reactions, leads to the reduction of hydrogen ions by electrons originating from the oxidation reactions. The evolution of hydrogen can occasionally cause the breaking of the crust of corrosion product. If this occurs, further corrosion is possible.

Conclusions

A correlation seemed to exist between the microstructural characteristics of the steel substrates used and their corrosion performance when coated and immersed in solution of 3.5% wt NaCl. The steel which had the largest average number of sulphide inclusions produced the lowest corrosion resistance. On the other hand, the longest times for failure of the coated systems tested were associated with the substrate of lowest inclusions content. It was proposed that the inclusions type and content of the various steels studied was the probable cause for the differences found in their corrosion performance under immersed conditions.

Acknowledgements

The authors express their thanks to CNPq and IPEN-CNEN/SP (Brazil) for the financial support provided in this work and to the Corrosion and Protection Centre-UMIST (U.K.) for the provision of research facilities.

References

1. N.D. Tomashov, Y.N. Mikhailovskii, V.V. Leonov, *Corrosion*, 20 (1964): p. 125t.
2. N.D. Tomashov, Y.N. Mikhailovskii, V.V. Leonov, *Corrosion*, 20 (1964): p. 218t.
3. G.W. Walter, *Corrosion Science*, 26 1 (1986): p. 27.
4. W.W. Kittelberger, A.C. Elm, *Ind. Eng. Chem. Prod. Res. Dev.*, 38 (1946): p. 695.
5. R.N. Miller, *Materials Protection*, 7 (1968): p. 35.
6. E.L. Koehler, *Corrosion*, 40 1 (1984): p. 5.
7. W. Funke et al, *Journal of Coatings Technology*, 58 741 (1986): p. 79.
8. J.G.de Souza, MSc. Thesis, UMIST, 1980.
9. R.R. Wiggle, A.G. Smith, J.V. Petrocelli, *Journal of Paint Technology*, 40 (1968): p.174.
10. J.V. Standish, *Ind. Eng. Chem. Prod. Res. Dev.*, 24 (1985): p.357.
11. D.L. Jordan, *Advances in Corrosion Protection by Organic Coatings*, (Cambridge, U.K.: J.D.Scantlebury, M. Kendig, 1989), p. 30.
12. G. Wranglén, *Corrosion Science*, 14, (1974) : p. 331.

Table 1 - Elemental composition of steels studied.

Steel	MS 1	LAS 1	MS 2	LAS 2
C	0.20	0.11	0.058	0.076
Si	0.04	0.47	0.012	0.36
Mn	0.67	0.78	0.24	0.36
S	0.028	0.010	0.012	0.009
P	0.011	0.013	0.011	0.093
Cr	n.d.	0.50	n.d.	0.88
Ni	0.016	0.02	0.02	0.013
Mo	n.d.	n.d.	0.01	n.d.
Co	0.005	0.007	0.006	0.006
Cu	0.01	0.32	0.03	0.28
Ti	0.003	0.03	0.003	n.d.
Al	0.002	0.03	0.046	0.035
Sn	0.004	0.006	0.013	0.007
Fe	balance	balance	balance	balance

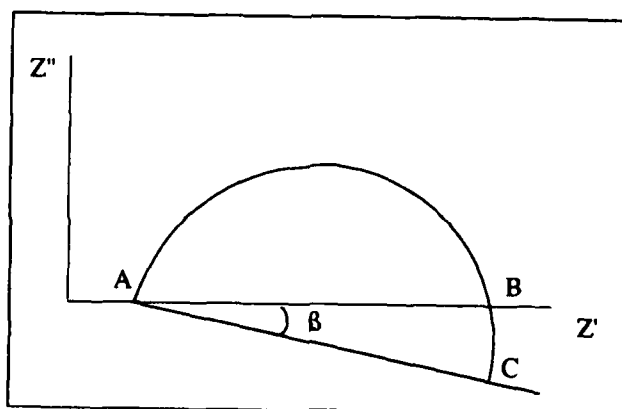


Figure 1 - Nyquist plot used for estimating R_{pf} from the chord AC (β is the depression angle).

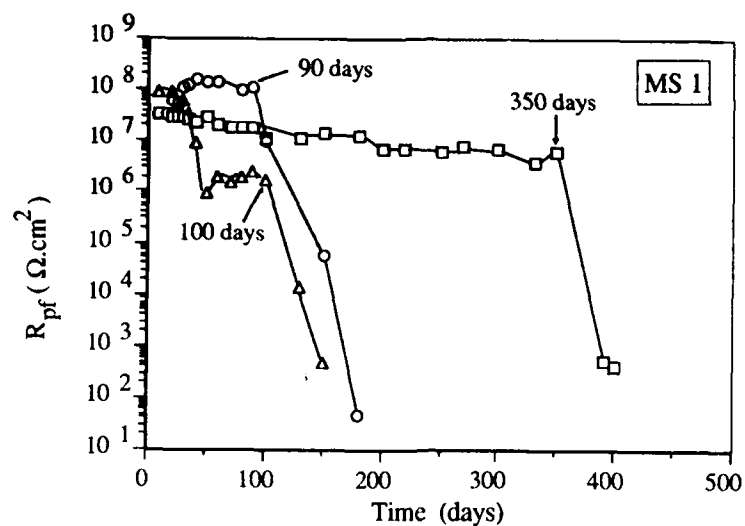


Figure 3 - Evolution of R_{pf} with immersion time for MS 1 specimens.

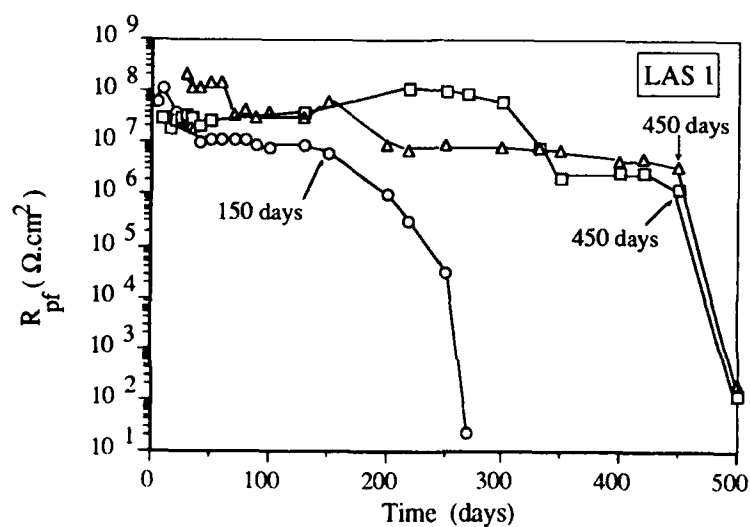


Figure 4 - Development of R_{pf} with immersion time for LAS 1 specimens.

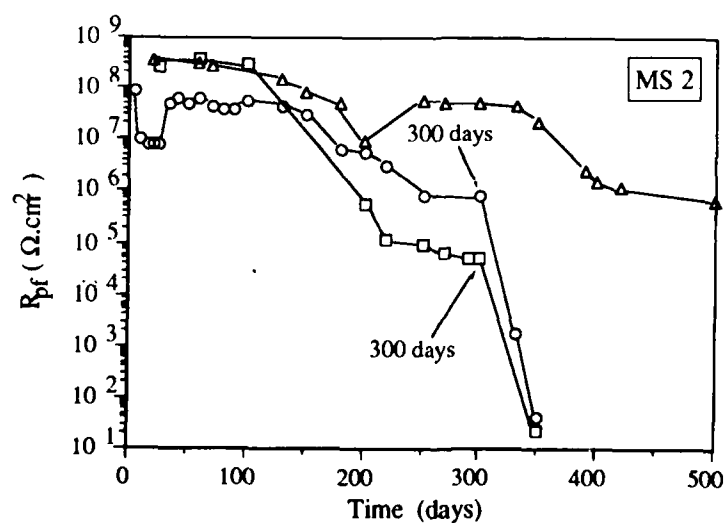


Figure 5 - Progress of R_{pf} with immersion time for MS 2 specimens.

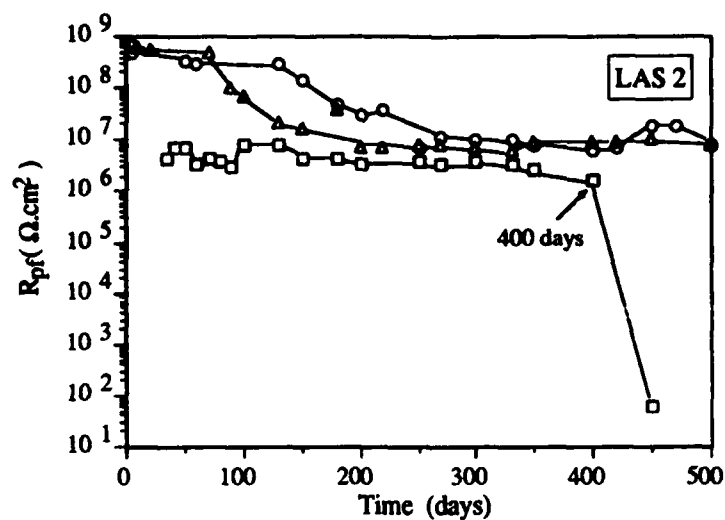


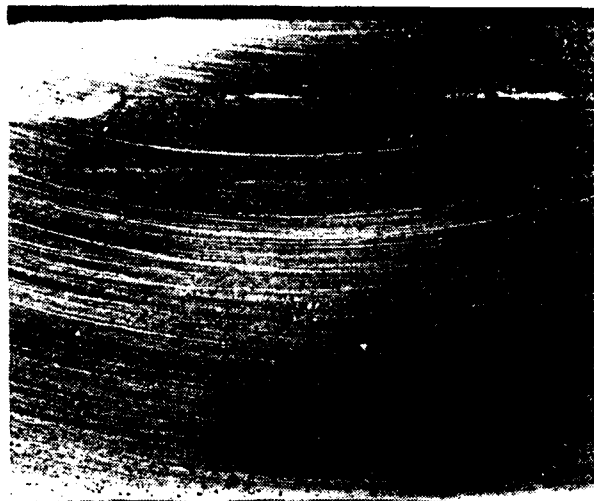
Figure 6 - Changes of R_{pf} with immersion time for LAS 2 specimens.

Table 2 - Time for coating failure and decay in resistance.

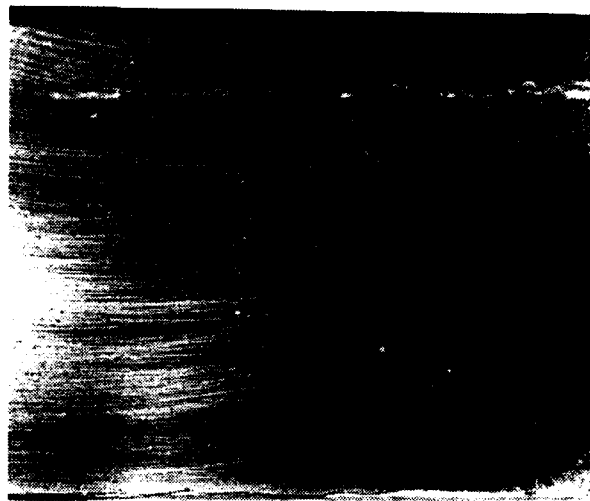
Substrate	time (days) for $R_{pf} \leq 10^6 \Omega \cdot \text{cm}^2$	time for failure (days)
MS 1 (1)	40	150
MS 1 (2)	100	180
MS 1 (3)	200	390
MS 1 (4)	always $>10^6 \Omega \cdot \text{cm}^2$	did not fail
LAS 1 (1)	90	250
LAS 1 (2)	330	500
LAS 1 (3)	200	500
MS 2 (1)	200	350
MS 2 (2)	390	did not fail
MS 2 (3)	180	350
LAS 2 (1)	35	450
LAS 2 (2)	200	did not fail
LAS 2 (3)	300	did not fail

Table 3 - Characteristics of most common inclusions in the steels used.

Steel	Average number of inclusions/ cm^2	Most common types	Shape
MS 1	(6040±560)	mainly MnS $\text{Al}_2\text{O}_3/\text{SiO}_2/\text{MnO}$	elongated round
LAS 1	(3020±1600)	mainly SiO_2 $\text{Al}_2\text{O}_3/\text{MnS}/\text{Cu}_2\text{O}$ TiO_2	round round round
MS 2	(2020±380)	mainly MnS Al_2O_3	lens round
LAS 2	(1440±100)	SiO_2 Al_2O_3 $\text{Al}_2\text{O}_3/\text{MnS}$	round round lens



(a)



(b)



(c)



(d)

Figure 7 - Coated steels after 30 days exposure to the chloride solution
(a) MS 1, (b) LAS 1, (c) MS 2, (d) LAS 2

Why the Improved Performance of Phosphoric Acid Pretreatments Under Aluminium Hydroxide Addition

ELISABETE ALMEIDA and DULCINEA PEREIRA

Serviço de Corrosão e Protecção de Materiais, DTM, INETI
1699 Lisboa Codex (Portugal)

M.O. FIGUEIREDO

Centro de Cristalografia e Mineralogia, I.I.C.T.

Alameda Afonso Henriques, 41, 4ºE,

1000 Lisboa (Portugal)

V.M.M. Lobo

Universidade de Coimbra, 3000 Coimbra (Portugal)

M. MORCILLO

Unidad Corrosion y Proteccion, CENIM

Av. Gregorio del Amo, 8, Madrid (ESPAÑA)

Abstract

This work presents the main results of an experimental study carried out with rust pretreatments based on phosphoric acid solutions, under addition of aluminium hydroxide.

Because the transformation of rust steel surfaces by phosphoric acid solutions depends strongly of the interfacial conditions, the first step of this work was clear definition of rust formation conditions and of a reproducible technique for brushing them to a known degree of SIS 055900. After that, the best range of acid concentration was optimized in the case of phosphoric acid solutions and of solutions saturated with aluminium hydroxide.

Several characterization techniques were used such as scanning electronic microscopy (SEM), energy dispersive spectrometry (EDS), infrared spectrometry (FTIR) and x-Ray diffraction (XRD) to interpret the phenomenon rust transformation. The results obtained allow to conclude for a best anticorrosive behaviour of phosphoric acid solutions saturated with aluminium hydroxide and to understand the main reasons for this improvement of anticorrosive behaviour.

Key terms: rusted steel surfaces, pretreatments, phosphoric acid, aluminium hydroxide.

Introduction

Although the study of rust pretreatments based on phosphoric acid have already a long history, this kind of pretreatments being among the oldest rust converters, today it is possible to find very controversial literature about this subject^[1-4]. Recently, it was possible to verify that the rust conversion action of phosphoric acid solutions depends strongly on the interfacial conditions^[5-6]. Either acid solution concentration^[5-6] or steel surface weathering conditions^[6] have a significant influence on the rust conversion mechanisms developed by this kind of pretreatments.

In this work, we investigate the main reasons for the best anticorrosive behaviour of the pretreatments, in which aluminium hydroxide is added to phosphoric acid solutions. With this purpose the anticorrosive behaviour of the rust conversion layers, their structure, chemical composition and solubility properties are compared. The adhesion of paint coatings to different rust conversion layers was also evaluated.

Experimental

Steel Substrates Used

The experimental work was carried out on mild steel according to ISO 630^[7] rusted during 10 months in a low-contaminated atmosphere field station^[6] and brushed using an automatic and reproducible technique^[8] to a degree CSt2 as described in standard SIS 055900^[9].

Pretreatments Used and Their Application

As pretreatments phosphoric acid solutions at 14,6% (w/w) and 33,2% (w/w), were used, because the rust conversion layers obtained with intermediate concentrations seem to show the best results for painting, under the actual steel surface weathering conditions^[6]. Similarly, the acid solutions concentrations used when saturated with aluminium hydroxide were 27,3% (w/w) and 38,6% (w/w).

For each sample with a 150 cm² area of corroded and subsequently well brushed steel surface, 0,7 ml of pretreatment solution were spread on the surface in a cross motion, as a paint, with the aid of a perfectly clean and dry little brush.

The surfaces pretreated were dried in laboratory during 24 hours at 23 ± 2°C before any evaluation test was performed.

Surface Characterization

Visual and microscopic observations

The surfaces were observed visually and with an optical microscope Olympus SHZ equipped with an Olympus camera OM-2 SP and also a JEOL JSM-35CF scanning electron microscope (SEM) equipped with an energy-dispersive X-ray spectrometer, Tracor Northern. Before SEM/EDS observations the surfaces under study were coated with a carbon film using a vacuum evaporator JEOL JEE-4X.

X- Ray Diffraction (XRD)

XRD was performed directly on the steel surface using a Rigaku D/MAX II C diffractometer either operating at 45 KV-20 mA with

a curve graphite crystal monochromator and a broad focus cobalt source, or at 45 KV - 30 mA with a copper tube and a nickel filter. The samples were scanned up to $85^\circ 2\theta$ with a speed of $2^\circ 2\theta \text{ min}^{-1}$. Only in two cases XRD was performed on powders scraped from steel surfaces.

IR Absorption Spectrometry

Infrared absorption spectra of the surface corrosion products, before and after pretreatments, were obtained on KBr pellets using a Mattson instrument model Galaxy 6030 and a microcomputer IBM system/2 model 55 SX with software FTIR/FIRST for data acquisition and processing.

Solubility measurement

After 24 hours of contact of the rust conversion layers with 18 ml of destilated water, in a perspex cell of 19mm of diameter, the electrolyte was homogeneized and retired for a glass, where it was acidified with one drop of HCl. Iron and phosphorous were determined in this solution by absorption molecular spectrometry, using a spectrometer Pye Unicam SP 300. Iron determination was based on the ortophenantroline complex method^[10]. The phosphovanadomolibdate complex method was used for phosphorous evaluation^[11].

Paint Coating Appllication and its Behaviour

A paint system composed by $150 \pm 25 \mu\text{m}$ of an epoxy-poliamide primer contaning aluminium as a pigment (P) and a finish coat urethane with titaneo dioxide (F). Was applied on a large number of panels with the four different rust conversion layers using a laboratory Doctor Blade applicator^[13]. The total dry thickness of the paint coating was $245 \pm 15 \mu\text{m}$.

Paint adhesion

The paint adhesion was evaluated according to ISO 4624^[13]. Under these conditions, the results were assessed as breaking force (expressed in Newton), breaking strength (in MegaPascal) and nature of failure. The last item, expressed in %, can either be by cohesion inside the material itself-Rust Conversion Layer (RCL); Primer (P) and Finishing Coat (F)-or by adhesion between two different materials (RCL/P, P/F and F/G-adhesive). The adhesive used to settle the metallic piece for catching to the pull-off machine was of the cyanoacrilate type. An Instron instrument, series 1100 of 10 Ton, connected to a microcomputer Hewlet Packard HP 85 was used for the pull-off test.

Anticorrosive behaviour

The anticorrosive behaviour was evaluated by direct exposure of the rust conversion layers in laboratory atmosphere ($23 \pm 2^\circ\text{C}$ and $50 \pm 5\% \text{ RH}$) and by indirect exposure, after paint coating application (2.4), either in a humidity cabinet^[14] or

in the natural atmosphere of Lumiar/Lisboa test site.^[6-15]
Coating degradation was evaluated according to ISO 4628.^[16]

Results and Discussion

The steel surfaces used in the present study were codified according to their surface preparation as shown in Table 1.

The morphology of the studied rust conversion layers (RCL) is quite different as can be seen on figs 1 and 2. The lower acid solution concentration leads to the formation of a white-bluish RCL with a granular structure. The addition of $\text{Al}(\text{OH})_3$ to H_3PO_4 solutions seems to lead to RCL with smaller grains size in a more compact structure.

The crystalline species identified in these RCL by XRD are mainly hydroxides - lepidocrocite, FeOOH , and minor goethite, $\alpha\text{-FeOOH}$ - and iron phosphates.^[6] Occasionally, a spinel - type oxide (- $\text{Fe}_2\text{O}_3/\text{Fe}_3\text{O}_4$) was also detected. No crystalline phase specific for aluminium could be traced in the XRD spectra.

Broad bands were noticed in the XRD Spectra of the white bluish RCL, positioned around the main reflection of vivianite, a ferrous phosphate hydrated^[6] phase with formula $\text{Fe}_3(\text{PO}_4)_2 \cdot 8\text{H}_2\text{O}$ in accordance with IR data^[6].

On the other hand, heigher concentrations of H_3PO_4 (with or without aluminium hydroxide) lead to formation of RCL with a pattern indicating an amorphous state. This glassy state is known as "phosphate glass"^[18], being attributed to disordering by rotation about hydrogen bridges in the material resulting from concentrated acid solutions.

The glassy RCL, present some regions almost continuous and others, as can be seen on micrographs a2), a3) and b2), in fig. 2, more or less heterogeneously broken. The addition of $\text{Al}(\text{OH})_3$ to H_3PO_4 solutions seems to contribute to densify the material relaxing the thin cracks of the glassy RCL. When these surfaces are exposed for some months to normal atmosphere, they behave differently as a function of $\text{Al}(\text{OH})_3$ addition. After 12 months of exposure, the RCL obtained with H_3PO_4 solution at 33,2%(w/w) showed some iron corrosion points, but the structure remained similar. On the contrary, the structure of RCL obtained with the H_3PO_4 solution at 38,6% and saturated with $\text{Al}(\text{OH})_3$, change more or less continuously as can be seen on micrographs b3) of figs 1 and 2. The change observed, leads to the growth of spirals similar to that reported by W. Kleber^[19]. The advance of this growth theory consists in the concept that, during growth, permanent steps exist and that there after, growth points may occur. Therefore a two-dimensional nucleus is not necessary in this case and growth can proceed even with a small supersaturation. This microstruture seems to be typical of the

begining of crystalization, and, in the case of RCL, it may imply a better order in the final structure.

Although this last RCL, had the best anticorrosive behaviour under laboratory atmosphere, it could not resist^[14] under a paint coating and exposed to humidity in a cabinet^[16] or in an open atmosphere^[16], for more than 10 days and 13 months respectively, before blistering formation. As can be seen on Tables 2 and 3, in both exposure situations the best anticorrosive behaviour is presented by RCL obtained with H_3PO_4 solutions activated with $Al(OH)_3$ addition. However, any one of the studied RCLs showed an anticorrosive behaviour so good as that obtained with the same paint coating applied on a rust-free steel surface (codified by 1 on Table 1).

The best behaviour of RCL obtained with phosphoric acid solutions saturated with $Al(OH)_3$, can probably be explained by the solubility properties of the newly-formed layers, as can be seen from Table 4. On the other hand, results listed on Table 5, show that all RCL studied improve significantly the paint adhesion on CSt2 steel surfaces. This improvement is specially significant at the level of RCL cohesion.

Conclusions

From results obtained in the present study it seems possible to draw the following conclusions:

- In low-grade aggressive atmospheres, the pretreatments based on H_3PO_4 , if correctly choosed and enhancing the paint adhesion forces, may improve the anticorrosive behaviour of the paint coatings having heigh impermeability;
- Better anticorrosive behaviour, can be observed with pretreatments based on H_3PO_4 saturated with $Al(OH)_3$. In spite of improving not so much the paint adhesion forces, these pretreatments allow the formation of RCL with heigher binding power and lower water solubility;
- Any of these pretreatments showed to "converte" completely the rust steel surfaces. It was always possible to verify the presence of $FeOOH$ in the brown-black RCL and beneath the white-bluish RCL. The later seem to result from the incipient evolution of the amorphous white products towards vivianite, $Fe_3(PO_4)_2 \cdot 8H_2O$, a blue crystalline phase that owes its colouring to the coexistence of Fe^{II}/Fe^{III} , with instabilization of valencies and correlative light absorption phenomena.
- The aluminium hydroxide added in the pretreatments, does not seem to develop any additional crystalline phase. The main reason for this may well be the recognized incompatibility of simultaneous accomodation of Fe and Al in the crystalline structures of the common and most stable phosphates^[20]. The known phosphating inhibition by aluminium^[21] has probably the same origin. On the other hand, the growth spirals observed after atmospheric exposure of the RCL obtained with heighly concentrated acid solutions saturated with $Al(OH)_3$, have no particular expression in the X-ray diffractograms.

- The global results so far obtained, seem to confirm published electrochemical data, showing that this kind of pretreatments do not effectively block the corrosive activity of rust^[22]. In this situation, they must not be recommended for use under aggressive atmospheres or beneath permeable paint coatings.

Acknowledgements

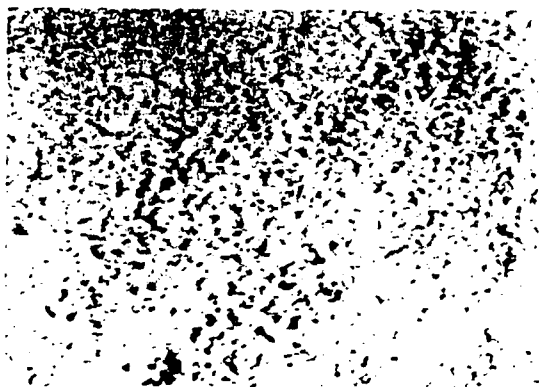
E. Almeida and M. Morcillo would like to thank the European Communities Commission (Agreement 7210/KB 931 and 932) for financial support and to all INETI staff that collaborate in this work, specially to Teresa Magalhaes and Joao Seabra.

References

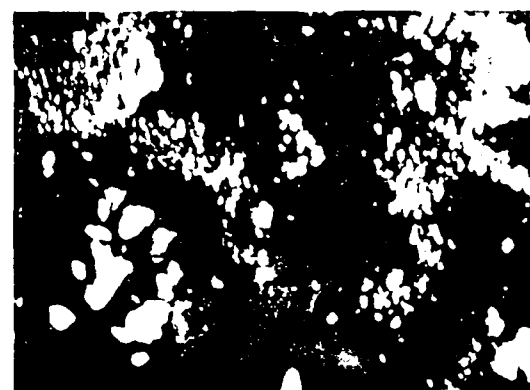
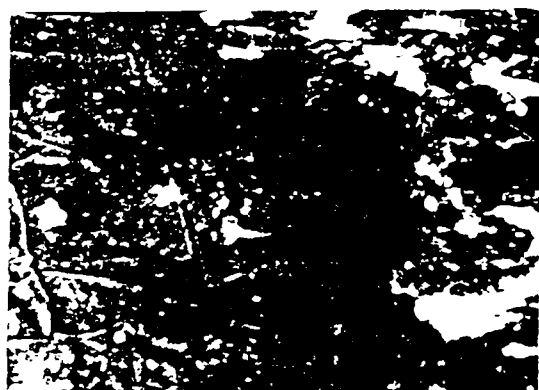
- 1 - Westchester, J., Metal Finish., Dec. (1966): p74.
- 2 - Hendry, M., "Reader Reponse on Rust Converter", Journ. of Protect. Coat. and Lin., 2, 8, (1985): p18.
- 3 - Frondistou Yannas, S., Journ. of Protect. Coat. and Lin., 3, (1986): p26-35.
- 4 - Alvarez, Z.E., Callozo, I. y Valdés, D.: Rev. Iber. Corr. y Prot., XVII, 1, (1987): p35-38.
- 5 - A.N. Nigam, R.P. Tripathi and K. Dhoot, Cor. Sic., 30, 819, (1990): p799-803.
- 6 - E. Almeida, D. Pereira, J. Waerenborgh, J.M. Cabral, M.O. Figueiredo, V.M. Lobo and M. Morcillo, Prog. in Org. Coat., 21, 4, (1993): p327-338
- 7 - ISO 630 - Structural Steels, Geneve, Switzerland, (1980).
- 8 - E. Almeida and M. Morcillo, "Protective Pretreatments of Rusted Steel Surfaces", CECA, Agreements Nos 7210/KB/931 and 932, LNETI/CENIM, Report Nº 1, (1988).
- 9 - SIS 055900 - Pictorial Surface Preparation Standard for Painting Steel Articles, (1967).
- 10 - Vogel, A.I., "Química Analítica Cuantitativa", Vol.II, Editorial Kapeloz, 2ª Edición, Buenos Aires, (1969).
- 11 - I.M. Kolthoff and P.J. Elving, "Treatise on Analytical Chemistry", Part II, Vol.5, 1ª Ed., Interscience Publishers, (1961).
- 12 - ASTM D 823-87 - Producing Films of Uniform Thickness of Paint, Varnish and Related Products on Test Panels, Method E, ASTM, Vol. 06.01, USA, (1990).
- 13 - ISO 4624 - Paints and varnishes - Pull-off test for

adhesion (1978).

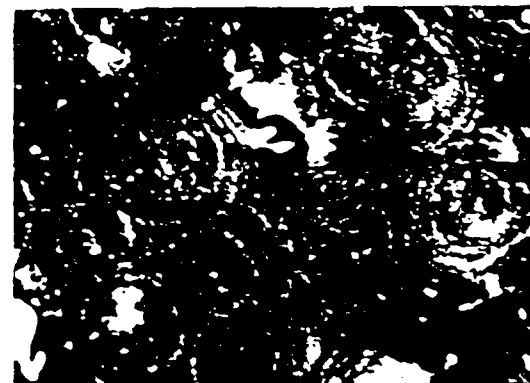
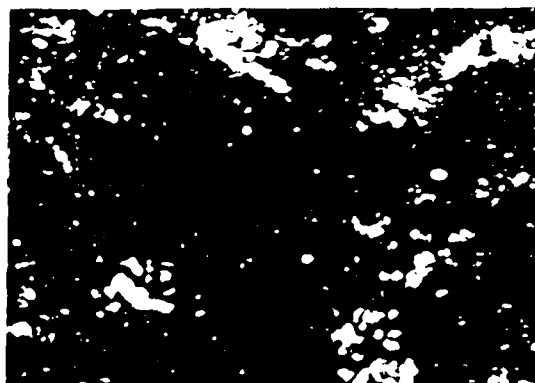
- 14 - DIN 50017 - Method of Test in Damps Heat Atmospheres (1963).
- 15 - ISO/DIS 8565.2 - "Metaux et Alliages - Essai de Corrosion Atmosphérique. Prescription Générales de l'Essai in Situ".
- 16 - ISO 4628 - "Evaluation of Degradation of Paint Coatings. Designation of Intensity, Quantity and Size of Common Types of Defects", (1984).
- 17 - W. Machu, Werkstoffe Korrosion 14, (1963): p273-279.
- 18 - H. Krebs - Fundamentals of Inorganic Chemistry, McGraw-Hill, London, (1968): p350.
- 19 - W. Kleber - An Introduction to Crystallography, Veb. Verlag. Technik. Berlin (1970): p117.
- 20 - Duncan McConnell, Mineralogical Magazine, June, 40, (1976): p609-10.
- 21 - J.C. Mason "Double Liaison. Chem. Peintures", May/Jun. (1966): p367-368.
- 22 - J.C. Galvan, S. Feliu Jr., J. Simancas, M. Morcillo, J.M. Bastidas, E. Almeida and S. Feliu, Elect. Act. 37, 11, (1992): p1983-85.



a1)at 14,6% and after 24 hours b1)at 27,3% and after 24 hours



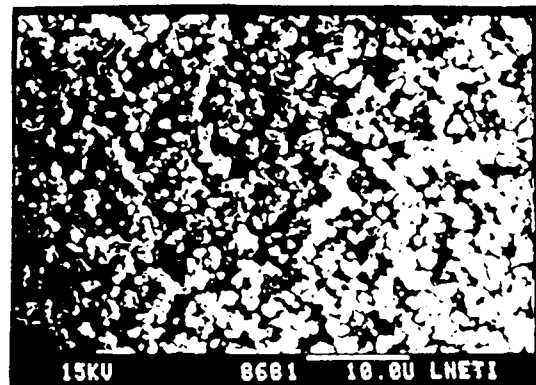
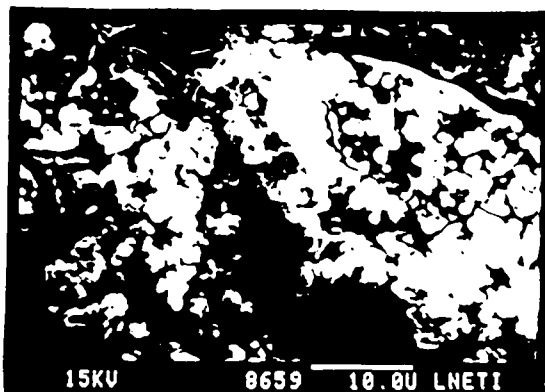
a2)at 33,2% and after 24hours b2)at 38,6% and after 24 hours



a3)at 33,2% and after 12 months b3)at 38,6% and after 12months

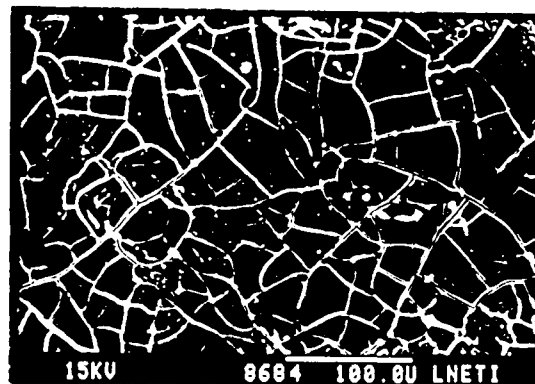
a) Pretreated with H_3PO_4 solu - b) Pretreated with H_3PO_4 solu -
tions tions saturated with $Al(OH)_3$

Fig.1 - Some results obtained by optical microscopy on the RCL under study.



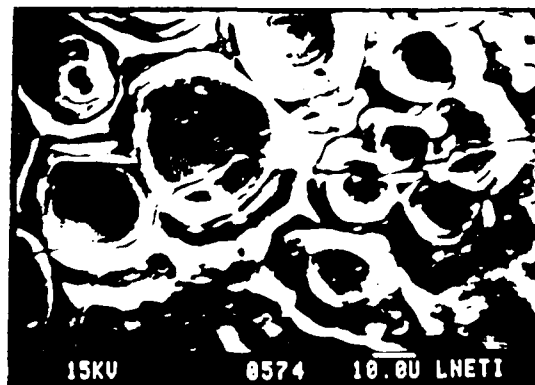
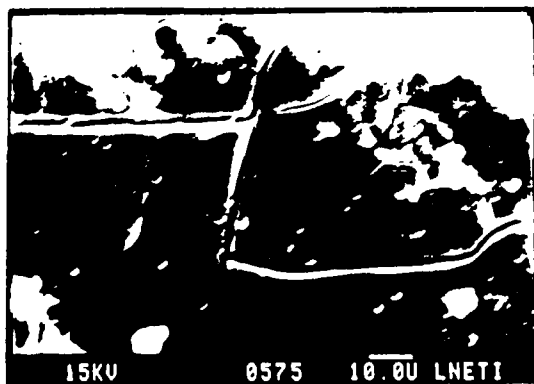
a1) at 14,6% and after 24 hours

b1) at 27,3% and after 24 hours



a2) at 33,2% and after 24 hours

b2) at 38,6% and after 24 hours



a3) at 33,2% and after 12 months
a) Pretreated with H_3PO_4 solutions

b3) at 38,6% and after 12 months
b) Pretreated with H_3PO_4 solutions saturated with $Al(OH)_3$

Fig.2 - Some SEM results obtained with pretreated surfaces at different times of exposure to laboratory atmospheres.

TABLE 1
STEEL SURFACES CODIFICATION

SURFACE CODE	PREVIOUS SUR- FACE PREPARA- TION ^[9]	PRETREATMENT APPLIED	PAINT COATING	
			YES	NO
1	C Sa 2 1/2	----	x	-
2	C St2	----	-	x
3	C St2	----	x	-
4	C St2	H ₃ PO ₄ at 14,6% (w/w)	-	x
5	C St2	H ₃ PO ₄ at 14,6% (w/w)	x	-
6	C St2	H ₃ PO ₄ at 33,2% (w/w)	-	x
7	C St2	H ₃ PO ₄ at 33,2% (w/w)	x	-
8	C St2	H ₃ PO ₄ at 27,3% (w/w) saturated with Al(OH) ₃	-	x
9	C St2	H ₃ PO ₄ at 27,3% (w/w) saturated with Al(OH) ₃	x	-
10	C St2	H ₃ PO ₄ at 38,6% (w/w) saturated with Al(OH) ₃	-	x
11	C St2	H ₃ PO ₄ at 38,6% (w/w) saturated with Al(OH) ₃	x	-

TABLE 2
ANTICORROSIVE BEHAVIOUR OF STEEL SURFACES PAINTED
a) After exposure in humidity cabinet^[14]

SUR- FACE CODE	BLISTERING ^[16] FORMATION VERSUS EXPOSURE TIME									
	48 H	72 H	4 D	7 D	8 D	10 D	11 D	12 D	14 D	19 D
1	0	0	0	0	0	0	0	0	0	0
2	* 3(S2)n.e.	Idem	Idem	** 2(S3)g	3(S4)g	Idem	Idem	Idem	Idem	3(S5)g
4	0	0	0	0	0	0	0	0	0	2(S4)n.e.
6	0	*** 2(S2)l	2(S2)l	2(S2)g	3(S2)g	Idem	Idem	Idem	3(S3)g	2(S4)g 3(S4)n.e.
8	0	0	0	0	0	0	0	0	2(S2)l	3(S3)l
10	0	0	0	0	0	2(S2)l	3(S3)l	3(S3)g	3(S3)g	3(S3)g

* Near edges

** Generalized

*** Localized

TABLE 3
ANTICORROSIVE BEHAVIOUR OF STEEL SURFACES PAINTED
b) After exposure at Lumiar/Lisbon test site

SURFACE CODE	BLISTERING[16] FORMATION VERSUS EXPOSURE TIME(MONTHS)						
	2	3	8	10	13	16	19
1	0	0	0	0	0	0	0
2	0	0	1(S2)n.e.	2(S2)g	2(S2)g	2(S3)g	3(S3)g
4	0	0	0	2(S3)n.e.	Idem	Idem	Idem
6	0	0	0	2(S3)n.e.	Idem	Idem	2(S3)g
8	0	0	0	0	0	0	2(S3)l
10	0	0	0	0	2(S3)n.e.	Idem	2(S3)g

TABLE 4
RESULTS OF SOLUBILITY TEST ($\mu\text{g.cm}^{-2}$)

SURFACE CODE	Fe CONTENT	P EXPRESS IN PO_4^{3-}
2	22.9	----
4	17.8	76.8
6	51.5	337.1
8	7.5	3.7
10	29.8	642.4

TABLE 5
RESULTS OF INITIAL PAINT ADHESION^[10]

SURFACE CODE	BREAKING FORCE (N)	BREAKING STRENGTH (MPa)	NATURE OF FAILURE					
			RCL	RCL/P	P	B/F	F	F/G
1	1768	5.6	--	--	65	--	10	25
2	430	1.4	85	--	15	--	--	--
4	1382	4.4	75	--	20	--	--	5
6	1537	4.9	15	55	20	--	--	10
8	1223	4.0	25	40	25	--	--	10
10	971	3.1	10	80	10	--	--	--

A Unique Plasma Spray Process to Create Corrosion Control Surfaces*

G. Sweet and W.W. Bristowe

*** Poster paper - Paper not available for publication.**

Evaluation of Corrosion Resistant Coatings for Mild Steel*

M.K. Trivdi, H.H. Mandalia and C.D. Mital

* Poster paper - Paper not available for publication.

Electrocorrosion-inhibiting Behaviour of Flame
Retarding PVC Pressure-sensitive Adhesive Tape

Wan-rong Tao
East china Univ. of Chemical Technology
PO Box 377
200237 Shanghai, P.R.China

Hong-hua Ge
East china Univ. of Chemical Technology
PO Box 377
200237 Shanghai, P.R.China

Yi Qing
East china Univ. of Chemical Technology
PO Box 377
200237 Shanghai, P.R.China

Abstract

Flame retarding PVC tape is a pressure-sensitive adhesive tape which is composed of polyacrylate adhesive and flame retarding PVC film. It has been used in the colour television.

In this paper electrocorrosion coefficient of flame retarding PVC pressure-sensitive adhesive tape was measured by using self made instrument; Sample's optimums were explored; Practicability of the instrument was evaluated and corrosion mechanism was discussed.

The experiment results show that: 1. This instrument is practicable in accurately testing the electrocorrosion coefficient. 2. Five formulas having excellent electrocorrosion-inhibiting behavior identical with imported tape's from Japan have been found out. 3. It's explained also that the main factor to affect the electrocorrosion coefficient is catalyzer and for the tested copper wire, the main corrosion medium is moisture air including volatilized matter from catalyzer and water.

Key terms: electrocorrosion coefficient, adhesive tape, polyacrylate

Introduction

Pressure sensitive adhesive tape is widely used in television industry^{1,2}. In a television, pressure-sensitive adhesive tape can be found at about more than 30 parts, including those one sided and two sided to ligate conducting wire, cover the welding hole on the printing circuit plate, prevent shock and resist heat and voltage, so the research for exploiting the pressure sensitive adhesive tape with many excellent performance, in which people are greatly intrested, is very active. Flame retarding PVC pressure sensitive adhesive tape used for binding up the erasing coil in colour television is one of that kind.

For the colour television's reliable quality and stable performance, not only the excellent performance of every element, but also the good anticorrosion with the effect of condition is required. The research in this field is not very popular at present. In this paper, the electrocorrosion coefficient of the pressure sensitive adhesive tape which is composed of polyacrylate adhesive and flame retarding PVC film was measured by using self made instrument; Practicability of the instrument was evaluated; Sample's optimums were explored and corrosion mechanism was discussed. The pressure sensitive adhesive tape has been successfully used to bind up erasing coil in the colour television.

Experimental Procedure

I. Preparation of pressure-sensitive adhesive tape

Weighed a certain amount of polyacrylate adhesive, added a proportional cross linking agent and catalyzer, diluted with certain dissolvent to suitable concentration, then spread it to PVC film, and heated and cross linked under the fixed temperature for several minutes. After these procedures, pressure-sensitive adhesive tape has been obtained.

II. The self made instrument to measure electrocorrosion coefficient

With the naked copper wire as electrode arm and adhesive as electrolyte, oxidizing reaction happens on anode copper wire and reducing reaction happens on cathode after electrization. The tensile strength ratio of anode copper wire to cathode copper wire after reaction is defined as the electrocorrosion coefficient.

$$\eta = \sigma_+ / \sigma_- \quad (1)$$

where η ----- electrocorrosion coefficient;
 σ_+ ----- tensile strength of anode copper wire, g;
 σ_- ----- tensile strength of cathode copper wire, g.

The diagram of the experiment instrument is showed in figure 1.

III. Preparation of samples

A. Preparation of standard samples³

1. The preparation of samples was required in the clean laboratory.
2. Operating staffs wore clean gloves, wiped rigid insulating plate with alcohol or acetone, then rinsed the cellulose acetate cloth with distilled water, and aired it. After that, it was not permitted to be touched directly by hand.
3. Put a cellulose acetate cloth with the length of 150 mm and width of 25 mm on the rigid insulating plate, and added two naked copper wires with same diameter on it. The diameter of the naked copper wire was from 0.18 mm to 0.20 mm. Then extended and fixed the naked copper wire along the slot of rigid insulating plate with appropriate pulling force.
4. Made the standard sample as described in figure 3 according to the applying method described in figure 2, then rolled back and forth for 5 times with the rolling instrument, whose weight was 2 kg. When rolling, naked copper wire should not be twisted and cellulose acetate cloth should not wrinkled. After

rolling, the sample should be airtightened.

5. The sample was 150 mm long and 25 mm wide. On one side of the sample, the leadind copper wire with necessary length should be kept for the connection with the power supply.

B. Preparation of non-standard sample

Replacement of cellulose acetate cloth by adhesive tape according to the method described in III - A, could get non-standard sample.

IV. Testing method³

1. Poured the distilled water into the glass container mentioned in figure 1, then connected according to the figure, and the sample should be hung in the airtightened testing container under free condition. A couple of electrodes could hang seven samples which could not contact the container wall, and there should be intervals between every two samples.

2. The testing temperature was $50^{\circ}\text{C} \pm 1^{\circ}\text{C}$. Connected with power supply after half an hour's preheating and then began to calculate the testing time. The testing voltage was $250\text{v} \pm 5\text{v}$ and the testing time was 20 hours.

3. After testing, removed the cellulose acetate cloth and the naked copper wire.

4. Tested the tensile strength of anode copper wire and cathode copper wire respectively by using the tension testing machine(AG 2000A electron universal testing machine). The copper wire's effective testing length was 100 mm and its extending speed was 100 mm/min.

5. Calculated η according to formula (1) and showed the testing results with the average, maximum and minimum values of seven data. When the average value was more than 1, fixed it as 1.

Results and Discussion

1. Evaluation of the testing instrument's practicability

A. Strength test of the blank naked copper wire

To test the system error and the error caused by the copper wire itself and the existent defect, blank test was conducted to the copper wire(table 1). To test the tensile strength by the AG 2000A electron universal testing machine, the sample was lengthened and the middle working area was marked. All the fractures in the working area could be recognized as the effective fracture.

The testing results showed that the average value was $0.48 \times 10^9 \text{Pa}$ and the relative error was 6.2%. When testing the electrocorrosion coefficient, such kind of error should be taken into account.

B. Evaluation of the repeatability

The instrument's practicability was evaluaed by repeating the test with yellow adhesive tape which was the domestic polyamide adhesive tape with the electrocorrosion coefficient of 0.95, and the black adhesive tape which was the self-made flame retarding PVC adhesive tapc(table 2). Table 2 shows that the

electrocorrosion coefficient of yellow adhesive tape is 0.95 and the data obtained is 0.96; The relative error is 4.2% which is within the relative error scope of the naked copper wire, and many data of the black adhesive tape is between 0.98 and 1.00, so this instrument can be used to evaluate the adhesive tape's electrocorrosion-inhibiting behavior.

II. The relationship between the electrocorrosion coefficient of the adhesive tape and the testing time

According to the testing standard, the testing period is 20 hours. From figure 4, we can see the electrocorrosion coefficient is almost stable in the first 10 hours, and the curve tends to smooth after 16 hours. So for the accurate testing of the electrocorrosion-inhibiting behavior, the testing period shall be more than 16 hours.

III. Electrocorrosion-inhibiting behavior of the black adhesive tape

According to the relationship between monomer component and behavior of the acrylate adhesive^{4,5}, we composed polyacrylate A, selected proportional cross linking agent I (synthetic resin with hydroxide radical; 3%), changed the type and amount of the catalyzer and the cross linking condition, then got five kinds of pressure-sensitive adhesive tape whose electrocorrosion coefficient was tested together with the Japan-made adhesive tape. For the result please refer to table 3. The result shows that η which is more than 0.9 satisfies the requirements of binding up the erasing coil and there is no apparent corrosion on the exterior of copper wire after experiment.

IV. Corrosion mechanism of the adhesive tape

After finding out the adhesive tape's electrocorrosion, its corrosion mechanism shall be discussed for the effective control of corrosion.

A. The effect of cross linking time on the electrocorrosion coefficient

To discuss the main factors affecting the electrocorrosion-inhibiting behavior, we first took the manufacturing procedure of the adhesive tape into consideration. That is to say, determined the electrocorrosion coefficient under various cross linking condition and the effect of the cross linking condition on it(see table 4).

The results show that for the above formulas, whether there is catalyzer or not, electrocorrosion does not happen provided the cross linking condition can ensure the completion of cross linking reaction.

B. Analysis of the main corrosion components

The main components of the formulas in this paper are polyacrylate, cross linking agent and three kinds of catalyzer 1, 2, 3 with different activity. We studied the effect of every single component on η , found out the elements of corrosion, and then discussed the cause of electrocorrosion.

In order not to have additional error, yellow adhesive tape with less

electrocorrosion was used as the carrier of cross linking agent and catalyzer, and PVC film as the carrier of resin. For the results, please refer to table 5. Table 5 shows that the resin A and cross linking agent 1, which were in the adhesive tape all alone and took part in the reaction, do not appear apparent corrosion in single existence. For catalyzer 1 and catalyzer 3, no corrosion signal can be seen from η , but from the tensile strength of the acted copper wire, actual corrosion can be seen. For example, the maximum of the cathode copper wire's tensile strength acted by catalyzer 1 is $0.44 \times 10^9 \text{Pa}$, while the minimum is $0.42 \times 10^9 \text{Pa}$; The maximum of the anode copper wire's tensile strength is $0.44 \times 10^9 \text{Pa}$, while the minimum is $0.38 \times 10^9 \text{Pa}$. The corresponding data of the copper wire's tensile strength acted by catalyzer 3 are: cathode 0.45, 0.34; anode 0.41, 0.37. All of these data are obviously lower than those of the naked copper wire's tensile strength, which is caused by corrosion, but η is still not very small because the difference of the tensile strength between cathode copper wire and anode copper wire is small. So the corrosion of catalyzer 1 and 3 is only the metal's general corrosion and has little to do with electrization. For catalyzer 2, apparent electrocorrosion is found out. The stripped anode copper wire appears grey and the surface is full of corrosion product, while there is almost no change for the cathode copper wire in appearance. The same happens on the data of the tensile strength. This shows the main corrosion element of every formula components is catalyzer and the main effect is catalyzer 2 for electrocorrosion.

C. The effect of catalyzing condition on η

Among the effects of single component, catalyzer 2 had strong electrocorrosion behavior, but the adhesive tape made from it had high η . So we imitated the cross linking procedure to heat the yellow adhesive tape applied with catalyzer 2 and added the amount of catalyzer 2 to 20%(table 6, 7), then we could discuss the effect of cross linking temperature and the amount of catalyzer. The experiment shows that when heating and cross linking, some parts of the catalyzer volatilize, corrosion elements decrease and electrocorrosion coefficient rises, but the main effect is the amount of catalyzer. When the amount of catalyzer reaches 20%, the electrocorrosion coefficient is still very high. The reason for low electrocorrosion coefficient of the yellow adhesive tape spread with catalyzer 2 is that the amount of catalyzer is much more than 20%. There is no effect on electrocorrosion coefficient because on preparation of the adhesive tape, the amount of catalyzer 2 is only 2% and heating is done when cross linking.

D. Study on the electrocorrosion medium

There are two possibilities to be electrocorrosion medium, one is with the catalyzer remaining in the adhesive on the adhesive tape as main medium; The other is that the remaining catalyzer volatilizes under certain temperature and moisture and forms the corrosion environment, while the adhesive shields and protects the copper wire. To determine which kind the adhesive tape's electrocorrosion belongs to, the contrast experiment was done between the non-standard and standard samples. For the results, please refer to table 8. To standard sample which was tested under 50°C , the catalyzer's volatilizing

elements remaining in the adhesive tape met moisture and slight electrolytic cell was formed, so oxidizing and reducing reactions happened between anode copper wire and cathode copper wire, causing the corrosion of anode copper wire; To non-standard sample, slight electrolytic cell could not be formed because of the isolation between the air, water and copper wire, so adhesive tape's electrocorrosion procedure was greatly restrained. It is concluded that the main medium causing the decrease of electrocorrosion coefficient is the second case.

By study on the electrocorrosion mechanism, the main factors affecting the adhesive tape's electrocorrosion are found out and the following measures can be taken to control corrosion:

1. Use the catalyzer having weak or little corrosion behavior.
2. During the preparation procedure of adhesive tape, control the amount and volatilization of catalyzer and decrease the remaining amount in the adhesive tape.
3. On using, decrease the remaining catalyzer's volatilization and the air moisture, avoid the formation of slight electrolytic cell.

Conclusion

1. Self-made instrument for testing electrocorrosion coefficient can be used to evaluate the adhesive tape's electrocorrosion behavior.
2. Acid catalyzer is the main element causing electrocorrosion and the medium of electrocorrosion is air, including volatilized matter from catalyzer and water.
3. The electrocorrosion behavior of the tested flame retarding PVC pressure-sensitive adhesive tape satisfies the requirements of colour television.

Reference

1. 李子東, 实用粘接手冊 (上海, 上海科技出版社, 1987), p.317.
2. 茅百明, 粘合剂, 5(1983):p.27.
3. HG 4 1550-84, Standard of Chemical Industry Ministry of P.R.China.
4. Dunning, R. Henry, Pressure Sensitive Adhesive, formulations and Technology, (Park Ridge N.J., Noyes, 1977), 428p.
5. 福沢敬司, 粘着技術 (高分子刊会, 1978)

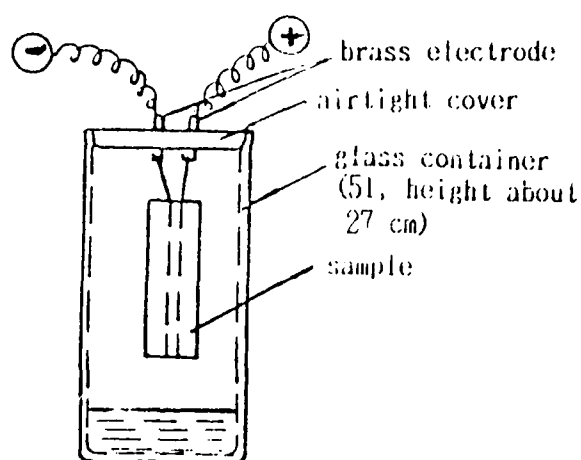


Figure 1. Diagrammatic sketch of η testing instrument

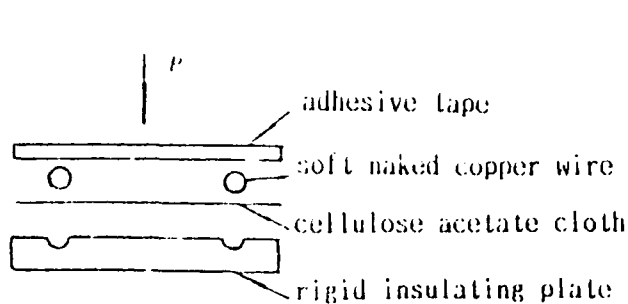


Figure 2. Applying diagram of sample

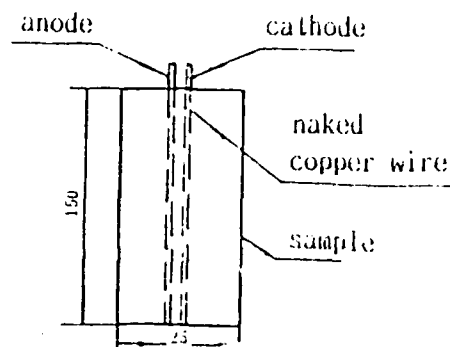


Figure 3. Size of sample

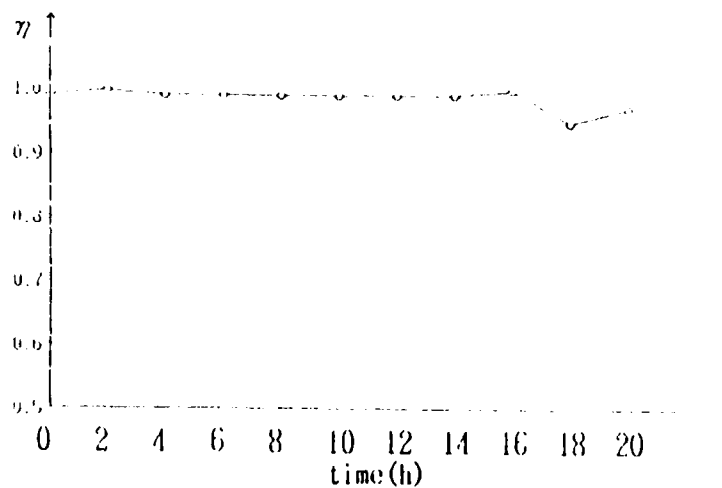


Figure 4. The relationship between the η of the block adhesive tape and testing time

Table 1. Tensile Strength of The Naked Copper Wire

tensile strength	0.47	0.47	0.48	0.49	0.49	0.50
10 ⁹ Pa	0.47	0.48	0.49	0.49	0.49	0.50

Table 2. Evaluation of The Repeatability of
The Electrocorrosion Coefficient

times	η Value of yellow adhesive tape			η Value of black adhesive tape		
	average	maximum	minimum	average	maximum	minimum
1	0.98	0.99	0.96	0.98	1.02	0.91
2	0.96	0.98	0.94	1.00	1.04	1.00
3	0.94	0.99	0.88	0.93	1.02	0.72
4				0.98	1.06	0.72
5				0.98	1.00	0.93
average value	0.96			0.97		
relative error	4.2%					

Table 3. Electrocorrosion Coefficient of The Black Adhesive
Tape and The Imported Adhesive Tape

No.	η value			remarks
	average	maximum	minimum	
1	0.97	1.01	0.93	catalyzer 1, 3, 4%, 80°C, 7 min.
2	1.00	1.03	0.97	catalyzer 1, 2, 4%, 80°C, 7 min.
3	0.98	1.03	0.92	catalyzer 1, 2, 4%, 80°C, 10 min.
4	0.96	0.98	0.92	130°C 7 min.
5	0.95	1.00	0.87	130°C 14 min.
6	0.91	0.96	0.79	adhesive tape imported from Japan

Table 4. Electrocorrosion Coefficient under Various Cross Linking Condition

cross linking condition	η value			remarks
	average	maximum	minimum	
130°C 10 min.	0.95	0.99	0.87	catalyzer 1, 2, 4% catalyzer 1, 2, 4%
7 min.	0.96	0.98	0.92	
80°C 10 min.	0.98	1.03	0.92	
7 min.	0.99	1.03	0.96	

Table 5. The Effect of Every Component on η

components	η value		
	average	maximum	minimum
catalyzer 1	0.95	1.01	0.90
2	0.56	0.72	0.48
3	0.98	1.01	0.90
cross linking agent 1	0.98	1.02	0.90
resin A	1.00	1.02	0.99

Table 6. The Effect of Heating Condition on Electrocorrosion Coefficient

component	η value without heating			η value after heating		
	average	maximum	minimum	average	maximum	minimum
catalyzer 2	0.56	0.72	0.48	0.70	0.78	0.55

Table 7. The Effect of The Amount of Catalyst
on Electrocorrosion Coefficient

amount of catalyst	η value			remarks
	average	maximum	minimum	
catalyst 1, 2; each for 2% catalyst 2; 20%	1.00 0.98	1.03 1.00	0.97 0.96	resin A; cross linking agent I 80°C, 7 min.

Table 8. The Electrocorrosion Coefficient of Standard
Sample and Non-standard Sample

component	η value of standard			η value of non-standard		
	average	maximum	minimum	average	maximum	minimum
catalyst 2	0.56	0.72	0.48	0.94	1.02	0.79